Developing novel methods for the generation of 3D retinal organoids from rat and macaque pluripotent stem cells

Madeleine Yen Mei Carter

Thesis submitted to Newcastle University for the degree of Doctor of Philosophy (PhD)

Biosciences Institute

Faculty of Medical Sciences

July 2022

Abstract

Pluripotent stem cells (PSCs) can be differentiated toward certain lineages using chemical, spatial and temporal cues. They can form 3D structures, termed organoids, which replicate the cellular diversity and organisation of native tissue along the timeline of embryological development. Retinal organoids (ROs) can represent the stratified complexity of native retina *in vitro* and therefore have huge potential for pre-clinical studies, biomedical research and the development of therapeutics for retinal disease. The generation of ROs from animal models such as macaque and rat is relevant for drug development as these are commonly used species for the safety assessment of candidate therapeutic agents.

By using a method combining generation of retinal progenitor cells, through an intermediate stage of adherent culture, and suspension culture in media used for the maturation of mouse ROs, rat embryonic stem cells (ESCs) were differentiated into 3D organoids. Using morphological characterisation, protein and gene expression assays, rat organoids developed phase-bright neural retina, and cells expressing retinal progenitor (Pax6/CHX10), retinal ganglion (SNCG/RBPMS) and photoreceptor (RCVRN) cell markers. However, the stratified cellular organisation typical of the retina was lacking after 28 days in culture. Comparison with mouse ESC-derived ROs showed variable responses to the same culture conditions indicating species-specific differences.

By adapting the timeline of human RO differentiation protocols to the shorter gestation of the macaque, induced pluripotent stem cell (iPSC)-derived organoids were generated which maintained typical retinal morphological features and cell marker expression at day 120. Macaque organoids show the sequential expression of neural-epithelia (Rax, Pax6, Sox2), photoreceptor precursor (Crx), photoreceptor (OPN1SW, OPN1LW/MW, RHO), interneuron (AP2α, PRKCα) and Müller glia (CRALBP) cell markers indicating some retinal development and maturation. Macaque iPSC lines showed variable responses with RPE conditioned media and IGF1-based protocols improving morphology and photoreceptor marker expression in one cell line.

These results develop the understanding of mammalian *in vitro* retinal differentiation by showing the capacity of rat and macaque PSCs to differentiate using known retinal stimulating factors. Further research should optimise cellular organisation to better replicate the retinal structure.

Acknowledgments

No research project is done in isolation, every piece of research comes within the context of the work done before and leads to the studies that follow. Therefore, I would like to acknowledge the incredible amount of work that led up to this project within the Lako lab group and around the world on retinal organoid research.

I would like to thank my supervisors Prof. Linda Lako, Dr Valeria Chichagova and Dr Birthe Dorgau for their supervision, expertise, advice and for constantly pushing me to find the next step.

My supervisory panel members Prof. David Steel and Dr Evelyne Sernagor were very supportive and helped me to improve my research and become a better scientist throughout my PhD.

Thanks to the NC3R charity who funded this project and supported my dissemination of this research at the ARVO conference 2022.

My friends, colleagues and bench pals at the Centre for Life have been instrumental in keeping me focused, challenged and sane throughout my PhD studies, so thank you to the Stem Cell lab members, past and present, and especially Maria, Rob, Ivo, Joe, Avril, Rodrigo, Jack, Anastassia and Jules for all the much-needed pastries, coffees and chats!

Thanks to my friends outside the lab, pub club at Bar Loco and especially my partner David Shapira who have been so consistently supportive and inspirational.

This thesis is dedicated to my grandmother, Theresa Kim Lui Repton, who always supported my studies and curiosity, taught me perseverance and my multiplication tables, and showed that living her life with Retinitis Pigmentosa would not affect her sense of enjoyment, generosity and family.

1923 - 2020

Table of Contents

List of Figures

List of Tables

List of Abbreviations

Abbreviation	Definition
°C	Degrees Celsius
AC	Amacrine cell
AMD	Age-related Macular Degeneration
BC	Bipolar cell
bFGF	basic Fibroblast growth factor/FGF2
CC	Connecting cilium
cDNA	coding deoxyribonucleic acid
-CM	Conditioned media
CO2	Carbon dioxide
ECM	Extra-cellular matrix
EFTF	Eye-field transcription factor
ESC	Embryonic stem cell
FBS	Foetal bovine serum
GCL	Ganglion cell layer
HC	Horizontal cell
IF	Immunofluorescence
IGF1	Insulin growth factor 1
IHC	Immunohistochemistry
INL	Inner nuclear layer
INZ	Inner nuclear zone
IPL	Inner plexiform layer
iPSC	Induced pluripotent stem cell
IRD	Inherited retinal disease
IS	Inner segment
MEF	Mouse embryonic fibroblast
MG	Müller glia
MITF	Microphthalmia-associated transcription factor
mRNA	Messenger RNA
NE	Neuroepithelium
NHP	Non-human primate
NR	Neural retina
NRPC	Neuroretinal progenitor cell
NSC	Neural stem cell
OC	Optic cup
OCT	Optical coherence tomography
OCT	Optimal cutting temperature compound
ONL	Outer nuclear layer
ONZ	Outer nuclear zone
OPL	Outer plexiform layer
OS	Outer segment
OV	Optic vesicle
PFA	Paraformaldehyde

PR	Photoreceptor
PSC	Pluripotent stem cell
qPCR	quantitative real time polymerase chain reaction
RA	Retinoic acid
RCVRN	Recoverin
RGC	Retinal ganglion cell
RHO	Rhodopsin
RLBP1	Retinaldehyde binding protein 1
RNA	Ribonucleic acid
RO	Retinal organoid
RP	Retinitis pigmentosa
RPC	Retinal progenitor cell
RPE	Retinal pigmented epithelium
SFEBq	Serum-free embryoid body formation with quick aggregation
TF	Transcription factor
UV	Ultraviolet light
wp	well plate

Chapter 1 Introduction and Literature review

1.1 Biology of the retina: importance, structure and function

The eye has evolved independently across many different animal groups however, the camera-type eye found in vertebrates is able to capture the highest optical resolution (Land & Nilsson, 2012). The transparent cornea and lens focus light entering the eye, converging it to the back of the eye onto the retina (Fig. 1.1A) (Sung & Chuang, 2010). The retina, or neural retina (NR), is a specialised laminated tissue responsible for converting light into electrical signals, via a process called phototransduction, that the brain can interpret as images. The highly organised laminar architecture of the retina is composed of multiple layers of interconnected neuronal cells that work together to perform this function (Sung & Chuang, 2010). In mammals five major classes of neuronal cells including photoreceptor cells (PRs), bipolar cells, horizontal cells, amacrine cells, and retinal ganglion cells (RGCs) contribute to its layered composition (Fig. 1.1B/C).
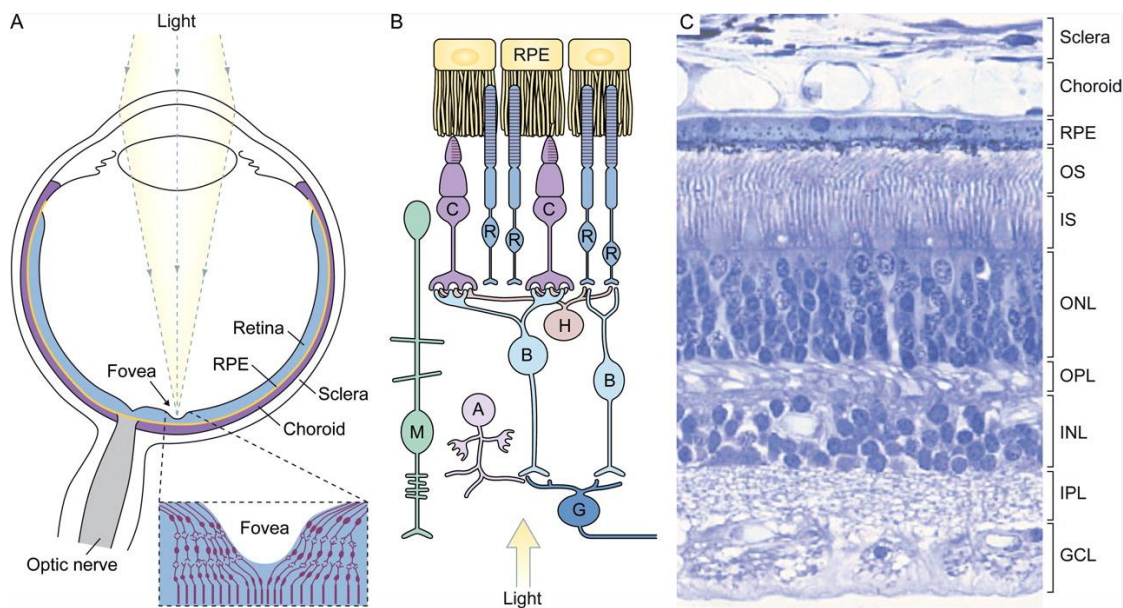
Figure 1.1. The location and cellular structure of the mammalian retina. *(Sung and Chuang 2010)A: The structure of the eye and location of the retina. B: The organisation of the cells of the neural retina tissue. The axons of retinal ganglion cells form the optic nerve which is the output to the brain. C: The retina with sclera and choroid tissues (H & E –stained) showing its laminated structure. RPE=retinal pigmented epithelium, C=cone photoreceptors, R=rod photoreceptors, B=bipolar cells, H=horizontal cells, A=amacrine cells, G=retinal ganglion cells, M= Müller glia, OS=outer segment, IS=inner segment, ONL=outer nuclear layer, OPL=outer plexiform layer, INL=inner nuclear layer, IPL=inner plexiform layer, GCL=ganglion cell layer.*

The inter-cellular synapses between these neuronal cells are crucial for the transmission of electrical signals throughout the retina, ultimately leading to the formation of visual perception in the brain (W. Heavner & Pevny, 2012).

The photosensitive PRs, which comprise over 80% of cells in the mouse retina (Jeon et al., 1998), have specialised rod and cone shaped cilia comprising an inner and outer segment (IS/OS) (Fig. 1.1B) (Yau & Hardie, 2009). PRs are a highly specialised cell type and the anatomy of the OS' is unique among cilia. They contain many stacked "disks" formed of a bi-layered plasma membrane which house numerous membrane spanning proteins (opsins) which enable phototransduction (Fain et al., 2010).

1.1.1 Phototransduction

The highly sensitive process of phototransduction that occurs in PR OS' is initiated by the absorption of a photon of light by the visual pigment, which causes a conformational change in the opsin protein (Yau and Hardie, 2009). This, in turn, causes the activation of a signalling cascade leading to the activation of a G protein (transducin) and the hydrolysis of cyclic guanosine monophosphate (cGMP), resulting in the closure of cGMP-gated ion channels in the OS membrane and the hyperpolarisation of the photoreceptor cell (Fig. 1.2) (Palczewski, 2006). In darkness, free cGMP binds to and maintains the channels in an open position (Yau and Hardie, 2009). The hyperpolarisation of the PR membrane, caused by light, results in a decrease in the release of glutamate from pre-synaptic vesicles, which activates bipolar cells (Yau and Hardie, 2009).
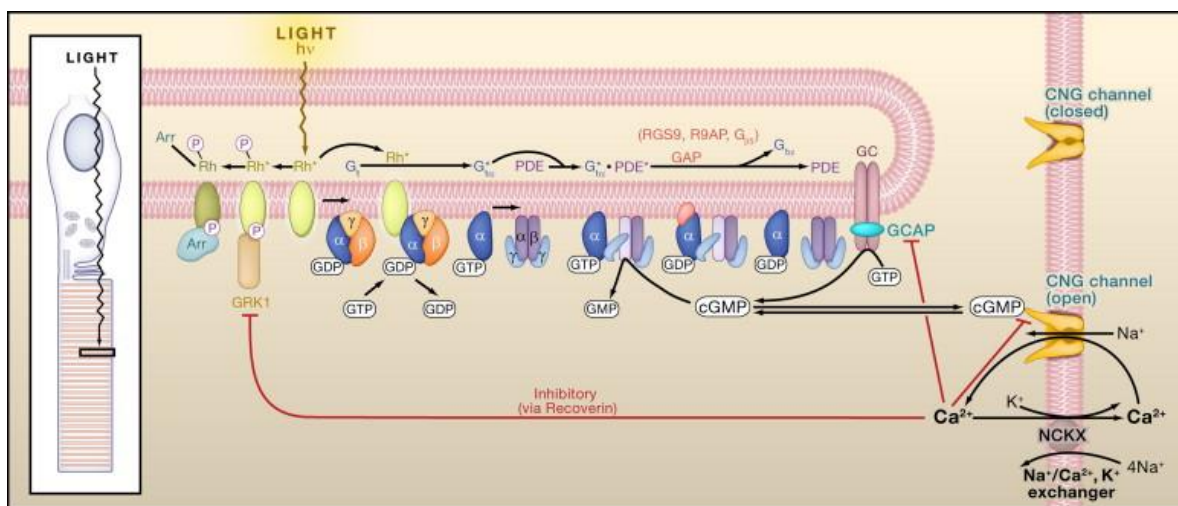
Figure 1.2. The process of transduction in a rod photoreceptor. The membrane spanning rhodopsin is activated by light (Rh*). This activates transducin (Gt*) which in turn stimulates PDE that hydrolyses cGMP and inhibits its ability to bind to cyclic-nucleotide-gated (CNG) channels. This blocks the inflow of calcium (Ca+) and sodium (Na+) (Yau and Hardie, 2009).

The opsins belong to the G-protein coupled receptor membrane-spanning family and exhibit huge diversity due to their early appearance in the evolution of complex life (Fain et al., 2010). Within the animal kingdom there are many sub-types of opsin and each PR class contains one type of opsin; in rods this is rhodopsin and in cones this is an opsin activated by different wavelengths of light (Yau & Hardie, 2009). PRs have different functionalities due to opsin variability. Rods, which contain the pigment rhodopsin, are adapted for sensitive vision in low light conditions. In contrast, cones, which contain different sub-types of opsin enable vision and colour detection in bright light conditions due to their receptivity to a wider range of light wavelengths (Yau & Hardie, 2009).

Primates have three cone types containing either: opsins optimised for detection of short wavelengths in the blue spectra (S/blue cones), mid wavelengths in the green spectra (M/green) and long wavelengths in the red spectra (L/red), and these vary in proportion depending on diurnal or nocturnal behaviour patterns (Wikler & Rakić, 1990). Another feature found in the primate retina is the fovea, an invagination found in the central macula region which is dense in cone PRs allowing for high acuity central vision (Fig. 1.1A) (Bringmann et al., 2018; Garita-Hernandez et al., 2019). The fovea is approximated in some non-primates as cats possess an "area centralis" and rabbits and shrews possess the "visual streak" which is a central area enriched for PRs and performs the same function as the fovea (Ahnelt and Kolb, 2000; Bringmann et al., 2018; Reichenbach and Robinson, 1995).

Cell nuclei of the PRs form the outer nuclear layer (ONL) and their processes contact bipolar and horizontal cells, forming the outer plexiform layer (OPL) (Fig. 1.1C). In response to light PRs release glutamate from their synapses which initiate the light response in bipolar cells (Sung & Chuang, 2010). Bipolar cells continue the synaptic transmission to the RGCs and these cell types form the major pathway for the signal to travel through the retina (Remington, 2012). The numerous, distinct forms of bipolar cells are classed into ON or OFF sub-types depending on the type of glutamate receptor, and rod or cone sub-types depending on the PR cell type they contact (Wan & Heidelberger, 2011; Yang, 2004). ON sub-types, which constitute all rod bipolar cells, depolarise in response to the light activation signal in the PRs, whereas OFF sub-types hyperpolarise in response to decreased glutamate release from PRs (Diamond, 2017; Yang, 2004). Bipolar cell nuclei are found tightly packed in the inner nuclear layer (INL) immediately adjacent to the PR synapses and are morphologically characterised by a large nucleus to cytoplasm ratio and thin axon (Fig. 1.1C) (Haverkamp, Haeseleer, et al., 2003).

Horizontal cells are also located in the INL and form synapses with PRs, bipolar cells and other horizontal cell subtypes in the outer plexiform layer (OPL) (Fig. 1.1B,C). They are a class of

interneurons which have several sub-types and mediate the synaptic transmission laterally (Remington, 2012). The nuclei of the interneuron class of amacrine cells are also found in the inner nuclear layer (INL) and ganglion cell layer (GCL) (Yau & Hardie, 2009). Amacrine cells are a diverse class of retinal interneurons which contact bipolar cells and RGCs and comprise many sub-types which mostly release an inhibitory neurotransmitter, GABA or glycine (Yan et al., 2020). The processes of amacrine, bipolar and RGCs form an interconnected layer in the inner plexiform layer (IPL) which transduce and modify the light response signal (Diamond, 2017).

Finally, RGCs and some displaced amacrine cells make up the innermost GCL (Fig. 1.1B,C). RGCs are post-synaptic to bipolar cells and are the output neurons of the retina as RGC axons form the optic nerve which leads out of the retina (Sung & Chuang, 2010). In the primate retina at least 17 sub-types of RGCs have been described, while in the mouse over 30 sub-types are found (Grünert and Martin, 2020). The sub-types can be characterised morphologically, by dendritic field and stratification in the IPL, and functionally, by response to light and gene expression profiling (Baden et al., 2016; Yan et al., 2020).

PR OS' are embedded within and closely interact with the RPE, a non-neural tissue which lies between the NR and the vascularised choroid (Fig. 1.1B,C) (Sung & Chuang, 2010). RPE cells play a crucial role in the visual transduction pathway by recycling the activated visual pigment, which is re-isomerised by RPE65 and CRALBP proteins, before it returns to the PRs ready to be activated (Luo et al., 2009; Yau & Hardie, 2009). The melanin-based pigment in RPE also plays an important protective role by absorbing harmful UV light before it damages the sensitive neurons of the retina (Bok, 1993). Furthermore, the RPE plays a role in phagocytosis and recycling of the disc membranes from the PR OS' which have rapid daily turnover (Bok, 1993).

Additionally, Müller glia cells, the major type of neuroglia in the retina, have their nuclei in the INL and span the depth of the retina, filling the extra-cellular space (Remington, 2012) (Fig. 1.1B). They provide structure and support to cells of the retina by regulating metabolism, neurotransmitter turnover, extracellular space, and ion and water content (Bringmann et al., 2009; Reichenbach & Bringmann, 2013). In addition, in the case of cone-mediated visual transduction, the activated visual pigment is re-isomerised within the Müller glia by CRALBP (Yau & Hardie, 2009).

1.2 Retinal disease and current therapeutic options

The complexity of the retina and its organisation of many interconnected and specialised cell types make it susceptible to disease. Prevalent degenerative retinal diseases are retinitis pigmentosa (RP)

and age-related macular degeneration (AMD) which result in chronic and irreversible loss of PR cells and cause visual impairment and blindness for millions of people globally (Shanks et al., 2013).

<u>1.2.1 Retinitis pigmentosa</u>
RP is a common form of inherited retinal degeneration (IRD) affecting approximately 1 in 4000 people worldwide and its onset can begin as early as adolescence (Verbakel et al., 2018). It is a heterogeneous family of diseases caused by genetic mutations in PR, RPE and cilia-related genes, of which at present approximately 80 have been identified (Daiger et al., 2015 "RetNet"). Inheritance patterns vary in autosomal dominant, autosomal recessive and X-linked types, making identification of the disease in patients with unaffected relatives more complex, and new mutations difficult to identify (Hartong et al., 2006). As well as manifesting as an isolated retinal condition, RP can also occur in syndromic disease, with retinal degeneration seen in patients with Usher's syndrome, Bardet-Biedl syndrome and other ciliopathies (Buskin et al., 2018; Tsang et al., 2018). In addition to PR-specific genes, genes specific to RPE and Müller glia cells, such as *MERTK* and *CRB1* respectively, have also been implicated in cases of RP (Hartong et al., 2006). The tyrosine kinase receptor MERTK is critical for rod PR OS turnover and CRB1 maintains retinal lamination and cell junctions between PRs and Müller glia cells (Lukovic et al., 2015; Pellissier et al., 2015). As PR function is intrinsically linked to other retinal cell types, such as Müller glia and RPE, RP can result from gene dysfunction in various retinal cell types.

Clinical presentation of RP varies significantly between patients but it is most commonly characterised by an initial loss of rod PRs which causes night blindness and loss of peripheral vision, followed by the degradation of cone PRs resulting in central vision loss and disruption of colour vision (Hartong et al., 2006). While retinal cells of the INL, including horizontal and amacrine cells, generally remain intact they have been observed to show abnormal growth such as neurite sprouting in areas of PR depletion (Fariss et al., 2000; Santos et al., 1997). Another common feature of IRDs is reactive gliosis caused by activation of the principal glial cells of the retina, Müller glia, in response to retinal damage or cell loss (Figure 1.3) (Ikelle et al., 2020; Subirada et al., 2018). Initially this has a neuroprotective effect as neurotrophic factors such as VEGF and antioxidants are released (Oku et al., 2002; Rodrigues et al., 2013). However, in chronic degenerative disease this becomes detrimental, as dysregulation of retinal homeostasis can cause neuroinflammation, neovascularisation and accelerates the progress of neurodegeneration (Bringmann et al., 2006; Sorrentino et al., 2016; Yoshida et al., 2013).
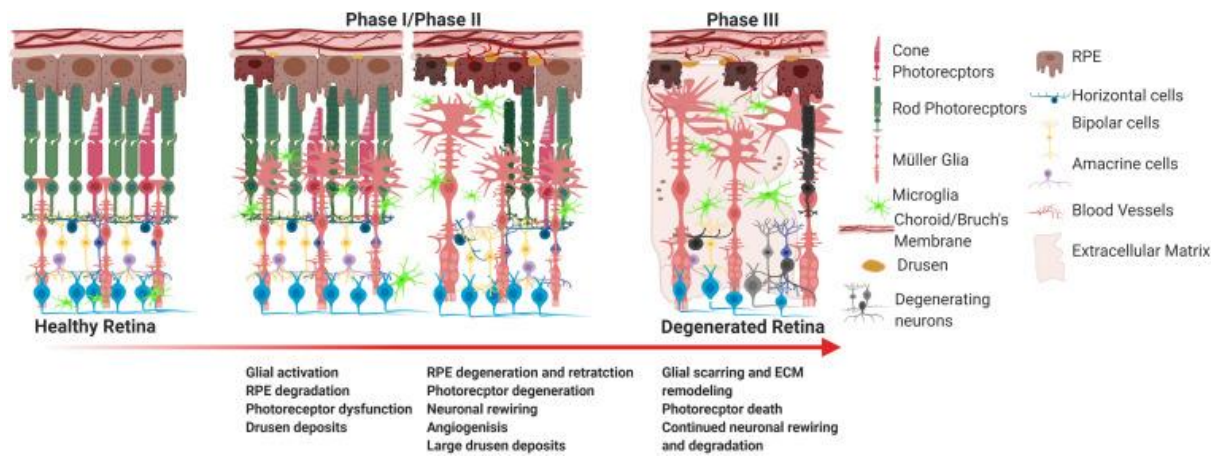
Figure 1.3. The process of retinal degeneration during disease progression showing the loss of cell types and remodelling of retinal structure (Ikelle et al. 2020).

The progression of RP usually begins in the second decade of life and can have a fast onset resulting in total blindness with 1-2 decades, or a slow progression resulting in partial blindness (Hartong et al., 2006). These factors and the ongoing deterioration of sight make it extremely disruptive to patient's quality of life.

1.2.2 Age related macular degeneration

AMD is a multifactorial condition which can be caused by genetic, age, behavioural and environmental risk factors (Joachim et al., 2018; Kaarniranta et al., 2011; Zhao et al., 2007). Risk factors including smoking, obesity, hypertension, chronic oxidative stress and inflammation have been strongly linked to the pathogenesis of the disease (Shaw et al., 2016). Currently, it is the leading cause of blindness in those aged over 65 in high income nations, with a prevalence of 43% in people over 85 while causing 5-6% of vision loss cases globally (Steinmetz et al., 2021; Xu et al., 2020).

AMD is characterised by a degeneration of RPE and PR cells in the macula region, which results in central vision loss (Cheung & Wong, 2014). The condition typically has an early stage where lipofuscin accumulates in the RPE and extracellular deposits of "drusen" are formed between RPE and Bruch's membrane (Figure 1.3) (Kaarniranta et al., 2011; Klein et al., 2004). It progresses to an atrophic or 'dry' or neovascular or 'wet' form where either retinal cells atrophy in the macula region or neovascularisation occurs resulting in inflammation and further degeneration (Nowak, 2006). The number of AMD sufferers alone has risen above 170 million and without treatment most patients will experience vision loss often with a rapid onset (Wong et al., 2014, 2014).

Despite their high prevalence, long-term and chronic effects, and cost to healthcare systems, current treatments for IRDs are limited. The heterogeneity of retinal disease, involvement of many distinct

cell types and the separation of the retina from the main vascular system complicates drug discovery and delivery. The symptomatic variability and the subjective nature of vision loss make clinical diagnoses of IRDs difficult and often patients may only be diagnosed after a substantial loss of PRs has occurred, which further limits treatment options.

1.2.3 Treatment options

However, there is light at the end of the tunnel, so to speak, as biomedical advancements in stem cell models, molecular understanding of disease and biomarker discovery, technological improvements in high throughput "-omic" studies and long-read genetic sequencing add to the knowledge and tools for treating retinal disease (Parfitt et al., 2016). Additionally, detection methods are improving and becoming more accessible as the cellular resolution 3D imaging technique optical coherence tomography (OCT) is now regularly included in NHS patient screenings (van Velthoven et al., 2007).

For patients with AMD, treatments consisting of repeated deliveries of anti-VEGF antibodies via intravitreal injection have helped to alleviate cases of neovascular AMD (Rosenfeld et al., 2006) (CATT research group., 2011). Although the overall incidence of AMD is increasing, the prevalence of blindness due to AMD decreased by 30% between 1990 – 2020 due to widespread adoption of anti-VEGF treatments and improved knowledge of risk factors (Steinmetz et al., 2021).

In the case of RP, advances have been made in clinical trials using natural small molecules such as vitamin A and E, and antioxidants including ascorbic acid to slow the disease progression in early stages, however this has little restorative effect in the later stages of disease when significant loss of PRs has already occurred (Berson et al., 2010; Komeima et al., 2006, 2007).

Gene therapy strategies for RP are being developed; however this approach is constrained by the complexity of genetic inheritance, the large number of affected genes and number of different affected cell types (Cideciyan et al., 2013; Miraldi Utz et al., 2018; Pellissier et al., 2015; Vandenberghe & Auricchio, 2012). At the time of writing only one gene therapy treatment for an IRD is clinically available following regulatory approval. Luxturna is an AAV-based gene therapy for the treatment of RPE65-associated Leber's congenital amaurosis (RPE65-LCA) and was approved by the FDA in 2017 (Ameri, 2018). The gene therapy delivers a corrected copy of *RPE65* to the affected RPE cells to restore the function of visual pigment processing (Redmond et al., 1998). The small size of the gene makes it an amenable target for gene therapy and its characterisation several decades ago together with the presence of a canine model of RPE65-LCA disease facilitated the drug discovery process and pre-clinical trials (Acland et al., 2001; Gu et al., 1997; Marlhens et al., 1997). However,

each gene therapy treatment requires an equivalent process of research, development and evaluation, making it a lengthy and costly way to treat IRDs.

Another broader stratagem for treating IRDs is that of optogenetics, which can be applied in any case of degenerative retinal disease where PRs are lost but other retinal cell types remain intact. Optogenetics works by targeting the remaining neural cells within the retinal circuitry and transforming them to become light-sensitive by the provision of a light sensitive microbial opsin protein (Garita-Hernandez et al., 2019). The approach can be adapted depending on the level of remaining intact neural-retinal cells giving it adaptability to patient conditions and the timing of diagnosis (McClements et al., 2020). Recently, the delivery of an optogenetic gene therapy in conjunction with visual goggles partially restored vision in an RP-affected patient who was previously limited only to light perception (Sahel et al., 2021). This study demonstrates the first case of patient restored vision using this technique and shows its promise for future treatment.

Another potentially powerful approach to restore vision is by the transplantation of PRs generated from pluripotent stem cells (PSCs). As PSCs have a potentially unlimited proliferative and differentiation capacity these can provide a renewable source of PRs which can be supplied to the defective retina to restore vision. The eye is particularly amenable to this type of transplantation experiment being "immune-privileged" and separated from the central immune system by the blood-retina barrier (Streilein, 2003). In this technique, PR precursors are injected into the sub-retinal space. The transplanted cells then engraft and integrate into the retinal architecture, and show some synapse formation with resident cells, or they participate in the transfer of genetic material and retinal proteins to host cells (Barber et al., 2013; Decembrini et al., 2014; Kruczek et al., 2017; Pearson et al., 2016).

Post-mitotic PR precursor cells showed the best initial success of transplantation, survival and engrafting into the retina and showed some restoration of visual function in mouse models of retinal degeneration (Decembrini et al., 2014; Gonzalez-Cordero et al., 2013). This suggests that some amount of plasticity supports transplanted cells to engraft and mature *in vivo*. Rigorous characterisation of the transplantable cells is required to confirm cell identity and ensure that undifferentiated cells which could potentially cause tumour development are not transplanted (Gasparini et al., 2019). Proof of concept pre-clinical studies have been performed in animal models with some success (Barber et al., 2013; Collin, Zerti, et al., 2019; Warre-Cornish et al., 2013) however, survival rates of transplanted rod precursors into the murine retina was found to be low (West et al., 2010). This can be improved by suppressing the immune system and local inflammatory pathways (Barnea-Cramer et al., 2016; Mandai et al., 2017).

This novel technique has some limitations on the delivery method and post-implant engrafting efficiency which is limiting the restoration of vision to a significant life-changing level at the moment. However, the use of retinal organoids as a cell source for retinal transplantation studies has significantly developed the field and further optimisation of this technology can provide a valuable and unique means of restoring vision.

In order to develop further suitable treatments for the myriad of retinal diseases pre-clinical testing is required. Currently much of this testing is performed using animal models including rodents and non-human primates (Penha et al., 2010; K. Zhang et al., 2012). However, results in rats and primates cannot be universally applied to humans or other species due to inherent differences in the biology of vision, metabolism and immunity (Mestas & Hughes, 2004; Sefton et al., 2015). With continued research and development organoid and cell-based assays there will be improved understanding of the molecular mechanisms of IRDs, improved platforms for drug development and subsequently, innovation of treatments.

1.3 Retinal development in vivo, cellular specification and genetic control, conservation through species and over time

The development of the eye is a highly regulated process conserved between all vertebrates (Martinez-Morales & Wittbrodt, 2009). Its specialised structure and commonality has made it an attractive organ to study and genetically, many of the transcription factors and pathways which shape the eye have been elucidated (S. S.-M. Zhang et al., 2002). Embryonically, first the neural tube is specified and from this the neural ectoderm arises, the optic vesicle (OV) then evaginates from the early eye-field in the neural tube and invaginates to form a bi-layered optic cup (OC) with NR on the apical side and presumptive RPE on the basal side (Fig. 1.4) (Martinez-Morales & Wittbrodt, 2009). Physical forces, genetic and molecular mechanisms are involved in this process (S. S.-M. Zhang et al., 2002). Primarily this is co-ordinated by a network of early eye-field transcription factors (EFTFs); Otx2, Pax6, Six3, Lhx2 and Rax which cross-regulate and have been shown by knockout studies and ectopic eye expression, in many species, to be crucial for correct eye development (Fig. 1.4) (Bailey et al., 2004; Goudreau et al., 2002; Zuber et al., 2003).

From the OC the developing neuroepithelium (NE) is further specified by the compartmentalisation of expression of EFTFs which become restricted spatially to determine presumptive NR, RPE and the optic stalk (Fig. 1.4) (S. S.-M. Zhang et al., 2002). From the OC tissue, the retina is specified which begins around gestational day (GD) 10 in the mouse embryo (Table 1.1). Other components that make up the complete eye such as the lens, ciliary muscles and vasculature are of epithelial, neural crest and mesenchymal origin (Fruttiger et al., 1996).

The role of signalling gradients including wingless-like proteins (Wnt), bone morphogenetic protein (BMP), fibroblast growth factor (FGF) and sonic hedgehog (Shh) molecules which are expressed in neural and neighbouring non-neural tissues have also been shown to play an important role in early retina specification (W. E. Heavner et al., 2014; Huang et al., 2015; Ohkubo et al., 2002). There is interplay between signalling gradients and gene expression in the developing retina. For example the Rax family of TFs have been shown to be essential for eye development, Rax is downstream of the BMP signalling pathway and lack of BMP4 causes lack of optic cup and lens formation (Bailey et al., 2004; Huang et al., 2015; Voronina et al., 2004). Growth factors such as IGF1 also have a stimulating role on neuronal progenitor proliferation and differentiation in the early developing retina (Hernandez-Sanchez et al., 1995). Moreover, combinations of patterning signals have been shown to have different effects on cellular proliferation than in isolation, suggesting an optimal balance of BMP, FGF and Shh signalling molecules are required for retinal tissue specification and growth (Ohkubo et al., 2002).
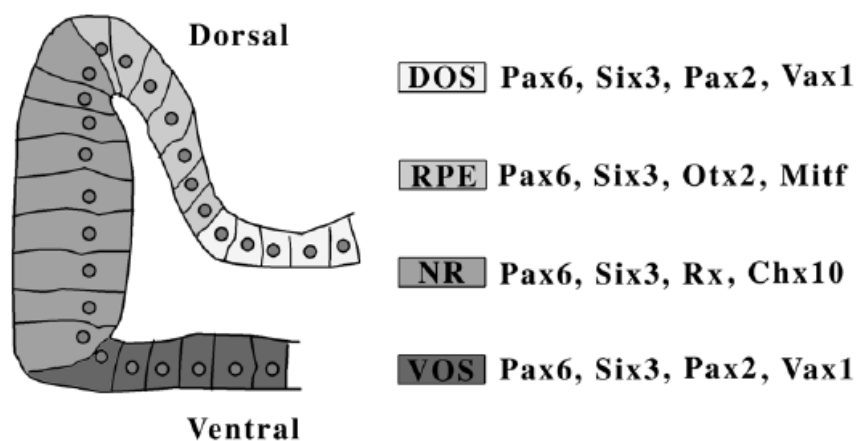
Figure 1.4. Key transcription factors regulating optic cup development (adapted from Zhang et al. 2002). The neuroepithelium evaginates from the neural tube (not shown) to form the optic vesicle showing distinct cellular areas expressing combinations of TFs, with presumptive neural retina specified at the apical side and presumptive RPE at the basal side. NR = Neural retina, RPE = retinal pigmented epithelium, DOS=dorsal optic stalk, VOS=ventral optic stalk.

The process of eye-field and subsequent retinal specification occurs commonly across all vertebrates however, the temporal staging of development is dependent on the length of gestation (Table 1.1). Seminal work performed by Hendrickson (1992) showed parallel timelines between human and

macaque retinal development in that the fovea is present in both human and macaque retina at 26-30% of gestational time and cone OS' appear by 65% gestational development in both species. Similar studies of rat and mouse retinal developmental time show broadly similar patterns of cell birth and structural development however, the rat has a longer period of post-natal maturation (Table 1.1) (Perry & Walker, 1980). Eye-opening in rodents occurs postnatally and is thought to be a crucial turning point for the development of the visual cortex, this occurs at a similar point for rat and mouse suggesting intrinsic retinal activity reaches maturity at approximately the same time (Table 1.1).

Studies investigating the process of eye formation, retinal cell generation and structural organisation using ex vivo tissue from relevant model species have been summarised in Table 1.1. Embryological studies from prior to gestational day (GD) 30 are not found for the macaque. The commonality of retinal development, timing and expression of regulating genetic factors, between human and macaque and between mouse and rat, is particularly relevant for this project and has been used to inform retinal differentiation method development.

Table 1.1. A comparative timeline of retinal development in vivo in clinically relevant species.

(Adapted from (Cruchten et al., 2017) *to include relevant developmental stages and species) (GD = gestational day, PND = post-natal day) (1*(Fernández-Nogales et al., 2019)*; 2*(Raedler & Sievers, 1975)*; 3*(Rapaport et al., 2004)*; 4*(Kuwabara & Weidman, 1974)*; 5*(Hendrickson, 1992)*, 6*(Townes-Anderson & Raviola, 1981)*, 7*(Sernagor et al., 2001)*, 8(Perry and Walker, 1980), 9*(Rochefort et al., 2009)*, 10*(Hoshino et al., 2017)*, 11(*(Rapaport et al., 1995)

Morphological feature and stage of retinal development	Human	Macaque	Mouse	Rat
Eye field defined	GD 17		GD 8	
Neural tube closed and optic stalk formed	GD 24			
Optic sulci converted into optic vesicles	GD 25		GD 8.5 - 9	GD 10
Optic vesicles contact surface ectoderm by which the lens placode forms	GD 27		GD 9.5 - 10	
Optic vesicles invaginate and form optic cup with optic fissures	GD 29	< GD 30[6]	GD 10.5	
Neural retina (NR) and retinal pigmented epithelium (RPE) domains are specified in the optic cup[1]			GD 9.5-10.5	
Postmitotic cell birth begins[3]	GD 52[10]	GD 27[3]	GD 11	GD 12
Pigment present in outer layer of optic cup (primitive RPE)	GD 33			
RPE is pseudostratified consisting of single row of cylindrical cells, connected to the optic stalk and the peripheral region of ora serrata. [2]		GD 45[11]		GD 13
Ciliary ganglion present	GD 37	GD 58	GD 12	GD 15[2]

Neural retina consists of inner neuroblastic layer, transient fiber layer of Chievitz, proliferative zone and outer neuroblastic layer	GD 42-45	<GD 51[5]		
Elongation of distal tip of retina to form ciliary marginal zone [1]			GD14.5-16.5	
Ganglion cells give rise to nerve fibre layer in neural retina	GD 45-48		GD16[7]	GD16[7]
The retinal ganglionic cell layer becomes a monocellular layer		GD 132 - 150[5]		PND 14-15
Inner plexiform layer formed in neural retina	GD 71-77	<GD 60[5]	GD 17	GD 17-18[2]
Outer plexiform layer in neural retina separate horizontal and bipolar nuclei from rudimentary rods and cones	GD 71-90[5]	GD 51 – 60[5]	PND 0	PND 4 (central region only) PND 8 (reaches the periphery)
Mitosis ceases in the neural retina	GD 100-120	GD 56-60[5]		PND 6
Primitive ciliary processes are forming from photoreceptors		GD 71[6]		
Outer segments formation begins in the neural retina	GD 150-180	GD 110[5]		
Retinal layers developed except at macula/centre	GD 240-280			PND 14
Birth	GD 270	GD 165	GD 19	GD 21
Eye opening	Birth	Birth	PND 12-14[9]	PND 15[5]
Eyes are morphologically fully developed	PN 2 years			PND 40[8]
Fovea fully developed	PN 6 years (estimated)	PN 1.5 years (estimated)	N/A	N/A

Of particular relevance to this project are anatomical and developmental differences between rat and mouse models. Rat and mice share similar retinal anatomy due to their close phylogeny and shared nocturnal behaviour, exhibiting low percentages of cone PRs, lack of a macula-like region, small lens and retinal size and maximal sensitivity in the S-opsin (Jacobs et al., 2001; Jeon et al., 1998; Watson, 2012). These species also share a similar gestation time, at 21 and 19 days respectively, which gives them a similar timeline of embryological development (Table 1.1).

Cytogenesis within the retina occurs in a regulated and time-dependent manner. Firstly, NE cells in the OC differentiate into retinal progenitor cells (RPCs), these proliferate by symmetric and asymmetric cell divisions differentiating chronologically into retinal ganglion, horizontal, cone PRs and amacrine cells in an early phase, and rod PRs, bipolar and Müller glia cells appearing in a second, later phase (Fig. 1.5a) (Hoshino et al., 2017; Livesey & Cepko, 2001; Mellough, Bauer, et al., 2019). Cell of each class arise first in the central retina then appear subsequently in the peripheral regions (Rapaport et al. 2004).

This order is largely conserved however timings differ between species according to gestation time. Cell "birthdating" experiments label postmitotic cells to temporally establish retinal cell differentiation *in vivo*. These have shown that within the macaque and the rat, which have gestation periods of 165 and 22 days respectively, cell genesis order is the same (Rapaport et al., 2004; Vail et al., 1991). However, it is more difficult to resolve the precise order of retinogenesis within shorter developmental timelines as the birth of different cell-types overlap. In the macaque retina the early phase of cell birth begins at gestational day (GD) 27 with the second phase from GD 43 onwards (Rapaport et al. 1991). In the mouse and rat the first phase of cell birth occurs at GD 10-18 and the second phase from GD 18 and post-natally (Fig. 1.5b) (W. Heavner & Pevny, 2012; Raedler & Sievers, 1975). This means, in the rat although a significant proportion of rod PRs, Müller glia and bipolar cells are generated in the first postnatal weeks, in the macaque ~96% of retinal cells are present by GD 120 (Table 1.1) (Rapaport et al., 2004; Vail et al., 1991). This advanced maturity in the primate correlates with the state of eye opening at birth; primates are born with eyes open, whereas in rodents this occurs in the 2-3 post-natal weeks (Table 1.1).
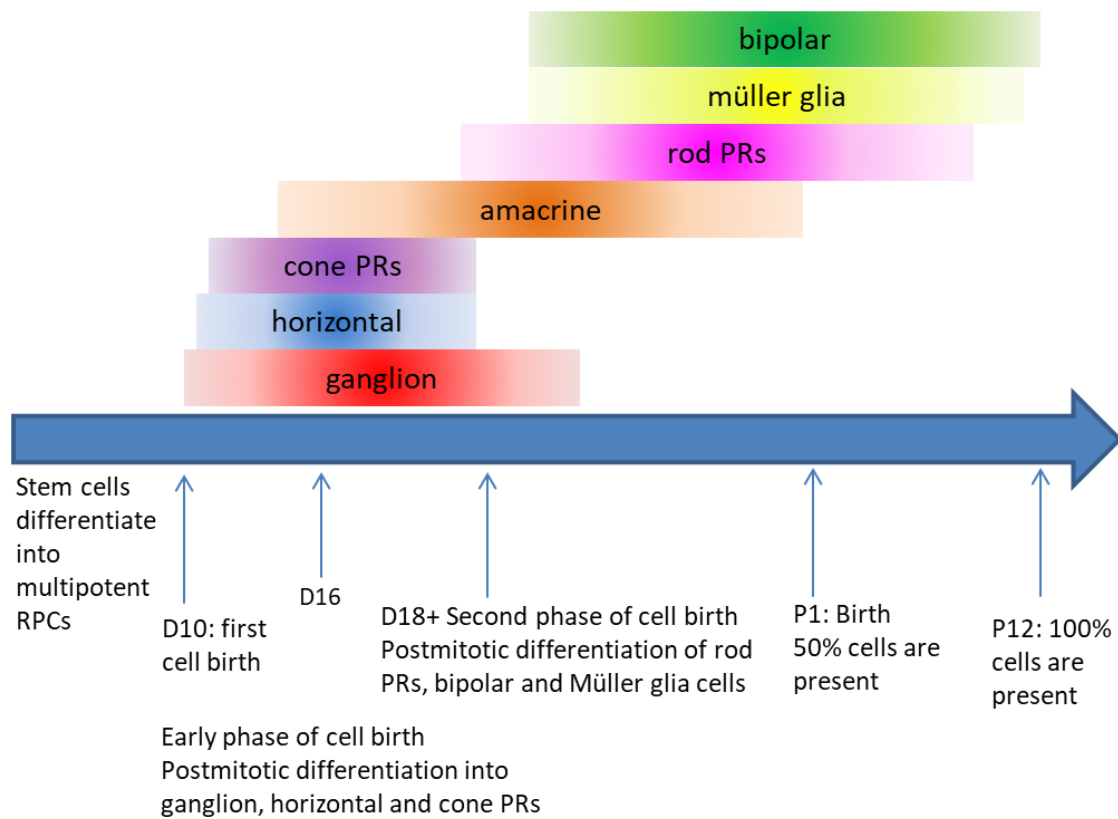
Model	Esrly phase		Second phase		
Rat:	D11	D16	D18	Birth	
Mouse RO:	D9	D15	D17	D20	
Macaque:	D27	D43	D70	D120	Birth
Human RO:	D60	D90	D150	D200	D270

Figure 1.5: (a) Timeline of retinogenesis in rat (data from Rapaport et al. 2004). D= day, P = post-natal day, RPC = retinal progenitor cell, RO=Retinal organoid. First phase of cell birth: Retinal ganglion cells arise first at embryonic D10, followed by horizontal and cone PR cells, they have similar patterns of cell genesis peaking between D14-16 and ceasing by D18. The first cone PRs are present at D11, peak between D14-15, and are generated up to D18. Amacrine cells arise next beginning genesis at D12, peaking at D15-19 and reaching total number by P2. Second phase of cell birth: Rod PRs are generated from D18 onwards, peaking from D21-P4. Followed by bipolar and Müller glia cell production which begins at D21 and peak between P2-4 and continue to be born following birth. (b) Comparative staging of cytogenesis and 1st and 2nd phases of cell birth in various animal retinal models. (Data from Rapaport et al. 2004, LaVail et al, 1991, Capowski et al. 2018, Völkner et al. 2016).

33

The cynomolgus macaque has a shorter gestation period of 165 days compared to that of other primates such as human (270 days) or chimpanzee (237 days) and correspondingly has a faster rate of retinal cell differentiation and development (Fürtbauer et al., 2010; Kiely et al., 1987). Based on life expectancy and the rate of presbyopia an approximate temporal ratio of 1:3 has been used by researchers when comparing ocular development throughout life between humans and macaques (Kiely et al., 1987).

The rat retina is still at an immature stage of development at birth lacking a mature PR layer while the OPL develops and divides the outer and inner nuclear layers between PND 4-8 (Table 1.1) (Cruchten et al., 2017). During the first 20 days following birth substantial morphological changes occur in the rat retina, with synaptic connections being formed between the PND 6-12 and retinal activity shown by electroretinogram signal present at PND 14 (Raedler & Sievers, 1975). PRs are not fully mature until PND 21 (Cruchten et al., 2017). Additionally there are differences spatially in timing of cell genesis between the central and peripheral areas of the retina, in rats cell birth in peripheral areas was an average of 2 days behind the central areas and the development of PRs (Rapaport et al., 2004). In humans cell genesis continues in the peripheral retina into adult life, far beyond cell birth in the central regions (Fernández-Nogales et al., 2019).

The process of cytogenesis in the primate retina also does not occur uniformly with cell differentiation in the central region of the retina beginning prior that in peripheral areas and reaching higher densities of PR cells (Grünert & Martin, 2020). The stepwise birth of retinal cells from a multipotent progenitor is similar to neurogenesis in the cerebral cortex as cells in the most basally located GCL arise followed by horizontal cells in the INL and cone PRs in the putative ONL (Otani et al. 2016). Accordingly, synaptogenesis in the retina occurs first in the inner plexiform layer IPL followed by the OPL once nuclear cell layers are defined (Table 1.1) (Hendrickson, 1992).

Further control of retinal cell quantity and distribution occurs after cellular differentiation. RGCs are the earliest neurons in the retina to differentiate however, many more cells are born than are present in the mature retina (Horsburgh & Sefton, 1987). The "excess" cells in the ganglion cell layer are removed in two phases by programmed cell death (Cusato et al., 2001; Horsburgh & Sefton, 1987).

Cells migrate to their correct positions within the retina and form synaptic connections with other neurons following cytogenesis (Ford & Feller, 2012). Synaptogenesis occurs concordantly with cytogenesis in the retina according to the order of cell birth and subsequently the temporal order of the process is the same between vertebrates. The first synaptic connections to form are in the IPL

between the early-born RGCs and amacrine cells, in mice and rat around GD 16, followed by horizontal cells and PRs making synaptic connections in the OPL around PND 0, then synaptic connections travelling apically-basally (vertically) through the retina are formed last when late-born bipolar cells contact RGCs (Blanks et al., 1974; Olney, 1968; Sernagor et al., 2001; Sharma et al., 2003). The formation of synaptic connections in the retina has been investigated in various animal models to investigate the mechanism and control of synaptogenesis. In mice it was seen that eye opening coincided with a decrease in synaptogenesis in the IPL but this was measured to be time-based and not dependent on light stimulus (Fisher, 1979). Blocking of cholinergic and glutamatergic transmission was found to impede RGC dendrite formation while ultra-structural studies have shown the initial branching of amacrine cells to be multi-directional until contact is reached with incoming afferent neuronal axons (Bodnarenko et al., 1995; Hinds & Hinds, 1983; Sharma et al., 2003). These studies implicate the release of neurotransmitters and cellular spatial organisation to be crucial to the process of synaptogenesis in the retina.

1.4 Relevance of using non-human primate models for retinal research

Anatomically, all non-human primates (NHPs), including macaques, share with humans unique features in the eye and visual pathway such as the fovea region which includes the macula, the specialised cone-rich central area in the retina. In both the macaque and human retina the density of cone PRs in this region reaches 160,000 to 200,000 cells/mm² (Picaud et al., 2019). This is high compared to the peripheral edges of the retina where cone density reaches 5,000 cells/mm² (Grünert & Martin, 2020). This is in contrast to most nocturnal rodent models which have an even distribution of rod and cone PRs throughout the retina and no foveal specialisation (Grünert & Martin, 2020). This specialisation is relevant when considering the biomedical and clinical research surrounding degenerative retina and macular diseases such as AMD which specifically affect this region of the retina. Another anatomical similarity shared only by members of the primate group, including humans and macaques, is trichromacy. This type of colour vision utilises three visual pigments resulting in three distinct cone opsins which show a spectral peak in the violet (shortwave, S), green (midwave, M) and yellow-green (longwave, L) spectral regions (Jacobs, 1993; Jacobs et al., 1991). This feature of the retina is unique to the primates among mammals and likely arose by convergent evolution once in the Old World primates, which includes both humans and macaques, and subsequently in the New World monkeys (Hunt et al. 1998).

The genus *Macaca* diverged from other primates around 5 million years ago and is widespread around the globe giving rise to a large range of adaptive genetic variation within macaque species (Shattuck et al., 2014). The cynomolgus macaque (*Macaca fascicularis*) and rhesus macaque

(*Macaca mulatta*) species are the most commonly used NHP models in biomedical research studies (Cauvin et al., 2015). This is due to their genetic and protein similarity, and their phylogenetic proximity to humans sharing more than 90% DNA sequence similarity with humans (Picaud et al., 2019). In addition, their wide distribution around the globe in many different habitats has resulted in adaptive evolution and wide genetic diversity akin to that present in humans (Shattuck et al., 2014). Although the cynomolgus and rhesus macaques are similar, the cynomolgus macaque is more commonly used in pre-clinical safety assessment due to practical reasons of a longer period of fertility annually and wider availability globally than the rhesus macaque (Cauvin et al. 2015). This restriction of rhesus macaque availability has subsequently led to less toxicological and pre-clinical data with which to support research studies.

As a model for retinal disease, cynomolgus and rhesus macaques possess the same susceptibility genes and genotype-phenotype correlations for inherited retinal diseases (IRDs) such as retinitis pigmentosa (RP) and achromatopsia (Y. Ikeda et al., 2018; Moshiri et al., 2019). The presence of naturally occurring retinal disease variants in captive populations of macaques demonstrates their importance as a model for retinal disease and development studies (Peterson et al. 2019, Moshiri et al. 2019). Due to its close genetic background the macaque is an invaluable NHP model for understanding the progression of retinal disease, discovery of disease-causing mechanisms in primates and for investigating potential treatments and cures for IRDs.

The relevance of the macaque for retinal research also rests on the anatomical similarities they share with humans as discussed above. The occurrence of animal models that accurately replicate human disease is vital to understanding the pathogenicity of disease and for assessing the safety, toxicity and efficacy of putative therapeutics. Furthermore, the use of NHP models is highly controlled and animal numbers are often limited, therefore the generation of *in vitro* NHP models would provide a valuable resource for pre-clinical studies.

1.5 Pluripotent stem cells; definition, their characteristics and applications

Pluripotent stem cells (PSCs) are found *in vivo* in the embryo (ESC) and have the unique ability of both symmetric, and asymmetric cell division which gives rise to a differentiated daughter cell as well as another stem cell by self-renewal (Evans & Kaufman, 1981). In effect this gives them unlimited proliferative potential. They are defined as being pluripotent, meaning they can differentiate into a cell of any identity (L. C. Stevens, 1970). They can be cultured *in vitro* in the presence of inhibitory factors which maintains their undifferentiated state and this makes them a powerful tool for developmental studies, as they can be employed to generate *in vitro* model cell

cultures and for cell replacement therapies (Smith et al., 1988; Thomson et al., 1998; Ying et al., 2008).

Challenges associated with the use of ESCs for research include the inherent variability between cell lines in differentiation potential arising from both genetic variation and culture technique (Osafune et al., 2008); Baker et al. 2007). Although, mostly stable, they also can develop chromosomal instabilities, such as trisomy, due to extended growth in cell culture environments (Canham et al., 2015; C. A. Cowan et al., 2004). Additionally, they are subject to strict regulation, for ethical reasons, which limits number of cell lines in use and thereby the variation of genetic backgrounds of the cell lines.

Since Takahashi and Yamanaka's ground-breaking development of induced pluripotent stem cells (iPSCs) (Takahashi & Yamanaka, 2006) we have been able to access the multipotent and proliferative potential of PSCs without the need for manipulation of embryonic tissues. By the ectopic expression of certain master transcription factors; *OCT3/4*, *SOX2*, *KLF4* and *MYC*, termed the "Yamanaka factors", somatic cells can be re-programmed to a pluripotent state (Yu et al., 2007). Mouse, primate, rat, pig and the somatic cells of many other species have been cultured and reprogrammed into iPSCs enabling a range of therapeutic and medical research uses (W. Li et al., 2009; H. Liu et al., 2008; Qin et al., 2007; Wu et al., 2010; Yu et al., 2007). iPSCs provide an unlimited cell source and starting point for *in vitro* cellular and organoid models, reduce ethical issues associated with the use of animals, and can be used for personalised medicine and autologous cell replacement therapies (Smith et al., 1988; Thomson et al., 1998; Ying et al., 2008).

iPSCs also present challenges and limitations for research as re-programmed cells can be affected by tumorigenic properties, epigenetic differences and low re-programming method efficiency (Attwood & Edel, 2019; Gore et al., 2011; Haridhasapavalan et al., 2020; Hussein et al., 2011; Kawamura et al., 2009; Lister et al., 2011). Furthermore, iPSC lines vary greatly in genetic background with up to 46% due to inter-individual differences (Kilpinen et al., 2017). The original tissue from which the iPSCs were derived and the DNA methylation state of the original cells can also contribute to varying differentiation potential of the derived iPSCs (de Boni et al., 2018; Roost et al., 2017). These inherent differences to iPSC lines mean that characterisation or pre-screening of cell lines may be required to assess their suitability for subsequent differentiation and production of specific cell types.

Despite these challenges, ESC and iPSC lines from many species have been derived, robustly maintained in culture and have the capacity to be directed into specific cell identities for a range of therapeutic and medical research uses (Buehr et al., 2008; Evans & Kaufman, 1981; W. Li et al., 2009;

H. Liu et al., 2008; Mitalipov et al., 2006; Qin et al., 2007; Thomson et al., 1998; Wu et al., 2009; Yu et al., 2007)

1.6 Use of pluripotent stem cells for the generation of in vitro organoid models

PSCs from multiple species can be directed to differentiate into specific cell types by exposure to chemical molecules, changes in the physical environment, and/or co-culture with other cell types, among other methods (Haruta et al., 2004; Shamir & Ewald, 2014). Since the development of protocols using PSCs to generate many cell types, the generation of organoids has become established in many fields. These are 3D cellular bodies replicating the structure, organisation, cellular diversity and function of a tissue found in the body (Fig. 1.6) (Dutta et al., 2017; Lancaster & Knoblich, 2014).

Organoids are typically generated using various cell culture techniques which act spatially, temporally and compositionally to control the local microenvironment of the cells in order to affect proliferation, restrict the developmental lineage, or encourage self-organisation in order to generate the complexities of a native tissue (Gjorevski et al., 2014; Lancaster & Knoblich, 2014; Meinhardt et al., 2014; D. Singh et al., 2018). Moreover specific proteins, molecules and morphogens can be directly added into the culture environment in order to stimulate known developmental pathways and specify cell fate (Carpenedo et al., 2009; Osakada et al., 2009; Xue et al., 2018). Techniques such as co-culture with neighbouring cell types found *in vivo* can help to mimic the inter-cell signalling patterns found locally to that tissue and improve differentiation outcomes (Hernandez-Sanchez et al., 1995; Yue et al., 2010).
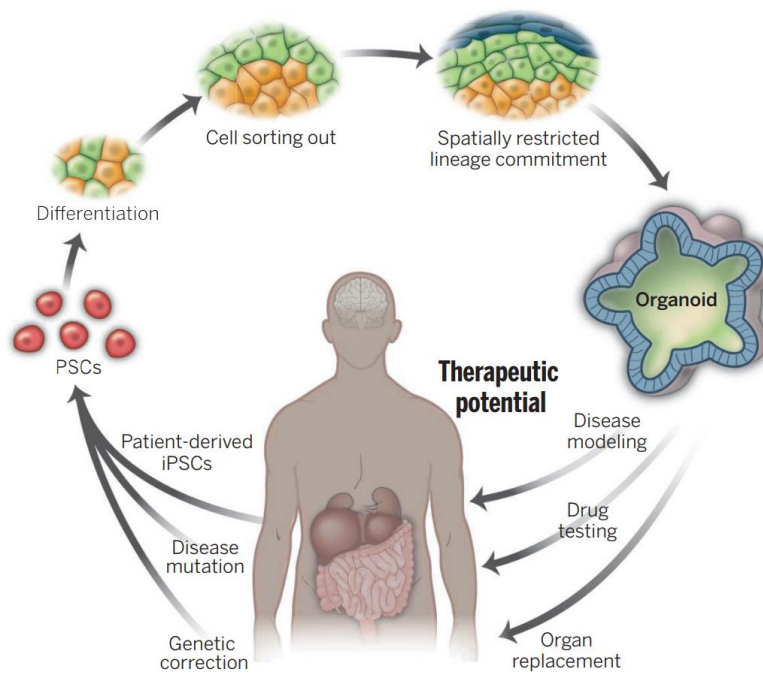
The potential of organoid technology for modelling disease progression, studying development and as an *in vitro* model for drug development and testing of therapeutics is vast (Fig. 1.6) (Dutta et al., 2017, Lancaster & Knoblich, 2014). To date, a wide range of organoid tissues have been derived from ESCs, iPSCs and organ-specific adult stem cells including the brain, retina, intestine, lung, liver and kidney (Assawachananont et al., 2014; Dye et al., 2015; Lancaster et al., 2013; McCracken et al., 2014; Takasato et al., 2015; Takebe et al., 2013). They are valuable as they possess the same genetic background as disease-affected patients and can thus be used as a model on which to accurately test gene therapy agents or for autologous cell replacement (Lane et al., 2020).

Organoids show distinct advantages as an innovative *in vitro* model system as they are cheaper, more amenable to experimental manipulation, higher-throughput and free from many of the ethical considerations faced by using live animal models (Lancaster & Knoblich, 2014). While retinal explant culture fully replicates a retinal system *in vitro*, the highly limited availability, high nutrient and oxygen demands and short lifespan of cells in culture makes it unfeasible for most research and development studies (Dodson et al., 2015; Schnichels et al., 2019). Furthermore, in contrast to 2D single cell type models organoids can largely replicate the structure and cellular diversity of a complex tissue arising from a single population of iPSC/ESC (Dutta et al., 2017; Lancaster & Knoblich,

2014). This makes organoid culture an attractive and useful model for studying the NR which has a highly organised 3D structure and consists of many distinct neuronal cell t

1.6.1 Applications of retinal organoids

Retinal organoids (ROs) derived from affected patient iPSCs have delivered timely assistance for disease modelling of retinopathies such as RP and Leber congenital amaurosis (Deng et al., 2018; Dutta et al., 2017). Now, study of how patient cell-line derived organoids respond to genetic factors in comparison with native tissue is advancing our understanding of the mechanisms of disease progression and predisposition to retinal disease (Rozanska et al. in press, (Buskin et al., 2018)). The advance of *in vitro* technology could not come at a more opportune time as it coincides with the increase of high-throughput transcriptomic studies used to assess development in a disease condition, for instance via the single-cell RNA-sequencing of organoids (Collin, Queen, et al., 2019; C. S. Cowan et al., 2020; Koo et al., 2012). Furthermore, *in vitro* differentiation protocol development allows the effects of gene expression pathways and extrinsic molecular signals on the precise temporal development of retinal cells to be studied in a readily accessible way (Collin, Queen, et al., 2019; C. S. Cowan et al., 2019; S. Kim et al., 2019; Lopez, Sangbae, et al., 2021; R. K. Singh et al., 2021; Sridhar et al., 2020; Zerti, Collin, et al., 2020). This could be important for elucidating species-specific effects of drug treatment and the underlying genetic and epigenetic mechanisms of disease.

One direct medical application of ROs is the facilitation of cell transplantation studies. Retinal cells differentiated from pluripotent precursors can be used to restore vision via transplantation in degenerative diseases such as RP and AMD, although currently this is limited by the successful integration of high quantities of cells and variable degree of post-transplant vision restoration (Barber et al., 2013; Collin, Zerti, et al., 2019; West et al., 2010). In mouse models of retinal degeneration the successful transplantation of PSC-derived PRs and restoration of vision has been achieved, however was shown to be dependent on the developmental stage of the PR cells (Gonzalez-Cordero et al., 2013; Gust & Reh, 2011; Pearson et al., 2012).

Transplantation of cone PR precursors into a retinal degenerative mouse model resulted in 1.5% cell integration however over half of the transplanted mice showed sight rescue indicating the potency of this technique (Zerti et al., 2021). There are challenges associated with the effective integration of transplanted PR populations, such as ensuring synapse formation between donor and host cells, and avoiding immune rejection. However, as PR cells lost via disease will not regenerate, this approach provides a unique way to restore viable light-responsive cell populations in late stage IRD patients. Further method development is needed, and the efficacy of transplantation could be further

improved by the detailed *in vitro* characterisation and study of the development of relevant cell types derived from and enabled by retinal cell models such as ROs.

Functional characterisation of some human ROs derived with current methods reveals a limited response to light which is comparable to that found in the neonatal mouse (Hallam et al., 2018; Zhong et al., 2014a). However, this is not commonly reported, likely due to the difficulty of generating OS maturity in PRs of ROs (Cora et al., 2019). Therefore, ROs can present a functional *in vitro* system suitable for modelling the tissue and studying disease progression and which are amenable to scalable production well suited for pre-clinical testing. The generation of ROs in a multi-well format produces an appropriate platform for the high-throughput screening of candidate drugs. This platform has been used to test retinal toxicological compounds efficiently and systematically and the RO response assessed by biochemical assays and transcriptomic analyses (Dorgau et al., 2022). The RO system as a tool for drug screening has further been validated by comparing the toxicological response data with that collected from *in vivo* studies (Dorgau et al., 2022).

Static cell culture
- x Nonphysiological cell/media ratio
- x No ECM
- x Only single cell types
- x No physiological interactions

Animal models
- x Different (phato-) physiology
- x Costs & availability (primates, large animals)
- x Lack of trichromacy, no macula
- x Ethical concerns

Ex-vivo
- x Short lifetime of explants
- x Limited availability
- x Inter-donor variability

- + Complex, stratified tissues
- + Most major retinal cell types
- + Complex interactions (e.g. ribbon synapses)
- + Long-living (>365d)
- + No ethical concerns

Organoids

- x Incomplete maturation
- x No persfusion (uncontrolled conditions, nonphysiological delivery of nutrients & compounds)
- x No RPE-PRC interaction
- x Lack of interphotoreceptor matrix

Figure 1.7. Showing the advantages and limitations of retinal organoids in comparison to current 2D cell models, in vivo models and tissue explants (from Achberger et al. 2019).

Clearly differences exist between the RO model and the retina *in vivo* and these should be considered for the purpose of analysis. Namely, they generate different ratios of PR types than are

found *in vivo*, they lack vasculature, they have a smaller size, and do not generate cells found in the retina which arise from non-neuronal progenitors, such as microglia (Figure 1.7). These differences to the retinal architecture may affect the maturity and timeline of development. For example, the process of vascularisation is intrinsic to the full development of the retina and microglia play an important immunological and supportive role during development and maturation (Fruttiger et al., 1996; Rouwkema et al., 2009; Silverman & Wong, 2018). Additionally, the integration of RPE with the retina is thought to be necessary for full maturation of PRs which is not guaranteed in current self-organising RO models (Akhtar et al., 2019; Bok, 1993; German et al., 2008). However, novel method developments aim to address these limitations and advance the retinal cell model further by incorporating microglia, RPE cells or RPE-secreted products and use microfluidics to better channel media and create incorporated retinal-vasculature or "retina-on-chip" systems (Achberger et al., 2019; Akhtar et al., 2019; Dorgau et al., 2019).

1.7 Strategies for retinal organoid cell culture

Eye-field induction and subsequent retinal development is a highly regulated process co-ordinated by genetic, chemical and environmental factors. Retinal cell specification *in vivo* occurs sequentially and involves cell-cell contact and exposure to diffusible signalling molecules as well as intrinsic genetic activity, which make up a complex and dynamic microenvironment (Bassett & Wallace, 2012; Zuber et al., 2003). RO formation and embryological retinal development share intrinsic developmental pathways which can be targeted during the generation of *in vitro* cell models.

Differentiation methods can generate mouse ROs which largely recapitulate retinogenesis *in vivo* (Fig. 1.8). In line with embryological development, the formation of neuroectoderm, polarised neuroepithelia (NE) and the optic vesicle (OV) is seen in the initial stages of mouse RO differentiation (Fig. 1.8) (Eiraku et al., 2011; Eiraku & Sasai, 2012; Kruczek et al., 2017).
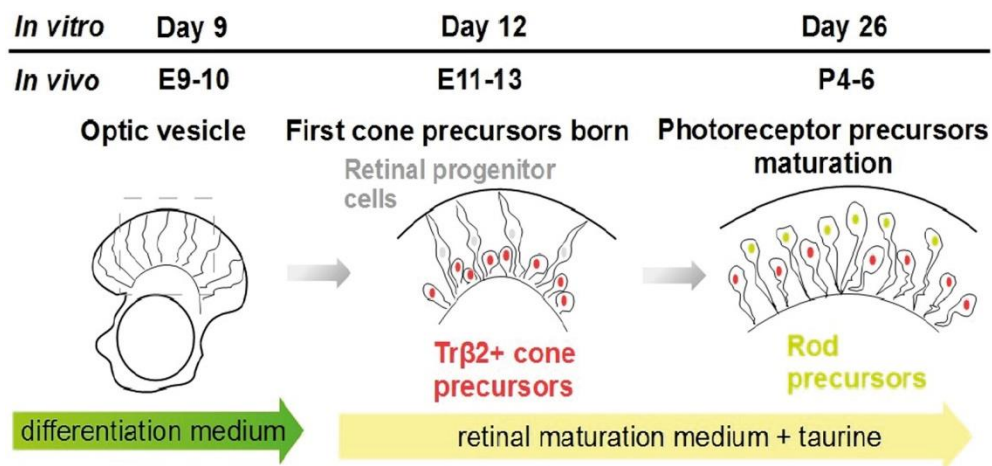
During the maturation period from day 10 onwards, the OV can invaginate to form the OC structure. Within the NE tissue the stepwise differentiation of multipotent RPCs into retinal cell subtypes occurs. This begins first with the appearance of RGCs from approximately day 10 and is followed subsequently by horizontal cells and cone PR precursors, amacrine and bipolar cells and finally the appearance of rod PR precursors and Müller glia cells at the final days of gestation (day 19-20) and into post-natal development (Fig. 1.8) (Eiraku & Sasai, 2012; W. Heavner & Pevny, 2012). Mouse ESC-derived ROs have been sustained in culture to day (D)26, which approximates post-natal day (P) 6, and produces mature PRs (Fig. 1.8) (Kruczek et al., 2017).

Studies have shown the dose-dependent and combinatorial effects of EFTFs *Pax6*, *Sox2* and *Rax* to be crucial for determining retinal fate in tissue (Xiang, 2013), indicating one way that the self-organisation model could work to carefully self-regulate the balance of these genetic factors of cell fate. As Sasai and others have suggested there is likely both complementary extrinsic and intrinsic signalling occurring in the retinal microenvironment, which enables signalling from neighbouring optic tissues to affect development and also allows the optic cup to self-pattern into NR in isolation (Sasai et al., 2012; Xiang, 2013). Exogenous application of signalling factors which target known pathways can activate master regulating factors and have a potent developmental effect. However, these may disrupt the local intrinsic signalling environment if not applied at the optimal dose or timepoint. This mechanism can be carefully exploited *in vitro* to stimulate retinal development, however requires careful modulation and optimisation.

1.7.1 Targeting signalling pathways in retinal cell development

As research groups have further built on methods for RO differentiation, techniques exploiting various cell culture parameters have been optimised. These include altering physical, spatial, molecular and cell-cell signalling and temporal factors. For example, known signalling pathways, such as Shh, BMP, FGF, IGF, Nodal and Wnt, have been targeted with exogenous small molecules to mimic the cues present in the developing native retina to guide the differentiation of PSCs toward a retinal fate (Table 1.2) (Hirami et al., 2009; H. Ikeda et al., 2005; Kuwahara et al., 2015; Lamba et al., 2006; Mellough et al., 2012; Nakano et al., 2012; Osakada et al., 2008, 2009; Zhong et al., 2014a).

Table 1.2. Summary of published methods using chemical, protein or growth factor additions to optimise in vitro retinal differentiation. Effect of signalling molecule is shown to be antagonistic (-) or agonistic (+) to the target pathway or receptor. (mESC = mouse ESC; mkESC = monkey ESC; hESC = human ESC; rESC = rat ESC; NSC = neural stem cell; NPC = neural progenitor cell; PND = post-natal day; RA = retinoic acid; PR = photoreceptor; RGC = retinal ganglion cell; Rx = Rax) EBs = embryoid bodies, NE = Neuroepithelium, Rcvrn = Recoverin, Rho = Rhodopsin.

Reference	Cell type	Chemical molecule/targeting protein	Target Pathway/ Receptor	Timepoint	Reported Effect
Ikeda et al. 2005	mESC	Dkk1 (100ng/mL) and Lefty-A (500ng/mL) Activin-A	Wnt (-) Nodal (-)	D0-5	Rax+/Pax6+ rostral neural progenitors
Osakada et al. 2009	mESC	CKI-7 (5uM) and SB431542 (5 uM)	Wnt (-) Nodal (-)	D0-D5	Increase Sox1, nestin and β -tubulin III
Osakada et al. 2008	mESC	(FCS (5%)) Activin-A (10 ng/mL)	TGF-β/Smad (+)	D3-5 D4-5	Induction of neural-retinal progenitors from Ebs
Osakada et al. 2008	mESC	DAPT (10 um)	Notch (-) (γ-secretase)	D10-20	Increase Crx (PR) from D16-20 and Pax6+/Islet1+ (GC). Decrease mitotic marker Ki67+.
Osakada et al. 2008	mESC	FGF (50 ng/mL), bFGF (10 ng/mL), Shh (3 nM), RA (500nM) and taurine (1 mM)	RARα receptor Shh (+) GABA/glycine receptor	D16-24 (FGF/bFGF) D16-28 (all others)	Generated rcvrn+/rho+ cells

Osakada et al. 2008	mkESC	Dkk1 (100ng/mL) and Lefty-A (500ng/mL)	Wnt (-) Nodal (-)	D0-18	Increase Rx+ Increase Crx+
Osakada et al. 2008	mkESC	RA (1 uM) and Taurine (100 uM) (N2 (1%))	RARα receptor GABA/glycine receptor	D90-120	Increase Crx+. Generated PR (cones and rhodopsin)
Yue et al. 2010	mkESC	RA (0.1 ug/mL) +co-culture with mkESC derived RPE	RARα receptor	3 weeks	Increased Rho+ cells to 25% by D10
Osakada et al. 2008	hESC	Dkk1 (100ng/mL) and Lefty-A (500ng/mL)	Wnt (-) Nodal (-)	D0-20	Increase Rx+
Osakada et al. 2008	hESC	RA (1 uM) and Taurine (100 uM)	RARα receptor GABA/glycine receptor	D90-140	Increase Crx+
Osakada et al. 2009	hESC	CKI-7 (5uM) and SB431542 (5 uM) Y-27632 (10 uM)	Wnt (-) Nodal (-) Rho/ROCK (-)	D0-D21 D0-15	Generated Ebs, Nanog and Oct ¾ expression decreased
Nakano et al. 2012	hESC	IWR-1e (3 uM)	Wnt (-)	D1-12	Counteract KSR supplementation to induce rostralisation
Nakano et al. 2012	hESC	(FBS (10%)) SAG (100 nM)	Smo (+)/Shh (+)	D12-18	Increased Rx+ cells and Sox2+ neural progenitors
Nakano et al. 2012	hESC	CHIR99021 (3 uM)	Wnt (+)	D15-18	Thinned NE but subsequently produced Mitf+ RPE
Mellough et al. 2012	hESC/ hiPSC	Noggin (1 ng/ml) Dkk1 (1 ng/ml) IGF-1 (5ng/ml) Lefty A (500 ng/ml) Shh (30 nM) T3 (40 ng/ml)	Wnt (-) IGF Nodal (-) Shh (+) TRα/TRβ (+)	D0-37	Increased Opsin gene expression
Kuwahara et al. 2015	hESC	BMP4 (1.5 nM)	BMP (+)	D6	Induced Rx followed by Chx10 expression
Kuwahara et al. 2015	hESC	CHIR99021 SU5402	Wnt (+) FGFR (-)	D18 – 24	Generated RPE in NR background

Qu et al. 2013	Mouse NSC explant	CHIR99021	Wnt7a (+)		Increase neurogenesis
Wang et al. 2014	rESC	EGF (20ng/mL) bFGF (20ng/mL)	EGFR/Ras (+) FGFR/Ras-Mapk (+)	D11	Proliferation of NPCs
Yourey et al. 2000	Rat retinal explant PND1	EGF	EGFR/Ras (+)	PND1 – 10	Increases cell proliferation (~30%)
Yourey et al. 2000	Rat retinal explant PND1	FGF2/bFGF (0.1-1 ng/mL)	FGFR/Ras-Mapk (+)	PND 1 – 10	Increases cell proliferation (~45%) and rho+
Kelley et al. 1999	In vivo rat pup	Retinoic acid (RA)	RARα receptor (+)	E18/E20	Increased rod PR, decreased amacrine
Lillian & Cepko 1992	Rat progenitor cells explant	TGF-a bFGF aFGF	FGFR/Ras-Mapk (+)	E15-18	Increased proliferation
Qu et al. 2015	rESC (Da8-16)	IWR-1e (3uM)	Wnt (-)	D0-8	Counteract KSR (20%) to generate neuroectodermal identity Ebs.

Differentiation methods using the addition of extracellular signalling molecules have been derived for the generation of retinal cells and organoids from rodent ESCs and iPSCs. The use of EB formation in 3D suspension and a directed culture technique targeting the Wnt and Nodal pathways with the addition of protein compounds; Wnt inhibitor Dkk1, Nodal inhibitor LeftyA, FBS and Activin-A (DLFA) successfully differentiated mESC to retinal precursor cells expressing *Rax* and *Pax6* (Table 1.2) (H. Ikeda et al., 2005).

Further improvements have been made on the culture method by testing chemical molecules CKI-7 (Wnt inhibitor) and SB431542 (Nodal inhibitor) assessing their capacity to act on the same pathways as recombinant proteins Dkk1 and Lefty-A (Table 1.2) (Osakada et al., 2009). The efficiency of this differentiation in mouse PSCs was comparable and the advantages of using small molecules which are non-biological products include reducing the risk of immune rejection, stable activity, low batch-batch variability (high purity) and their low cost. Furthermore, application of CKI-7 and SB431542 significantly increased gene expression of neural marker *Sox1* at day 5 in organoid culture and *Nestin*

and *ß3-tubulin* cells at day 8, demonstrating effective NE differentiation using mESC (Osakada et al. 2009, Table 1.2).

To target later stages of retinal development and cell differentiation *Rax*+ cells generated from mESC using this method were purified by FACS at day 9 and subsequently treated with the Notch inhibitor DAPT from day 10-20 (Osakada et al., 2008). DAPT is an indirect inhibitor of the Notch signalling pathway, which is critical for progenitor proliferation in the retina (Mills & Goldman, 2017). The Notch pathway is active in RPCs and Müller glia and therefore its disruption is likely to cause neuronal differentiation and potentially loss of structure (Jadhav et al., 2006; Mills & Goldman, 2017). Application of DAPT in mESC-derived ROs increased PR precursors expressing *Crx*, from day 16-20, suppressed differentiation inhibitors and decreased the number of mitotic cells (Table 1.2) (Osakada et al., 2008). This evidence confirms the hypothesised role for DAPT to steer mitotic progenitor cell fate towards post-mitotic PR precursors.

The FGF and Shh signalling gradients have been implicated in the early patterning of the developing retina and the generation of rod PR precursors (Levine et al., 2000; Zuber et al., 2003). RA is also present at high concentrations in the developing vertebrate retina from the OC stage, while *in vitro* studies culturing embryonic rat retinal cells showed RA addition increased rod PR generation (Table 1.2) (Kelley et al., 1999; Levine et al., 2000). Based on findings from animal development *in vivo*, growth factors and chemicals have been tested to improve rod PR generation in mouse RO culture. The Sasai group tested aFGF (50 ng/mL), bFGF (10 ng/mL), Shh (3 nM), RA (500nM) and taurine (1 mM) which were added in combination from day 16 to DAPT-treated mESC-derived PR precursors and this facilitated their effective differentiation towards rod PR cells expressing *Rcvrn* and *Rhodopsin*, however these factors had no effect on cone PR populations (Table 1.2) (Osakada et al., 2008).

In embryological development taurine is the most common amino acid in the ocular tissues and in the retina specifically, taurine is important for PR development and acts as a cryoprotectant against stress related neurological pathologies (Ripps & Shen, 2012). Abundant taurine circulating in the immature rodent NR is downregulated on maturity suggesting it plays a key role in development (T. L. Young & Cepko, 2004). It has also been implicated to control neuronal differentiation, migration and act as a neuromodulator as it contacts both GABA and glycine receptors and is present throughout the CNS (Kilb & Fukuda, 2017). As such, taurine is included in culture media during the maturation phase of *in vitro* RO differentiation and acts to increase PR precursors, as shown by increased *Crx* and *Rhodopsin* expression (Osakada et al., 2008) (Table 1.2).

1.7.2 Serum-free generation of retinal organoids

In contrast to studies adding exogenous signalling factors, seminal work by the Sasai group demonstrated the self-organising capability of mouse and human stem cells into 3D laminated retinal structures when cultured in minimal media conditions (Eiraku et al., 2011; Eiraku & Sasai, 2012; Nakano et al., 2012). This method termed "serum-free embryoid body formation with quick aggregation" (SFEBq) uses plates with low surface adhesion to spatially promote the quick aggregation of a defined number of stem cells to form an embryoid body (EB) which can then be exposed to a variety of retinal growth factors (Fig. 1.9) (Eiraku & Sasai 2012). Crucially, very few growth factors, signalling molecules or stimulants are included in the early culture stages instead exploiting the intrinsic and reinforcing cell-cell signalling to generate neuroectodermal tissue (Sasai et al., 2012).
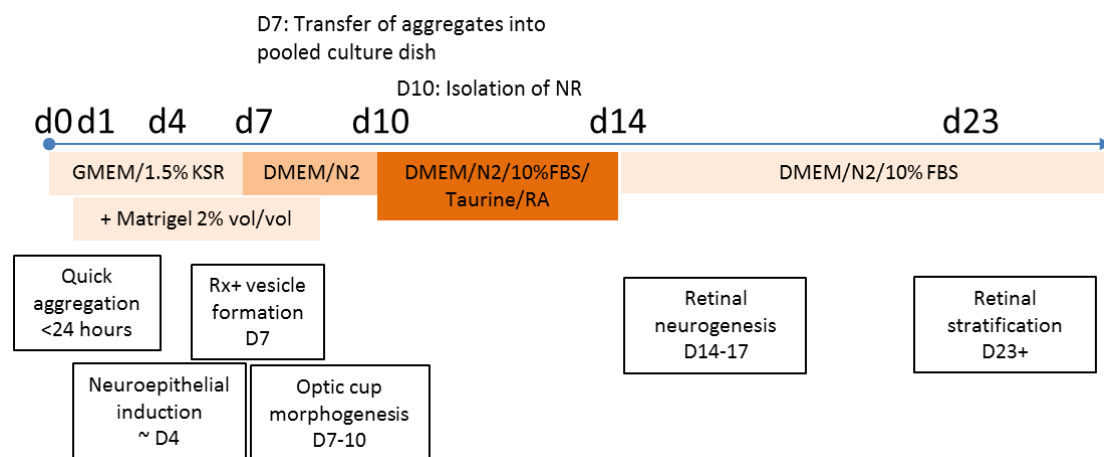
Figure 1.9. Schematic shows SFEBq culture protocol used with mESC (Rx-GFP line) for generation of 3D retinal organoids (adapted from Eiraku & Sasai 2012). DMEM = DMEM-F12. Retinal stimulants include retinoic acid (RA), taurine and N2 supplement. Rx+ = Rax expression.

The SFEBq method informed the initial rat and macaque differentiation experiments described in this thesis. In this method the addition of extra-cellular matrix (ECM)-rich Matrigel at day 1 supports the development of NE tissue which is characterised by a phase-bright lamina surrounding the periphery of the organoid (Eiraku & Sasai, 2012). The organoids are pooled from day 7 -10 and the culture media includes the neural supplement N2 which supports NE and RPC specification (Eiraku et al., 2011; Eiraku & Sasai, 2012) (Fig. 1.9). The phase-bright OV is manually dissected from the main body of the organoid at day 10 (Fig. 1.9). Retinal maturation media added from day 10 includes the signalling molecules taurine (T) and retinoic acid (RA) in addition to N2 supplement and foetal bovine

serum (FBS) (Fig. 1.9). From day 14 onwards the organoids are cultured in the maturation media without RA/T however FBS and N2 supplement is included to support growth and long term culture (Fig. 1.9).

The general development of ROs can be classified into distinct phases which are morphologically distinct and occur in parallel in the embryonic retina (Capowski et al., 2018). These include firstly, efficient embryoid body (EB) formation, followed by specification to neuroectoderm, and generation of neuroepithelial (NE) tissue consisting of multipotent and heterogenous retinal progenitor cells (RPCs), followed by differentiation of the distinct retinal cell subtypes, and finally cell migration and synaptogenesis to form a fully laminated retinal structure. Published culture techniques which have been used to control these phases of RO development are further discussed here.

1.7.3 Embryoid body formation
Methods to generate EBs from PSCs vary in technique and importantly affect the size of organoids and subsequently the efficacy of NE and optic vesicle (OV) growth.

Some groups have used aggregates of stem cell colonies lifted directly from stem cell maintenance, with partial enzymatic dissociation to form clumps which become EBs. These are then cultured by gradual addition of neural induction media (NIM) to induce a change to neuroectoderm. This was shown to be effective in human PSC cell culture (Lamba et al., 2006; Meyer et al., 2009, 2011).

Other groups have fully enzymatically dissociated stem cell colonies and re-plated a discrete quantity of cells in individual chambers or wells in order to form uniform EBs of a specific density (Eiraku & Sasai, 2012; Hallam et al., 2018; Kuwahara et al., 2015; Nakano et al., 2012). While this method is effective for generating large quantities of uniform EBs efficiently in a multi-well format, it requires maintenance of many separated small volumes. This technique generates EBs which are uniform following plating however isolates the organoids from the paracrine signalling from neighbouring organoids which could lead to more intra-batch heterogeneity.

In the early stages of development, following plating of the stem cells, various supplements have been included in the culture media such as the extra-cellular matrix (ECM) proteins laminin and Matrigel, to facilitate effective re-aggregation of the dissociated stem cells and promote the integrity of the developing neuroepithelium, the myosin inhibitor Blebbistatin and Rho-kinase inhibitor (ROCKi), Y-26362, to promote aggregation of the cells and reduce apoptosis prompted by dissociation (Chichagova et al., 2019; Eiraku & Sasai, 2012; Nasu et al., 2012; Zhong et al., 2014a). These components have improved cell re-aggregation efficiencies and allowed for greater organoid heterogeneity.

To spatially affect the formation of EBs various well shapes have been trialled, including 100mm Petri dishes and V and U-shaped tissue culture multi-well plates. When these well surfaces are coated with gelatin or a hydrophilic polymer coating (Lipidure) this creates a low-attachment surface preventing cell adhesion and promoting cell-cell over cell-substrate interactions (Hallam et al., 2018; Meyer et al., 2009; Völkner et al., 2016). Another way to spatially promote aggregation into EBs is the "hanging drop" technique which uses the surface tension of media to encapsulate cells in a micro-volume drop (Z. Wang et al., 2012; Wobus et al., 1991, 2002). This approach physically restricts the volume around the cells causing them to aggregate without the addition of the ECM component. This reduces the method cost and manipulation of the cells, however the EBs later require transferring to larger volumes as they proliferate. Due to the need for a relatively high-throughput system for drug development and safety assessment studies, the 96-well plate system is attractive as it allows for the individual trialling of compounds on each organoid.

This method has been validated by many research groups with cell lines including mouse and human ESC (mESC/hESC) and iPSC (miPSC/hiPSC) (Decembrini et al., 2014; Hallam et al., 2018; Kruczek et al., 2017; Ueda et al., 2018; Völkner et al., 2016). This method shows a developmental timeline which re-capitulates what is seen *in vivo* with minimal exogenous assistance (Fig. 1.9) (Capowski et al., 2018; Eiraku & Sasai, 2012; Völkner et al., 2016). Further optimisations to the SFEBq method have improved the differentiation efficiency, length of cell culture and enhanced the production of specific retinal cell subtypes by the addition of growth factors such as IGF1 and B27 (DiStefano et al., 2017; Felemban et al., 2018; Mellough et al., 2015; D. Singh et al., 2018; Zerti, Dorgau, et al., 2020) (Table 1.3).

Table 1.3. Reviewing and comparing some published methods for inducing retinal organoid differentiation from murine stem cells. D= day, SFEBq = serum-free embryoid body forming method with quick aggregation, ESC = embryonic stem cell, NR= Neural retina, wp = well plate, RO = Retinal organoid, OC = optic cup, PR = Photoreceptor, IF = Immunofluorescence analysis.

Cell type	Plating strategy	Plating cell density	Media additions	Technique	Max. Age	Functional readout	Outcome	Reference
Mouse ESC Rx-GFP	SFEBq in 96-wp	3000-5000 cells/well	RA/T D10-14	Excision of NR at D10. Pooled culture from D7. 40% O2	D24	IF analysis and bright-field images	3D RO with lamination and all retinal cell types	*Eiraku & Sasai, 2012*
Mouse ESC	SFEBq, no excision	3000 cells/well	RA/T D14+, Serum-free from D14+	Pooled at D9, density lowered from D27+	D26-36	Gene expression + IF analysis. TEM	Enriched rod PRs	*Gonzalez-Cordero et al. 2013*
Mouse ESC Crx-GFP	SFEBq, no excision	3000 – 5000 cells/aggregate	N2, B27. Absence of serum. Matrigel +2days	Hyperoxia from D12+	D25	IF analysis, retina size	Enriched PRs and increased OC and RO size.	*Decembrini et al., 2014*
Mouse ESC hPax6-GFP	Modified SFEBq	1500-9000 cells/aggregate	DAPT (D12-14/ 16-18)	Trisection of organoid at D10	D21	Gene expression + IF analysis	Enriched cone/rod PRs. Greater proportion of NR+ organoids	*Völkner et al., 2016*
Mouse ESC GFP-opsin	Modified SFEBq with 96-wp	3000 cells/well	Trans-RA (D14-16), DAPT	Pooled at D9	D26-30	Gene expression + IF analysis	Enriched cone PRs	*Kruczek et al., 2017*

Mouse iPSC Nrl-eGFP	Modified SFEBq with 96-wp	3000 cells/well	5% KSR, AGN193109 (D0 – 10). Removal of FBS at D10	Excision at D23	D30	Gene expression + IF analysis	Enriched PRs	*Ito et al., 2017*
Mouse ESC Nrl-eGFP	Modified SFEBq	3000 cells/well	9 cis-RA; Taurine, IGF1 from D10.	Rotating bioreactor from D10. Dissection vs. intact. 5% O2 to D10; then normoxia.	D25-32	IF analysis and transcriptomics	Increase S-cone PRs, larger size. Enhanced ciliogenesis	*DiStefano et al., 2017*
Mouse iPSC Nrl-eGFP	Modified SFEBq	3000-4000 cells/well	9-cis RA/trans-RA, 1% FBS, T3, BMP4, DAPT	Pooled culture from D9. 40% O2	D35	IF analysis	Enriched rod + S-/M- opsin PRs	*Ueda et al., 2018*

DiStefano et al. optimised the SFEBq protocol, for mESC retinal differentiation, by altering the culture media components and spatial parameters of the physical culture environment to improve retinal differentiation outcomes (Table 1.3) (DiStefano et al., 2017). By performing comparative experiments they identified 9-cis RA to improve the generation of mature, polarised S-cone photoreceptor cells (PRs), and IGF1 to support PR differentiation, and the survival of interneurons (DiStefano et al., 2017). Notably, they also included retinal stimulants RA/T continuously in culture media beyond day 10. Further beneficial modifications included the use of a rotating bioreactor from day 10 onwards to improve waste removal and nutrient circulation. Organoids were also dissected or kept intact at day 10 or these were pooled in mixed culture from day 7 onwards, which increased the size of neural retina (NR) structures (DiStefano et al., 2017). Overall, this study shows that some modified techniques from mouse RO culture can be used to derive rat retinal cells at early stages of differentiation however more specific optimisations are required. Due to the reported success of this method to generate RPCs at day 16, this method was used to attempt generation of a laminated ROs from rESC in this thesis.

The developmental timeline of laboratory rats is close to that of mouse with similar gestation periods of 22 and 20 days respectively (King, 1913; Murray et al., 2010). Furthermore, retinal development and the order of retinogenesis, discussed in section 1.4 and Table 1.1, is conserved between the species indicating the potential for cross-species specific differentiation methodology (W. Heavner & Pevny, 2012; Rapaport et al., 2004).

Factors which may need to be optimised for effective rat RO differentiation include the initial seeding density of stem cells, the culture media formulation, and the timing of culture protocols. This can be informed by previous research investigating culture of rat neural or retinal cell or tissue explants. In studies such as these, the culture conditions of the cells have been adapted for optimal survival and proliferation of rat neurons, for example by the inclusion of triiodothyronine (T3) and N2 and B27 supplements (Bottenstein & Sato, 1979; Ientuile et al., 1984; Sevilla-Romero et al., 2002) (Table 1.2). Additionally, this can be informed by known differences in physiology and retinal anatomy, for instance, as the embryological size of rats is larger than that of mice this may affect the optimal cell density or quantity for effective embryoid body (EB) formation.

1.7.4 Manual manipulation of organoids
The SFEBq method derived by Sasai and colleagues (Eiraku & Sasai, 2012) relies on the isolation, by manual excision, of the optic vesicle/cup (OV/OC) from mouse-derived ROs, at day 10 to derive laminated retina. This technique relies on the recognition of the characteristic morphology of the NE

tissue and the temporal progression of retinogenesis over time. However, this method limits the amount of retinal tissue which can be generated as low percentages of ROs generate fully evaginated OV/OC. To counteract this, other groups omit the excision resulting in increased retinal tissue and cell yield as well as generation of mature PRs (Decembrini et al., 2014; Gonzalez-Cordero et al., 2013) (Table 1.3).

Eye-field induction efficiency in mouse ROs is also dependent on cell-seeding density however this was found not to correlate with evaginations of OVs (Völkner et al., 2016). By immunofluorescence (IF) analysis of the presumptive NR and RPE markers; Lhx2, Mitf and Rax, it was shown that the identity of NR and RPE was determined on a molecular and spatial level rather than depending on the structural development of OV/OCs (Völkner et al., 2016). To improve and increase the retinal differentiation efficacy in organoid culture, trisection of the entire mESC-organoid at day 10 was shown to derive three times as much retinal NE tissue (Völkner et al., 2016). Further method optimisations entirely omitted the manual isolation of OV/OC tissue, maintaining retinal lamination throughout the organoid in an effort to increase the quantity of PRs (Decembrini et al., 2014).

Further modifications to the physical cell culture environment includes the use of rotating bioreactors to improve nutrient availability and effective waste removal from the culture system (DiStefano et al., 2017). The use of a rotating chamber to culture mESC-derived EBs alongside static culture of both intact and dissected ROs identified key culture parameters important for the development of retinal cell types, such as cone PRs, and found that constant rotation increases organoid size (DiStefano et al., 2017). By comparing transcriptomic data from ROs to the mouse retina, the authors found that the period of neural-retina (NR) development was accelerated from 10 or 14 days in static culture to 7 days (DiStefano et al., 2017).

1.7.5 Transitioning to adherent 2D culture

Many studies have generated distinct retinal cell types by first forming EBs in suspension followed by plating on a 2D biopolymeric surface (coated with poly-d-lysine, ornithine or laminin) to generate an adherent cell culture system (H. Ikeda et al., 2005; Osakada et al., 2008; Qu et al., 2015; Zhong et al., 2014a). This technique builds on early neuronal cell culture methods which generate mature neurons in a 2D system coated with an optimal substrate to support cell proliferation (Y. Li et al., 2014; G. T. Young et al., 2014). This is an effective method as it promotes a high, uniform media to cell ratio increasing the accessibility of diffusible molecules and relative oxygen exposure. Decreased oxygen levels have a profound effect on the developing CNS and *in vitro* studies show chronic anoxia reduces retinal RGC survival and proliferation (Ortega et al., 2017). These protocols exploit

alterations in the physical environment to promote neural cell growth, however it is worth noting that this is in combination with chemically directed culture conditions to direct and support cell differentiation.

The technique of adherent 2D culture has been effective for generating retinal tissue and multipotent retinal progenitors from EBs. Re-plating EBs into 2D culture facilitates the outgrowth of neural rosettes, generation of retinal progenitor cells and NE tissue sometimes in the form of OV/OC (Mellough et al., 2012; Osakada et al., 2008; Zhong et al., 2014a). The transition to adherent growth alone may be sufficient to induce NE growth but substrate coatings which have supported retinal cell proliferation are; the ECM and protein rich substrates of Matrigel, poly-d-ornithine and various laminins (Fligor et al., 2018; Shibata et al., 2018; G. T. Young et al., 2014)

To develop retinal tissue from hESC and hiPSC the 2D culture technique was applied from day 30-60 to expand RPCs from EBs in combination with supplemented media components (Mellough et al., 2012). The presence of bipolar, branching RPCs were strikingly seen proliferating on the poly-d-orthinine and laminin coated substrate from the main body of the organoid 5 days following plating (Fig. 1.10). The cell density increases and mature retinal marker gene expression (*OPSIN*, *RECOVERIN*, *ARR3*, *RPE65*) as well as neurite formation was observed in cells 30 days after plating (Mellough et al., 2012).
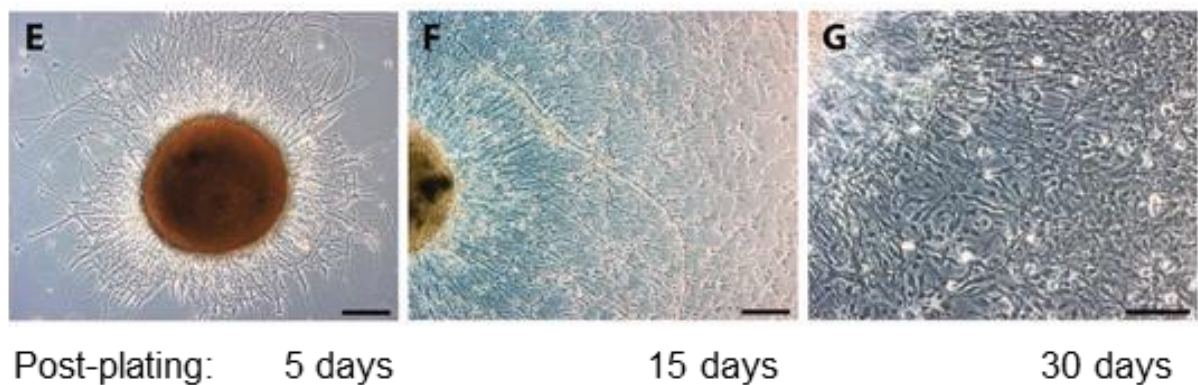
Figure 1.10. Bright-field images showing cell proliferation in 2D adherent culture from human PSC derived EBs. Scale bar = 200 µm (E, F), = 100 µm (G). (data from Mellough et al. 2012).

Plating in 2D generates an overall greater yield of NE tissue when compared with the low efficiency of OV/OC structures typical in the SFEBq system (C. S. Cowan et al., 2019; Eiraku & Sasai, 2012; Regent et al., 2020). Subsequent formation of 3D ROs from 2D cultures is performed by manually lifting the adherent, newly proliferated RPCs and re-plating them into low-attachment plates for further suspension culture. This can be done in a targeted way, by isolating those areas with

optically bright NE tissue and a recognisable and characteristic OV/OC formation. These structures derived from hiPSCs effectively re-formed in 3D culture and had high neural-retinal identity with 50-70% of cells positive for the RPC marker *VSX2* (Zhong et al., 2014a).

Additionally, to improve time and labour efficiency, adherent cells have been detached and lifted in a non-targeted way using "checkerboard" scraping where the total cell monolayer is manually separated by horizontal and vertical divisions and lifted indiscriminately (C. S. Cowan et al., 2019; Regent et al., 2020). As well as increasing the yield of overall retinal structures generated, compared with the manual excision of retinal structures in 2D, this method has been reported to generate a higher proportion of RPE-tissue within the ROs which subsequently are re-formed (Regent et al., 2020).

The ROs formed following a period of 2D adherent culture show the same morphological structure and histological organisation as in the native retina and transcriptomic analysis shows generation of mature retinal cell types can be achieved (C. S. Cowan et al., 2019). However, as a strategy for the purposes of drug development and safety assessment it is less attractive due to the technical challenges and additional time required for the separation and maintenance of the organoids which are returned to 3D suspension culture.

1.7.5.1 Rodent-specific adherent culture studies

The adherent culture method was shown to be effective at generating retinal progenitor cells and tripoint neural progenitors from rat PSCs. Qu et al. (2015) differentiated RPCs from rESCs using adherent plating. Firstly, a modified SFEBq technique (Eiraku & Sasai 2012), was used to generate EBs at a defined cell density of 5000 cells/well. Then, at either day 10 or 14, EBs were transferred to adherent culture and at day 16 the RPCs were characterised by retinal gene and protein expression (Fig.1.11) (Qu et al., 2015). The adherent culture system affects cell differentiation in combination with signalling and growth factors present in the media. The initial media to support differentiation into neuroectoderm modified the SFEBq mESC media by increasing KSR to 20% and including the Wnt inhibitor IWR-1e (Qu et al., 2015). This inhibitor was shown by Nakano et al. (2012) to counteract the caudalising effect of the high concentration of KSR to cause a rostralising effect in developing hESC-derived ROs (Table 1.2). Compared with mESC differentiations, a higher cell plating density of 5000 cells/well was used and rat ESC were exposed to a lower concentration of Matrigel (1%) at day 1 which was maintained until day 8 (Qu et al., 2015). Differentiation media including 10% KSR and 10% FBS in minimal base media was used from day 8 - 14 when the media was changed to the maturation media (DMEM-F12, 10% FBS and N2) or until day 16 when the RPCs were collected

(Qu et al., 2015). At either day 10 or 14 cells were cultured adherently and at day 16 the RPCs were assessed for neural-retinal gene and protein expression, *Pax6, Rax* and *Lhx2,* neural-retina progenitor marker *Chx10* and neuronal markers *Nestin*, *GFAP* and *Tuj1* (Qu et al., 2015). This novel method confirms the capability of rat PSCs to be directed in culture towards a retinal fate using chemical signals to modulate pathways known from mouse and human derived methods to affect retinogenesis.
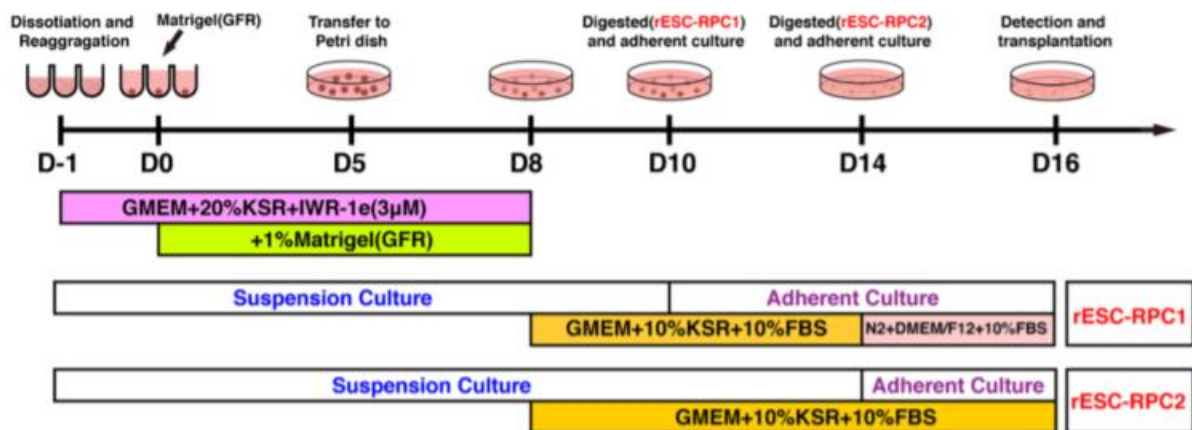
Figure 1.11. Retinal differentiation protocol to generate retinal progenitor cells (RPCs) from rESC (from Qu et al. 2015). This method adapted the SFEBq Sasai-based protocol to include a higher concentration of KSR, addition of IWR-1 between day 1-8, a modified maturation media and adherent cell culture. RPCs were harvested at day 16 for characterisation and transplantation studies.

The RPCs showed expression of neural-retinal and progenitor markers; *Chx10, Otx2* and *Lhx2*, however at significantly lower levels than in primary control cells (Qu et al., 2015). Levels of neuronal markers, *GFAP*, *Nestin* and *TUJ1* were much higher than in primary RPC controls, indicating a propensity of the rESCs to differentiate towards neuronal lineages. The cells were collected at day 16 and further matured *in vivo* following transplantation into rat eyes, thereby maturation *in vitro* was not shown. This work demonstrates the ability of immature NR cells to be derived from rESC using known differentiation factors and cell culture techniques however requires further study and optimisation to generate a 3D retinal model. Due to the reported success of this method to generate RPCs at day 16, this method was used to attempt generation of a laminated ROs from rESC in this thesis. To achieve this the method was adapted to extend the culture of rESC-derived organoids beyond day 16 and retinal stimulants including RA/T were applied.

The adherent culture strategy has been effective for the generation of tripotent neural progenitors from rESC (Z. Wang et al., 2012). To date, a method for the derivation of mature 3D rat ROs has not been published, so this study is informative as a culture method specifically developed for rat PSCs.

Key findings from this paper include the use of the hanging-drop method to generate EBs within a micro-volume drop (30 µL). The media includes N2 and B27 and mouse embryonic fibroblast (MEF) conditioned media (CM), Rho kinase inhibitor (ROCKi) Y-27632, and two inhibitors used to maintain pluripotency (CHIR99021 and PD0325901) and notably does not include Matrigel (Z. Wang et al., 2012). rESC-derived EBs were formed by day 4 upon removal of the inhibitors from the media and expression of neuroectodermal marker *Nestin* is detected. At day 8, EBs were seeded into poly-D-lysine and laminin coated tissue culture plates to generate neural progenitor cells in adherent culture (Z. Wang et al., 2012). The formation of neural rosette structures was seen 4-5 days after plating and the culture media was kept as N2B27 with the additional supplementation of bFGF and EGF (Table 1.2)(Z. Wang et al., 2012). The adherent cells which rapidly proliferated in the monolayer culture stages were characterised as NE progenitor cells of a maturity approximately equivalent to those isolated from rat brains at gestational day (GD) 14.5 by their elongated, bipolar morphology, expression of cell proliferation marker Ki67 and neural progenitor markers Nestin, Sox2, Pax6 and Olig2 (Z. Wang et al., 2012). Interestingly, the culture media used to generate rat EBs differed entirely from that used with mouse PSCs in the retinal SFEBq method and consisted of N2B27 with MEF-conditioned media (CM) and ROCKi, and with lowered concentrations of the inhibitory compounds (2i: PD0325901 and CHIR99021) to support aggregation and survival between day 0-2. After day 5 the EBs were transitioned to N2B27 media rich in neural growth factors (Z. Wang et al., 2012).

As this project aims to differentiate rat PSCs towards a NR identity, which arises first from the neuroectoderm around E8-9 (Table 1.1), the methodology from these studies is particularly relevant to derive neural progenitor cells from rESC, which could later be exposed to retinal stimulating factors.

1.7.5.2 Primate specific adherent culture methods

Few studies have shown the potential of NHP PSCs to be differentiated towards a retinal lineage using robust culture methods. Those studies which have used NHP PSCs to generate retinal cells in culture using this strategy will be discussed here alongside the methods derived using human PSCs which have informed them.

In hESC culture, early application of CK1-7 and SB431542 (Wnt and Nodal inhibitors) generated RPCs (*RAX*, *MITF* and *SIX3* expressing cells) (Osakada et al., 2009). The expression of progenitor markers gradually decreased as retinogenesis occurred and differentiation into functional RPE cells was also achieved by day 60 in culture. Addition of RA and taurine (RA/T) from day 90-140 promoted PR differentiation determined by increased PR marker expression (Table 1.2; Osakada et al. 2008).

In a similar way macaque ESC (mkESC) were cultured with serum-free differentiation media including Dkk1 and Lefty (SFEB/DL) between day 0-18, which generated aggregates with 42% of Rax+/Pax6+ cells at day 30 (Table 1.2; Osakada et al. 2008). The addition of RA/T and N2 supplement in FBS-free culture media from day 90 onwards significantly increased PR (Crx+) cells from 26% to 71% on day 120 (Osakada et al., 2008). Differentiated cells were also positive for M/L and S opsin cone PR markers. In total 35% of cells were PR-like cells using this method. Other retinal cells expressing amacrine, bipolar, RGC and Müller glia markers were generated, and these typically were found in the same regions although a laminated structure was lacking (Osakada et al. 2008). After 40 days in culture some cells expressed Mitf and co-expressed Pax6 denoting the identity of RPE. After day 90 these cells expressed the mature RPE cell markers RPE65 and ZO-1 (Osakada et al. 2008).

A further *in vitro* study supports the proactive effect of RA on NHP PR development, shown by the adherent co-culture of mkESC with mkESC- derived RPE cells and exposure to RA, which reduced the required culture length for mature cell marker expression and increased rhodopsin expression five-fold to 25% (Yue et al., 2010) (Table 1.2).

Therefore, the culture method of SFEB/DL and RA/T factors has the capacity to differentiate NHP cells to a neural-retinal identity and subsequently direct cells toward a mature PR fate in combination with adherent culture and co-culture with retinal cell types, however fully laminated retinal structures have not been derived, and functionality was not assessed in these early studies.

Further chemical modulation of hESC differentiation by Nakano et al. (2012) showed the low KSR concentration (1.5%) used with mESC culture was insufficient to generate NE from human PSCs, and 20% KSR was required. The caudalising effect of the increased serum replacement was counteracted by the addition of a Wnt inhibitor (IWR-1e) (Table 1.2; Nakano et al., 2012). The ECM and protein rich component Matrigel (1%) was added from day 2-12 of culture to facilitate NE and OC formation, similarly to mouse and rat differentiation experiments (Eiraku and Sasai, 2012, Qu et al., 2015). ROCKi, Y-27632, was added at plating to avoid dissociation-induced apoptosis. An effective enhancer of retinal differentiation was application of 10% FBS from day 12-18 in combination with SAG (hedgehog (Shh) and indirect Wnt agonist) (Table 1.2). This increased the amount of Rax+ cells to

70% and cells co-expressed *VSX2* and *PAX6* indicating NR identity. 3D hESC-derived ROs were placed into pooled culture at day 12, which may have further contributed to successful retinal development (Nakano et al., 2012).

Further development of hESC-derived retinal culture by Kuwahara et al. (2015) applied BMP4 recombinant protein at day 6 in place of Matrigel to establish a dorsal-ventral axis and generate NE tissue (Table 1.2). Subsequent co-treatment with Wnt agonist CHIR99021, and FGFR antagonist SU5402 from day 18-21 induced the thinning of NE, inhibited NR differentiation and generated Mitf+ cells and RPE (Table 1.2; Kuwahara et al., 2015). Interestingly, earlier treatment with CHIR99021 from day 15-18 increased Mitf+ cells without suppressing *VSX2* and shows the critical time-dependent action of the Wnt pathway in retinal development. When this exposure was removed, NR continued to thicken and develop, producing organoids with a balanced composition of NR and RPE (Kuwahara et al., 2015). The application of these molecules was subsequently termed "induction-reversal". This study also maintained ROs in a DMEM-F12 maturation media with RA/T to enable long-term NR culture (Kuwahara et al., 2015).

Another human RO differentiation method which has improved method efficacy and production of PR cells has been developed and optimised in the Lako lab group. This method omits BMP4 and Matrigel, in favour of a minimal media containing B27 supplement, KSR and insulin growth factor 1 (IGF1) to generate OVs at a high efficiency (Table 1.2) (Mellough et al., 2012, 2015). The addition of IGF1 throughout development significantly increased OVs and key retinal progenitor and eye-field markers such as Pax6 and Vsx2 in hESC cultures (Mellough et al., 2015). Continued supplementation with IGF1, B27 and N2 supplements throughout differentiation also led to formation of PR cells expressing mature markers such as recoverin, bassoon and rhodopsin (Mellough et al., 2015). Another interesting finding from this study showed that the emergence of mature PR markers was accelerated in the presence of IGF1 in the culture media and the PR cells were generally maintained longer compared to the un-supplemented condition and other published methods.

Due to the application of several factors in combination, the causative agent cannot be readily identified. However, T3, is known to control gene expression via the TRβ2 receptor, which is expressed throughout the retina and whose activity coincides with cone PR genesis in the mouse retina (Applebury et al., 2000; Ng et al., 2009). Furthermore, T3 has been shown to control L/M cone specification in the human retina (Eldred et al., 2018) and its use in other human RO differentiation protocols from day 37, in combination with RA/T, has a proactive effect on retinal lamination and structure (Eldred et al., 2018; Wagstaff et al., 2021).

Further optimisations to this IGF1 method included the addition of Rho-kinase inhibitor (ROCKi), Y-27632 in the initial stages of plating, and FBS, RA/Taurine, T3 and concentrated lipids added later in differentiation (Dorgau et al., 2019; Zerti et al., 2021b). Despite the additional supplementation of stimulatory retinal factors, the addition of IGF1 continued to show a significant increase on recoverin expression and long-term maintenance of OV structures (Zerti et al., 2021b).

Studies have shown that human retinal differentiation techniques such as SFEBq and Wnt/Nodal inhibition for early NE generation and RA/T for retinal maturation can differentiate macaque ESCs to neural-retinal identity and subsequently toward mature PR fate (Table 1.2) (Osakada et al., 2008; Yue et al., 2010). However, to date only one recent publication has documented the generation of 3D ROs from NHP stem cells (Lopez et al., 2021b). This group used a combination of published human retinal differentiation methods to generate 3D retinal tissue from rhesus macaque iPSCs (Kuwahara et al., 2015; Meyer et al., 2011; Zhong et al., 2014a).

The method used neural induction media (NIM) as the culture media for EB formation, BMP4 addition at day 6, followed by plating in adherent 2D culture to generate morphologically neuroepithelial (NE) tissue, which was then sub-cultured in 3D suspension in low-attachment plates (Lopez et al., 2021). A combination of B27 supplement, RA/T and Activin-A was used in the maturation media applied between day 30-80. Activin-A was purported to play a role in stimulating exit from the cell cycle which in this case could be useful for triggering a change away from RPC proliferation towards retinal cell differentiation. The organoids were characterised by morphology and temporal staging to classify 3 stages of retinogenesis, as suggested by Capowski et al., which occurred approximately 30% earlier than in human PSC derived organoids (Capowski et al., 2018; Lopez, Kim, et al., 2021). At the final stage of differentiation (day 125) mature PR makers were detected by transcriptomic and IF analysis, alongside other retinal markers for bipolar cells and Müller glia, and a structured retinal lamina was seen (Lopez, Kim, et al., 2021). (Lopez, Kim, et al., 2021). Despite using the same timeline of culture conditions as in human RO differentiation, the progression of retinal development was seen to be faster in the rhesus macaque derived organoids, suggesting an intrinsically faster rate of retinogenesis. This study shows it is possible to generate macaque organoids with mature retinal cell identity including PRs, a laminated structure and retinal gene expression. However, the efficiency of generating 3D ROs which had the full laminated structure was significantly lower at 1.4-4.7% compared to human ESC differentiation (26%) (Lopez, Kim, et al., 2021).

A key finding of interest to this project is the accelerated development of retinogenesis within the derived organoids, as mature PR markers were detected at day 105 compared with day 150 in human ROs (Lopez et al. 2021). This study was published after the experimental lab work on my project had been completed, hence the efficacy of the culture method was not evaluated on cynomolgus macaque iPSCs.

These studies confirms that use of signalling molecules that are physiologically active in the native retina can have the same proactive effect in cell culture models. As retinal histogenesis is a highly conserved process co-ordinated by core transcription factors and developmental pathways, optimisations shown in hPSC culture provide targets for effective signalling pathways and can inform differentiation methods used with other related species such as macaque. Furthermore, chemical stimulation has now been shown to be effective in stimulating retinogenesis from rhesus macaque iPSCs as well as demonstrating the differences in temporal staging of retinal development between macaque and human PSCs when exposed to the same environmental conditions.

1.7.6 Developmental timing of primate organogenesis
Comparative studies on cortical development from PSCs of various primate species, including human, chimpanzee and macaque show that the timeline of neurogenesis is species-specific and intrinsically regulated (Otani et al., 2016).

To investigate the mechanisms affecting the larger brain size and cortical thickness of higher order primates, Otani et al differentiated human, chimpanzee and macaque PSCs towards a cortical fate *in vitro*. Primate NE cells which had been differentiated generated neuronal classes in a fixed temporal order at a rate equivalent to that seen *in vivo*. In the macaque model, expression of late order neurons was seen 20 days before that of chimpanzee and human. Furthermore, the species-specific rate of developmental timing was conserved in both adherent and 3D laminated cell culture models.

This was shown to be due to a divergence in progenitor capacity which shows that NE progenitor cells have longer periods of symmetric proliferative division, and longer cell cycle length leading to an overall greater number of neurons in primates compared to rodents, as well as in humans compared to macaques (Figure 1.12) (Otani et al., 2016).
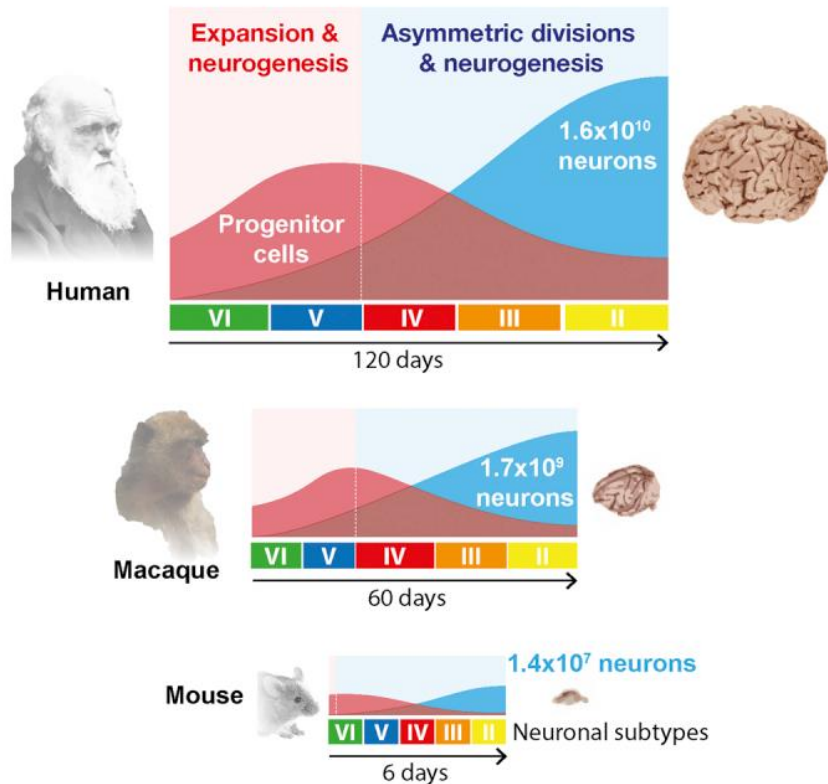
Figure 1.12. Comparison of developmental time during cortical cell expansion in vivo between species of interest. Although the phases of development are conserved between mouse, macaque and human, the overall length of the expansion period is longer in humans leading to an increased number of neurons (from Otani et al. 2016).

Another recent study compared in vitro cortical brain organoid development between humans and other NHP species showed a conserved gene, *ZEB2*, which controls the switch from proliferative to neurogenic state in NE progenitor cells (Benito-Kwiecinski et al., 2021a). This study confirmed species-specific and endogenously regulated gene expression which resulted in a delayed onset of neurogenesis in humans compared to chimpanzee and gorilla which both have shorter gestation times and fewer neurons overall. The demonstration of species-specific intrinsically regulated timeline of development in the brain indicates the possibility that neurogenesis in the primate retina may be similarly regulated.

1.7.7 RPE conditioned media or co-culture approach to retinal differentiation

RPE cells have been shown to play a role in the proliferation of RPCs and the structural organisation of the NR, potentially due to the secretion of diffusible factors including trophic factors IGF1, bFGF,

63

PDGF, IL-6, IL-8, MCSF and TGF-β, which are secreted by RPE cells *in vitro* (Sheedlo & Turner, 1996a). Additionally, there is a structural, supportive and neuroprotective role provided by the RPE in the form of ECM proteins, such as laminins and collagen, and growth factors, including vitronectin and complement factors (Al-Ubaidi et al., 2013; Neugebauer et al., 1991; A.-G. Wang et al., 2006). Furthermore, the close proximity found between the RPE and NR in the native retina suggests RPE-PR contact and replication of the microenvironment in which they interact are important for PR differentiation and maturation (Bok, 1993; Redmond et al., 1998). Studies have used this knowledge to support retinal cell differentiation *in vitro*, by the addition of various ECM components (Dorgau et al., 2019) and RPE/NR co-culture techniques (Akhtar et al., 2019; Ghareeb et al., 2020). Relevant studies applying these techniques in rodent and primate culture will be discussed here.

1.7.7.1 Rodent-specific methods

The addition of RPE conditioned media (-CM) to rat RPCs cultured from embryonic and neonatal explants was shown to promote cell proliferation, survival and maturation in culture. Retinal explants isolated at GD 16, GD 18 and PND 2 were cultured with RPE-CM and subsequent RPC-like cells which arose were sub-cultured and analysed by immunostaining for retinal cell markers. Cells from PND 2 expressed mature PR markers opsin, arrestin and neuron-specific enolase (NSE) (80%), and glial marker CRALBP (20-30%) while less than 1% expressed the early NE marker, nestin. Cells derived from GD 16 retina were positive for nestin (67%), opsin (81%), arrestin (76%), CRALBP (18%) and NSE (18%). This shows a differentiation potential of RPCs in line with native retinogenesis (Ford & Feller 2012). Interestingly, the proportion of cone PR cells (opsin+/arrestin+) was also found to align with that in native retina (Sheedlo & Turner 1996).

In the same study, RPCs from GD 16 rat retina were exposed to defined growth factors previously identified from RPE secretions and expected to stimulate retinal mitosis (R. M. Anchan et al., 1991; Lillien & Cepko, 1992). After 7 day exposure to components; EGF, PDGF, MCSF, bFGF, NGF, TGF-β and TGF-α, minimal retinal cell proliferation was produced (Sheedlo & Turner 1996). These results show that RPE secretes a factor(s) which promotes the survival, proliferation and maturation of RPCs which could not be replicated by the addition of serum and other known growth factors. These likely include ECM proteins. Additionally, it suggests that exogenous signalling factors play a key role in the determination of retinal cell fate.

The role of RPE in aiding maturation of PR cells was also seen in explant culture of retina-RPE constructs. Isolated neonatal rat retina (PND 0-4) was isolated with or without RPE tissue attached and cultured *in vitro* to determine the effect of RPE on the subsequent development of the retina.

This is relevant as rat PRs mature throughout post-natal weeks (M. Anchan et al., n.d.; Caffé et al., 1989; Pinzón-Duarte et al., 2000) (Table 1.1). Both retina only and retina-RPE explants showed retinal development, cell differentiation and synaptic formation at approximately the same time point as *in vivo*. The addition of RPE aided the morphology of connecting cilia in PRs and the morphology of OS' compared with retina only explant (Pinzon-Duarte et al. 2000). This experiment showed that RPE was not required for the process of cell differentiation, synaptogenesis and inner retinal lamination in retinal explant culture, however full maturation of PRs was facilitated by the interaction with RPE tissue.

Another group used gerbil retina for dissociation studies and development studies. By enzymatically disrupting cells from their structure and plating *in vitro* they investigated the intrinsic and extrinsic determinants of retinal cell organisation and maturation (Bytyqi et al., 2007). Gerbil neonatal eyes were used as the model because they have significant post-natal maturation and a higher proportion of cone PRs than either mouse or rat, due to their diurnal lifestyle (Bytyqi et al., 2007; Huber et al., 2010). The re-aggregation of dissociated retinal cells from PND 1 embryos into retinal spheres was achieved and the structural organisation was determined by immunohistochemistry for cell and lamina-specific proteins which showed organisation into IPL-like layers (Bytyqi et al., 2007). The addition of RPE-CM produced a higher level of organisation within the re-aggregated spheres with GCL, IPL and INL lamination clearly present. However, PRs were absent in both types of spheres indicating lack of complete cellular maturation *in vitro* (Bytqi et al. 2007).

Furthermore, in the RCS rat, a model with degenerate retina and impaired PR and RPE growth, transplantation of pigmented rat neonatal RPE cells into the subretinal space rescued PRs. PR OS' increased in length from 2 to 18 μm between day 14-21 after transplantation in comparison to controls which had no OS' and shorter IS' in the PR layer (N. Lin et al., 1996). This shows that *in vivo* healthy RPE has a profound impact on development in the retina and is able to initiate repair mechanisms, new growth and maturation.

In summary, rat cultures of immature retinal cells at embryonic or neonatal stages, which are likely to be a mix of pre and post-mitotic cells, and approximate organoid culture, when supplemented with RPE-CM show improved cell organisation, survival, proliferation and maturation. Dissociated gerbil retinal tissue re-capitulated the formation of the retina developmentally (Bytyqi et al., 2007; Matthias et al., 2018) showing the addition of RPE or Müller glia cell supernatants to result in improved cellular organisation and viable cultures could be kept until day 15. Co-culture of retina-RPE explant tissues isolated the same original eye show a less significant effect of RPE on the

organisation and migration of cells in the developing retina; however, the removal of RPE caused a detrimental effect to PR maturation (Pinzón-Duarte et al., 2000).

1.7.7.2 Primate-specific methods

The differentiation of mkESC into retinal cells has been achieved by co-culture with mkESC-derived RPE (Yue et al. 2010). Cells expressing the PR markers recoverin and rhodopsin were generated, and interneuron cell expression was also detected by calbindin and PKC expression. Remarkably, this was achieved in un-supplemented ESC culture media, with PR marker expression appearing after 10 days (Yue et al., 2010). Further supporting the stimulating effect of RA on primate PR development, Yue et al. (2010) added RA to the maturing macaque ESC-RPE co-culture, which reduced required culture length and increased rhodopsin expression five-fold in approximately 25% of cells. This co-culture method removed the requirement for serum supplementation and resulted in Rhodopsin+ cells after 10 days, thereby showing a stimulating effect of RPE on primate retinal maturation and PR development as well as effective use of co-culture in primate retinal cell systems.

The use of RPE conditioned media (RPE-CM) has been used in the generation of human ROs, as a supplement in culture media at a ratio of 1:3 from day 18 (Dorgau et al., 2019). Interestingly, no significant differences were observed in generation of NE and RPE in human ESC-derived ROs at the early to mid-stages of differentiation (day 35-90) (Dorgau et al., 2019). However, by the later stages of differentiation (day 150) a significant increase in rod PR cells and synaptic connections was seen in the RPE-CM supplemented condition (Dorgau et al., 2019). Additionally, this culture method showed generation of all major retinal cell types by day 150 organised in a structured lamina with the presence of mature features such as connecting cilia in the PRs and synaptic contacts between cells (Dorgau et al., 2019). The addition of de-cellularised RPE isolated from bovine eyes also improved rod and RPE cell marker expression in comparison to ROs supplemented with de-cellularised neural retina extract or the un-supplemented control. This method tested RPE addition in a background of the IGF1 culture method which includes B27 and N2 supplements, IGF1, and T3, which have been shown to improve PR generation and retinal structure in human RO generation (Mellough et al., 2015). This study further supports the use of RPE-derived components to improve RO maturation and suggests allogeneic tissues can be used as a source for these components.

Overall, differentiation methods using solely 2D culture have the propensity to differentiate human and macaque PSCs into various retinal cell types including RPE, RGCs and PR cells which are often found disorganised in populations of mixed cell identity (Osakada et al. 2009). The macaque retinal cells which were generated in these published studies have significant limitations in representing the

full cellular diversity of the retina as well as the 3D laminated structure. However, the culture environment that is used to sustain macaque PSC-derived retinal cells *in vitro* is informative for future development and optimisation of retinal cell differentiation and organoid culture methods.

1.8 Analysis and characterisation of retinal organoid differentiation efficacy

In order to validate the various differentiation methods and compare method optimisations it is necessary to characterise ROs throughout differentiation for retinal cell generation, organisation and an organised and laminated retinal structure. Furthermore, functional analysis of ROs by assessing the light-responsiveness, using multi-electrode arrays and patch-clamping, importantly confirms the maturity and functionality of the *in vitro* retinal tissue and validates the model system for toxicology testing (Hallam et al., 2018). The parameters which have been used by research groups as a standard for correct retinal development include organoid morphology, protein expression, gene expression, transcriptomic analyses and comparison with embryonic or mature retina (Collin, Queen, et al., 2019; C. S. Cowan et al., 2019; Zerti, Collin, et al., 2020).

As is known by molecular investigation of TFs, the early NR is specified by the co-expression of *Pax6*, *Rax* and *Chx10* which distinguishes it from neighbouring presumptive RPE which is identified by the absence of *Rax* and presence of *Pax6*, *Mitf*, and *Otx2* (Fig. 1.2) (Bäumer et al., 2003; S. S.-M. Zhang et al., 2002). These factors are known to be crucial for regulating development and cell differentiation temporally and spatially throughout retinogenesis and thereby are appropriate markers for study in RO culture. Assessment of these factors by gene expression analysis enables the efficacy of RO differentiation techniques to be evaluated at key stages of differentiation (Meyer et al., 2009; Zuber et al., 2003).

Additionally, groups have derived specific transgenic reporter lines, such as *Crx*-eGFP, which enable visualisation of retinal development in live cells and derived samples (Collin, Zerti, et al., 2019; Decembrini et al., 2014; Ito et al., 2017; Lam et al., 2019). This is a valuable technique which allows for the confirmation of correct retinal gene temporal expression and spatial mapping throughout the phases of differentiation.

In terms of protein expression, there are known markers of retinal cell subtypes which can be used for the identification of cells within a mixed model or organoid. These have been identified in analysis of native retina and specific antibodies have been derived and validated to enable use (Pérez de Sevilla Müller et al., 2017; Rodriguez et al., 2014; Samson et al., 2009). However as in the case of bipolar, RGC and amacrine cells there are many distinct subtypes and protein marker expression is variable between them (Ekström & Johansson, 2003; Haverkamp, Ghosh, et al., 2003;

Haverkamp & Wässle, 2000; Hinds & Hinds, 1983). Often these proteins are expressed at various stages in development and within different cells of the CNS at various timepoints, such as Vsx2/Chx10 which is known to act in RPCs to control proliferation during early retinogenesis, while it also controls bipolar cell genesis in the mature retina (Livne-bar et al., 2006). In this case one can find a common marker which is ubiquitous, such as gamma-synuclein (SNCG) for RGCs, use a marker specific for a distinct subtype, such as ChAT for cholinergic starburst amacrine cells, or use a combination of markers such as PKC- α and GO- α for rod ON bipolar cells, in order to definitively identify the cell type (Famiglietti & Sundquist, 2010; Haverkamp, Haeseleer, et al., 2003; Rodriguez et al., 2014). Furthermore, although retinogenesis is a highly conserved process in vertebrates with homologous gene and protein families, between different species there may be different patterns of protein expression within homologous cell types, such as is found in the 10 subtypes of bipolar cells in the mouse retina (Haverkamp, Haeseleer, et al., 2003).

Morphological characterisation of developing ROs is an important marker of method efficacy and known retinal features such as phase-bright NE, OV/OC growth and PR generation can be visualised by microscopy throughout differentiation. These features have been used to classify human RO development into three stages, distinguishable by eye (Capowski et al., 2018). Interestingly, the morphological staging is comparable with other mammalian species such as mouse and macaque (Lopez, Kim, et al., 2021; Völkner et al., 2016). Transmission electron microscopy (TEM) also lends itself well to organoid analysis. It can be used to determine the presence of specific intracellular structures such as OS disks and characterise the maturity and organisation of PRs and other retinal cells in the developing organoid (Gonzalez-Cordero et al., 2017; Zhong et al., 2014a).

These morphological stages of retinal development can further be linked to gene and protein expression profiles by performing single-cell transcriptomic and proteomic analyses on ROs. Recent studies have used transcriptomic analyses to compare the developmental trajectories of ROs to native retina and this enables the stages of cell fate branching and specification to be studied in depth (Capowski et al., 2018; Collin, Queen, et al., 2019; C. S. Cowan et al., 2020; S. Kim et al., 2019; Zerti, Collin, et al., 2020). This is a powerful technique which also enables classification of the full cellular diversity found in ROs throughout differentiation. However, currently it is an expensive technique to employ thereby limiting the number of cells/organoids which can be assessed. Another challenge presented by this technique is the disruptive cell dissociation methods required to isolate cells from mature ROs. High quality and unbiased analyses require optimisation of the dissociation techniques to avoid loss of fragile cell types and to maintain the cellular diversity within the sample (Fadl et al., 2020).

Generally, in *in vitro* development, there is heterogeneity seen between individual organoids or low efficiencies of organoid generation within a batch. This may arise from intrinsic cell line variability or may indicate the efficiency of the culture technique (Chichagova et al., 2020). This impacts the sampling technique for measuring and comparing between samples as organoid selection can result in a non-representative sample. These molecular measures along with the overall homogeneity of the organoids generated within batch, are all parameters which can be further improved by method optimisation and cell culture techniques.

1.9 Current pre-clinical animal models

Whilst common in practice, using animal models for pre-clinical testing has significant drawbacks including the lengthy, costly nature and ethical consideration due to perform such studies. Currently, *in vivo* NHP studies are regarded as the 'gold standard' for generating pre-clinical research data although a high percentage of late-stage trials suffer failure due to lack of efficacy or toxicity problems in humans (Luni et al., 2014). Furthermore, despite physiological similarities the use of animal models does not help to explain the reasons for off-target effects in human trials.

Animal testing is also constrained by biological differences that exist between species such as genetic complexity and gestation time. For retinal testing specifically, all rodent species lack the specialised central retinal areas including the fovea. Mice and rat, which are the most common mammals used in biomedical research in the UK, are nocturnal so lack the specialised "visual streak" region of densely packed cone PRs and bipolar cells that diurnal rodents such as gerbils possess (Great Britain et al., 2020; Huber et al., 2010). Additionally, in both mice and rats there exist different ratios of rods to cone PRs throughout the retina compared with humans, and rodents completely lack the L-opsin in cone PRs which registers red light (Applebury et al., 2000; Szél et al., 1996).

Using animal models which are phylogenetically and physiologically close to human, such as the macaque, is better for modelling and trialling candidate drugs and therapies aimed for restoration of sight loss in humans. As such, NHP models are inherently more suitable for drug development and safety assessment studies. Advancing the range and specificity of *in vitro* animal cell models to become closer to representing the biology of the retina is essential to validate and progress the use of cellular models. This includes optimising the methods for mammalian *in vitro* retinal differentiation to improve the cellular composition and functionality within the organoids, as well as generating models from species which are suitable for the drug development industry.

Validation of ROs can be performed through molecular analysis, functional characterisation and toxicological response evaluation, which can then support their use in pre-clinical studies and reduce the amount of live animals required. Additionally, validation of animal cellular models will be informative for the adoption of human ROs as a valid model system. Improvements to human *in vitro* cellular models will support advances in personalised genetic therapeutics which is limited in animal models (Luni et al., 2014).

<u>1.10 Project aims</u>

This project aims to develop and optimise published protocols to derive ROs from rat and macaque iPSCs for use as an *in vitro* model system for pre-clinical testing of therapeutics for retinal disease. Cell culture strategies including spatial, chemical and temporal manipulation as have been discussed here will be investigated.

Although mouse and human ROs have been developed and characterised in the past 8 years, the species selected herein have not been assessed for this purpose (Kuwahara et al., 2015; Ueda et al., 2018; Zhong et al., 2014b). These species are relevant organisms to study as they are currently widely used in pre-clinical trials and drug development studies (Great Britain et al., 2020; Sieving et al., 2006). Furthermore, the industrial sponsors of this project (Novartis, Merck and Roche) have indicated these species would be the most desirable for immediate use in pre-clinical trials and drug discovery. Data already derived from *in vivo* studies will facilitate the direct comparison with the *in vitro* RO model and this has the potential to reduce and eventually replace the use of animals for medical research. Additionally, the generation of robust organoids from model organisms will allow us to assess the developmental differences to humans and better inform the use of animal models in a wider clinical sense.

This would represent a huge step forward in the transition away from traditional *in vivo* testing towards a novel, scalable, easier to study and more clinically effective way to treat retinal disease. This is in line with the aims of NC3R. Therefore, the aims of the project are:

1. To develop methods for the robust generation of 3D retinal organoids from rat and macaque iPSCs in a multi-well plate format to enable systematic studies of drug testing and development.
2. To characterise the PSC-derived organoids for retinal morphology, protein and gene expression using molecular, immunological and microscopy techniques.

Chapter 2

Chapter 2 Materials and Methods

Unless otherwise stated all experimental procedures were carried out by the author.

2.1 Cell culture

2.1.1 Mouse embryonic fibroblast (MEF) cell culture

Culture vessels were coated with a 0.2% gelatin solution and incubated for 1 hour prior to use.

Live primary MEFs, strain CF1 (Merck-Millipore, PMEF-CFL) were thawed into 10 mL culture media (Table 2.1), centrifuged at 300g for 4 minutes, re-suspended in culture media, counted using a cell counting chamber and plated at a density of 1.15 x 106 cells per 25 cm2 flask. Cells were cultured and passaged when confluent (every 2 – 4 days) at a ratio of 1:3 until passage 5 using 0.05% Trypsin-EDTA (Life Technologies, 25300096). At this point cells were mitotically inactivated by irradiation using a Faxitron CP-160 radiation machine with an exposure of 120 kV, 4 mA for 7 minutes.

Irradiated MEFs (iMEFs) were placed back in the incubator for 1 hour minimum before storing frozen or they were detached enzymatically and re-seeded for immediate use. iMEFs were plated at the appropriate density of 5 x 105 cells per 9.6 cm2 for rat and mouse stem cells or 3 x 105 cells per 9.6 cm2 for macaque stem cells.

Table 2.1. Mouse embryonic fibroblast culture media

Component	Supplier/Cat. No.	Final Concentration
DMEM with Glutamax	Life Technologies/21885108	-
FBS	Gibco/10270106	10%
Non-Essential Amino Acids	Gibco/11140	1x
Penicillin/Streptomycin	Gibco/15140	1%

2.1.2 Rat stem cell culture

An induced pluripotent stem cell (iPSC) line was obtained from Dr C. Merkl (Technische Universität München, Freising, Germany), derived by viral transduction of pluripotency inducing genes (*OCT4*, *SOX2*, *CMYC* and *KLF4*) (Merkl et al., 2013). This cell line was initially cultured by Dr. V. Chichagova as per the published study and named "CM iPSC" (Table 2.2). Additional rat embryonic stem cell (ESC) and iPSC lines were obtained from Dr X. Aranguren (University of Navarra, Health Research Institute of Navarra, Pamplona, Spain); 2 iPSC cell lines which were re-programmed with lentiviral expression of *OCT4*, *SOX2*, *KLF4* and mCherry reporter, and named "XA iPSC (9.9)" and "XA iPSC (9.5)" (Coppiello et al., 2017a) and one GFP-tagged ESC line isolated from a Sprague Dawley animal and named "XA

ESC (7.8)" (Coppiello et al., 2017b). These lines were cultured according to the original publication (Table 2.3).

An additional rat ESC line (rESC Da.c8 #464) was obtained from the Rat Research and Resource Centre (Missouri, US) (P. Li et al., 2008) and cultured according to the datasheet (Table 2.4).

Table 2.2. Rat iPSC "N2B27-2i" culture media (from Merkl et al. 2013). *ROCK inhibitor only included in cell culture media immediately post-thawing

Component	Secondary component	Supplier/ Cat. No.	Secondary concentration	Final Concentration
N2 medium	DMEM/F12	Gibco/31330095	-	1x
	N2 supplement	Life Technologies/17502001	1x	
	BSA fraction V	Life Technologies/15260037	100 µg/mL	
B27 medium	Neurobasal medium	Life Technologies /21103049	-	1x
	B27 supplement w/o Vitamin A	Gibco/12587	1x	
	Glutamax	Gibco/35050061	2 mM	
2-mercaptoethanol	-	Gibco/11140	-	0.1 mM
Penicillin/Streptomycin	-	Gibco/15140	-	1%
Rat LIF	-	Biotechne/NBP2-35263	-	1 µM
CHIR99021	-	Sigma/SML1046	-	3 µM
PD0325901	-	Sigma/PZ0162	-	0.5 µM
*ROCKi (Y-27632)	-	Chemdea/CD0141	-	5 µM

Table 2.3. Rat iPSC culture media (from Coppiello et al. 2017a). 1Inclusion generates 2i media, 2Inclusion generates 3i media. *ROCK inhibitor only included in cell culture media immediately post-thawing.

Component	Secondary component	Supplier/ Cat. No.	Secondary concentration	Final Concentration
N2 medium	DMEM/F12	Gibco/31330095	-	1x

Component		Supplier/Cat. No.		Final Concentration
	N2 supplement	Life Technologies/17502001	1x	
B27 medium	Neurobasal medium	Life Technologies /21103049	-	1x
	B27 supplement w/o Vitamin A	Gibco/12587	1x	
2-mercaptoethanol	-	Gibco/11140	-	0.1 mM
Penicillin/Streptomycin	-	Gibco/15140	-	1%
Rat LIF	-	Biotechne/NBP2-35263	-	1 µM
[1,2]CHIR99021	-	Sigma/SML1046	-	1 µM
[1,2]PD0325901	-	Sigma/PZ0162	-	1 µM
[2]A83-01	-	Tocris/2939	-	1 µM
*ROCKi (Y-27632)	-	Chemdea/CD0141	-	5 µM

Table 2.4. rESC (RRRC #464) culture media. *To be added into media aliquots of 100mL and used within 1 week. ROCK inhibitor (10 uM) only included in cell culture media immediately post-thawing. 1 ROCK inhibitor only included in cell culture media immediately post-thawing

Component	Supplier/Cat. No.	Final Concentration
DMEM/F12	Gibco/31330095	-
N2 supplement	Life Technologies/17502001	0.5x
Neurobasal media	Life Technologies /21103049	-
B27 w/o Vit. A	Gibco/12587	1x
Glutamax	Gibco/35050061	0.5x
2-mercaptoethanol	Gibco/11140	0.1 mM
Pen/Strep	Gibco/15140	1x
*CHIR99021	Sigma/SML1046	3 uM
*PD035901	Sigma/PZ0162	0.5 uM
*Rat LIF	Biotechne/NBP2-35263	1 uM
[1]ROCKi (Y-27632)	Chemdea/CD0141	5 µM

Culture media for CM iPSC included 2 inhibitors; GSK3β inhibitor CHIR99021 and MEK1/2 inhibitor PD0325901, as described in Merkl et al. 2013 (Table 2.2). For XA cell culture it was recommended to

thaw cells using media with 3 inhibitors, additionally including ALK5 inhibitor A83-01, and following several passages to change to XA 2i media from Coppiello et al. 2017a (Table 2.3).

Rat ESC line #464 was cultured with the addition of rat leukamia inhibitory factor (LIF) (Table 2.4). Additionally, Rho kinase inhibitor (ROCKi), Y-27632, was included in all rat PSC culture media immediately post-thaw, to prevent single-cell induced apoptosis (Table 2.2, 2.3, 2.4).

Briefly, a vial of cells was thawed, transferred into a falcon tube and PSC culture media added up to 10 mL volume. Cells were centrifuged at 200g for 4 minutes, supernatant was discarded and cell pellet was re-suspended in 2 mL culture media supplemented with 5 µM ROCKi. Cell volume was plated onto prepared iMEFs in a final volume of 2 mL per well of a 6-well plate.

Cell passaging of iPSCs was performed every 2 - 4 days by washing briefly with DPBS, addition of ~1 mL Accutase (Stem Cell Technologies, 07920) per well of a 6 well plate to lift colonies which were held in a tube for 3 – 4 minutes before dilution at 1:3 with culture media. Cell suspension was centrifuged at 200g for 4 minutes and cell pellet re-suspended and plated at a splitting ratio of 1:4 – 1:6.

Rat ESCs were passaged similarly however due to their weak adherence, cells were first removed from adherent culture by gentle pipetting in fresh culture media, collected into a tube and centrifuged at 200g for 4 minutes. The cell pellet was re-suspended in Accutase (1ml/well) for 3 minutes before dilution with ESC culture media, centrifugation then plating at a splitting ratio of 1:4 – 1:6.

All rat stem cell lines were plated onto iMEFs prepared at a seeding density of 52,000 cells/cm^2.

Cells were frozen and stored by detaching and dissociating colonies as reported above for passaging, and the cell pellet was re-suspended in freezing media consisting of 90% FBS, 10% DMSO and 5 µM ROCKi. Cells were aliquotted into cryovials, placed into a Mr Frosty ® freezing container (Nalgene) and stored at -80°C before transfer to the vapour phase of liquid nitrogen for long term storage.

2.1.3   Mouse stem cell culture

Mouse ESC line E14 was obtained from K. Gassner (Llobet-Navas research group, IDIBELL Bellvitge Biomedical Research Institute, Spain) and cultured according to her protocol (Table 2.5). Seeding density was 4.5 x10^4 cells/cm2. Cells were cultured successfully both on MEF feeder cells and feeder-free on 0.2% gelatin-coated 6-well plates. Cells were passaged when confluent, approximately every 2-3 days and were detached using 0.05% Trypsin-EDTA (Life Technologies, 25300096) and split at a ratio of 1:5 onto freshly prepared iMEFs or gelatin-coated plates.

Table 2.5. Culture media for mESC. *LIF to be added on the day of use to aliquots of 100 mL.

Component	Supplier/Cat. No.	Final Concentration
DMEM/F12	Gibco/31330095	-
KSR	Life Technologies/A3181502	20%
Non-Essential Amino Acids	Gibco/11140	0.1 mM
Glutamax	Gibco/35050061	1x
2-mercaptoethanol	Gibco/11140	0.1 mM
*Mouse LIF	ESGRO/ESG1106	1000 L

2.1.4   Rodent retinal differentiation methods

Differentiation protocols were adapted from published protocols for mouse and human retinal organoid differentiation and are found in Table 2.9-2.11 and appendices A and B.

96-well U-bottom plates (TPP/ 92097) for organoid culture were coated with Lipidure solution (AMSbio, AMS.52000011GB1G)- (1 g/200 mL 100% Ethanol) by adding 50 µL/well and evaporating overnight. Plates were UV sterilised prior to use. Adherent plating differentiation methods used 6 well-plates coated with Matrigel. These plates were pre-coated at 1mg/well for 1 hour at 37°C. Organoids were seeded at a density of 32 organoids/well. Plating methods and consumables were kept consistent between all experiments.

Rat iPSC/ESCs were detached and dissociated to single cell suspension by incubation with Accutase for 5 minutes. Cell concentration was adjusted to 2-5 x 10^4 cells/mL with retinal differentiation media and 100 µL cell suspension was plated per well. Rho kinase inhibitor (ROCKi) Y-27632 at 5 µM was supplemented into media for initial cell plating to reduce single-cell induced apoptosis and improve initial cell aggregation.

Condition 1 (C1) method was based on the serum-free embryoid body with quick aggregation method (SFEBq) developed by Eiraku & Sasai (Eiraku & Sasai, 2012) and performed as follows: following cell plating in differentiation media (Table 2.6), diluted growth factor-reduced Matrigel (Corning, 354230) was added at 20 µL/well to a final concentration of 2% v/v on day 1 of differentiation (24 hours after plating). Half media changes were carried out every 2 days from day 1 – 12 and media was changed to retinal maturation media 1 and 2 (Table 2.7, 2.8) on days 7 and 10 respectively. RA/T were supplemented on the day from day 10-14. Media was half-changed every 3 days from day 14 onwards.

Table 2.6. Rat retinal differentiation media (Eiraku & Sasai 2012). C2 media includes AGN193109 addition. Media used from day 0-7/9.

Component	Supplier/Cat. No.	Final Concentration
GMEM	Gibco/11710035	-
Non-Essential Amino Acids	Gibco/11140	0.1 mM
Sodium pyruvate	Life Technologies/11360	1 mM
2-mercaptoethanol	Gibco/31350	0.1 mM
Knockout Serum Replacement	Life Technologies/A3181502	1.5 %
Penicillin/Streptomycin	Gibco/15140	1%
ROCKi (Y-27632)	*Chemdea/CD0141*	*5 µm*
(AGN193109)	*R & D systems,5758*	*0.1 µm*

Table 2.7. Rat retinal maturation media 1 (Eiraku & Sasai 2012). Media used from day 7-10

Component	Supplier/Cat. No.	Final Concentration
DMEM/F12, Glutamax	Gibco/31330093	-
N2 supplement	Life Technologies/17502001	1%
Penicillin/Streptomycin	Gibco/15140	1%

Table 2.8: Rat C1 retinal maturation media 2 (components L-Taurine and RA were added to media fresh before addition) (Eiraku & Sasai 2012). Media used from day 10 onwards with RA/T included only from day 10-14.

Component	Supplier/Cat. No.	Final Concentration
DMEM/F12, Glutamax	Gibco/31330093	-
N2 supplement	Life Technologies/17502001	1%
FBS	Gibco/10270106	10%
Penicillin/Streptomycin	Gibco/15140	1%
L-Taurine (T)	*Sigma/T8691*	*1 mM*
Retinoic acid (RA)	*Sigma/R2625*	*0.5 µm*

Variants of this methodology were tested on rat stem cells and termed C1-C5 (Eiraku & Sasai, 2012; Kruczek et al., 2017; Kuwahara et al., 2015; Ueda et al., 2018) (Table 2.9, Appendix A). Media components were kept consistent in terms of catalogue number and supplier throughout.

All novel methods tested on the XA ESC line in chapter 3 used an initial seeding density of 3500 cells/well are summarised in Table 2.10

For methods with excision of tissue, surgical scalpel and micro-scissors were used to manually cut the phase-bright neuroepithelium or budding optic vesicle structures from edges of 3D organoids at either day 7 or 10 of differentiation, in sterile conditions. These cut portions were pooled in 24- well low-attachment tissue culture plates at a density of 21 sections per well.

Table 2.9. Summary table of experimental conditions tested for retinal differentiation on rat PSC lines based on published protocols. D = day of differentiation experiment. OV = optic vesicle, OC = optic cup, NE = neuroepithelium, RA = retinoic acid, wp = well plate, (m/h) ESC = (mouse/human) embryonic stem cell.

Reference/ Model	Cell line	Condition	Cell/well	Culture media summary	Plating strategy
Eiraku & Sasai, 2012 / mESC	CM iPSC	C1	2000/3500/5000	D0-7: GMEM/1.5% KSR	96 wp
	XA iPSC 9.5	C1	2000/3500	D1: 2% Matrigel	96 wp
				D7-10: DMEM/N2	
	XA ESC	C1	2000/3500	D10-14: DMEM/N2/10% FBS/RA/Taurine	96 wp
				D14+: DMEM/N2/10% FBS	
	XA ESC	C1	3500	Media change to maturation media at D5	Excision of OV at D7/10 then pooled
	XA ESC	C1	3500	Media change to maturation media at D7	Excision of OV at D7/10 then pooled
	XA iPSC 9.5 and 9.9	C1	3500	D0-7: GMEM/1.5% KSR	96 wp
				D1: 2% Matrigel	
				D7-10: DMEM/N2	
Ueda et al., 2018 / mESC	CM iPSC	C2	2000/3500/5000	D0-9:GMEM/KSR/AGN193109	96 wp
	XA iPSC 9.5	C2	2000/3500	D1: 2% Matrigel	96 wp
	XA ESC	C2	2000/3500	D9-14: DMEM/N2/1% FBS	96 wp
				D14-23: DMEM/N2/1% FBS/ RA/Taurine	
	CM iPSC	C3	2000/3500/5000 cells/well	As C2 but with 9-cis RA instead of RA (D14-23)	96 wp

Kuwahara et al., 2015 / hESC	CM iPSC	C4	2000/3500/5000	No Matrigel, D2: BMP4, FBS 10%, RA/Taurine (D10-14)	96 wp
Kruczek et al., 2017 / mESC	CM iPSC	C5	2000/3500/5000	D0-D9: GMEM/1.5% KSR D1: 2% Matrigel D9-14: DMEM/N2 D14+: DMEM/N2/RA/Taurine	96 wp
DiStefano et al. 2018 / mESC	XA iPSC 9.5 and 9.9	Expt 8	3500	D0-7: GMEM/1.5% KSR D1: 2% Matrigel D7-10: DMEM/N2/2-mercap. D10-18:DMEM/N2/Taurine/9cis-RA/IGF-1 D18+: DMEM/N2/Taurine/9cis-RA/IGF-1/B27-VitA/2% FBS	96 wp

Table 2.10. Retinal differentiation methods tested on rat XA ESC line using novel methods.

NB: Plating cell density for every condition in table was 3500 cells/well. DMEM-F12/Glutamax abbreviated to DMEM. Abbreviations: D = day, C = condition, wp = well plate, BF = bright-field, RA = retinoic acid, IHC = Immunohistochemistry analysis.

Cell line	Condition	Media addition	Culture summary	Plating strategy
XA ESC	Expt 6/C1	D0-10: GMEM/1.5% KSR D1: 2% Matrigel	Extending the minimal plating media stage from day 7 to day 10.	96 wp
XA ESC	Expt 6/C2	D0-10: DMEM/1.5% KSR D1: 2% Matrigel	Testing alternate richer plating media until D10.	96 wp
XA ESC	Expt 6/C3	D0-7: GMEM/1.5% KSR D7-10: DMEM/N2/10% FBS/Taurine/RA D1: 2% Matrigel	Acceleration of maturation media addition from D14 to D7.	96 wp
XA ESC	Expt 6/C4	D0-7: DMEM/1.5% KSR D7-10: DMEM/N2/10% FBS/Taurine/RA D1: 2% Matrigel	Acceleration of maturation media addition from D14 to D7 and use of DMEM base.	96 wp
XA ESC	Expt 7/C1	D0-7: GMEM/1.5% KSR D7-25+: DMEM/N2/10% FBS/Taurine/RA D1: 2% Matrigel	Removal of D7-10 media – addition at D7 with retinal stimulants.	96 wp until end/ 96 wp then pooled at D7
XA ESC	Expt 7/C2.1	D0-5: GMEM/1.5% KSR D5-10: DMEM/N2/2% FBS/Taurine/RA D10-25+: DMEM/N2/10% FBS/Taurine/RA D1: 2% Matrigel	Earlier change (D5) to retinal maturation media.	96 wp then pooled at D7

XA ESC	Expt 7/C2.2	D0-5: GMEM/1.5% KSR D5-25+: DMEM/N2/2% FBS/Taurine/RA D1: 2% Matrigel	Earlier change (D5) to retinal maturation media. Lower serum concentration.	96 wp then pooled at D7
XA ESC	Expt 7/C2.3	D0-5: GMEM/1.5% KSR D5-10: DMEM/N2/2% FBS/Taurine/RA D10-25+: DMEM/N2/10% FBS/IGF-1/Taurine/RA D1: 2% Matrigel	Earlier change (D5) to retinal maturation media. Addition of IGF-1 (100ng/mL) from D10 onwards.	96 wp then pooled at D7
XA ESC	Expt 7/C2.4	D0-5: GMEM/1.5% KSR D5-10: DMEM/N2/2% FBS/Taurine/RA D10-25+: DMEM/N2/10% FBS/T3/Taurine/RA D1: 2% Matrigel	Earlier change (D5) to retinal maturation media. Addition of T3 (0.5nM) from D10 onwards.	96 wp then pooled at D7
XA ESC	Expt 7/C3	D0-7: GMEM/1.5% KSR D7-14: DMEM/N2/2% FBS/B27-VitA/Taurine/RA D14-25+: DMEM/N2/2% FBS/2x B27-VitA/Taurine/RA D1: 2% Matrigel	Addition of B27-Vit A (1x) supplement from D7 and low serum.	96 wp then pooled at D7
XA ESC	Expt 7/C4.1	D0-7: GMEM/1.5% KSR D7-25+: DMEM/N2/DAPT/10% FBS/Taurine/RA D1: 2% Matrigel	Addition of DAPT (10 µM) from D7 onwards	96 wp then pooled at D7
XA ESC	Expt 7/C4.2	D0-7: GMEM/1.5% KSR D7-10: DMEM/N2/10% FBS/Taurine/RA D10-25+: DMEM/N2/DAPT/10% FBS/Taurine/RA D1: 2% Matrigel	Addition of DAPT from D10 onwards	96 p then pooled at D7

82

2.1.5 Mouse and Rat ESC retinal differentiation

Mouse ESC were cultured and detached for plating as described. The differentiation protocols are taken from published literature (DiStefano et al., 2017; Eiraku and Sasai, 2012) summarised in Table 2.9 and Appendix C. To separate the feeder cell layer, mESCs were plated in 0.2% gelatin coated plates for 30 minutes prior to seeding according to Eiraku and Sasai (Eiraku and Sasai, 2012). Cells were plated at a seeding density of 3000 cells per well in Lipidure-coated low attachment 96-well plates. Following plating, diluted growth factor-reduced Matrigel (Corning, 354230) was added at 20 µL/well to a final concentration of 2% vol/vol on day 1 of differentiation (defined as 24 hours after plating).

Retinal differentiation methods which were used on rESC (RRRC) and mESC are summarised in Table 2.11.

Table 2.11. Summary of differentiation methods and cell culture conditions tested on RRRC rESC cell line (rESC DA-EC8 #464) and mESC in chapter 4. Methods were taken from published research differentiating mESC or rESC into neural or retinal progenitor cells (NPCs/RPCs) with various modifications. BF = bright-field, wp = well-plate, D = day, C = condition.

Reference/Cell type/Condition	Cell line	Plating density	Media addition	Culture summary	Plating strategy
Eiraku & Sasai, 2012 (mESCs)	mESC	3000 cells/well	D0-7: GMEM/1.5% KSR D1: 2% Matrigel D7-10: DMEM-F12/N2 D10-14: DMEM-F12/N2/10% FBS/RA/Taurine D14+: DMEM-F12/N2/10% FBS	SFEBq from Sasai protocol with no further modifications.	96 wp
DiStefano et al. 2018 (mESCs)	mESC and rESC DA-EC8	3000 cells/well	D0-7: GMEM/1.5% KSR D7-10: DMEM-F12/N2/2-mercap. D10-18: DMEM-F12/N2/Taurine/9cis-RA/IGF-1 D18-26+: DMEM-F12/N2/Taurine/9cis-RA/IGF-1/B27-VitA/2% FBS D1: 2% Matrigel	Supplement-rich.	96 wp
Qu et al. 2015 (rat-RPCs)	rESC DA-EC8	3500/5000 cells/well	D0-9: GMEM/20% KSR/IWR1-e D9-14: GMEM/10% KSR/ 10% FBS D14-26+: DMEM-F12/N2/10% FBS/Taurine/RA D1 and D6: 1% or 2% Matrigel	Higher KSR and IWR1-e. Lower matrigel (from Nakano et al. 2012).	96 wp then pooled at D6

Wang et al. 2012 (rat-NPCs)/ Qu et al. 2015 (rat-RPCs)	rESC DA-EC8	3500/5000 cells/well	D-2-0: N2B27 2i (rESC media) D0-9: GMEM/20% KSR/IWR1-e D9-14: GMEM/10% KSR/ 10% FBS D14-26+: DMEM-F12/N2/10% FBS/Taurine/RA D0/1 and D6: 1% Matrigel	2 day induction period as 'EBs'. Matrigel addition at either D0 or D1.	96 wp then pooled at D6
Wang et al. 2012 (rat-NPCs)/ Qu et al. 2015 (rat-RPCs)	rESC DA-EC8	3500 cells/well	D-2-0: N2B27 2i (rESC media) D0-9: GMEM/20% KSR/IWR1-e D0 and D6: 1% Matrigel	2 day induction period as 'EBs'. Matrigel addition at D0.	96 wp then pooled at D6
Wang et al. 2012 (rat-NPCs) (3D)	rESC DA-EC8	3000 cells/well or drop	D0-2: N2B27 2i:MEF-CM + Y-27632 D2-4: N2B27 2i:MEF-CM D4-5: N2B27:MEF-CM D5-11: N2B27	Generate EBs then plate in 2D to induce NPCs and expose to retinal stimulants	96 wp (30uL or 100uL)
Wang et al. 2012 (rat-NPCs) (3D)	rESC DA-EC8	Floating colonies (various size)	D0-2: N2B27 2i:MEF-CM + Y-27632 D2-4: N2B27 2i:MEF-CM D4-5: N2B27:MEF-CM D5-11: N2B27	Generate EBs then plate in 2D to induce NPCs and expose to retinal stimulants	Pooled in low attachment 6 wp
Qu et al. 2015 (rat-RPCs) + novel modifications. (C1)	rESC DA-EC8	3000 cells/well	D0-9: GMEM/20%KSR/IWR1-e/Y-27632 D9-14: GMEM/10%KSR/10%FBS D14+: DMEM-F12/N2/10% FBS/Taurine/RA D1 and D6: 1% Matrigel (variant) D9-14: +/- SAG	Generate organoids in 96wp using chemical stimulants, pool at D6 and expose to retinal stimulants.	96 wp then some pooled in low attachment 6 wp at D6.

85

			(variant) D9+: DMEM-F12/N2/10% FBS/Taurine/RA (variant) D11-20: +/- DAPT		
Qu et al. 2015 (rat-RPCs) + novel modifications.(C2)	rESC DA-EC8	3000 cells/well	D0-4: GMEM/20%KSR/IWR1-e/SB-431542/Y-27632	Similar to C1 with inclusion of SB-431542 to improve EB generation.	96 wp
Wang et al. 2012 (rat-NPCs) (3D) + novel modifications.(C3)	rESC DA-EC8	3000 cells/well or drop	D0-2: N2B27 2i:MEF-CM + Y-27632 D2-4: N2B27 2i:MEF-CM D4-5: N2B27:MEF-CM D5-14: N2B27 D14+: DMEM-F12/N2/10% FBS/Taurine/RA (variant) D9-14: +/- SAG (variant) D9-14: +/- SAG, bFGF (variant) D17+: +/- IGF-1	Generate neural EBs in droplets then plate in 2D to induce NPCs, re-plate in 3D and expose to retinal stimulants.	30uL drops in 96 wp, some plated in 2D at D5 and re-plated in 3D at D11 or D14.

2.1.6 Macaque stem cell culture

Macaque (*Macaca fascicularis*) iPSC lines were obtained commercially from JCRB cell bank (Japan). The 3 iPSC lines were originally derived by introduction of reprogramming transgenes Oct 3/4, Sox2, Klf4 and c-Myc from liver cells (cyfH1 and cyfH5) and skin cells (cynS1).

The iPSC culture method was taken from a published study deriving cynomolgus iPSCs (Shimozawa, 2016). Briefly, cells were thawed into 10 mL iPSC culture media (Table 5.1), centrifuged at 200g for 4 mins, re-suspended in 1 mL of iPSC media supplemented with 10 μM Rho kinase inhibitor (ROCKi) Y-27632. Cells were plated onto iMEFs prepared as described in Methods 2.1.

Cells were passaged every 3 – 8 days when large colonies had formed either by using Accutase (Stem cell technologies, 07920) or collagenase IV (200 U/mL) to lift and partially dissociate whole colonies into smaller clumps and split at a ratio of 1:4 - 6. Alternatively, cells were passaged by manually dissociating large confluent colonies without enzymatic treatment and split at an approximately similar ratio. Macaque iPSCs were maintained on a feeder layer of irradiated MEF cells (iMEF), which were plated at a density of 3×10^5 cells in 9.6 cm^2 as described in 2.1.1.

Macaque iPSCs were also maintained as a feeder-free monolayer as per Wunderlich et al. on Matrigel-coated tissue culture plates (Wunderlich et al., 2012). Briefly, culture dishes were coated with growth factor reduced Matrigel (SLS, 354230), diluted at 1 mg/12 mL in DMEM/F12 media (Gibco/31330095) and 1 mL plated per 9 cm^2 then incubated for 1 hour. iPSCs were dissociated into single cells by incubation with Accutase for ~5 mins and filtered through 40 μm cell strainer. Cells were suspended in MEF-CM supplemented with 20 μM ROCKi and bFGF (100 ng/mL) and plated at a density of 1000 – 2000 cells/cm^2. Cells were passaged as single cells when confluent (~4 - 6 days).

Table 2.12. Primate stem cell culture media (from Shimozawa, 2016) ROCKi only included in cell culture media immediately post-thawing.

Component	Supplier/Cat. No.	Final Concentration
DMEM/F12	Gibco/31330095	-
Knockout Serum Replacement	Life Technologies/A3181502	20%
Glutamax	Gibco/35050061	1x
Non-Essential Amino Acids	Gibco/11140	1x
Penicillin/Streptomycin	Gibco/15140	1%
2-mercaptoethanol	Gibco/31350	0.1 mM
Human recombinant LIF	Biolegend/ 716404	10 ng/mL

| Human recombinant basic FGF | Peprotech/100-18B | 4 ng/mL |
| ROCKi (Y-27632) | Chemdea/CD0141 | 20 µM |

2.1.7 Macaque retinal differentiation methods

The methods used for macaque retinal differentiation were taken from published literature and documented in Table 2.13 and Appendix B. These were tested and adjusted to the shorter gestation of a macaque (165 days) to that of a human (270 days) using a factor of 0.61.

Macaque iPSCs were detached as for passaging and replated at the desired plating density in 200 µL/well volume in Lipidure coated U-bottomed 96-wp (TPP/ 92097). The cells aggregated and were further matured in a series of culture media with various retinal growth stimulants and small molecules detailed in Table 2.13.

Organoids were matured within 96-wp which were stored in an incubator set to maintain 37®C with 5% CO_2 and 20% O_2. Throughout differentiation they were imaged by a bright-phase microscope and collected for molecular analysis.

In some samples exposed to the IGF1 method/C3 the effect of pooling the individual organoids was tested. These organoids were removed at day 16 from 96-wp using a plastic Pasteur pipette and transferred into ultra-low attachment (Corning, 3471) or Lipidure-coated 6-wp at a density or 16 organoids/well for maturation in pooled suspension culture.

Table 2.13. Summary of macaque differentiation methods tested on iPSC lines (H1, H5 and S1) and data output. Methods were taken from published research differentiating human stem cells into retinal organoids with various modifications. CHIR99021/SU5402 added for induction-reversal (IR) methods only. BF = bright-field, wp = well-plate, D = day, SFEBq = serum-free embryoid body formation with quick aggregation, RA = retinoic acid.

Reference/ Method	Cell line	Plating density	Media addition	Summary of culture method
Kuwahara et al. 2015 with human timing /C2.1	S1 and H5	6000 and 9000 cells/well	D0-18: IMDM/F12, KSR (10%), Lipids (1%), 1-thioglycerol (450uM), Glutamax (1x), Pen/Strep (1x)+ Y-27632 (20uM) D6: BMP4 (1.5nM) D18-24: DMEM/F12, Glutamax (1x) N2 (1%), FBS (10%), Pen/Strep (1x) **(CHIR99021 (3uM), SU5402 (5uM))** D24+: DMEM/F12, Glutamax (1x) N2 (1%), FBS (10%), Pen/Strep (1x), Taurine (0.1mM), RA (0.5uM)	SFEBq aggregation and EB formation, maturation in 96wp with addition of IR molecules for RPE stimulation from D18-24.
Kuwahara et al. 2015 with modified timing/C2.3	S1, H5 and H1	9000 cells/well	D0-11: IMDM/F12, KSR (10%), Lipids (1%), 1-thioglycerol (450uM), Glutamax (1x), Pen/Strep (1x)+ Y-27632 (20uM) D4: BMP4 (1.5nM) D11-15: DMEM/F12, Glutamax (1x) N2 (1%), FBS (10%), Pen/Strep (1x) **(CHIR99021 (3uM), SU5402 (5uM))** D15+: DMEM/F12, Glutamax (1x) N2 (1%), FBS (10%), Pen/Strep (1x), Taurine (0.1mM), RA (0.5uM)	Same as above but timing adjusted to macaque gestation length. Addition of IR molecules for RPE stimulation from D11-15.
Kuwahara et al. 2015 with modified	S1, H5 and H1	9000 cells/well	D0-11: IMDM/F12, KSR (10%), Lipids (1%), 1-thioglycerol (450uM), Glutamax (1x), Pen/Strep (1x)+ Y-27632 (20uM) D4: BMP4 (1.5nM)	Same as C2.1 but timing adjusted to macaque gestation length. Addition of IR molecules for RPE stimulation

timing and RPE-CM/C2.4			D11-15: DMEM/F12, N2 (1%), FBS (10%), Pen/Strep (1x), Taurine (0.1mM), RA (0.5uM)s, **CHIR99021 (3uM), SU5402 (5uM))** D15+: (DMEM/F12, Glutamax (1x) N2 (1%), FBS (10%), Pen/Strep (1x), Taurine (0.1mM), RA (0.5uM)):RPE-CM	from D11-15. Media from D15 includes 1/3 macaque RPE-CM to improve photoreceptor maturation.
Dorgau et al. 2019 with modified timing /C3 (IGF1)	S1, H5 and H1	9000 cells/well	D0-11: DMEM/F12, B27 (2%), KSR (20%), NEAA (1%), Glutamax (1%), Pen/Strep (1x), IGF-1 (5 ng/mL) D11-18: DMEM/F12, B27 (2%), FBS (10%), NEAA (1%), Glutamax (1%), Pen/Strep (1x), IGF-1 (5 ng/mL), Taurine (0.1mM), RA (0.5uM) D18+: DMEM/F12, B27 (2%), N2 (1%), FBS (10%), NEAA (1%), Glutamax (1%), Lipids (1x), Pen/Strep (1x), IGF-1 (10 ng/mL), Taurine (0.1mM), RA (0.5uM), T3 (40ng/mL)	IGF-1 induced protocol with macaque adjusted timing. Organoids were pooled in 6wp at D16 or matured in 96wp throughout.

2.1.8   Dissection and isolation of control primary tissue

Control retinal tissue was obtained from a male Sprague Dawley rat aged 58 days old. Rat eyes were dissected to isolate optic cup structures consisting of sclera, RPE and retina by Drs. L. Armstrong and D. Zerti. One optic cup was fixed in 4% PFA (Santa Cruz, 30525-894) for 1 hour, dehydrated in 30% sucrose and embedded in optimal cutting temperature solution (OCT: CellPath, KMA-0100-00A) and stored at -20°C by Dr V. Chichagova for protein expression analysis. Retina was dissected from another optic cup, washed with PBS and stored in ~1 mL of RNAlater (Sigma, R0901) at -80°C for gene expression analysis.

Retinal tissue was obtained from an adult female rhesus macaque (*Macaca mulatta*) aged approximately 4 years. The tissue was surplus to an ongoing study directed by Prof. Stuart Baker (Institute of Neuroscience, Newcastle University), which was approved by the relevant Ethics Review Board of Newcastle University. One eyecup was dissected and fixed by placing in 2% PFA (Santa Cruz, 30525-89-4) overnight at room temperature. On the following day the eye was washed with PBS twice and outer musculature, lens and cornea removed by dissection and all components were placed in 30% sucrose in a fridge overnight. Once dehydrated the eye cup was embedded using OCT and stored at -20°C. Macaque retina was dissected from another optic cup, washed with PBS and stored in ~1 mL of RNAlater at -80°C for gene expression analysis.

2.1.9   Macaque RPE explant culture

Retinal tissue was obtained from an adult female rhesus macaque (Macaca mulatta) aged approximately 4 years. The tissue was surplus to an ongoing study directed by Prof. Stuart Baker (Institute of Neuroscience, Newcastle University), which was approved by the relevant Ethics Review Board of Newcastle University. The anterior part of the eye was removed together with the vitreous and the RPE was manually lifted from the choroidal membrane using fine forceps. Pieces of RPE tissue were washed in culture media (Table 2.14) and plated in Matrigel-coated cell culture plates. After reaching confluency cells were passaged using Tryple Select (Gibco, 12563), re-plated and fed with culture media 3 times weekly.

Table 2.14. RPE culture media

Component	Supplier/Cat. No.	Final Concentration
Advanced RPMI 1640	Gibco/R7388	-
Knockout Serum Replacement	Life Technologies/A318150	10%
B27 supplement	Gibco/17504	2%
Glutamax	Gibco/35050061	1%
Penicillin/Streptomycin	Gibco/15140	1x

2.2 Pluripotency assessment

To assess the pluripotency of the primate iPSCs, a commercially available live cell staining reagent was obtained (BioTracker 529 Green Dye (Merck, SCT029)) and prepared according to the manufacturer's instructions. Briefly, 1 vial of dye (10 µg) was dissolved in 4.8 µL DMSO to give a 5 mM stock solution. This was further diluted in 12 mL of iPSC media (Table 5.1) to give a cell stain solution at 2 µM. This stain solution was added to a total of 6 culture wells (2 mL/well) and incubated for 3 hours. The cell stain was removed and 1 mL DPBS added to enable clearer imaging. The cell staining was visualised using an Axiovert fluorescent microscope.

2.3 Immunofluorescence analysis

Organoid samples from all species were treated similarly. Samples were washed briefly with DPBS and fixed by adding 4% PFA for 40 minutes at room temperature. Samples were washed with DPBS thrice for at least 5-15 minutes to remove PFA. Samples were covered with 30% sucrose solution and stored overnight (12-20 hours) at 4°C. After the samples had dehydrated, they were transferred to moulds (CellPath, GAD-1000-10A) and sucrose was removed. Samples were embedded using OCT, frozen and stored at-20°C. Sample blocks were sectioned using a cryostat (Leica, CM1860) at a thickness of 10 µm and preserved on glass slides (SuperFrost, Menzel). Primary retinal samples were sectioned at a thickness of 20 µm.

Slides were air-dried and sections separated using ImmEdge pen (VectorLabs, H-4000), washed thrice with PBS to remove OCT from tissue and blocked with 5% goat or donkey serum, 0.3% Triton-X in PBS at room temperature for 1 hour. Primary non-conjugated antibodies were diluted in 1% BSA (Sigma, A9418), 0.3% Triton-X in PBS and applied to sections after removal of blocking buffer. A range of concentrations were tested and the most suitable are reported in Table 2.15 and 2.17. Samples were incubated with antibodies overnight at 4°C.

Primary antibody solution was removed by washing thrice with PBS for 10-15 minutes. Secondary antibody conjugated to fluorophores Alexa488, Alexa647, Alexa546 (Thermofisher) or Cy3 (Jackson Immuno-Research Laboratories) (Table 2.18) were diluted in 1% BSA, 0.3% Triton-X in PBS and applied to sections at room temperature for 1 hour. Secondary antibody solution was removed by washing thrice with PBS for 10-15 minutes. Nuclear counterstain Hoechst (Sigma, B2261) was diluted in Vectashield at 1:2000 (VectorLabs, H-1000), applied to sections and slides were sealed with a glass coverslip (Menzel, 15747592).

2.3.1   Rat control tissue: Antibody validation

To identify cells within rat ROs, IHC conditions and antibody specificity were first validated using rat retinal tissue (Table 2.15). Primary antibodies were applied to retinal sections at a range of concentrations and with fluorophore-conjugated secondary antibodies. Immunofluorescence (IF) was evaluated in comparison to a negative control consisting of organoid sections with only secondary antibody applied (Fig. 2.1). Each antibody showed herein displayed immunoreactivity above background levels and retinal localisation consistent with expectations from the published literature denoting retinal cell identity (Fig. 2.1; Table 2.16).

Table 2.15. List of primary antibodies used for IHC on primary and organoid rat tissue.

Antibody	Cat. No.	Host species	Source	Dilution
Pax6	PRB-278P	Rabbit	Biolegend	1 in 200
Rax	ARP31926-P050	Rabbit	Aviva	1 in 200
Vsx2	HPA003436	Rabbit	Sigma	1 in 50
Chx10/Vsx2	SC-21692	Goat	Santa Cruz	1 in 100
OPSN-SW	AB5407	Rabbit	Abcam	1 in 200
OPSN-MW	AB5405	Rabbit	Abcam	1 in 200
Calbindin D28K	AB1778	Rabbit	Abcam	1 in 200
Recoverin	AB5855	Rabbit	Abcam	1 in 1000
Prox1	AB5474	Rabbit	Abcam	1 in 1000
Hu C/D	A21271	Mouse	Thermofisher	1 in 200
Rhodopsin	MAB5356	Mouse	Merck-Millipore	1 in 200
Rhodopsin (Ret-P1)	O4886	Mouse	Sigma	1 in 200
SNCG	H00006623-M01A	Mouse	Abnova	1 in 500
CRALBP	AB15051	Mouse	Abcam	1 in 200
ChAT	AB144P	Goat	Merck-Millipore	1 in 500
RPE65	AB13826	Mouse	Abcam	1 in 200
Best1	AB2182	Mouse	Abcam	1 in 500
ZO-1	61-73000	Rabbit	Invitrogen	1 in 200

Troponin I	AB19615-500	Mouse	Abcam	1 in 200
Neun	MAB377	Mouse	Merck-Millipore	1 in 100
Nestin	611658	Mouse	BD Biosciences	1 in 500
Ki67	AB15580	Rabbit	Abcam	1 in 200
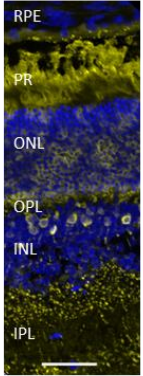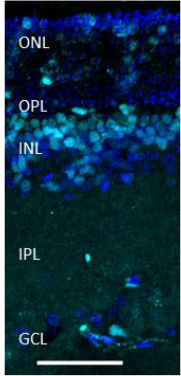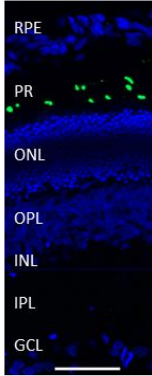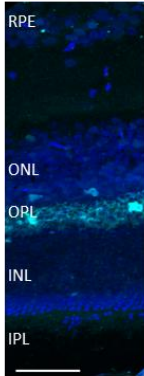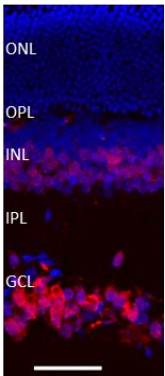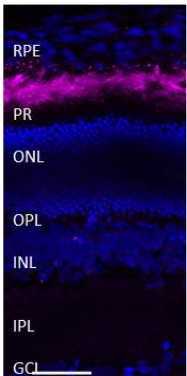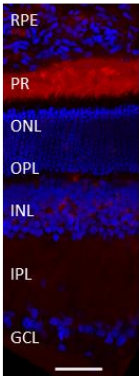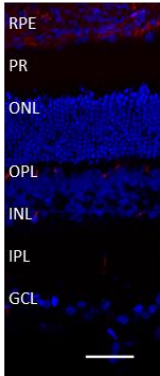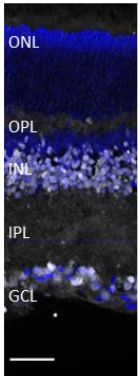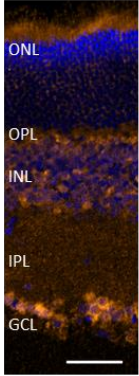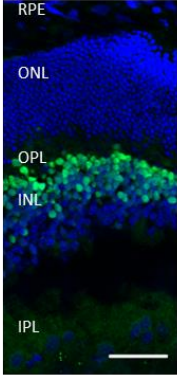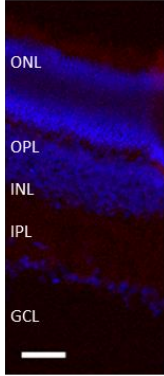
Recoverin (PR and bipolar)	Prox1 (Horizontal and amacrine)	OPSN-SW (blue cone PR OS)	Calbindin-D28K (Horizontal)
Hu C/D (RGCs and amacrine)	Rhodopsin (Rod PR)	Ret-P1 (Rod PR)	Secondary only
Pax6 (Horizontal and amacrine)	Rax (RGCs, bipolar and Müller glia)	Vsx2 (Bipolar)	Secondary only

Figure 2.1. Validation of retinal primary antibodies in adult rat retina showing target cell types. Secondary only = negative control. Scale = 50µm. RPE=retinal pigmented epithelium, PR=photoreceptors, ONL=outer nuclear layer, OPL=outer plexiform layer, INL=inner nuclear layer, IPL=inner plexiform layer, GCL=ganglion cell layer, OS = outer segment, ((r) = red, (y)= yellow, (g) = green.

Fig. 2.1 (continued)

SNCG (RGC)	CRALBP (Müller glia)	Best-1 (RPE)	RPE65 (RPE)	Secondary only
PKC-α (Bipolar)	Recoverin (y) + SNCG (r) (PRs/bipolar and RGC)	OPN-MW (g) + RetP1 (r) (red cone PR OS and rod PR OS)	Chx10 (Bipolar)	Secondary only
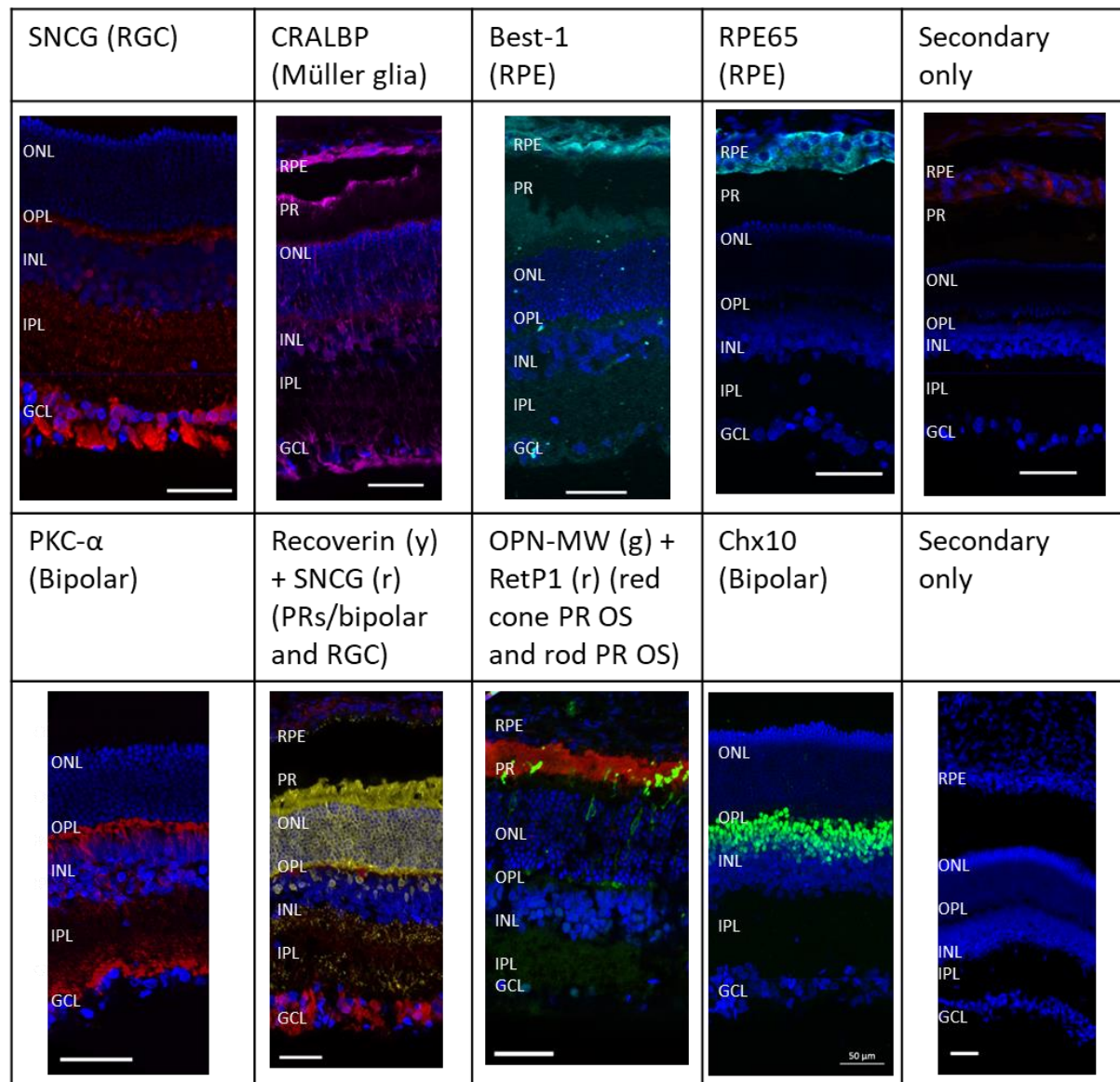
Pax6 is an important regulator of neural-retinal (NR) development and is expressed in various cell types during embryogenesis and retinal maturation, in these results Pax6 was detected in the INL and GCL which likely correspond to horizontal, amacrine and RGCs (Fig. 2.1). This localisation is in accord with published sources for mature rat retina expression (Table 2.16; Volkner et al., 2018). The rod bipolar cell marker PKC-α was detected in the OPL, throughout the INL and in the upper boundary of the GCL (Fig. 2.1). This is in accordance with its localisation in the native mouse retina, where it is found throughout the axon terminals of the cells (Haverkamp et al., 2003). All other antibodies displayed in Figure 2.1 are correctly localised to their predicted cell type (Table 2.16)

96

As these antibodies will be used to analyse samples from developing organoids in the day 5-25 stages the most appropriate experiment control for antibody validation would be embryonic rat retina. However, it was not possible to obtain these tissue samples. On occasions where the protein localisation varies between embryonic and post-natal stages of development, such as Pax6 and Rax, these differences are highlighted in Table 2.16, however a positive staining in adult retina and lack of signal in the secondary antibody only control was considered to validate the use of the antibody for rat tissue at all stages of development. The appropriate antibody concentrations were determined by these experiments and the same conditions and imaging techniques were used for subsequent analyses.

Table 2.16. Primary antibodies validated for use in adult rat retina. Predicted cell type informed by published research. Rat retinal location and dilution factor determined by the experiments described in this report. RGC = retinal ganglion cell, RPC = retinal progenitor cell, NR = neural retina, PR = photoreceptor, GCL = ganglion cell layer, INL = inner nuclear layer, OPL = outer plexiform layer, RPE = retinal pigmented epithelium.

Antibody	Predicted target cell type	Rat retinal location reported herein	Primary reference	Dilution
Pax6	Mature: RGC, horizontal & amacrine	Mature retina; GCL & INL	Volkner et al.2018	1 in 200
	Embryonic: RPCs in NR, eye field	-		
Rax	Mature: RGC, bipolar cells and Muller glia	Mature retina; GCL, INL, PR	Meyer et al. 2009	1 in 200
	Embryonic: RPCs in NR, eyefield	-		
Vsx2	Mature: Bipolar cells	Mature retina; INL	Livne-bar et al. 2006	1 in 50
	Embryonic: RPCs in NR, eyefield	-		
Chx10 (Vsx2 homologue)	(as Vsx2)	Mature retina: INL		1 in 100
OPN-SW	Cone PRs (short (blue) wavelength subtype)	PRs	Insinna et al. 2012	1 in 200
OPN-MW	Cone PRs (medium/long (green/red) wavelength subtype)	PRs	Insinna et al. 2012	1 in 200

Calbindin D28K	Horizontal cells including synapses	OPL	Bytyqi et al. 2007	1 in 200
Recoverin	PRs and bipolar cells	PRs and INL, plexiform layers	McGinnis et al. 1999	1 in 1000
Prox1	Horizontal & amacrine	Mature retina; INL and GCL	Dyer et al. 2003	1 in 1000
	Embyonic: RPCs	-		
Hu C/D	RGC and amacrine	GCL/INL	Ekstrom & Johansson 2003	1 in 200
Rhodopsin	Rod PRs	PR	McKay et al. 2009	1 in 200
Rhodopsin (Ret-P1)	Rod PRs	PR	Chidlow et al. 2011	1 in 200
SNCG	RGC	GCL, plexiform layers	Soto et al. 2008	1 in 500
CRALBP	Müller glia & RPE	GCL, processes throughout retina, RPE	Livne-bar et al. 2006	1 in 200
RPE65	RPE cytoplasm	RPE	Chidlow et al. 2011	1 in 200
Best1	RPE membrane	RPE	Bakall et al. 2003	1 in 500
PKC-α	Rod bipolar cell nuclei and axon terminal	INL/OPL/IPL	Haverkamp et al. 2003	1 in 200

2.3.2   Macaque control tissue: Antibody validation

Antibodies for retinal-cell specific markers were applied to control retinal tissue from Macaca mulatta. Those which showed specific localisation within the retina were carried forward using the same experimental conditions for analysis of macaque iPSC derived organoids (Table 2.17).

Table 2.17. List of primary antibodies used for IHC on primary and organoid macaque tissue.

Antibody	Cat. No.	Host species	Source	Dilution
Vsx2/Chx10	HPA003436	Rabbit	Sigma	1 in 50
Rhodopsin	MAB5356	Mouse	Merck-Millipore	1 in 200
Recoverin	AB5585	Rabbit	Abcam	1 in 1000
CRALBP	AB15051	Mouse	Abcam	1 in 200

Prox1	AB5475	Rabbit	Abcam	1 in 1000
SNCG	H00006623-M01A	Mouse	Abnova	1 in 500
ChAT	AB144P	Goat	Merck-Millipore	1 in 500
Pax6	PRB-278P	Rabbit	Bioloegend	1 in 200
OPN1LW	AB5405	Mouse	Merck-Millipore	1 in 200
OPN1SW	AB5407	Mouse	Merck-Millipore	1 in 200
Crx	H00001406-M02	Mouse	Abnova	1 in 100
Sox2	MAB2018	Mouse	Merck-Millipore	1 in 200
Otx2	AB114138	Rabbit	Abcam	1 in 200
Rax	SC-271889	Mouse	Santa Cruz	1 in 500
GO-α	MAB3073	Mouse	Merck-Millipore	1 in 500
Ki67	AB15580	Rabbit	Abcam	1 in 200
PKCa	SAB4502354	Rabbit	Sigma	1 in 100

Table 2.18. List of secondary antibodies used for IHC on primary and organoid tissue

Antibody (λ)	Cat. no.	Host sp.	Source	Dilution
Donkey α-goat Alexa (647)	A21447	Donkey	ThermoFisher	1 in 800
Goat α -rabbit Cy3 (555)	111165003	Goat	Jackson ImmunoResearch	
Goat α -mouse Alexa (647)	A21237	Goat	ThermoFisher	
Goat α -rabbit Alexa (488)	111545144	Goat	Jackson ImmunoResearch	
Goat α -mouse Cy3 (555)	115165003	Goat	Jackson ImmunoResearch	
Donkey α -mouse Alexa (546)	A10038	Donkey	ThermoFisher	

Antibodies were applied in various concentrations to sections of adult macaque retina and assessed by IF analysis for positive signal and correct localisation within the expected cells of the retina (Fig. 2.2, Table 2.19). Those that showed the expected pattern of expression were used in future sample analysis on primate stem-cell derived organoid samples with the same experimental conditions (Table 2.19).
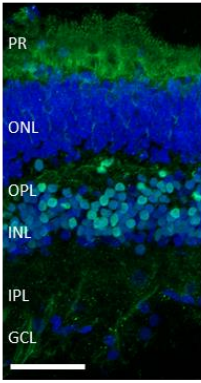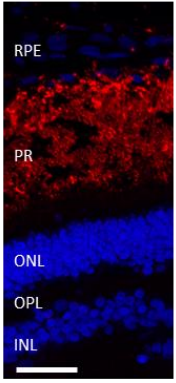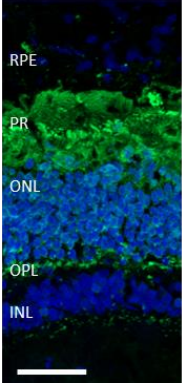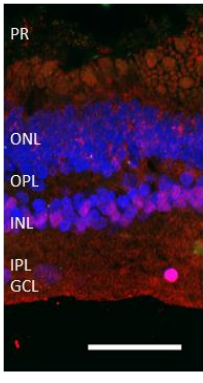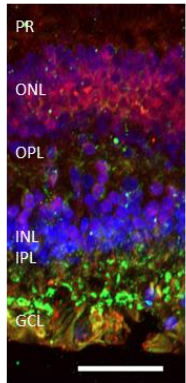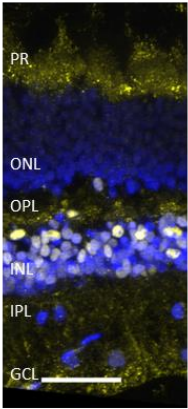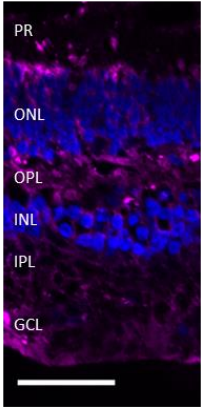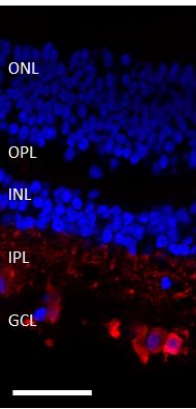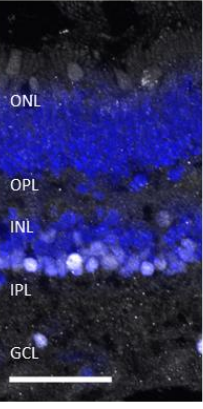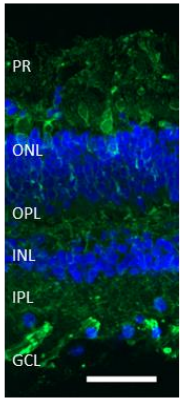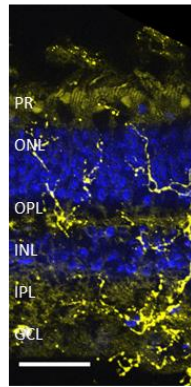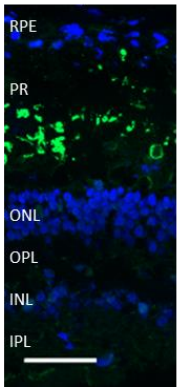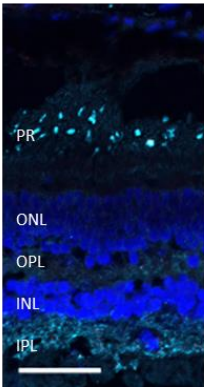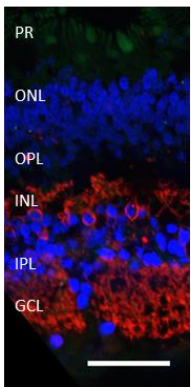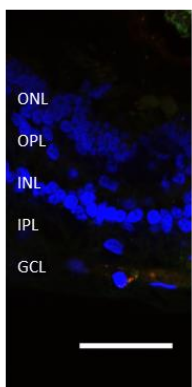
Figure 2.2. Validation of retinal primary antibodies in adult macaque retina showing target cell types. RPE=retinal pigmented epithelium, RGC = retinal ganglion cell, PR=photoreceptors, OS = outer segment, ONL=outer nuclear layer, OPL=outer plexiform layer, INL=inner nuclear layer, IPL=inner plexiform layer, GCL=ganglion cell layer, gr = green. Negative control contained secondary antibodies only. Scale bar = 50 μm.

Table 2.19. Primary antibodies validated for use in adult macaque retina. Predicted cell type informed by published research. Primate retinal location and dilution determined by the experiments described in this report. RPE=retinal pigmented epithelium, RGC = retinal ganglion cell, PR=photoreceptors, OS = outer segment, ONL=outer nuclear layer, ONBL=outer neuroblastic layer, OPL=outer plexiform layer, INL=inner nuclear layer, IPL=inner plexiform layer, GCL=ganglion cell layer.

Antibody marker	Predicted target cell type	Primate retinal location reported herein	Primary reference	Dilution
Pax6	Mature: RGC, horizontal & amacrine	Mature retina; GCL & INL	(Völkner et al., 2016)	1 in 200
	Embryonic: RPCs in NR, eyefield	-		
PKCa	Bipolar cells	GCL, INL	(Haverkamp, Haeseleer, et al., 2003)	1 in 100
Vsx2/Chx10	Mature: Bipolar cells	Mature retina; INL	(Livne-bar et al., 2006)	1 in 50
	Embryonic: RPCs in NR, eyefield	-		
OPN1SW	Cone PRs (short wavelength (blue))	PR OS'	(Insinna et al., 2012)	1 in 200
OPN1LW	Cone PRs (medium/long wavelength (green/red))	PR OS'	(Insinna et al., 2012)	1 in 200
Recoverin	PRs and bipolar cells	PR and INL, plexiform layers	(McGinnis et al., 1999)	1 in 1000
Prox1	Horizontal	Mature retina; INL	(Dyer et al., 2003)	1 in 1000
	Embryonic: RPCs	-		
Rhodopsin	Rod PRs	PR	(McKay et al., 2009)	1 in 200
SNCG	RGC	GCL, plexiform layers	(Soto et al., 2008)	1 in 500
CRALBP	Müller glia & RPE	GCL, processes throughout retina, RPE	(Livne-bar et al., 2006)	1 in 200
ChAT	Starburst amacrine cells	GCL/INL	(I.-B. Kim et al., 2000)	1 in 500
Crx	Mature: Post mitotic PRs Embryonic: developing PRs (ONBL)	ONBL/PR	(Glubrecht et al., 2009)	1 in 100
Sox2	RPCs, amacrine and MG	INL/MG	(Y. Lin et al., 2009)	1 in 200
GO-α	Bipolar cells	OPL, INL, IPL	(Eliasieh et al., 2007)	1 in 500

Arrestin 3	Cone PRs	PR/ONL/IPL	(Glubrecht et al., 2009)	1 in 100

IF was evaluated in comparison to sections with only secondary antibody applied (Fig. 2.2). Each antibody showed herein displayed immunoreactivity above background levels and specific localisation consistent with expectations from the published literature (Fig. 2.2; Table 2.19). In occasions where the protein expression varies between embryonic and post-natal stages of development, such as Pax6 and Rax, these differences are highlighted in Table 2.19, however a positive staining in adult retina and lack of signal in the negative control was considered to validate the use of the antibody for all macaque retinal tissue. The appropriate antibody concentrations were determined by these experiments and the same conditions and imaging techniques were used for subsequent analysis.

2.3.3   Image analysis

Images of live organoids were collected throughout the differentiation process to assess organoid morphology or appearance of retinal features using the bright-field phase of an Axiovert microscope. Images of fluorescently labelled organoid samples were captured using Zeiss Axioimager microscope and Zeiss Zen blue software.

2.4 Gene expression analysis

2.4.1   RNA extraction and quantification

RNA extraction was performed using Promega ReliaPrep RNA Tissue Miniprep system (Promega, Cat: Z6111) as per kit instructions. Briefly, cell pellets were incubated with lysis buffer (containing 1-thioglycerol) and vortexed to homogenise. Primary retinal tissues were additionally homogenised using Precellys Evolution homogeniser (run conditions: 6500rpm, 2 x 25sec cycles, 10sec interval) with the addition of Precellys ceramic bead kit (CK28-R/2ml). Sample lysate had 100% isopropanol added and was passed through an RNA-binding minicolumn. Column was washed and minicolumn membrane was incubated with DNase I mix for 15mins. Column was washed with column wash and RNA wash to remove buffers and contaminating DNA. Finally, bound RNA was eluted from membrane using 15 or 30 µL Nuclease-free water.

RNA quantity and purity was checked using a Nanodrop 2000 spectrophotometer. Acceptance criteria for RNA samples was set at concentrations >125ng/ µL and absorbance A 280/260 values between 2.0-2.2 and A 260/230 between 1.7-2.3.

2.4.2   Turbo DNase treatment

Following extraction RNA samples were treated with TURBO DNase I (Ambion, AM1907) as per kit instructions with the following parameters. Sample had 1 µg of RNA or 1.25 µg per 10 µl reaction

volume to enable cDNA synthesis with 800ng/8 µl input RNA or 1000ng/8 µl. Samples were kept on ice and diluted to the appropriate concentration with nuclease-free water then a mix of DNase buffer (0.1x reaction volume) and 1 µl of enzyme was added per reaction. Samples were incubated at 37°C for 30 mins. DNase Inactivation Reagent was then vortexed thoroughly and added (0.1x reaction vol.) and samples incubated for 5 minutes at room temperature. Samples were then centrifuged at 10000g for 90 seconds and the clear RNA supernatant was removed and stored at-80°C or immediately processed into cDNA.

2.4.3   cDNA synthesis
cDNA was synthesised from 0.5 or 1 µg input of RNA using GoScript Reverse Transcription Kit (Promega, Cat: A5001) as per kit instructions. Briefly, RNA was incubated with random primers at 70°C for 5 minutes then chilled on ice. A mastermix of 0.5mM dNTPs, 3.75 mM MnCl2, GoScript reverse transcriptase, ribonuclease inhibitor and 1x reaction buffer was prepared and added to RNA for a reaction volume of 40 µL. This was run in PCR machine with reaction conditions: anneal at 25°C for 5 minutes, extend at 42°C for 60 minutes, then inactivation of RT enzyme at 70°C for 15 minutes. cDNA samples were stored at -20°C.

2.4.4   End-point PCR
Polymerase Chain Reaction (PCR) setup for primer validation consisted of a mastermix containing 1 µM forward and reverse primers (each), dNTPs, GoTaq G2 enzyme (Promega, M784), 1x green reaction buffer (Promega, M791), Nuclease-free water and 12.5 ng of sample cDNA (assuming 100% RT efficiency) in a total reaction volume of 10 µL. Reaction conditions were initial denaturation step at 95°C for 2 minutes, then 30 cycles of (denaturation at 94°C for 20 seconds, annealing at 60°C for 30 seconds, 72°C for 15 seconds), then final extension of 75°C for 5 minutes.

PCR products were analysed by gel electrophoresis in 2% agarose gel alongside a 1kb ladder to visualise size and efficacy of amplification.

2.4.5   Primer design
Primer sequences for retinal rat genes were designed by myself except Rax, Pax6, Vsx2 and Mitf which were designed by Dr. V. Chichagova (Table 2.20). Primer sequences for rat housekeeping genes *GAPDH*, *MAPK1* and *B2M* were designed by myself or taken from Rocha-Martins et al. (Rocha-Martins et al., 2012) as specified in Table 2.20. Primers designed for species-specific detection and use in end-point PCR were designed to have amplicon length < 600 bp (Table. 2.21). Primate retinal gene primers were designed by myself, except *NANOG*, *OCT4*, *SOX2* and *GAPDH* which were designed by Dr. V. Chichagova (Table 2.22). All primers were designed to target sequences crossing

exon-exon junctions. Criteria was set for primer melting temperature at 60°C and amplicon length to be 70-200 base pair (bp) to ensure efficient amplification in qPCR reactions.

Table 2.20. Rat candidate primer sequences and properties. [1]Sequences designed by Dr V. Chichagova, [2]Sequences for GAPDH2 primers were taken from Rocha-Martins et al. 2012. Tm denotes melting temperature (°C) as determined by Primer BLAST tool on NCBI.

Primer Name	Sequence (5' - 3')	Length/ bp	Tm/°C	Product size/bp
[1]Rax_2 F	CCCGGAGTTCGAAGCTACTC	20	60	184
[1]Rax_2 R	TTCCAGCTCGTGCAGTTGAT	20	60	
[1]Vsx2_3 F	GGCTACTGGGGATGCACAAA	20	60	105
[1]Vsx2_3 R	CCTGCTCCATCTTGTCGAGTT	21	60	
[1]Mitf_2 F	AAGAGAGCTCACAGCGTGTA	20	59	167
[1]Mitf_2 R	CCGGATCGTTTGACTTGGGA	20	60	
[1]Pax6_2 F	CAGAACAGTCACAGCGGAGT	20	60	149
[1]Pax6_2 R	CCGTTGGACACCTGCAGAAT	20	60	
[2]MAPK1 F	TGTTGCAGATCCAGACCATG	20	58	132
[2]MAPK1 R	CAGCCCACAGACCAAATATCA	21	58	
[2]B2m F	CGAGACCGATGTATATGCTTGC	22	59	114
[2]B2m R	GTCCAGATGATTCAGAGCTCCA	22	60	
GAPDH F	GGACCAGGTTGTCTCCTGTG	20	55	184
GAPDH R	AGAGGGCACCAAACCTTCAG	20	56	
Nestin1 F	ACTCTGCTTTTCCAGACCCCA	21	61	175
Nestin1 R	CTGGCCTGAAGGAACTCCTGA	21	61	
Otx2_1 F	CTTTAAGGAGTGCGGCTCCA	20	60	128
Otx2_1 R	CCCTGAACCACACTAGGCAG	20	60	
Lhx2_1 F	GACTACTACAGGCGGTTCTCTG	22	60	196
Lhx2_1 R	CGAAGTGCAAGCGGCAATAG	20	60	
Brn3b_3 F	AGAGCTTGTCTTCCAACCC	19	61	120
Brn3b_3 R	GTGGTGGTGGCTCTTACTC	19	61	
Rcvrn_1 F	GAGATCGTCATGGCTATTTTCAA	23	57	98
Rcvrn_1 R	CAGATCTTCTCAGCCCGCTT	20	60	
Rho_2 F	TTGGAGGTGAAATCGGCCTG	20	60	189
Rho_2 R	CCTCGGGGATGTACCTGGAC	20	61	
Rbpms_2 F	CTGCATGCCCAGTGTTTCTCT	21	61	118
Rbpms_2 R	CTGCAGTGGGTTGATACGTGA	21	60	
Rpe65_1 F	CATGTCACAGATTCATCCGCAC	22	60	91
Rpe65_1 R	GGAAAAGCACAGGTGCCAAA	20	60	
Arr3_1 F	GGTGAGAGAGCAGTGGCTACC	21	62	96
Arr3_1 R	TGCTGTTGGAGCTTTCTAGCTT	22	60	
Nrl_2 F	ATGCAGGGAAAAGGGACACCA	21	62	100
Nrl_2 R	TGGCAGAGACCTCGTAGTCA	20	60	
Opn1mw_1 F	AACTTGGCAGTTGCTGACCT	20	60	142
Opn1mw_1 R	GGCCTGTGATCCCACATAGT	20	59	
Opn1sw_1 F	AACAATCGTAACCACGGGCT	20	60	118
Opn1sw_1 R	AGGCCCGGAACTGCTTATTC	20	60	
Rom1_1 F	TGCCTTGGCTCACTACAAGG	20	60	189
Rom1_1 R	TTGCTCTGGATCCGGTCAAC	20	60	
Mertk_2 F	CTGCTTCTGCGGGTTTGTTC	20	60	179
Mertk_2 R	GGCTTTGCAAGGTAAGCTCG	20	60	

Crx F	GCCTCACTATTCTGTCAACGC	21	60	170	
Crx R	CTGGGTACTGGGTCTTGGC	19	60		
Prox1 F	TGCAGGAAGGATTGTCACCC	20	60	195	
Prox1 R	GACGCGCGTACTTCTCCATC	20	60		
Calb1_1 F	AGCGCTCTCTCAAACTAGCC	20	60	114	
Calb1_1 R	CCACTTCCATCAGCGTCGAA	20	60		

Table 2.21. Rat and Mouse-specific primer sequences and properties. Used in end-point PCR for species-specific selection.

Species	Primer Name	Sequence (5' - 3')	Length/ bp	Tm/°C	Product size/bp
Rat	Pax6 Rat F	CTAAGGATGCTGAACGGA	18	60	129
	Pax6 Rat R	GTTGGTGTTTTCTCCCTG	18	60	
Mouse	Pax6 Mouse F	CTAAGGATGTTGAACGGG	18	60	129
	Pax6 Mouse R	GTTGGTGTTCTCTCCCCC	18	60	
Rat	Sox2 Rat F	GGGTGCAAAAGAGGAGAGTAA	21	60	446
	Sox2 Rat R	TTCCTTGTCTGTAACGGTCCTT	22	60	
Mouse	Sox2 Mouse F	GGGTGCAAAAGAGGAGAGTAG	22	60	530
	Sox2 Mouse R	TTCCTTGTTTGTAACGGTCCTA	22	60	
Rat	Nanog Rat F	GATTCCTCGCCGATGCCTGCC	22	60	172
	Nanog Rat R	CAGACAGCTTTAGCTTGGGAT	22	60	
Mouse	Nanog Mouse F	AACGCCTCATCAATGCCTGCA	21	60	169
	Nanog Mouse R	TTGAGAGCTTTTGTTTGGGAC	21	60	
Rat	Oct4 Rat F	CAGCCAGACAACCATCTGC	19	60	215
	Oct4 Rat R	GCAGAAACATGTTCTCCAGGT	21	60	
Mouse	Oct4 Mouse F	CAGCCAGACCACCATCTGT	19	60	215
	Oct4 Mouse R	TCAGAAACATGGTCTCCAGAC	21	60	
Rat	Vsx2 Rat F	CGTCATGGCTGAGTACGGC	19	60	261
	Vsx2 Rat R	TTGTCGAGTTTGGGCAGGA	19	60	
Mouse	Vsx2 Mouse F	GCGTCATGGCTGAGTATGGT	20	60	262
	Vsx2 Mouse R	TTGTCGAGCTTGGGCAGGG	19	60	

Table 2.22. Primate primer sequences and properties. *Sequences designed by Dr V. Chichagova.

Primer Name	Sequence (5' - 3')	Length/ bp	Tm/°C	Product size/bp
*Nanog-F	AATACCTCAGCCTCCAGCAGATG	23	62	148
*Nanog-R	TGCGTCACACCATTGCTATTCTTC	23	62	
*OCT4-F	GAGAACCGAGTGAGAGGCAACC	22	62	166
*OCT4-R	CATAGTCGCTGCTTGATCGCTTG	23	62	
*SOX2-F	TTGTTCGATCCCAACTTTCC	20	56	200
*SOX2-R	ACATGGATTCTCGGCAGACT	20	59	
*GAPDH F	TGCACCACCAACTGCTTAGC	20	61	87
*GAPDH R	GGCATGGACTGTGGTCATGAG	21	61	
PAX6 2 F	CCTCCTTCACATCTGGCTCC	20	60	188
PAX6 2 R	ATAACTCCGCCCATTCACCG	20	60	
RAX F	CACGACTTTCACCACGTACC	20	59	183
RAX R	GAGGACACTTCCAGCTTCTCC	21	60	
VSX2 F	ACGGAGCTACCAGAAGACAG	20	59	168
VSX2 R	GGCAGACTTGAGGATGGACTC	21	60	

RCVRN F	AGGACGTGAAGCTCCTTCCA	20	61	160
RCVRN R	TCAAACTGGATCAGTCGCAG	20	58	
RHO F	CCATGAGCAACTTCCGCTTC	20	60	150
RHO R	AGTAGTCGATTCCGCACGAG	20	60	
RLBP1 F	CGCGAAAGTTCAACGTGGG	19	60	124
RLBP1 R	CCAGCTTCAATGGTACAGCG	20	60	
RPE65 F	CCCTCCTGCACAAGTTTGAC	20	60	86
RPE65 R	CATTGCCCGTACGTAAGCATC	21	60	
ARR3 F	GAAACGGGACTTCGTGGACC	20	60	142
ARR3 R	CACTTCCAAGTCATCACGGC	20	60	
NRL F	GCTGAGTCCTGAAGATGCCA	20	60	170
NRL R	TTAGCTCCCGCACAGACATC	20	60	
OPN1SW F	CAACAACCGTAACCATGGGC	20	60	127
OPN1SW R	CATGATGTGAGCTTGGAACTGC	22	60	
OPN1MW F	TTCTTCGCATGCTTTGCTGC	20	60	186
OPN1MW R	GAGTTCAGAGCCGTCGTCAA	20	60	
AP2A1 F	CATGGCTTTGCTGGCTGACC	20	62	193
AP2A1 R	GAAGAGATACATGCGGCCTAGA	22	59	
CALB1 F	CACAGCCTCACAGTTTTTCGAG	22	60	182
CALB1 R	TCCCATCATCTCTTTGCCCAT	21	60	
CRX F	GCCTCACTATTCTGTCAACGC	21	60	170
CRX R	CTGGGTACTGGGTCTTGGC	19	60	
PROX1 2 F	TGCAGGAAGGATTGTCACCC	20	60	195
PROX1 2 R	GACGCGCGTACTTCTCCATC	20	61	
MITF 2 F	CCTCCGATAAGCTCCTCCAG	20	60	130
MITF 2 R	TCTGTTGCATGAATTGGGCC	20	58	
RBPMS 2 F	TTCAGGAGGAGGAGGTCCG	19	60	171
RBPMS 2 R	CTGCTTCTGAGCGACTGTCA	20	60	
PRKCA 2 F	GGAGAGGGACGTGAGAGAAC	20	60	116
PRKCA 2 R	AGTTTTCTGCTCCTTTGCCG	20	60	

2.4.6 Rat control tissue: Primer validation

Primers were validated for use in rat retinal tissue by analysing the amplification of gene products from control adult rat cDNA by end-point PCR. Negative "no RT" controls were generated from a cDNA synthesis reaction using control cDNA as a template and omitting reverse transcriptase. Primers were designed to span exon junctions of genes and, in the case of pluripotency genes *SOX2*, *NANOG* and *OCT4* and neural-retinal genes *PAX6* and *CHX10*, to distinguish between rat and mouse species.

The housekeeping genes *GAPDH*, *MAPK1* and *B2M* were chosen based on research investigating stable gene expression in rat tissue at embryonic and post-natal development (Rocha-Martins et al. 2012), and a selection of primer sets for each were tested.

Primer sets *GAPDH3*, *MAPK12* and *B2M2* produced bright bands of the correct product size denoting efficient and specific amplification from adult rat cDNA. They were further tested on iPSC and rat organoid cDNA to confirm their suitability for future experiments (Fig. 2.3). All these primers showed specificity of binding as they produced a single gene product of the predicted size shown by a clear band and no band was seen in the negative controls. Primer sets *GAPDH3* and *MAPK12* were chosen for use in future experiments due to consistent band intensity between samples.

	Neg.	No RT control			iPSC cDNA			Organoid cDNA		
	Gapdh3	Gapdh3	B2 m2	Mapk1 2	Gapdh3	B2m2	Mapk 1 2	Gapdh3	B2m2	Mapk1 2
SIZE(bp)	-	-	-		184	114	132	184	114	132
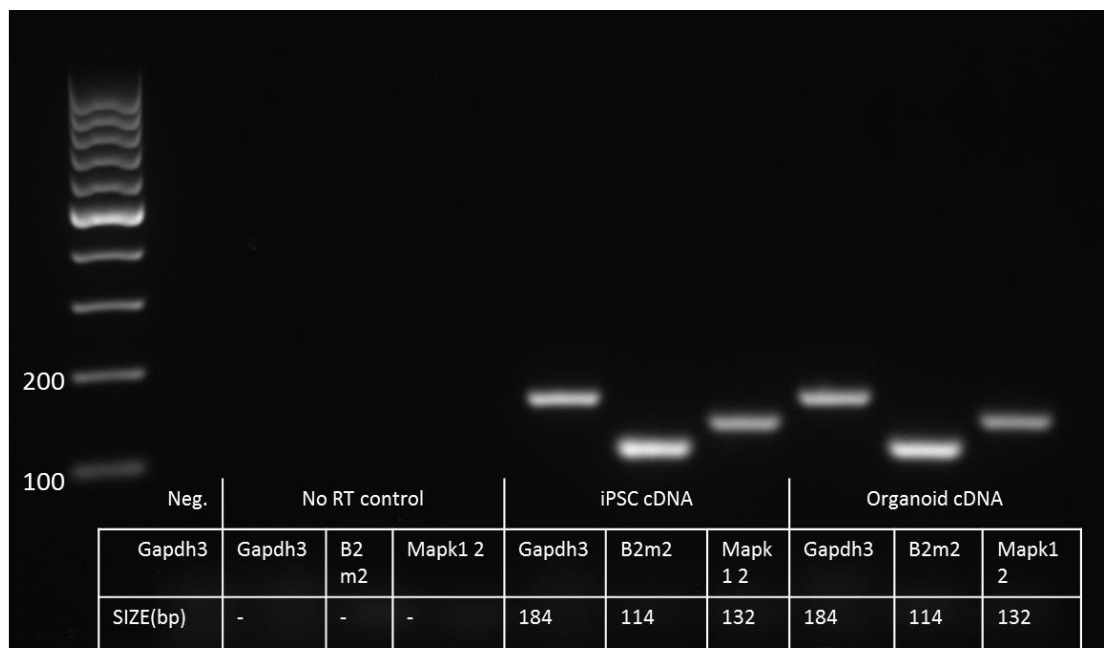
Figure 2.3. Validation of candidate primers for housekeeping genes using sample cDNA. In figure annotation, top line is sample input; negative control contains no template, No RT control produced from CM iPSC RNA in the absence of reverse transcriptase, cDNA produced from CM iPSC (iPSC) or CM iPSC derived organoid sample RNA (organoid). Middle line shows primer sets used. Size row denotes expected length of amplicon in base pairs (bp). Ladder shows 100 bp markers.

A set of primers were designed to target the neural-retinal genes *NESTIN*, *OTX2, LHX2* and *BRN3b* and validated by RT-PCR using rat retina cDNA as a template (Fig. 2.4a,b). These are expressed early in retinal specification and would be used to assess RO identity in the early stages of differentiation along with other EFTFs. The primer sets which will be used for analyses are Nestin_1, Otx2_1, Lhx2_1 and Brn3b_1 as these showed a single amplification of a single product using rat retinal cDNA and a negative result in the no RT control sample (Fig. 2.4a, b). Neither of the primer sets designed for *SOX2* were suitable as multiple products have been amplified (Fig. 2.4a).
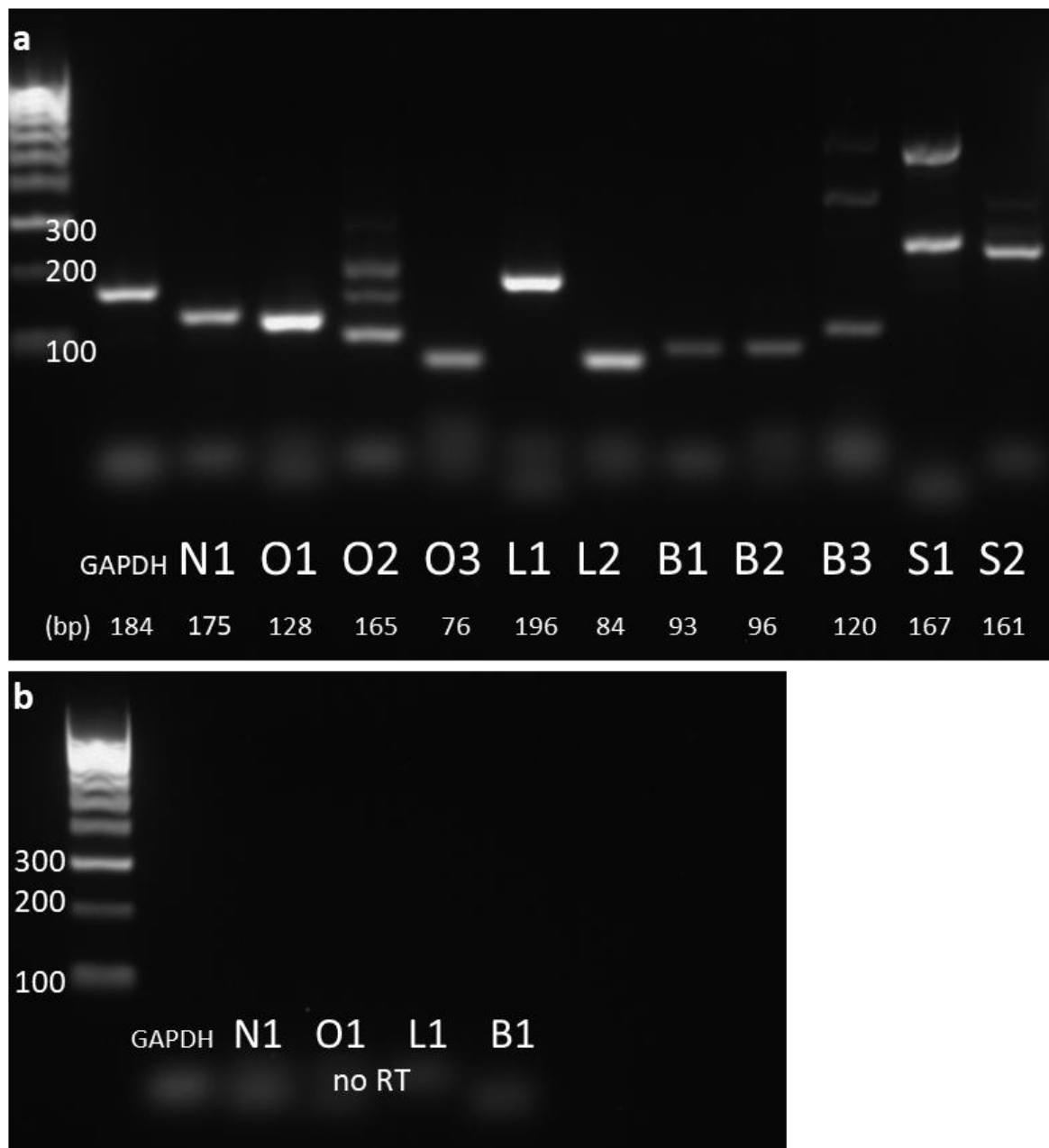
Figure 2.4. Validation of candidate primers for retinal genes of interest using rat primary retinal tissue cDNA. N=Nestin, O = Otx2, L = Lhx2, B = Brn3b, S = Sox2 (a) Shows primer amplification on rat template cDNA (b) Shows primer amplification on negative control sample containing no RT cDNA. (c) Shows Rax, Vsx2, Pax, Mitf candidate primer amplification on rat template cDNA (d) Shows primer amplification on no RT samples. Ladder shows 100 bp markers. Size row denotes expected length of amplicon in base pairs (bp).

C

PRIMER:	Neg. control	Rax1	Rax2	Rax3	Vsx2_1	Vsx2_2	Vsx2_3	Vsx2_4	Pax6_1	Pax6_2	Mitf1	Mitf2	Mitf3
SIZE (bp):	-	197	184	88	71	108	105	70	112	149	162	167	169

d

Rax1   Rax2 Rax3 Vsx2_1 Vsx2_2 Vsx2_3 Vsx2_4 Pax6_1 Pax6_2 Mitf1 Mitf2 Mitf3
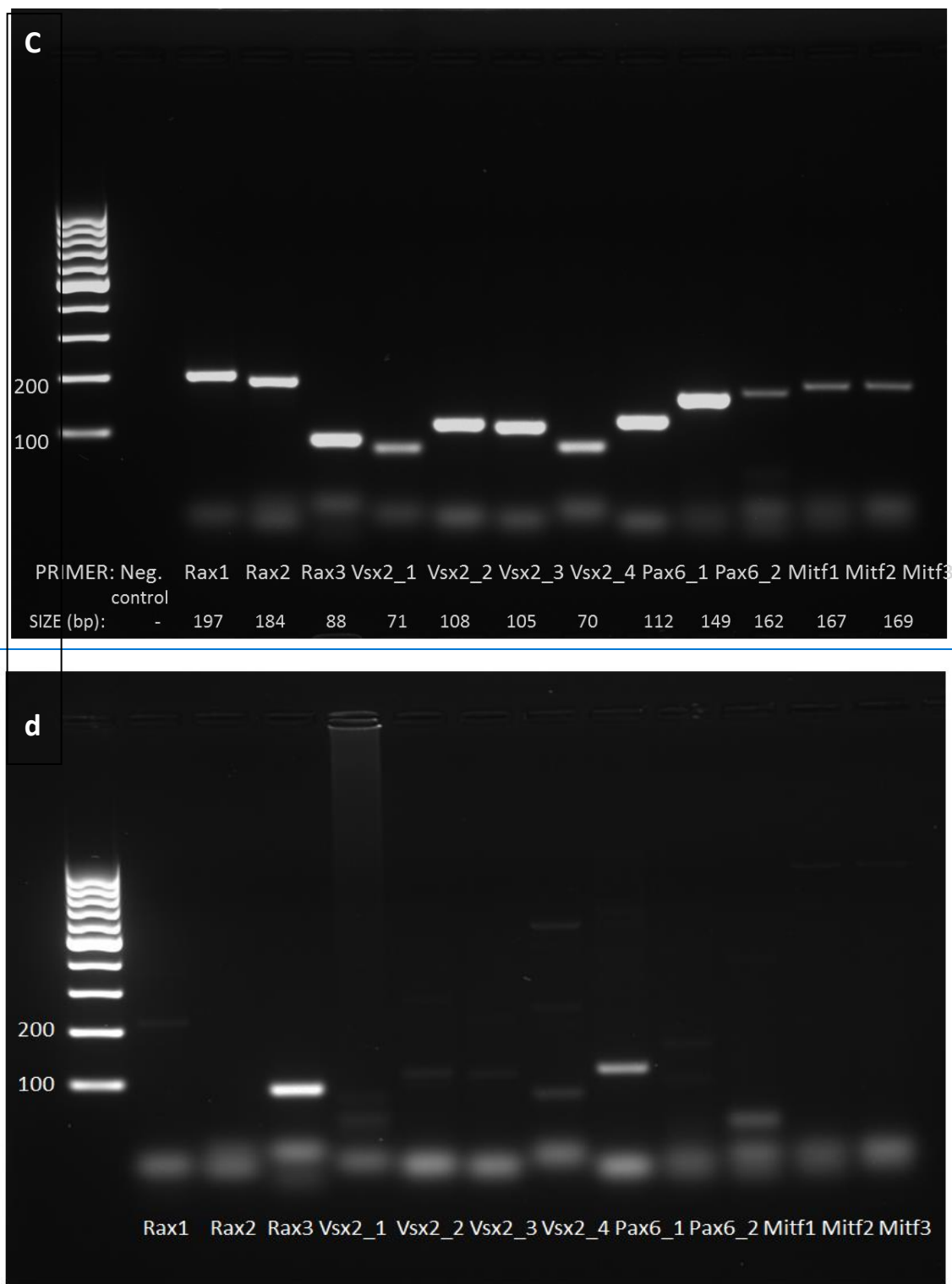
Primer sets for each of the neural-retinal genes of interest Rax, Pax6, Vsx2 and Mitf were also validated against adult rat cDNA by PCR (Fig. 2.4c). Multiple primer sets were tested for each gene and those which were used for analysis are Rax_2, Vsx2_3, Mitf_2 and Pax6_2 as these showed the

110

brightest band of product at the correct size using retinal cDNA as the template (Fig. 2.4c) while also showing no amplification from the no RT control (Fig. 2.4d).

A further panel of primer sets for mature retinal genes were tested on rat retina cDNA for their specificity (Fig. 2.5). Following the same validation criteria the following primer sets were chosen for sample analysis due to amplifying a single product at the correct length; Recoverin_1, Rhodopsin_2, RBPMS_2, Arrestin3_1, Nrl_2, OPN-S_1, OPN-M_1, Rom_1 and Calb_1 (Fig. 2.5).
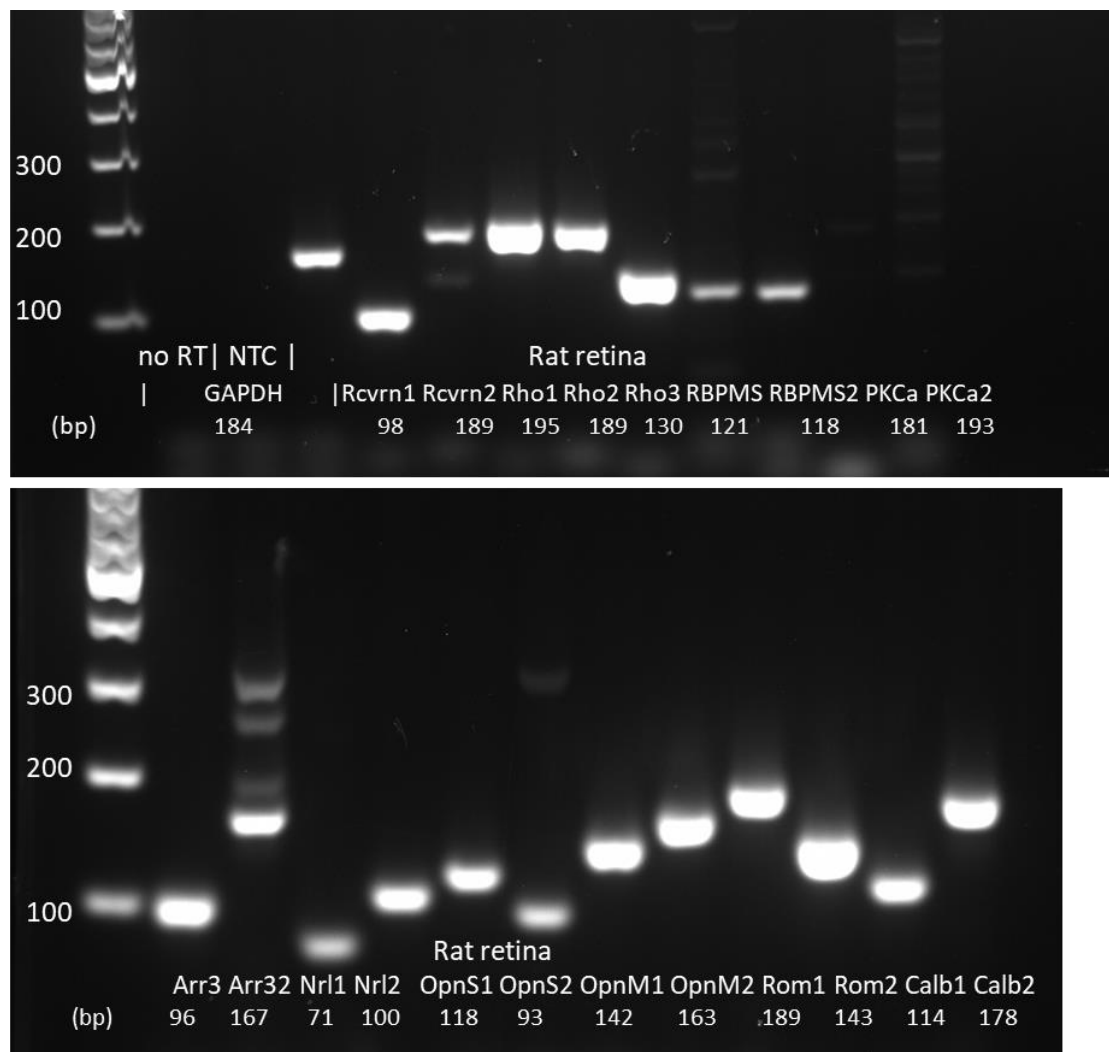
Figure 2.5. Validation of candidate primers for mature retinal genes of interest using primary rat retinal cDNA. Ladder shows 100 bp markers. Size row denotes expected length of amplicon in base pairs (bp). NTC = no template control.

2.4.7   Validation of primers for retinal genes on macaque samples

Primers cross-specific for *Macaca mulatta* and *Macaca fascicularis* were designed to target pluripotency and retinal cell-specific genes and tested by end-point PCR on cDNA from adult

macaque retina (Table 2.22). The resulting amplicons were visualised by gel electrophoresis and those generating a single amplicon of anticipated length were used for analyses of macaque iPSCs and their derived organoid samples (Fig. 2.6).

Those which showed no amplification (*PAX6, MITF, RBPMS, PKCα* and *PROX1*) were discarded (Fig. 2.6a). These target genes were found to have multiple exons and differential gene splicing, so primers were re-designed to target constitutively expressed exons and re-tested, which achieved a positive result (Fig. 2.6b).
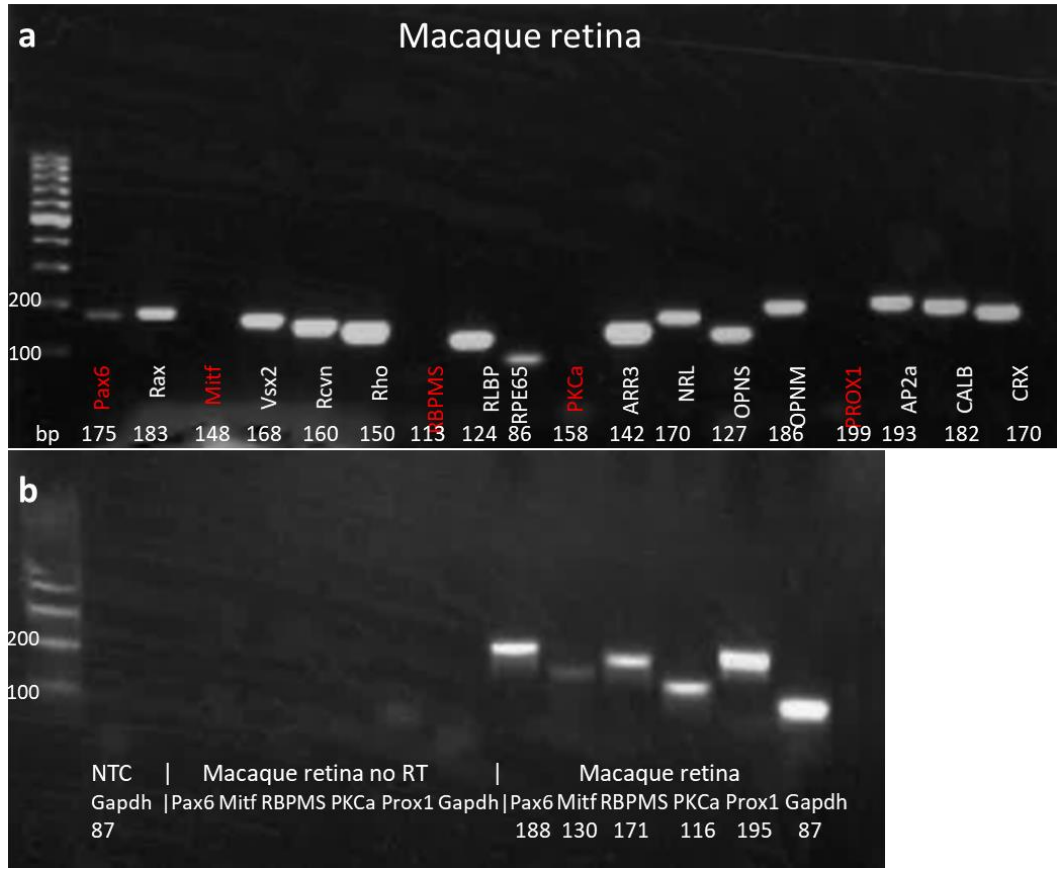
Figure 2.6. Validation of primate retinal gene primers. Electrophoresis gel visualising results of PCR with candidate retinal gene primers applied to macaque adult retina cDNA. Expected amplicon length in base pairs (bp). (a) Those highlighted in red were deemed unsuitable for further analysis. (b) Analysis of re-designed primers with successful amplification. NTC = No template control.

2.4.8   Quantitative PCR

Quantitative PCR (qPCR) was set up with mastermix of 1 µM forward and reverse primers (each), GoTaq qPCR mix and CXR reference dye (Promega, A6001), 12.5 ng cDNA sample and nuclease-free

112

water in a reaction volume of 10 µL. Reaction conditions were: 40 cycles of 95°C for 15 seconds and 60°C for 1 minute, finalizing with a melt curve stage.

Assays were performed using a QuantStudio 7 Flex Real-Time PCR System (Applied Biosystems), using SYBR green reaction technology (Promega). Relative gene expression changes were calculated using the comparative delta Ct method (Livak and Schmittgen, 2001). Ct results of the target genes were normalized to the Ct of the reference gene Gapdh (ΔCt); ΔCt then normalised to the ΔCt of the reference sample, giving the (ΔΔCt), finally the fold change in expression (RQ) was determined (2-ΔΔCt).

2.4.9   Statistical analyses

All statistical tests were performed using Prism (GraphPad, USA). The standard errors of all means (SEM) were calculated and shown graphically as error bars. Statistical significance was tested using two-way ANOVA (Dunnett statistical hypothesis for multiple test correction) and depicted graphically as asterisk: * = p-value < 0.05, ** = p-value < 0.01, *** = p-value <0.001, **** = p-value <0.0001.

Chapter 3

Chapter 3 Rat retinal differentiation using iPSC and XA ESC cell lines

3.1 Rat retinal differentiation strategy

In this chapter the "Sasai method" (termed C1), and Sasai-based differentiation method variants (termed C2, C3, C4, and C5) were tested on rat PSC to assess if mouse RO differentiation methods apply to rat PSCs (Fig. 3.1).
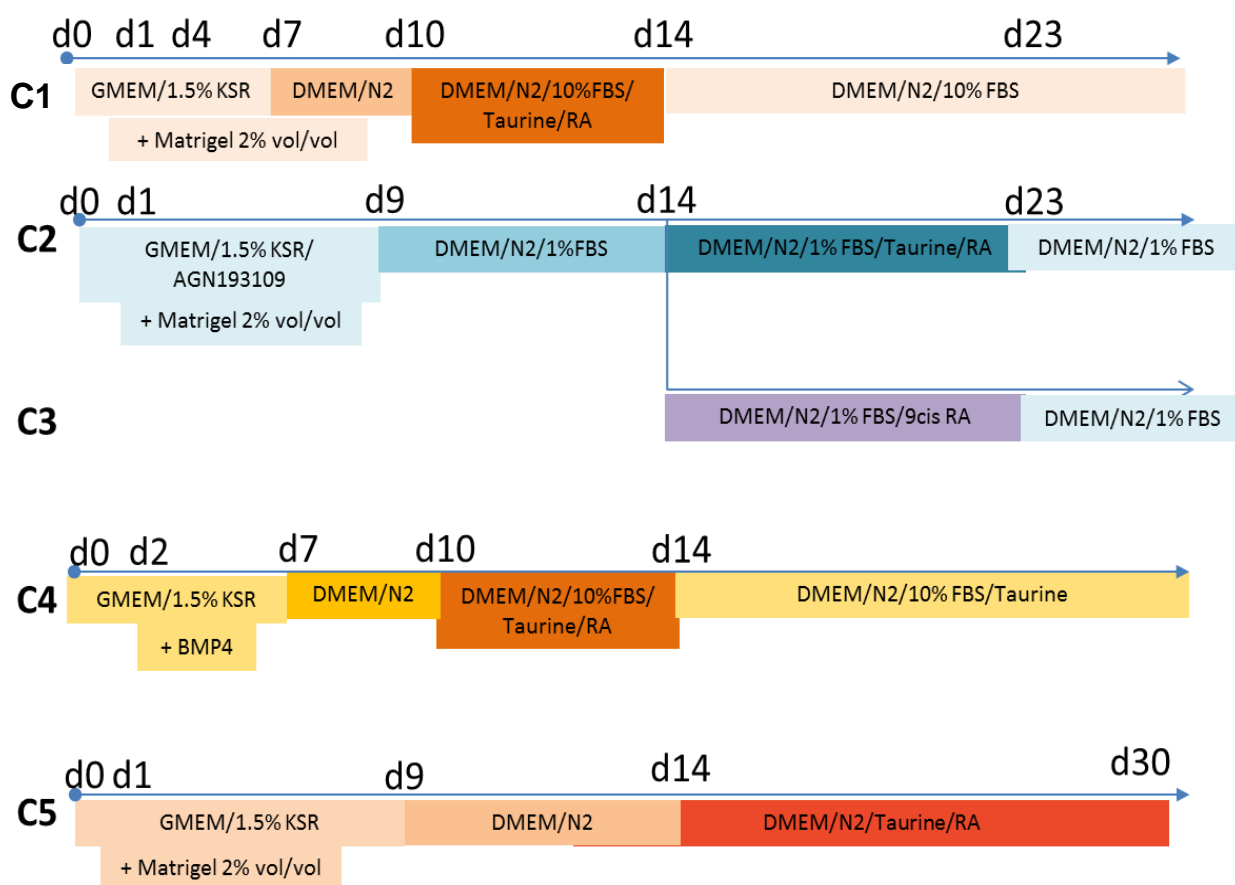
Figure 3.1: Schematic showing published retinal organoid differentiation protocols tested on rat iPSC (CM iSPC, XA iPSC) and ESC (XA ESC) with various media compositions and time of addition of various components. C = condition.

The differentiation methods tested in this chapter considered the method optimisations and retinal differentiation outcomes achieved with mouse PSCs in the literature. Various parameters of RO differentiation methodology, such as media composition, cell plating density and excision of OV structures were applied to rat PSCs and the findings are reported in the chronological stages of retinal differentiation as follows: 1. Effective re-aggregation of stem cells upon plating, 2. NE development and OV/OC formation, 3. Retinal cell differentiation in rat PSC derived organoids and culture method adaptation and 4. Generation of pigmentation in rat PSC (XA ESC) derived organoids.

To date, no published studies have demonstrated the generation of ROs from rat PSCs. The successful derivation of rat ROs is relevant for toxicology and developmental biology studies as it will enable the comparison of *in vivo* to *in vitro* retinal cell models. These cell-based models could therefore provide a platform for the validation of 3D ROs to be used in pre-clinical studies and improve drug discovery and toxicology studies. Additionally, rat ROs have the potential to aid retinal research in rodents by facilitating autologous transplantation studies using rat models of retinal degeneration such as the RCS rat.

3.2 Chapter aims

The aim of this chapter was to test and develop a method for rat PSC differentiation to ROs using a combination of mouse and human RO protocols and known retinal cues.

For this study we obtained 3 rat iPSC lines and 1 ESC line from collaborators Dr C. Merkl and DrX. Aranguren. The rat PSC-derived organoids were subsequently characterised for morphology, and retinal marker expression throughout differentiation, using microscopy, immunohistochemistry and RT-qPCR. This analysis was performed using primary rat retinal tissue as a positive control and validated primers and antibodies. The validation of the differentiation methods using mouse PSCs is described in chapter 4.

3.3 Results

3.3.1 Differentiation of rat PSC derived organoids

Differentiation experiments were performed using 3 rat iPSC lines (CM iPSC, XA iPSC 9.5 and XA iPSC 9.9) and 1 ESC line (XA ESC) which were cultured as per Methods (Table 3.1. Further novel method adaptations were tested on the XA ESC line and are summarised in Methods Table 3.2. Various cell plating densities were assessed in the differentiation experiments, namely 2000, 3500 and 5000 cells/well for CM iPSC line and 2000 and 3500 cells/well for the XA ESC line (Table 3.2). These densities were chosen in line with cell densities used for mouse PSC differentiation which range from 2000 – 5000 cells/aggregate with 3000 cells being commonly used (Table 1.3).

3.3.1.1 Effective re-aggregation of stem cells upon plating

Rat stem cells were maintained in culture as per Methods (2.1.2). All stem cell lines showed tight edged colony growth typical of pluripotent stem cells (Fig. 3.2).
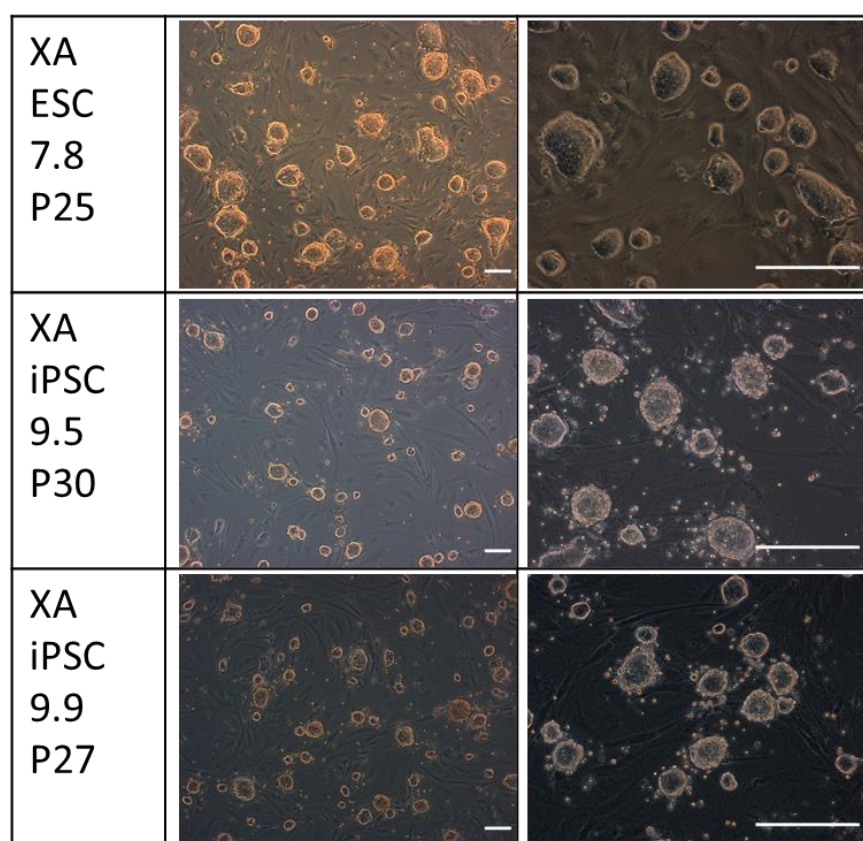
Figure 3.2 Bright-field images showing the representative morphology of rat stem cell lines cultured on iMEF feeder cells. Scale = 200 µm.

The morphology of early stages of differentiation in rat iPSC organoids (CM iPSC), differentiated with the conditions (C) 1/2/3/5 appeared similar to those reported from mouse ESC differentiation (Eiraku & Sasai 2012). Rat iPSCs (CM iPSC) formed uniform spherical aggregates by day 3 and developed phase-bright NE at the external edge of organoids by day 5 (Fig. 3.3). This morphology was seen in three cell plating densities; 2000, 3500 or 5000 cells/well (Fig. 3.3). In C4 (Matrigel-/BMP4+), there was a lack of aggregation of cells at day 2, and no smooth defined edge around the periphery of the organoids at day 3 (Fig 3.3). Subsequently these organoids did not develop the thick NE lamina by day 5 as is seen in the other SFEBq-conditions (Fig. 3.3). BMP4 is present in the developing optic vesicle but is also a determinant of mesodermal specification in the mouse embryo (Johansson & Wiles, 1995; Ohkubo et al., 2002), therefore it's addition at this timepoint may have prompted differentiation towards a mesodermal lineage. This was later confirmed by the presence of beating troponin 1+ cells generated in 100% organoids in C4 (Fig. 3.4).

		CM iPSC		
		2000	3500	5000
D3	C1/5			
	C2/3			
	C4			
D5	C1/5			
	C2/3			
	C4			
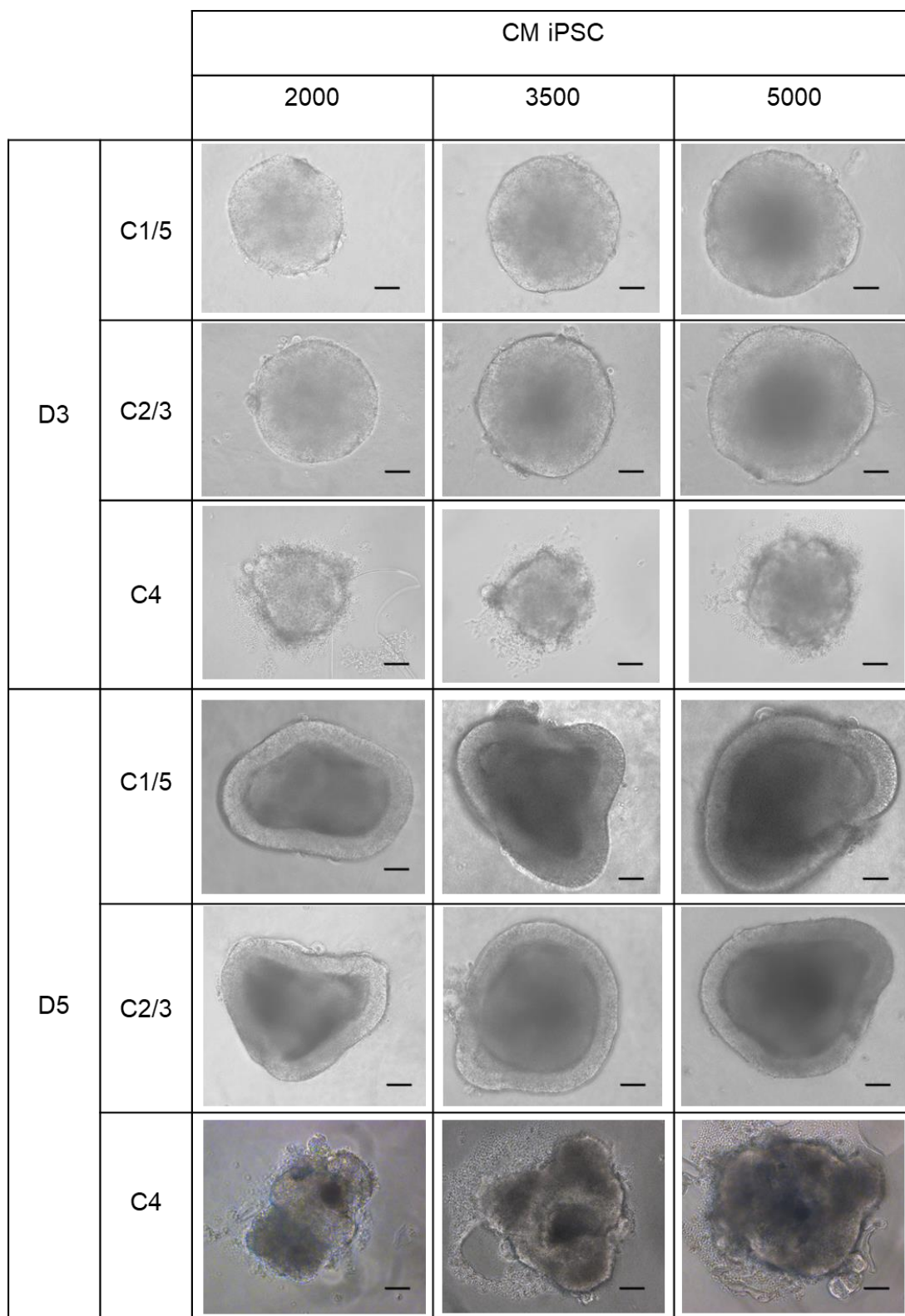
Figure 3.3. Bright-field morphology showing the effective re-aggregation of rat iPSC (CM iPSC) at day 3/5 after plating. Cells were plated at either 2000, 3500 or 5000 cells/well. C = Condition. D = day. C1/5 and C2/3 have been exposed to Matrigel at day 1 of differentiation. C4 lacks Matrigel and has been exposed to BMP4 at day 2. N (experiment) = 1, n (organoid) = 288. Scale bar = 100 μm.
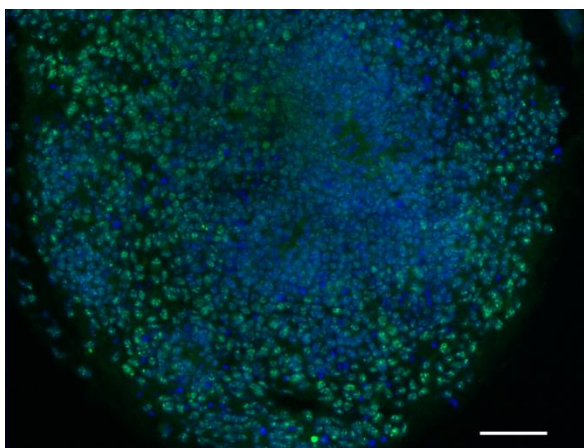
Figure 3.4 Confirmation of non-neural identity of CM iPSC derived organoids by troponin staining at D10 (C4/5000 cells). Hoe=Hoescht (nuclear dye). Scale bar = 50 μm.

Quantification of organoid morphology in the first 9 days of differentiation confirmed that the most effective methods for generating organoids with NE and retinal morphology were C1, C2/3 and C5 (Fig. 3.5). C4 showed no examples of retinal morphology by day 5 (n=96) (Fig. 3.5). The lowest cell density of 2000 cells/well showed good initial development with the highest percentage of organoids (50-100%) developing NE structure at day 3 in every condition (Fig. 3.5). However, this density generated low efficiencies of retinal morphology at day 7; 33% compared to 67% in 3500 or 5000) (Fig. 3.5). The most effective plating cell density for the generation of NE throughout day 3-7 was therefore, 3500 cells/well in C1, 2 and 3 which had NE morphology in 33-83% organoids at day 7 (Fig. 3.5). The highest plating density of 5000 cells/well showed the lowest percentage of retinal morphology development at day 3 in every condition (33-67%), however by day 7 was comparable to 3500 cells/well in the best conditions (67-83%) (Fig. 3.5).

These results show that mouse SFEBq-based differentiation methods including Matrigel can initially generate NE, in contrast to BMP4 addition (Fig. 3.3, 3.5). These results suggest that a higher cell plating density may be required for rat RO generation than mouse. However, the results also show that maintenance of NE and retinal morphological development beyond day 7 was restricted across all methods and cell densities (Fig. 3.5).

120

Condition	Cell density	D3	D5	D7	D9
C1	2000	100%	50%	33%	0%
	3500	83%	67%	67%	0%
	5000	67%	50%	67%	0%
C2/3	2000	100%	50%	33%	0%
	3500	83%	83%	83%	0%
	5000	67%	100%	83%	0%
4	2000	50%	0%	0%	0%
	3500	44%	0%	0%	0%
	5000	33%	0%	0%	0%
5	2000	100%	50%	17%	0%
	3500	83%	67%	33%	0%
	5000	67%	50%	67%	0%

Figure 3.5. Quantification of CM iPSC-derived organoids with retinal morphology derived with differentiation methods C1, C2, C3, C4 and C5 with a plating density of either 2000, 3500 or 5000 cells/well as assessed by bright-field morphology between day 3-9. Green = high efficiency, red = low efficiency N (experiment) = 1.. D3: n (organoid) = 96, D5: n=96, D7: n=80, D9: n=64.

Based on the highest differentiation efficiency achieved at day 3 using plating densities of 2000 and 3500 cells/well with the CM iPSC line of 83-100%, these two densities were tested on other rat stem cell lines (XA ESC and XA iPSC 9.5) (Fig. 3.6) and taken forward for further optimisation.

		XA ESC		XA iPSC 9.5	
		2000	3500	2000	3500
D3	C1				
	C2				
D5	C1				
	C2				
D7	C1				
	C2				
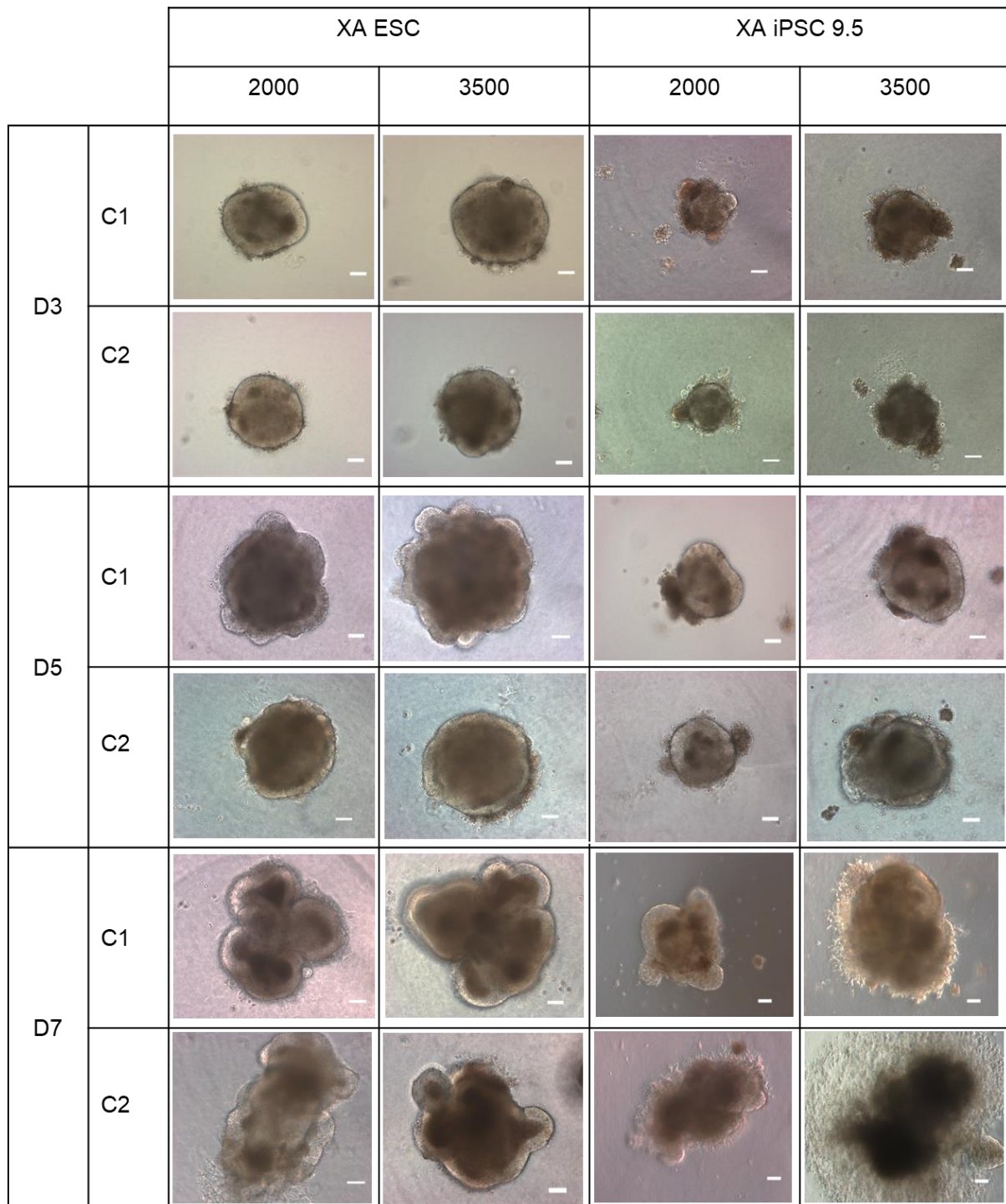
Figure 3.6. Representative bright-field morphology showing the effective re-aggregation and development of neuroepithelium between day 3 and day 7 in rat PSC-derived organoids (XA ESC and XA iPSC 9.5 lines). Cells were plated at either 2000 or 3500 cells/well. C = Condition. D = day. . N (experiment) = 1, n (organoid) = 144. Scale bar = 100 μm.

XA ESC differentiation at 2000 and 3500 cells/well showed quick and effective aggregation by day 3 and development of NE at day 5, followed by further development of the NE and growth of optic vesicle-like structures at day 7 (Fig. 3.6). XA iPSC differentiated in the same conditions showed incomplete aggregation at day 3, and the organoids from both conditions and cell densities had a less defined edge, smaller size and less rapid growth than XA ESC-derived organoids (Fig. 3.6).

At day 5 there was development of a thick phase-bright lamina of NE which was more common in C1 organoids than C2 in both lines and similar between the cell densities (Fig. 3.6). At day 5 17% of XA iPSC organoids show NE morphology with C1 3500 cells/well, compared with 50% of XA ESC organoids with the same method (Fig 3.7).

By day 7 there are clear differences between the cell lines; morphologically XA ESC organoids at day 7 maintained a bright layer at the outer periphery, whereas the majority of XA iPSC organoids did not (Fig. 3.6). At day 7 NE morphology was quantified and 50% of XA ESC organoids (n=120) showed positive NE morphology compared to 17% of XA iPSC organoids with the best method (C1 3500) (Fig. 3.7). The most effective condition, shown by the quantification of 40% of organoids with NE morphology at day 9, was C1 and 3500 cells/well with the XA ESC line (Fig. 3.7b).

At day 7 there was a loss in structure in the XA iPSC organoids in both conditions and cell densities (Fig. 3.6). C2 generated around 7% of XA iPSC organoids with NE morphology at day 7 which decreased to less than 2% at day 9 (Fig. 3.7a). The differentiation efficiency of XA iPSCs was significantly lower than XA ESC-organoids with less than 5% organoids showing NE morphology at day 9, with the best method (Fig. 3.7a).

Despite organoid development showing NE and OV structures, beyond day 7 the morphology of the XA ESC organoids across both conditions and cell densities deteriorated, and the phase-bright tissue was lost in 100% of organoids by day 14 (Fig. 3.7b).
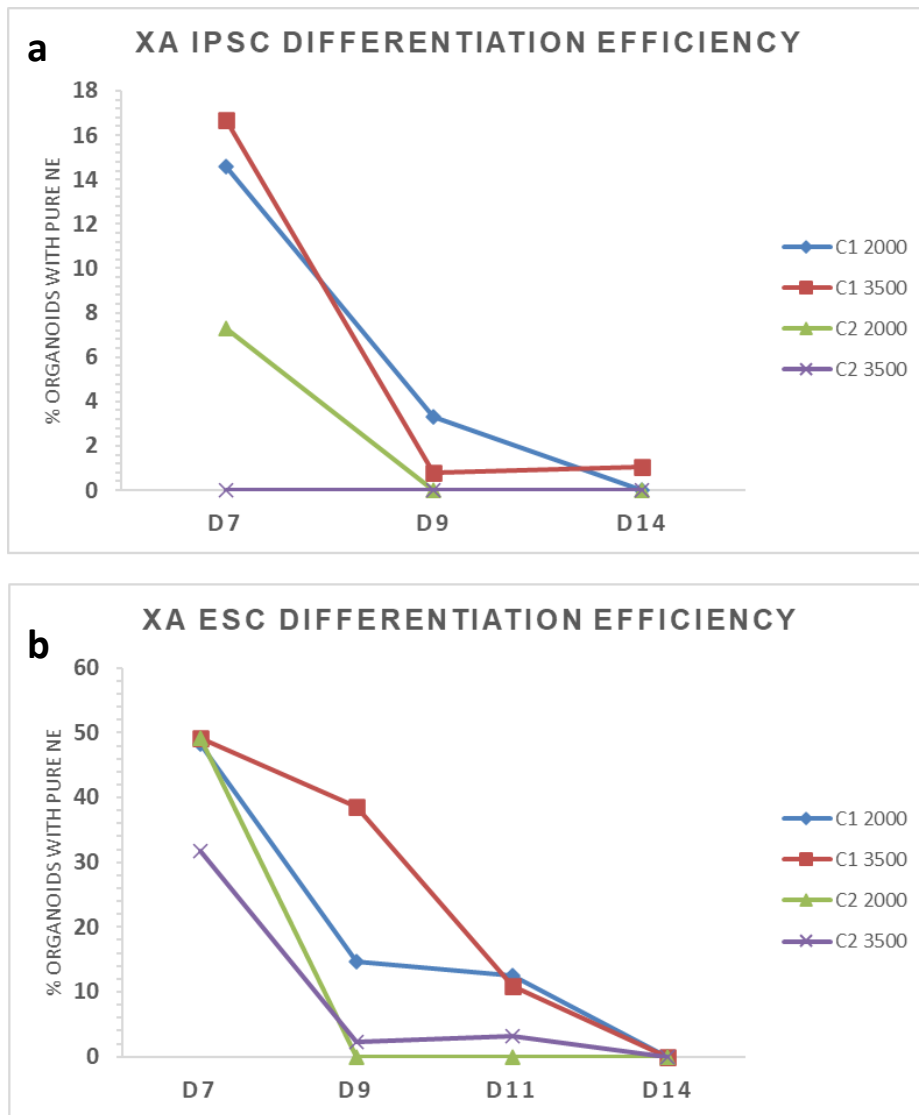
Figure 3.7. Quantification of organoids with complete neuroepithelium (NE) morphology between day (D) 7 and 14 of differentiation with condition (C) 1 and 2 with a plating density of either 2000 or 3500 cells/well in (a) XA iPSC (b) XA ESC. N (experiment) = 1. D7: n (organoid) =120, D9: n=96, D11: n=72, D14: n=60

In conclusion, several known retinal differentiation protocols were tested on 3 rat PSC lines at 2 or 3 cell plating densities. The SFEBq-based methods using a minimal plating media and the addition of Matrigel at day 1 (C1, C2, C3) showed the induction of re-aggregation of stem cells and development of NE by day 5 in CM iPSC, XA ESC and XA iPSC lines. Retinal morphology was lost in organoids generated from all cell lines beyond day 7, however XA ESC-derived organoids showed the best maintenance of putative NE over time. Based on morphology and efficacy of differentiation, the unmodified Sasai protocol (C1) with 3500 cells/well plating density showed the highest efficacy of retinal morphological development in both CM iPSC and XA ESC lines. Therefore, this will be used as

a control condition for future experiments. The identity of the putative NE which is present in this condition between day 5-7 will be investigated as the next stage of organoid development.

3.3.1.2 Neuroepithelial development and optic vesicle or cup formation

The observance of an optically bright lamina of tissue at day 5-7 around the periphery of the rat PSC-derived organoids is temporally in alignment with published results from studies using mouse PSC and embryological rat retinal development (Table 1.1) (Kruczek et al., 2017). To confirm that the tissue observed in rat PSC-derived organoids (XA ESC and CM iPSC) is of NE identity, both protein and gene analysis was performed.
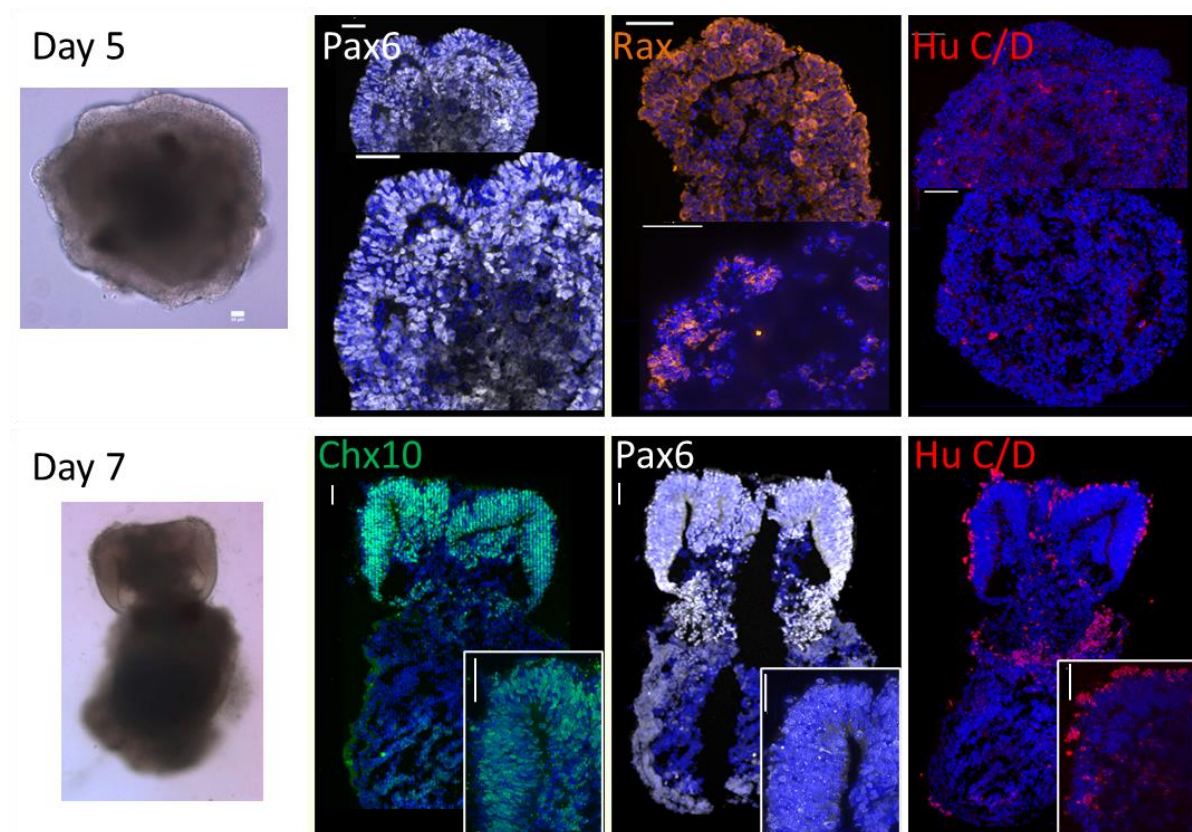
Figure 3.8. Representative bright-field morphology and immunohistochemistry analysis of XA ESC-derived organoids sampled at day 5 and day 7. Markers for eye-field transcription factors (Pax6) and (Rax), retinal progenitor cell (Chx10) and RGC/amacrine cells (Hu C/D) were assessed to confirm the neuroepithelial identity of the organoid tissue. Red signal in day 5 Hu C/D panel is background level only. N (organoid) = 8. Inset box shows higher magnification. Samples nuclear counterstained with Hoescht (blue). Scale bar = 50 μm.

At day 5 there was clear presence of Rax and Pax6 in the tissue lamina at the periphery of the organoids corresponding to the phase-bright regions seen by bright-field microscopy (Fig. 3.8). This confirms the identity of the phase-bright tissue as neuroepithelial.

Pax6 and Chx10 were detected at day 7; moreover, co-localisation of these two markers was restricted to the areas which show a defined and phase-bright morphology by bright-field microscopy (Fig. 3.8). These findings indicate the development of retinal progenitor cells (RPCs) within this region.

The marker for RGCs and amacrine cells Hu C/D was assessed, as RGCs are the earliest cells to differentiate within the retinal lamina in rat at ~GD 11 (Table 1.1). Hu C/D was not detectable in organoids at day 5 however at day 7 there were positive cells at the periphery of the organoids on the external edge of the NE (Fig. 3.8). This is directly inverted to their localisation found in the native retina.

The quantification of relative cell types was not performed for these samples, therefore the IHC data collected in this section is informative only to characterise the stage of retinal development and not to compare between conditions.

The XA ESC organoid samples from this differentiation could not be analysed for gene expression due to inefficient RNA extraction from cell pellets. This would have been informative for validating the immunohistochemistry results in Figure 3.8.

Retinal gene expression was analysed by RT-qPCR in CM iPSC organoids sampled at day 5 and 7 (Fig. 3.9) which showed the presence of phase-bright NE at day 5 (Fig. 3.3). Samples were collected from 8 – 16 organoids and gene expression fold change was quantified using the comparative ΔΔ Ct method by normalising against an undifferentiated iPSC control collected at day 0. *Mapk1* was used as an endogenous housekeeping gene to normalise expression. Two independent biological repeats were analysed.
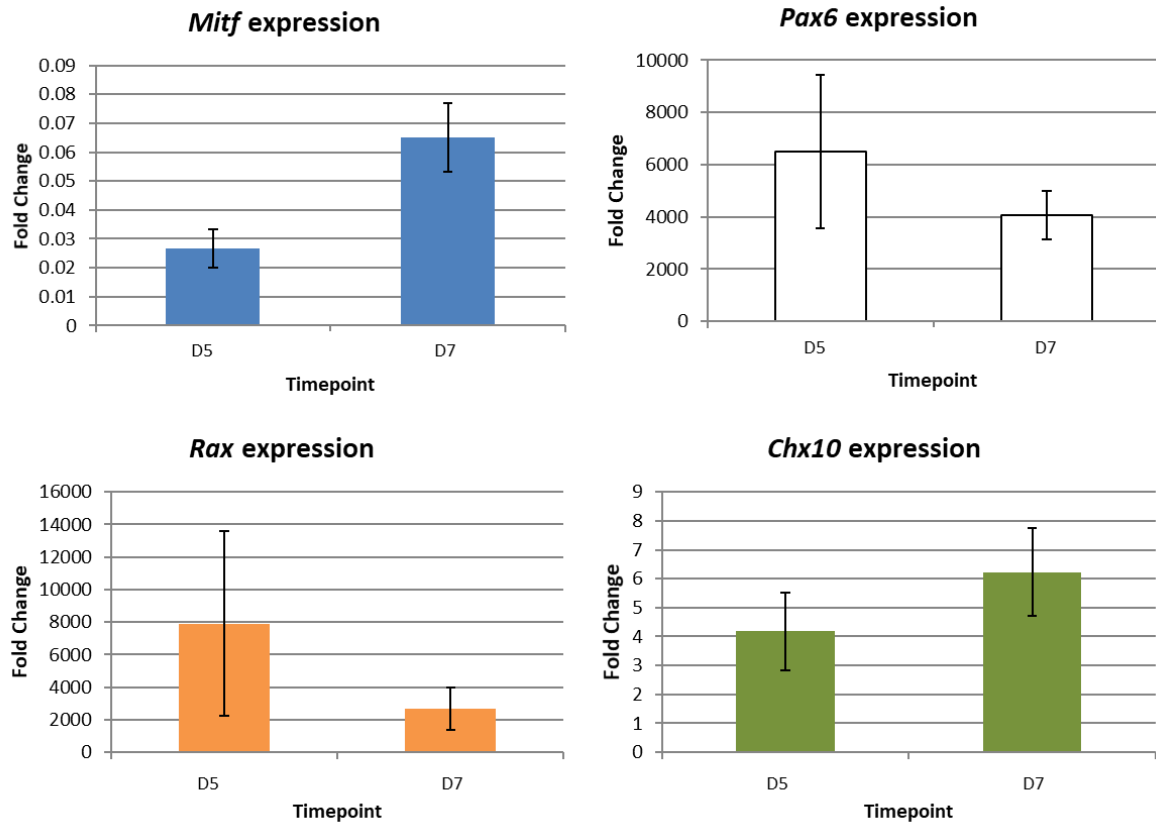
Figure 3.9. Gene expression of neural-retinal transcription factor genes: Mitf,, Pax6 and Rax, and retinal progenitor cell marker Chx10 showing fold change in CM iPSC-derived organoids with C1 and 3500 cells/well. Relative expression normalised to undifferentiated iPSC which have fold change of 1. D = Day. N (experiment) = 2. Error bars show SEM. Values analysed with Student's t-test showed no significant differences between timepoints.

The eye-field transcription factors (TF) Pax6 and Rax showed an increase in expression at day 5 by a factor of 6000-fold (Pax6) and 8000-fold (Rax) relative to iPSC (Fig. 3.9). There is a large degree of error in these measured values which may be explained by organoid variability both within and between biological replicates. The lower end of the values shows gene expression 4000-fold (Pax6) and 2000-fold (Rax) higher than at day 0 confirming upregulation of these genes during the first 5 days of differentiation. At day 7 both Pax6 and Rax expression decreased from day 5, although this is not significant when interrogated using the Student's t-test (Fig. 3.9). However, at day 7 the values remain high at ~4000-fold (Pax6) and 2000-fold (Rax) compared to day 0 (Fig. 3.9).

This decrease between day 5-7 may be indicative of a transition towards more specific retinal identity as eye-field transcription factor genes are turned off, or it may indicate a restriction of

marker expression to regions of the organoid becoming more defined as presumptive retina. It could also represent a downregulation in expression due to a lack of support in the environmental conditions.

The expression of *Chx10* was increased by 4-fold at day 5 and 6-fold at day 7 on average compared to day 0 (Fig. 3.9). The increase between day 5-7 was not significant. However, an increase in *Chx10* is expected in normal development as RPCs are specified and proliferate by asymmetrical division.

The expression of *Mitf*, a TF linked to the specification of presumptive RPE within the optic cup, was also assessed. This showed increased expression of a much lower magnitude than the other genes assayed for with an upregulation of 0.025-fold at day 5 increasing to 0.065-fold by day 7 (Fig. 3.9). No pigmentation was observed to develop in these organoids, primarily because this cell line was derived from the albino Fischer rat strain (Merkl et al., 2013).

In conclusion, markers known to support specification of the eye-field and presumptive retinal tissue were detected in rat PSC-derived organoid samples using protein and gene expression assays. These samples were from 2 cell lines which showed characteristic NE morphology at day 5 and 7. Detection of Rax/*Rax* and Pax6/*Pax6* in day 5 samples was confirmed indicating specification of the eye-field in the phase-bright areas now defined as NE tissue. The presence of Chx10/*Chx10* in day 7 samples confirms further retinal development by the generation of RPCs. Additionally, the presence of Hu C/D at day 7 shows early cell specification of RGC or amacrine cells, albeit at an inverted location compared to native retina. Organoid structure shown by tissue sectioning shows OV structures. It would be informative to perform IHC analysis for CM iPSC-organoids and RT-qPCR for XA ESC-organoid samples to improve the characterisation of the samples and enable direct cell line comparison.

3.3.1.3 Retinal cell differentiation in rat PSC derived organoids

As the presence of NE tissue in both CM iPSC and XA ESC organoids deteriorated beyond day 7 (Fig. 3.5, 3.7), adaptations were made to the Sasai protocol (C1) between day 5 - 10. It was hoped that these modifications would help support NE and retinal structures beyond day 10. Furthermore, the presence of retinal cell markers would be measured by gene or protein assays to confirm whether any change in morphology is reflected in retinal cell generation. These experiments were performed using the XA ESC line as this showed the greatest maintenance of NE tissue over time.

<u>Excision experiments</u>

Firstly, it was hypothesised that culture of organoids in 96-wp beyond day 7 without excision of NE tissue was detrimental. Therefore, manual excision of OV structures at an early stage of development was hypothesised to reduce any counteractive developmental effects from the non-NE tissue. This approach has been used in other publications to isolate retinal tissue in mouse ROs (Eiraku & Sasai, 2012; Völkner et al., 2016).

Therefore, despite the initial aims of the project to generate ROs in a 96-wp format, the excised organoid regions were pooled with the aim to improve differentiation outcomes.

As OVs developed in the rat XA ESC organoids from day 7 (Fig. 3.6) and OC invagination is predicted to occur *in vivo* between GD 8-9 (Table 1.1) two timepoints for excision were tested on XA ESC organoids. These were performed alongside a control which was kept intact. In each sample multiple organoids were sampled randomly from a larger pool.

Organoids were first generated in 96-wp using C1 and a plating cell density of 3500 cells/well, then removed and pooled in culture at day 7 and either immediately or at day 10 had the OV region excised and transferred to pooled culture in 24-wp (Fig. 3.10a). After <24h cut regions formed structures with a continuous phase-bright edge as described in Eiraku & Sasai (2012).

Time	Excision day	Retinal marker expression				
		Chx10	Pax6	Hu C/D	RCVRN	Rho
D14	Uncut (n=4)	100%	100%	100%	0%	-
	D7 (n=4)	75%	100%	100%	0%	-
	D10 (n=5)	20%	100%	100%	0%	-
D26	Uncut (n=4)	0%	100%	100%	50%	25%
D30	D7	Y*	Y*	Y*	Y*	Y*
	D10	Y*	Y*	Y*	Y*	Y*
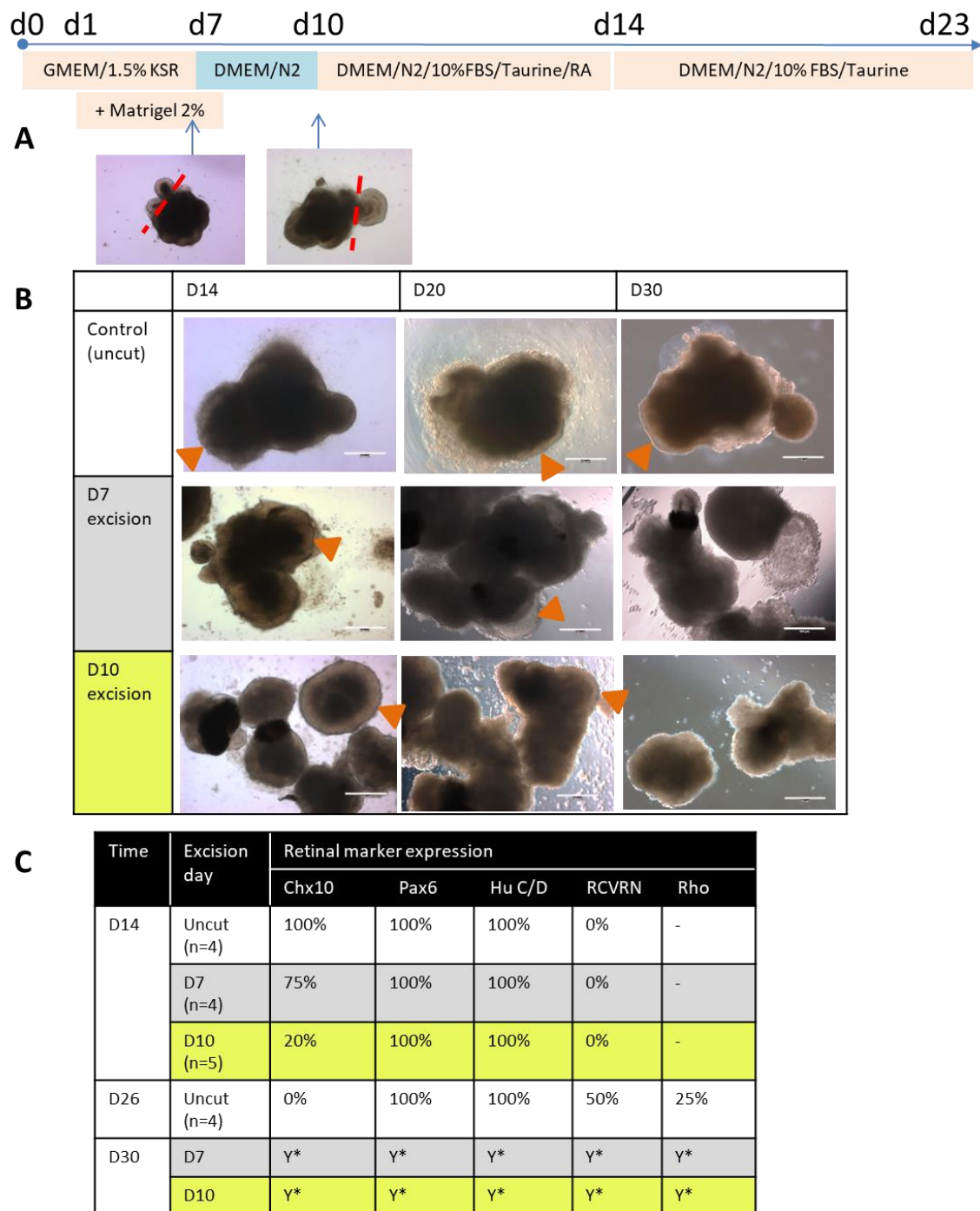
*Figure 3.10. Comparing between excision of optic vesicles from rat XA ESC organoids at day 7 or 10 of differentiation. (a) Culture method, NB: excised regions were pooled in culture following excision (b) Representative bright-field morphology of organoids throughout culture (c) Summary of IHC results from day 14, 26 and 30 samples. Eye-field transcription factors (Pax6) and (Rax), retinal progenitor cell (Chx10), RGC/amacrine cells (Hu C/D), PR marker (Rcvrn) and rod PR marker (Rho) were assessed in uncut, excised at D7 or excised at D10 samples. Orange arrows denote NE morphology. N (experiment) = 1. Scale bar = 500 μm. *Expression not quantified.*

The cut conditions showed good viability post-excision, reforming into whole individual organoids with an outer border with the majority composed of phase-bright NE tissue at day 14 (Fig. 3.10b). This contrasts with the uncut condition which at day 14 has lost much of the phase-bright NE tissue (Fig. 3.10b). By day 20, in the uncut sample most of the NE tissue has deteriorated into an undefined mass around the periphery of the organoid, as was seen in previous experiments (Fig. 3.10b). In both the day 7 and day 10 excision samples there is some retention of the NE however it has also been partially between day 14 -20 (Fig. 3.10b). At the latest sampling point, day 30, there were no organoids showing a distinct layer of bright NE in the day 7 or day 10 excision condition, however in the uncut condition there was a less significant loss (Fig. 3.10b).

Due to the tendency of some excised organoids to fuse together and form one larger structure, quantitative comparison of retinal protein markers at later stages of differentiation was difficult to perform. To mitigate this challenge the excised regions could have been transferred into individual wells following excision, however this was not tested in this study.

By recording the presence or absence of a retinal marker within a sample of multiple organoids, the protein expression in the excised and uncut conditions was compared semi-quantitatively in addition to qualitative comparison. All markers were present at day 30 in the day 10 excision condition whereas the uncut and day 7 excision conditions both lacked Chx10 (Fig. 3.10c).

Sample	Chx10	Pax6	Hu CD	RCVRN	Rho
D26 uncut n=4	N	Y	Y	Y	Y
D30 (D7 excision)	N	Y	Y	Y	Y
D30 (D10 excision)	Y	Y	Y	Y	Y
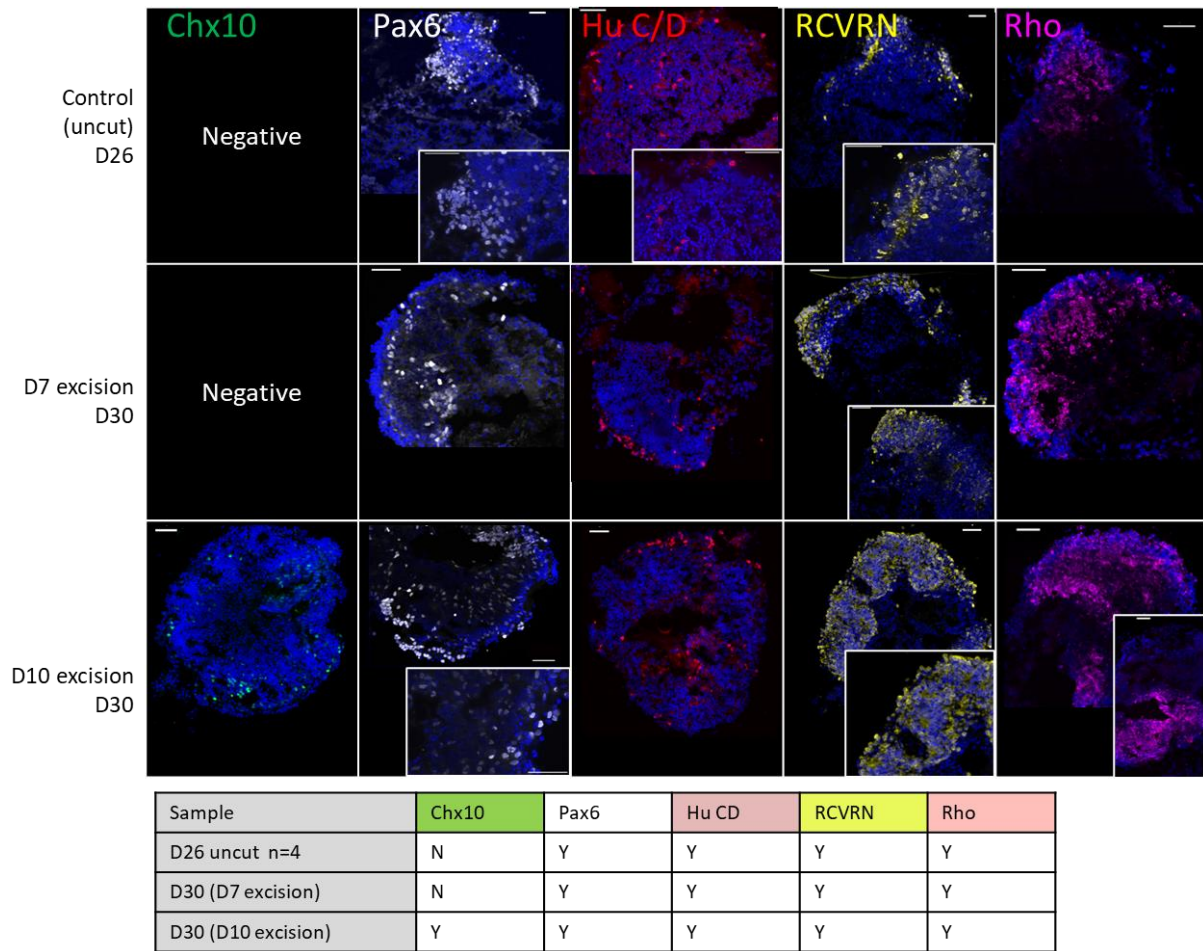
Figure 3.11. Comparing retinal protein expression between excised or uncut rat XA ESC organoid samples at day 26 or 30. Markers for eye-field transcription factor (Pax6)), retinal progenitor cell (Chx10), RGC/amacrine cells (Hu C/D), PR marker (Rcvrn) and rod PR marker (Rho) were assessed. Samples nuclear counterstained with Hoescht (blue). Boxes show higher magnification panels.N (experiment) = 1. Scale bar = 50 µm

However, although markers were present, cellular expression and localisation did not match native rat retina. Cells positive for PR markers recoverin (Rcvrn) and rhodopsin (Rho) were found in all conditions, and these are widely distributed around the organoid outer edge (Fig. 3.11). In terms of spatial orientation, in all conditions RGCs were localised to the outer edge of the organoids as were recoverin and rhodopsin suggesting a lack of retinal lamination (Fig. 3.11).

To summarise, the retinal morphology appeared improved in the excision conditions as non-retinal features were reduced, the prevalence of phase-bright edges was observed throughout the organoids and IHC marker signals were stronger than the uncut control. Furthermore, organoids from the condition excised at day 10 showed the presence of RPC and bipolar cell marker Chx10 at a late stage which most likely indicates development of bipolar cells. This was lacking in the uncut

control. In addition, the presence of mature PR markers recoverin and rhodopsin was observed throughout the outer edge of the organoids, which is promising and warrants further investigation. From IHC analysis we conclude that retinal cellular specification and some maturation is occurring throughout differentiation, and excision induces retinal marker expression at the later stage of differentiation. However, all conditions show mis-localisation of some retinal cell populations (e.g., RGCs) indicative of a lack of correct cell organisation and retinal lamination. It was difficult to quantify differences between organoids generated in the excision experiments as they had fused together. By semi-quantitative and qualitative assessment the excision at day 10 has improved retinal differentiation outcomes from day 14-30.

Culture media supplementation

In this set of experiments changes were made to the media composition, timepoints of media addition and spatial environment of the organoids, by either keeping them in 96-well plates (wp) or pooling them together in culture in low attachment 24-wp (Fig. 3.12).
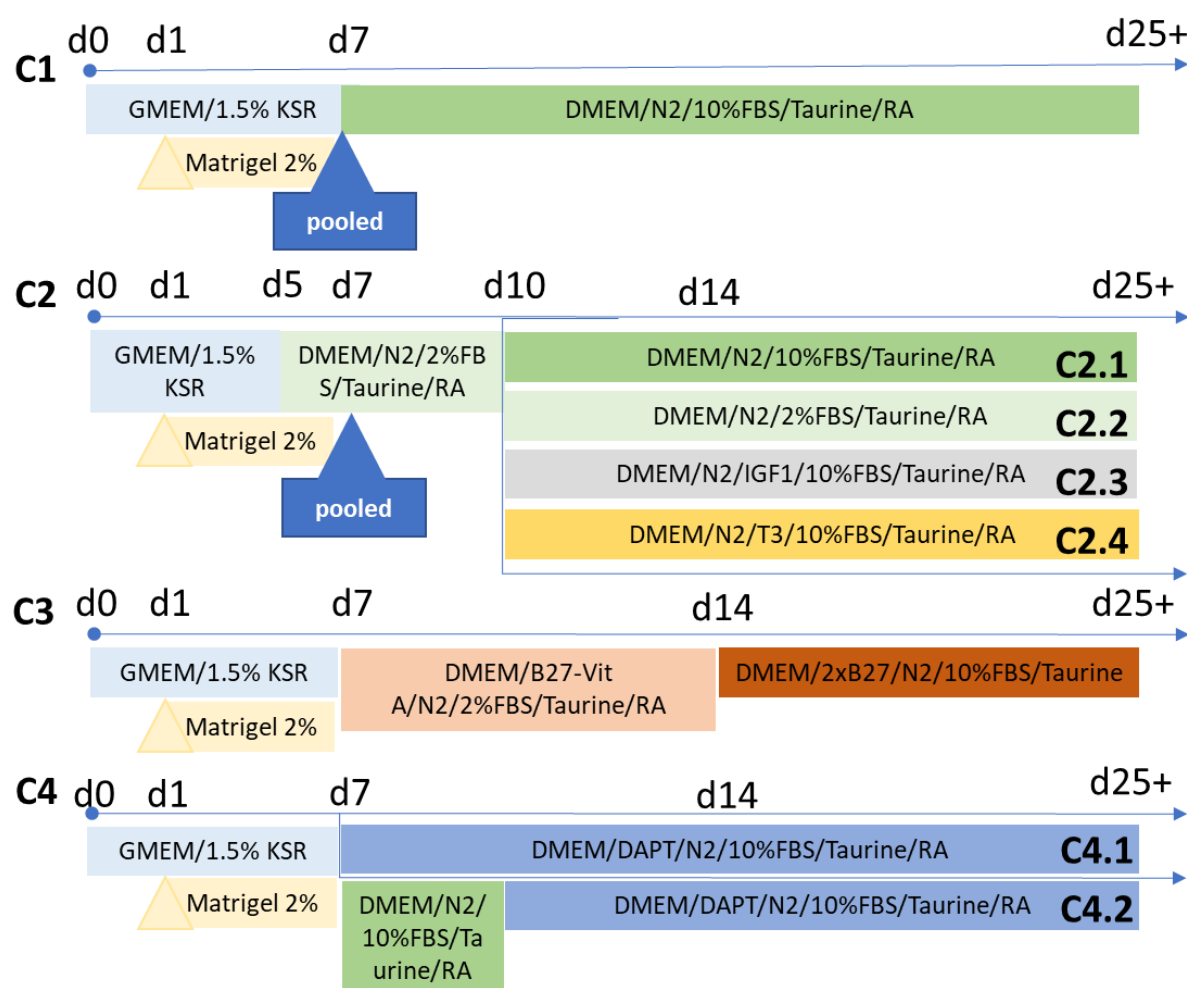
Figure 3.12. Schematic of retinal differentiation culture conditions including supplementation of retinal cues tested on rat XA ESC line (Conditions summarised as Experiment 7 in Table 3.8). Retinoic acid (RA) was removed from media at day 14.

To test the hypothesis that accelerating the addition of maturation media, which includes neuralising supplement 'N2', retinoic acid (RA), taurine, and FBS would improve retinal differentiation by accelerating the support of developing NE, the Sasai (C1) method was adapted (Fig. 3.12). In C1 the maturation media is added from day 7 (instead of day 10) consistently until the end of differentiation.

Modifications made to the Sasai SFEBq method in C2 were hypothesised to improve retinal structure and presence of mature retinal cells from studies generating mouse PSC-derived ROs (Table 1.3, Fig. 3.12). In C2 the maturation media is added earlier at day 5 instead of 10 (Fig. 3.12). From day 10 the C2 condition includes either the unmodified maturation media with 10% FBS (C2.1), or a lower percentage of FBS (C2.2), or with retinal stimulants such as IGF1 (C2.3), or T3 (C2.4) (Fig. 3.12). It was hypothesised that these method variants would have a positive impact on retinal development as suggested by mouse RO differentiations and rat retinal explant studies (Table 1.2, 1.3; Distefano et al., 2017; Sevilla-Romero et al., 2002, Decembrini et al., 2014). Organoids derived in these conditions were pooled in culture from day 7 in order to improve allow inter-cellular paracrine signalling between organoids and enable stimulation by IGF1.

Another method variant, condition 3 (C3), includes the addition of the retinal supplement used often in neuronal differentiations, B27-supplement, which is used in some optimised mouse retinal organoid differentiation protocols (Decembrini et al., 2014; DiStefano et al., 2017). This also accelerates the timepoint of addition to day 7 of a richer maturation media including RA/T, N2 and FBS alongside B27 (Fig. 3.12).

Finally, the condition termed condition 4 (C4) tests the addition of Notch pathway inhibitor DAPT at 10 µM in the maturation media from either day 7 or 10 onwards (Fig. 3.12). This was reported to accelerate cell cycle exit during mESC retinal differentiation and encourage differentiation of PR (Osakada et al., 2008).

The development of organoid morphology and protein expression and cellular identity was compared throughout stages of differentiation up to day 14.

The morphology of the aggregates formed after plating was good in all conditions with quick aggregation by day 1, phase-bright NE evident between day 3-5 with further development of OVs seen by day 7 (Fig. 3.13).

Method	D1	D3	D5	D7
C1/3/4				
C2				

Method	D10	Method	D14	Method	D14
C1		C1		C2.1	
C2		C1 (96 wp)		C2.2	
C3		C3		C2.3	
C4		C4 (DAPT d7+)		C2.4	
		C4 (DAPT d10+)			
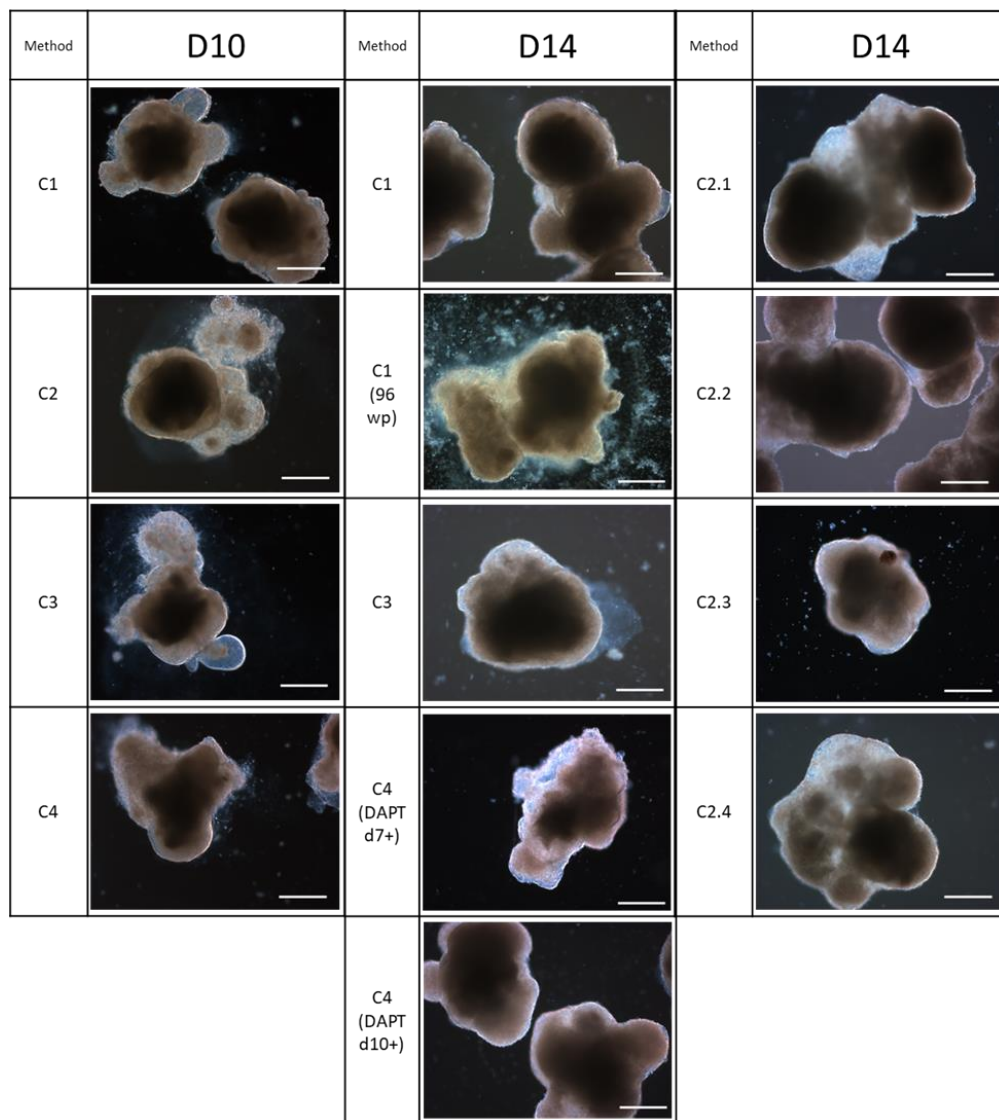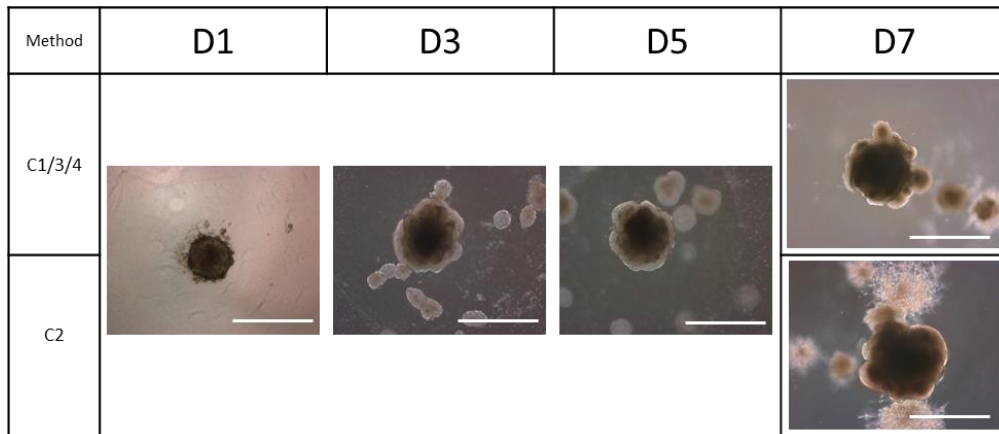
Figure 3.13. Representative bright-field morphology showing the effective aggregation and development of neuroepithelium and retinal morphology in XA ESC-derived organoids until day 14 in experiment 7. C = Condition. D = day. In C4 DAPT is added either from day 7 (d7+) or day 10 (d10+) onwards. N (experiment) = 1, n (organoid) = 144. Scale bar = 500 μm.

There was continued positive morphology in all conditions (C1-4) up to day 10 (Fig. 3.13). At day 10 organoids generated in C1 and C3 showed the most promising morphology with very bright OVs formed of NE tissue illustrated by microscopy (Fig. 3.13). In other conditions, such as C2 and C4, there is also presence of regions of defined NE however OVs are less bright and defined (Fig. 3.13).

The retinal morphology generated in these organoids was not quantified due to insufficient number of high-throughput images being collected at each timepoint. Therefore, the images shown in Fig. 3.13 are illustrative of each condition but cannot be used to quantitatively compare differentiation efficacy between conditions.
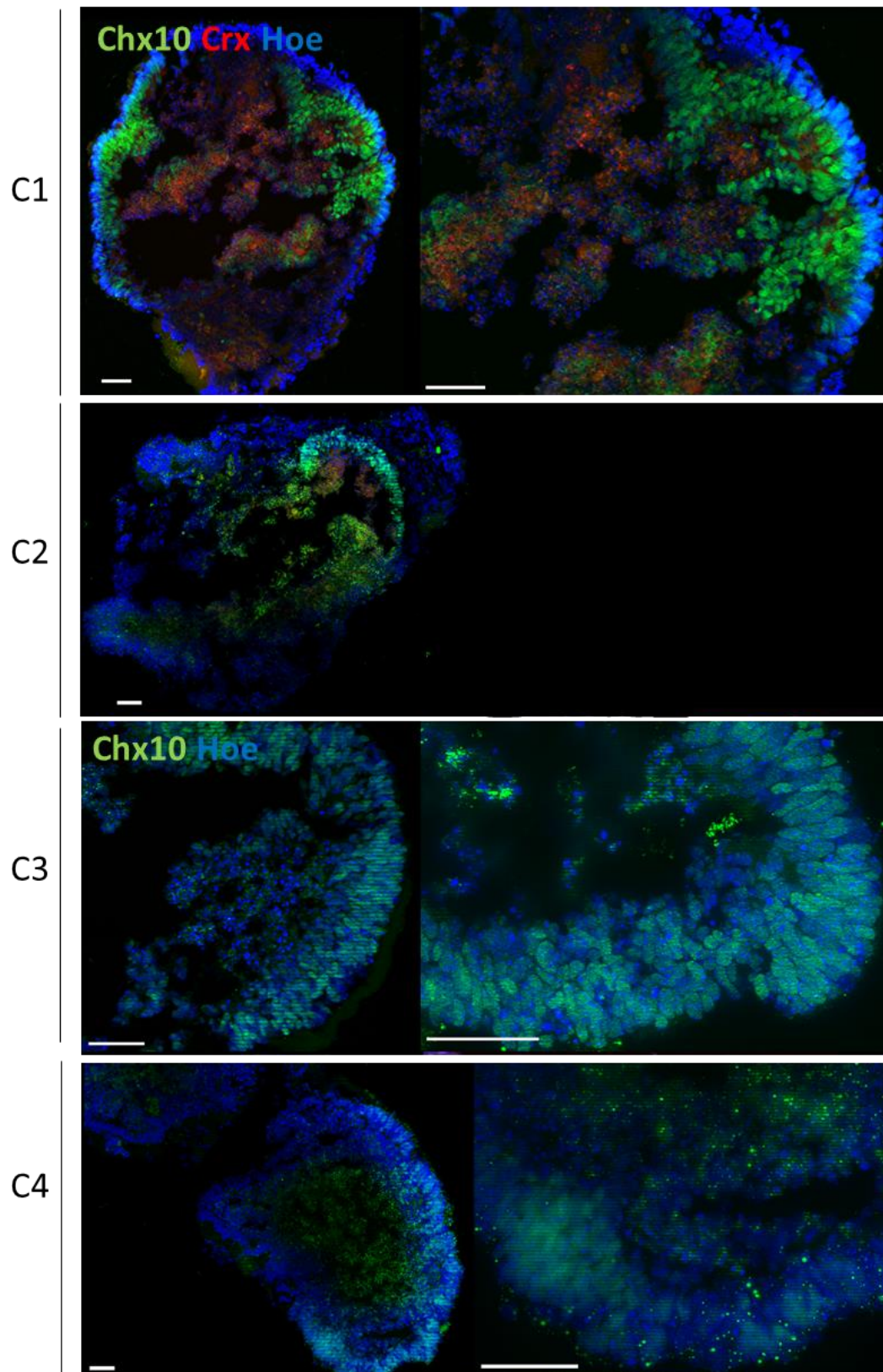
Figure 3.14. Presence of retinal progenitor cell marker Chx10 detected at day 10 of differentiation in rat XA ESC organoids. Red signal for Crx staining in C1 and C2 samples is background levels only. Samples nuclear counterstained with Hoescht (Hoe). n = 8. Scale bar = 50µm. C = condition.

This was accompanied by clear Chx10 expression in rosette structures below the apical edge in C1 and at the periphery of C3 organoid samples (Fig. 3.14). These regions in C1 and C3 correlate with Pax6 expression where signal is localised to tightly packed columnar nuclei at hinged regions of the organoid periphery (Fig. 3.15). Furthermore, the RGC/amacrine cell marker Hu C/D is also detectable at locations basal to the periphery (Fig. 3.15). This is good evidence for neural-retinal identity and generation of RPCs present in these structures which is further supported by their characteristic optically bright NE morphology which was seen at day 10 (Fig. 3.13). The marker for PR precursor cells, Crx, was assessed in C1 and C2 samples however only background levels of reactivity were observed (Fig. 3.14).

RPC marker Chx10 is present to some extent in C2 organoids however it could only be detected at a relatively low (10x) magnification suggesting weak expression and this effect is further seen in C4 samples (Fig. 3.14). In C2 samples Pax6 and Chx10 expression are detected in a lamina of cells while Hu C/D expression is detected in a cluster of cells at the periphery of the organoid indicating a lack of retinal lamination (Fig. 3.14, 3.15). In C4 samples bright Pax6 signal does not localise clearly to organised nuclei (Fig. 3.15). Together with lack of clear Chx10 expression this suggests this method is ineffective for generating NE in this cell line (Fig. 3.15). This is further supported by morphology where the apical edge of C2 and C4 organoids are dimmer and bordered by regions of cells with non-retinal morphology (Fig. 3.13).
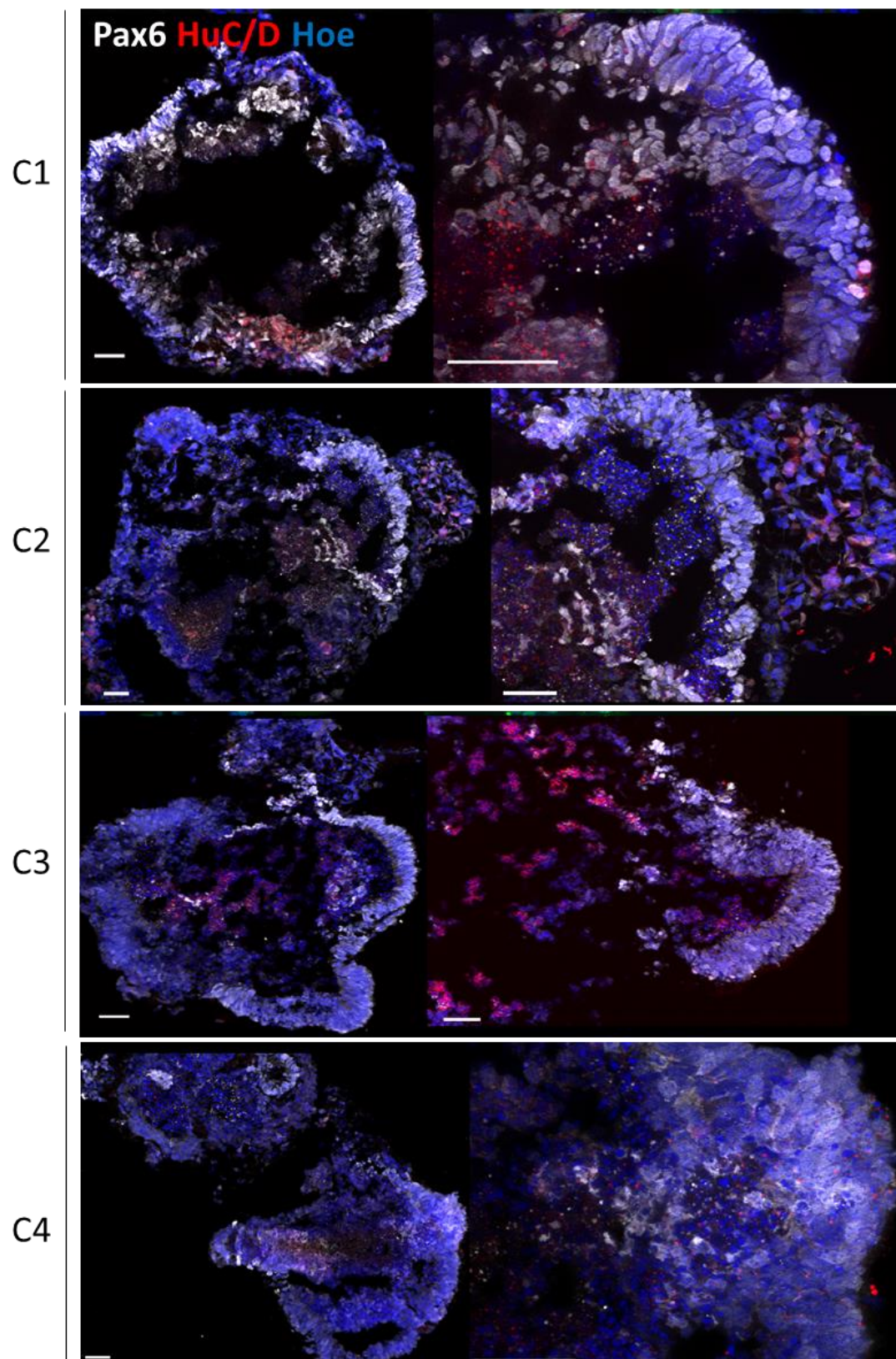
Figure 3.15. Presence of neural-retinal transcription factor Pax6 and RGC/amacrine cell marker Hu C/D detected at day 10 of differentiation in rat XA ESC organoids differentiated in experiment 7. Samples nuclear counterstained with Hoescht (Hoe). n = 8. Scale bar = 50µm. C = condition.

Further retinal development was assessed morphologically and by other retinal cell markers using IHC. Maintenance of phase-bright NE was seen to some extent in C1 (pooled), C2.3, C3 and C4.1 however in the remaining conditions the optical brightness and structural definition of the NE tissue declined (Fig. 3.13). Retinal protein analysis of C1 (pooled) samples showed the presence of RPCs (Chx10+) and RGCs (SNCG+) in organoids (Fig. 3.16a, c). However, analysis for NE cells (Pax6), PR progenitor cells (Crx), PRs (Rcvrn) and S-cone PRs (OPN-S), showed no true expression pattern (Fig. 3.16a, b, c).
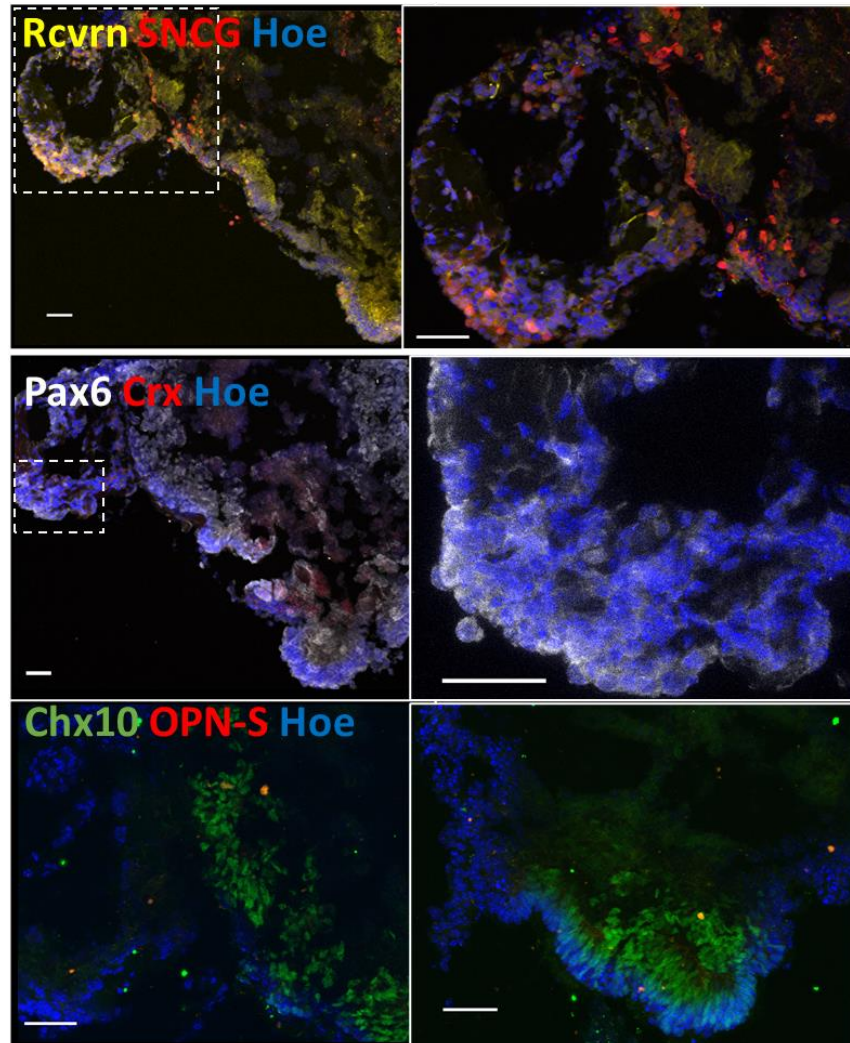
Figure 3.16. Presence of RGC cell marker SNCG and RPC marker Chx10 detected at day 14 of differentiation in rat XA ESC organoids differentiated using C1 in experiment 7. (a) Rcvrn and SNCG co-stain (b) Pax6 and Crx co-stain (c) Chx10 and OPN-S co-stain. Retinal markers Rcvrn, Pax6, Crx and OPN-S show background expression levels only. Samples nuclear counterstained with Hoescht (Hoe). Dashed boxes show area of magnification in right panels. N (experiment) = 1. n (organoid) = 8. Scale bar = 50μm.

IHC data for other conditions are summarised in Table 3.1. IHC analysis showed all conditions, except C4.2, by day 14 generated RGCs (SNCG+) (Table 3.1). C4.2 showed diffuse staining of RPC marker Chx10 at day 10, suggesting lack of RPC differentiation may have impacted RGC generation (Fig. 3.14) However, across all conditions other retinal markers were lacking, with only C1 (pooled) expressing Chx10 at day 14 (Fig. 3.16c, Table 3.1). Other conditions with positive morphology (C2.3, 3) showed bright staining for PRs (Rcvrn) however the localisation of positive cells was not found at apical regions indicating lack of progressive retinal structural organisation from NE stage onwards (Table 3.1).

Table 3.1. Summary of IHC analysis on day 14 XA ESC-derived organoids from experiment 7. Key: + = positive signal localised correctly, ~ = weak positive expression not correctly localised, - = no clear expression. Markers assessed are those indicative of neural-retinal development. Summary of assessment of morphology for this stage and presence of RPE-like pigmentation.

Marker / Condition	Rcvrn	SNCG	Pax6	Chx10	S-opsin	Morphology	Pigment
1 (pooled)	-	+	-	+	-	~	+
1 (96 wp)	-	+	-	-	-	-	-
2.1 (10% FBS)	~	+	-	-	-	-	-
2.2 (2% FBS)	-	+	-	-	-	-	-
2.3 (IGF1)	~	+	-	-	-	+	+
2.4 (T3 10nM)	-	+	~	-	-	~	-
3 (B27)	~	+	~	-	-	+	+
4.1 (DAPT D7+)	-	+	-	-	-	+	-
4.2 (DAPT D10+)	-	-	-	-	-	+	-

The morphology of organoids deteriorated from day 14 onwards in all conditions therefore, IHC analysis was not performed for later timepoints. Pigmented patches were observed in C1 (pooled), C2.3 and C3 at day 14 indicating successful retinal cell differentiation (Table 3.1). These conditions had positive retinal morphology suggesting RPE was generated (Fig. 3.17).
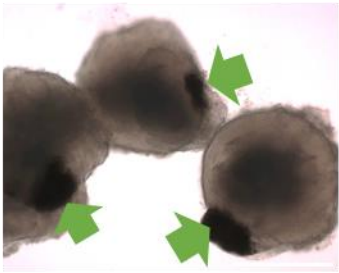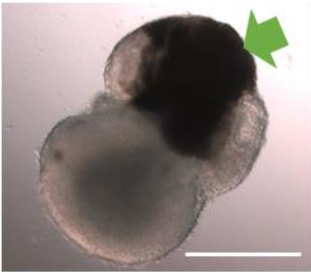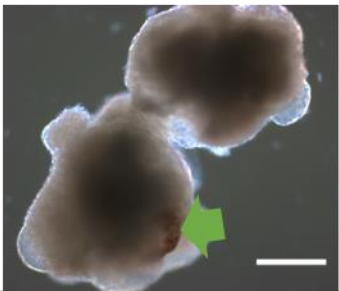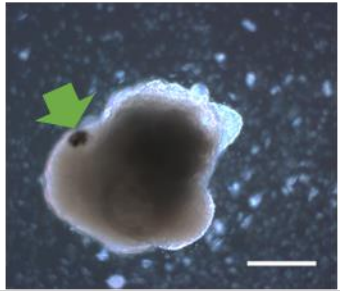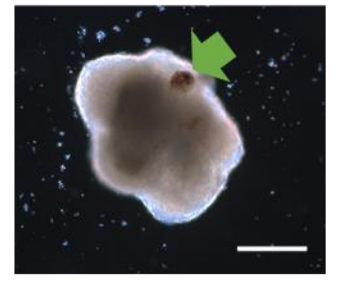
	D14 (pooled)	D14 (96 wp)	D17 (pooled)
Expt 5/C1			-
Expt 7/C1		-	
Expt 7/ C2.3		-	-

Figure 3.17. Evidence of pigmented cell growth from XA ESC-derived organoids in differentiation experiments 5 and 7. Green arrows show pigmented presumptive RPE. Scale bar = 500 μm. C = condition. D = Day.

In summary, methods testing the addition of growth factors such as B27 (C3) and IGF1 (C2.3) to the media compositions had a beneficial effect on RO morphology and development. These conditions showed the most promising retinal characteristics with prolonged maintenance of phase-bright tissue which co-localised with retinal protein marker expression and pigmented patches (Fig. 3.17; Table 3.1). The addition of Notch inhibitor DAPT at day 7 in C4.1 reduced the prevalence of definitive Pax6+/Chx10+ neural retina (Fig. 3.14, 3.15) as well as the RGC marker in comparison with all other conditions (Table 3.1). Pooling of organoid improved both the morphology and prevalence of retinal protein markers (Table 3.1; Fig. 3.13-15). None of the conditions showed retinal lamination or convincing retinal development beyond approximately day 17.

3.3.2 Investigating the source of pigment in rat PSC cell line-derived retinal organoids

Interestingly, the XA ESC cell line was reported to be generated from an albino rat (personal communication, Dr Xabier Aranguren, UNAV (2017)). This warranted further molecular investigation into the underlying source of the pigmentation seen in XA ESC-derived organoid samples. It was suggested by the research scientist that the cell line may be contaminated with wild-type mouse ESCs. To investigate this a mESC line was obtained from an academic colleague (K. Gassner IDIBELL Bellvitge Biomedical Research Institute, Llobet-Navas research group) and cultured to obtain mouse cDNA as a positive control for analysis. Primers were designed to target cDNA sequences for pluripotency genes *Sox2*, *Oct4* and *Nanog* specific to either rat or mouse species. RT-PCR was carried out on all rat and mouse stem cell lines as well as a biological negative control (iMEFs). The primers were found to be species-specific as they selectively amplified one set of genes in either the rat or mouse stem cell samples (Fig. 3.18). However, in the reactions from XA ESC cDNA, amplicons were generated using both rat and mouse-specific primers for *Oct4* and *Nanog* suggesting contamination of the rat XA ESC line with mouse ESCs. (Fig. 3.18).
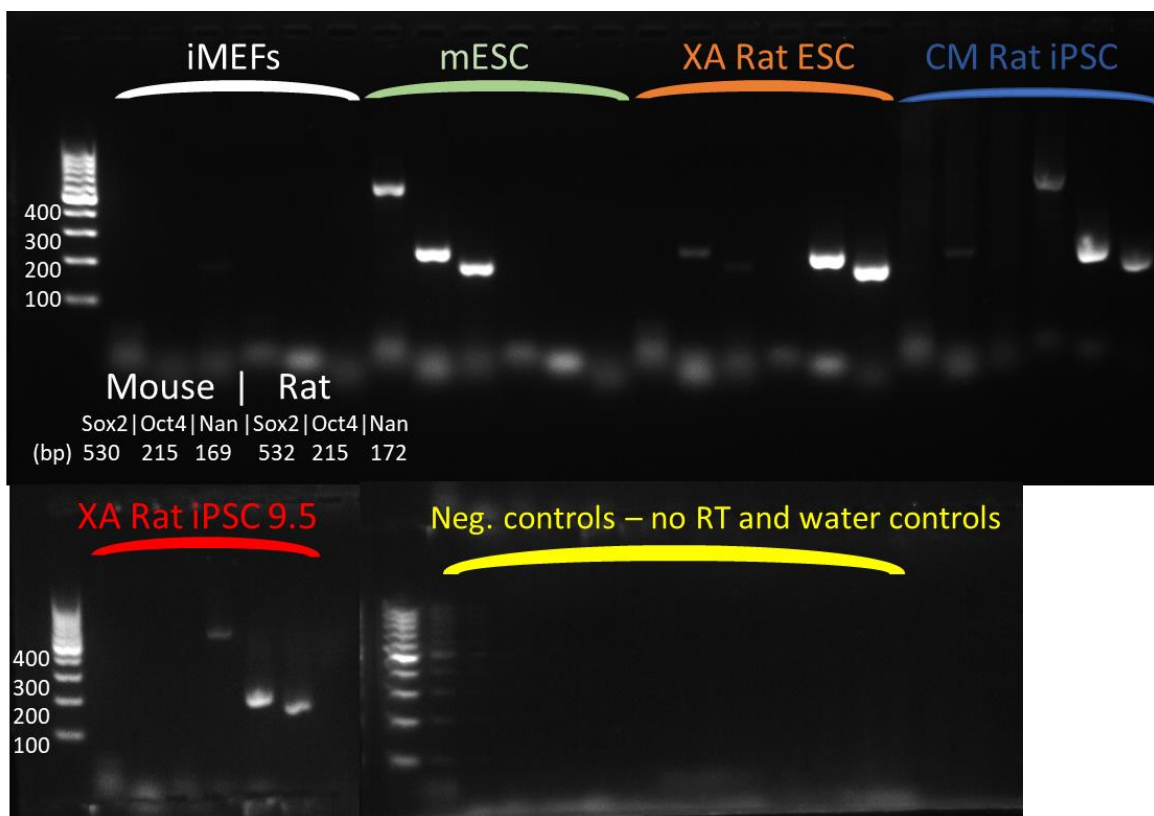
Figure 3.18. RT-PCR assessment of rat (XA ESC, CM iPSC, XA iPSC 9.5) and mouse (mESC) stem cell lines and irradiated MEF (iMEF) cDNA using rat or mouse species-specific primers for pluripotency genes Sox2, Oct4 and Nanog (Nan). Sequence of reactions was kept the same as annotated for "iMEFs". Negative control samples include no reverse transcription (RT) samples and water only.

To further investigate this finding, RT-PCR was carried out in a similar way using cDNA extracted from XA ESC-derived ROs which appeared pigmented from day 14. Mouse and rat retina cDNA samples were used as species-specific positive controls and iMEF cDNA as a biological negative control. Organoid cDNA generated from an alternate rat cell line (CM iPSC) which showed positive retinal morphology at day 5 was also analysed. Primer pairs were designed to target exon-spanning species-specific sequences for *Pax6* and *Chx10*.

The primers were found to be species-specific as they selectively amplified one set of genes in either the rat or mouse retina samples (Fig. 3.19). An amplicon was detected in the rat retina sample using mouse *Chx10* primers at a length of > 400 base pairs (Fig. 3.19). This is much larger than the two splice forms expected from this reaction which are lengths of 205 and 262 base pairs. It was found that amplicons for *Pax6* and *Chx10* were generated using mouse-specific primers on XA ESC-derived organoid cDNA in addition to a faint band seen for rat specific *Pax6* (Fig. 3.19). These amplicons are detected in both the day 10 and 14 samples suggesting the samples have been contaminated with mouse gene amplicons. As the negative controls (no RT and water) do not show any amplification of mouse or rat genes this likely did not occur during preparation of the PCR reactions. As the mouse-specific transcripts are also detected in the XA ESC samples this is indicative that the organoids are not derived from a pure population of rat cells but from a mixed culture of mESC and rESC. Amplicons from neither rat nor mouse-specific primers were detected in organoids derived from an alternate rat iPSC line (CM) therefore this sample was re-analysed (Fig. 3.20).
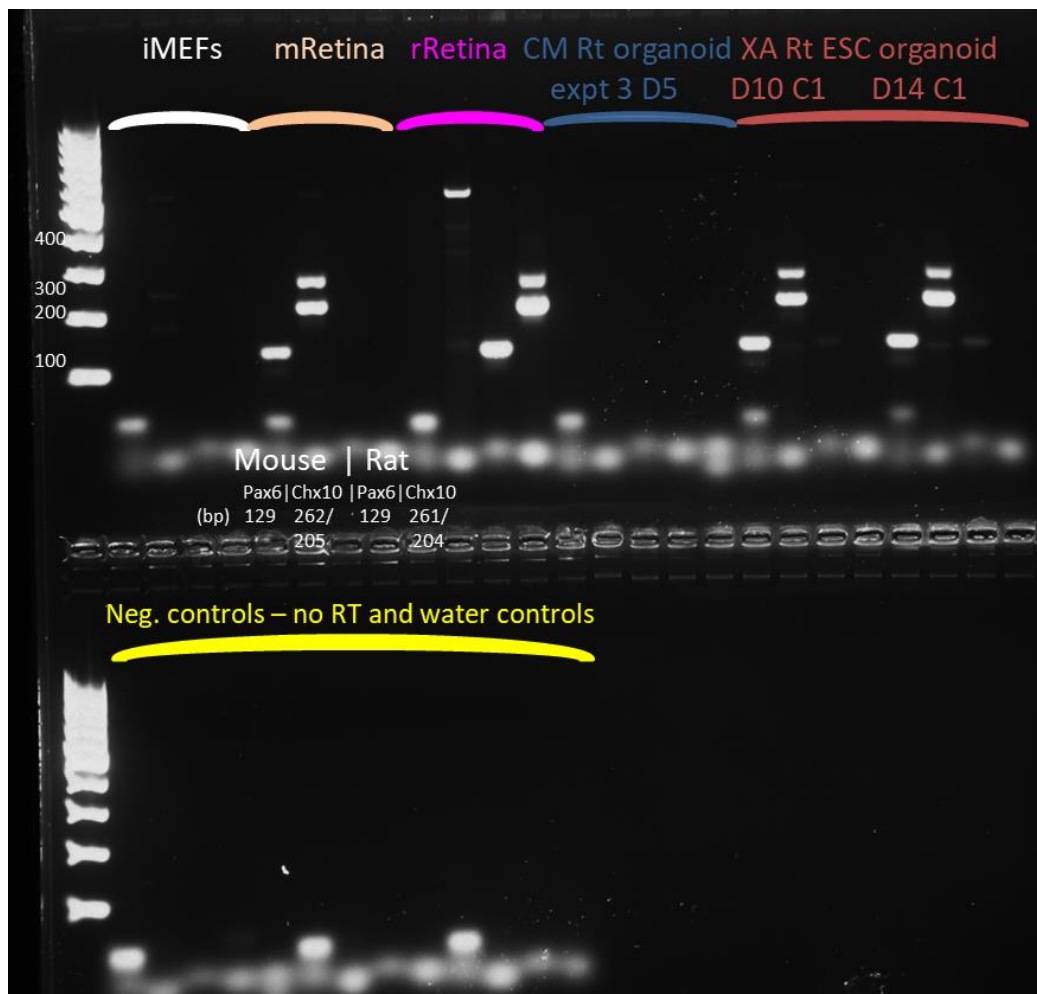
Figure 3.19. RT-PCR analysis of neural-retinal genes using species-specific primers for Pax6 and Chx10 on cDNA samples of; iMEFs as a negative control, mouse retina (mRetina) and rat retina (rRetina) as species-specific positive controls and on rat CM iPSC derived organoids and rat XA ESC derived organoids which showed pigmentation. The sequence of retinal primers was consistent between samples as annotated for "mRetina".. D = Day, C = Condition.

The use of both native mouse and rat retina in this PCR alongside the sample cDNA and positive results was considered to validate the specific primer pairs used for this analysis. Similarly, for the primer sets for pluripotency genes *Nanog*, *Sox2* and *Oct4* these are considered to be valid for use due to the clear, single bands of expected length generated in the mESC and rESC control cDNA samples.

Assessment of another CM iPSC-derived organoid sample using mouse and rat specific primers was performed to resolve the amplification of a product using mouse specific *Oct4* primers in the iPSC line (Fig. 3.18), and the lack of product amplification from CM iPSC organoid sample cDNA (Fig. 3.19). Gene expression analysis of cDNA from CM iPSC organoid sample (D5 C1 5000 cells/well) shows

expression of rat retinal gene markers (Rt Pax6 and Rt Chx10) as well as rat-specific pluripotency expression (Rt Sox2, Oct4 and Nanog) and shows no amplification for either mouse retinal genes (Ms Pax6 and Chx10) or mouse pluripotency gene markers (Ms Nanog and Oct4) (Fig. 3.20).

GENE	Gapdh	Rt Pax6	Rt Chx10	Ms Pax6	Ms Chx10	Rt Sox2	Rt Oct4	Ms Nanon	Ms Oct4	Rt Nanog	Gapdh	Rt Pax6	Rt Chx10	Ms Pax6	Ms Chx10
bp	184	129	261/204	129	262/205	446	215	169	215	172	184	129	261/204	129	262/205
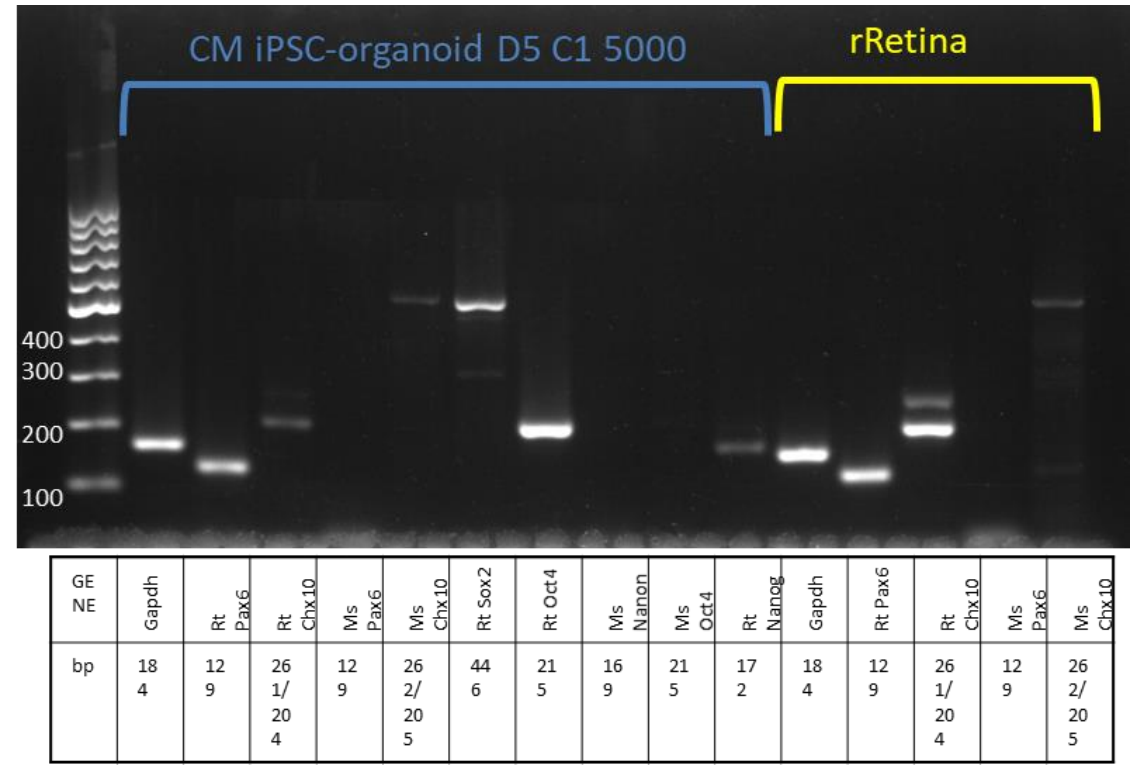
*Figure 3.20. RT-PCR analysis of pluripotency (Sox2, Oct4 and Nanog) and neural-retinal genes (Pax6 and Chx10) using species-specific primers on cDNA samples of; rat retina (rRetina) and on rat CM iPSC derived organoids. Expected amplicon size is listed below gel lane in base pairs (bp). Rt = Rat, Ms = Mouse, D = Day, C = Condition, * = Unspecific binding.*

The band amplified using the Ms Chx10 primers is of a much larger size than expected indicating non-specific binding to another product (Fig. 3.20; asterisk). Additionally, this band is also seen in the rat retina sample indicating that it is not of mouse origin (Fig. 3.20). Therefore, this organoid sample was not contaminated with mouse PSC, in contrast with XA ESC-organoids which show strong amplification of retinal genes with mouse specific primers (Fig. 3.19). This also suggests the CM iPSC line was not contaminated with mouse cells or gene products prior to the differentiation of these cells.

In summary, species-specific gene amplification via RT-PCR of the XA ESC line shows the expression of mouse alongside rat transcripts pluripotency genes *Oct4* and *Nanog*, and organoid samples

derived from this line also show expression of mouse retinal genes *Pax6* and *Chx10*. This line was effective at generating organoids with NE and OV morphology which may have arisen from the mouse cells.

This data together with the fact that the rat XA ESC cell line was originally derived from an albino animal, suggests the pigmented cells in XA ESC-derived organoids have been generated from contaminating mouse stem cells. These cells have likely developed alongside the rat cells throughout organoid differentiation and given rise to retinal cells of mouse identity. This could be conclusively confirmed by the use of species-specific primers for RPE-specific genes such as *RPE65*.

The alternate rat PSC lines (CM iPSC and XA iPSC) tested in this chapter did not generate pigmented organoids and do not show gene expression of mouse identity as determined by RT-PCR indicating their suitability for the generation of rat ROs in the future.

3.4 Discussion

3.4.1 Rat PSC culture

The method to culture all rat PSC lines used two chemical inhibitors and Leukaemia Inhibitory Factor (2i/LIF). These were based on the published methods they were originally derived with. The rat PSC culture method differs to that used for mouse PSC culture, however, was able to maintain rat PSC colonies with a characteristic, smooth, domed appearance with tight borders. Adherence to the feeder cell layer was poor and large colonies often detached, therefore the sub-passaging technique was carefully controlled to reduce cell loss.

3.4.2 Rodent retinal tissue shows specific reactivity of primers and antibodies

To validate the techniques used for analysis of retinal cell identification in rat ROs, rat and mouse primary retinal tissue was obtained for use as a positive control. Antibodies for known retinal differentiation markers were tested on rat retinal tissue by immunohistochemistry to validate them for organoid screening.

Although the use of rat and mouse adult retina can be used to validate the general use of antibodies and primers for that species, as a calibrator for quantitative gene expression there are some caveats. As retinal markers can be expressed in multiple cell types with different expression levels during embryonic and adult stages, the best calibrator for organoid gene expression would be rat retinal tissue collected at the relevant gestational stages. This has been achieved in studies which use human ROs and embryonic retinal samples to temporally align the retinal development in organoids with that of native retina and enable the accurate staging of retinogenesis (Collin, Queen, et al.,

2019; C. S. Cowan et al., 2020). In this case it was not possible to obtain embryological samples as the adult rat tissue was only available as a surplus from other ongoing research projects.

Therefore, in this chapter, the undifferentiated iPSC sample was used as a calibrator for rat organoid gene expression. In the very early stages of development this allows a more meaningful measure to be calculated showing any transition towards the neural-retinal identity as an upregulation in gene expression.

3.4.3   Limited retinal development with iPSC line and mouse Sasai protocol

The differentiation protocols C1-5 were developed in studies using mESC (Eiraku & Sasai, 2012; Kruczek et al., 2017; Ueda et al., 2018) or human ESC (Kuwahara et al., 2015) and were first tested on the rat iPSC and ESC lines without any modification (Fig. 3.1). Organoid samples were analysed for retinal differentiation efficiency by assessing organoid morphology and gene and protein expression of known markers for retinal cellular identity.

The experiments showed initial success with effective cell aggregation and development of phase-bright NE tissue achieved in the early stages of differentiation between day 1-7.

It was shown that methods adding Matrigel at day 1 resulted in uniform and spherical cell aggregation, as seen in mouse PSC-derived organoids using the SFEBq culture technique (Eiraku & Sasai, 2012). The addition of Matrigel is notable as it is rich in ECM-proteins including laminin, usually expressed and secreted by neighbouring RPE cells (Aisenbrey et al., 2006). The addition of other defined proteins present in ECM has been shown to promote NR development, and in some cases induce transdifferentiation of RPE cells into neuronal cells *in vitro* (Dorgau et al., 2019; Reh et al., 1987). This suggests the addition of Matrigel improves retinal cell culture likely by a combination of the physical support and signalling molecules (Benton et al., 2014).

In the early stages of differentiation both C1 and C2 methods and two/three cell plating densities generated morphology of NE tissue in CM iPSC and XA ESC-derived organoids between day 3 -9 (Fig. 3.6, 3.7). Gene and protein expression analysis of early retinal marker genes confirmed the NE identity of the tissue by IHC and RT-qPCR of early-stage organoid samples (day 5 and 7) (Fig. 3.8, 3.9).

From day 10 onwards there was a loss in NR morphology seen in rat PSC-derived organoids (Fig. 3.7). The phase-bright smooth edge was replaced by an irregular darkened organoid periphery and OV-like protrusions from the organoid were lost in place of uncharacteristic, disrupted structures

suggestive of a loss of retinal identity. This was not confirmed molecularly; however, the change from the typical NR morphology showed significant divergence from retinal development.

Rat iPSC (CM iPSC and XA iPSC) derived organoids were more susceptible to this change compared to XA ESC-derived organoids (Fig. 3.6). Within the ESC-derived organoids plating density had an effect with 3500 cells/well showing the least non-retinal morphology (Fig. 3.7). Moving forward I decided to use exclusively the XA ESC line for differentiation optimisation experiments with the aim of applying the most effective method onto iPSC lines. Focusing on method development with 1 line later had significant implications when the XA ESC line was found to be contaminated.

3.4.4   Method adaptations including excision of ROs and retinal stimulant supplementation

It was hypothesised that an explanation for the loss in NR morphology seen from day 9 was that phase-bright NE regions of the organoid were not excised from the main organoid as performed by the Sasai lab using the same culture protocol (Eiraku & Sasai, 2012). This approach has the benefit of separating visible retinal structures from mis-differentiated cell types which may have an undesirable effect on the course of retinal differentiation (Decembrini et al., 2014).

To evaluate this method the excision of NR regions and pooling of excised regions in a 24-wp format was tested compared to culture in 96-wp. Comparing between excision at day 7 or 10 showed no substantial difference; however, the excised conditions did show a difference to the uncut control condition in terms of retinal protein marker expression and retinal morphology. Due to the experimental design of pooling the excised regions together, it was difficult to quantify any significance due to the excision. Furthermore, the labour-intensive nature of manual excision experiments is a significant disadvantage to a culture method which aims to deliver a high throughput testing platform. The optical brightness of the NR was reduced between day 20-30 in the excised conditions however, IHC analysis showed continuous layers of Rcvrn+ and Rho+ cells at the apical edges of the organoids at day 30 indicating long term maintenance of PR cells. In light of the later investigation of XA ESC line fidelity, this positive retinal development in the samples may be due to contaminating mouse cells present in the XA ESC line.

In order to further improve culture conditions various method adaptations were made including; to accelerate the addition of retinal maturation media which includes factors hypothesised to support retinal growth namely RA/T and N2. The rationale for earlier inclusion of N2 supplement, a factor developed to support neuronal growth, is to reduce non-retinal differentiation. N2 supplement is a synthetic serum-free additive containing a defined mixture of growth factors shown to have a

supportive effect on neuronal cell development (Bottenstein and Sato, 1979). It was derived to replace the need for serum addition which also supports neuronal growth and cell proliferation, however, has an undefined composition and can exhibit batch variability (Bottenstein and Sato, 1979).

N2 and B27 supplements were derived for the optimised growth and culture of neuronal cells and the maintenance of rat embryonic neurons (Brewer et al., 1993; Brewer and Cotman, 1989). The addition of these supplements were therefore tested at an early stage of differentiation in experiment 7/C3 to evaluate these supplements (Brewer et al., 1993; Brewer and Cotman, 1989).

The addition of molecules T3 (triiodothyronine) and DAPT to cell culture media were also tested based on studies showing them to have a proactive effect on retinal development and lamination *in vivo* and *in vitro*. T3 is known to play a role in the development of the CNS of all mammals (Di Liegro, 2008). Specifically, in the rat retina it is important for retinal lamination, as shown by T3 deficient models which have reduced retinal thickness and decreased retinal growth at the perinatal stage (Sevilla-Romero et al., 2002). A study on thyroid hormone metabolism in the rat retina showed a peak in T3 production at PND 5 suggesting a role in synaptogenesis in the retina (Ientuile et al., 1984). Other groups have added T3 to mouse ESC and human differentiation methods, in combination with other molecules BMP4 and DAPT, to improve the generation of opsin containing cells (Ueda et al., 2018; (Eldred et al., 2018; Wagstaff et al., 2021). Therefore, in experiment 7/C2 I tested the addition of T3 to culture at a time corresponding to the perinatal period of ~day 10-20 of differentiation to evaluate its potential to improve retinal structure.

The Notch pathway is active in RPCs and Müller glia and therefore stochastic disruption of it is likely to cause neuronal differentiation and loss of structure due to its expression by Müller glia (Mills and Goldman, 2017). Notch inhibitor DAPT has been used for promoting neuronal differentiation in human ESC cultures by confirming cell fate determination in Rax+/Pax6+ progenitors (Riazifar et al., 2014) and in retinal differentiation from mouse ESC Crx+ cells were stimulated to acquire photoreceptor cell identity (Osakada et al., 2008). To investigate these outcomes with rat organoid differentiation the addition of DAPT from day 7 or 10 within retinal maturation media was tested.

The results from these various method variants showed that the acceleration of retinal maturation media to day 7 and addition of B27 and N2 supplements and IGF1 improved retinal morphology and protein marker expression in XA ESC-derived organoids, thereby improving retinal differentiation from day 7 -14 (Table 3.1). However, it also gave rise to organoids with pigmented cells in these conditions from approximately day 14 onwards (Fig. 3.17). This is likely to represent the generation

of RPE cells, as these appeared alongside areas of positive retinal morphology and arose at an appropriate timepoint for RPE development (Table 1.1).

In vivo pigmentation is found solely in melanocytes (skin) and RPE cells, which are derived from the neural crest and optic cup (Miroslawa Cichorek et al., 2013; Mirosława Cichorek et al., 2013). To confirm that the pigmented cells in the organoids are putative RPE cells, RPE-specific gene expression could be assayed for using highly sensitive RT-qPCR. As *Mitf* primers were validated in rat tissue, future work could further investigate the identity of the pigmented cells in late-stage organoids by performing RT-PCR with species-specific primers.

3.4.5   Pigmentation showed identity of XA ESC line is mixed chimeric mouse/rat

The unexpected results showing pigmentation in the XA ESC-derived organoid samples, and gene expression analysis detecting mouse retinal transcripts in XA-ESC ROs indicate there are wild-type mouse retinal cells expressing those transcripts which are likely also responsible for the generation of the pigmented cells (Fig. 3.17). The presence of mouse pluripotency gene transcripts in the XA ESC samples further show the contamination from mouse cells originated in the starting stem cell population (Fig. 3.16). This was also later confirmed by the lab from which they were sent (Dr X. Aranguren, personal communication).

Interestingly, the expression of mouse *Oct4* and *Nanog* in the XA ESC sample is much less bright than that of the rat transcripts indicating a smaller relative population of mESC present however during differentiation the mouse specific *Pax6* and *Chx10* transcripts become dominant over the rat variants suggesting the conditions are favourable to support mouse ESC differentiation over rat. However, as PCR is not a quantitative method further quantitative analysis is required to verify this hypothesis. To confirm this RT-qPCR would need to be performed using a standard curve to quantify the relative amounts of rat and mouse specific transcripts produced at each stage throughout differentiation.

This could be performed to determine if rat cells are less responsive to the same RO differentiation conditions and may require different conditions that mESC. A way to further test this would be the concurrent differentiation of fluorescently labelled mouse and rat PSC with the same culture conditions to assess at which point development differs between the species. Mouse and rat ESC differentiation in parallel has been investigated in chapter 4 experiments.

The mixed identity of the XA ESC line invalidates the further use of this cell line for the generation of rat ROs as they will be chimeric. In light of the chimerism of the XA ESC line, the relevance of the method optimisations made with this line to inform general rat PSC retinal differentiation may be

questioned. As it seems the mouse cells in the mixed culture over-proliferated in comparison to the rat cells during the course of the differentiation the conditions may have been optimised preferentially towards mouse differentiation requirements rather than rat. Therefore, the optimisations found to have a positive impact on XA ESC retinal differentiation, such as B27 and IGF1 addition, excision and pooling of organoids will need to be first re-tested on a confirmed rat PSC line. Furthermore, it highlights the vigilance required for cell culture to avoid contamination of this kind and the need to perform independent verification of cell lines acquired from other sources.

Analysis of species-specific gene expression in the other rat PSC lines (CM iPSC, XA iPSC) used to generate organoids showed no contamination of mouse transcripts. These lines can therefore be used to generate rat ROs in future experiments and the data collected in this chapter from these cell lines can be used to inform future work. Moving forward another rat ESC line will be obtained, verified using species-specific primers, and exposed to adapted retinal differentiation protocols.

Chapter 4

Chapter 4 Rat and Mouse ESC retinal differentiations and method comparison

4.1 Modified rodent retinal differentiation methods

4.1.1 Serum free embryoid body formation with quick aggregation protocol

The serum free embryoid formation with quick aggregation (SFEBq) strategy for generating self-organising retinal organoids (RO) developed by the Sasai group was shown in the previous chapter to have some success generating 3D organoids from rat iPSC and a hybrid rat--mouse ESC line up to day 10 (Eiraku & Sasai, 2012).

~~Further beneficial modifications included the use of a rotating bioreactor from day 10 onwards to improve waste removal and nutrient circulation. Organoids were also dissected or kept intact at day 10 or these were pooled in mixed culture from day 7 onwards, which increased the size of neural retina (NR) structures (DiStefano et al., 2017).~~

In this chapter both the unmodified (Eiraku & Sasai, 2012) and the optimised SFEBq (DiStefano et al., 2017) (Fig. 4.1) differentiation methods will be used to differentiate mESC and a newly obtained rat ESC (rESC) line in parallel. mESC and rESC derived organoids will be compared in terms of morphological development and protein expression to enable validation of the SFEBq technique and a direct species-species comparison.
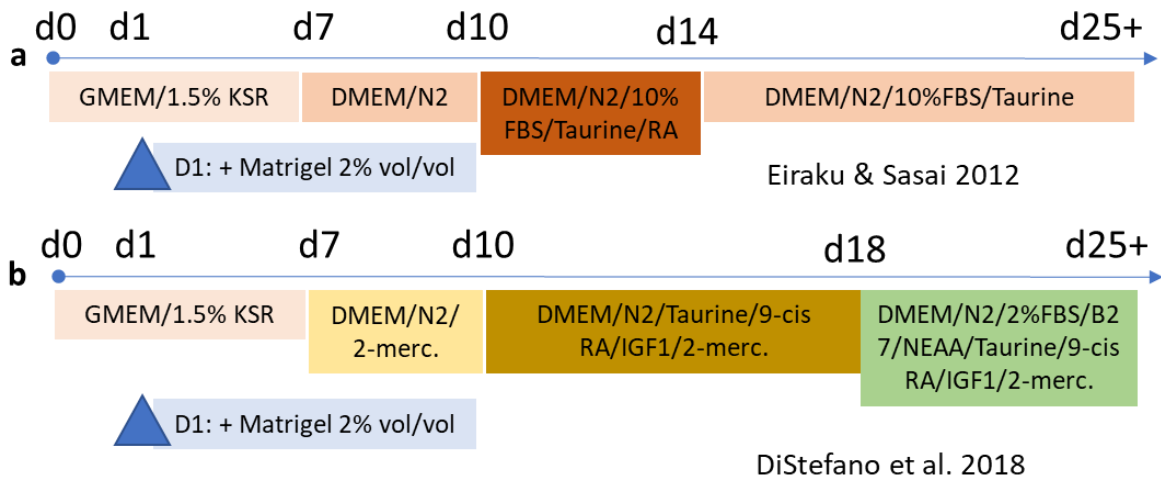
Figure 4.1. Comparison of retinal organoid differentiation protocols published for mouse ESC (a) Sasai protocol using serum-free embryoid body formation with quick aggregation technique (SFEBq) (Eiraku & Sasai, 2012) (b) Adapted SFEBq method supplementing IGF1, 9-cis RA and B27 to the culture media (DiStefano et al. 2018). DMEM = DMEM-F12.

4.1.2   Chemically directed approaches

In previous rat differentiation experiments, difficulties were encountered with the maturation of the rat pluripotent stem cell (PSC) derived organoids using the SFEBq methods published for mouse differentiation, as retinal morphology of the structures deteriorated beyond day 9.

In addition to performing a validation of SFEBq methods using mESC, it is hypothesised that effective rat retinal differentiation requires optimisation. Therefore, in this chapter neural and retinal differentiation methods published for rat PSCs will be used to provide another basis for the derivation of 3D ROs from rESCs.

The condition termed "C1", tested on rESC consists of the media components used in the Qu et al. method from day 0-14, followed from day 14 by the retinal maturation media used in the Sasai protocol (Eiraku & Sasai, 2012). Additional method variants (C1 +SAG) were tested in parallel, with media additives hypothesised to improve retinal maturation and development.

The addition of SAG, which acts on the smoothened (Smo) pathway to stimulate sonic hedgehog (Shh) and Wnt pathways, was tested between day 9-14 as this has been implicated in the stimulation of RPC growth in mouse retina (Y. Wang et al., 2005). SAG was specifically chosen as it has also been shown to increase RPC proliferation in human RO differentiation experiments using the SFEBq technique (Nakano et al., 2012) (Table 1.2).

The addition of Wnt inhibitor CK1-7, Nodal inhibitor SB-431542, and Activin-A in the media applied during early rESC differentiation (C2; Fig. 4.~~3~~2, C4; Fig. 4.~~4~~3) was based on the use of these molecules between day 0-5 to effectively differentiate neural-retinal organoids from mESC (Osakada et al. 2009) (Table. 1.2). These molecules were also effective for EB generation between day 0-21 in hESC differentiation protocols implying conservation of these developmental mechanisms between mammalian species.

The ECM-rich component Matrigel has both been included and excluded in effective mouse RO differentiations (Osakada et al. 2009; Eiraku and Sasai 2012). Previous differentiation experiments in chapter 3 ~~(3.3.4)~~ using rat CM iPSC and XA ESC lines showed effective EB and NE formation with Matrigel addition ~~(Fig. 3.8, 3.10)~~. Therefore, C1 and C2 included Matrigel supplementation to generate EBs (Fig. 4.~~3~~2, 4.~~4~~3).

The growth factor IGF1, has been implicated to have a proactive role in PR development in both rodent and human RO differentiation *in vitro*, therefore, method variations C3 (Fig. 4.~~4~~3) included

IGF1 from day 17 onwards, at a time window correlating with PR maturation *in vivo* (Table. 1.1) (DiStefano et al., 2017; Mellough et al., 2015).

The method variations in C3 were also informed by the use of fibroblast growth factor (FGF) which has been effective in studies using rat retina explant tissue for re-aggregation and maturation studies (Table 1.2) (Lillien & Cepko, n.d.; Yourey et al., 2000) (Fig. 4.4~~3~~).
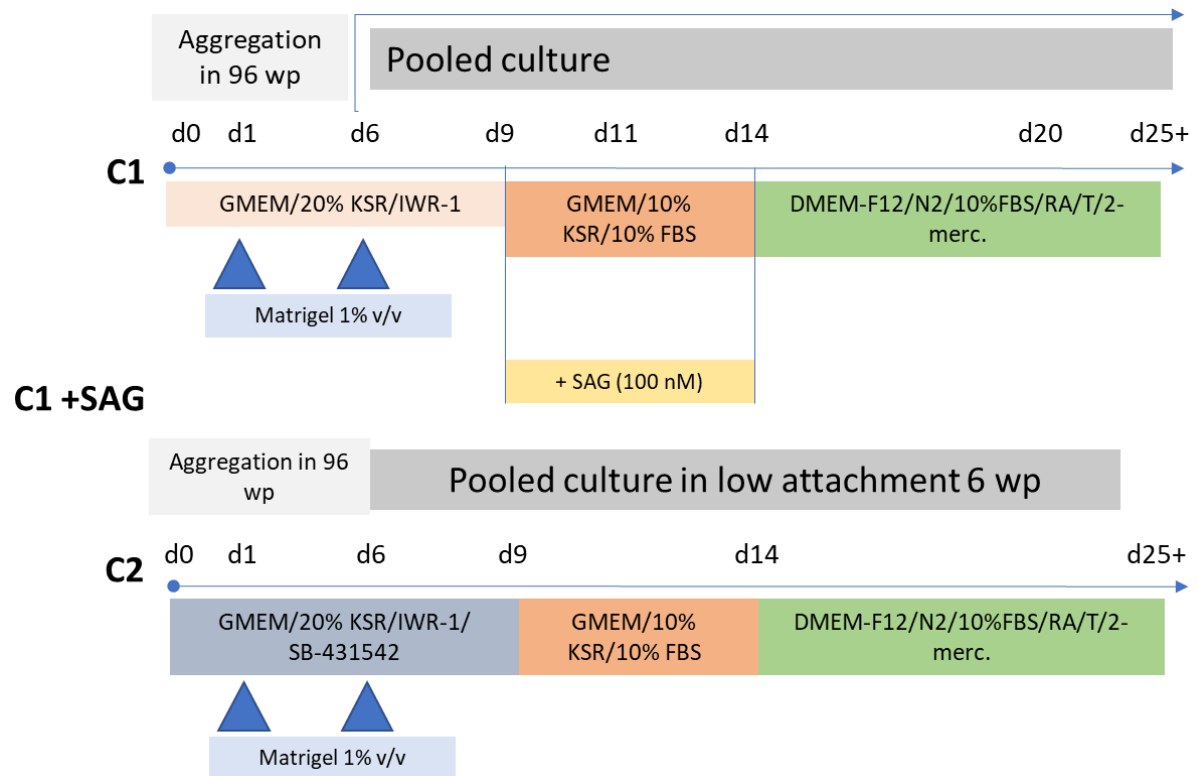
Figure 4.2. Schematic of retinal differentiation methods using chemical signalling molecules based on Qu et al. method tested on rESC: Condition (C) 1 and 2. D = day. Wp = well plate.

To test the capacity of rESC (RRRC) to proliferate into RPCs, a stage of adherent cell culture was included in the development of retinal differentiation methods in this chapter. This stage of adherent culture was applied from day 5, following EB formation (Fig. 4.3). RPCs were subsequently manually detached, following proliferation, to re-aggregate them in 3D suspension culture from either day 11 or 14. Cell aggregates were then cultured in a retinal maturation media, containing FBS, N2 supplement, RA and taurine (Fig. 4.3). It is hypothesised that generation of RPC cells are subsequent maintenance in known retinal stimulants would support specification of mature retinal cell types and the development of a laminated retina structure.

157
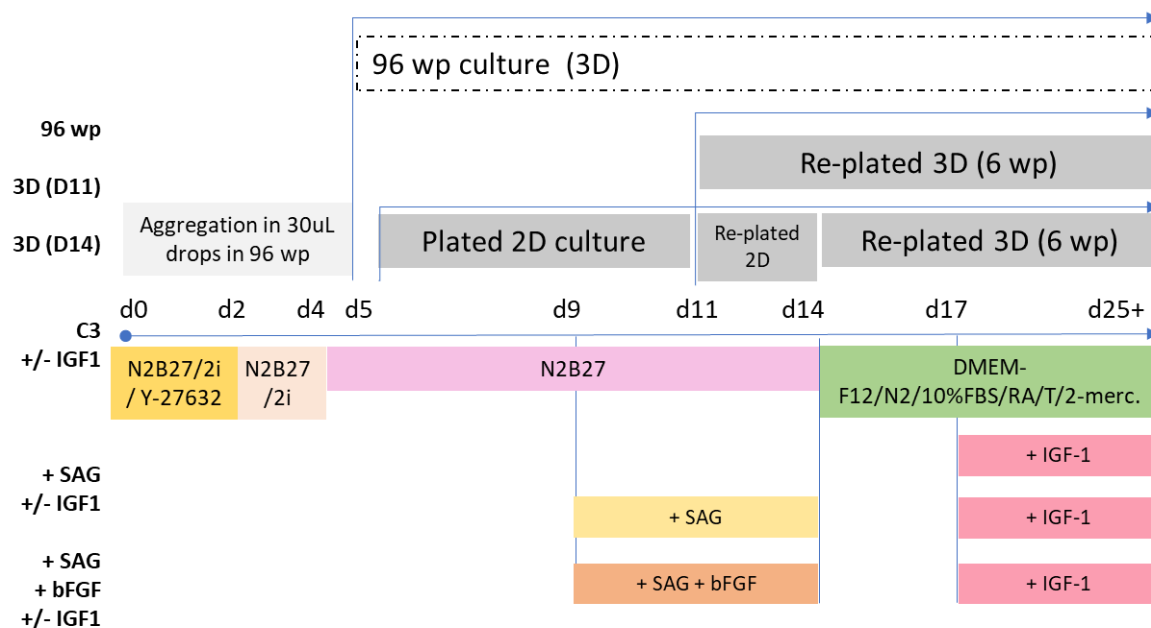
Figure 4.3. Schematic of differentiation methods using adherent culture technique and chemical stimulant addition tested on rESCs: C3. D = Day. Wp = well plate. RA = retinoic acid, T = taurine. 2i = CHIR99021 and PD0325901.

4.2 Chapter aims

A validated rat ESC line (rESC Da.c8 #464) was obtained commercially from the Rat Research and Resource Centre (Missouri, US) in order to facilitate a new round of retinal differentiations. In addition, a mouse ESC line was obtained so that a direct comparison could be made throughout the process of differentiation. This was subject to retinal differentiation by a published protocol to firstly confirm the efficacy of the method in the lab and secondly to enable a direct rat to mouse developmental comparison.

This chapter assessed the new rESC line capacity for retinal differentiation with mouse-specific methods. This was followed by testing additional strategies of differentiation methods shown to be effective on rat stem cells for neural and retinal cell specification, such as adherent cell plating. Furthermore, differentiation methods were modified to incorporate adherent culture and chemical small molecules and growth factors in combination, shown to have a stimulatory effect on *in vitro* rat retinal cell culture or explant growth. These various approaches were tested in order to progress from challenges encountered in the first chapter of the project with applying methods derived for mouse PSCs differentiation directly to rat PSCs.

4.3 Results

4.3.1 Pluripotency characterisation of rat ESC (RRRC) line

To move forward a new rESC line was obtained from the Rat Research and Resource cell bank (RRRC, Missouri, USA) generated from a Dark Agouti (pigmented) line (#464 DA.c8), hereafter referred to as rESC (RRRC). The rESCs were cultured as per the protocol provided by RRRC and showed typical tightly-edged stem cell colony morphology (Fig. 4.4).
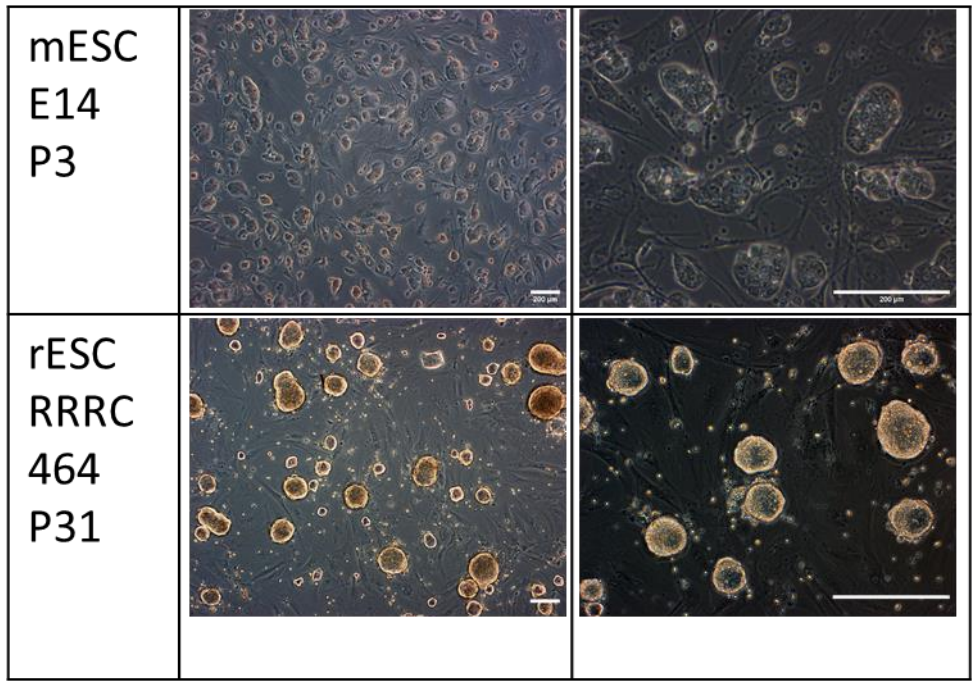
Figure 4.4 Bright-field images showing the morphology of mouse and rat stem cell lines cultured on iMEF feeder cells. Scale = 200 μm

The line has been characterised for pluripotency by the RRRC. To confirm this and the species identity in a similar method to the previous rat cell lines, rESCs were cultured and assessed by RT-PCR using species-specific primers for pluripotency genes (Fig. 4.5). Only amplicons for *Sox2, Oct4* and *Nanog* with rat-specific primers were generated confirming the correct identity of the cell line and its suitability for use in future retinal differentiation experiments.
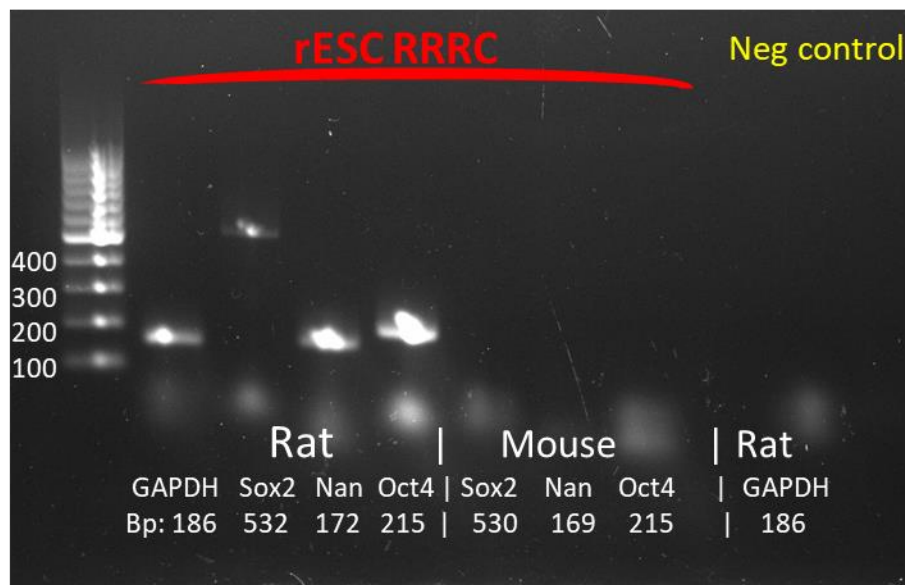
Figure 4.5. RT-PCR analysis using species-specific primers for pluripotency genes Sox2, Oct4 and Nanog (Nan) confirming species identity and pluripotency of RRRC rESC line at passage (P) 26. Bp = shows the expected amplicon length in base pairs. Negative (Neg) control sample contains no RT cDNA.

4.3.2   Mouse ESC comparison with rat ESC retinal differentiation

To confirm the efficacy of several RO differentiation protocols, the widely used SFEBq protocol derived by Eiraku & Sasai for mESC differentiation (Eiraku & Sasai 2012) and an optimised version including retinal growth factors IGF1, B27, and 9-cis RA, (DiStefano et al. 2018) were both tested on mESC . These experiments aimed to replicate and validate the published studies using mESC. These would also help to confirm whether the differentiation method or the difference between rat and mouse responses is causing the lack of effective retinal differentiation seen in previous experiments with rat iPSCs. These experiments were performed with the organoids kept in suspension in 96-wp throughout differentiation rather than pooled culture or excision in order to enable comparison of the media culture components and avoid fusion of the retinal structure.

With both methods the morphological development of mESC was characteristic of retinal differentiation as phase-bright NE tissue was observed by day 5, optic vesicles (OVs) developed by day 7 followed by invagination and optic cup (OC) formation, in one example, by day 10 (Fig. 4.6). Organoids were grown in 96 well-plates (wp) and there was continued growth of the whole organoid and retinal structures with the maintenance of phase-bright neural retina (NR) throughout later stages of differentiation (day 14-21) (Fig.4.6).

160

Method	D5	D7	D10
Sasai (mESC)			
DiStefano (mESC)			

Method	D14	D17	D21
Sasai (mESC)			
DiStefano (mESC)			
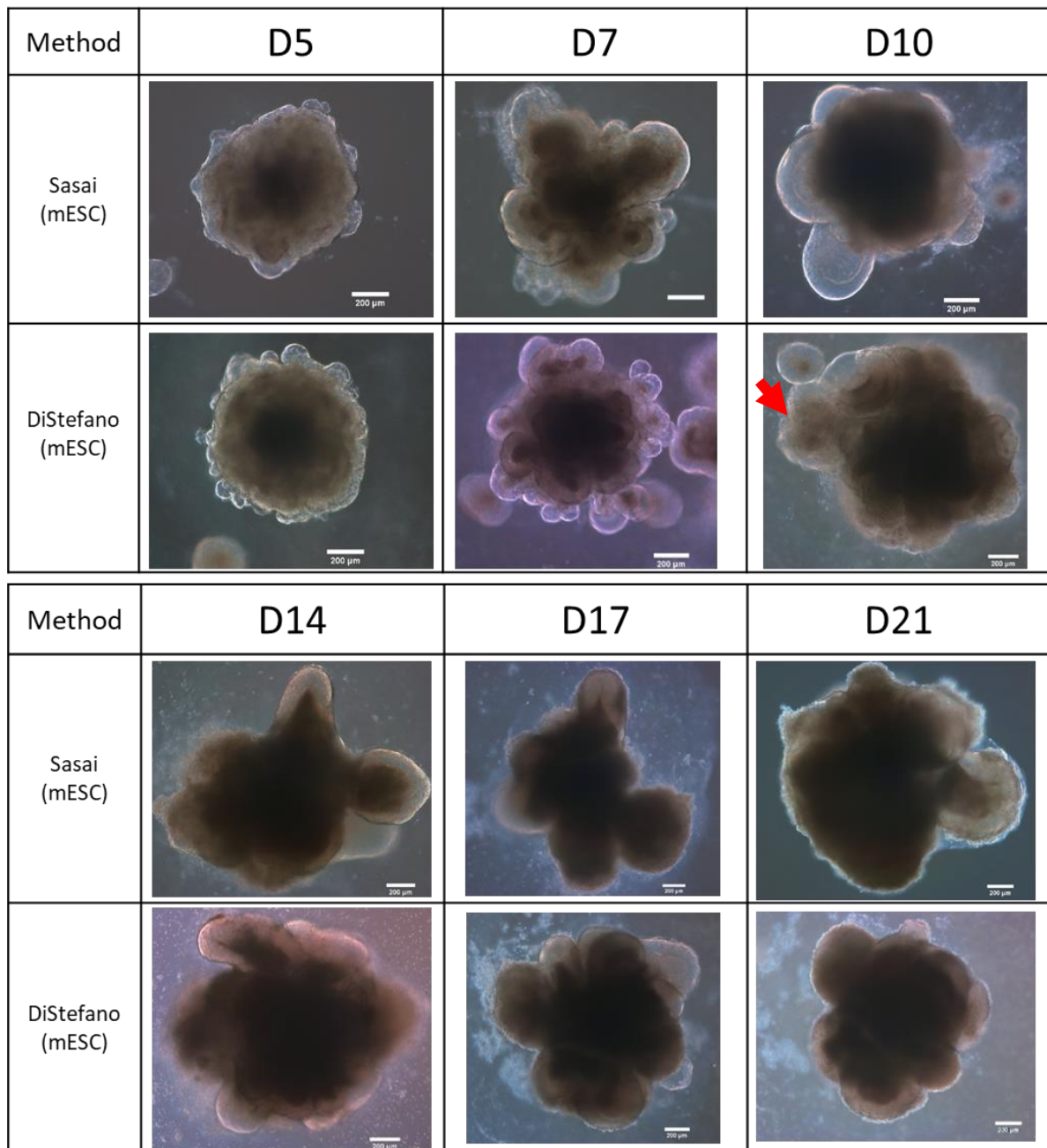
Figure 4.6. Representative bright-field images show developing retinal morphology throughout differentiation of mESC using two published methods. Red arrow denotes optic cup formation. D = day. Representative images of experiment N = 1, organoid n = 384. Scale bar = 200 µm.
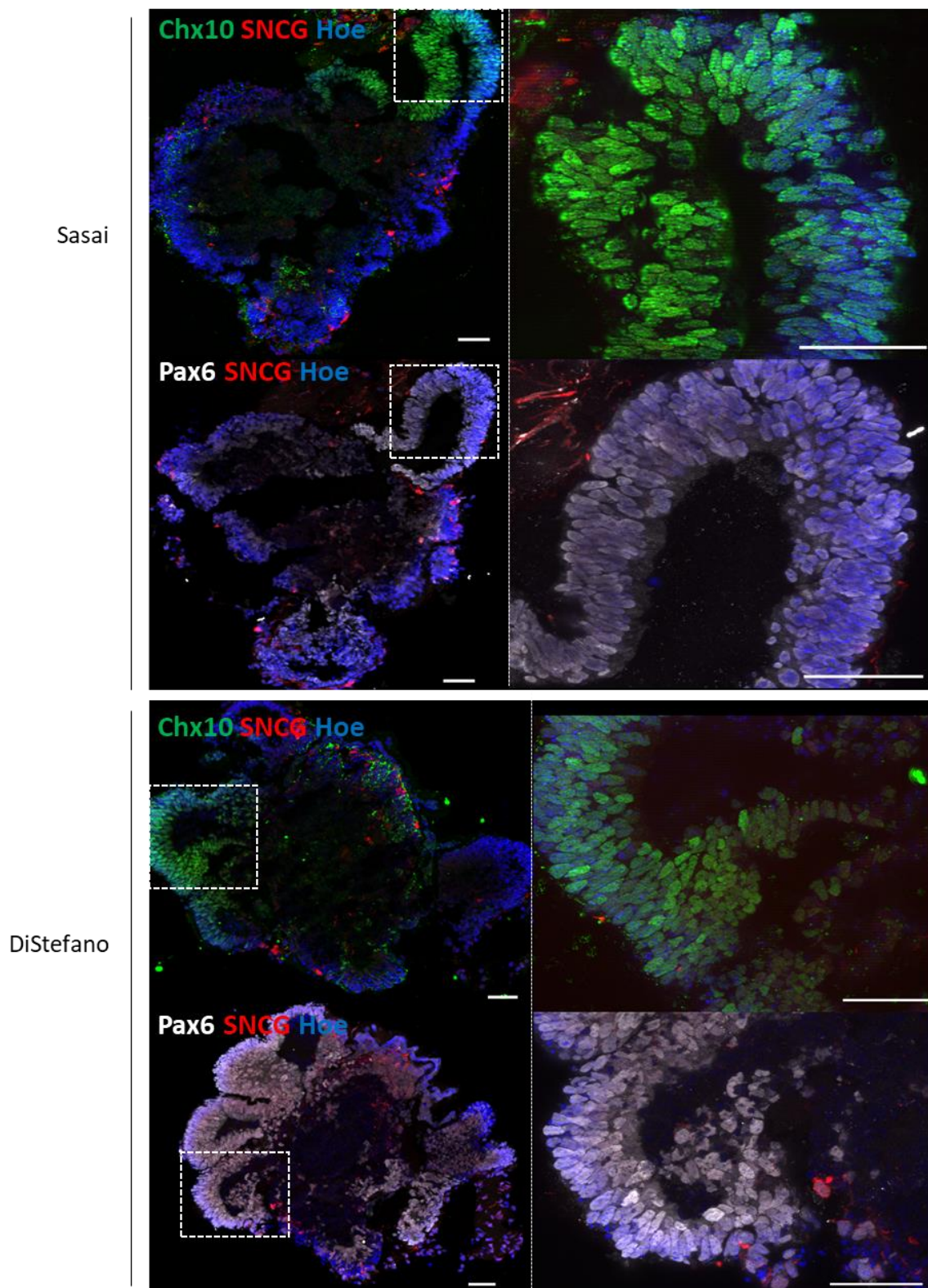
Figure 4.7. IF analysis confirming presence of neuroepithelium (Pax6) and RPCs (Chx10) in mESC organoids derived using two published methods (Sasai or DiStefano) at day 10 of differentiation. Sections counterstained with nuclear dye Hoescht (Hoe). Boxes show areas of magnification. Representative images of experiment N = 1, organoid n = 384. Scale bar = 50 µm.

Immunofluorescence (IF) analysis of organoid samples confirmed retinal cell identity in organoids from both conditions. At day 10 tightly packed laminar nuclei at the periphery of the organoids exhibited expression of Chx10 and Pax6 denoting their identity as NR with the presence of retinal progenitor cells (RPCs) (Fig. 4.7). Due to their shape and localisation in distinct lobes at the organoid periphery these regions likely correspond to the phase-bright NE regions visible by bright-field microscopy (Fig. 4.6).

Further analysis of mESC organoids derived with both the Sasai and DiStefano differentiation methods at day 14 showed continued maintenance of Chx10+/Pax6+ NE with the further development of hinge folding, a process which occurs *in vivo* in the NR prior to the invagination of the OC (Fig. 4.8). As these cells are only found in partial areas of the organoid, these regions likely correlate with the optically bright edge seen in organoids derived with both methods in Fig. 4.6. IF analysis using the Neun antibody, a marker for newly born neurons, shows no cells expressing Neun within the NE lamina (Fig. 4.8).
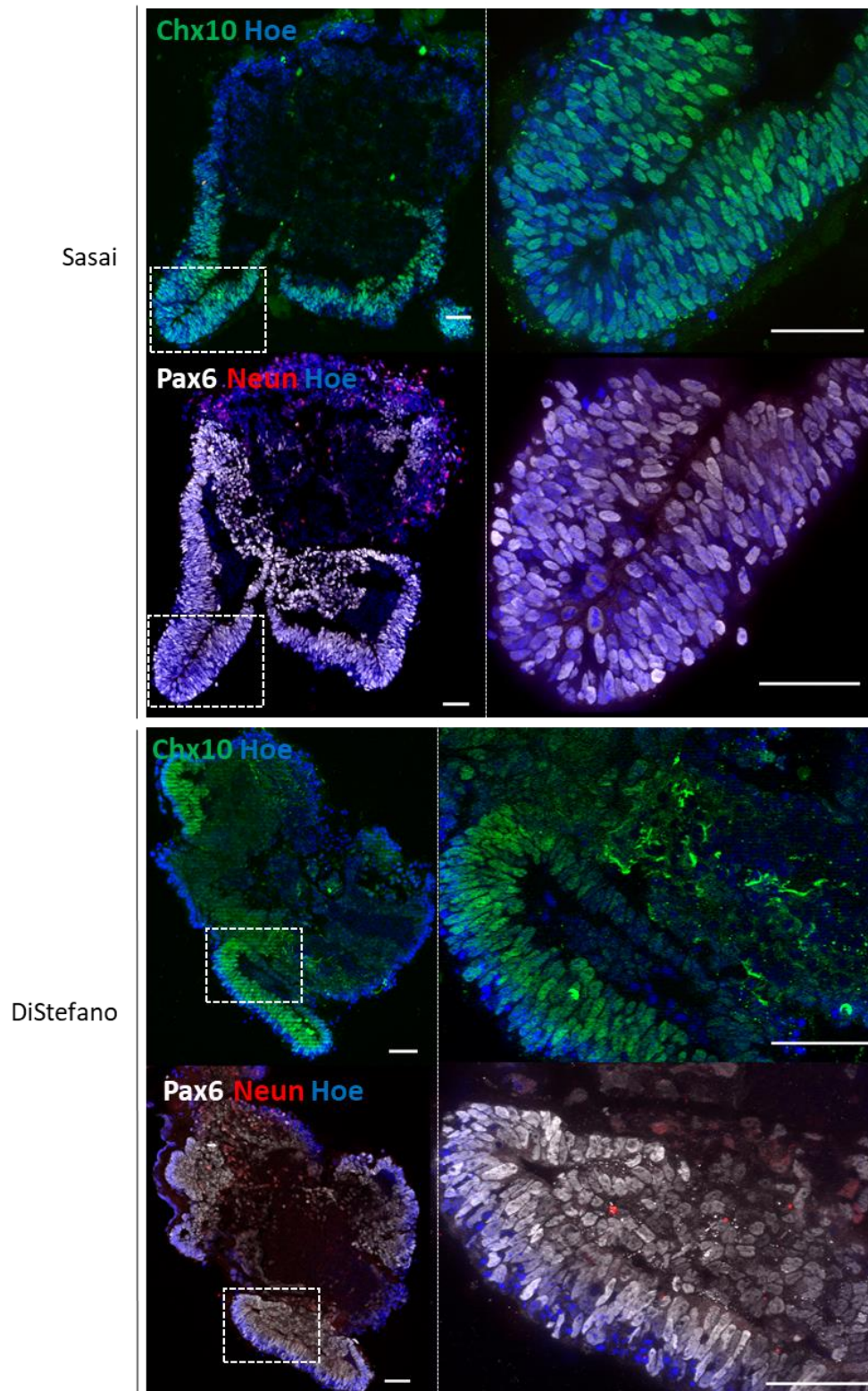
Figure 4.8. IF analysis confirming presence of neuroepithelium (Pax6) and RPCs (Chx10) in mESC organoids derived using two published methods (Sasai or DiStefano) at day 14 of differentiation. Sections counterstained with nuclear dye Hoescht (Hoe). Boxes show areas of magnification. Representative images of experiment N = 1, organoid n = 384. Scale = 50 μm.

By day 21 the bright NR regions are maintained in both conditions although the morphology of the central body of the organoid deteriorated (Fig. 4.6). Supporting the continued maturation of the NR, IF analysis at day 21 shows the presence of mature PR marker recoverin (Rcvrn) within OV structures aligned at basal side of the organoids in both conditions (Fig. 4.9, 4.10). Evidence of structural lamination in these regions is observed, however the expression of retinal ganglion cell (RGC) marker SNCG is present on the apical side of the organoids resulting in an inverted apical-basal polarity of the NR in the Distefano method condition (Fig. 4.9).
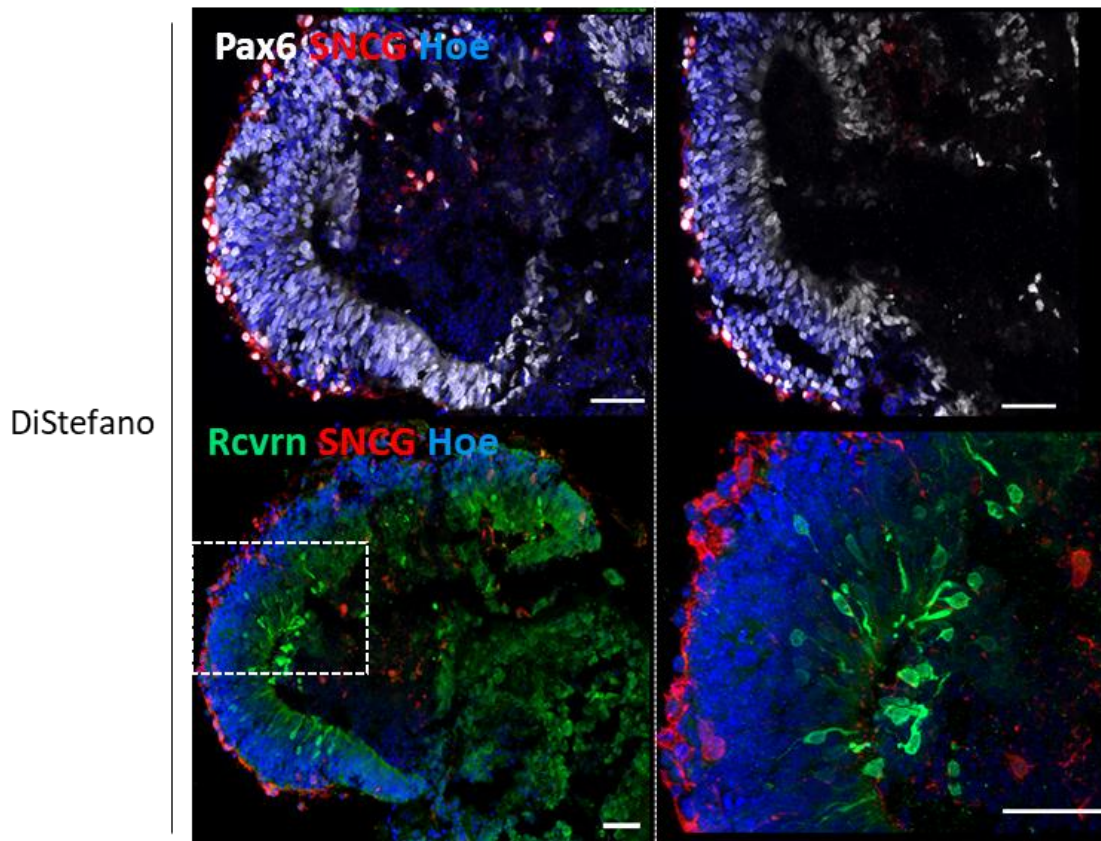
Figure 4.9. IF analysis confirming presence of retinal cell markers recoverin (Rcvrn), SNCG and Pax6 in mESC organoids derived using DiStefano method at day 21 of differentiation. Sections counterstained with nuclear dye Hoescht (Hoe). Boxes show areas of magnification. Representative images of experiment N = 1, organoid n = 384. Scale = 50 μm.

In mESC organoids derived with the Sasai method the retinal lamination is less defined with cells expressing SNCG found on both sides of the NR lamina indicating a lack of structural organisation (Fig. 4.10). Pax6 is also present throughout the apical and basal layers in both conditions indicating a layer of interneurons or the presence of RPCs (Fig. 4.10).
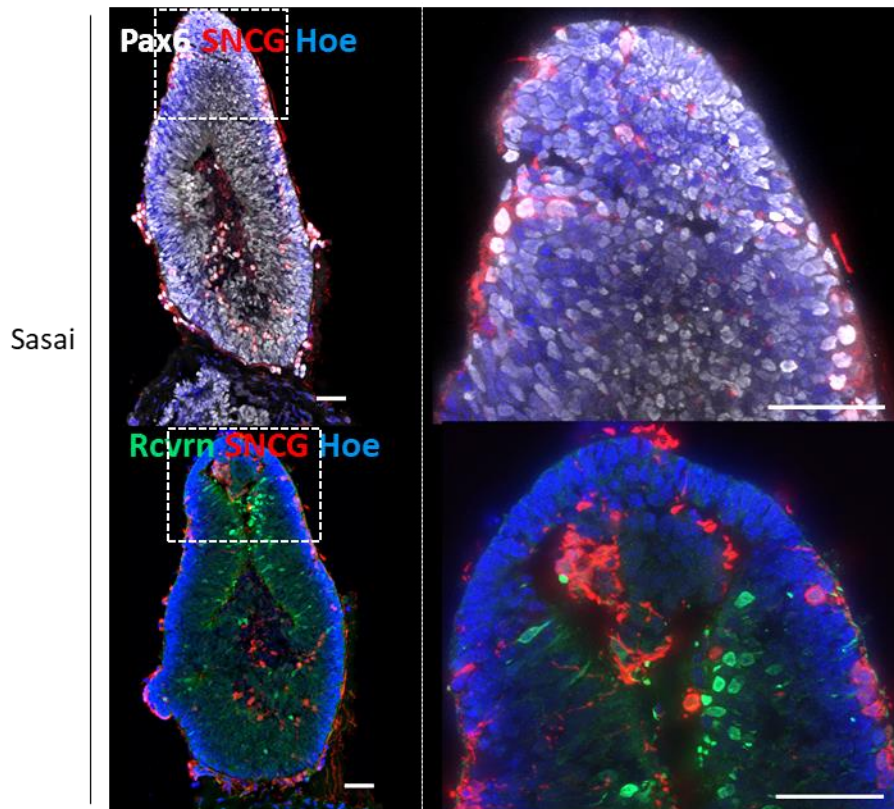
Figure 4.10. Analysis confirming presence of retinal cell markers recoverin (Rcvrn), SNCG and Pax6 in mESC organoids derived using two published Sasai method at day 21 of differentiation. Sections counterstained with nuclear dye Hoescht (Hoe). Boxes show areas of magnification. Representative images of experiment N = 1, organoid n = 384. Scale = 50 μm.

In conclusion, the mESC differentiation experiments assessing two published methods show that 3D ROs can be generated in suspension using the SFEBq strategy with both Sasai and DiStefano culture media conditions. These organoids morphologically show the development of a phase-bright NE lamina and OV/OC structures at timepoints in accordance with published studies and *in vivo* development (Fig. 4.6). Assessment of cellular identity and localisation within the organoids showed RPC (Chx10) and NE (Pax6) markers to localise in OV structures between day 10-14 (Fig. 4.7, 4.8). By day 21 (Fig. 4.9, 4.10) organoids derived in both conditions have matured and generated RGCs and PRs in OV regions. The optimised culture media used in the DiStefano method generated improved organisation of RGC and PR cells relative to each other, although an inverted lamination is seen throughout the tissue (Fig. 4.19). In comparison, Sasai-derived ROs showed no retinal lamination as SNCG+ cells are distributed throughout the NR tissue (Fig. 4.10). This experiment confirms that SFEBq protocols including known retinal stimulants, are sufficient to generate mESC-derived ROs which show retinal morphology and approximate the timeline of mouse retinogenesis *in vivo*. This

method validation suggests that testing rat PSC lines with these methods will reveal whether they have the capacity to respond to these conditions or whether further rat-specific method adaptations are required for RO generation.

4.3.3 Testing the capacity for retinal differentiation from rat ESC (RRRC) line

To assess the potential of rESC (RRRC) line for retinal differentiation, the DiStefano differentiation method that was most effective in mESC differentiation was tested. The direct chronological comparison of organoid morphology highlighted steps of the method that were less effective and require optimisation for successful differentiation from rESC. Clear species-specific differences can be seen from day 1; despite the same plating cell density, the mESC aggregates are larger with a tightly defined edge indicating improved re-aggregation (Fig. 4.11). Between day 1-5 the mESC-derived organoids continued to generate the clear, phase-bright edge resembling NE tissue and OVs develop (Fig. 4.11). These OVs developed and became more defined by day 7 (Fig. 4.12). However, the rESC-derived organoids lost definition as the outer edge became progressively more disorganised and unstructured from day 1-7 (Fig. 4.11). In 100% of organoids rESC-organoids did not show any development of phase-bright NE tissue.

Species	D1	D3	D5	D7
Rat (rESC)				
Mouse (mESC)				
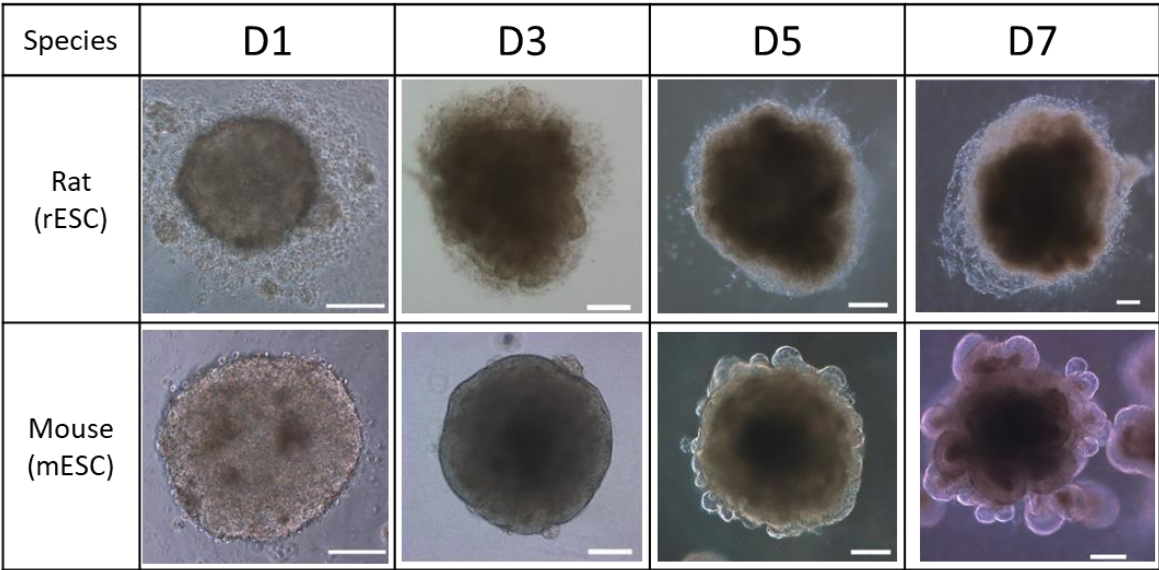
Figure 4.11. Representative morphological comparison of mESC vs rESC (RRRC) derived organoids using the DiStefano method for retinal differentiation. Representative images of experiment N = 1, organoid n = 384. Scale bar = 200 µm. D = Day.

In summary, the rESC (RRRC) line differentiated with the modified SFEBq method (DiStefano et al., 2017) was ineffective at generating organoids with characteristic retinal morphology within the first 10 days of differentiation. Molecular analysis was not performed on these samples due to the lack of

NE development. Direct temporal comparison with mESC differentiation revealed significant species-specific differences at the initial stages of the differentiation process.

Due to the contrast in species response, differentiation methods derived for use with rat PSC were instead tested and evaluated for their efficacy at generating RO morphology, and retinal protein and gene expression. A summary of the differentiation experiments performed on the rESC (RRRC) line is shown in Table 4.1.

Table 4.1. Summary of rat differentiation methods tested on RRRC rESC cell line (rESC DA-EC8 #464) and data output. Methods were taken from published research differentiating mESC or rESC into neural or retinal progenitor cells (NPCs/RPCs) with various novel modifications. BF = bright-field, IF = immunofluorescence, wp = well-plate, D = day, C = condition.

Reference (Cell type)	Name/ Results Section	Plating density	Media addition	Culture summary	Plating strategy	Observed morphological features	Data output
DiStefano et al. 2018 (mESCs)	Expt 9/ 4.3.3	3000 cells/well	D0-7: GMEM/1.5% KSR D7-10: DMEM/N2/2-mercap. D10-18: DMEM/N2/Taurine/9cis-RA/IGF-1 D18-26: DMEM/N2/Taurine/9cis-RA/IGF-1/B27-VitA/2% FBS D1: 2% Matrigel	Supplement-rich. Uses 9 cis-RA. Worked well with mESC.	96 wp	Poor morphology (fluffy) compared with mESC-derived organoids, differences seen from D1 (aggregation). Lack of bright-phase edge and OV-like structures.	BF images
Qu et al. 2015 (rat-RPCs)	Expt 10/ 4.3.4	3500/5000 cells/well	D0-9: GMEM/20% KSR/IWR-1e D9-14: GMEM/10% KSR/ 10% FBS D14-26+: DMEM/N2/10% FBS/Taurine/RA D1 and D6: 1% or 2% Matrigel	Higher KSR and IWR-1e. Lower Matrigel conc. (from Nakano et al. 2012).	96 wp then pooled at D6	Retinal and NE morphology seen until D14 in 1% Matrigel condition	BF images/ IF analysis at day 7/10/14

Wang et al. 2012 (rat-NPCs)/ Qu et al. 2015 (rat-RPCs)	Expt 10+11/ 4.3.4	3500/5000 cells/well	D-2-0: N2B27 2i (rESC media) D0-9: GMEM/20% KSR/IWR-1e D9-14: GMEM/10% KSR/ 10% FBS D14-26+: DMEM/N2/10% FBS/Taurine/RA D0/1 and D6: 1% Matrigel	2 day induction period as 'EBs'. Matrigel addition at either D0 or D1.	96 wp then pooled at D6	Lack of retinal morphology at D5/D7.	BF images.
Wang et al. 2012 (rat-NPCs) (3D)	Expt 12	3000 cells/well or drop	D0-2: N2B27 2i:MEF-CM + Y-27632 D2-4: N2B27 2i:MEF-CM D4-5: N2B27:MEF-CM D5-11: N2B27	Generate EBs then plate in 2D to induce NPCs and expose to retinal stimulants	96 wp (30uL or 100uL)	Good aggregation up to D3.	Experiment terminated at day 4 due to infection
Wang et al. 2012 (rat-NPCs) (3D)	Expt 12	Floating colonies (various size)	D0-2: N2B27 2i:MEF-CM + Y-27632 D2-4: N2B27 2i:MEF-CM D4-5: N2B27:MEF-CM D5-11: N2B27	Generate EBs then plate in 2D to induce NPCs and expose to retinal stimulants	Pooled in low attachment 6 wp	Good aggregation up to D3.	Experiment terminated at day 4 due to infection
Qu et al. 2015 (rat-RPCs) + novel modifications	Expt 13(C1)/ 4.3.4.1	3000 cells/well	D0-9: GMEM/20%KSR/IWR1-e/Y-27632 D9-14: GMEM/10%KSR/10%FBS D14+: DMEM/N2/10% FBS/Taurine/RA D1 and D6: 1% Matrigel (variant) D9-14: +/- SAG	Generate organoids in 96wp using chemical stimulants, pool at D6 and expose to retinal stimulants.	96 wp then some pooled in low attachment 6 wp at D6.	Good aggregation, NE and retinal morphology up to D17 in pooled culture, deterioration in 96wp from D12.	BF images. IF analysis and RT-qPCR

Qu et al. 2015 (rat-RPC) + novel modifications	Expt 13(C2)/ 4.3.4.1	3000 cells/well	D0-4: GMEM/20%KSR/IWR1-e/SB-431542/Y-27632 D1 and D6: 1% Matrigel	Similar to C1 with inclusion of SB-431542 to improve EB generation.	96 wp	Poor morphology compared to C1 at D4.	BF images. Terminated at day 4
Wang et al. 2012 (rat-NPC) (3D) + novel modifications	Expt 13(C3)/ 4.3.4.2	3000 cells/well or drop	D0-2: N2B27 2i:MEF-CM + Y-27632 D2-4: N2B27 2i:MEF-CM D4-5: N2B27:MEF-CM D5-14: N2B27 D14+: DMEM/N2/10% FBS/Taurine/RA (variant) D9-14: +/- SAG (variant) D9-14: +/- SAG, bFGF (variant) D17+: +/- IGF1	Generate neural EBs in droplets then plate in 2D to induce NPCs, re-plate in 3D and expose to retinal stimulants.	30uL drops in 96 wp, some plated in 2D at D5 and re-plated in 3D at D11 or D14.	Good aggregation in drops, promising retinal morphology in re-aggregates in 3D maintained long-term up to D30.	BF images. IF analysis and RT-qPCR

4.3.4   Differentiation experiments using rESC and rat optimised SFEBq protocols

5   Methods to be tested on rESC (RRRC), which had been published for their use with rat PSC lines are shown in Fig 4.12 and described further in Table 4.1. Notable culture alterations used by Qu et al. (2015) and not previously tested on our rat PSC lines include; the increase of KSR to 20%, Wnt inhibitor IWR-1e between day 0-9, and the decrease in Matrigel concentration from 2% to 1% which is replenished in media for the first 9 days of culture. The Qu et al. method also pooled organoids in culture at day 6 and plated in adherent culture from day 9. This published method reported generation of RPCs (Pax+/Rax+) from rESC by day 16 with a plating cell density of 5000 cells/aggregate (Qu et al., 2015).
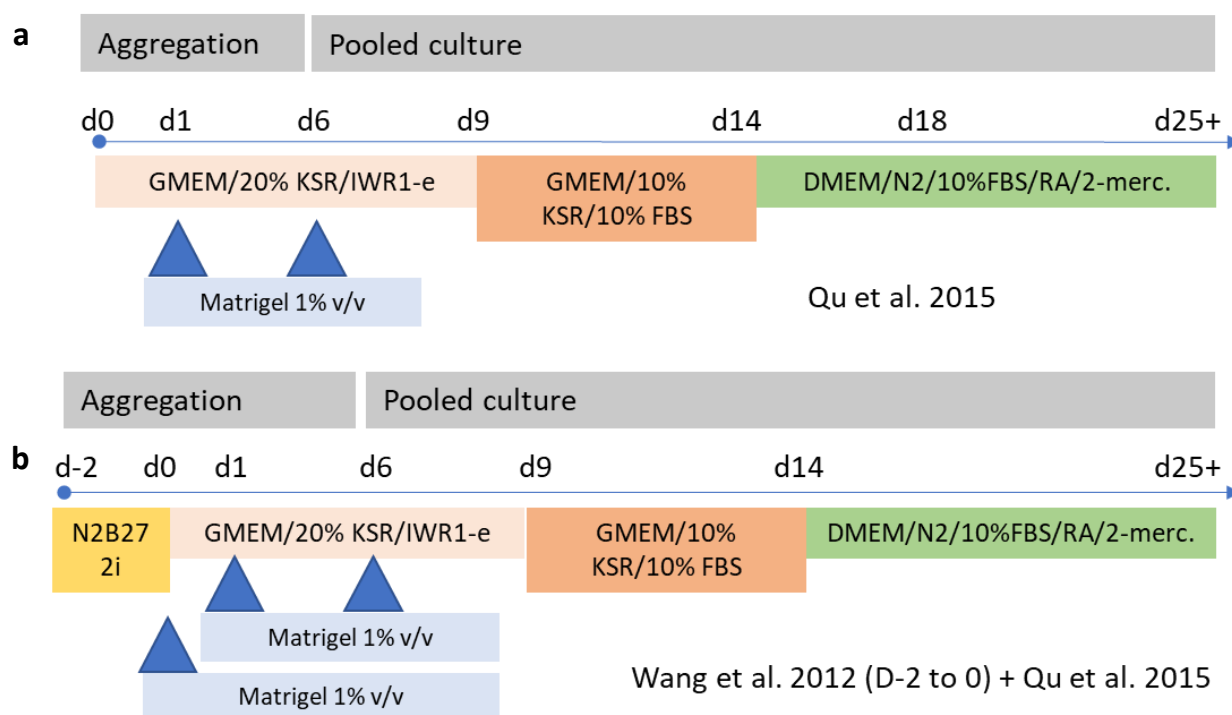
Figure 4.12. Schematic comparison of differentiation methods tested on rESC (RRRC) published (a) for generation of RPCs from rESC (Qu) and (b) novel hybrid method using a 2- day induction period post-plating (Wang + Qu). DMEM-F12 abbreviated to DMEM. D = day.

This protocol was tested in part; organoids were pooled from day 6 onwards however, cultured in 3D suspension throughout differentiation. This format is more amenable for the project aim of using ROs for toxicology analysis. The culture media used by Qu et al. (2015) was applied from day 0 -14, followed by the retinal maturation media used by Eiraku & Sasai (2012) from day 14 onwards (Fig. 4.12a). To bridge the gap between this experiment and what had previously been tested, two plating cell densities of 3500 or 5000 cells/well and both Matrigel concentrations of 1% and 2% were tested on rESC (RRRC) (Table 4.1).

The Wang et al. (2012) method uses the rESC culture media to generate EBs and gradually removes the 2 inhibitors (CHIR99021/PD0325901) which maintain pluripotency at day 0-5, causing differentiation to NPCs. This method and a novel hybrid method using this plating media (N2B27 2i) in a two-day step prior to the addition of culture media from Qu et al. method was also tested on rESC (RRRC) (Fig. 4.132b; Table 4.1).
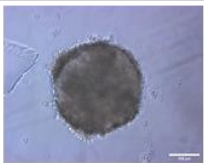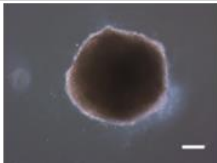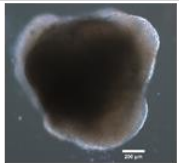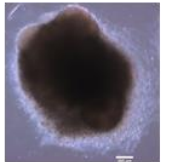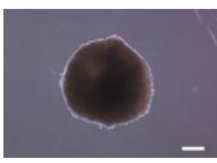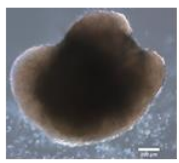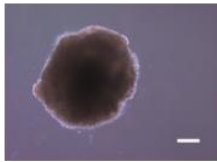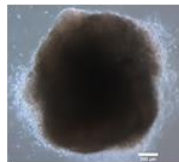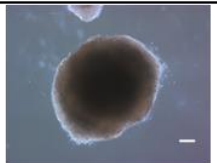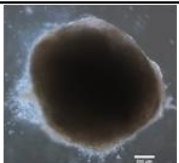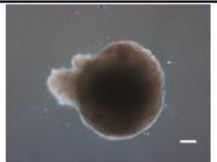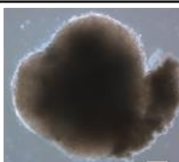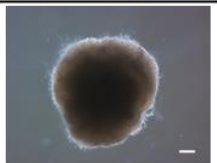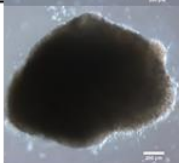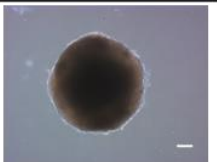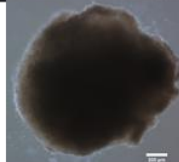
Method	Variation	D1	D5	D9
Qu	3500 cells D1 mat. 1%			
	3500 cells D1 mat. 2%	N/A		
	5000 cells D1 mat. 1%			
	5000 cells D1 mat. 2%			

Method	Variation	D-1	D3	D7
Wang/ Qu	3500 cells D0 mat. 1%			
	3500 cells D1 mat. 1%	N/A		
	5000 cells D0 mat. 1%			
	5000 cells D1 mat. 1%			

Figure 4.13. Representative bright-field morphology of rESC-derived organoids using rat specific protocols with Qu or Wang/Qu methods (described in Fig. 4.12). Putative NE morphology highlighted by red arrows. Variation of methods include plating density of 3500 or 5000 cells/well. Representative images of experiment N = 1, organoid n = 384. Scale bar = 200 µm. D = day. Mat. = Matrigel.

Morphological assessment of the rESC-derived organoids generated using these methods was promising, showing improved aggregation 1 and 4 days after plating (Fig. 4.13, D1/D-1 and D5/D3), compared to rESC-derived organoids using the SFEBq method (Fig. 4.11). Organoids derived with the Qu et al. method and 1% Matrigel went on to develop a prominent phase-bright edge, highlighted by red arrows, 9 days after plating which was not seen in the Wang/Qu method organoids (Fig. 4.13, D9/D7).

Those organoids with promising retinal morphology at day 9 from the Qu et al. conditions (Fig. 4.13) continued to develop a retinal-like morphology with a thickening of phase-bright NE at day 10, which was maintained until day 14 (Fig. 4.14).
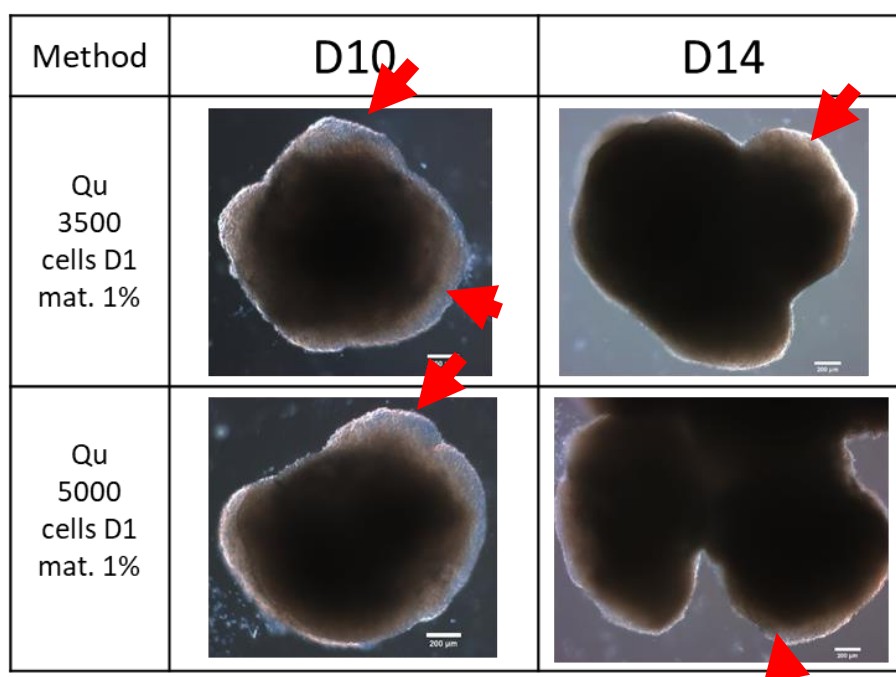
Figure 4.14. Bright-field morphology of rESC-derived organoids showing positive retinal morphology derived by Qu method variation with Matrigel (mat.) application at 1% vol/vol and seeding density of 3500 or 5000 cells/well. Representative images of experiment N = 1, organoid n = 384. Putative NE morphology highlighted by red arrows. Scale = 200 μm.

These conditions, which generated characteristic retinal NE morphology (Fig. 4.14), were further analysed using IF for the presence of NR markers in organoids sampled at day 7, 10 and 14 of differentiation.

At day 7, both the 3500 and 5000 cells/well "Qu/1% Matrigel" conditions showed a band of Pax6+ cells at the organoid periphery which did not co-express the neuronal marker Neun, which indicates

eye-field specification (Fig. 4.15). However, these nuclei lacked the columnar organisation seen in mESC-organoids which is typical of developing NE. There were also SNCG+ cells present in these regions indicating RGC generation (Fig. 4.16). No typical staining for recoverin (Rcvrn) was observed (Fig. 4.15). This is in line with the expected timeline of rat retinogenesis.

Qu
3500 cells
1% mat.

Qu
5000 cells
1% mat.
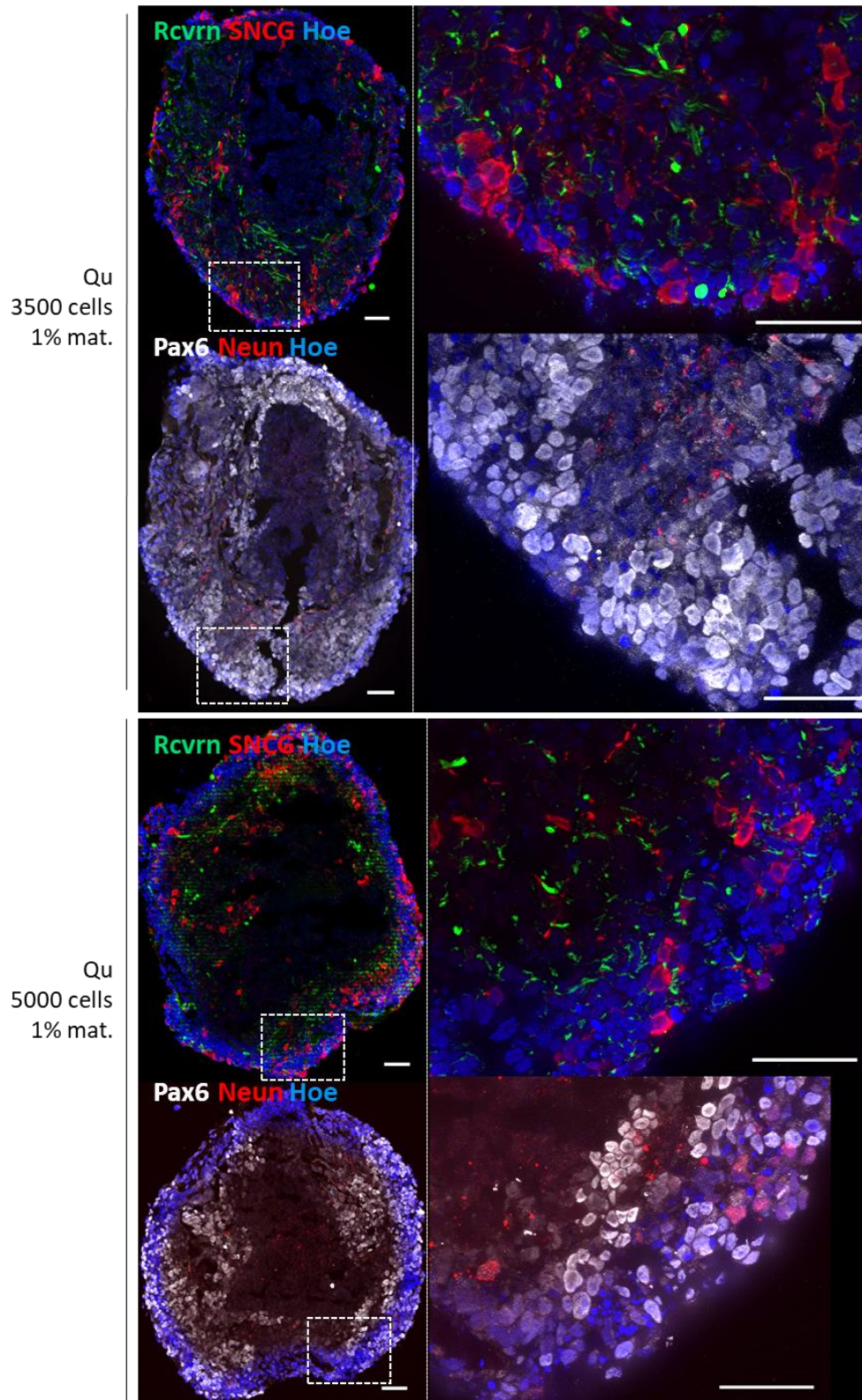
Figure 4.15 IF analysis for eye-field TF (Pax6), neuronal (Neun) and retinal cell markers (SNCG, Rcvrn) on rESC-organoids at day 7 derived with "Qu" method (3500 or 5000 cells/well). Sections counterstained with nuclear dye Hoescht (Hoe). Boxes show areas of magnification. Representative images of experiment N = 1, organoid n = 8. Mat = Matrigel. Scale bar = 50 µm.
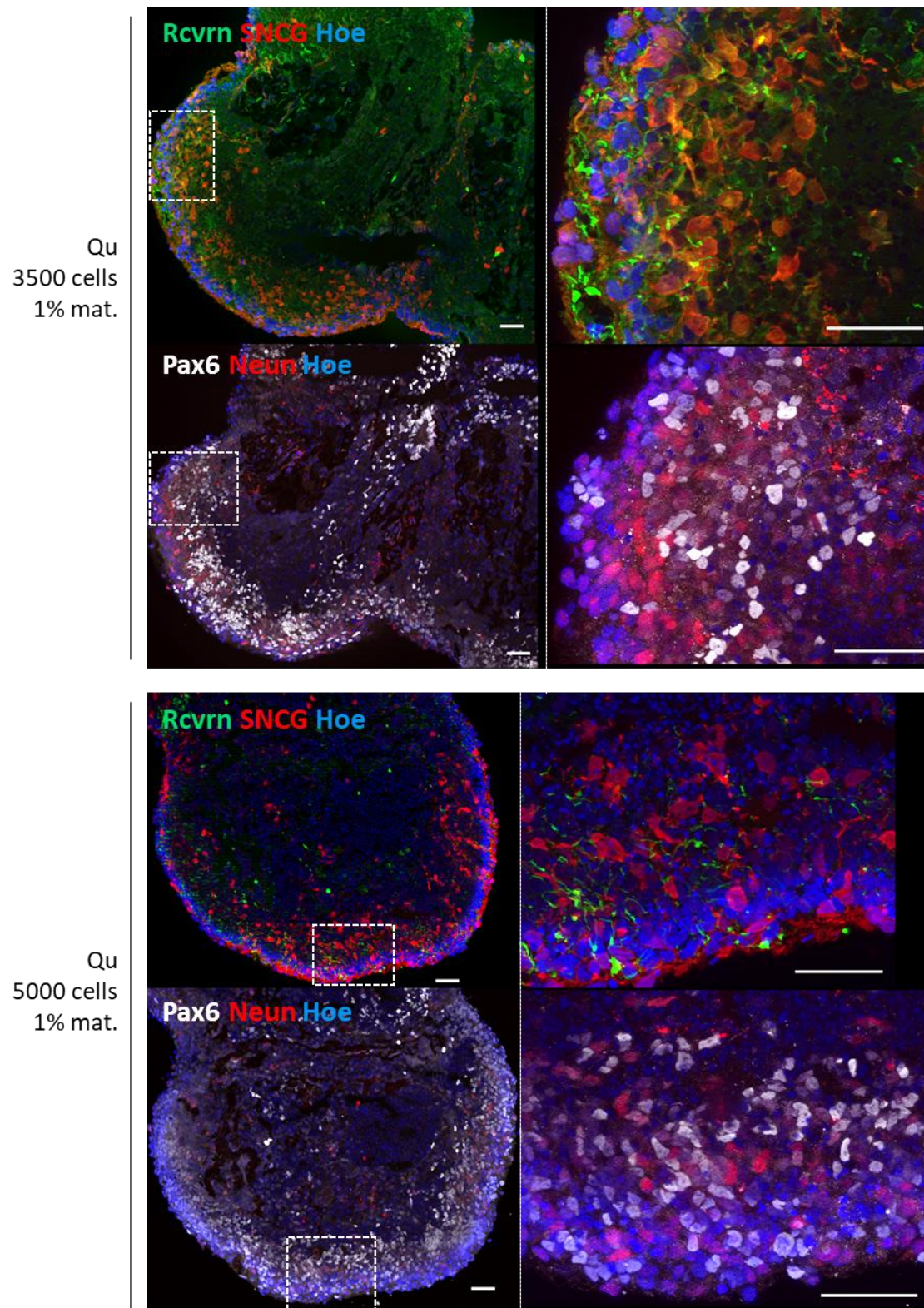
Figure 4.16 IF analysis for eye-field TF (Pax6), neuronal (Neun) and retinal cell markers (SNCG, Rcvrn) on rESC-organoids derived at day 10 derived with "Qu" method (3500 or 5000 cells/well). Sections counterstained with nuclear dye Hoescht (Hoe). Boxes show areas of magnification. Representative images of experiment N = 1, organoid n = 8. Mat = Matrigel. Scale bar = 50 μm.

At day 10 peripheral areas at the apical edge of the organoids, of both cell densities, have a layer of Pax6+ interspersed with Neun+ cells indicating the mixed neural-retinal identity of those areas (Fig. 4.16). These likely correspond to the phase- bright edges seen by bright-field microscopy (Fig. 4.14). Cells positive for SNCG were found at the apical edge of the organoid, whereas Rcvrn+ cells were found on the basal aspect, indicating a developing inverted lamination (Fig. 4.16).

At day 14, SNCG was observed in cells at the apical edge of the organoids derived in both cell density conditions (Fig. 4.17). This shows the capacity of the culture conditions to generate RGCs by this timepoint and localisation indicates a developing inverted laminar structure. The pan-PR marker Recoverin is not present in either condition although it was also lacking at the same timepoint in developing mESC organoids (Fig. 4.17; Fig. 4.8). In the 3500 cells/well condition Pax6 and Rax are observed in cell nuclei at cell-dense peripheral areas suggesting eye-field specification although they lack the tight columnar arrangement typical of NE (Fig. 4.17).
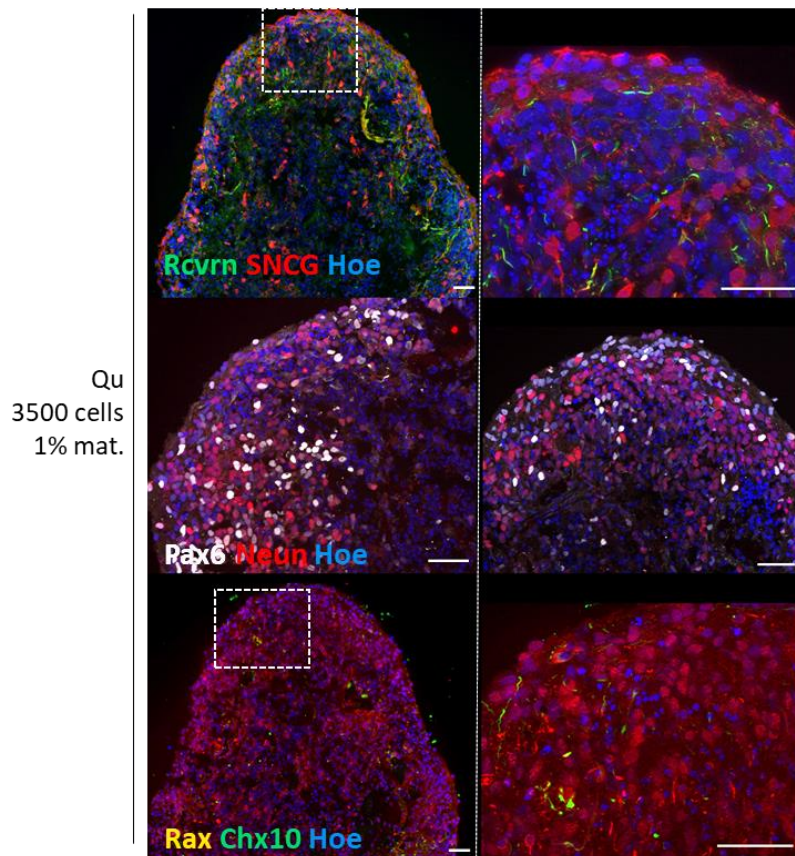
Figure 4.17. IF analysis for eye-field TF (Pax6, Rax, Chx10), neuronal (Neun) and retinal cell markers (SNCG, Rcvrn) on at day 14 derived with "Qu" method (3500 or 5000 cells/well). Sections counterstained with nuclear dye Hoescht (Hoe). Boxes show areas of magnification. Representative images of experiment N = 1, organoid n = 8. Mat = Matrigel. Scale bar = 50 μm.

Organoids derived in 5000 cells/well condition show similar expression of Pax6 and Rax although the organisation of Pax6+ cells is better defined (Fig. 4.17). Presence of SNCG and Neun is also comparable between the two cell density conditions (Fig. 4.17). Chx10 was not detected in either 3500 and 5000 cell/well conditions indicating the lack of RPCs or bipolar cells at this timepoint of differentiation (Fig.4.17).

(Figure 4.17 cont.)
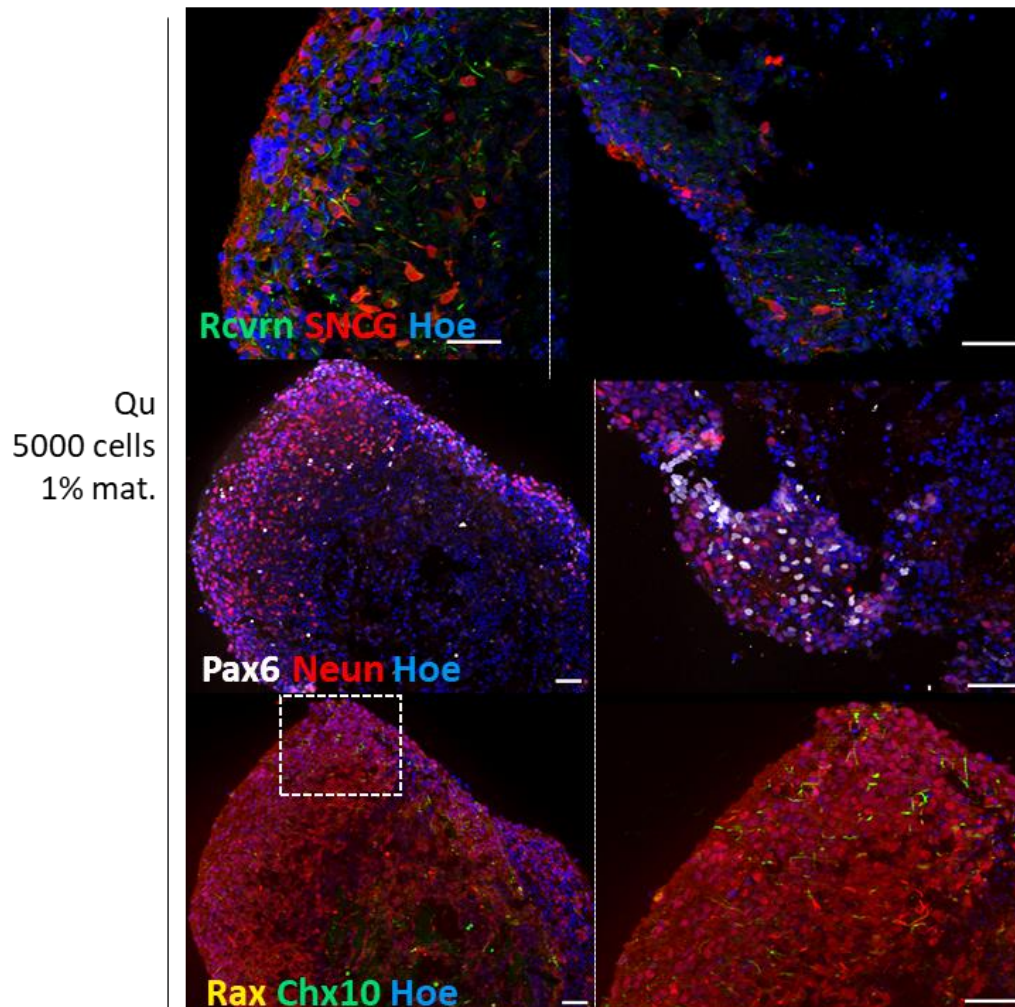
In summary, retinal morphology in rESC-derived organoids has been greatly improved from earlier experiments with the maintenance of phase- bright tissue and NE identity until day 14. The best culture conditions as determined by formation of NE were found to be with Qu et al. (2015) method using 20% KSR, chemical Wnt inhibitor IWR-1e and 1% Matrigel. Assessment of two plating densities showed little difference morphologically or by IF analysis. Similar protein presence of key retinal transcription factors (Rax/Pax6) was observed in both cell density conditions (Fig. 4.17).

The detection of Neun in a substantial region of cells found interspersed with Pax6+ cells, shows the propensity of differentiation into neuronal cell types between day 10-14 using this protocol. Due to both the SNCG and Neun antibodies being mouse-reactive, co-staining of these samples could not be performed. Without further specific staining for either neuronal or retinal cell subtypes it is difficult to draw conclusions about the identity of these cells being retina-specific or of other neurons. However, it does show the timeline of cell differentiation and specification to approximate that of RGCs in rat retinal cytogenesis (Rapaport et al., 2004).

A lack of laminated structure was observed between day 10-14 corresponding to the thinning and slight darkening of the phase- bright edge seen morphologically (Fig. 4.17). However, very similar results were obtained in in mESC organoids at the same time point of differentiation; hence this may not be indicative of a lack of capacity to generate PRs at a later stage.

These results show the capacity of rESC to generate ROs with similar morphology and marker expression from published findings (Qu et al., 2015). Use of novel methods and further culture of rESC-derived organoids generated at a stage beyond day 14 is now required to determine whether a retinal lamina with full cellular diversity can be generated.

4.3.4.1 Retinal differentiation method development using chemical stimulants (C1)

To build on the successful response of rESC to the altered plating media composition from previous experiments (4.3.3), further chemically induced differentiations were tested (Table 4.1). These included variations of the "Qu" method with the addition of Shh/Wnt stimulating molecules, SAG, from day 9 onwards to build on the presence of early eye field transcription factors previously detected at day 7 (Fig. 4.18, C1; Table 4.1). The lower concentration of Matrigel (1%) and pooling of culture at day 6 was repeated. An additional method variant (C2) involved the addition of chemical inhibitor of TGF-β/ALK4 pathway "SB-431542" in the plating media as it was reported by Osakada et al. (2009) to improve robust formation of EBs from day 0-5 in mESC (Fig. 4.18, C2).
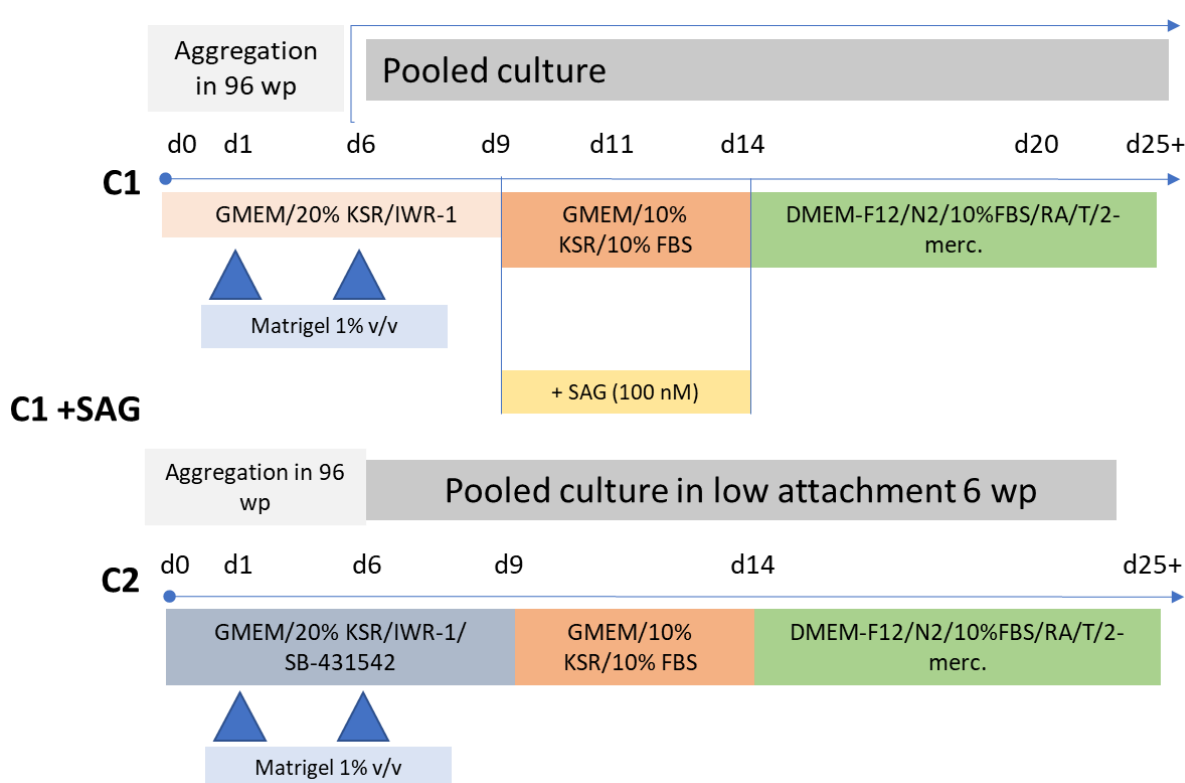
Figure 4.18. Schematic of differentiation methods using chemical signalling molecules, based on Qu et al. method tested on rESC: C1 and C2.

Comparison of the early stages of aggregation and morphological development of EBs between conditions 1 and 2 showed that C2 lacked uniformity and a clearly defined edge as was observed in C1 samples (Fig. 4.19). By day 4 the structure of the periphery of C2 organoids had deteriorated compared with C1 suggesting the combined effect of SB-431542 with Wnt inhibitor IWR-1e does not help robust formation of EBs in early stages of differentiation (n=768) (Fig. 4.19). This condition was subsequently terminated at day 5 to enable greater focus on more promising conditions.

Method	D1	D3	D4
C1			
C2			
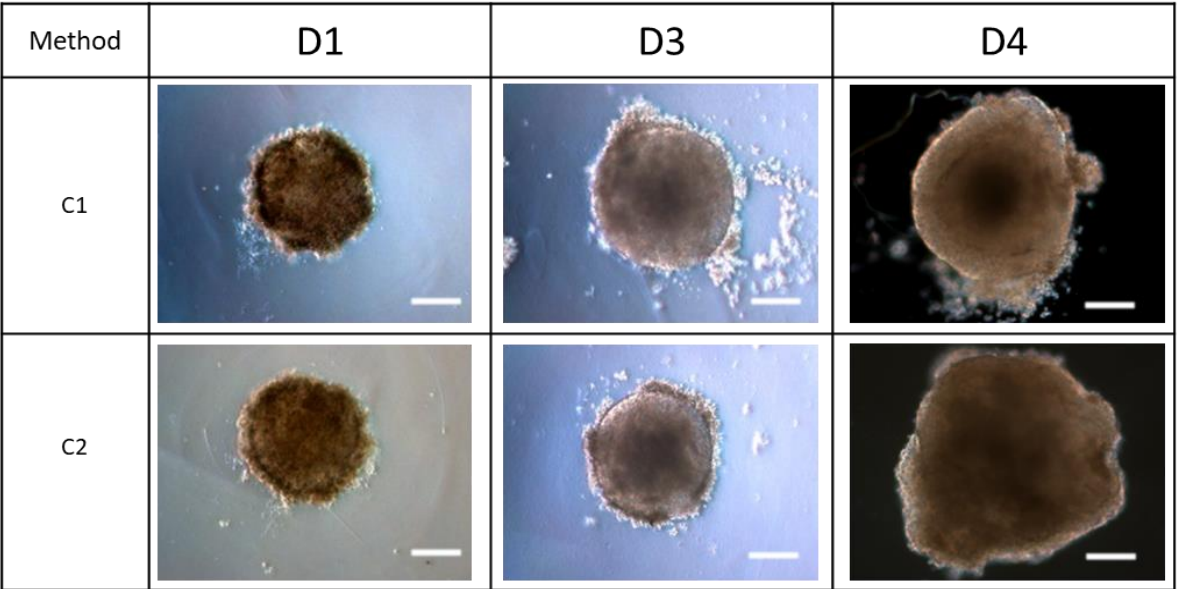
Figure 4.19. Representative bright-field morphology of rESC-derived organoids showing initial aggregation in C1 and C2. Representative images of experiment N = 1, organoid n = 768. Scale bar = 200μm.

C1 generated organoids with typical retinal morphology displaying some phase-bright tissue at the edges of the organoids at day 10-14 of differentiation (Fig. 4.20).

Method Variation	D7	D10	D14
C1 Pooled			
C1 Pooled + SAG			
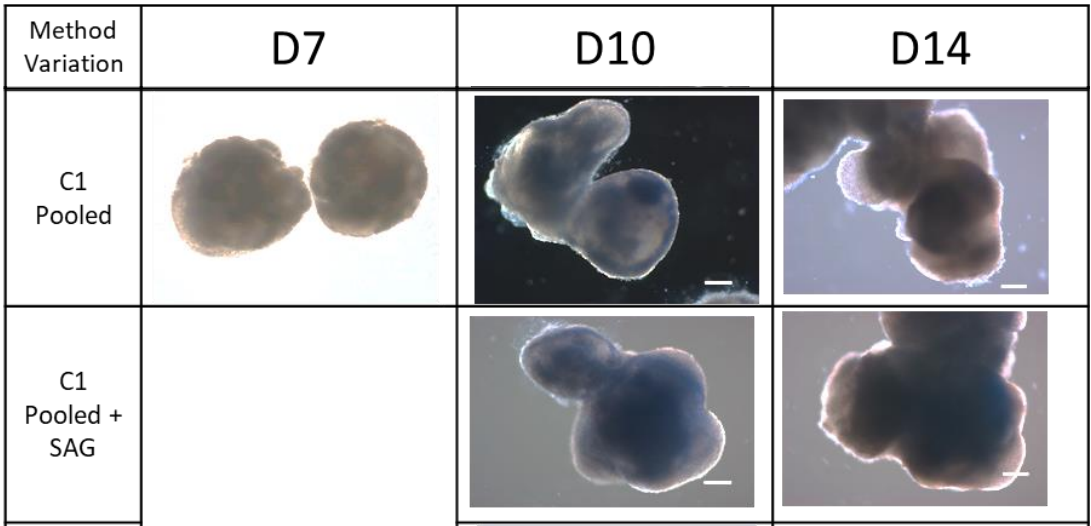
Figure 4.20. Representative bright-field morphology of C1 rESC-derived organoids in pooled culture conditions. Red arrows indicate putative phase-bright neuroepithelium. Representative images of experiment N = 1, organoid n = 384. D =day. Scale bar = 200 μm.

Morphologically it was difficult to definitively compare the effects of different retinal stimulants in culture as both variants showed some capacity for development of typical retinal morphologically such as phase-bright NE (Fig. 4.20, 4.21). Moreover, due to using pooled culture, organoids fused together. Both variants were sampled at day 24 and 28 for analysis of mature retinal proteins and gene expression analysis.

Figure 4.21. Representative bright-field morphology and development of C1 rESC-derived organoids in pooled culture throughout differentiation. Red arrows indicate putative neuroepithelium. Representative images of experiment N = 1, organoid n = 368. Scale bar = 500µm.

IF analysis assessing for the presence of RGC (SNCG) and PR (Rcvrn) markers was performed for C1 pooled organoids without any supplementation and the pooled condition with SAG added (+SAG).
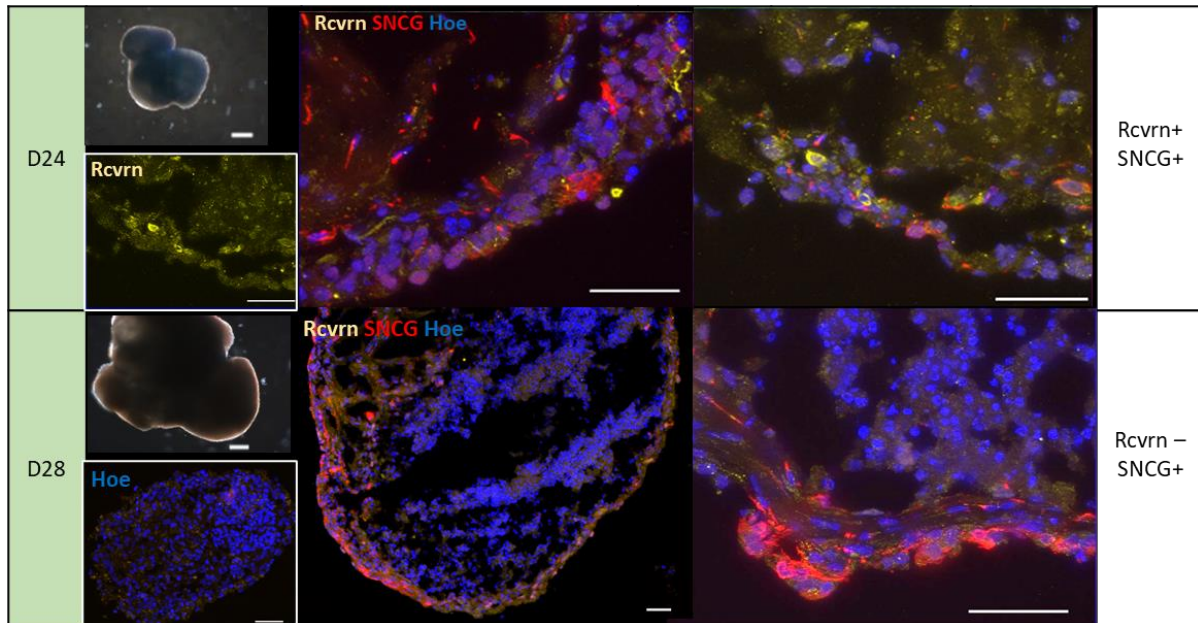
At day 24 there are Rcvrn+ cells at the periphery of the organoids which are found interspersed with SNCG+ cells (Fig. 4.22). The presence of Rcvrn+ cells was not detected in organoids sampled at day 28 although SNCG+ cells were clearly located around the periphery of the organoids (Fig. 4.22). The cell lamina where these retinal cells are found had also thinned between day 24-28 (Fig. 4.23).

Gene expression analysis was performed for retinal genes of interest on organoid cDNA collected at day 28 using RT-qPCR as described in Methods (2.3). As these samples were collected from a late timepoint in differentiation, one marker of early RPC expression (*Chx10*) was measured, which can also mark mature bipolar cells, whilst the remaining candidates are markers of mature retinal cell types; *RBPMS* for RGCs, *Rcvrn* for PRs, *CALB1* for horizontal cells, *Prox1* for horizontal and amacrine cells, *Crx* for post-mitotic PRs, *NRL* for rod PR precursors and *ARR3* for cone PR precursors. Validation of the primers was performed in Methods (2.5) and the analysis was performed using adult rat retina cDNA expression as a normalisation control, *GAPDH* as an endogenous control and the Delta Ct comparative method (Livak & Schmittgen, 2001).

Due to a limited pool of sample organoid cDNA eight retinal genes were assessed with the aim to confirm the expression of key PR, RGC and interneuron markers to capture the cellular diversity in C1-derived organoids.

As only one set of samples, generated from one differentiation experiment, has been analysed for RT-qPCR expression it is not possible to make conclusions as to the statistical significance of any differences between the conditions, so this data is informative only to show a pattern of trends, or in comparison with other cell culture strategies.

Although the retinal genes *Crx*, *Nrl* and *Arr3* were assessed, values of gene expression were considered too low for quantification (Ct >35). Therefore, these results are not shown.

At day 28 the expression of *Chx10*, *Rbpms*, *Rcvrn*, *Calb1* and *Prox1* was shown to be higher in C1 pooled organoids without the addition of SAG (Fig. 4.23).

Without confirmation using an additional marker for bipolar or RPCs it is not possible to determine whether the addition of SAG has caused a relatively lower *Chx10* expression is indicative of a loss of bipolar cells or RPCs in comparison to the C1 pooled sample.

The level of *RBPMS* expression is of a magnitude comparable to that of the mature rat retina and reflects a high level of RGCs in the organoids which is reflected in the SNCG presence observed by IF data (Fig. 4.23a, 4.22).
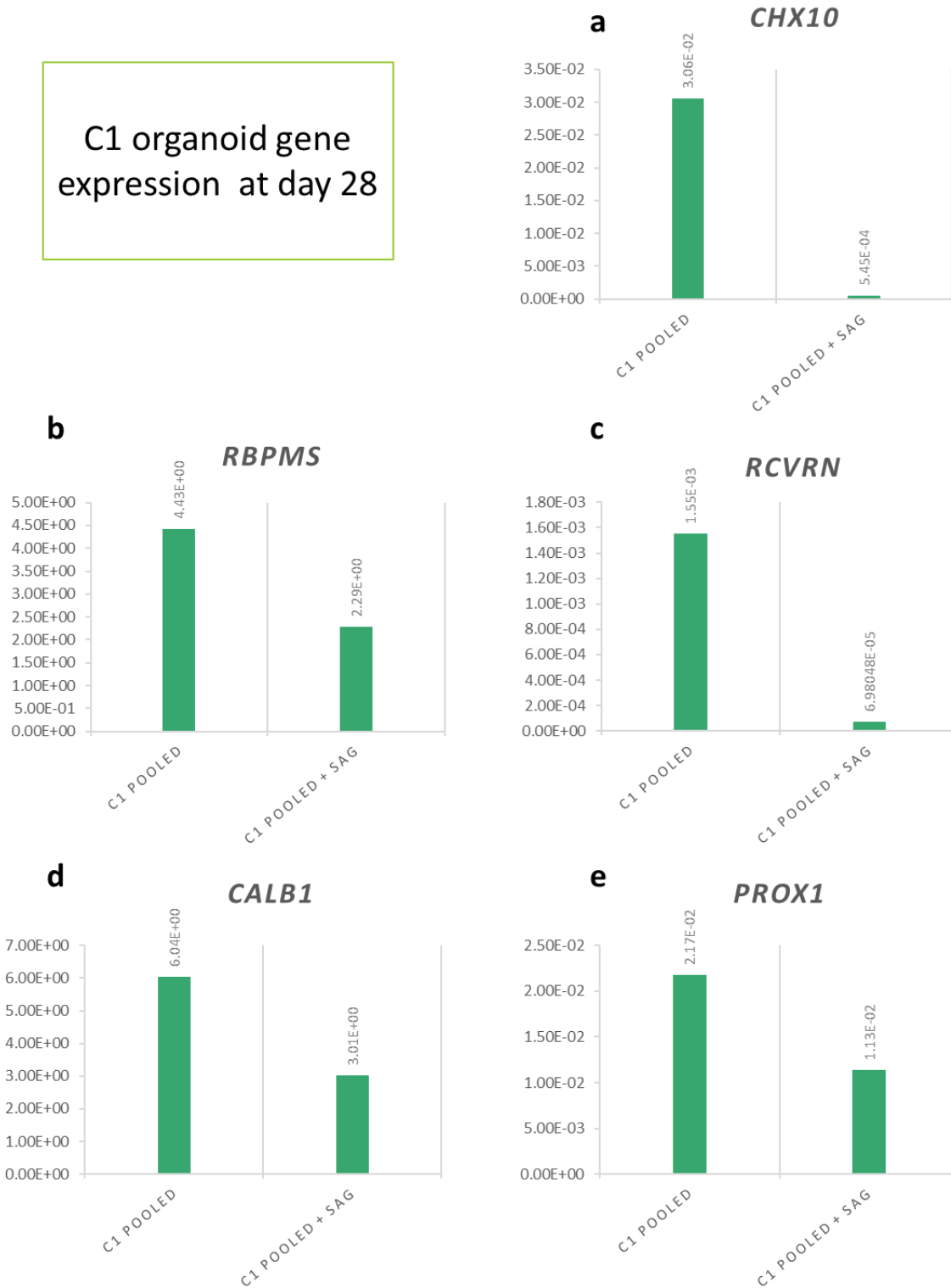
Figure 4.23. Gene expression of rESC-organoids derived with C1 methods at day 28 of differentiation normalised to adult rat retina (a) Chx10 for retinal progenitor cells (b) RBPMS for RGCs (c) Rcvrn for PRs (d) Calb1 for horizontal cells and (e) Prox1 for horizontal and amacrine cells. Calculated as relative fold change with arbitrary units. N (experiment)= 1, n (organoid) = 20.

In conclusion, long-term culture of organoids using pooled culture and the Qu et al. (2015) method generated organoids with NE morphology from day 10 until day 20 (Fig. 4.20, 4.21). Despite promising retinal like morphological features observed in the condition supplemented with the Shh agonist SAG, results from gene expression analysis at day 28 showed no improvement in key retinal gene expression (Fig. 4.23). This could suggest that the day 28 timepoint is too late to capture any improvements from this condition as retinal cells may not be present at this relatively late timepoint, which corresponds with stage PND 4-8 in rat embryological development. Earlier assessment of retinal gene and protein expression, for example at day 10, 14, and 17 would have been helpful to assess the response of cells to the earlier application of retinal stimulants.

Nevertheless, the IF and gene expression analysis both show RGCs and PR cells to be present in the organoids; however they lack the structural organisation and quantity seen in the native retina.

4.3.4.2 Retinal differentiation method development using hanging-drop method and adherent plating strategy culture (C3)

To improve retinal differentiation a different plating strategy was tested in C3 methods. This was informed by studies using an intermediate stage of adherent (2D) culture to generate retinal precursor cells from both human and mouse PSC (Zhong et al., 2014; Osakada et al. 2008). Methods plating EBs in 2D to generate multipotent neural and retinal progenitor cells from rESC were also informative (Qu et al., 2015; Z. Wang et al., 2012). Variations of the Wang et al. (2012) method with the novel addition of retinal stimulants at key developmental timepoints is shown in Fig. 4.24 (Table 4.1). These methods and results described in this section are referred to as "condition 3/C3". These methods were used with rESC (RRRC) to derive EBs in suspension using the "hanging-drop" technique which were then plated in 2D culture at day 5. The cells which proliferated were then manually detached and re-plated in 3D suspension culture at either day 11 or 14, and from day 14 they were exposed to retinal maturation media containing 10% FBS, N2, Taurine and RA (Fig. 4.24).
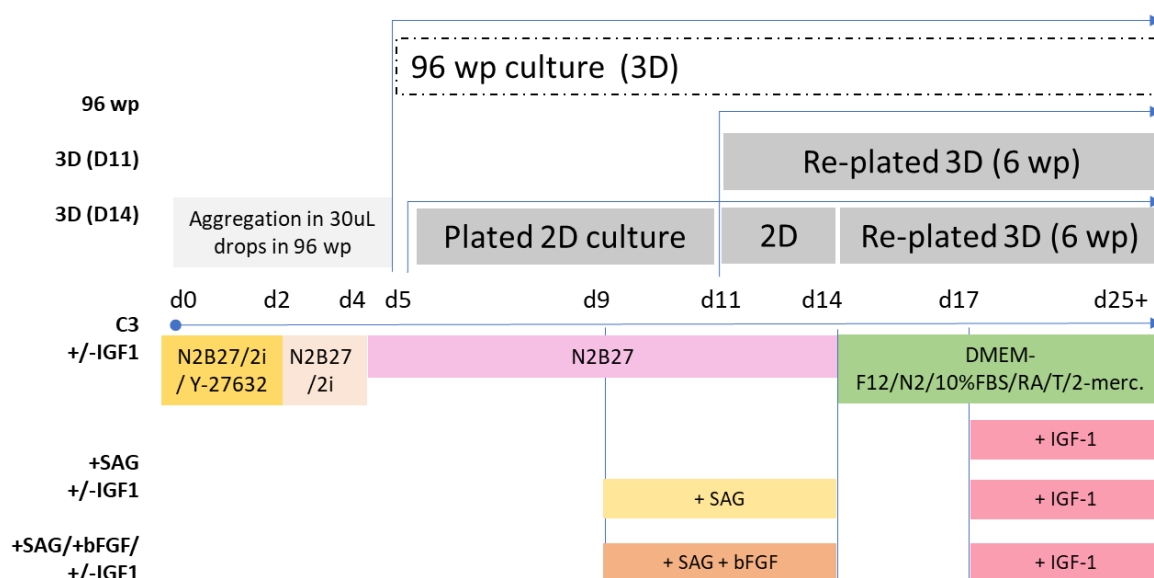
Figure 4.24: Schematic of differentiation methods using adherent culture technique tested on rESC in C3. D = Day. Wp = well plate.

With these adaptations I intended to first generate robust EBs and NR precursor cells and subsequently add retinal stimulants to increase retinal or PR progenitors at appropriate developmental timepoints. These included SAG during eye-field specification at day 9, to increase Rax+ and Sox2+ neural-retinal progenitors (Nakano et al. 2011); the addition of bFGF to increase cell proliferation and neural progenitors (Yourey et al. 2000; Wang et al. 2012) and the addition of IGF1 at day 17 aimed to stimulate PR progenitors and cone PRs (Table 1.2, DiStefano et al. 2017, Mellough

et al. 2015; Zhou et al. 2015). The aim was to re-plate RPCs from 2D into suspension culture following their expansion thereby re-aggregating purified RPCs as a 3D organoid to achieve retinal lamination. The length of timing for 2D plating was informed by the Wang et al. (2012) and Qu et al. (2015) publications, and cell proliferation observed following attachment.
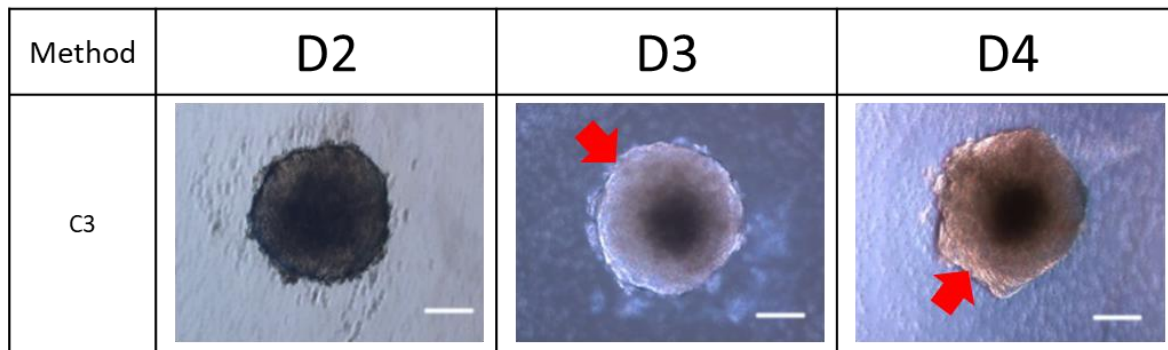
Figure 4.25. Representative bright-field morphology of rESC aggregation and embryoid body formation using hanging-drop method: C3. Experiment N = 2, organoid n= 864. Red arrows indicate putative neuroepithelium. D=Day. Scale bar= 200 µm.

Dissociated rESC (RRRC) were plated using the hanging-drop method, with 3000 cells within a single drop of media (30 µL). These showed good aggregation and uniform EB growth and morphology by day 4 (Fig. 4.25). Formation of EBs was successful using this strategy without Matrigel in 100% of organoids (n=864). Adherent culture began at day 5 when EBs were plated onto Matrigel-coated 6 well plates. This resulted in the generation of morphologically distinct cell populations of epithelial, NE and branching neuronal identity proliferating from day 8-14 (Fig. 4.26).

Method	D8	D10	D14
C3 2D			
C3 2D + SAG			
C3 2D + SAG + bFGF			
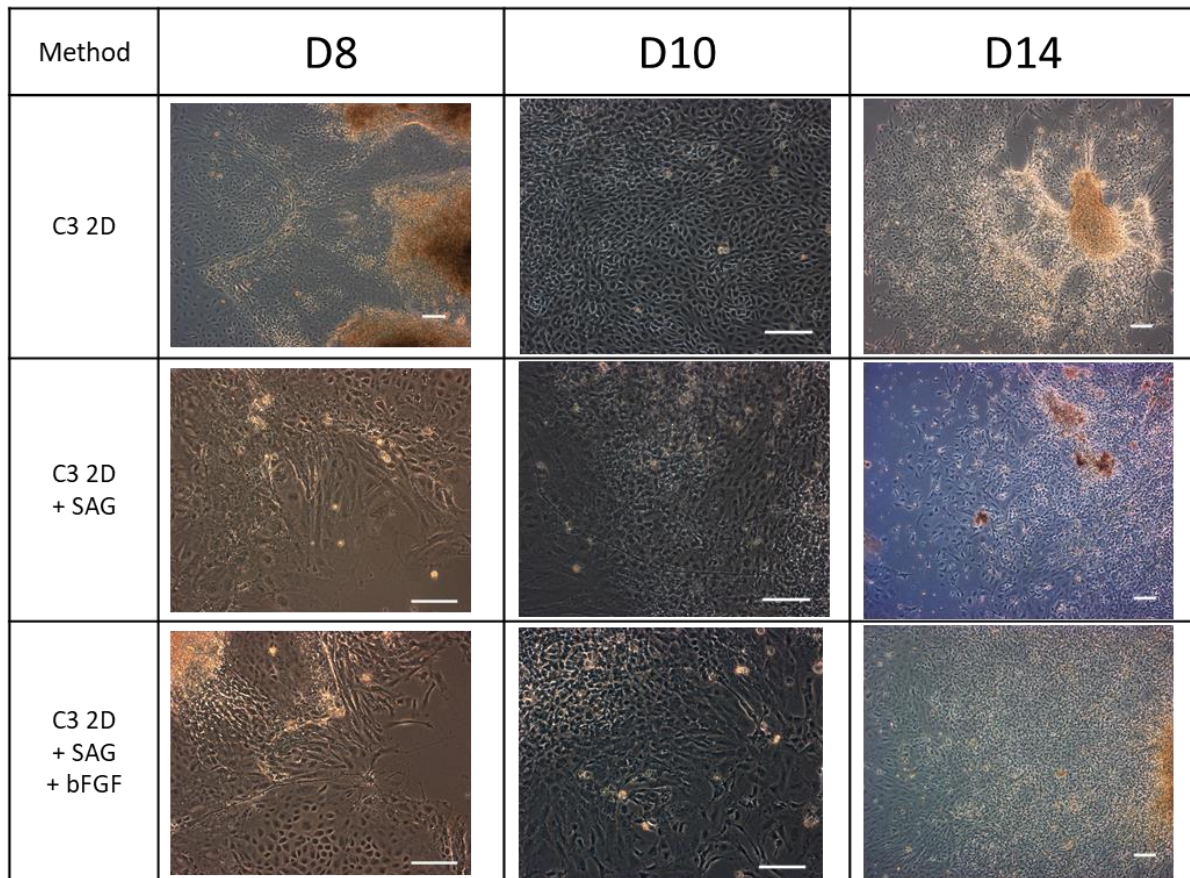
Figure 4.26. Representative bright-field morphology of rESC-derived embryoid bodies plated in 2D adherent culture at day 5 and the proliferation of neural-epithelial progenitor cells shown in red circles: C3. N (wells) = 8. Scale bar = 200 μm. D = day.

The cells in 2D were characterised by rapid proliferation and distinctive morphology of bipolar cells branching from areas of bright, tightly clustered cells (Fig. 4.26). This aligns with the reported timeline of development seen in the Wang et al. publication (Z. Wang et al., 2012).

A sample of adherent cells was fixed for IF analysis with proliferation marker Ki67 and NR progenitor cell markers Sox2, Nestin and Pax6. At day 11 the adherent cultures showed the presence of Sox2+ cells tightly clustered together in clumps which were not positive for Pax6 (Fig. 4.27). Pax6 expression was not detected in multiple samples (Fig. 4.27). Cells expressing both Ki67 and Nestin were present, indicating actively proliferating neural progenitor cells (Fig. 4.27).
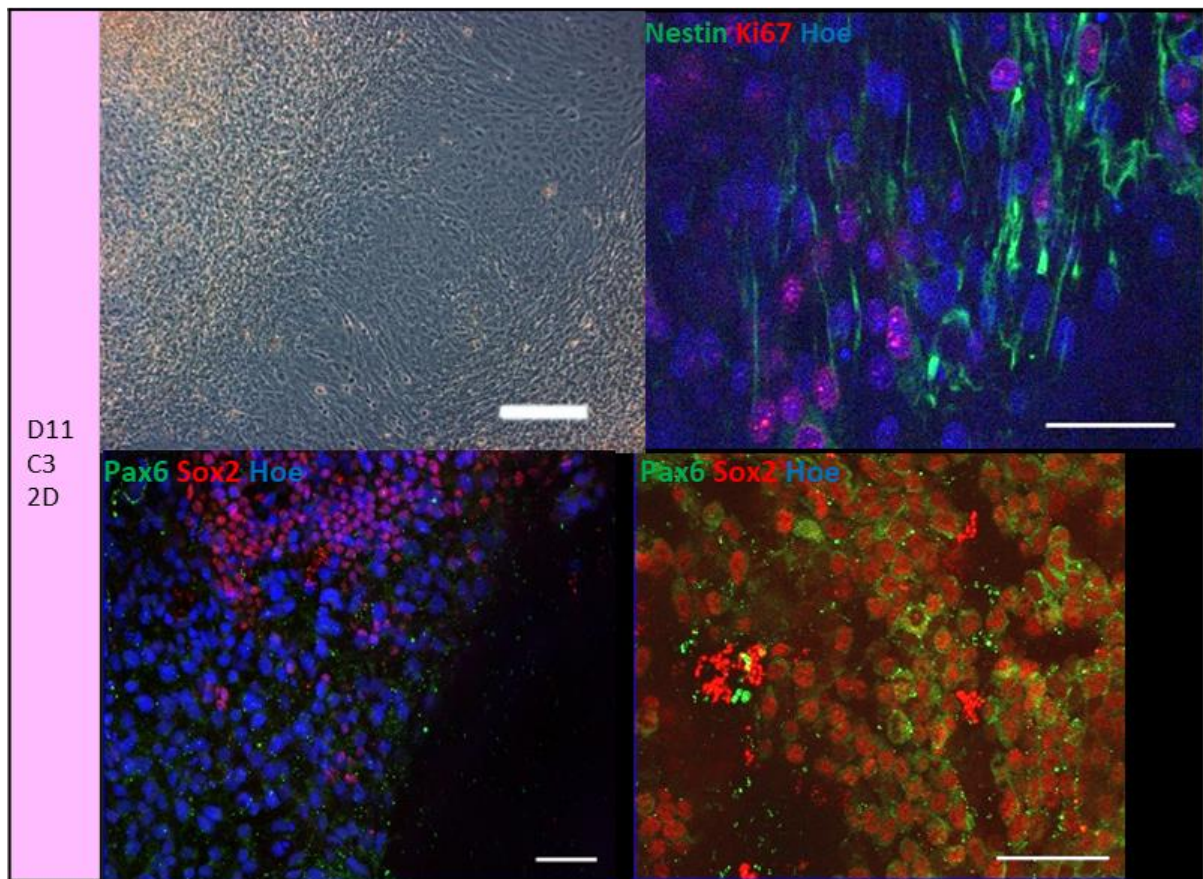
Figure 4.27. Representative bright-field morphology and IF analysis of adherent cells derived from rESC-EBs in C3 at day 11 of differentiation, 6 days following plating using proliferation marker Ki67, and neural-retina progenitor markers Pax6, Sox2 and Nestin. Nuclei counterstained with Hoescht (Hoe). Images are representative of 3 wells. Scale bar (BF) = 200µm. Scale bar (IF) = 50 µm.

At either day 11 or 14 these sub-populations with the bipolar, branching morphology of neural-epithelial progenitor cells were detached mechanically and re-plated in suspension culture where they quickly re-aggregated in 3D organoids that displayed promising retinal morphology (Fig 4.28). Following the addition of retinal maturation media and IGF1 supplementation the re-formed aggregates continued to develop and maintain phase-bright edge and newly budding structures emanating from the main body were observed (Fig. 4.28).

Method Variation	D14/D17	D17/20	D24/27	
			- IGF-1	+ IGF-1
C3 (D11)				
C3 (D11) + SAG				
C3 (D11) + SAG + bFGF				
C3 (D14)				
C3 (D14) + SAG				N/A
C3 (D14) + SAG + bFGF				
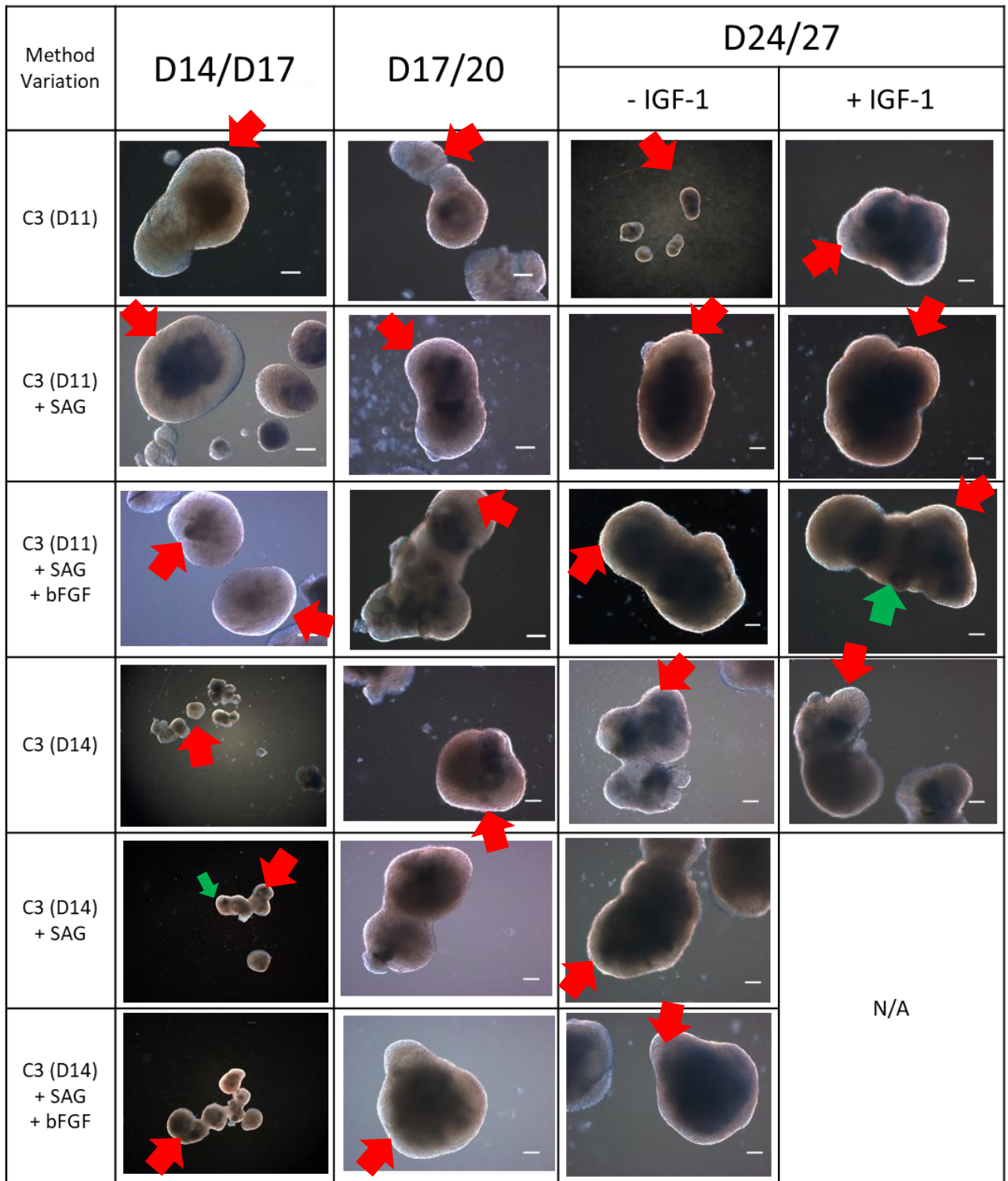
Figure 4.28. Representative morphology of re-formed rESC-derived aggregates re-plated in 3D culture on either day 11 or 14 in C3 method: Timepoints were chosen to reflect the same period elapsing following re-plating in 3D, e.g. D14/17 = 3 days post-plating. Red arrows indicate putative NE; Green arrows indicate putative RPE. D= day. N/A = no sample available. Scale bar = 200 μm.

These conditions were cultured until day 28 or 38 depending on sample availability. The prolonged culture time was intended to allow sufficient retinal maturation following an extension of the progenitor growth stage caused by 2D culture for 6 or 9 days. Throughout this period the structures did not deteriorate, although the putative NE lamina thinned from day 27, as has been seen to some extent in the later stages of all previous differentiation experiments (Fig. 4.29).
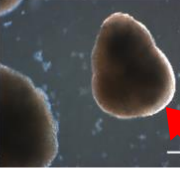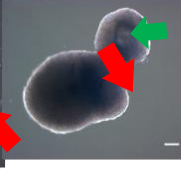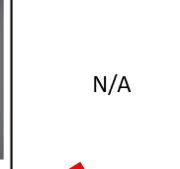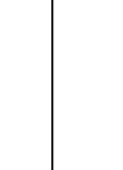
Figure 4.29. Representative bright-field morphology of re-aggregated rESC-derived organoids plated in 3D suspension culture on either day 11 or 14 with-/out addition of IGF-1 from day 17. Red arrows indicate putative neuroepithelium; green arrows indicate putative RPE. N/A indicates no sample was available. Scale bar = 200 μm. D = day.

In addition to maintenance of NE, dark areas approximating developing RPE were observed from day 20 in C3 organoids (Fig. 4.28, 4.29). Those re-plated on day 14 showed pigmented patches earlier than those on day 11, at 6 days post-plating (Fig. 4.28). This suggests that maintaining culture in 2D for 3 further days contributes to either progenitor maturity or propensity to develop into RPE. In the condition re-plated at day 11, these pigmented patches are maintained at day 30 where they are observed to form a crescent structure to the base of NE (Fig. 4.29).

A subset of organoids in C3 were kept in 96-wp throughout differentiation, without the 2D culture. Promising retinal features were observed, such as an outer periphery of NE at day 10 and thin bands of putative phase-bright NE apparent from day 20-27 (Fig. 4.30). Despite the overall size of organoids remaining small and a lack of defined OV/OC structures, this promising morphology constitutes a clear improvement from organoids generated in 96-wp previously with Sasai SFEBq methods (Table 4.1) which suggests the culture media used in C3 might better support neural-retinal differentiation

from rESC while 2D plating could improve organoid structure by eliminating non-NE progenitors at an early stage.
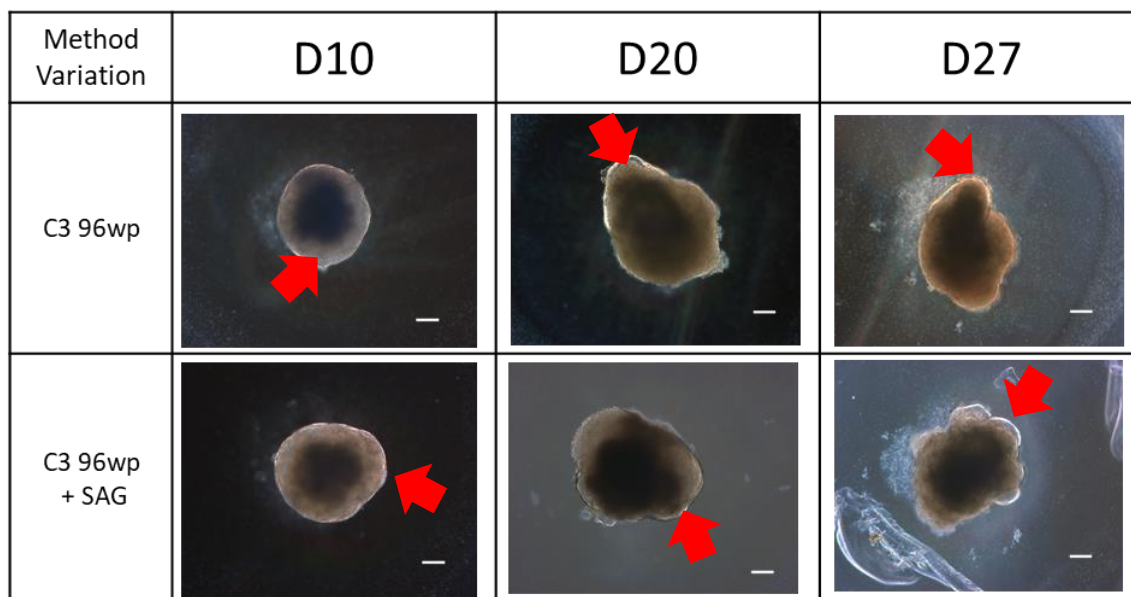
Figure 4.30: Representative bright-field morphology of rESC-derived organoids generated in 96-wp format with C3 conditions. Red arrows indicate putative neuroepithelium. Scale bar = 200 µm. D= day.

To identify and characterise the cells within the rESC-derived organoids, samples were collected for RT-qPCR and IF analyses.

To enable the molecular comparison of C3 methods on NE and retinal cell development the markers for RPCs (Chx10), NE (Pax6), RGCs (SNCG) and PRs (Rcvrn) were tested on samples collected at day 20 and 28. In conditions re-plated at day 11 this equates to 9 and 17 days after re-plating and for re-plated at day 14 condition this equates to 6- and 14-days post-plating. The results have been summarised in Table 4.2.

To correlate the morphology of the organoids with protein expression in a meaningful way the summary table is presented linking marker expression with its localisation within the organoids (Table 4.2). Retinal structure was characterised by a band of tightly packed columnar nuclei forming the outer edge of the organoid in a manner characteristic of NE. This analysis revealed that despite optically bright putative areas of NE from day 20 persisting until day 30 there was not a strong structural arrangement of cells which expressed retinal markers, especially Rcvrn and Pax6 (Fig. 4.28, 4.29). Although SNCG+ were always found at peripheral areas of NE, "~" generally indicates SNCG+ cells are present at the peripheral edge of the organoids, or one cell deep in a thin layer (Table 4.2).

The conditions C3 3D (D14) + SAG and C3 3D (D14) + SAG + bFGF were not analysed at day 20 due to an insufficient number of organoids in culture. As the morphology of the organoids remained promising these were instead kept for analysis at day 28 when it was hypothesised that the retinal cells would have a more mature phenotype.

The most promising conditions as determined by IF analysis at day 20 and 28 are represented in bold text in Table 4.2. All samples showed a decrease between day 20 to 28 in the percentage of organoids with Rcvrn+ cells as well in Pax6+ cells (Table 4.2). However, SNCG+ cells were retained in all conditions. The organoids cultured in 96-wp continuously and in the "C3 3D (D14) + SAG + bFGF" condition showed no evidence of Rcvrn+ cells present (Table 4.2). Additionally, the condition "C3 3D (D11) + SAG + bFGF + IGF1" which showed promising retinal morphology at day 27 and marker expression at day 20 lacked Rcvrn and Pax6 expression at day 28 (Fig. 4.28, Table 4.2). This suggests these conditions are insufficient to support PR development. Interestingly, these are from different lengths of plating suggesting it may be the media components rather than the length of time or pooling of culture conditions which require optimisation.

Table 4.2 Summary of IHC analysis on day 20 rESC (RRRC)-derived organoids using C3 methods. Morphology Key: + = region of NE lamina with retinal marker, ~ = retinal marker and some localisation to retinal structure, - = lack of defined structure correlating with retinal marker. Markers assessed are those indicative of neural-retinal development; Rcvrn = PRs, SNCG = RGCs, Chx10 = RPCs/bipolar, Pax6 = RPCs/interneuron. Detection is shown as a percentage of organoids within a sample of 3-6 organoids in total which showed marker presence by IHC. The most promising conditions for each timepoint are highlighted in bold.

Timepoint	Condition	Retinal marker				Morphology
		Rcvrn	SNCG	Chx10	Pax6	
D20	C3 96wp	75%	75%	0%	0%	~
	C3 96wp + SAG	100%	100%	0%	0%	~
	C3 3D (D11)	50%	100%	0%	100%	~
	C3 3D (D11) + IGF1	66%	100%	0%	100%	~
	C3 3D (D11) + SAG	100%	100%	0%	0%	~
	C3 3D (D11) + SAG +IGF1	0%	100%	0%	0%	~
	C3 3D (D11) + SAG + bFGF	100%	100%	0%	35%	-
	C3 3D (D11) + SAG + IGF1 + bFGF	100%	100%	0%	100%	~
	C3 3D (D14)	100%	100%	0%	60%	~
	C3 3D (D14) + IGF1	100%	100%	0%	100%	~
D28	C3 96wp	0%	80%	0%	0%	~
	C3 3D (D11) + SAG + bFGF	33%	100%	0%	33%	-
	C3 3D (D11) + SAG + bFGF + IGF1	0%	100%	0%	0%	~
	C3 3D (D14)	60%	100%	0%	40%	~
	C3 3D (D14) + SAG	66%	100%	0%	0%	~
	C3 3D (D14) + SAG + bFGF	0%	100%	0%	33%	
	C3 3D (D14) + IGF1	80%	100%	0%	50%	~

Two conditions which showed good morphology and the greatest percentage of organoids with SNCG+ and Rcvrn+ cells at day 20 and 28 were the C3 3D D14 conditions with and without the addition of IGF1 (Fig. 4.28, 4.29, Table 4.2). The IF analyses show Rcvrn+ cells at the periphery of the organoids neighbouring SNCG+ cells and accompanied by phase-bright NE morphology (Fig 4.31). The Rcvrn expression, as shown by the single fluorophore panel, was above background levels, and remains present at day 28 in the non-supplemented condition (Fig. 4.31). The expression pattern is extra-nuclear however differs from PRs in the mature retina (Fig. 4.31).
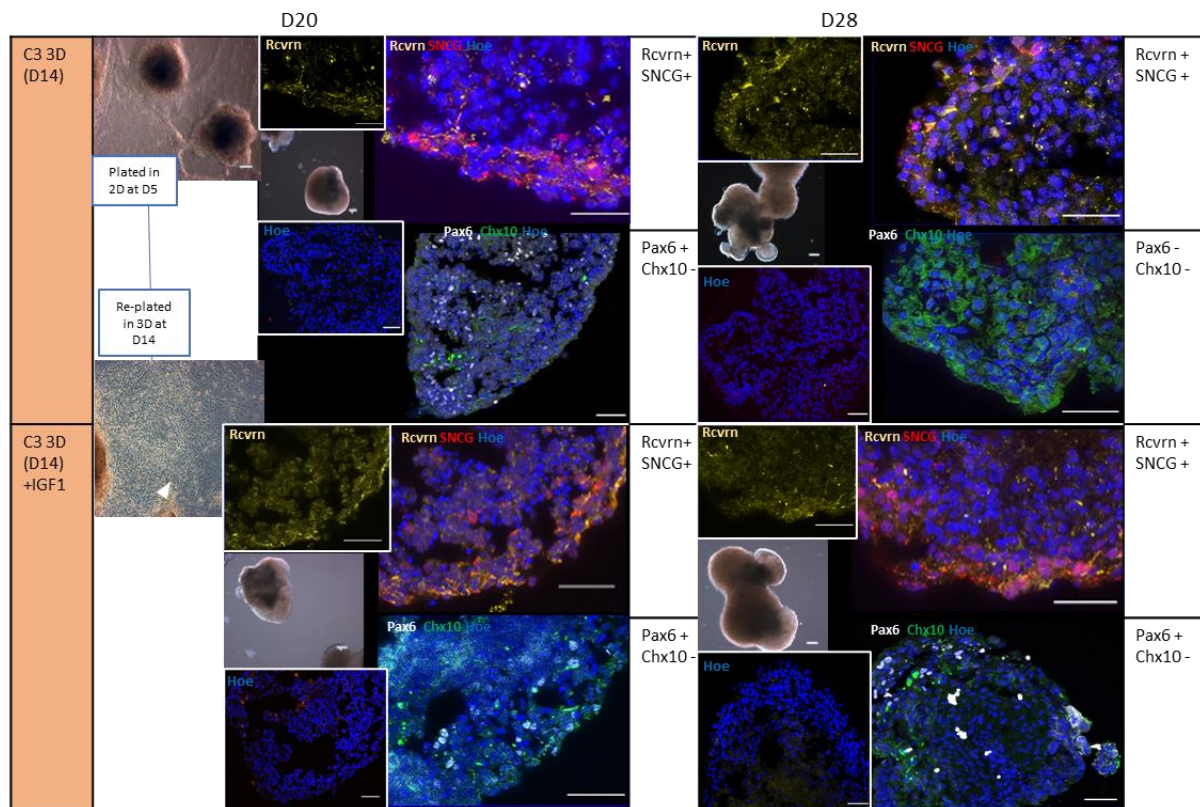
Figure 4.31. Representative bright-field morphology and IF analysis of C3 rESC-derived organoids assessing for RGC (SNCG), PR (Rcvrn), RPC (Chx10) and NE marker (Pax6) at day 20 and 28 of differentiation. Nuclei counterstained with Hoescht (Hoe). Negative control images labelled with secondary antibodies shown as Hoescht only panels. Scale bar (BF) = 500µm. N(experiment) = 1, n (organoid) = 8. Scale bar (IF) = 50µm.

Organoid morphology, as determined by IF analysis, lacks columnar nuclei and stratification of the native retina. SNCG+ and Rcvrn+ cells were not aligned with an apical-basal polarity indicative of retinal lamination (Fig. 4.31). Pax6 was expressed in some cells in both conditions at day 20 and in the IGF1 condition at day 28 (Fig. 4.31). Chx10, which stains nuclei of RPCs and bipolar cells,

dependent on developmental stage, showed staining above background levels, however the expression pattern was extra-nuclear and did not correspond to primary retinal tissue (Fig. 4.31).

Gene expression analysis was performed on C3 derived organoids similarly to C1. Analysis for *Crx*, *Nrl*, and *Arr3* showed no quantifiable data (Ct>35) and therefore are not shown here. As only a single set of samples has been analysed for RT-qPCR expression it is not possible to make conclusions as to the statistical significance of any differences between the conditions, so this data is informative only to show a pattern of trends, or comparison with other culture strategies (C1) (Fig. 4.23).

In comparison to C1, the magnitude of *Rcvrn* was at least a factor of $x10^2$ lower in C3 samples in some cases ($x10^{-5}$ or $x10^{-6}$ vs $x10^{-3}$) which is surprising given the pronounced NE morphology seen in late stages at day 27 and beyond in C3 (Fig. 4.28, 4.29) which is not seen in C1 organoids. Furthermore, Rcvrn expression was detected at day 28 in C3 3D D14 (+/- IGF1) samples (Fig. 4.31). Low gene expression may reflect a low overall proportion of Rcvrn+ cells within the organoid sample.

Expression of RGC marker, *RBPMS,* and horizontal cell marker *Calb1* was high, at a level comparable to that of the adult retina indicating significant generation of RGCs and interneurons (Fig. 4.31). This supports the IF analysis which showed SNCG+ cells at day 20 and 28 across all C3 methods (Table 4.2).

The addition of SAG to the 96-wp or 3D conditions did not cause a drop in retinal gene expression as was seen in C1 samples (Fig. 4.32). Although, in terms of retinal protein expression, addition of SAG resulted in loss of Pax6 expression in C3 3D conditions compared to the un-supplemented condition (Table 4.2).
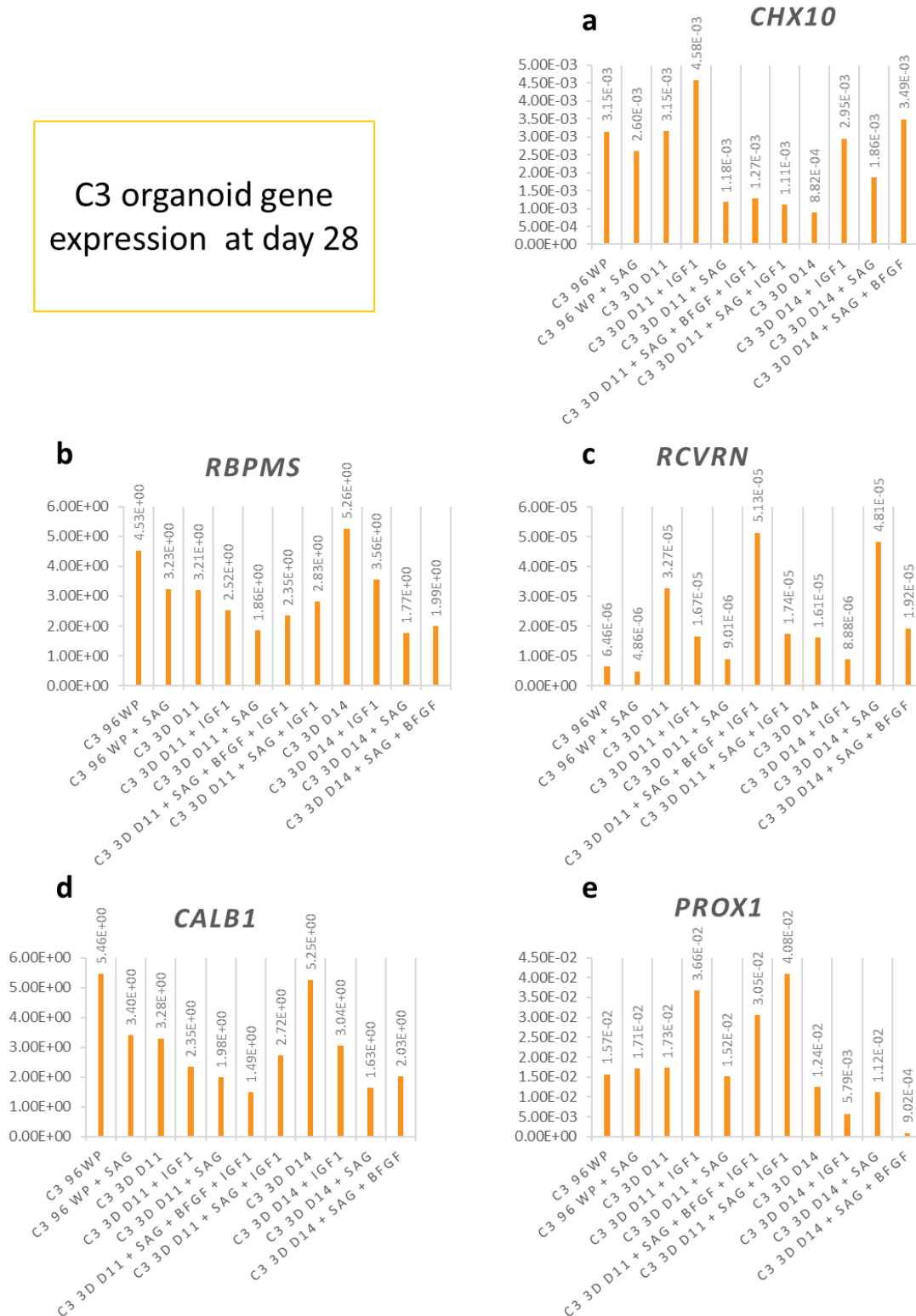
Figure 4.32. Gene expression of rESC-organoids derived with C3 methods at day 28 of differentiation normalised to adult rat retina (a) Chx10 for RPCs (b) RBPMS for RGCs (c) Rcvrn for PRs (d) Calb1 for horizontal cells and (e) Prox1 for horizontal and amacrine cells. Calculated as relative fold change with arbitrary units. N (experiment)= 1, n (organoid) = 20.

In conclusion, organoids derived in C3 conditions showed effective re-aggregation of stem cells and EB formation without the addition of Matrigel, which is useful for deriving a chemically defined protocol free of animal-derived compounds. In light of the lower retinal gene expression seen between organoids generated in C3 and C1 it would be informative to characterise the EBs immediately prior to plating at day 5 to identify differences at an early stage of culture.

The adherent stage of plating effectively generated an expanding population of progenitor cells with a neural identity as determined by Sox2/Nestin/Ki67 staining (Fig. 4.27), corroborating data published by Wang et al. (2012). Nonetheless, the lack of PR expression at day 28 compared with C1 and the absence of laminated NE suggests that maintenance and/or differentiation of mature retinal cells did not occur. Further characterisation of these cells using the retina-specific progenitor markers Rax and Chx10 should be performed during and following adherent plating, to determine whether further adaptations to the culture method could be used to generate a population of cells enriched for retinal rather than neural progenitor cells. A delay in retinal cell specification could follow the transition from 2D to 3D as the stage of RPC expansion has theoretically been extended during adherent culture. However, cells cultured in 2D until day 14 did not show improved expression compared to those re-plated earlier at day 11.

These preliminarily results show that rESC (RRRC) can be cultured adherently and readily re-form 3D organoids in suspension however, they lack a laminated retinal structure at day 28. Analysis at timepoints before and after day 28 would reveal whether organoids were in the process of development or if the window for retinal cell specification had passed. Furthermore, analysis of independent experiment replicates is required to confirm these results.

4.4   Discussion

4.4.1   Mouse retinal differentiation

Obtaining and differentiating a mESC line was valuable to confirm the efficacy of published retinal differentiation methods and give insight into the correct timeline of retinogenesis *in vitro*. This enabled time-matched comparisons between rat and mouse cell lines which showed critical differences in aggregation efficiency and early development (day 0-7; Fig. 4.11). This prompted a review of differentiation methods used specifically on rat PSC (Qu et al., 2015; Z. Wang et al., 2012) followed by their modification and application to rESC (RRRC).

In retrospect, as this differentiation experiment was performed once, additional testing of the Sasai SFEBq method on the rESC (RRRC) line would have been useful to confirm this conclusion.

The mESC experiments also confirmed earlier findings differentiating the chimeric XA ESC line which found the addition of B27 supplement and IGF1 in Conditions 2.3 and 3 (Experiment 7) generated the best examples of retinal morphology, protein expression and generation of pigment (Fig. 3.12, 3.13). This was supported by mESC differentiation using the DiStefano et al. (2018) method, which supplements the culture media with IGF1 from day 10 and B27 from day 18. This method was found preferential for generating NR with a laminated organisation compared to the Sasai SFEBq method (Fig. 4.10).

A potential cause for the differences between rat to mouse response to the same culture conditions could be linked to the stem cell intrinsic capacity for differentiation. Mouse ESC are reported to have a ground or naïve state of pluripotency compared with the primed state held by primate ESCs, which approximates the limited pluripotency of rodent epiblast stem cells (EpiSC) (Guo et al., 2009; Nichols & Smith, 2009). Rat ESCs, unlike mESC, when cultured *in vitro* express high levels of trophoblast stem cell factors, have a higher level of genome instability and show lower efficiency of germ-line competence (Guo et al., 2009; Hong et al., 2011). These differences may suggest variant pluripotency states held by rESC which differentiate them from mESC and could affect their developmental and differentiation capacity *in vitro*.

4.4.2   Rat ESC differentiation

Obtaining a genuine rESC line from the RRRC enabled confident evaluation of previously untested differentiation methods. Conditions testing published rESC differentiation protocols performed by Qu et al. (2015) included both 1% and 2% concentrations of Matrigel and plating densities of 3500 and 5000 cells/well which aimed to bridge the difference between culture techniques previously tested. The rESC (RRRC) line responded well to the enriched plating media (20% KSR) including Wnt

inhibitor IWR-1e and 1% Matrigel, with both cell densities showing effective aggregation, some retinal morphology and retinal protein expression up to day 14 (Fig. 4.13-4.17). This was a significant development in the methodology showing the capacity of a rESC line to generate 3D organoids with retinal morphology and cellular identity and also corroborated published findings (Qu et al. 2015).

A higher concentration of KSR has a moderately caudalising effect which is counteracted in culture by the addition of the rostralising effect of Wnt inhibitor IWR-1e, these method adaptations used by Qu et al. (2015) for rESC differentiation were developed by Nakano et al. (2012) who showed more effective NE generation when differentiating hESC with these conditions. Additionally, the use of Matrigel at a lower concentration of 1% v/v, than previously trialled in the mouse based SFEBq methods, was shown to be preferentially better at generating rESC-organoids with prolonged retinal morphology. This was used by both the modified hESC method and rESC differentiation (Nakano et al., 2012; Qu et al., 2015).

IF analysis at day 14 confirmed NE identity of retinal structures by the widespread Pax6/Rax expression and development of RGCs as denoted by SNCG expression (Fig. 4.17). However, despite the expression of Pax6/Rax, the RPC marker Chx10 was absent (Fig. 4.17). This is also in accordance with the results from Qu et al. (2015) who show *Vsx2* (*Chx10* homolog) expression at a very minimal level of <10 fold in rESC-derived cells compared to 50000-fold for primary rat RPC cells. This could indicate the putative RPCs generated with this method do not have high *Chx10* expression at this stage due to culture conditions or are very few in number.

The improvements in retinal morphology in rESC-derived organoids accompanied by the IF analysis which shows RPC generation in experiment 10 (Table 4.1) is interesting as it unexpectedly suggests greater similarities of culture requirements between rat and human ESC than rat and mouse ESC. Further modification using techniques from human PSC organoid differentiation methods may therefore be appropriate to test on rESC to improve other stages of retinal differentiation.

4.4.3   Rat ESC differentiation optimisations using pooled culture and chemical supplementation

To develop further method optimisations to generate rat ROs, the Qu et al. (2015) method was tested again with the addition of retinal maturation media from day 14. Additionally, C1 methods in section 4.3.3.1 supplemented retinal growth stimulating molecules (Fig. 4.18). The rationale for SAG and IGF1 addition was based on method optimisations used in hESC retinal differentiation to increase PR precursors (Mellough et al., 2015; Nakano et al., 2012).

While C1 methods generated organoids displaying retinal NE morphology at day 14 and 17 in the non-supplemented and SAG variants, the prevalence of NE decreased from day 17-28 and pronounced OV structures were not seen (Fig. 4.20). Culture of ROs in pooled culture led to maintenance of NE morphology beyond day 14. This could be due to greater exposure to local paracrine signalling reinforcing correct retinal specification (Close et al., 2005), or improved media circulation generally in a larger volume. Protein analysis showed cells positive for Rcvrn at day 24, while none were detected at day 28.

Gene expression analysis at day 28 showed retinal gene expression of RGC and interneurons (*RBPMS* and *Calb1*) at a level comparable to native rat retina, which is partially confirmed by IF analysis and detection of SNCG. Expression of RPC/bipolar cell and PR markers, *Chx10* and *Rcvrn*, was much lower than that in mature rat retina, however the C1 sample showed much higher *Chx10* and *Rcvrn* expression than any variant of C3 methods (Fig. 4.23, 4.32). PR-specific markers, *Crx*, *Nrl* and *Arr3* were not expressed at detectable levels. Low PR gene expression at day 28 despite evidence of Rcvrn at day 24 suggests that maintenance and development of mature PR cells beyond a certain timepoint was lacking in the C1 condition. Earlier analysis of C1 samples, such as at day 20 would be informative to determine to what extent PR specification is occurring and whether the timeline aligns with *in vivo* development.

The C1 retinal differentiation methods from day 0 -14 were principally based on the Qu et al. (2015) publication which did not show maturation of the RPCs in *in vitro* culture. This prompts the possibility that the rESCs were not amenable to further maturation in the adherent system and could not be further matured in this way. This was seen to some extent in these results where a mature laminated retinal structure or expression of multiple retinal cell types was lacking. However, the results from these experiments show a promising starting point for further method optimisations for rESC differentiation.

4.4.4 Rat ESC differentiation optimisations using novel and hybrid adherent plating strategies

Further testing with rESC (RRRC), in C3 methods in 4.3.3.2, aimed to accelerate the rate of optimisation and screen a variety of alternate culture strategies that had been shown to work in retinal or neural culture from primarily rat PSCs (Wang et al. 2012; Qu et al. 2015).

The alternate "hanging-drop" method for generating robust embryoid bodies (EBs) was tested in C3 and successful in 100% of organoids (n = 864) (Fig. 4.25) and removes the need for Matrigel addition.

This provides a useful alternative which could be used to derive a fully defined culture protocol, which can improve organoid heterogeneity and is required for manufacturing production of cell models.

The method for EB formation which was adapted from the mouse ESC differentiation studies using Wnt and Nodal inhibitors (Osakada et al. 2008) in C2 methods was shown to be less effective at generating EBs with NE morphology. This was in contrast to the methods used for rESC differentiation including the prolonged addition of 1% Matrigel and increased KSR proportion ("Qu") and the hanging-drop method ("Wang"). This is further evidence for the effectiveness of specific rat-optimised methods, rather than the use of mouse differentiation protocols.

The adherent culture strategy reported by Wang et al. (2012) to specifically enhance and isolate proliferating NE progenitor cells was successfully used in C3 methods to generate re-aggregated 3D organoids with retinal morphology and thick phase-bright NE tissue which was maintained long term in culture (Fig. 4.28, 4.29). This step likely eliminates non-NE cells which could be causing degradation in organoids which were kept in 96 well plate (wp) format at later timepoints (Fig. 4.30).

Similarly to organoids derived with "Qu" conditions there was no detection of the RPC marker Chx10 by IF analysis in C3-derived organoids at either day 20 or 28. In this case, as Rcvrn cells are already present it is likely that RPC marker expression would have occurred prior to these timepoints. It would be possible to check this by performing molecular analysis at an earlier stage of differentiation to capture the RPCs before they mature.

The lack of expression of post-mitotic PRs (*Crx*), rod (*Nrl*) and cone progenitor (*Arr3*) markers despite detection of *Rcvrn* is interesting and suggests further IF analysis with PR or bipolar markers should be performed to better characterise the Rcvrn+ cells. The presence of Rcvrn and absence of Crx/Nrl/Arr3 could also suggest an immature phenotype as PRs may not yet have committed to specific rod or cone identity.

The gene expression analysis of key retinal markers, *Chx10* and *Rcvrn*, in C1 organoids are of a larger magnitude than any of the samples from C3 methods. As this is measured at a relatively late timepoint (day 28) this could indicate the methods using an intermediary 2D plating stage have delayed the process of retinal development and expression of mature cell markers. This is supported by the morphological characterisation of ROs which, in human differentiation experiments, have been generally classified into distinct stages by the Gamm et al. group. Their study showed an initial stage with a thick bright NE layer which peaked in size in "Stage 2" of development followed by a thinner lamina with a brush border for the more mature "Stage 3" of organoid development

(Capowski et al., 2018). If we consider rat RO development to occur along a common developmental staging, the morphology of organoids derived with adherent plating in C3 conditions show a peak in NE laminar thickness later than those in the C1 methods. This could be suggestive of a delayed differentiation process which would be reflected in a longer period of retinal gene expression which could be quantified several stages after day 28.

4.4.5   Further work

Assessing the later stages of organoid development, at day 20 and 28, by IF analysis with the proliferation marker Ki67 in combination with markers such as Pax6 would reveal if the cells are still in the stages of differentiation or if cells are terminally differentiated. This would determine whether adherent plating stages had, as expected, extended the stages of RPC generation and thereby delayed the onset of maturity in 3D re-aggregated organoids.

During the later stages of differentiation, dark pigmented patches of cells were seen in organoids with NE morphology derived using C3 3D conditions (Fig. 4.29). These could be further investigated using IF analysis for RPE-specific markers such as Mitf, for immature stages, and RPE-65 for mature stages, to determine if putative RPE has arisen in these organoids.

Although long-term maintenance in culture is sometimes desirable and should result in maturing retinal cell organisation and synaptogenesis the results here often show decreased retinal protein expression at day 28 compared to day 20. This could indicate that there is the capacity to develop into retinal-like organoids earlier in the differentiation timeline which is not sustained at the day 28 stage.

Given the success of generating re-aggregated organoids in 3D using 2D adherent plating strategy, and the positive retinal gene and protein expression generated in C1-derived organoids using the modified "Qu" method, it would be informative to test the adherent plating strategy from day 8 in combination with the Qu et al. media components from day 0-14, followed by further retinal maturation media and supplementation with IGF1.

Furthermore, another independent repeat of the rESC differentiations was performed, using the culture conditions from C1 (Modified "Qu") and C3 (Hanging-drop and adherent plating) methods. Analysis of these replicates would confirm whether effects from the method modifications were statistically significant. Unfortunately, due to limitations of time, the analysis of these samples was not carried out.

Despite the lack of generation of laminated tissue, there was maintenance of the 3D organoid structure beyond previous timepoints of differentiation where phase-bright tissue degraded. Furthermore, there was significant generation of RGCs in rESC-derived ROs, evidenced by protein and gene expression analysis. The reliable generation of rESC-RGCs may be informative for the development of therapeutics and tissue modelling for glaucoma or other diseases which are characterised by loss or damage to RGCs.

Therefore, the outcomes from these method modifications and differentiation experiments provide an informative starting point for the further development of *in vitro* rat retinal differentiation.

Chapter 5

Chapter 5 Macaque retinal differentiations

5.1 Macaque retinal differentiation strategy

As retinal histogenesis is a highly conserved process co-ordinated by core transcription factors and developmental pathways, optimisations shown in hPSC culture can inform differentiation methods used for related non-human primate (NHP) species such as macaques.

Based on these reports, the development of novel differentiation protocols for generating NHP retinal organoids (ROs) should consider the overall accelerated timeline of development in primates with shorter gestation periods compared with humans. Therefore, this chapter will test the application of retinal differentiation methods adjusted to the relatively shorter gestation length of the macaque, which is hypothesised to better support the process of retinal differentiation.

Studies indicate a role for IGF1 supplementation to improve PR generation and long-term maintenance in human RO cultures (Mellough et al., 2015; Dorgau et al., 2019). As IGF1 receptors are widely expressed throughout the macaque PR layer, similarly to expression patterns in the native human retina (Rodrigues et al., 1988; Waldbillig et al., 1991), it is conceivable that IGF1 can be applied for similar positive developmental effects in macaque RO culture. Based on this research the

The stimulatory effect of RA/T supplementation on macaque PR generation and the effective results achieved in various human RO differentiation methods supports their use for further RO method development and therefore these have been tested in this chapter for generation of macaque ROs. These culture methods provide a relevant starting point for the development of novel retinal differentiation methods for macaque iPSCs (Fig.5.1).

Retinal differentiation of macaque ESCs using solely 2D culture has the capacity to develop into a limited range of retinal cell types, including RPE, RGC and PR cells, however these are found disorganised in populations of mixed cell identity (Osakada et al. 2009). Therefore, in this chapter, the use of the 96-well plate (wp) system to generate 3D organoids in suspension culture was tested in preference to adherent culture in 2D plates.

The strong effect of RPE-CM supplementation seen on macaque ESC differentiation and on human ROs suggest beneficial effects to PR generation in primate ROs and therefore RPE-CM supplementation was tested in this chapter for the retinal differentiation from macaque iPSCs (Fig. 5.1).
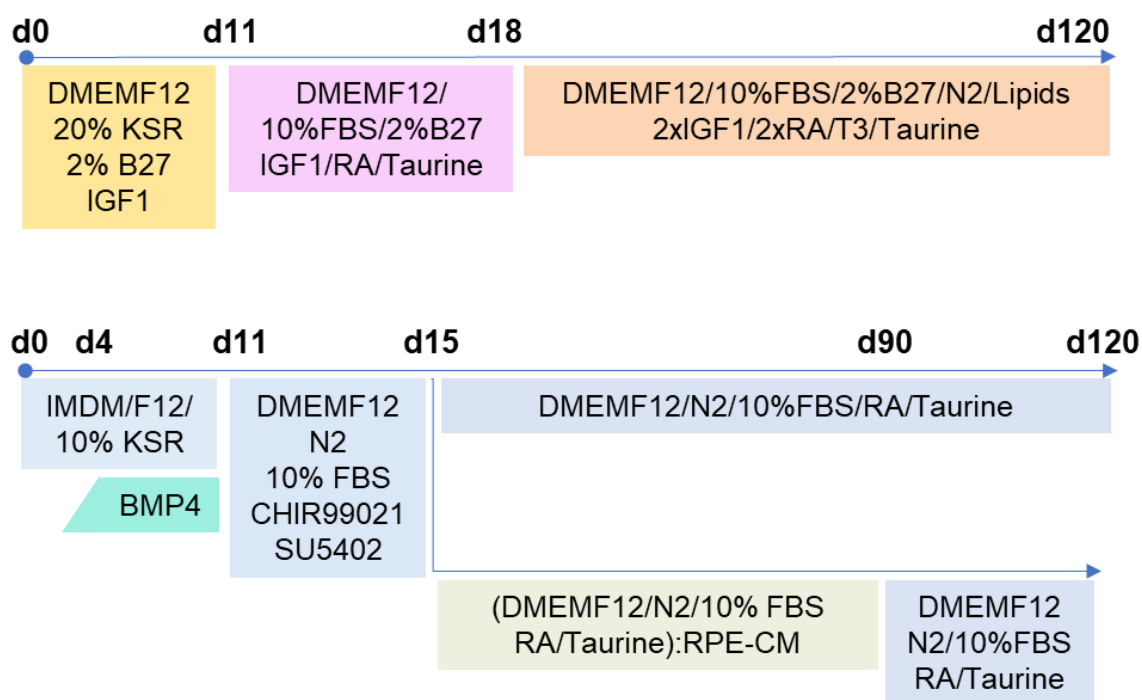
Figure 5.1. Schematic describing the optimised protocol variants assessed for macaque retinal organoid differentiation using a contracted timeline (up to day 120), IGF1 culture and RPE-CM media addition between day 15-90.

5.2 Chapter aims

The aim of this chapter was to derive 3D ROs from three lines of commercially available cynomolgus macaque (*Macaca fascicularis*) iPSCs. Published differentiation protocols reported to work with human PSCs were used as a baseline and novel method adaptations were included such as the alteration of the timing of culture protocols and inclusion of signalling molecules and RPE-CM hypothesised to enhance retinal differentiation.

The derived macaque organoids were characterised for structure and cellular identity and diversity. This included analysing the morphological development, retinal protein and gene expression and cellular structure using immunohistochemistry (IHC), RT-qPCR, and bright-field microscopy. This data enables the comparison of differentiation methods and iPSC lines in the efficiency and efficacy of retinogenesis.

The derivation of a method to generate an *in vitro* NHP retinal model would be a significant and novel development for the field of retinal organogenesis. It would be immediately utilisable in pre-clinical studies investigating the safety and action of retinal disease therapeutics. In addition, it would provide a model to comparatively study primate retinal development and enable identification of human-specific mechanisms of disease.

5.3 Results

5.3.1 Adaptation of primate stem cells to feeder-free culture conditions

According to the culture protocol used by the iPSC manufacturers (Shimozawa, 2016) iMEF feeder cells were used as a substrate on which to expand the macaque stem cells. These cells formed large colonies consisting of tightly packed cells with a high nuclei to cytoplasm ratio (Fig 5.2). These colonies showed highly defined edges (Fig. 5.2).
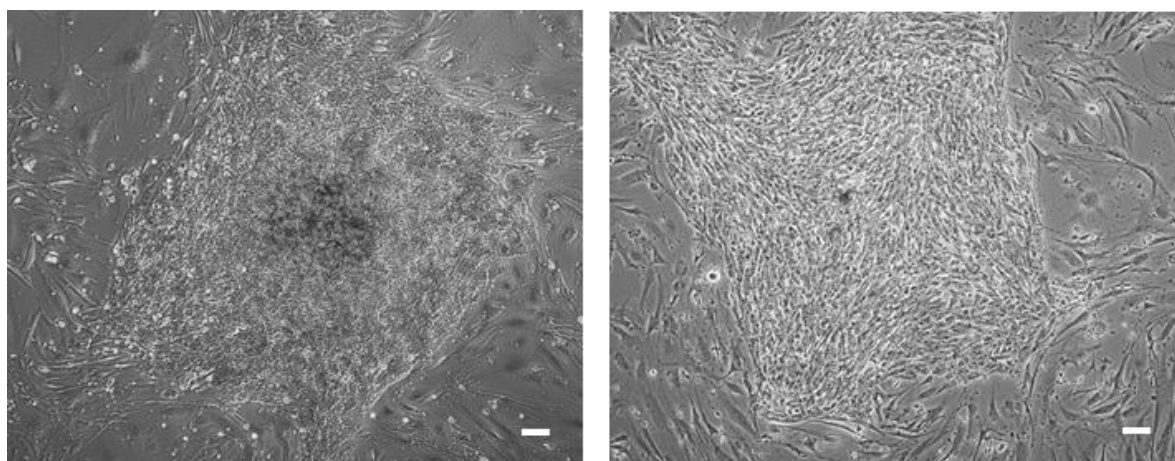
Figure 5.2. Macaque iPSCs (H1 line) grown on iMEF feeder cells. Cells imaged on a phase-contrast microscope 5 days after seeding. Scale bar = 100 µm

As human ESC and iPSC have been successfully adapted to feeder-free culture conditions using Matrigel as a surface substrate this same culture technique was applied to macaque iPSCs in an effort to streamline the culture process and remove a degree of non-uniformity that comes from using feeder cells. The protocol details for seeding density and passaging technique were used from a published study (Wunderlich et al., 2012). The recommended seeding densities ranged from 1000 – 2000 cells/ cm^2 which is represented by the three plating densities of 9000, 13500 and 18000 cells per well of a 6wp (9.6cm^2)(Fig. 5.3). Following plating, cells were sparsely distributed in the wells and the culture with the highest plating density achieved confluency 7 days after plating (Fig. 5.3).
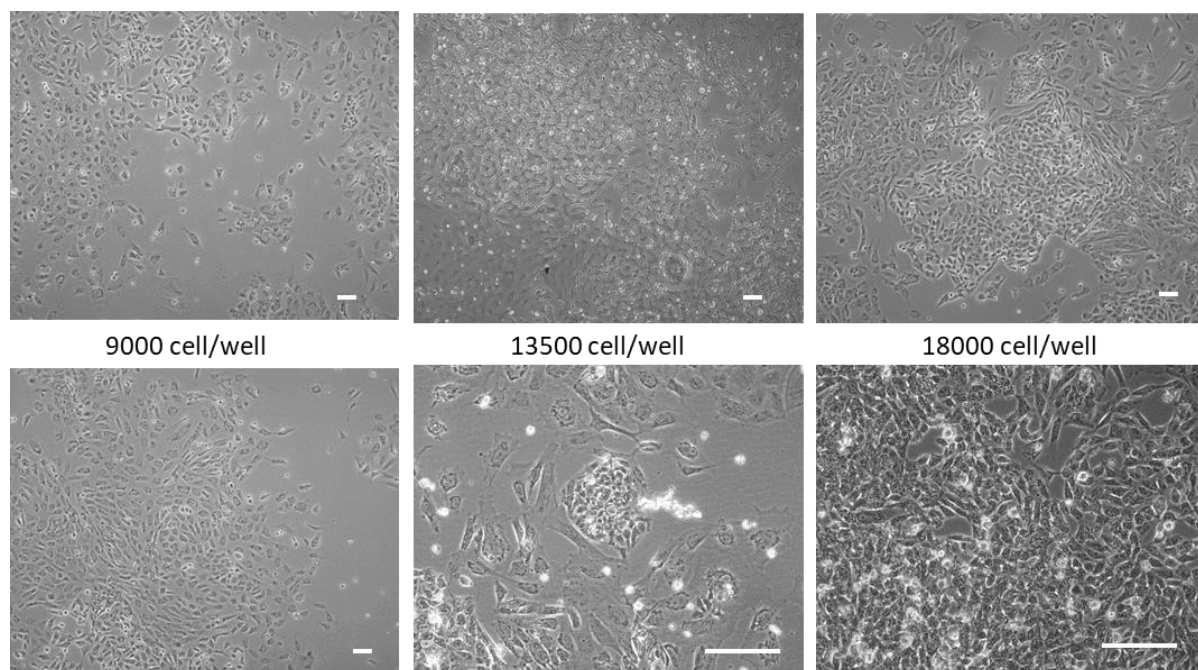
Figure 5.3. Macaque iPSCs (H1 line) grown as a monolayer in feeder-free conditions on Matrigel coated plates at 3 seeding densities. Cells imaged on a phase-contrast microscope 7 days after seeding. Scale bar = 100 μm.

The morphology of the iPSCs grown in feeder-free conditions lacked the tight clustering and definition of colony edges seen in cultures grown on iMEF feeder cells (Fig. 5.3, 5.2). Cells in the lower density conditions of 9000 and 13500 cells/well showed an epithelial-like cell morphology (Fig. 5.3). Therefore, it was necessary to determine whether these cultures retained their pluripotency. To achieve this RNA was extracted and assayed for the expression of known pluripotency genes *NANOG*, *SOX2* and *OCT4* and a housekeeping gene *GAPDH* (Fig. 5.4).

Alongside the macaque iPSC samples, a human iPSC cell line (AD4/WT3) was analysed to act as a positive control (Melguizo-Sanchis et al., 2018). All cell samples assayed showed a uniform level of *GAPDH* expression which provides a useful baseline for comparison of other gene expression levels. All macaque iPSC samples excepting "d" (H1 grown on iMEFs with no tightly packed colonies) showed positive expression of all pluripotency markers (Fig. 5.4). The cell sample "b" (H1 grown on Matrigel in a 12-wp) showed relatively lower expression of *OCT4* and *NANOG* compared with other cell samples (Fig. 5.4) indicating a higher proportion of cells in this sample were not pluripotent.
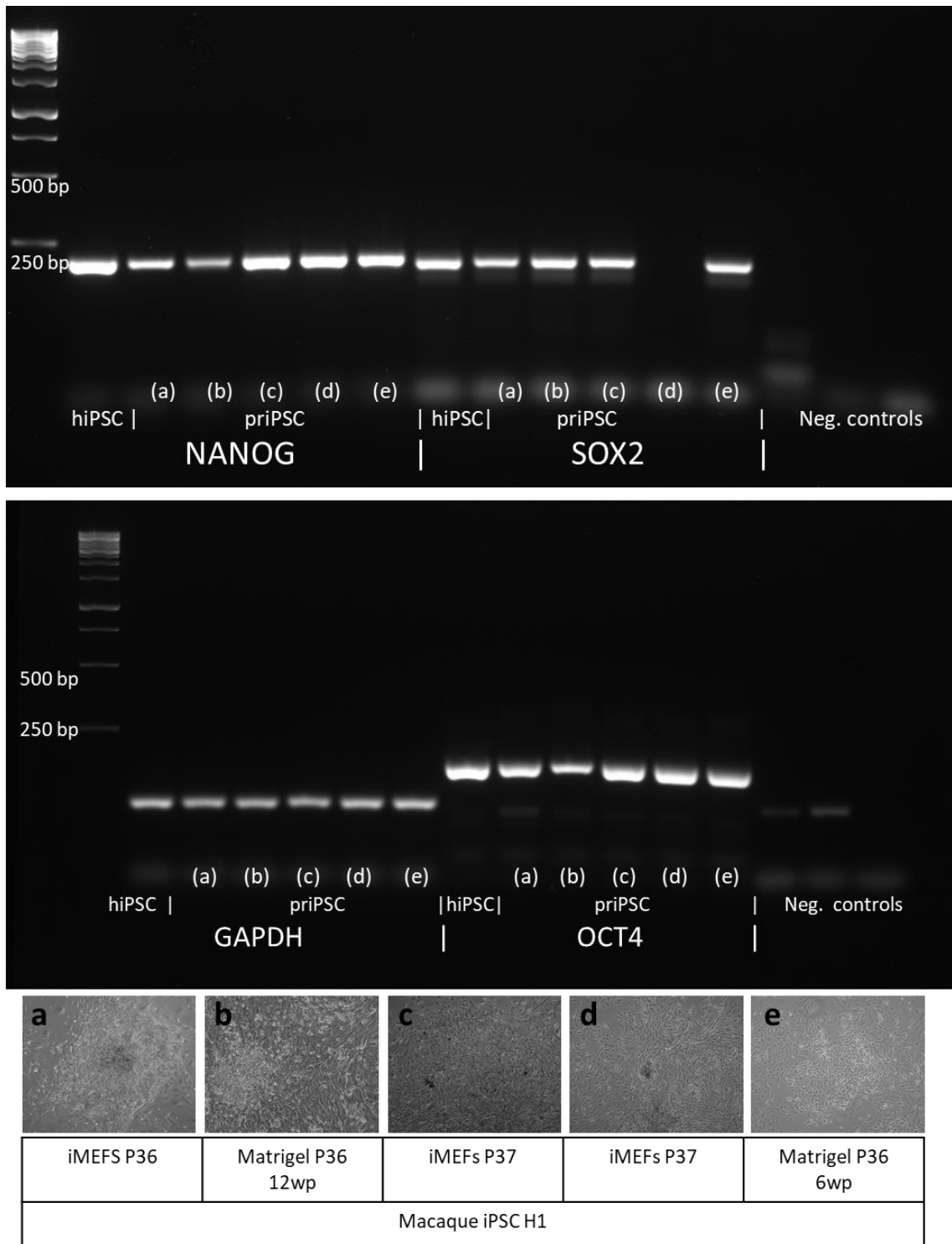
Figure 5.4: Pluripotency gene expression analysis of macaque iPSC (priPSC) H1 RNA samples cultured on iMEFs and in feeder-free conditions (Matrigel). A human iPSC (hiPSC) line (WT3) was analysed as a positive control. P = passage number. Negative controls include "No RT" and water samples.

To further validate the pluripotency of the macaque iPSCs and to characterise their visual identity, a commercially available pluripotency cell stain was applied to macaque iPSCs (S1, H5 and H1) cultured in parallel on iMEFs and Matrigel. The co-localisation of the fluorescent green stain with the densely packed cells towards the centre of the colonies cultured on iMEFs is apparent for all cell lines (Fig. 5.5). The cells grown on Matrigel are positive for the pluripotency stain when they are clustered together, this type of growth is less prevalent in the S1 cell line where all the cells on Matrigel show only background levels of expression (Fig. 5.5). Furthermore, as a visual aid this technique enables the future identification of cells with a morphology expected to correlate with pluripotency.
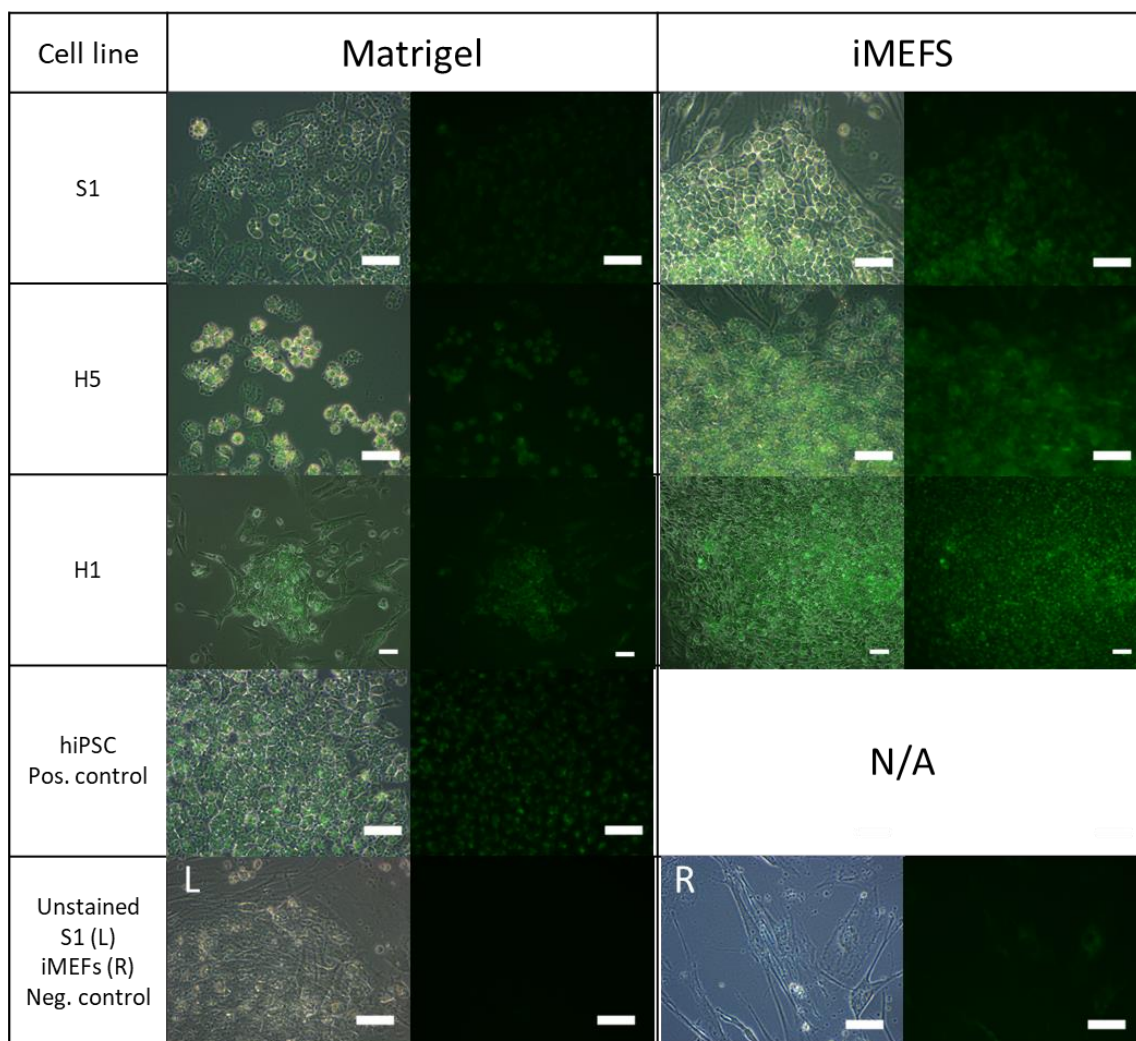
Figure 5.5. Application of Biotracker pluripotency cell stain to macaque iPSC lines (S1, H1 and H5) cultured on Matrigel or iMEF feeder cells. Human iPSC line (AD4) grown in usual conditions on Matrigel used as a positive control. Unstained S1 cells (L) and stained iMEFs (R) imaged as a negative control. Scale bar = 100 μm.

Overall, these analyses shows that the substrate for culturing the cells is not the main determinant of the cells' retained pluripotency as both those on Matrigel and iMEFs showed a degree of pluripotent gene expression and binding to pluripotency indicator dye (Fig. 5.4, 5.5). However, the formation and structure of cells in tightly packed colonies with high expression of pluripotency dye can only be observed under iMEF culture conditions. Henceforth, cells were cultured solely on iMEFs as visually it was possible to distinguish those with a morphology known to correlate with pluripotency and therefore enable quick and robust culture. Furthermore, the manual passaging technique was used as it most reliably ensured re-plating of sufficiently large cell clumps which showed the brightest staining with the Biotracker pluripotency dye. All three iPSC cell lines (H1, H5 and S1) were able to be cultured reliably using this technique. Their pluripotency was considered validated and therefore their suitability for retinal differentiation experiments was confirmed.

5.3.2   Optimising the timing of retinal differentiation methods to the macaque gestation length

The SFEBq method was first shown as a technique for the self-organisation of stem cells by the Sasai group. The EBs generated from both mouse and human ESC/iPSCs differentiated, under specific cell culture conditions, into 3D ROs broadly comprising the structure and cellular diversity of the native retina (Eiraku et al., 2011; Eiraku & Sasai, 2012; Nakano et al., 2012). Therefore, this method was tested on the macaque iPSC lines to establish whether they were capable of 3D self-organisation induced by the SFEBq technique in a 96-wp format.

The SFEBq differentiation protocol was further optimised, by the Sasai group and others, to improve the method efficiency and the generation of specific cell types within the RO model. Kuwahara et al. (2015) modified the method by including the brief addition of the small molecules CHIR99021 and SU5402 between days 18-24 of hESC differentiation. These were termed "induction -reversal molecules" for their stimulatory effect on the growth of retinal pigmented epithelium (RPE) and resulted in the generation of a retinal organoid comprising both RPE and neural retina. Both the un-modified and the Kuwahara/Sasai variant including the induction-reversal molecules were initially tested on macaque iPSCs (Fig. 5.8). The addition of Matrigel was not tested during macaque iPSC differentiations, instead the BMP pathway stimulant BMP4 was added at day 6 which was shown in hiPSC differentiation to reliably generate neural retina (NR) (Kuwahara et al., 2015).

Further novel variations to the Kuwahara/Sasai method (Kuwahara et al., 2015) were tested including the adjustment of the culture method timeline to the relatively shorter gestation of

macaque embryonic development, these conditions are termed (NHP) compared to those with human timing (H) (Fig. 5.8). The addition of macaque RPE-CM to the culture media of the Kuwahara/Sasai differentiation method was also tested, in an effort to improve PR generation and retinal structure (Fig. 5.8).

Finally, a protocol used for the differentiation of human PSC including IGF1 and other retinal growth factors was tested for macaque retinal differentiation using macaque-adjusted timing, and termed C3 (Dorgau et al., 2019; Mellough et al., 2015) (Fig. 5.8). The full method media components are listed in Table 5.3.

These differentiation methods were tested on macaque iPSC lines in parallel and where possible using the same starting population of cells to reduce technical variation.
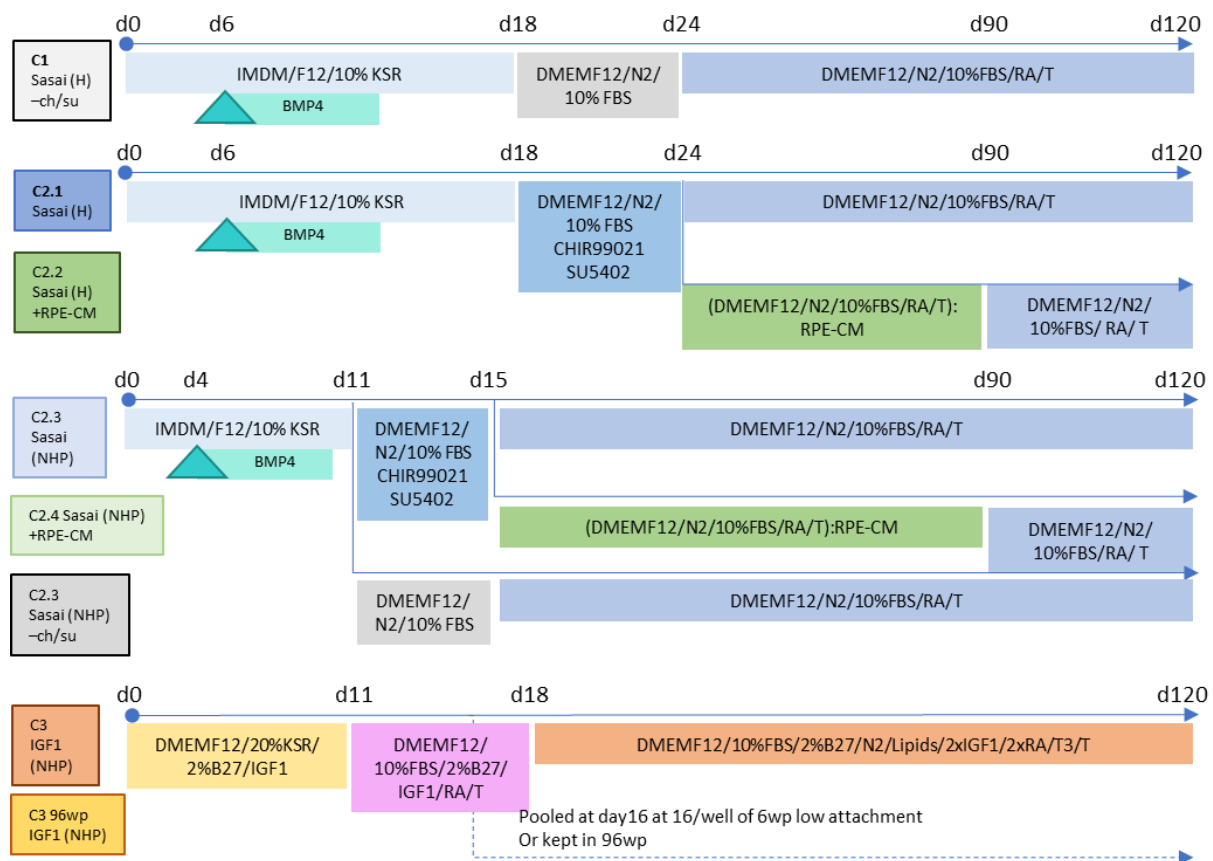
Figure 5.8: Outline of method setups tested on macaque iPSC lines showing media composition and timepoints of addition. Those based on the Sasai protocol (C1, C2.1, C2.2, C2.3, C2.4) and those using IGF1 based protocol. ch/su = CHIR99021/SU5402, RA = retinoic acid, T = Taurine, RPE-CM = RPE conditioned media, (H) = human timing (NHP) = Non-human primate (Macaque) timing.

216

A novel method adjusting the culture timeline of the "Sasai" protocol to the shorter gestation of macaque was tested on 3 cynomolgus macaque iPSC lines; S1, H5 and H1. The time adjustment was based on the ratio of 165 days of macaque gestation to the human 270 days (Fig. 5.8). It was hypothesised this program of culture conditions would better align with the intrinsically faster program of development and enhance the subsequent retinal development and cell differentiation from macaque iPSCs.

In these experiments, the organoids were sampled throughout differentiation. They were maintained in culture, where possible, until day 120 which is expected to correlate with day 200 of human RO development. By day 120 in macaque retinal development *in vivo*, approximately 96% of cells are expected to be present (Fig. 5.1). Therefore, RPE, PR and Müller glia cells which arise latest in retinogenesis are expected to be detectable in macaque RO cultures at this timepoint (Fig. 5.1).

The morphology of S1 organoids derived with the Sasai method with macaque-adjusted timing (Sasai (NHP)) showed an optically bright layer of neural retina (NR) that was maintained until day 120 (Fig. 5.9a). The efficiency of the NHP timing method was also improved with close to 100% of organoids exhibiting a complete smooth phase-bright neuroepithelial (NE) edge from day 8-50 in contrast to 35-75% in the human timing (Sasai (H)) condition (Fig. 5.9b). Following day 50 there was a substantial loss of retinal morphology in S1 organoids in both conditions however around 35% of organoids in the NHP condition were still morphologically retinal by day 120 compared to <5% in the Sasai (H) condition (Fig. 5.9a,b)

Generation of organoids with a characteristic retinal morphology with effective aggregation and NE development was achieved with H5 iPSCs and NHP adjusted timing (Fig. 5.9c). Retinal morphology was generally lost in H5 organoids derived with human (H) timing following day 70 whereas in the NHP timing method it is maintained until day 120 (Fig. 5.9c). Due to deterioration of the H5 Sasai (H) organoids the final timepoint (day 120) was not analysed.

A third macaque iPSC line, H1, was assessed for retinal differentiation capability using Sasai methods with macaque-adjusted timing (NHP). Unfortunately, the organoids generated with the inclusion of induction-reversal molecules became unusable due to an infection so only the condition tested without CHIR99021/SU5402 (-ch/su) could be analysed. H1 organoids from this method showed effective aggregation following plating and development of positive retinal morphology including phase-bright putative NE between day 9-50 (Fig. 5.9d). However, the putative NE tissue deteriorated from day 50 onwards (Fig. 5.9d).
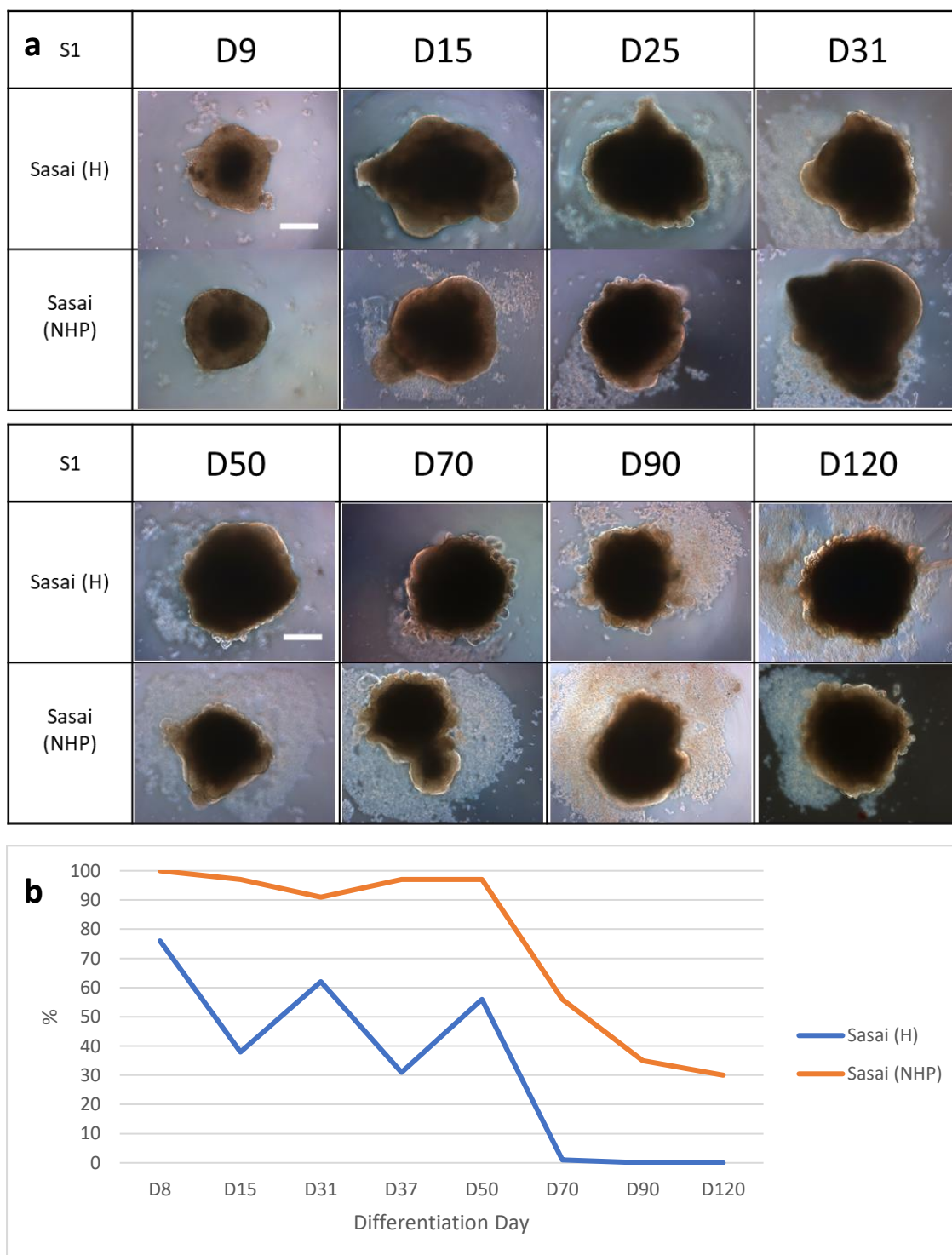
Figure 5.9: Comparing organoids throughout differentiation with Sasai protocols using human (H) or macaque (NHP) adjusted timing. (a) Representative morphology of S1 organoids throughout differentiation showing presence of bright neural retina (b) Efficiency to generate S1 organoids with retinal morphology n = 294. (c) Representative morphology of H5 organoids with Sasai (H) and (NHP) adjusted timing. n = 196. (d) Representative morphology of H1 organoids with Sasai (NHP) adjusted timing without CHIR99021/SU5402 (-ch/su), n =196. D = Day. Scale bar = 100 µm.

H5	D9	D15	D21	D31
Sasai (H)				
Sasai (NHP)				

H5	D50	D70	D90	D120
Sasai (H)				NA
Sasai (NHP)				
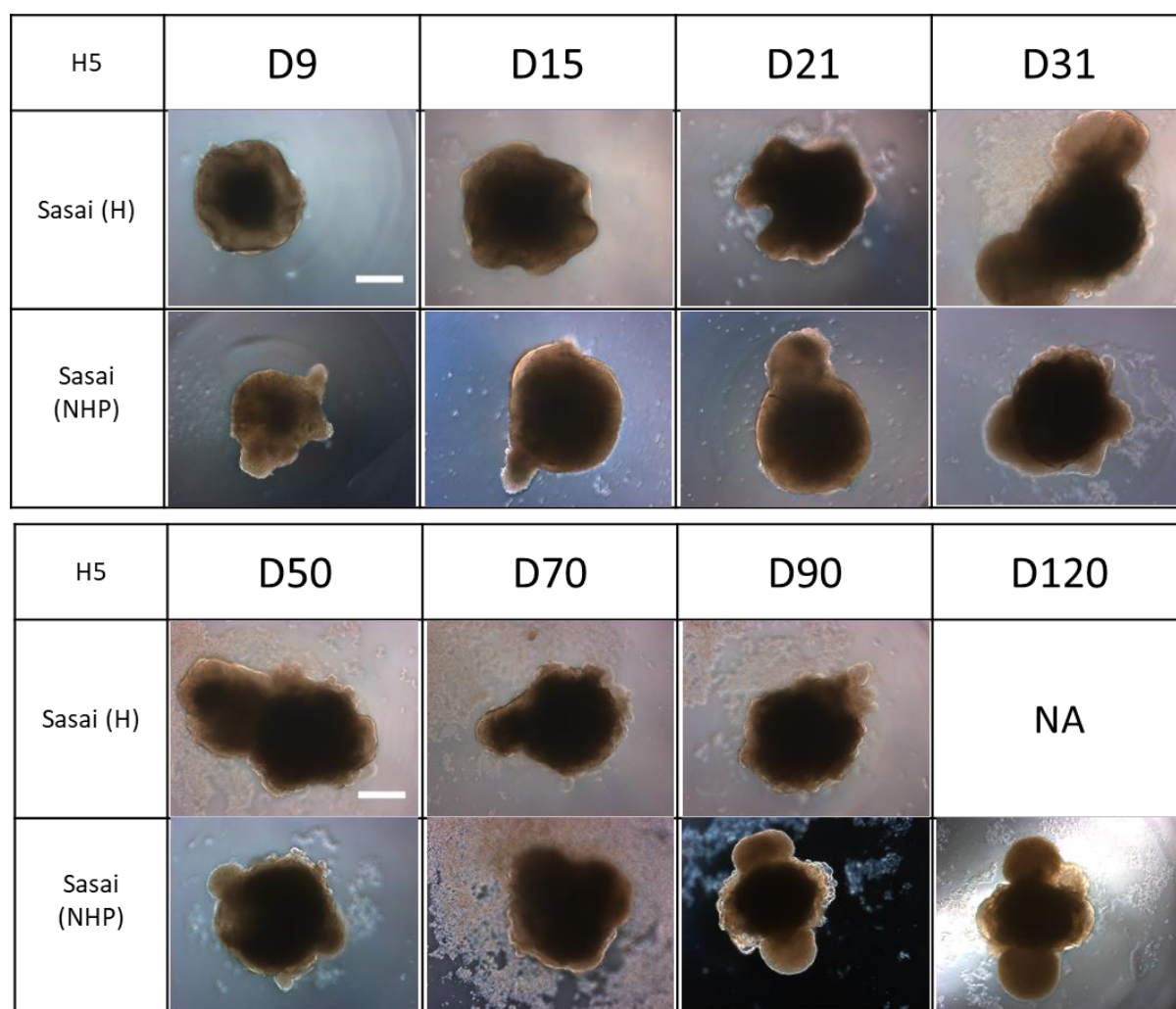
In summary, organoids derived from 3 macaque iPSC lines with the Sasai SFEBq based culture method show effective aggregation and the development of characteristic phase-bright putative NE tissue. The conditions using the NHP adjusted timing method show the prevalence and maintenance of this retinal morphology at a greater proportion and length of time in both the S1 and H5 organoids compared with the human timing method. In order to characterise the identity of the cells within the putative NE, protein and gene expression analysis was performed on organoid samples.

5.3.2.1 Molecular analysis of early-stage macaque organoids derived with NHP timing adjusted methods

To assess the identity of the putative NE and confirm the structural development and localisation of retinal cells within the organoids, IF analysis was performed. NE and retinal markers were assessed at the expected timepoint(s) of their expression to characterise the staging of organoid

development. At each timepoint, at least 6 organoids were sampled, processed and representative images collected. To corroborate protein expression analysis, gene expression analysis by RT-qPCR was performed on S1 and H5 organoid samples. Each differentiation experiment using the S1 cell line was independently performed twice. Relative gene expression was normalised to adult macaque retinal tissue and *GAPDH* used as an endogenous control using the $2^{-\Delta\Delta Ct}$ method. Each sample was collected from at least 10 organoids. Statistical analyses using two-way ANOVA with multiple comparisons was performed at each timepoint between conditions as described in Methods 2.5.

In organoid samples from day 9 – 15 expression of the eye-field transcription factors Rax, Pax6, Otx2 and neuroectodermal/neural stem cell marker Sox2 was assessed, and Sasai methods with either human (H) or macaque (NHP) timing were compared.
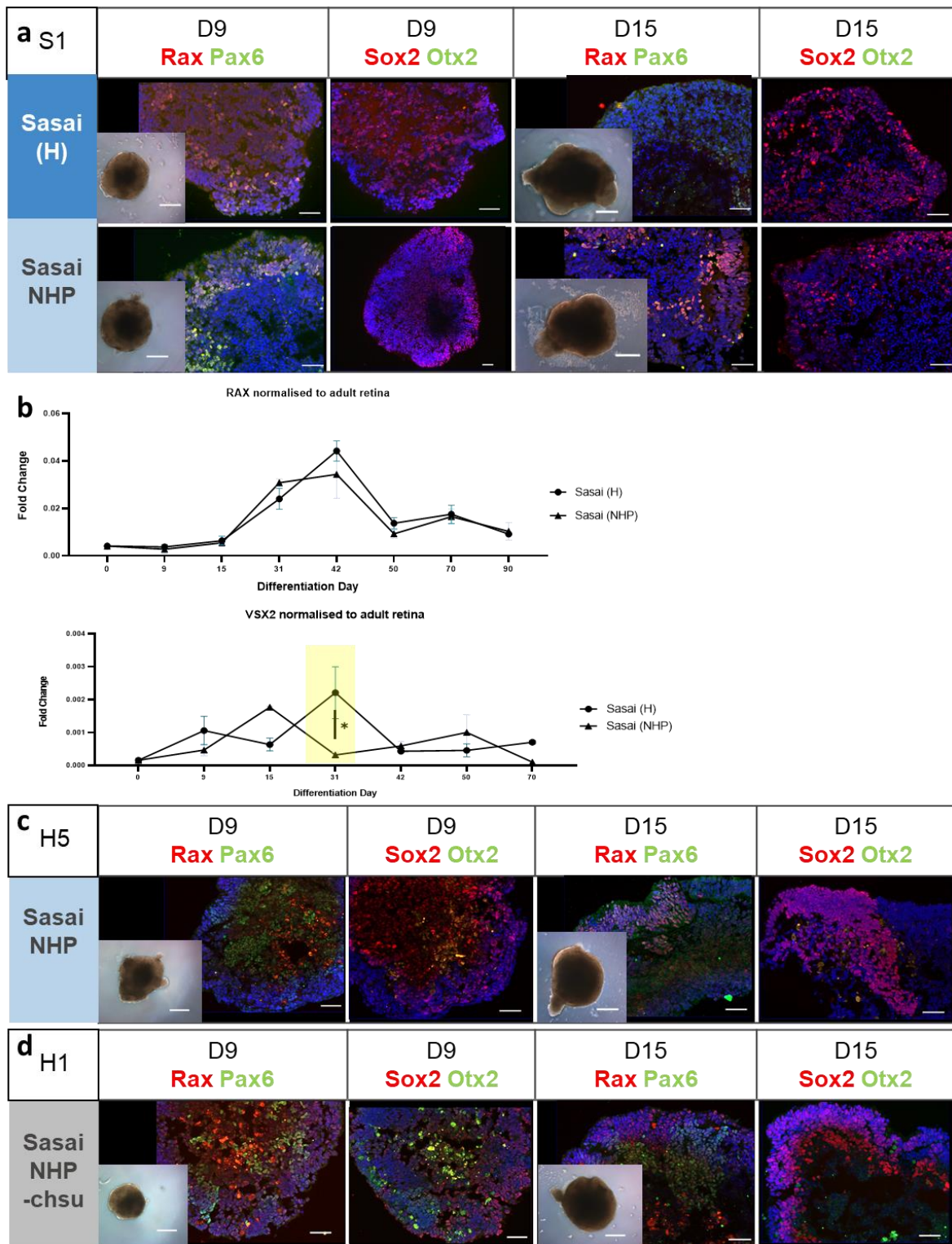
Figure 5.10. Expression of eye-field transcription factor Rax, Pax6, Otx2 and neuroectodermal Sox2 markers comparing Sasai condition with human (H) and macaque (NHP)-specific timing. (a) S1 organoids (b) Gene expression of S1 organoids. Error bars show SEM. N=2. * = p-value < 0.05, ** = p-value < 0.01, *** = p-value <0.001, **** = p-value <0.0001. (c) H5 organoids (d) H1 organoids derived without CHIR99021/SU5402 (-chsu). D = day.

In S1 organoids Rax and Pax6 co-localise in cells at the periphery of organoids, regions expected to correspond to the phase-bright areas seen by bright-field microscopy (Fig. 5.10a). In both conditions Sox2 is expressed throughout the organoid at day 9 becoming restricted to peripheral regions by day 15 (Fig. 5.10a). This correlates with the appearance of phase-bright tissue and confirms neuroectodermal differentiation with specific regions of eye-field specification (Fig. 5.10a). A notable difference is the continued presence of Rax at day 15 in the S1 (NHP) timing samples but not in the (H) samples (Fig. 5.10a). Otx2 was not detected in any S1 samples (Fig. 5.10a). Gene expression analysis of *RAX* shows expression levels between day 9-15 are relatively low with peak expression in samples from both conditions occurring between day 15-50 indicating continued retinal specification (Fig. 5.10b). Expression of retinal progenitor cell (RPC) marker *VSX2* peaks later in samples generated using the human timing condition at day 31 at levels significantly higher than in the NHP timing condition (Fig. 5.10b). Expression of *VSX2* was not detectable beyond day 70.

In H5 organoids Pax6 and Rax are expressed in cells between day 9 – 15 but these are not located in a thick peripheral band consistently as in S1 (NHP) derived organoids but distributed throughout the organoid (Fig. 5.10c). These markers co-localise in cells at day 15 indicating the presence of NE tissue at the periphery of organoids (Fig. 5.10c). Similarly to S1 samples Sox2 expression is distributed throughout the organoid at day 9, then restricted to peripheral areas at day 15 which also matches the areas of optically bright tissue (Fig. 5.10c). Similarly to S1 samples Otx2 was not detected in H5 samples (Fig 5.10c).

H1 organoids derived with the Sasai (NHP) condition without induction-reversal molecules (-ch/su) showed Rax expression throughout organoids between day 9 - 15 with some Rax- cells found to be Pax6+ (Fig. 5.10d). Sox2 was also expressed in cells throughout the organoids becoming more spatially restricted by day 15, as seen in the S1 and H5 samples (Fig. 5.10d). A notable difference seen in H1 organoids compared to both S1 and H5 is the presence of Otx2+ cells seen at day 9 (Fig. 5.10d). Up to day 11 this condition has identical media composition to the Sasai (NHP) condition therefore, this difference likely represents a cell line specific effect or variation within the sample.

In conclusion, at the early stages of differentiation, expression of neuroectodermal marker Sox2 and eye-field transcription factors Rax and Pax6 are observed in the areas characterised by the presence of phase- bright NE. This confirms the development and identity of NE tissue expressing specific eye-field markers. This expression pattern is seen in all cell lines excepting H1 samples which also express Otx2 transiently at day 9. As this marker is lacking in H5 and S1 organoids this may be due to cell line differences. Analysis of later stages of organoid development in terms of protein and gene

expression will show whether these cell lines generate mature PR and other retinal cells over the course of differentiation. Gene expression of the RPC marker, VSX2, was seen to peak earlier in S1 organoids derived with the NHP-adjusted timing method.

5.3.2.2 Molecular analysis of mid-stage macaque organoids derived with NHP timing adjusted methods

Next, organoid samples were analysed at timepoints during the mid-stages of differentiation (day 50-90) for PR and bipolar cell marker Rcvrn and RGC marker SNCG/RBPMS to determine if retinal cell differentiation was occurring and NE tissue was developing retinal lamination.

In S1 organoids some laminated areas at day 50 are seen in Sasai (H) and (NHP) conditions, with Rcvrn+ cells found in a linear arrangement towards the base of the organoid edge and adjacent to SNCG+ cells (Fig. 5.11a). This arrangement could suggest inversion of retinal cell lamination, or that the Rcvrn+ cells are bipolar cells which would then be correctly positioned between RGCs basally and developing PRs (Fig. 5.11a). At day 70 and 90 both S1 samples (H) and (NHP) show SNCG+ cells with developing axons are present adjacent to Rcvrn+ cells (Fig. 5.11a). However, throughout this time period Rcvrn+ cells are localised in the interior of the organoid while SNCG+ cells are sparsely located with axons found at the outer edge of the organoids indicating mis-localisation of developing PR/bipolar cells and lack of a laminated structure (Fig. 5.11a).
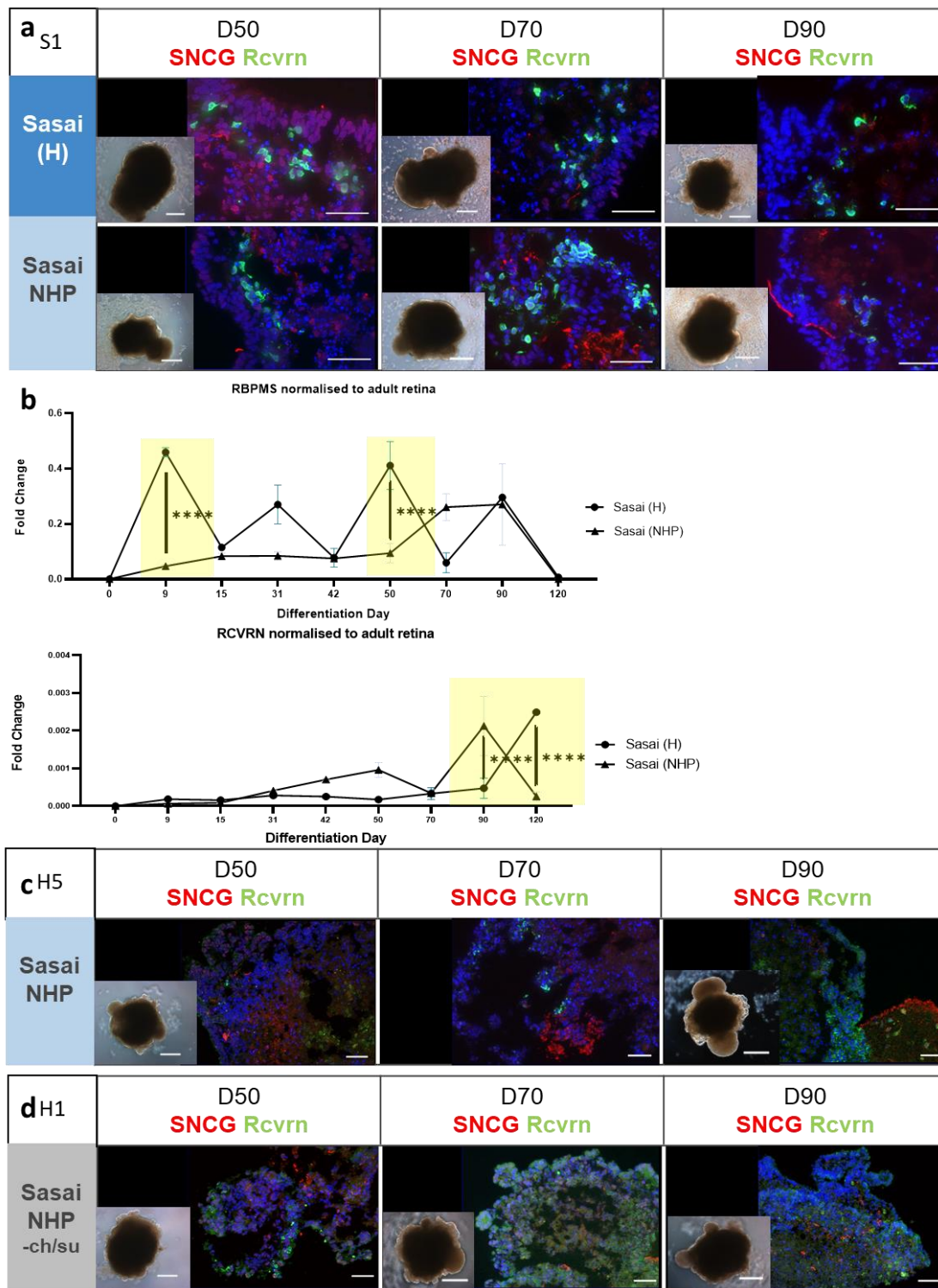
Figure 5.11. Expression and localisation of RGC (SNCG/RBPMS) and PR/bipolar (Rcvrn) cells comparing Sasai conditions with human (H) and macaque (NHP)-specific timing. (a) S1 organoids, (d) Gene expression of S1 organoids shown as fold change normalised to adult macaque retina. Error bars show SEM. N=2. * = p-value < 0.05, ** = p-value < 0.01, *** = p-value <0.001, **** = p-value <0.0001. (c) H5 organoids, (d) H1 organoids derived without CHIR99021/SU5402. D = day.

Although the RGC marker SNCG appears similar between timing conditions in S1 samples, expression of *RBPMS* is significantly higher (p<0.0001) in the human timing condition at day 9 and 50 when expression levels peak at around 0.5-fold that in the native retina (Fig. 5.11b). However, in the NHP timing condition *RCVRN* expression peaks at a level significantly higher than the human timing condition at day 90 (p<0.0001), earlier than the peak seen in the human timing condition at day 120 (Fig. 5.11b).

In H5 organoids, Rcvrn+ cells are generated later than in S1 and H1 organoids as none were detected at day 50 (Fig. 5.11c). By day 70 there are Rcvrn+ cells which appear within the central areas of the organoid, adjacent to SNCG+ cells however a laminated structure is lacking (Fig 5.11c). At day 90 Rcvrn+ cells are localised to a continuous peripheral region indicating correct localisation for PRs, however SNCG+ cells are located in a neighbouring apical edge indicating lack of a laminated retinal architecture (Fig. 5.11c).

H1 organoids derived with the Sasai (NHP) method without CHIR99021/SU5402 at day 50 show prevalent Rcvrn+ cells surrounding the edge of organoids with SNCG+ cells found within the body of the organoids in an arrangement approximating that of retinal structure (Fig. 5.11d). At day 70 and 90 Rcvrn+ cells remain localised at the peripheral edge of the organoids and SNCG+ cells are noted basally to them, in the correct relative orientation, in contrast to S1 organoids (Fig. 5.11d/a).

In conclusion, during the mid-stages of differentiation, organoids from all cell lines develop the presence of both PR and RGC markers. Rcvrn+ cells are observed in S1 and H1 organoids from day 50 onwards. In H5 organoids they arise later from day 70. RGC marker SNCG is present from day 50 in all conditions and cell lines. Comparison between S1 organoids derived with human or NHP timing showed no difference in marker localisation however RBPMS was significantly decreased in the NHP timing method. RCVRN expression peaked significantly earlier in the NHP timing condition. This timepoint of increased RCVRN expression at day 90 is more aligned with that seen in macaque gestational development corresponding with both rod PR and bipolar cell development (Fig. 5.1). The most striking differences were seen between cell lines. H1 and H5 organoids showed Rcvrn+ cells correctly localised to the outer periphery of organoids at day 90 whilst S1 organoids showed internal Rcvrn+ cells throughout day 50-90. Further investigation using PR-specific markers and assessment of later timepoints would indicate whether Rcvrn+ cells and retinal structure are developing.

5.3.2.3 <u>Analysis of late-stage macaque organoids derived with NHP timing adjusted methods</u>

To investigate the presence and localisation of PRs in phase- bright NE tissue observed in organoids at day 120 the PR opsin markers; OPN-S, OPN-ML, and Rhodopsin (Rho), were assessed in organoid samples from day 90 and 120. Co-staining with RGC marker SNCG was performed to identify areas of retinal lamination and polarity of PRs.

At day 90 in S1 organoids generated with the Sasai (H) method there is expression of cone opsin markers (OPN-S/OPN-ML) marking some cells at the periphery of the organoids (Fig. 5.12a). Rhodopsin expression is lacking throughout this area and no structured lamina is observed (Fig. 5.12a). In comparison the organoids generated with the Sasai (NHP) method show a continuous band of cone opsin (OPN-S/OPN-ML) expressing cells at the organoid periphery which are arranged in a laminar layer approximating the ONL in the retina (Fig. 5.12a). Staining in (NHP) samples shows extra-nuclear expression and axon formation indicating improved maturation of cone PRs using this method (Fig. 5.12a). Rhodopsin expression is lacking, as only background reactivity is seen, and SNCG expression is also absent, indicating loss of RGCs and lack of a laminated retinal structure (Fig. 5.12a). In contrast, gene expression analysis of the PR precursor marker *CRX* and cone PR marker *ARR3* show significantly higher peak expression in samples generated with human timing methods (Fig. 5.12b). The magnitude of expression levels is low indicating a smaller proportion of these cell types in organoid samples compared with the native retina (Fig. 5.12b). Both *CRX* and *ARR3* peak at day 31 which corresponds with the gestational development of cone PRs, which occurs between day 30-90 and precedes PR marker expression at day 50 (Fig. 5.12b, 5.1).

In H5 organoids generated with the (NHP) method there is a thin, one cell thick, border of S cone opsin (OPN-S) positive cells found at the peripheral edge of the organoids at day 90 similar to the S1 Sasai (H) samples (Fig. 5.12c, a). The OPN-S marker is more prevalent than OPN-ML and Rhodopsin is not present in any cells showing background expression only (Fig. 5.12c). This narrow lamina aligns with the Rcvrn+ cells seen in previous staining at day 90 (Fig. 5.11c). SNCG+ cells are also absent in these regions close to the OPN-S/OPN-ML+ cells indicating lack of fully laminated retina (Fig. 5.12c).

H1 organoids at day 90 showed both OPN-S and OPN-ML expression in cells located at the outer edge of organoids (Fig. 5.12d). These cells show, similarly to the S1 (NHP) samples, extra-nuclear expression of OPN-S and OPN-ML with some axon formation from the cells while Rhodopsin expression is absent (Fig. 5.12d). SNCG+ cells are detected basally to OPN-S and OPN-ML positive cells indicating correct relative localisation however they do not form a continuous lamina of cells (Fig. 5.12d).
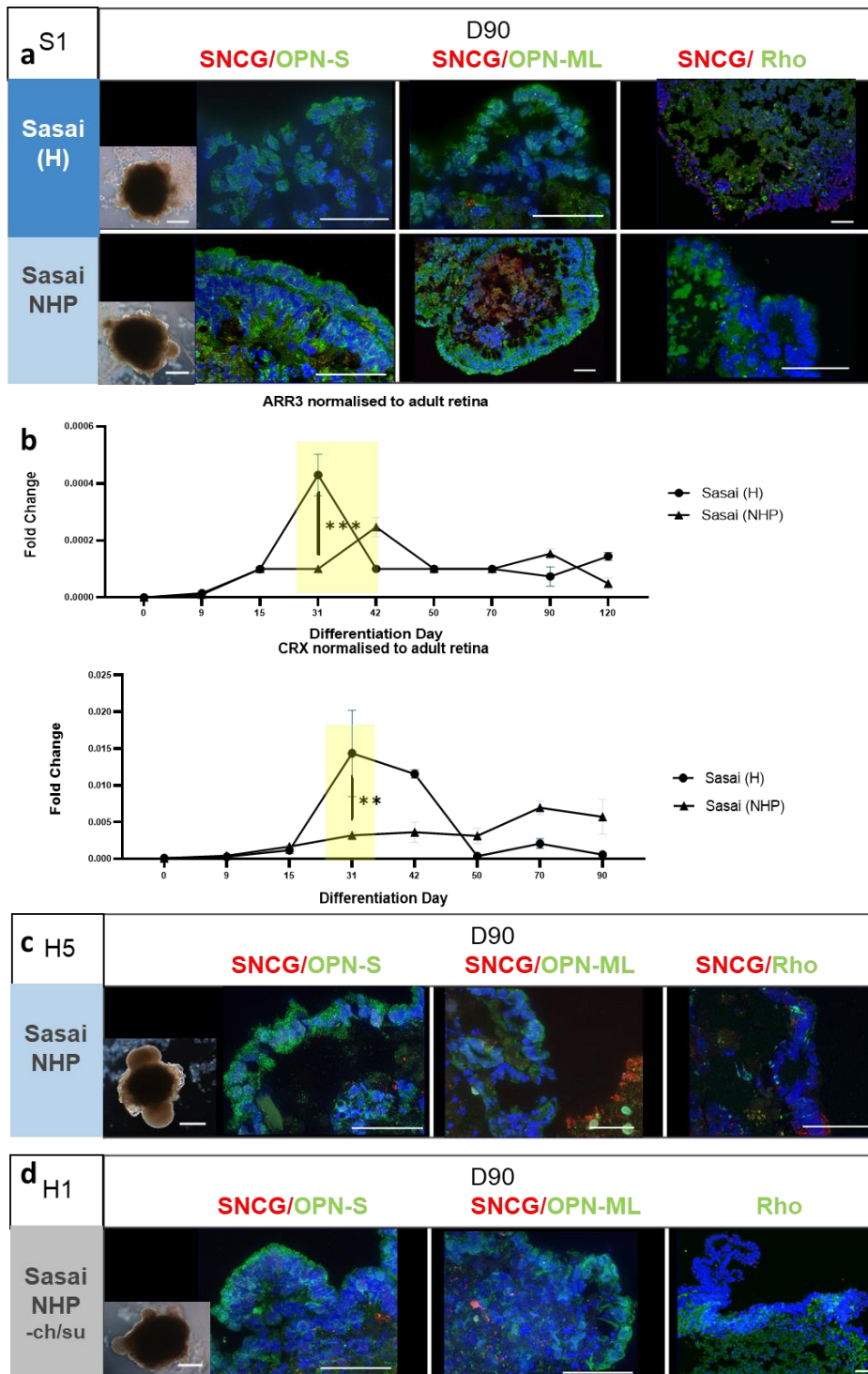
Figure 5.12. Expression of RGC (SNCG/RBPMS), S-cone (OPN-S), M/L cone (OPN-ML) and rod (Rho) cells comparing Sasai method with human (H) and macaque (NHP) timing. (a) S1 organoids (b) Gene expression shown as fold change normalised to adult macaque retina for S1 organoids. Error bars show SEM. N=2. * = p-value < 0.05, ** = p-value < 0.01, *** = p-value <0.001, **** = p-value <0.0001. (c) H5 organoids, (d) H1 organoids. Green reactivity in Rho panels is background levels only. D = day.

S1, H5 and H1 organoids sampled at day 120 were assessed for the presence of cell types generated latest such as rod PRs and Müller glia cells, in addition to cone PRs and RGCs.

At day 120 S1 organoids derived with Sasai (NHP) method show OPN-S and OPN-ML expression is retained in cells at the peripheral edge with continued axon formation however the structure of an ONL lamina seen at day 90 in (NHP) samples is not detected (Fig. 5.13a). In both (H) and (NHP) conditions there is presence of CRALBP+ cells in the proximity of OPN-ML+ cells (Fig. 5.13a). In the Sasai (H) samples OPN-ML and OPN-S expression is comparable to Sasai (NHP) samples (Fig. 5.13a). Atypical localisation of SNCG is seen in some cell nuclei located in the OPN-S cell layer at the outer edge of the organoids in both the (H) and (NHP) timing conditions and Rhodopsin+ cells are absent (Fig. 5.13a). The expression of the Müller glia marker *RLBP1* steadily increases after day 42, peaking in both conditions at day 120 however is significantly higher in the (H) sample at its peak (Fig. 5.13b).

H5 organoids derived with the Sasai (NHP) method show some OPN-S+ and OPN-ML+ cells however these do not show axon formation seen in S1 samples (Fig 5.13c, a). The samples were also negative for Rhodopsin and Rcvrn in the same areas (Fig. 5.13b). As organoid morphology showed a loss of phase-bright neural retina to a greater extent than H5 organoids derived with other methods, these were not further analysed with other mature markers such as CRALBP.

H1 organoids generated with the exclusion of induction-reversal molecules (-CHIR99021/SU5402) show phase-bright NR and OPN-S/OPN-ML expression at day 90 (Fig. 5.12d). At day 120 these show maturing OPN-S+ PRs, basic lamination with RGCs located basally to Rcvrn+ cells and CRALBP+ cells within the lamina of cone PRs (Fig. 5.13d). Additionally, a bipolar-specific cell marker (GO-α) was tested in combination with Rcvrn to identify whether it co-localised with Rcvrn in bipolar cells. Rcvrn+ cells at the periphery did not co-express GO-α indicating these are not of bipolar cell identity (Fig. 5.13d). The presence of Arr3 was also detected in cells lining the outer edge supporting the marker expression of OPN-S and OPN-ML (Fig. 5.13d).
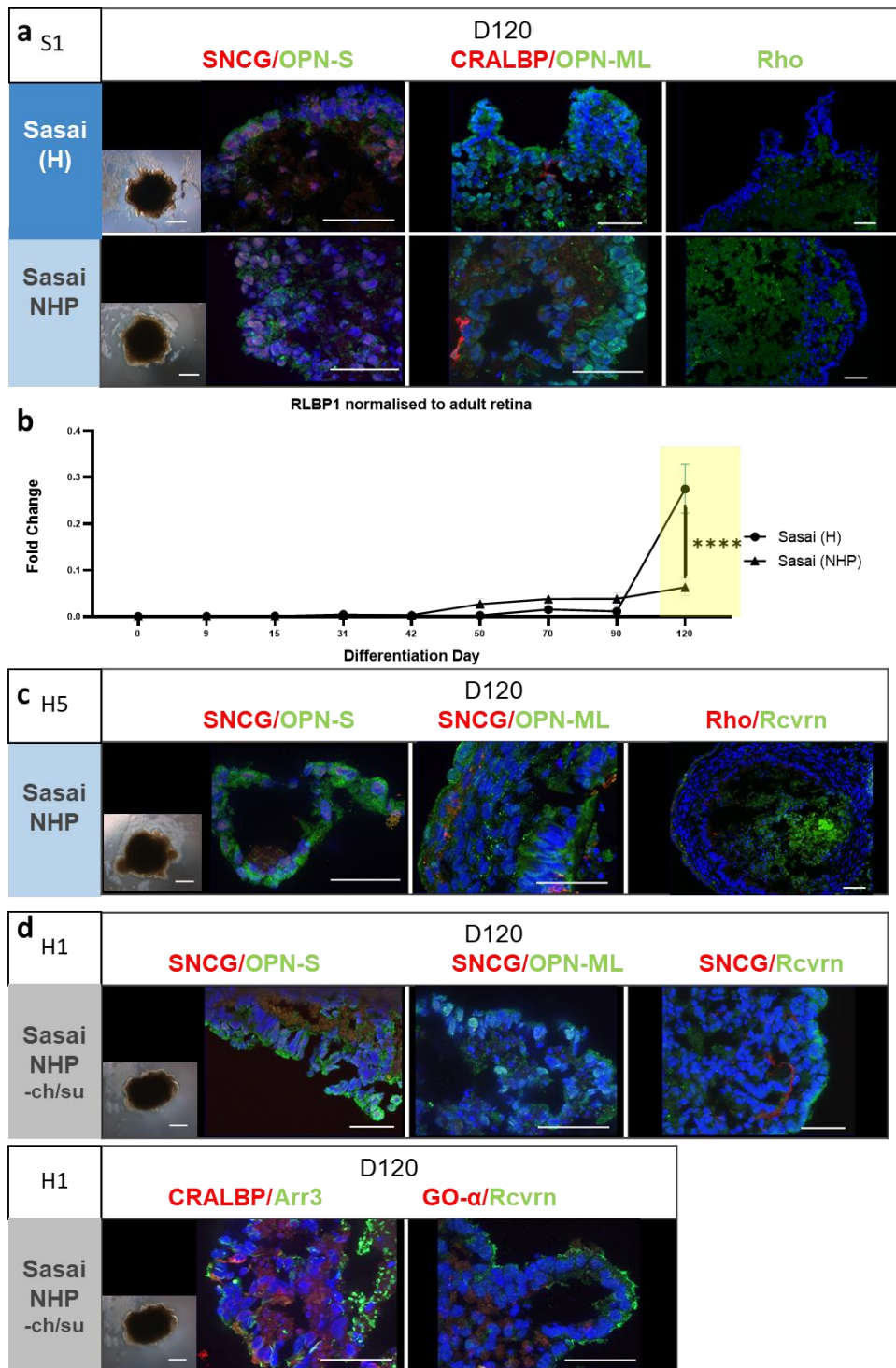
Figure 5.13. IF analysis for RGC (SNCG), S-cone (OPN-S), M/L-cone (OPN-ML), rod (Rho), PR/bipolar (Rcvrn), Müller glia (CRALBP/RLBP1), cone PR (ARR3) and bipolar (GO-a) cells comparing Sasai method with human (H) and macaque (NHP) timing. (a) S1 organoids (b) Gene expression in S1 organoids shown as fold change normalised to adult macaque retina. Error bars = SEM. N=2. * = p-value < 0.05, ** = p-value < 0.01, *** = p-value <0.001, **** = p-value <0.0001. (c) H5 organoids, (d) H1 organoids. Green reactivity in Rho panels is background levels only. D = day

Interneuron cell expression was assessed in S1 organoids by gene expression analysis using known markers throughout differentiation. Gene expression of horizontal cell marker *PROX1* peaked between day 15-31 in both conditions (Fig. 5.14). This aligns with horizontal cell genesis which begins in the native macaque retina in the first phase of cell birth (Fig. 5.1). *PROX1* was not detected beyond day 50 and no significant differences were observed between conditions.

The marker for bipolar cells, *PRKCA*, shows a gradual and steady increase from day 15 onwards reaching a peak at day 70 in both conditions, which is in line with gestational development (Fig. 5.14). Relative expression levels are high, peaking at~0.3-fold of adult macaque retina and no significant differences were observed between conditions throughout differentiation (Fig. 5.14).

The marker for mature amacrine cells, *AP2A*, peaks earlier, between day 31-42, in NHP timing condition, and at day 50 in human timing condition (Fig. 5.14). The expression level of *AP2A* is high in both conditions reaching ~0.4-fold of adult macaque retina expression at the peak (Fig. 5.14). Following peak expression *AP2A* expression decreases in both conditions reaching a level comparable to day 0 by 120 (Fig. 5.14). The expression of both conditions aligns with cytogenesis in the macaque retina as amacrine cells are born early in the second phase of cell birth with cell numbers reaching a peak between day 56-85 and production ceasing by day 110 (Fig. 5.1).

A critical transcription factor for RPE development, *MITF* peaks between day 50-90 in both conditions and shows significantly higher expression in the NHP-adjusted method at day 70-90 (Fig. 5.14). Relative expression of *MITF* is comparable to the levels seen in adult macaque retina rising to around 2-fold that of the adult at day 70 (Fig. 5.14). As *MITF* plays an important role in the formation of RPE within the retina this may indicate RPE generation at these stages in development although no pigmented cells were visible in organoid samples.
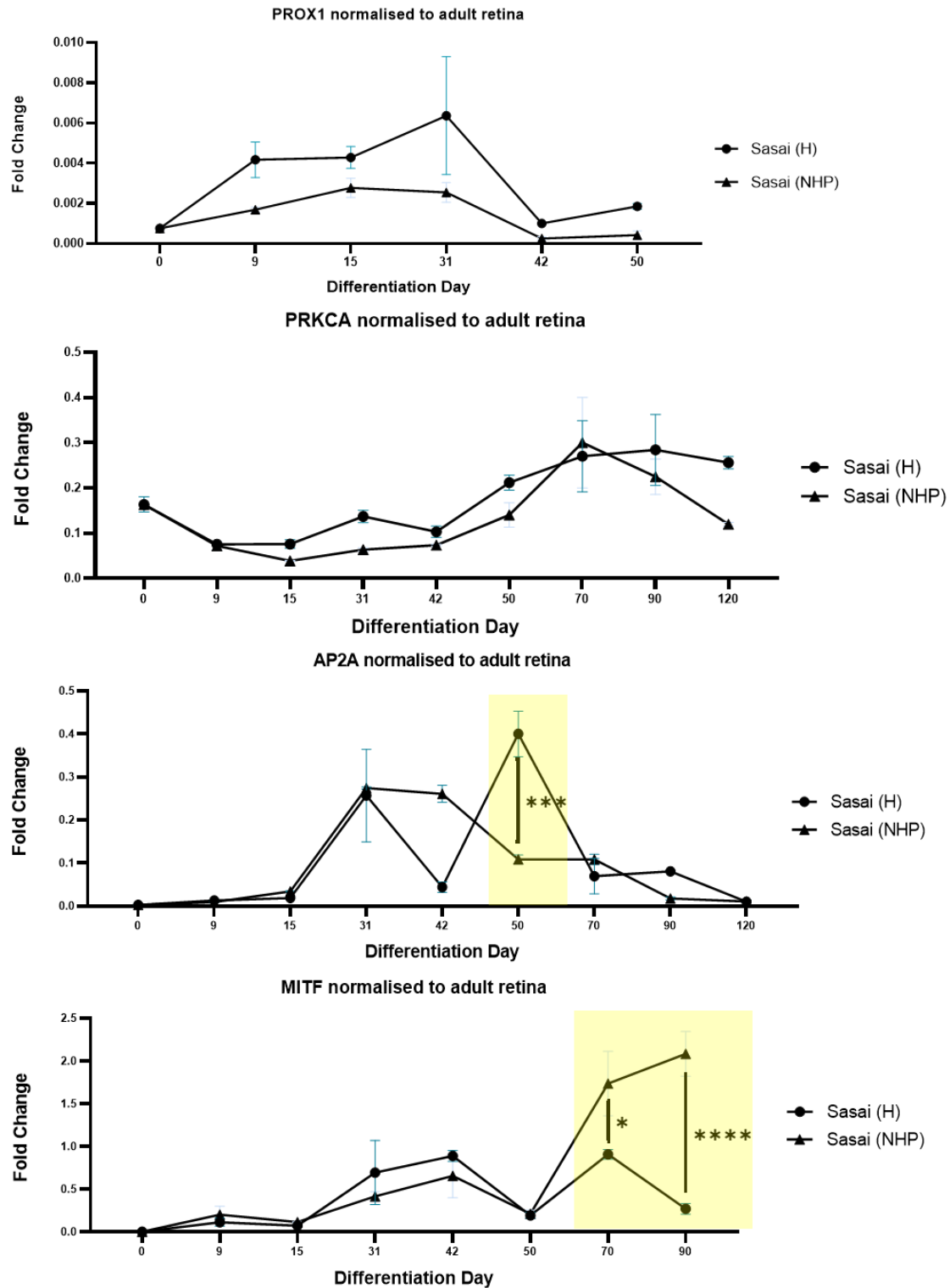
Figure 5.14. Gene expression analysis of S1 organoids throughout differentiation comparing Sasai condition with human (H) and macaque (NHP)-specific timing. Gene expression shown as fold change normalised to adult macaque retina. 10-24 organoids per sample. Error bars show SEM. N=2. * = p-value < 0.05, ** = p-value < 0.01, *** = p-value <0.001, **** = p-value <0.0001.

In conclusion, at day 90 all cell lines show similar prevalence of phase-bright tissue at the periphery of the organoids and cone opsin markers in cells correctly localised to the organoid periphery. The S1 organoids derived with NHP timing show improved OPN-S and OPN-ML cell structure however lower levels of gene expression for cone PR markers. In S1 organoids at day 120, OPN-S, OPN-ML and Müller glia marker presence is retained in both timing conditions although the expression is localised to the nuclear membrane indicating lack of IS/OS development (Fig. 5.13a). Expression of CRALBP is seen alongside OPN-ML+ cells in the "H" timing condition and in the "NHP" condition there are CRALBP+ cells located in a region located basally to OPN-ML cells indicating a maturing retinal structure in both conditions (Fig. 5.13a).

Gene expression of *RLBP1*, *ARR3* and *CRX* are significantly higher in the organoids generated using human timing methods at timepoints aligning with gestational development (Fig. 5.13b). The gene expression of interneuron markers (*AP2A*, *PRKCα*, *RAX*), PR precursors (*CRX*, *ARR3*), and mature markers for PRs (*RCVRN*) and Müller glia cells (*RLBP1*) in S1 organoids throughout differentiation show profiles correlating with the order of cytogenesis in the embryonic macaque retina. Additionally, of note is the low magnitude of gene expression of *PROX1*, *VSX2, ARR3* and *CRX* which were < 0.01 that of adult macaque retina expression (Fig. 5.14, 5.10b, 5.12b). The low levels might be explained by the non-uniformity of the organoids and fewer cell numbers compared to ubiquitous expression in mature retinal cell types of native retina.

Despite some retinal gene expression being increased in the S1 "H" timing samples, organoid morphology was improved and maintained to a greater extent in NHP timing condition (Fig. 5.9a,b). Additionally, several key retinal markers, such as *VSX2* and *RCVRN* showed earlier expression in the "NHP" condition than in "H" timing samples which aligns with gestational cytogenesis. The RPE marker *MITF* was also significantly higher in the "NHP" than in the "H" timing condition at late stages of differentiation.

The morphology and retinal marker expression in H5 samples from the "NHP" condition was similar to S1 organoids at early (Fig. 5.10c) and late stages (Fig. 5.13c). However, H5 organoids showed later expression of Rcvrn and lack of a laminated structure at day 90 (Fig. 11c, 12c). In H5 samples at day 90 OPN-S and OPN-ML markers are seen in the "NHP" condition (Fig. 5.13c) however, H5 organoids did not show maturation of cone PR cells between day 90-120.

H1 organoids show cone opsin, Müller glia and Rcvrn localised in cells at the peripheral edge indicating continued maturation of PR cells and correct structural organisation of the retinal lamina between day 90-120 (Fig. 5.12d, 5.13d). Gene expression analysis would confirm if this cell line

expressed the genes in greater amounts than in the S1 cell lines, as by IF analysis the retinal cell structure is improved.

Overall, the protein expression of macaque organoids at the late stages of differentiation show the S1, H5 and H1 lines to be capable of generating mature retinal cell markers and basic retinal structure in parts. Direct comparison of the "NHP" and "H" timing methods in S1 samples shows that early media addition does not significantly improve retinal marker expression although morphology and some cellular structure is improved.

Mature rod PR markers were not found to be expressed in any cell line at the latest stage of development, indicating a bias towards cone PR production or lack of rod PR maturation using the Sasai retinal differentiation methods. Assessment with an immature rod-specific marker such as NRL would help to determine this.

5.3.3 Adding RPE-CM to macaque retinal organoid differentiation methods

The addition of RPE-conditioned media (-CM) to *in vitro* mammalian retinal culture has been shown to aid retinogenesis and PR maturation (Dorgau et al., 2019; Sheedlo & Turner, 1996b), as well as RPE co-culture facilitating macaque ESC differentiation towards retinal cells (Yue et al., 2010). No pigmented RPE cells were generated in H5 and S1 organoids with the Sasai culture methods therefore, it was hypothesised that RPE-CM supplementation would be effective in stimulating PR growth, encouraging the growth of RPE and maintenance of the retinal structure generally. To test this, RPE cells were isolated from primary macaque retina and cultured *in vitro* as an explant to generate the media from an appropriate primary tissue source.

Culture media used for hiPSC-derived RPE was used for macaque explant RPE culture and found suitable to maintain RPE growth up to 1 passage post plating (P1). Beyond P2 cells transdifferentiated losing the tight cell-cell adhesion seen at P1 characteristic of RPE growth and instead showed an elongated, fibroblastic morphology (Fig. 5.15). RPE-CM was collected daily from confluent cultures at P1.

Passage number	Macaque Eye 1	Macaque Eye 2
explant		
P1		
P2		
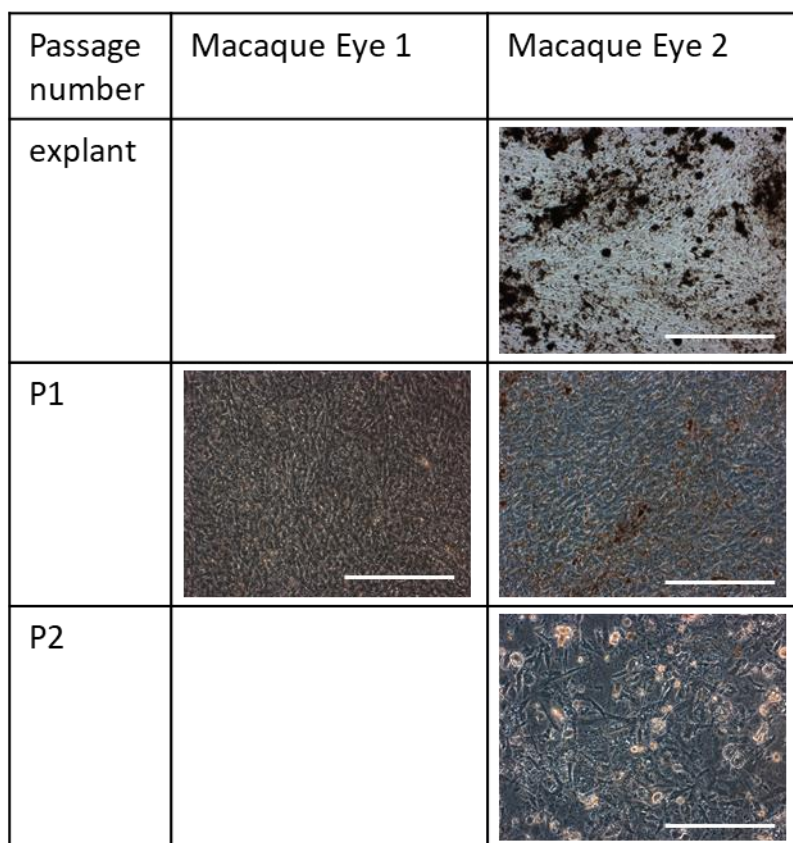
Figure 5.15. Representative bright-field images of macaque RPE explant cell culture on two occurrences showing the morphology of cells immediately following plating and 1 or 2 sub-passages (P1, P2). Scale bar = 500 μm

The timepoint for the addition of RPE-CM corresponds with the change to retinal maturation media. The Sasai condition with macaque (NHP) adjusted timing was therefore tested with the addition of RPE-CM at day 15 (Fig. 5.8). The maturation media was adapted to include a proportion of the conditioned media at a 1:3 ratio which was found to have a proactive effect on rod PR generation in human RO derivation (Dorgau et al., 2019). The data in this section was collected from organoids generated using the S1 and H5 cell lines only. The development and maintenance of retinal cell types and structure was compared throughout differentiation. The organoids were assessed by IF analysis for retinal protein expression throughout differentiation; to identify any differences in retinal cell generation and photoreceptor maturation. Gene expression analysis of S1 and H5 organoid samples generated in RPE-CM supplemented conditions was performed using RT-qPCR. Relative gene expression was calculated in the same way as previously for S1 samples.

S1 organoids generated with the RPE-CM supplemented condition and un-supplemented condition with (NHP) adjusted timing both show growth of smooth, phase-bright neural retina (NR) from day 31 which is maintained to some extent until day 120 (Fig. 5.16a). The efficiency of both methods to generate organoids with retinal morphology is also similar with ~100% of organoids at day 8 and maintained until day 120 in ~40% of organoids (Fig. 5.16b).
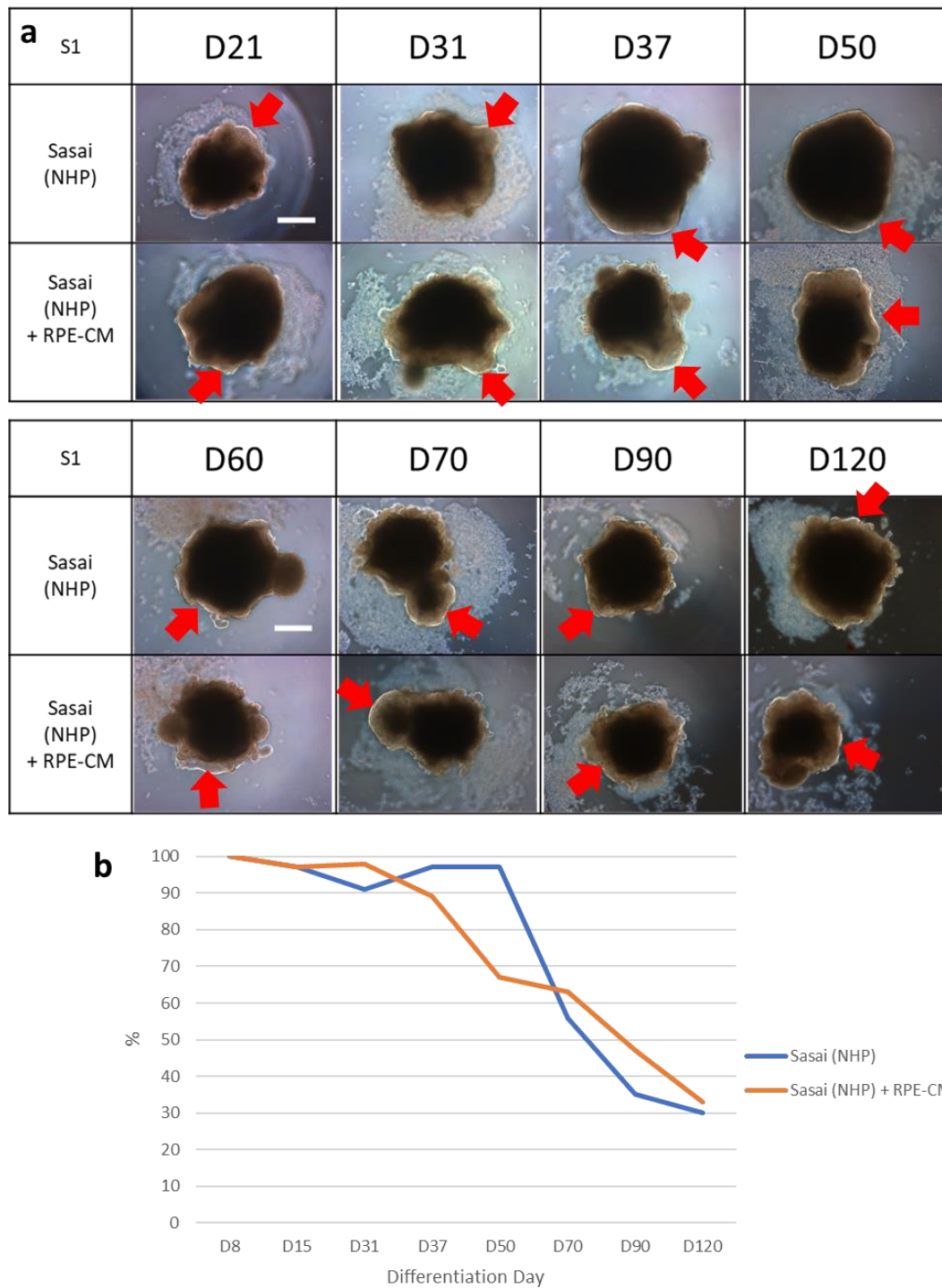
Figure 5.16. Addition of RPE-CM makes no significant difference to macaque RO morphology, method efficiency or early retinal marker expression in S1 organoids. (a) Representative morphology of S1-derived organoids throughout differentiation, red arrows indicating presence of bright neural-epithelia (b) Efficiency of method to generate organoids with retinal morphology D = Day. Scale bar = 100 µm. n = 144. (c) Relative gene expression of RAX and VSX2 shown as fold change normalised to adult macaque retina. Error bars = SEM. N = 2.

236
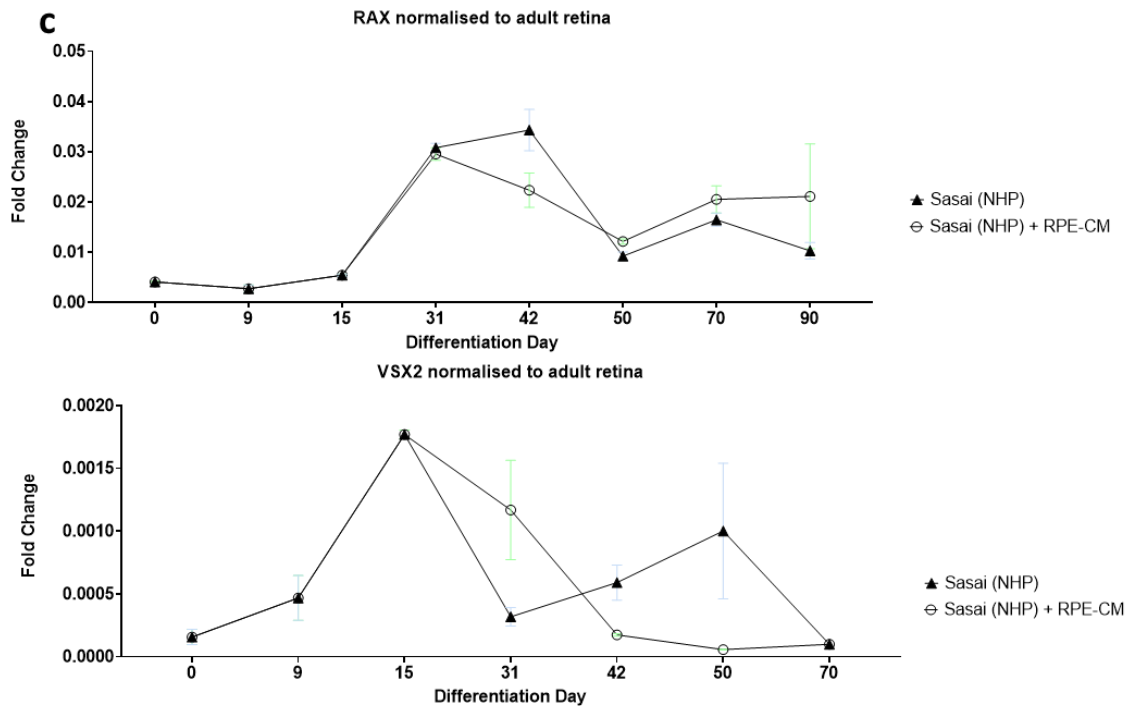
Early marker expression of the eye-field transcription factor *RAX* and the RPC marker *VSX2* show expression peaks between day 31-42 and day 15 respectively (Fig. 5.16c). This is in accordance with development of RPCs *in vivo* and specification of phase-bright NE *in vitro* (Fig. 5.16a, 5.1). No significant differences were seen between conditions supplemented with RPE-CM in *RAX* and *VSX2* expression which supports the morphological data (Fig. 5.16c).

Furthermore, using the H5 line, organoids were generated which showed some smooth, bright putative NE tissue at day 15, however throughout differentiation this thinned and decreased in optical transparency in both conditions (Fig. 5.17a). The expression of early eye-field and RPC markers *RAX* and *VSX2* was 10-fold lower than relative expression in S1 samples for the same timepoints however the timeline of expression aligns between cell lines (Fig. 5.17b). This is in accordance with morphological data where the NE layer is more apparent in S1 organoid samples between day 21-50 (Fig. 5.16a). No significant differences in *RAX* and *VSX2,* or PR precursor marker *CRX* expression resulted from RPE-CM supplementation up to day 70 of differentiation (Fig. 5.17b).

The addition of RPE-CM in the Sasai-based maturation media generated organoids from both S1 and H5 cell lines with a characteristic retinal morphology of phase-bright NE. Similar timelines of peak *RAX* and *VSX2* expression was seen between S1 and H5 samples in both conditions. However,

method efficiency and early retinal cell marker gene expression was not improved by RPE-CM supplementation.
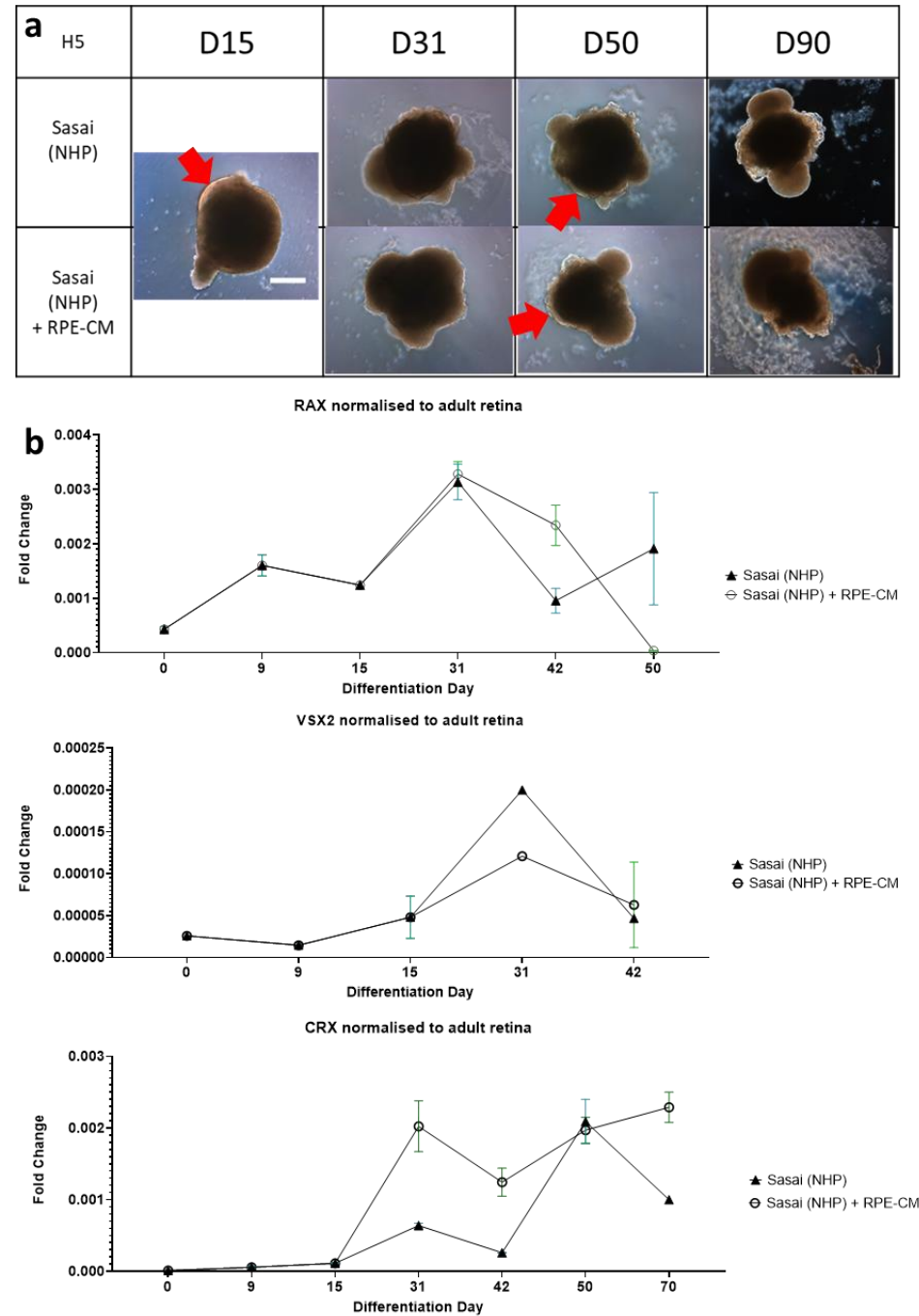
Figure 5.17. Addition of RPE-CM makes no significant difference to macaque morphology or early retinal marker expression in H5 organoids. (a) Representative morphology of H5-derived organoids throughout differentiation, red arrows showing presence of bright neuro-epithelia. Scale bar = 100 μm. n = 144. (b) Relative gene expression of RAX, VSX2 and CRX shown as fold change normalised to adult macaque retina. Error bars = SEM. N =2.

5.3.3.1 Molecular analysis of macaque organoids derived with RPE-CM supplementation

As Crx marks post-mitotic PRs and Ki67 marks actively proliferating cells, these markers were analysed in macaque ROs at the mid-stages of differentiation. IF analysis of S1 samples shows the formation of a thick lamina of tightly packed, with Crx+ columnar cell nuclei seen only in the Sasai (NHP) + RPE-CM condition at day 50 (Fig. 5.18a). This cell lamina thins by day 70 although Crx+ expression remains. The un-supplemented conditions show Crx+ cells at the periphery of the organoid however the characteristic organisation of the structure is lacking. Ki67 expression is only correctly expressed in cell nuclei at day 70 in the Sasai (NHP) + RPE-CM condition (Fig. 5.18a).

These data show that although there is no significant quantitative difference of *CRX* expression between the RPE-CM supplemented and non-supplemented conditions, the localisation of Crx+ cells and lamina structure is improved by RPE-CM addition in S1 organoids (Fig. 5.18a, b).

Furthermore, assessing for Rcvrn in S1 organoids between day 50 – 90 shows the RPE-CM supplemented condition produced correct localisation of Rcvrn+ cells in the tissue lamina at the organoid periphery indicating a positive effect that RPE-CM might have on PR positioning and maturation (Fig. 5.18c). At day 90 Rcvrn+ cells have not migrated to the outer periphery in either condition and although there are Rcvrn+/SNCG+ cells present in both conditions they are found internally within the organoid (Fig. 5.18c). Gene expression analysis shows a significant increase in Rcvrn at day 90 in the un-supplemented condition compared to the RPE-CM condition (Fig. 5.18d). These data suggests that although there is a positive impact of RPE-CM addition on the localisation of Rcvrn in S1 organoids, at day 90 they have not subsequently developed the mature laminated structure, and the proportion of Rcvrn+ cells is much lower in macaque ROs compared to adult macaque retina (Fig. 5.18c,d). The greatest expression was seen in the un-supplemented condition with peaks at day 50 and 90, approximating the gestational timeline for PR generation in the retina (Fig.1.5), however overall magnitude levels were low.
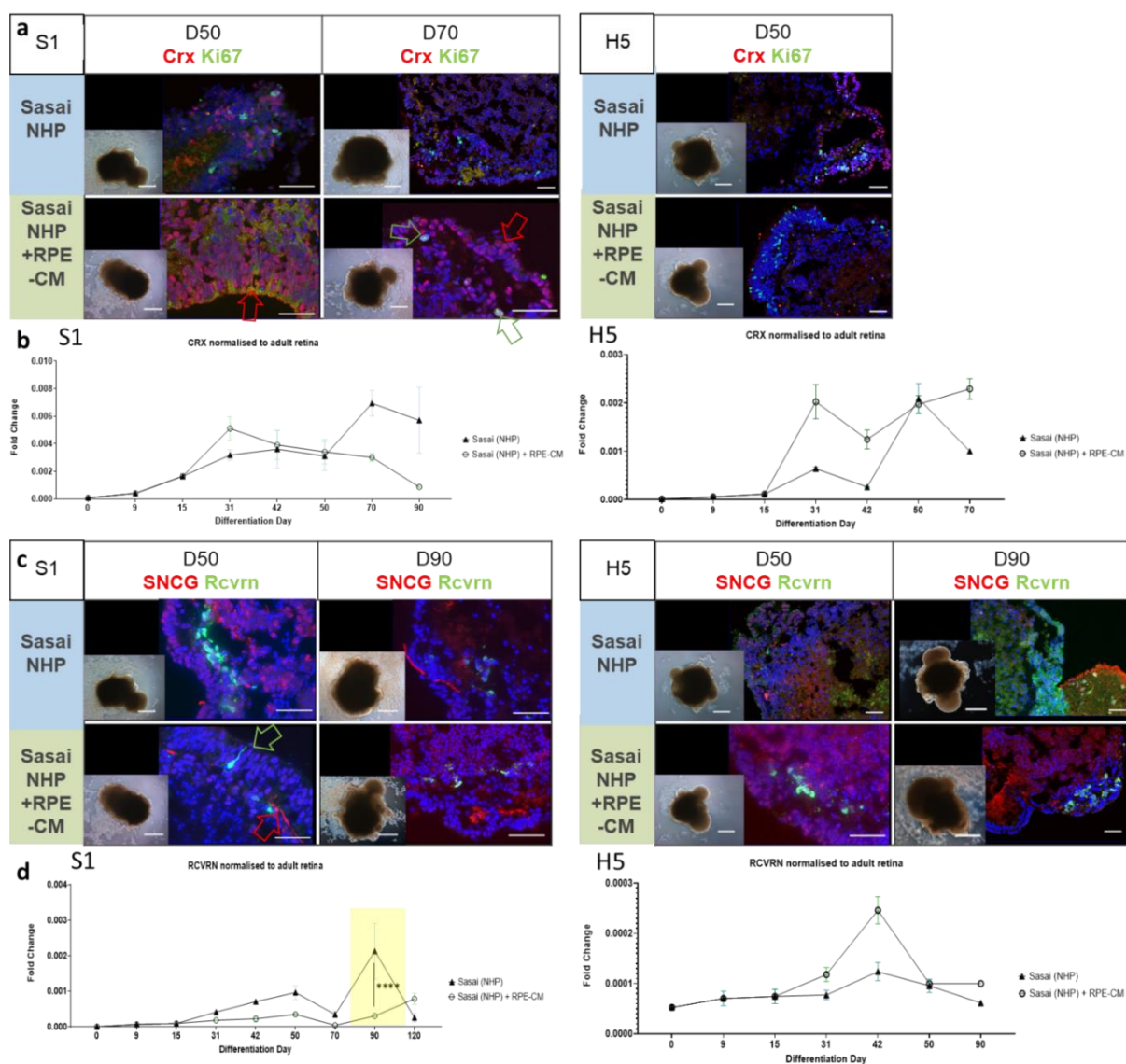
Figure 5.18. Comparison of RPE-CM addition on PR precursor generation in S1 and H5 organoids. (a) Representative IF analysis for PR precursor (CRX) and proliferation marker (Ki67). Arrows highlight correct marker expression. (b) Gene expression of CRX. (c) IF analysis for PR/bipolar (Rcvrn) and RGC marker (RBPMS). (d) Gene expression of RCVRN. Error bars = SEM. * = p < 0.05, ** = p < 0.01, *** = p <0.001, **** = p <0.0001. N = 2.

No significant differences were observed in *CRX* or *RCVRN* marker expression in H5 samples at similar timepoints (Fig. 5.18). Furthermore, the magnitude of expression was 10-100-fold lower in H5 samples compared with S1, indicating low efficiency of cell generation at these timepoints.

To assess PR development and maturation, IF and gene expression analysis for cone (ARR3, OPN-S, OPN-ML) and rod (Rho, NRL) specific markers, as well as Müller glia cells (CRALBP/RLBP1), was performed on S1 and H5 organoids sampled at day 90 and 120.

240

In S1 organoids IF analysis of cone PR markers OPN-S and OPN-ML show expression and localisation in cells lining the outer periphery of the organoids in a lamina structure (Fig. 5.19a). In the RPE-CM supplemented condition there is also a layer of SNCG+ cells found basally to these indicating correct orientation of PR cells and structure of retinal lamination (Fig. 5.19a). This improvement is also seen by gene expression analysis where *ARR3* expression rises significantly higher in RPE-CM supplemented S1 organoids from day 90-120 (Fig. 5.19b). At day 120 OPN-S and OPN-ML expression remains present in cells at the outer periphery of organoids, however SNCG+ cells are no longer present basally to them in the RPE-CM condition indicating lack of maintenance of RGCs within the laminated retinal structure (Fig. 5.19a). Analysis of Müller glia marker CRALBP showed expression in cells neighbouring OPN-ML+ cells in both conditions, in an orientation similar to that seen in native macaque retina (Fig. 5.19a, 5.7). Expression of the corresponding gene *RLBP1* shows a significant increase between day 90-120 in the RPE-CM supplemented condition compared with the un-supplemented condition (Fig. 5.19b).

In H5 samples there is a similar expression pattern of OPN-S+ and OPN-ML+ cells which are present in the peripheral organoid cell layer at day 90 in both conditions (Fig. 5.19c). Although samples were not analysed for protein expression at day 120, gene expression analysis shows that RPE-CM addition significantly increases *ARR3* and *RLBP1* at day 90 although expression levels of *RLBP1* are lower in magnitude than S1 samples (Fig. 5.19d). As Müller glia cells are among the last to arise during the process of retinogenesis this expression pattern is in accordance with native retinal development.

In both cell lines the expression of *RBPMS* is not significantly affected by RPE-CM addition (Fig. 5.19b, d).

These results corroborate the analysis of S1 organoids at earlier timepoints where Rcvrn and Crx localisation is improved by RPE-CM addition at day 50. This shows that cone PR expression is significantly increased in the RPE-CM supplemented condition when analysed at later timepoints with appropriate localisation within the outer tissue lamina (Fig. 5.19a, b)
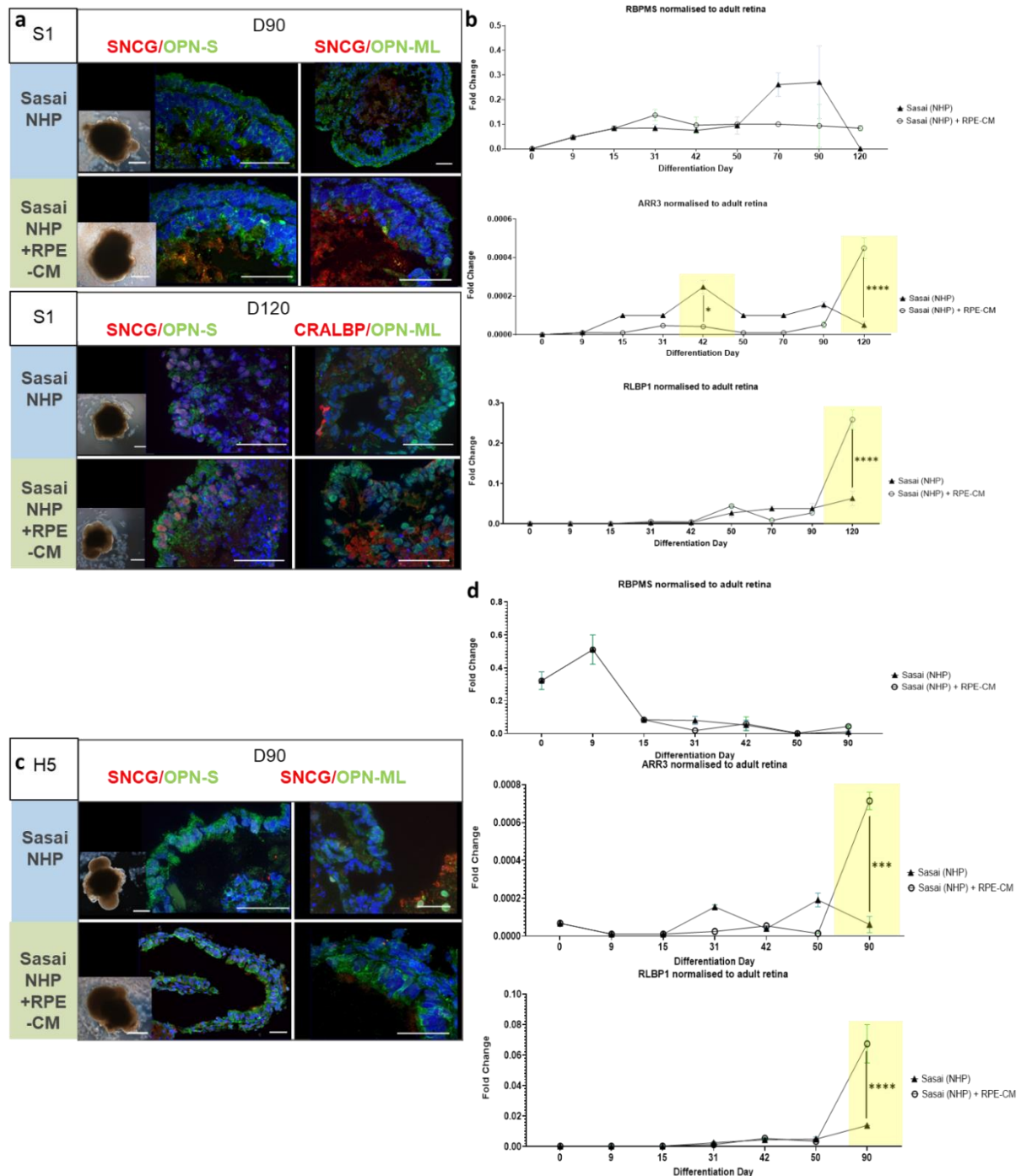
Figure 5.19. RPE-CM addition significantly increases cone PR marker (OPN-S and OPN-ML/ARR3) expression and shows correct localisation in S1 and H5 organoids. Relative gene expression shown as fold change normalised to adult macaque retina. Error bars = SEM. N =2. * = p < 0.05, ** = p < 0.01, *** = p <0.001, **** = p <0.0001. (a) IF analysis in S1 samples at day 90 and 120. (b) Gene expression analysis of RBPMS, ARR3 and RLBP1 in S1 organoids (c) IF analysis of cone opsin and RGC marker (SNCG) at day 90 in H5 organoids (d) Gene expression of RBPMS, ARR3 and RLBP1 in H5 organoids.

Analysis of rod PR-specific markers in H5 organoids at day 90 revealed the presence and correct localisation of Rhodopsin in the RPE-CM supplemented condition, with correct organisation of SNCG+ cells located in the basal lamina at day 90 (Fig. 5.20a). Corresponding gene expression analysis of rod-specific marker *NRL* showed an increase from day 50-90 in the RPE-CM supplemented condition compared to the un-supplemented condition although this was not significant (Fig. 5.20b). The overall magnitude of *NRL* was low compared with native retina which is supported by the low quantity of Rhodopsin+ cells detected in organoids by IF analysis (Fig. 5.20).
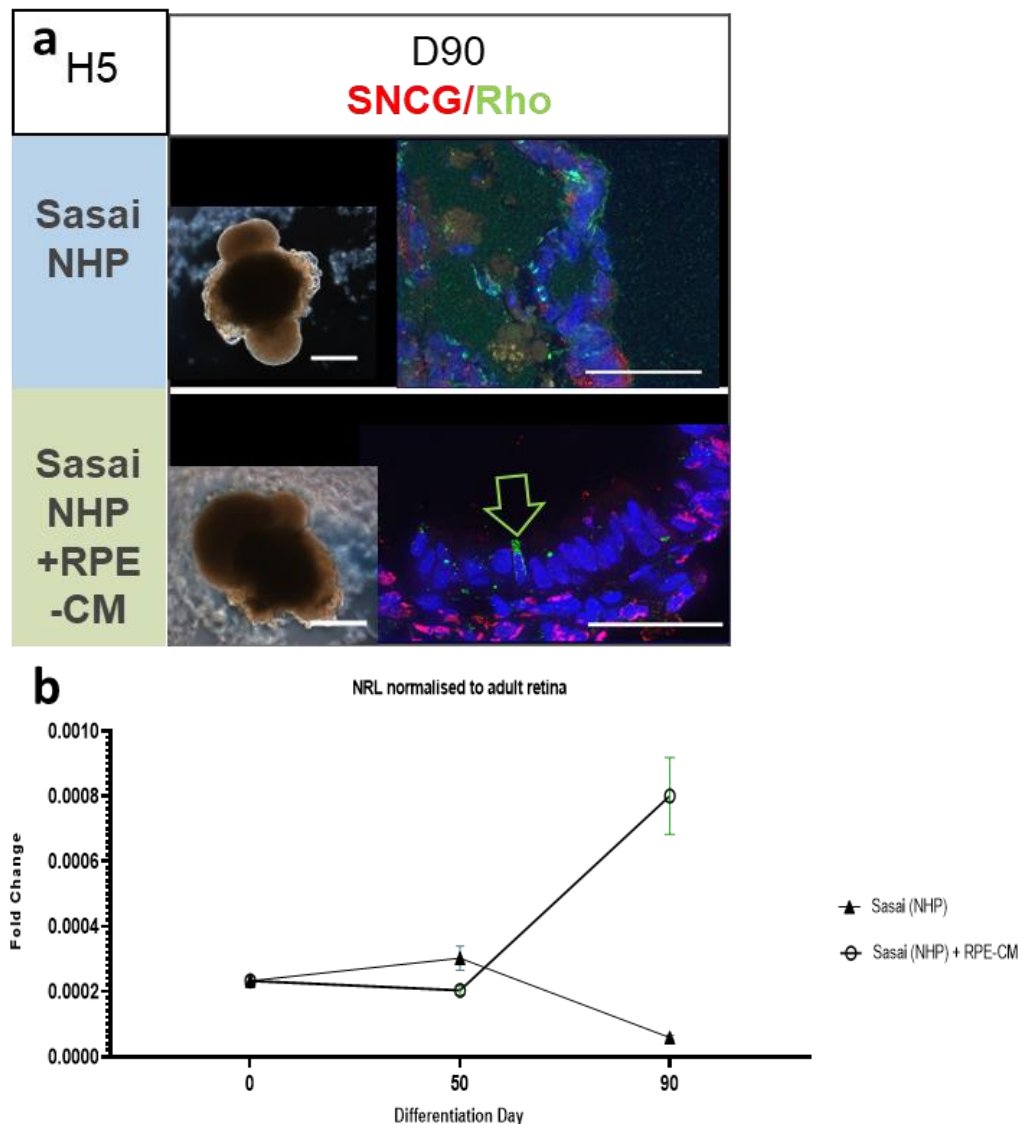
Figure 5.20. RPE-CM addition improves rod PR marker (Rho/NRL) expression and shows correct localisation in H5 organoids. (a) Arrowhead showing correct localisation of Rhodopsin+ cell in RPE-CM supplemented condition at day 90. Background expression levels only in NHP sample (b) Gene expression analysis of rod marker (NRL). Error bars = SEM. N=2.

Gene expression analysis was also performed for interneuron cell markers which shows upregulation of amacrine cell marker *AP2A* and bipolar marker *PRKCA* in H5 organoids, however in S1 organoids the only significant difference shows bipolar gene marker *PRKCA* is reduced at day 70 in comparison to the un-supplemented condition (Fig. 5.21a). The expression of *AP2A* in S1 organoids was not significantly affected (Fig. 5.21a).
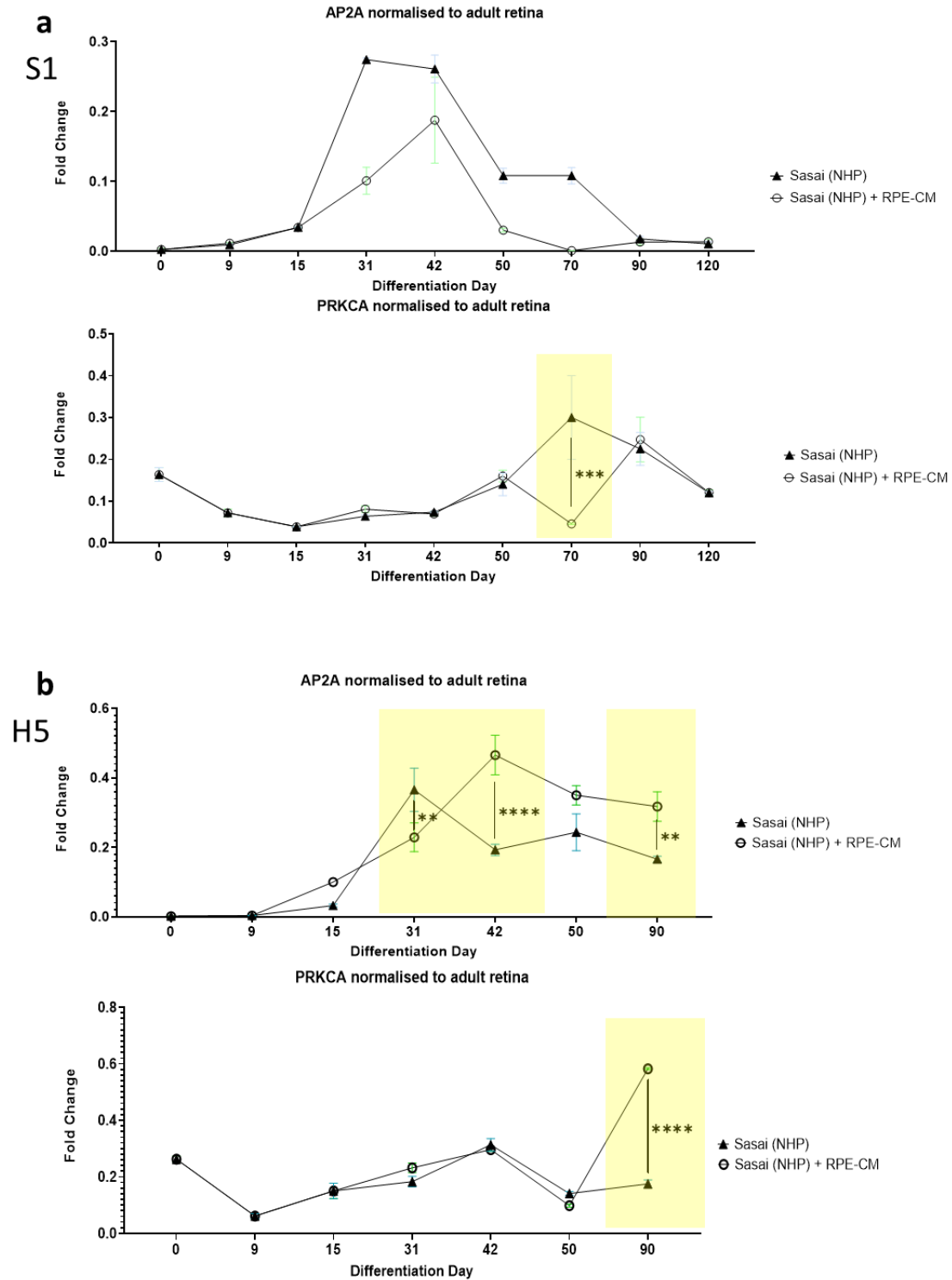
Figure 5.21. Relative gene expression shown as fold change normalised to adult macaque retina.
*Error bars = SEM. * = p-value < 0.05, ** = p-value < 0.01, *** = p-value <0.001, **** = p-value*
<0.0001. (a) RPE-CM addition reduces bipolar cell (PRCKA) gene expression in S1 organoids (N = 2) (b)
RPE-CM increases amacrine (AP2A) and bipolar cell (PRKCA) expression in H5 organoids (N =1).

245

In contrast to the results from S1 organoids, the expression of interneuron markers in H5 organoids shows a significant increase of *PRKCA* at day 90 and significantly higher *AP2A* expression from day 42-90 in the RPE-CM supplemented condition (Fig. 5.21b). The timeline of *AP2A* expression corresponds with that of the native retina as amacrine cells are born in the retina between day 42-70 (Fig. 5.1). *AP2A* expression is relatively high reaching half that of native retina at peak expression (Fig. 5.24). This result suggests RPE-CM addition might have a stimulatory effect on amacrine cell production, in some cell lines.

The expression of the RPE marker *MITF* was also analysed in H5 and S1 ROs throughout differentiation and is seen expressed at late stages of differentiation at levels comparable to mature macaque retina (Fig. 5.22). Interestingly, in S1 organoids *MITF* expression is significantly higher between day 50-70 in the RPE-CM supplemented condition, whereupon the un-supplemented condition increases to become significantly higher at day 90 (Fig. 5.22a). This earlier increase suggests RPE-CM supplementation accelerates expression of *MITF* compared to the un-supplemented condition.
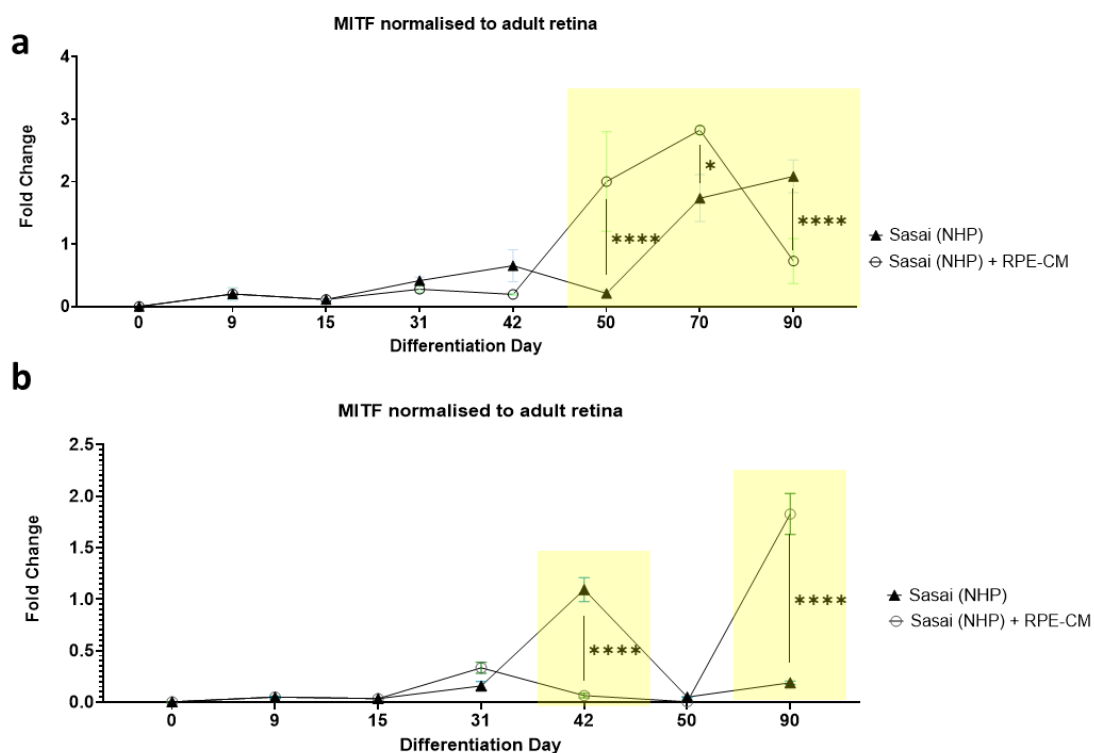
Figure 5.22. RPE-CM addition improves MITF expression at late stage of macaque retinal differentiation in (a) S1 organoids N=2 (b) H5 organoids N=1. Relative gene expression shown as fold change normalised to adult macaque retina. Error bars = SEM. * = p-value < 0.05, ** = p-value < 0.01, *** = p-value <0.001, **** = p-value <0.0001.

The timing profile in S1 organoids with the RPE-CM supplemented condition therefore aligns more closely with the embryological timing found in the macaque where peak RPE cytogenesis occurs between GD 27 – 85 (Table 1.2) (Rapaport et al., 1995).

In H5 organoids the *MITF* expression was also significantly increased in the RPE-CM condition however the timing profile varied to that seen in S1 organoids. Firstly, the early peak of *MITF* in the un-supplemented condition at day 42, seen in both cell lines, was significantly higher in H5 samples (Fig. 5.22). The RPE-CM condition then showed peak expression at day 90 compared to day 70 in S1 samples (Fig. 5.22b). However, the magnitude of H5 expression, as seen for other retinal genes, was lower than that in S1 samples (Fig. 5.22). Furthermore, the H5 samples for day 70 was not analysed resulting in lower temporal resolution than in S1.

5.3.3.3 Conclusions of using RPE-CM for macaque retinal organoid generation

RPE-CM supplementation does not show an effect on early retinal marker expression however improved the localisation and expression of PRs and Müller glia cell markers within the retinal tissue structure from day 50 onwards in both cell lines.

Due to limited sample cDNA genes expressed in the early stages of retinal development such as *RAX*, *VSX2*, and *CRX* were not analysed in samples later than day 70. The RGC marker, *RBPMS*, peaked at day 9, prior to RPE-CM supplementation and no significant differences were seen between conditions (Fig. 5.19b, d). The early peak seen in H5 organoids is in line with gestational development as RGCs are the first retinal cell type to be born (Fig. 5.1).

Cell generation and retinal gene expression improvements made by RPE-CM addition were observed including the presence of rod marker expression in H5 organoids and the significantly increased expression levels of cone PR and Müller glia markers in both S1 and H5 cell lines. The magnitude of the impact was different between cell lines however the overall trend was similar with both lines generating organoids with significantly higher *ARR3* and *RLBP1* expression at later stages of differentiation with RPE-CM addition. In S1 organoids there was no detection of Rhodopsin or *NRL* in samples above background level, therefore the protein and gene expression results indicate the emergence and maturation of cone PR cells, but a lack of rod PRs.

H5 organoids derived in RPE-CM conditions could not be analysed at day 120 due to an insufficiency of organoid quantity. However, H5 organoids derived with the un-supplemented condition were analysed for PR-specific markers at day 120 showing OPN-S+ and OPN-ML+ cells and lack of Rhodopsin expression (Fig. 5.13c). Positive cone and rod PR marker expression at day 90 in the RPE-CM condition suggests retinal maturation might continue to develop and would be worth assessing

in future experiments. Additional timepoint analysis of H5 organoids (day 70 and 120) by repeat differentiation experiments would be informative in order to identify the stage and limits of PR development with these method supplementations. Earlier peaks in PR mature marker expression in H5 organoids compared to S1 indicate cell line differences in expression timelines (Fig. 5.19).

Lower levels of *ARR3* expression were seen between day 15-50 in S1 and H5 samples with RPE-CM addition from both cell lines in comparison with the un-supplemented condition. Cytogenesis of cone PRs during gestational development occurs from GD 27 (Fig. 5.1) (Vail et al., 1991). Therefore, these results suggest that RPE-CM supplementation from day 15 disrupts cone PR generation in the early phase of retinogenesis but supports cone generation at later stages of differentiation. Therefore, the timing of RPE-CM addition could be delayed to correct this. However, investigation with other early cone-specific PR markers, such as *RXRG* and *ONECUT1*, is first required to confirm this.

Changes to interneuron cell expression patterns caused by RPE-CM supplementation include the significant increase of *AP2A* and *PRCKA* expression in H5 organoids at mid and late stages of differentiation respectively, however this was not supported by analysis of S1 samples (Fig. 5.21). Interneuron protein expression analysis was not performed due to time constraints; however this could be used to assess if *AP2A* and *PRCKA* expressing cells were correctly localised in relation to PR cells.

MITF expression is of a much higher magnitude than all previously discussed genes, at levels comparable and higher than native retina (Fig. 5.22). Peak *MITF* expression in the RPE-CM condition is significantly higher than the un-supplemented condition but varies in time between cell lines (Fig. 5.22). This significant increase suggests that RPE-CM addition has a stimulatory effect on RPE development in macaque ROs.

5.3.4 Using the IGF1 method for macaque retinal organoid differentiation

5.3.4.1 Comparing organoid morphology in IGF1 condition between cell lines

In parallel to assessing the Sasai based methods for macaque retinal differentiation, another method termed "IGF1" was tested on all three macaque iPSC lines (S1, H5 and H1). This protocol has been developed and optimised in the Lako lab to produce ROs from hiPSC and hESC lines (Zerti et al., 2021, Dorgau et al., 2019; Mellough et al., 2015). The culture media includes IGF1 as well as other retinal growth stimulants such as B27 supplement from day 0 of differentiation (Fig. 5.8). It also differs from the Sasai protocol by the lack of BMP4 or Matrigel at early timepoints and includes T3 and Lipids in the maturation media used from day 18 onwards (Fig. 5.8). Additionally, to enhance the effect of IGF1, the organoids are pooled at a density of 16 organoids/well when cultured in the maturation media. Both techniques of 96-wp and pooled culture were tested in macaque iPSC differentiation experiments. The timing of the IGF1 protocol was adjusted to macaque (NHP) timing in the same way as the Sasai (NHP) conditions (section 5.3.4, 5.3.5) to support the shorter gestational timeline and enable comparison between these methods.

The organoids were observed throughout differentiation and bright-field images were collected for morphological comparison and assessment of NE development. Counts were made throughout differentiation of organoids showing characteristic retinal morphology to calculate method efficiency. Additionally, organoids were sampled and analysed for gene and protein expression as performed in previous sections.

With all macaque cell lines the IGF1 method produced organoids which developed thick, optically bright tissue approximating NE from day 21 onwards (Fig. 5.23). One noticeable disadvantage of using the IGF1 method with the pooling technique, compared with 96-wp, is it results in organoids fusing together. This increases the overall size of the organoids whilst decreasing the total surface area of peripheral NE limiting the access to nutrients for the cells in the interior of the organoids.

S1 organoids between day 70-120 generated in 96-wp show limited areas of NE thinner than the pooled condition and the NE appearance in both IGF1 conditions is less optimal than in Sasai conditions (Fig. 5.23a). The efficiency of the IGF1 method to generate S1 organoids with a retinal morphology is similar to that of the Sasai (NHP) methods from day 0 to 40 (Fig. 5.23b). Between day 40-80 organoids with retinal morphology decline in both conditions and by day 90-120 this stabilises at 20-30% of organoids with retinal morphology (Fig. 5.23b).
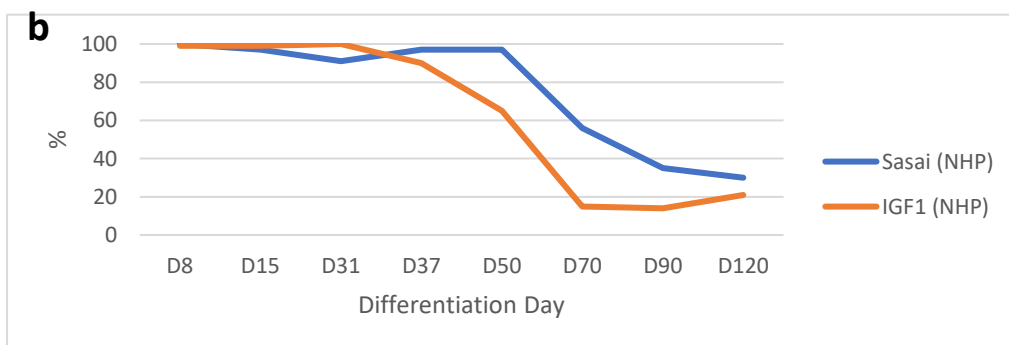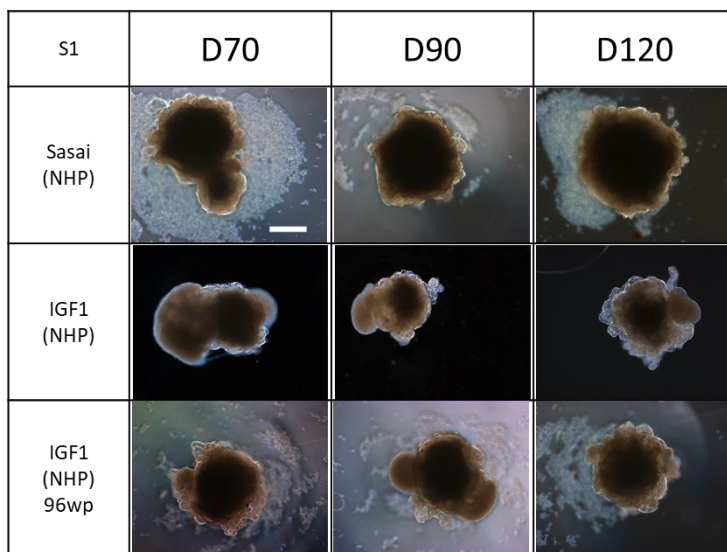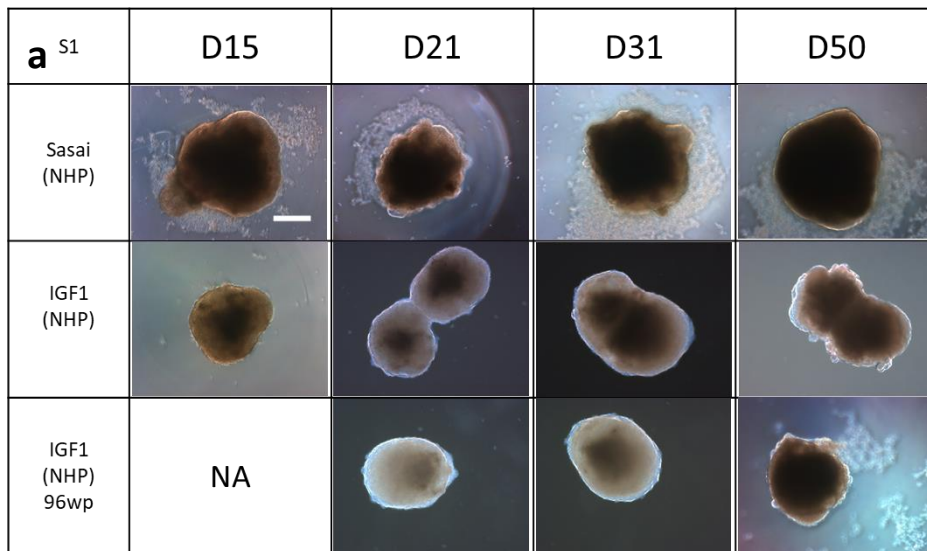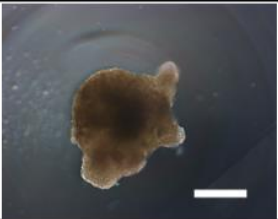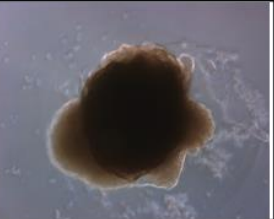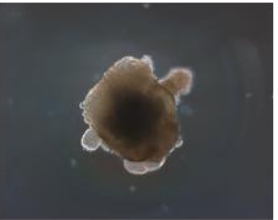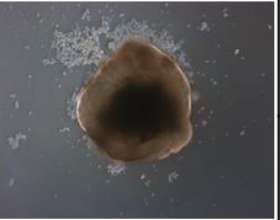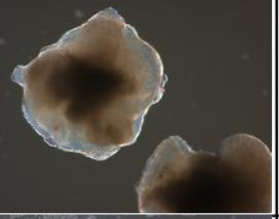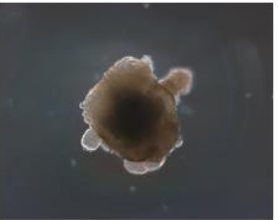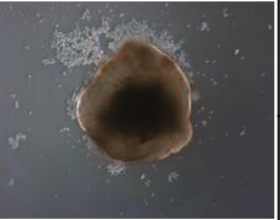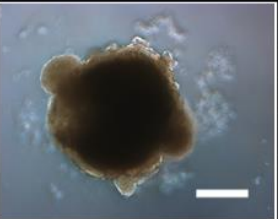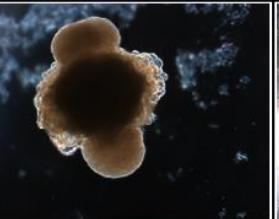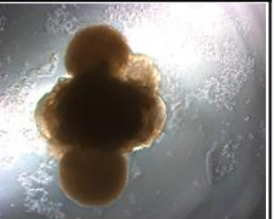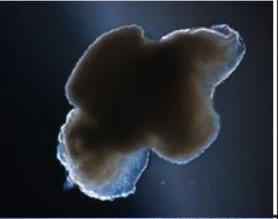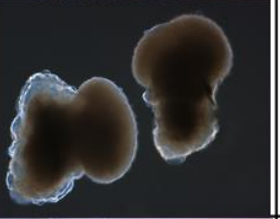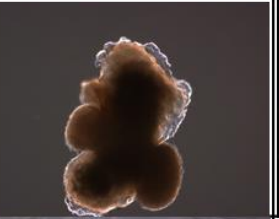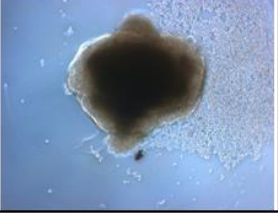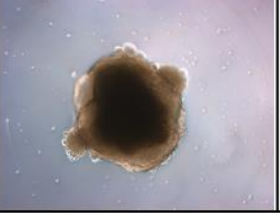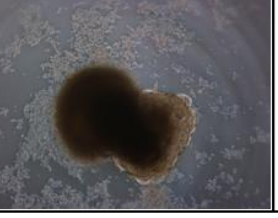
Figure 5.23.

Comparing macaque organoids throughout differentiation using the Sasai or IGF1 methods with macaque timing (NHP). (a) Representative morphology of S1 organoids (b) Efficiency of method to generate S1 organoids with retinal morphology (n = 288)., (c) Representative morphology of H5 organoids, (d) Representative morphology of H1 organoids. D = Day. Scale bar = 100 µm. N/A = not applicable, ND = not determined.

C H5	D9	D15	D21	D31
Sasai (NHP)				
IGF1 (NHP)				
IGF1 (NHP) 96wp				

H5	D50	D70	D90	D120
Sasai (NHP)				
IGF1 (NHP)				
IGF1 (NHP) 96wp				

d H1	D9	D15	D21	D31
Sasai (NHP) -ch/su				
IGF1 (NHP)				
IGF1 (NHP) 96wp	N/A	N/A		

H1	D50	D70	D90	D120
Sasai (NHP) -ch/su				
IGF1 (NHP)				ND
IGF1 (NHP) 96wp				ND
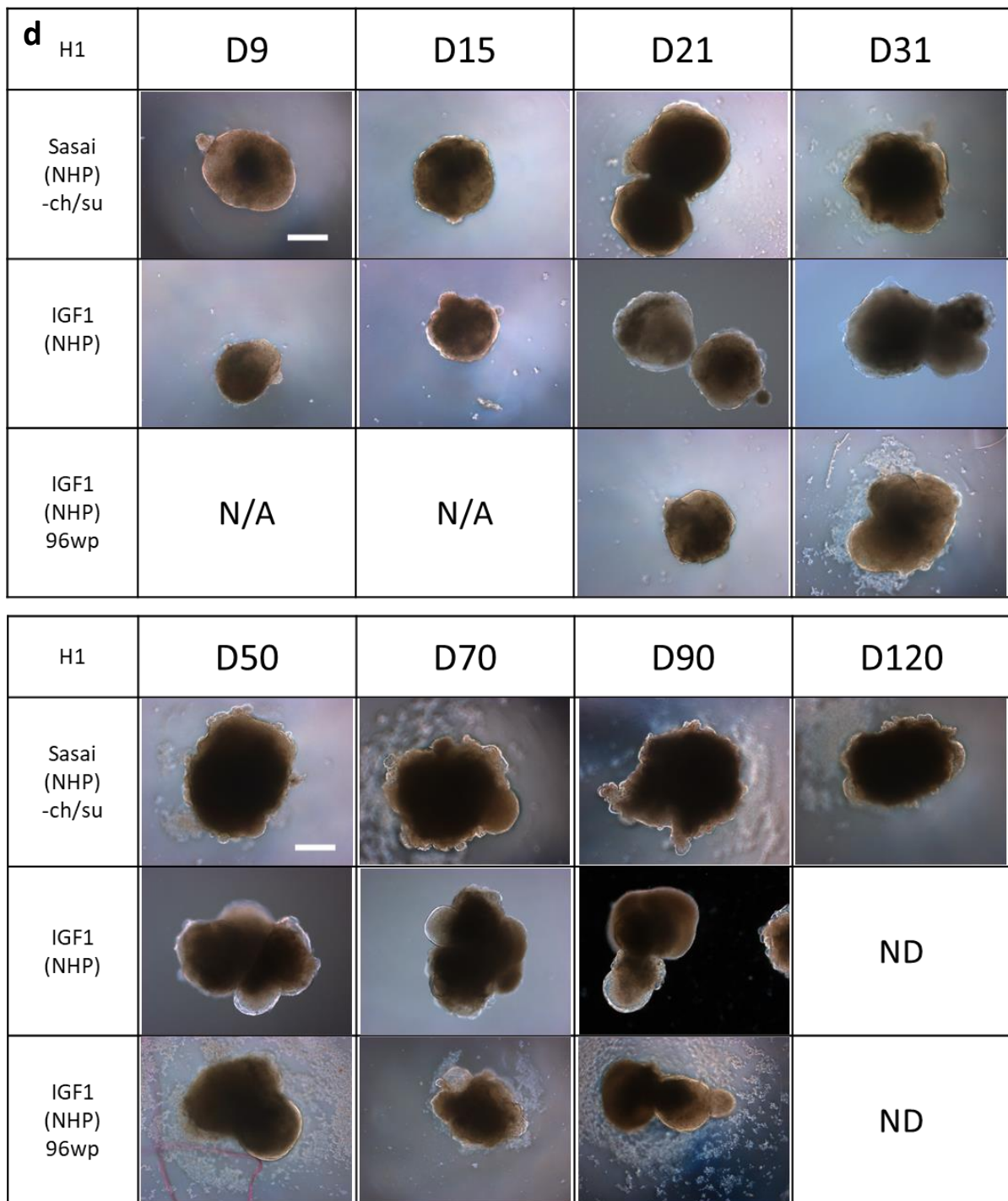
H5 organoids derived with the IGF1 method in both 96-wp and pooled culture retained thick NE until day 120, despite fusing together, which was especially prevalent from day 20-70 in the pooled condition (Fig. 5.23c). The NE layer was better maintained throughout differentiation in IGF1 samples compared to organoids generated with Sasai methods (Fig. 5.23c). Throughout differentiation, H5 organoid morphology in IGF1 conditions was more rounded, thick and bright

compared with S1 organoids indicating potential differences between cell lines in response to the culture conditions (Fig. 5.23a,c).

H1 organoids generated in both the IGF1 conditions also showed development of a bright putative NE layer, this was at a slightly later timepoint than seen in the S1 and H5 organoids becoming defined at day 50 in pooled organoids (Fig. 5.23d). Similarly to the S1 and H5 samples the H1 organoids in the IGF1 96-wp condition developed a thinner layer of bright NE than in the pooled samples which was maintained until the final timepoint of day 90 (Fig. 5.23d). Due to limited H1 iPSC proliferation there were insufficient organoid samples available to maintain these in IGF1 culture until day 120.

In summary, differentiation of 3 macaque iPSC lines using the IGF1 method with NHP timing can generate organoids with putative NE maintenance throughout timepoints relevant to retinal development. H5 organoids show the best morphological examples of NE in both IGF1 conditions between day 50-120 while S1 organoids showed greater loss in retinal morphology than H5 or H1 from day 40 onwards.

5.3.4.2 Molecular analysis in early-stage organoids generated in IGF1 method

Protein and gene expression analysis was carried out for retinal markers using validated antibodies and macaque specific primers to confirm retinal cell identity and compare between methods. Although IF analysis from Sasai (NHP) samples has been discussed previously in sections 5.3.4 and 5.3.5, the results are shown here in order to directly compare between the Sasai and IGF1 methods with the macaque (NHP) adjusted timing. The H5 and S1 lines were analysed for retinal gene expression using the same methods described previously and will be discussed in the following sections.

Due to constraints of time, the H1 samples, which were not maintained until day 120, have not yet been analysed for gene expression. Therefore, H1 sample protein expression data will be discussed separately in section 5.3.6.5.

Firstly, organoids at an early stage of development prior to pooling (day 5-15) were assessed for the presence and localisation of eye-field transcription factors Rax, Pax6 and Otx2 and the neuroectodermal marker Sox2.

In order to highlight the difference between the IGF1 and Sasai methods, the gene expression results for the most significantly different variation of the IGF1 method has been shown in gene expression graphs. For S1 samples this was the pooled variant and for H5 samples this was the 96-wp variant.
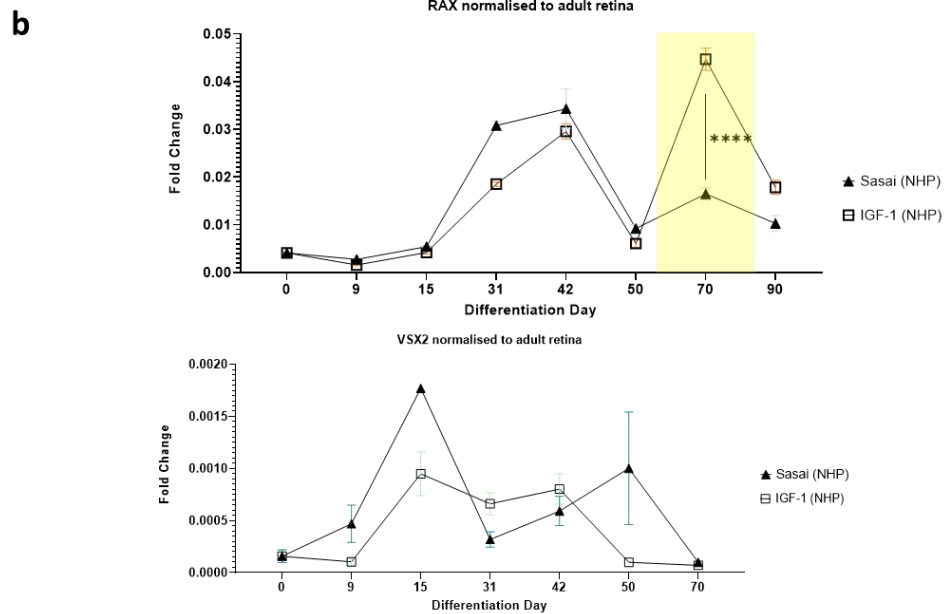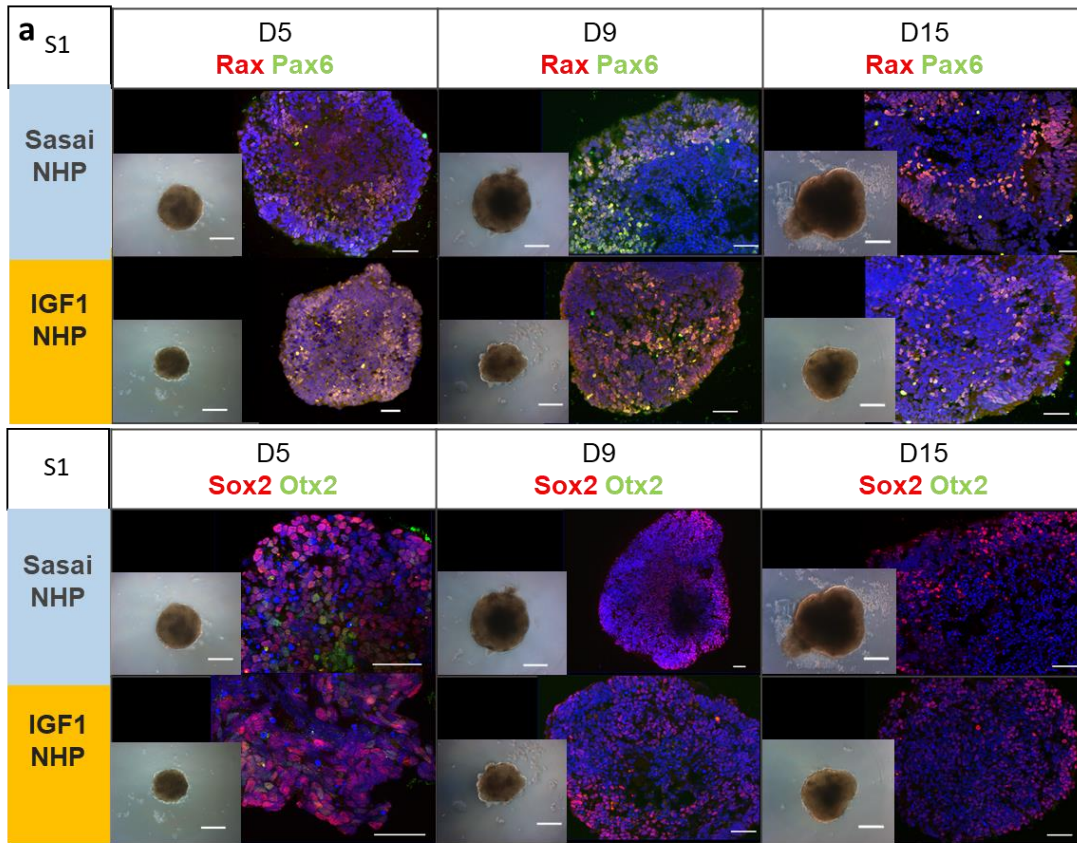
Figure 5.24. Assessing for eye-field genes (RAX, PAX6, and OTX2), neuroectodermal (SOX2), and RPC marker (VSX2) in S1 organoids (a) Representative IF analysis. D= day. Scale (BF) = 500µm, (IF) = 50µm. (b) Relative gene expression shown as fold change normalised to adult macaque retina. Error bars = SEM. N=2. * = p-value < 0.05, ** = p-value < 0.01, *** = p-value <0.001, **** = p-value <0.0001.

Expression of retinal markers at day 5 in S1 organoids generated using the IGF1 method was comparable to the Sasai method with co-expression of Rax/Pax6 and Sox2 expression in cells distributed throughout the organoid (Fig. 5.24a). At day 9 in Sasai organoids the expression of Rax/Pax6 is spatially restricted to the peripheral areas of the organoid whereas IGF1 samples retain widespread distribution of Rax/Pax6+ cells until day 15 (Fig. 5.24a). In S1 Sasai samples, Sox2 was expressed throughout organoids at day 5 and 9 then restricted to peripheral areas at day 15 whereas IGF1 samples show Sox2 expression throughout the organoid between day 5-15 (Fig. 5.24a) Therefore, IF analysis confirms NE identity and shows activity of neural-retinal regulatory transcription factors in these cells (Fig. 5.24a).

Retinal genes hypothesised to be expressed in the early stages of development; *RAX* and *VSX2,* were assessed in S1 samples up to the day 90 timepoint. Expression of *RAX* showed two peaks at day 42 and 70 in both conditions, with significantly higher expression in the IGF1 conditions at day 70 compared to the Sasai condition (Fig. 5.24b). *RAX* levels of expression at the early stage of differentiation when IF analysis was performed in comparison is much lower (Fig. 5.24b). The later peak may be linked to the stimulatory role that *RAX* plays on PR and interneuron specification, suggesting the IGF1 method is beneficial for PR generation in S1 organoids.

Expression of *VSX2* was not significantly altered in the IGF1 condition, and both methods show peak expression between day 15-50 which is in line with the gestational development of RPCs (Fig. 5.1). Throughout differentiation there was no significant differences in *VSX2* expression between conditions (Fig. 5.24b). However, the magnitude of gene expression is low at 1-2 x 10^{-3} -fold suggesting a low proportion of RPCs in RO tissue compared to adult macaque retina (Fig. 5.24b). *VSX2* expression was not detected in samples beyond day 70.
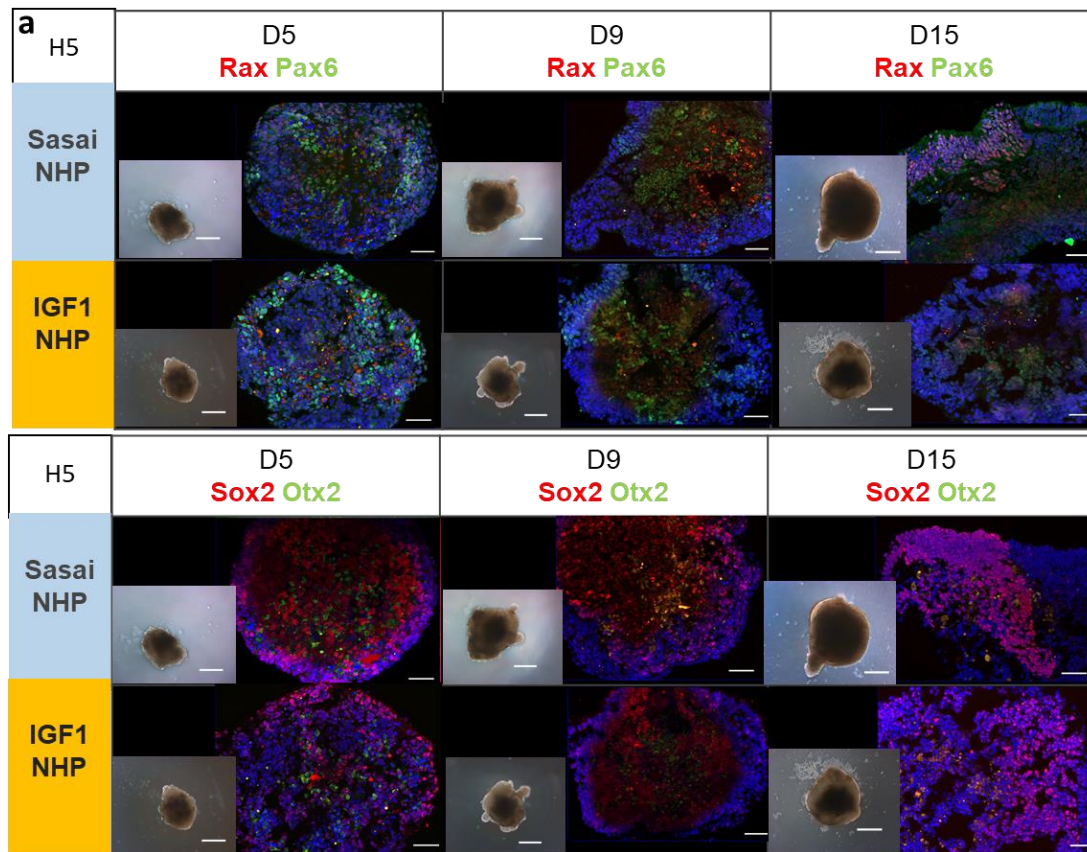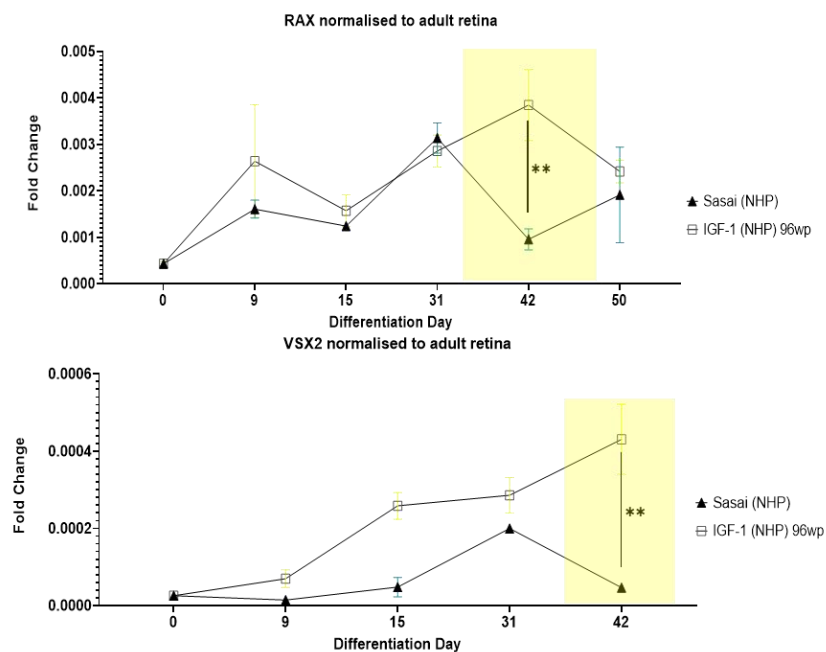
Figure 5.25. Assessing for eye-field genes (RAX, PAX6, and OTX2), neuroectodermal (SOX2), and RPC marker (VSX2) in H5 organoids (a) Representative IF analysis. D= day. Scale (BF) = 500μm, (IF) = 50μm. (b) Relative gene expression shown as fold change normalised to adult macaque retina. Error bars = SEM. N=2. * = p-value < 0.05, ** = p-value < 0.01, *** = p-value <0.001, **** = p-value <0.0001.

In H5 organoids generated using the IGF1 and Sasai methods, Rax/Pax6 are co-expressed in cells in the peripheral areas of organoids from day 5 – 9 (Fig. 5.25a). At day 15 in the Sasai samples, Rax/Pax6 co-localise in cells at the periphery of the organoids marking early NR tissue (Fig. 5.25a). This expression pattern is absent in the IGF1 sample as Rax is not detected at day 15 (Fig. 5.25a). Sox2 was expressed throughout the organoid in day 5-9 in H5 Sasai samples becoming restricted to the peripheral regions by day 15, whereas IGF1 samples show Sox2+ cells throughout the organoids from day 5-15 (Fig. 5.25a). Notably Otx2 staining was negative in all samples from both S1 and H5 throughout day 5-15 indicating a lack of transcription factor activation. This may be due to later expression of this marker.

Gene expression analysis of *RAX* supports IF data as expression levels rise from day 0-9 in both conditions, before decreasing at day 15 (Fig. 5.25b). The expression of *RAX* peaks in both H5 samples between day 31-42, with the IGF1 pooled condition expressing a significantly higher level of *RAX* at day 42 than the Sasai sample (Fig. 5.25b). *RAX* was not detected in samples from day 50-90. This early peak was also seen in S1 IGF1 and Sasai samples (Fig. 5.24b), however S1 organoids also showed a second peak of *RAX* at day 70 which was not seen in H5 samples assessed from day 50-90 (Fig. 5.25b). As *RAX* is known to be expressed in macaque RPCs, RGCs and amacrine cells sequentially throughout development this expression pattern is in alignment with gestational development (Table 5.4, Fig. 5.1). The magnitude of *RAX* in H5 organoids was also a factor of 10 lower than those levels seen in S1 organoids (Fig. 5.25b, 5.24b).

The expression of *VSX2* increases in both Sasai and IGF1 conditions from day 9 onwards and reaches a significantly higher peak in the IGF1 condition, double that of Sasai conditions at day 42 (Fig. 5.25b). This indicates RPCs are being generated in both conditions over this period. After this timepoint it was not detected in samples from either condition. In comparison to S1 *VSX2* expression, H5 *VSX2* levels are similarly low as was seen in *RAX* expression analysis, the maximum H5 expression reaching approximately 1/3 of that of S1 organoids (Fig. 5.25b, 5.24b).

In conclusion, organoids derived using the IGF1 method show similar morphology at the early stages of differentiation with all cell lines generating small, rounded organoids with phase-bright NE. The greatest definition of NE is seen at day 15 in the H5 organoids while S1 organoids show lack of definition of phase-bright tissue at this stage (Fig. 5.22).

Developing NE is expected to co-express the eye-field transcription factors Rax/Pax6 as well as the neuroectodermal and proliferation marker Sox2. IF analysis shows S1 organoids in the IGF1 condition have NE marker presence throughout organoids from day 5-15 with less spatially defined expression

than in the Sasai condition (Fig. 5.24a). This could suggest a delay in retinal development in the IGF1 condition. Similarly, H5 organoids derived using the IGF1 method show expression of Rax/Pax6 and Sox2 throughout organoids between days 5-9 indicating a developing but less defined eye-field area (Fig. 5.25a). Gene expression analysis shows RAX is significantly upregulated in IGF1 samples of both S1 and H5 samples although at different timepoints. These peaks are later than when eye-field specification occurs suggesting the IGF1 condition is affecting an increase in interneuron cell expression as RAX marks retinal cell types in the early and mature macaque retina (Fig. 5.12). The IGF1 condition also resulted in significantly higher levels of VSX2, although this was only seen in one cell line (H5) and expression levels were relatively low indicating a small effect.

5.3.4.3 Molecular analysis in mid-stage organoids generated in IGF1 method

During the middle stages of organoid differentiation, between days 50-90, protein expression of PR and RGC markers was performed and compared with gene expression analysis for markers of the same cell types. This enables the maturation of the NE tissue identified in early-stage organoids to be analysed in terms of structural definition alongside quantitative comparison between methods.

In S1 IGF1 organoids the PR/bipolar cell marker Recoverin (Rcvrn) was expressed in cells between day 50-90, clustered within the organoid interior (Fig. 5.26a). Rcvrn+ cells do not form a tightly packed layer at the periphery in either Sasai or IGF1 samples, as would be expected in the developing retina. In both conditions RGC marker, SNCG, is expressed in cells adjacent to Rcvrn+ cells throughout days 50-90 however, SNCG+ cells are less prevalent in the IGF1 sample at day 70-90 (Fig. 5.26a). Structurally minor differences are seen between S1 Sasai and IGF1 samples. In both samples SNCG and Rcvrn+ cells are similarly disorganised with Rcvrn+ cells found within the organoid and lack of retinal lamination (Fig. 5.26a).

RBPMS is a marker for the earliest born cells in the retina, RGCs, as such the expression pattern is expected to peak early. In the S1 organoids generated in the IGF1 condition there is a significant increase in RBPMS day 15-50 reaching a peak of ~0.5-fold of native retina expression (Fig. 5.26b). The timing and relatively high magnitude is supported by the detection of RGC-specific protein SNCG which is widely seen in S1 organoids at day 50 (Fig. 5.26a). This early peak is not seen in Sasai samples, although expression levels increase from day 0 and remain around 0.1-fold during this period (Fig. 5.26b). Later in differentiation RBPMS increases in both conditions between day 70-90, which is not expected from the profile of retinal cytogenesis, and may reflect a second phase of RGC birth, as RBPMS is not expressed in other retinal cell types (Fig. 5.26b, 5.1).

Analysis of PR protein markers does not show notable differences between conditions throughout day 50-90 however a significant increase in CRX expression in S1 organoids derived with the IGF1 condition precedes RCVRN expression at timepoints aligning with PR specification in gestational development, i.e., day 42 and 70 (Fig. 5.26b, 5.1). Furthermore, RCVRN expression showed a steady increase from day 15 onwards in all conditions and peaks at day 90 in both conditions (Fig. 5.26b). The IGF1 sample shows significantly higher RCVRN expression at its peak than the Sasai sample (Fig. 5.26b). These data indicate that the IGF1 method has a stimulatory effect on RGC and PR gene expression at appropriate times in RO development.
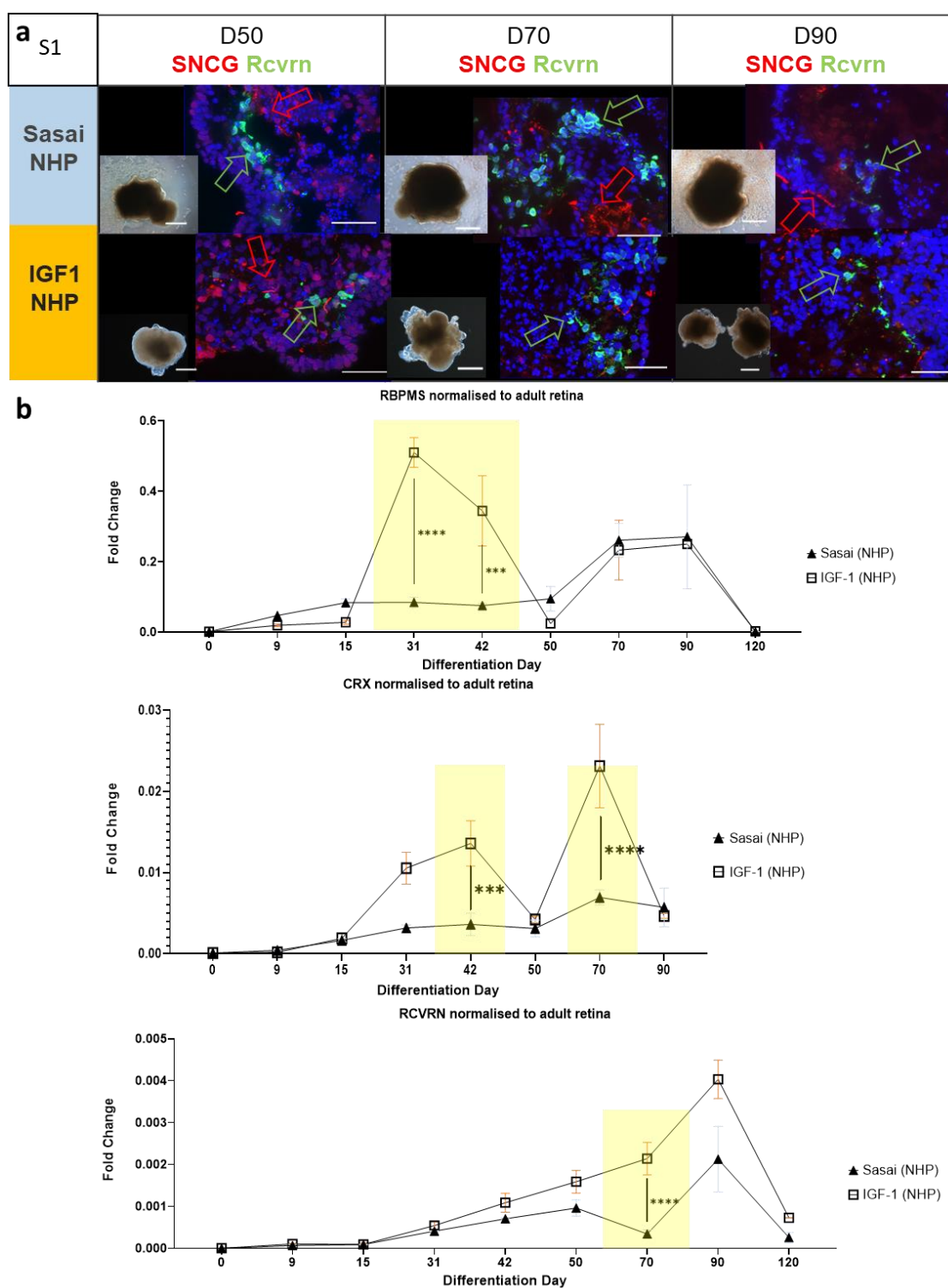
*Figure 5.26. Assessing for RGC genes (SNCG/RBPMS), PR precursors (CRX) and bipolar/PR cells (RCVRN) in S1 organoids (a) Representative IF analysis. D= day. Scale (BF) = 500µm, (IF) = 50µm. Arrows indicate correct expression pattern (b) Relative gene expression of RBPMS, CRX and RCVRN shown as fold change normalised to adult macaque retina. Error bars = SEM. N=2. * = p-value < 0.05, ** = p-value < 0.01, *** = p-value <0.001, **** = p-value <0.0001.*

H5 organoids generated with the IGF1 pooled method show Rcvrn+ cells neighbouring SNCG+ cells from day 50-90 (Fig. 5.27a). Between day 50-70 these are located within the organoid however at day 90 in the pooled condition Rcvrn is expressed in cells forming a continuous layer at the outer edge of organoids organised in a structure approximating that of native retina (Fig. 5.27a). This correct localisation of Rcvrn is also seen in the Sasai sample at day 90, however SNCG+ cells are also found at the peripheral edge of the organoid (Fig. 5.27a). In the IGF1 96-wp sample Rcvrn+ cells remain in the organoid interior, adjacent to SNCG+ cells (Fig. 5.27a).

The expression of *RBPMS* in H5 samples peaks in the first 15 days of differentiation indicating early generation of RGCs (Fig. 5.27b). The expression in Sasai samples peaks at day 9 with levels approximately half that of the adult macaque retina, while IGF1 samples do not show significant upregulation from high base expression levels at day 0 (Fig. 5.27b). *RBPMS* expression is not significantly different between conditions and decreases in both conditions from day 15-50, after which levels are negligible up to day 90 (Fig. 5.27b). This pattern of expression aligns with gestational development (Fig. 5.1).

CRX expression shows significantly higher expression in H5 IGF1 samples than in the Sasai sample at timepoints between day 31-50 (Fig. 5.27b). Peak expression levels between day 15-50 correlate with the timeline for cone PR generation (Fig. 5.27b. 5.1). H5 organoid samples show a comparable timeline of *CRX* upregulation and magnitude of expression to S1 organoids indicating a stimulatory effect of the IGF1 method, independent of cell line (Fig. 5.27b, 5.26b).

Furthermore, in the IGF1 condition *RCVRN* expression increases significantly higher than in Sasai samples from day 31-90 (Fig. 5.27b). This upregulation follows *CRX* upregulation confirming that PRs are being stimulated in the IGF1 condition. Although the magnitude of *RCVRN* is low, it is comparable to the level seen in S1 samples (Fig. 5.27b, 5.26b).
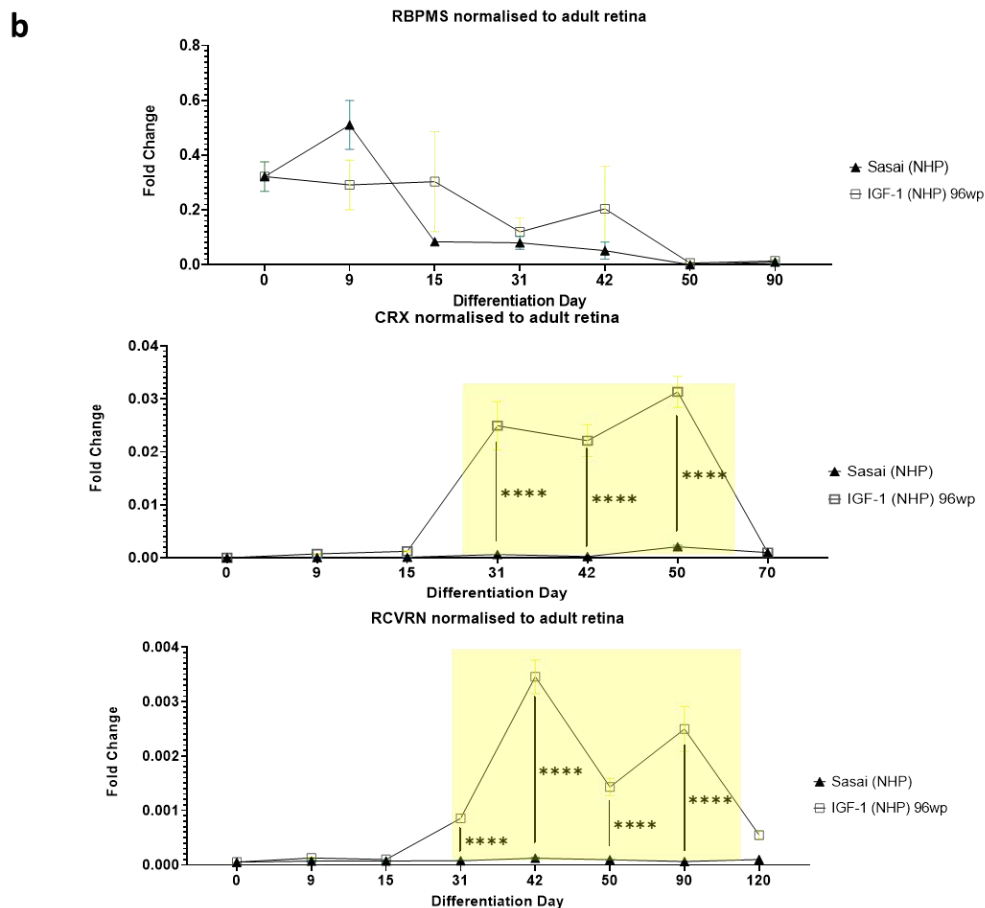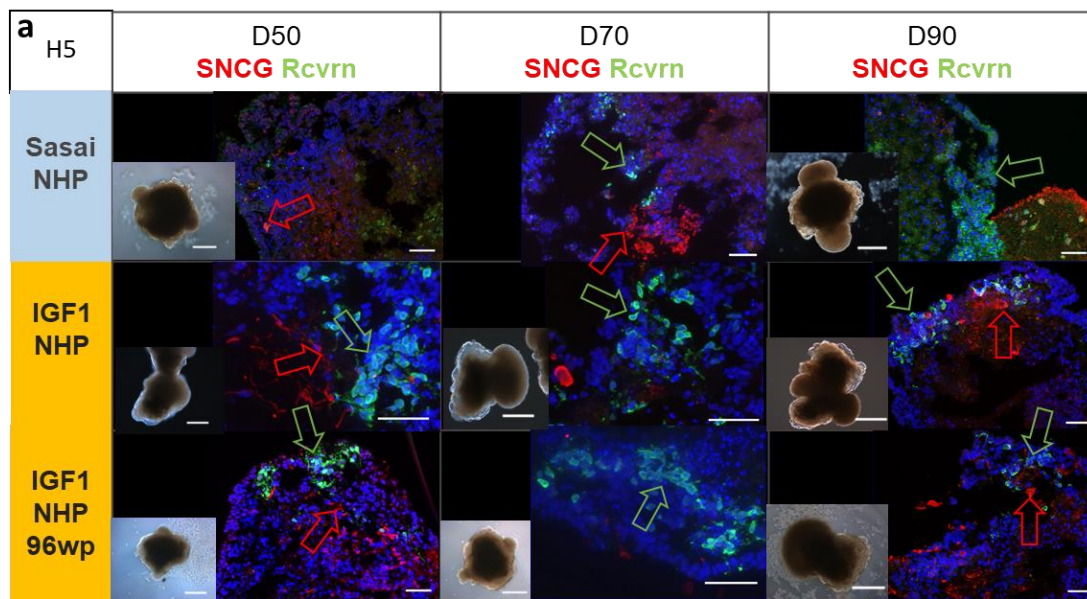
Figure 5.27. Assessing for RGC genes (SNCG/RBPMS), PR precursors (CRX) and bipolar/PR cells (RCVRN) in S1 organoids (a) Representative IF analysis. D= day. Scale (BF) = 500µm, (IF) = 50µm. Arrows indicate correct expression pattern (b) Relative gene expression shown as fold change normalised to adult macaque retina. Error bars = SEM. N=2. * = p-value < 0.05, ** = p-value < 0.01, *** = p-value <0.001, **** = p-value <0.0001.

In conclusion, this analysis shows that the IGF1 method significantly increased PR marker expression in both H5 and S1 cell lines at timepoints correlating with PR generation during embryogenesis. In addition, the correct cellular organisation and localisation of PR and RGC cells at the peripheral organoid edge was only observed in H5 samples generated with the IGF1 condition (Fig. 5.27). Incidentally, these samples also show characteristic retinal morphology with thick phase-bright NE maintained until day 90 (Fig 5.23c).

These results indicate that the IGF1 method improves PR cell localisation and generation with both cell lines showing the same effect. Positive PR marker expression in H5 samples was supported by retinal organoid morphology.

The analysis of RGCs shows the IGF1 method to have a significant stimulating effect on S1 samples although this did not result in improved cellular organisation. An increase in *RBPMS* expression was not seen in H5 IGF1 samples, which may be due to the high base level expression quantified in day 0 samples. *RBPMS* is an RNA binding protein which selectively marks RGCs in the mammalian retina (Nasir-Ahmad et al., 2021; Rodriguez et al., 2014) therefore its role in H5 iPSC samples is not clear. Furthermore, S1 iPSC samples at day 0 show negligible *RBPMS* expression indicating it is not essential for stem cell maintenance.

5.3.4.4 Molecular analysis in late-stage organoids generated in IGF1 method

Analysis of PR-specific markers was performed on S1 and H5 organoids sampled at the latest stages of differentiation, from day 90-120. This included assessment of the cone PR marker, Arr3, cone PR specific opsins, OPN-S and OPN-ML, and the rod PR opsin, Rhodopsin (Rho). At the day 120 timepoint the Müller glia cell marker, CRALBP, was assessed as it arises in the retina at the latest stage of cytogenesis. Finally, the bipolar specific marker GO-α was assessed to differentiate between staining of bipolar and PR cells by Rcvrn.

Analysis of S1 organoids at day 90 using opsin specific antibodies shows clear structural differences in the NR layer between the Sasai and IGF1 conditions. In the Sasai sample OPN-S and OPN-M/L are expressed in a continuous tightly packed cell layer lining the outer edge of the organoids (Fig. 5.28a). There is stratification of cell nuclei and axon projection in the basal direction (Fig. 5.28a). In comparison, few cells in the IGF1 samples express OPN-S or OPN-M/L and these lack the structured retinal organisation seen in the Sasai sample (Fig. 5.28a). However, OPN-S+ and OPN-M/L+ cells in the IGF1 96-wp condition are localised at the peripheral organoid edge and adjacent to SNCG+ cells indicating correct cellular organisation (Fig. 5.28a). This is not seen in the Sasai condition where no

presence of SNCG+ cells is detected in the regions of opsin+ cells (Fig. 5.28a). In neither IGF1 nor the Sasai condition was Rho detected at day 90 (Fig. 5.28a). Gene expression analysis for Rho shows extremely low levels of expression relative to mature macaque retina, corroborating its lack of detection by IF analysis (Fig. 5.28a, b). Despite these low levels, expression is significantly upregulated in the IGF1 sample at day 120, indicating some positive method effect (Fig. 5.28b).
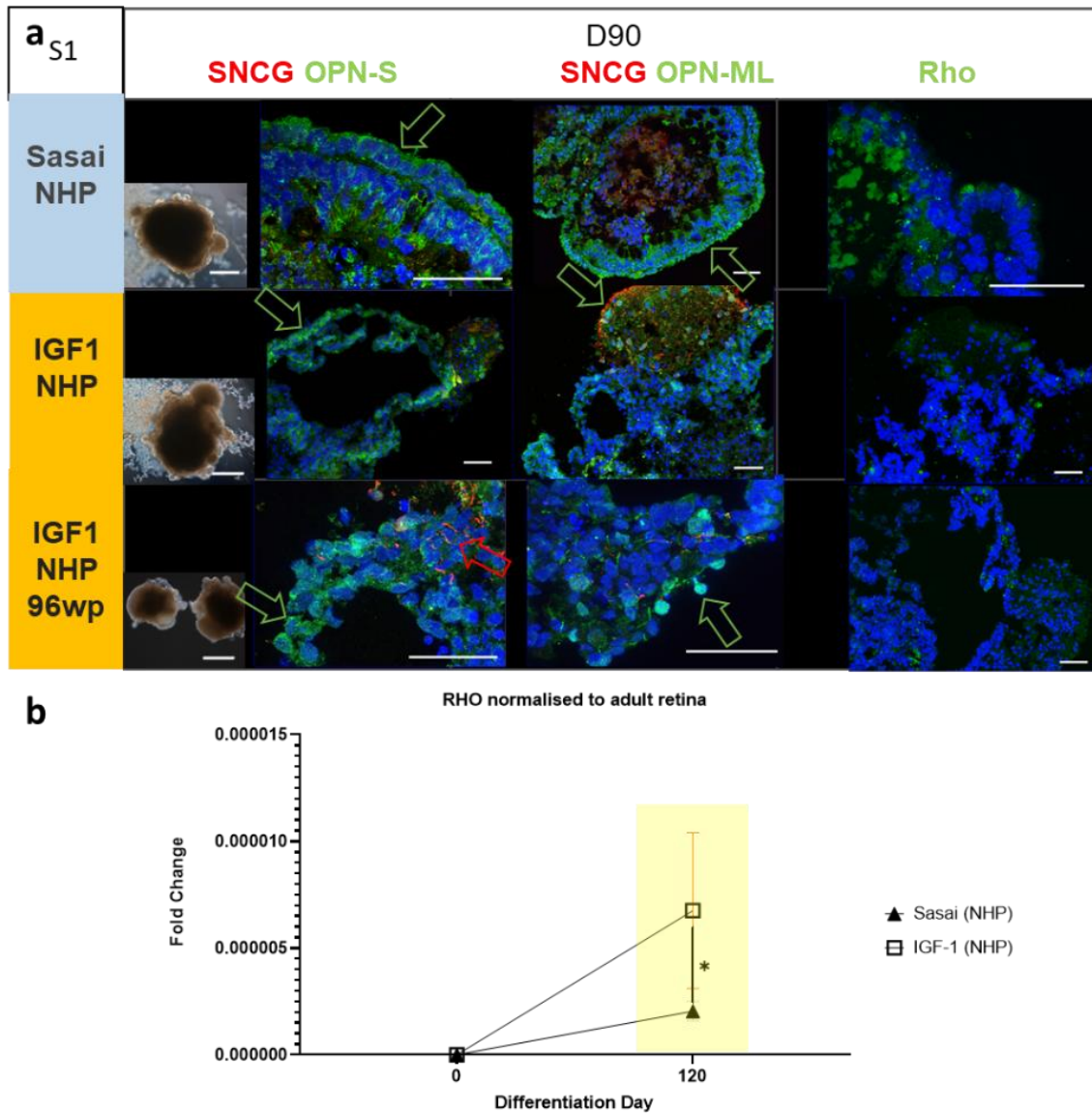
Figure 5.28. Assessing for RGCs (SNCG), cone PR (OPN-S, OPN-ML) and rod PR cells (RHO) in S1 organoids (a) Representative IF analysis. D= day. Scale (BF) = 500µm, (IF) = 50µm. Arrows indicate correct expression pattern. ND = Not determined. Green staining in Rhodopsin panels is background level. (b) Relative gene expression shown as fold change normalised to adult macaque retina. Error bars = SEM. N=2. * = p-value < 0.05, ** = p-value < 0.01, *** = p-value <0.001, **** = p-value <0.0001.

At day 120 S1 organoids in the IGF1 condition express the cone PR markers OPN-S and OPN-ML in cells at the periphery of the organoids however the structure in the cell layer in the IGF1 pooled condition is disrupted (Fig. 5.29a). Expression of OPN-ML in the IGF1 pooled condition shows limited maturation of the positive cells; however they are located in regions with CRALBP+ cells indicating correct relative localisation of mature cell types (Fig. 5.29a).
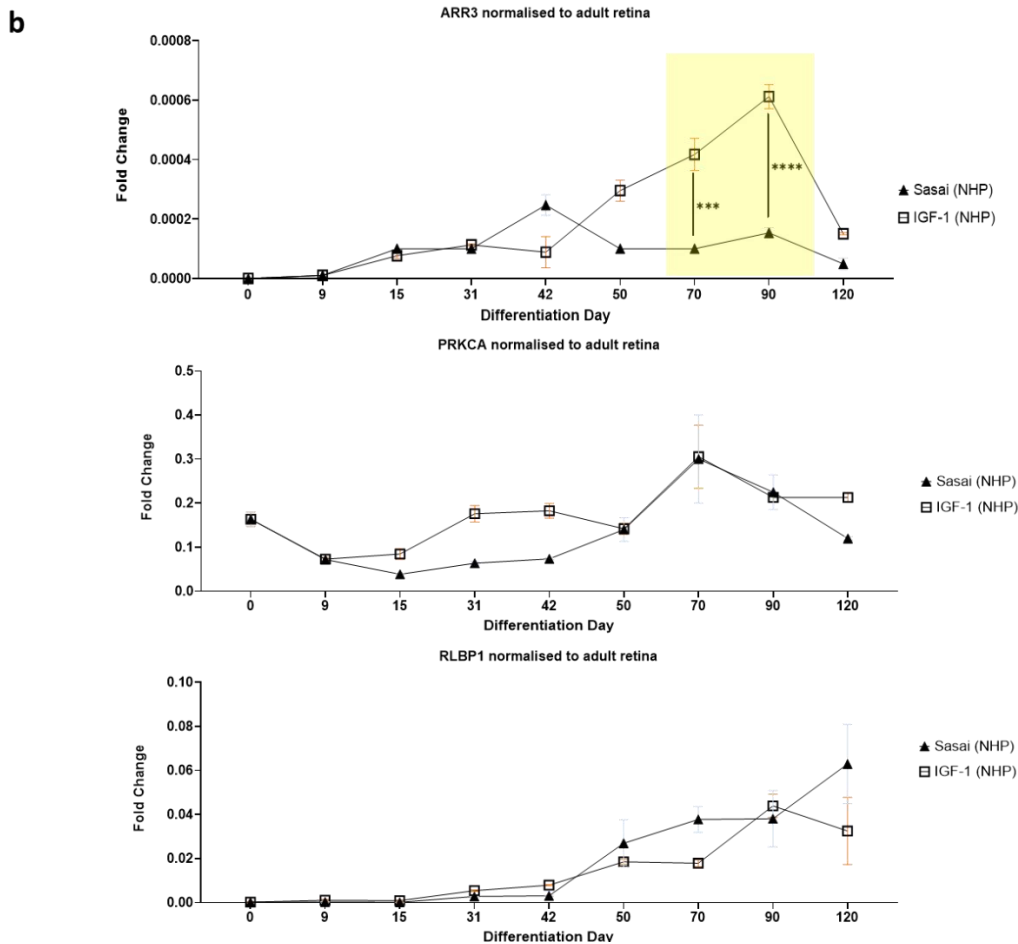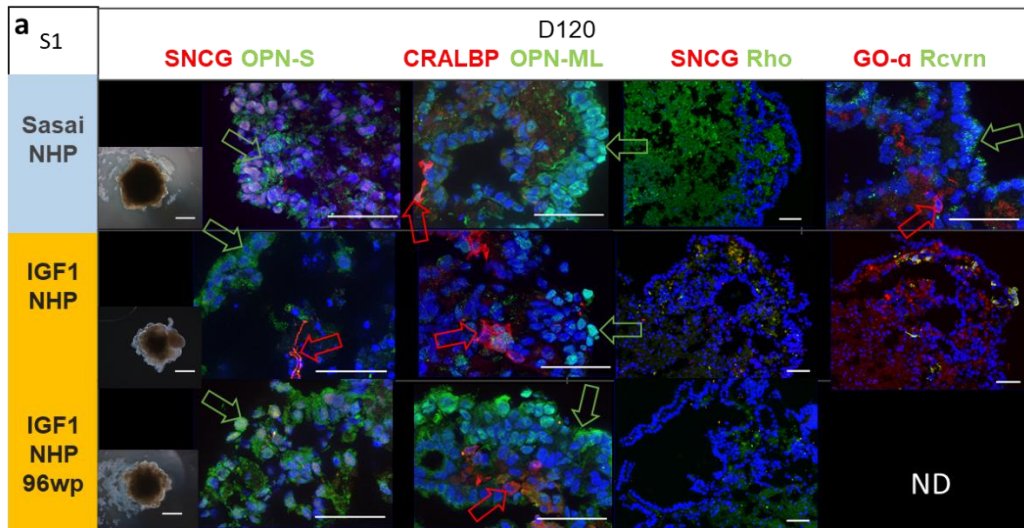
*Figure 5.29. Assessing for RGCs (SNCG), cone PR (OPN-S, OPN-ML, ARR3), rod PR (RHO), Muller glia (CRALBP/RLBP1), bipolar (GO-a, PRCKA) and bipolar/PR marker (RCVRN) in S1 organoids (a) Representative IF analysis. D= day. Scale (BF) = 500μm, (IF) = 50μm. Arrows indicate correct expression pattern. ND = Not determined. Rhodopsin panel staining is not above background level (b) Relative gene expression shown as fold change normalised to adult macaque retina. Error bars = SEM. N=2. * = p-value < 0.05, ** = p-value < 0.01, *** = p-value <0.001, **** = p-value <0.0001.*

The expression of OPN-M/L in the IGF1 96-wp condition compared to the pooled condition shows improved organisation of cells in a continuous layer with some formation of axons from the basal side of the cell nuclei, this shows a more complete tissue lamina arrangement (Fig.5.29a). There is no detected presence of Rho in the S1 day 120 sample indicating lack of development of mature rod PRs with all methods (Fig. 5.29a). Co-staining with GO-α and Rcvrn in the S1 IGF1 pooled sample shows co-expression of these markers indicating a population of bipolar cells (Fig. 5.29a). In comparison the Sasai sample showed distinct populations of Rcvrn+/GO- α at the peripheral edge of organoids- and Rcvrn-/GO- α+ cells basally to these cells indicating the correct localisation and structural arrangement of PR and bipolar cells, respectively (Fig. 5.29a).

Gene expression analysis of cone PR marker *ARR3* in S1 samples shows that the IGF1 condition results in significantly higher peak expression levels between day 70-90 compared to the Sasai condition (Fig. 5.29b). The Sasai condition shows an earlier peak in *ARR3* expression at day 42, which aligns with the gestational development of cone PRs (Fig. 5.29b). The magnitude of *ARR3* is low compared to the mature retina (Fig. 5.29b). Sample comparison between methods at day 120 shows strong, continued expression of cone opsin markers in the IGF1 condition.

The expression of the bipolar cell marker, *PRKCA*, increases early in the IGF1 conditions with expression levels approximately double that of the Sasai condition between day 15-42 (Fig. 5.29b). Following this *PRKCA* increases to peak at day 70 at the same time and level as in the Sasai sample before tapering off (Fig. 5.29b). This aligns with the timeline for production of bipolar cells in the developing macaque retina (Fig. 5.1).

The Müller glia marker *RLBP1* shows an increase in expression levels throughout differentiation reaching peak expression levels at the latest timepoints of day 120 in Sasai samples, and day 90 in the IGF1 sample (Fig. 5.29b). As Müller glia cells are among the latest to arise in retinogenesis this confirms the correct sequential timeline of development is occurring in S1 ROs in both conditions.

Looking at H5 organoids less of a structural difference was seen between Sasai and IGF1 conditions at day 90 than in the S1 samples (Fig. 5.30a, 5.29a). Clear extra-nuclear expression of OPN-S and OPN-ML was seen in both the Sasai and IGF1 conditions in cells lining the outer edge of the organoids (Fig. 5.30a). This layer however was only one cell thick and in IGF1 conditions some limited expression of SNCG+ cells were seen in the adjacent cell layer (Fig. 5.30a). Notably the H5 organoid from the IGF1 pooled condition shows Rhodopsin expression in a small number of cells in the outermost cell layer, which is not seen in the Sasai condition (Fig. 5.30a).

Gene expression analysis of rod PR markers confirm the positive effect of the IGF1 method on rod cell generation as both *NRL* and *RHO* are significantly upregulated compared to Sasai samples (Fig. 5.30b). The rod progenitor marker *NRL* shows peak expression at day 50, prior to the upregulation of the mature rod marker *RHO* which increases up to day 120 (Fig. 5.30b). These results indicate IGF1 conditions improve rod PR protein and gene expression in H5 RO differentiation.
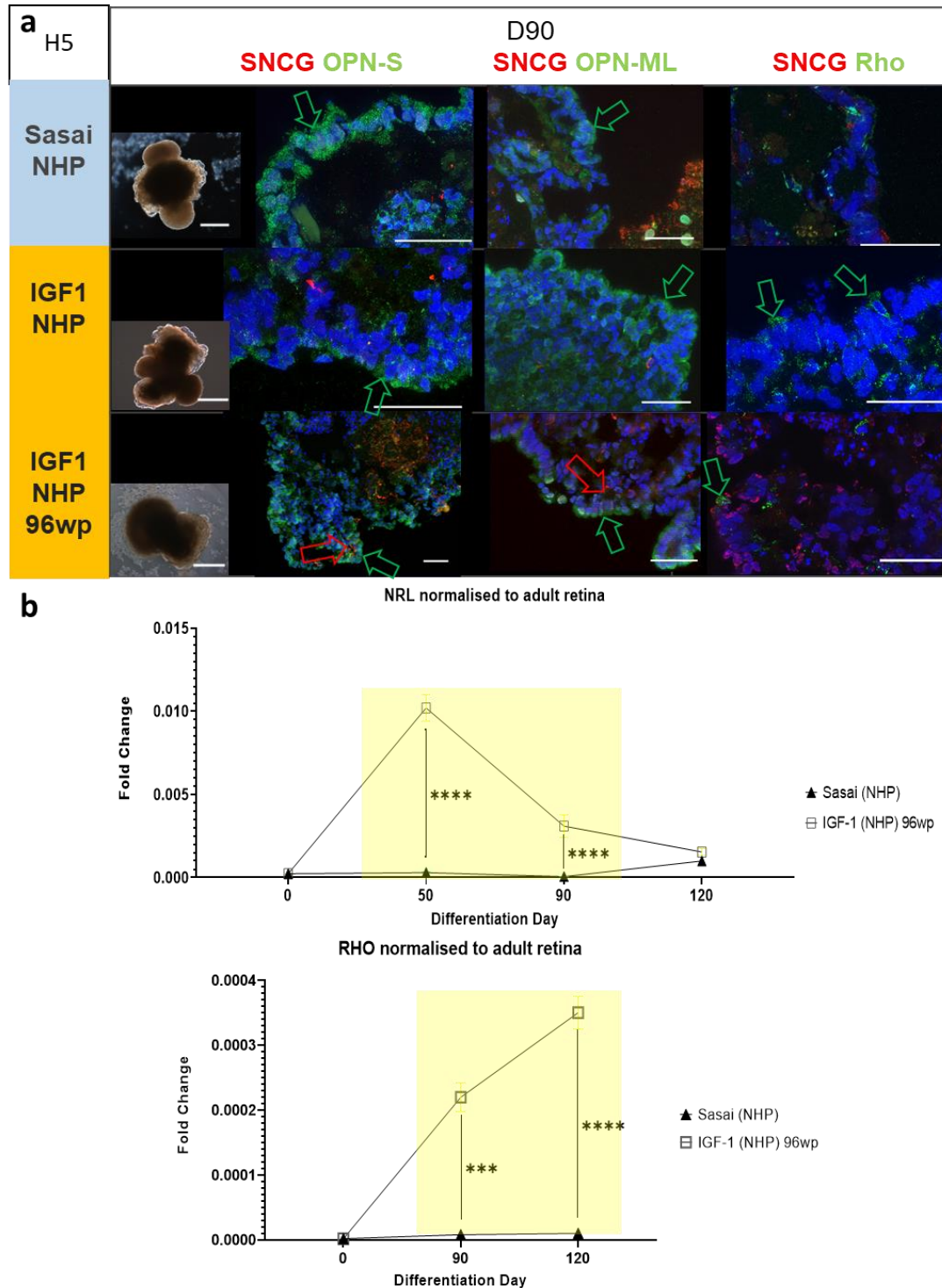
Figure 5.30. Assessing for RGCs (SNCG), cone PR (OPN-S, OPN-ML) and rod PR cells (RHO, NRL) in H5 organoids (a) Representative IF analysis. D= day. Scale (BF) = 500µm, (IF) = 50µm. Arrows indicate correct expression pattern. (b) Relative gene expression shown as fold change normalised to adult macaque retina. Error bars = SEM. N=2. * = p-value < 0.05, ** = p-value < 0.01, *** = p-value <0.001, **** = p-value <0.0001.

At day 120 the H5 samples from the IGF1 conditions show both cone opsin expression of OPN-S and OPN-ML in cells in the outer cell layer of the organoids (Fig. 5.31b). Although the opsin cell layer is only one cell thick, there is expression of SNCG+ cells in the area directly below OPN-S+ and OPN-ML+ cells (Fig. 5.31a). These cells show axon formation and overlay showing increased maturation and potentially formation of synapses (Fig. 5.31a). Furthermore, analysis of cone marker Arr3 shows expression in cells forming a continuous layer of tightly packed cell nuclei interspersed with CRALBP+ cells in a structure approximating the ONL of native macaque retina as determined in antibody validation experiments (Fig. 5.31a, 5.7).

The co-staining with Rhodopsin and Recoverin in H5 organoids at day 120 showed of the lack of Rhodopsin+ cells, indicating that their detection at day 90 marked a rare population of cells (Fig. 5.31a). There was detection of Rcvrn+ cells in the IGF1 96wp condition distributed within the centre of the organoid (Fig. 5.31a). Further analysis assessing Rcvrn in combination with GO-α show co-staining in all cells located within the centre of the organoid defining these cells as of bipolar cell identity rather than PRs (Fig. 5.31b). There is a distinct population of Rcvrn+/ GO-α- cells located at the periphery of the organoid which represent PR cells and show a lower intensity of Rcvrn expression that in the Rcvrn+/ GO-α+ bipolar cells (Fig. 5.31a).

The cone PR specific marker, *ARR3* shows the highest expression levels in IGF1 samples at day 42 and between day 90-120 when it is significantly higher than in the Sasai condition (Fig. 5.31b).

The expression of bipolar marker, *PRKCA*, shows high expression at day 0 indicating expression in the iPSC sample. This decreases and then increases from day 9-42 when it peaks in both IGF1 and Sasai samples (Fig. 5.31b). Additionally, IGF1 samples show a later increase from day 70-120 (Fig. 5.31b). This is more in line with gestational development of bipolar cells which are generated in the second phase of cell birth (Fig. 5.1).

The expression of *RLBP1* in the IGF1 condition increases at day 42 to double that of the Sasai sample (Fig. 5.31b). Again at day 90 *RLBP1* peaks in the IGF1 sample significantly higher than the Sasai condition which shows peak expression at a level of approximately a third (Fig. 5.31b).
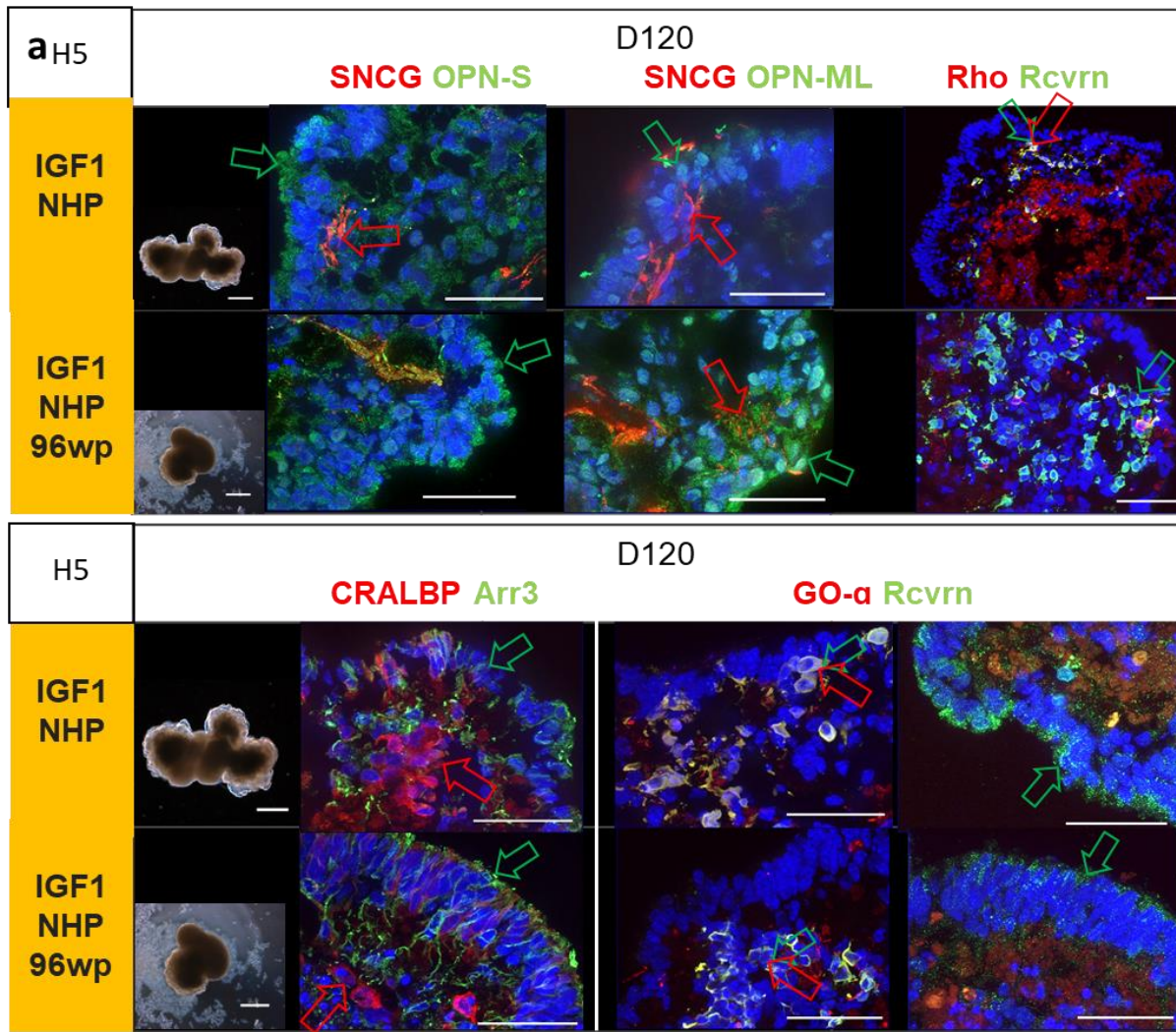
Figure 5.31. Assessing for RGCs (SNCG), cone PR (OPN-S, OPN-ML, ARR3), rod PR (RHO), Müller glia (CRALBP/RLBP1), bipolar (GO-α, PRCKA) and bipolar/PR marker (RCVRN) in S1 organoids (a) Representative IF analysis. D= day. Scale (BF) = 500µm, (IF) = 50µm. Arrows indicate correct expression pattern (b) Relative gene expression shown as fold change normalised to adult macaque retina. Error bars = SEM. N=2. * = p-value < 0.05, ** = p-value < 0.01, *** = p-value <0.001, **** = p-value <0.0001.

Other retinal genes which were found to be significantly differentially expressed between the IGF1 and Sasai methods are the horizontal cell marker, *PROX1*, and the RPE marker *MITF* (Fig. 5.32). In both cell lines *PROX1* is significantly higher in the IGF1 samples than the Sasai samples at day 42 (Fig. 5.32). This is in accordance with the timepoint for horizontal cell development *in vivo* (Fig. 5.1). This also corroborates earlier analysis which showed upregulation of *RAX* expression in both cell lines between day 31-42 (Fig. 5.24b, 5.25b).

b

ARR3 normalised to adult retina

PRKCA normalised to adult retina

RLBP1 normalised to adult retina
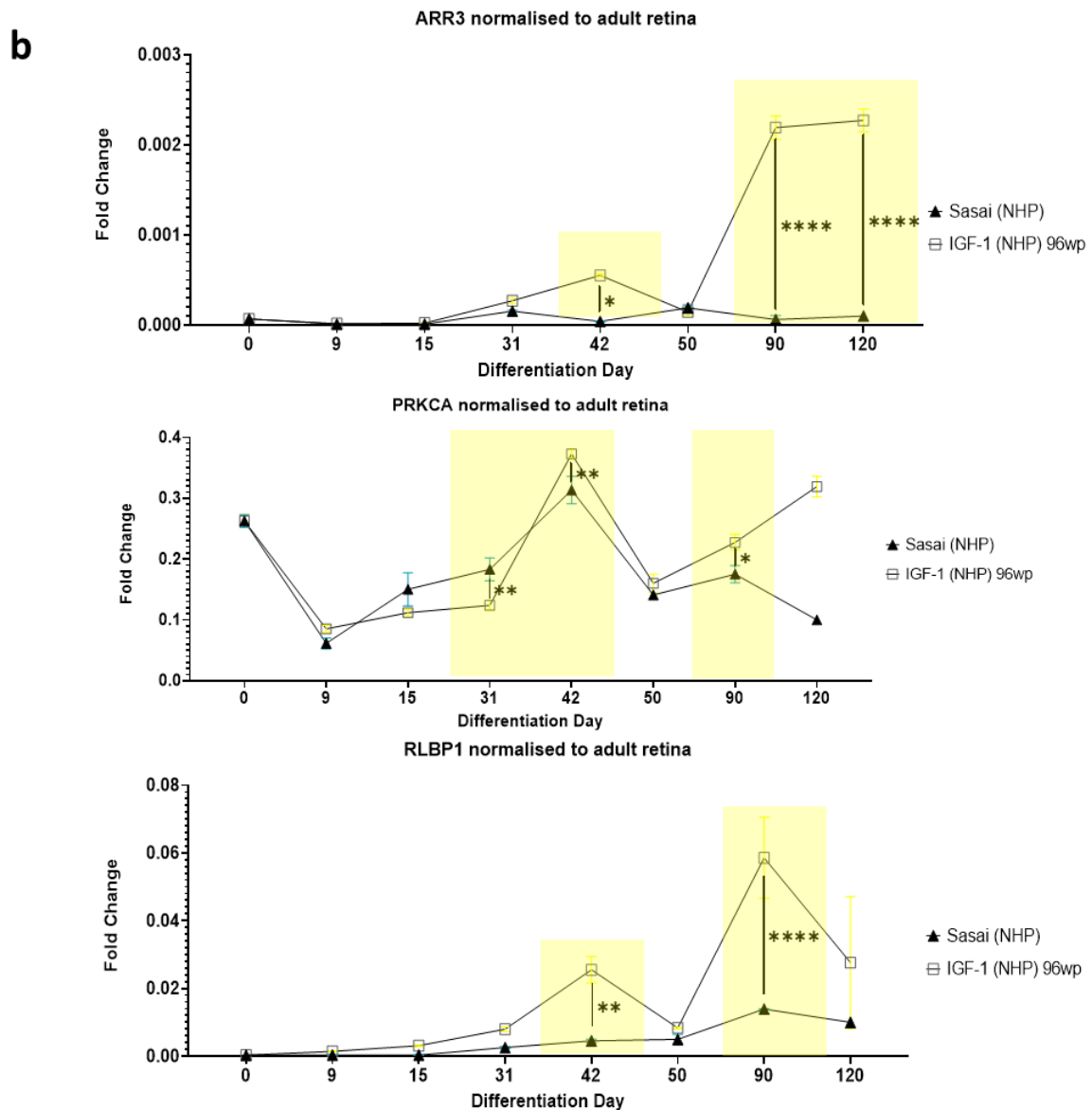
In S1 organoids *MITF* shows high expression levels increasing from day 70-90 in the Sasai and IGF1 pooled conditions to reach twice that of the adult macaque retina (Fig. 5.32a). In H5 organoids *MITF* reaches peak expression in the mid-stage of organoid development in the Sasai condition at day 42 (Fig. 5.32b). At this point it is significantly higher expressed in the Sasai method compared to the IGF1 condition at levels close to that of the native retina (Fig. 5.32b).

272
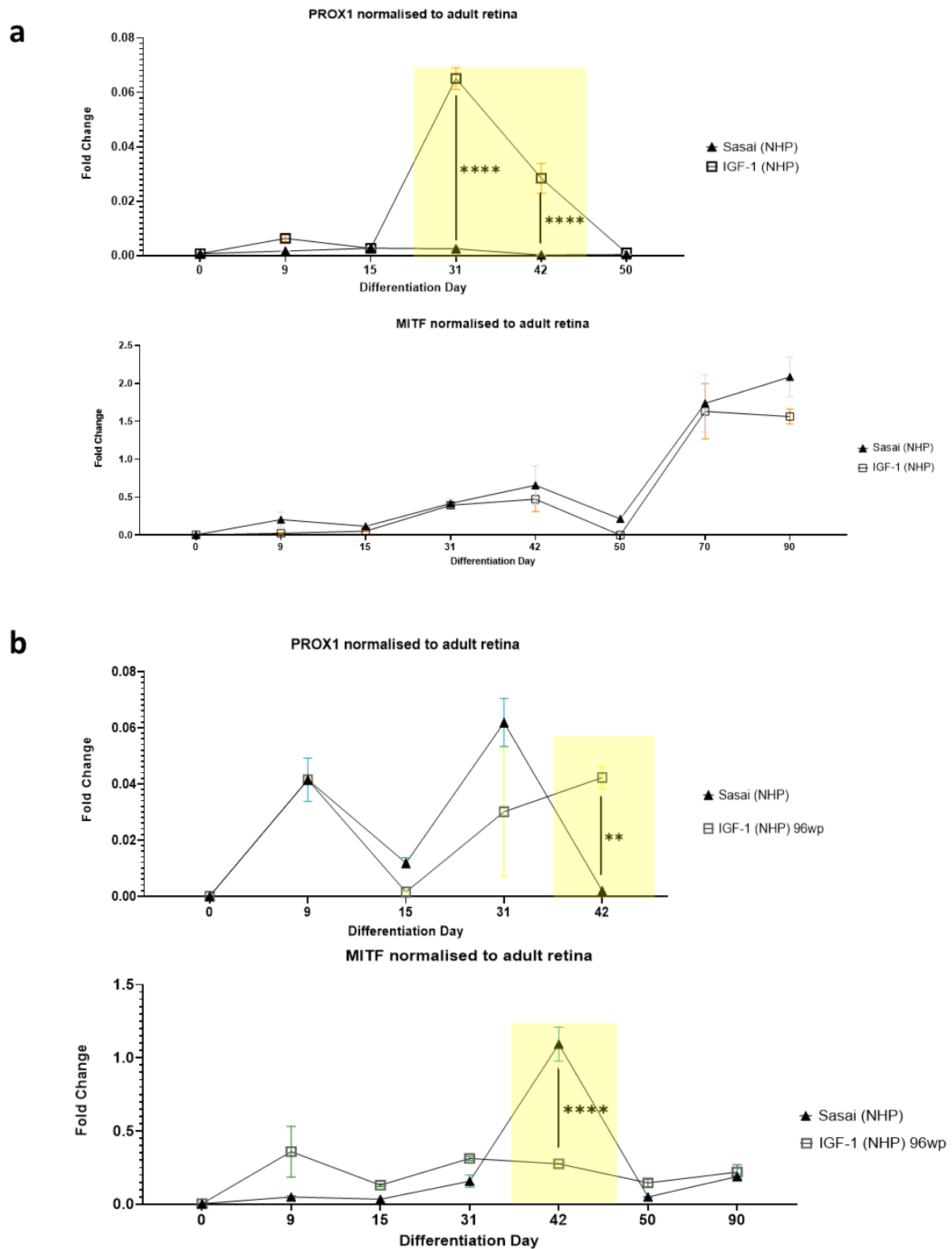
Figure 5.32. Relative gene expression shown as fold change normalised to adult macaque retina. Assessing for horizontal cell (PROX1) and RPE cell (MITF) expression in (a) S1 organoids. (b) H5 .N=2. organoids. Error bars = SEM. N-* = p-value < 0.05, ** = p-value < 0.01, *** = p-value <0.001, **** = p-value <0.0001.

273

To conclude, in H5 samples analysed from IGF1 conditions at the latest stages of development there is evidence of developing cone PRs and increasing maturity of the NR cell lamina with the presence of CRALBP+ cells and an organisation suggesting potential synapse formation between RGCs and PRs (Fig. 5.31a). In summary, these results show the development of a cone-dominated laminated retina with Arr3+ cells, bipolar cells (Rcvrn+/GO-α+), Müller glia cells (CRALBP+) and RGCs (SNCG+) organised correctly in the same region of retinal lamina (Fig. 5.31a).

A larger volume of organoids resulting in a reduced surface area to volume ratio would be expected to reduce diffusion and availability of nutrients in cells in the interior of the organoid. Despite this, there is prolonged maintenance, or less loss, of SNCG cells in both the S1 and H5 IGF1 samples from day 90 and 120 compared with Sasai conditions (Fig. 5.30a, 5.31a),

The co-staining using bipolar marker GO-α and Rcvrn at the latest stages of development was interesting as it shows that in macaque iPSC samples Rcvrn detection in cells is not sufficient to identify PR cell populations. As such, analysis using specific PR markers, such as the opsins, is more reliable for tracking populations of developing PRs and the results using this marker from earlier stages of analysis should be interpreted with this dual cell type specificity in mind. The co-localisation of GO-α with Rcvrn highlights that in S1 IGF1 samples there is less defined presence of PRs marked by Rcvrn.

Organoids generated from both S1 and H5 cell lines show predominantly cone PR specific marker expression with only a few cells in H5 samples showing rod PR marker expression (Fig. 5.29a, 5.30a). This could indicate that the method is unsuitable for rod PR production. Alternatively, it could indicate that mature rod PR markers have not developed yet. Analysis with an immature rod precursor marker such as NRL or sampling at a later timepoint would help to determine this.

Gene expression analysis supports these conclusions as PR specific markers are significantly up regulated in the IGF1 samples of both cell lines at timepoint aligning with their detection by IF analysis and developmentally appropriate times.

5.3.4.5 Comparing retinal protein expression in H1 retinal organoids generated with the IGF1 method

H1 organoids generated in both the IGF1 conditions also showed development of a bright putative NE layer, this was at a slightly later timepoint than seen in the S1 and H5 organoids becoming defined at day 50 in pooled organoids (Fig. 5.23d). Similarly to the S1 and H5 samples the H1 organoids in the IGF1 96-wp condition developed a thinner layer of bright NE than in the pooled samples which was maintained until the final timepoint of day 90 (Fig. 5.23d). Due to limited H1 iPSC

proliferation there were insufficient organoid samples available to maintain these in IGF1 culture until day 120.

In H1 organoids derived with Sasai (NHP -ch/su) method there are separate populations of Rax+ and Pax6+ cells and limited co-expression from day 5-15 (Fig. 5.33a). In H1 IGF1 samples, Rax/Pax6 are lacking in cells at day 5, while IF analysis shows Rax/Pax6 throughout the organoid at day 9 and Pax6+ cells remain present at day 15 (Fig. 5.33a). Sox2 is widely expressed throughout the organoids in both conditions at day 5 and 9, at day 15 becoming limited to cells in peripheral regions in Sasai samples, and absent in the IGF1 condition (Fig. 5.33a). In contrast to S1 and H5 samples, H1 organoids derived with the Sasai (-ch/su) condition express Otx2 in cells at the organoid periphery at day 9 (Fig. 5.33a). Of all cell lines, at this stage H1 organoids derived with IGF1 method show the most limited expression of NE markers losing Rax and Sox2 expression between day 9 and 15 (Fig. 5.33a).

H1 organoids show limited Rcvrn expression in cells at day 50 of both IGF1 conditions and the Sasai -ch/su condition (Fig. 5.33c). However, in all cases these cells are correctly localised to the outermost cell layer of the organoids, which the IGF1 96-wp sample shows some retinal organisation with RGCs located basally (Fig. 5.33c). At day 70 Rcvrn expression in the Sasai sample has decreased in intensity at the periphery of organoids while in the IGF1 condition Rcvrn+ cells remain bright at the outermost edge of the organoids (Fig. 5.33c). Additionally, SNCG+ cells and axon formation can be seen in the basal aspect of IGF1 organoids, which is not seen in the Sasai sample at day 70 (Fig. 5.33c). At day 90 in IGF1 samples Rcvrn is expressed in cells at the rounded outer edge of the organoids representing correct localisation (Fig. 5.33c). In comparison the smooth, rounded NE has been lost in the H1 Sasai -ch/su sample and Rcvrn+ cells are disorganised (Fig. 5.33c). Therefore the IGF1 method improves the cellular expression and localisation of key retinal markers in the organoid throughout day 50-90 of differentiation.

Further analysis of retinal gene expression will confirm if the IGF1 method also improved quantitative retinal marker expression. As has been seen in previous analyses for H5 and S1 samples, gene expression comparison can show definitive and significant differences between conditions, which by IF analysis appear similar.
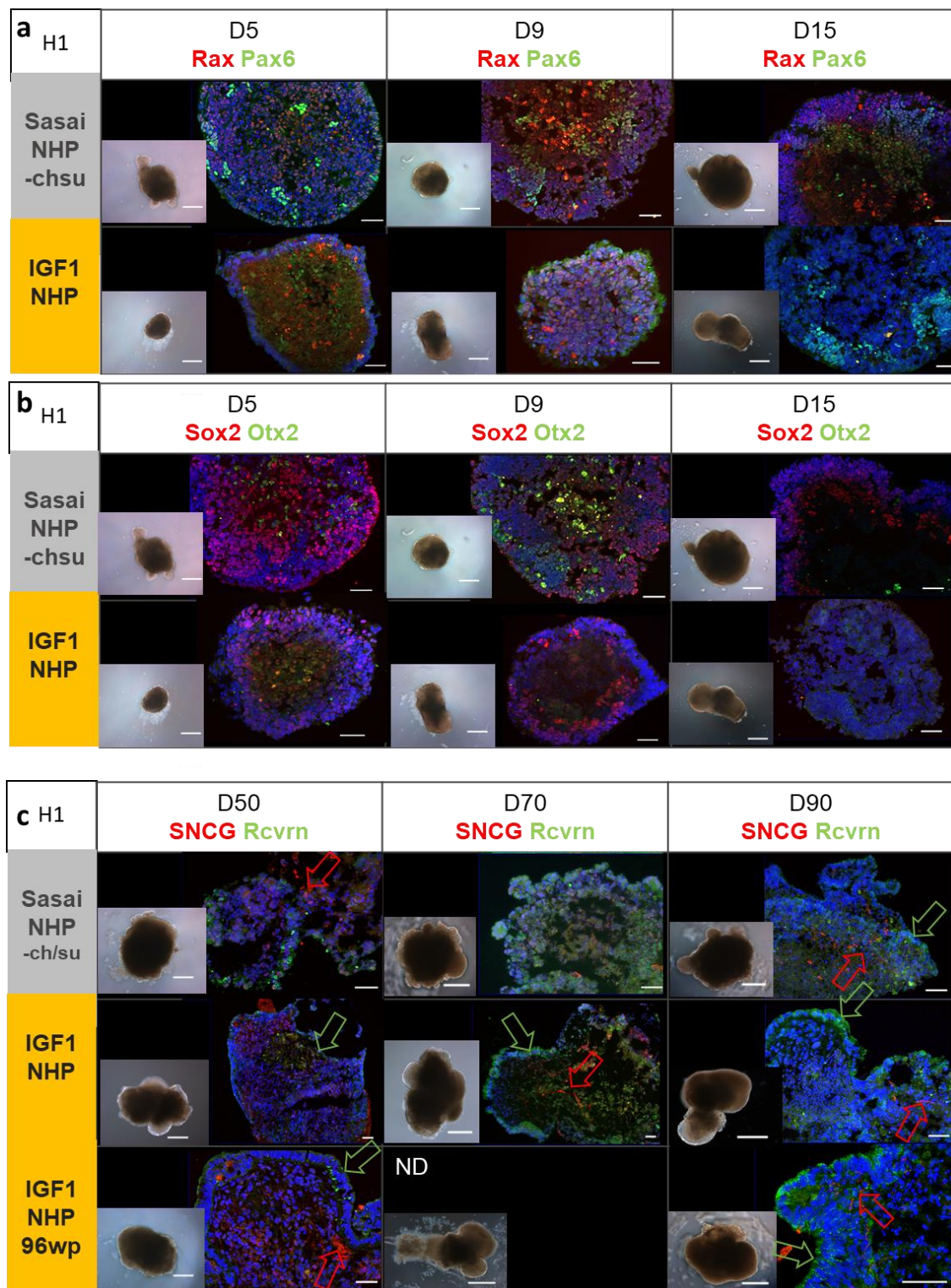
Figure 5.33. Representative IF analysis assessing for (a,b) neural-retinal TFs (Rax, Pax6, Otx2), neuroepithelial marker (Sox2) and (c) RGCs (SNCG) and bipolar/PR marker (RCVRN) in H1 organoids generated in Sasai without CHIR99021/SU5402 (-ch/su) and IGF1 methods with macaque adjusted timing (NHP). D= day. ND = not determined. N=2. Scale (BF) = 500μm, (IF) = 50μm. Arrows indicate correct expression pattern.

5.4   Discussion

5.4.1   Primate stem cells adaptation to feeder-free conditions

In this chapter I have tested the capability of three macaque iPSC lines to be cultured in feeder-free conditions. The results show that it is possible to grow the S1, H5 and H1 iPSCs on Matrigel as a monolayer without complete loss of pluripotency gene expression (Fig. 5.5, 5.6). This aligns with the findings of other groups who have adapted NHP stem cells for culture in feeder-free conditions (Ono, 2014). However, the morphology of the cells is altered and they lose the characteristic tightly packed colony structure which was shown by Biotracker staining to be definitive of pluripotency. In addition, key pluripotency gene expression *OCT4* and *NANOG* was decreased (Fig. 5.5, 5.6). Therefore, by culturing the cells in feeder-free conditions, an unknown proportion of cells will likely spontaneously differentiate. The Biotracker dye technique shows the advantage of the immediate visualisation of pluripotency which is very instructive for the future culture of the stem cells where passaging and quality control of cells is determined by eye.

Due to this technical advantage I opted to continue culture of the macaque iPSCs on iMEF feeder cells as strict quality control was able to be performed throughout culture and passaging. This likely enabled culture and differentiation to be performed on a purer population of iPSCs than if they were maintained as a monolayer.

However, in practice culturing macaque iPSCs on iMEFs and using a manual passaging technique limited the quantity of cells able to be generated through sub-culturing. In some cases, for example using the H1 cell line this led to an insufficiency of iPSCs for plating and differentiation into organoids. It would be useful to improve the scalability of culture experiments by either upscaling the size of iPSC culture plates to generate more cell colonies per passage, or to further investigate the use of a feeder free and enzymatic based passaging system for macaque iPSCs.

5.4.2   Adaptation of human retinal differentiation protocols onto macaque iPSCs

Applying published protocols from human PSC studies directly onto macaque iPSC successfully shows the capacity of S1 iPSCs to differentiate into retinal tissue. Analysis of known retinal cell markers showed SNCG+ and RCVRN+ cells paired with a characteristic optically phase-bright neuroepithelia lamina located at the periphery of the organoids generated with the Sasai method with human timing (Fig. 5.11). Gene expression also supported the detection of retinal cells throughout differentiation. These differentiation experiments crucially demonstrated the capability

277

of a macaque iPSC line to develop NE morphology and retinal marker expression using the SFEBq methodology.

The peak size of organoids was reached between day 25-50, where organoids had thick, bright NE morphology which is similar to that of stage 2 organoids as defined by morphological characterisation of developing human retinal organoids (Fig. 5.9a) (Capowski et al. 2020). The stage 2 of human RO development is usually observed between day 25-147 (Capowski et al. 2020). As the development of retinal structures was rapid during the first 20 days of growth and NE thinning was observed in retinal morphology from day 50 onwards it was hypothesised that macaque differentiation was occurring at an accelerated rate compared with human PSC differentiation. This led to the conclusion that the use of the same temporal parameters of the human culture conditions was insufficient to support macaque retinal cell maturation.

5.4.3   Improving macaque retinal differentiation by adjusting the timing of the culture programme

The novel method adaptation of adjusting the timing of the culture protocol was applied to generate organoids from 3 macaque iPSC lines with the additional aim of applying culture media, reagents and signalling molecules known to show a productive effect on retinal cell growth and differentiation. The timing adjustment was hypothesised to induce the process of retinal differentiation while better supporting the timeline of cell generation leading to less loss of retinal morphology and greater maturity of cell types.

The results from both S1 organoids showed the Sasai method with NHP adjusted timing improved the efficiency and maintenance of the retinal morphology in organoids until day 120 compared with application of human timing (Fig. 5.9a,b). It was the aim to also compare the H5 and H1 cell lines differentiated with both human and NHP timing Sasai conditions, however this was not performed due to lack of time and cell availability.

Analysis of the S1 organoids generated using NHP timing in comparison with human timing showed improved structure of opsin+ cells at day 90 with OPN-S and OPN-ML cell forming a tightly packed continuous layer which was not seen in the human timing samples (Fig. 5.12a). It also resulted in earlier expression of key retinal markers *VSX2* and *RCVRN* which showed peaks earlier than those generated with the human timing method (Fig. 5.10b, 5.11b). Despite good examples of mature retinal cell localisation and organisation in the NHP adjusted method, the gene expression results for

S1 samples showed significantly higher levels in the human timing samples for cone PR (*CRX* and *ARR3*) and Müller glia (*RLBP1*) markers (Fig. 5.12b, 5.13b).

Unfortunately, this direct comparison could not be performed for other cell lines due to lack of available samples. However, protein expression analysis of H5 and H1 samples derived with NHP timing methods also show presence of structured opsin+ cells in the peripheral cell layer of organoids at day 120 indicating generation of PR cells has been achieved using this method (Fig. 5.13c, d).

It would have been informative to perform gene expression analysis of H1 organoids from the Sasai (NHP) -ch/su condition as the IF analysis of samples at day 120 showed positive expression of mature PR markers such as OPN-S, OPN-ML, CRALBP, GO-α and Arr3 as well as correct localisation of these cells lining the peripheral edge of the organoids (Fig. 5.29).

Interestingly, a recent article has been published showing the generation of 3D ROs from rhesus macaque iPSCs (Lopez et al., 2021). This study shows the accelerated development of macaque ROs in terms of morphological features and expression of key retinal markers by protein expression analysis. Lopez et al., (2021) defines Stage 1, by the widespread presence of eye-field and NE markers including Rax, Pax6, Lhx2 and Otx2 as shown by IF analysis. In this chapter I have shown results determining the presence of Rax and Pax6 expression in S1/H1/H5 macaque derived organoids from day 5 -15 however gene expression of *RAX* peaks at day 42 (Fig. 5.10b).

Although the transcription factor Otx2 is known to be active at the OV stage of retinal development in mouse, its activity in developing primate retina is known to be present in post-mitotic committed PRs and to co-ordinate PR fate specification (Martinez-Morales & Wittbrodt, 2009; Muranishi et al., 2012; Zuber et al., 2003). In the recent derivation of ROs from rhesus macaque cells, Otx2+ cells were detected at day 44 (Lopez et al. 2021). The results in this chapter show that Otx2 was not expressed in S1 or H5 organoids at the earliest stages of NE specification, day 5-15, although Rax/Pax6 were expressed. However, it can be expressed in organoids at this stage as transient expression was seen in H1 organoids (Sasai -ch/su) condition at day 9 (Fig. 5.33b). As Rax/Pax6/Otx2 protein expression was not assessed in organoids beyond day 15 it is not possible to say when these markers expression arise in the conditions, however these organoids showed *RAX* expression at later timepoints and subsequently developed PR marker expression (Fig. 5.48-5.51). The IF analysis of samples at day 5-15 show that whether Otx2 is expressed or not, PR cells can be derived at later stages of differentiation.

The "stage 2" of human RO development is reported to occur approximately between day 25-147 and is defined by a thick phase-bright NE layer and an intermediate developmental stage (Capowski et al. 2019). IF analysis of human ROs shows an abundance of PR precursors expressing Crx and Otx2 as well as Rcvrn and the development of rod and cone specific markers such as NRL and ARR3 which are bordered internally with a hollow core (Capowski et al. 2019). In this results chapter S1 organoids show stage 2 characteristics of thick NE morphology and *CRX* expression peaks between day 31-42, which is in line with human developmental timing (Fig. 5.12b).

This is followed by development into "Stage 3" which show maturation of the outer nuclear layer (ONL) with rod and cone PRs present in a ratio of 4:1, morphologically the NR thins and a "brush border" is seen indicative of outer segment maturation of PR cells and Müller glia cells are finally present (Capowski et al. 2019). In human ROs this is reported to occur from day 180 onwards (Capowski et al. 2019). In the S1 and H1 samples generated with the NHP timing methods, the NR had thinned and CRALBP+ ,OPN-S+ and OPN-ML+ cells were present at day 120 indicating the presence of some stage 3 characteristics (Fig. 5.13). As these markers were also expressed in S1 samples in the human timing condition, and the timeline of retinal gene expression profiles were largely, excepting *VSX2* and *RCVRN*, identical between timing methods, the chronology of macaque retinogenesis may remain unaffected by culture media composition up to a point.

The temporal regulation of primate and rodent embryonic cell specification and development *in vivo* is shown by explant and chimeric transplantation studies to be cell-autonomous (Rayon & Briscoe, 2021). This suggests stem cell derived *in vitro* models replicate the species-specific temporal pattern of development and can be used to ask questions of the regulation of cell differentiation differences between species. This has been confirmed to some extent in these results, as macaque organoids from different timing conditions consistently showed the presence of mature retinal cell markers prior to timepoints reported in human.

Rhesus macaque ROs were reported to show stage 3 characteristics such as maturing PRs (IS/OS development) from day 105-120 (Lopez et al. 2021) which supports the intrinsic earlier differentiation of macaque cells. This was also seen in the data in this chapter as mature PR markers were observed and upregulated in cells from day 90-120 (Fig. 5.11-13).

5.4.4   Improving macaque retinal differentiation by addition of RPE-CM

Based on previous studies, the addition of RPE-CM to retinal maturation media was hypothesised to improve PR generation, retinal tissue structure and induce the formation of RPE tissue in the macaque organoids (Dorgau et al., 2019; Sheedlo & Turner, 1996b; Yue et al., 2010).

This was seen to a limited effect in these experiments. By performing gene expression analysis at many points throughout differentiation it was possible to study the timeline of retinal gene expression profiles and to observe when upregulation of these genes was occurring. Protein analysis for a reduced number of genes was also performed at timepoints throughout differentiation in order to correlate this with gene expression and observe the localisation and structure of cells within the retinal tissue. By testing two cell lines in parallel it was possible to observe if RPE-CM induced effects were consistent in different cell lines.

No significant differences were seen in organoid morphology or early marker expression (*RAX*, *VSX2*, *CRX*) in either cell line. This is in accordance with results published by Dorgau et al. in human ESC differentiation experiments where the addition of de-cellularised RPE or RPE-CM made no difference to the early development of ROs (Dorgau et al., 2019).

Gene expression analysis of early PR markers showed no significant increase in the RPE-CM condition in either cell line and in S1 organoids *RCVRN* showed peak expression in the un-supplemented condition at day 90 (Fig. 5.18). Despite lower or equivalent gene expression levels the organisation of Crx+ and Rcvrn+ cells within the peripheral RO tissue lamina in S1 organoids was clearly improved in the RPE-CM supplemented condition at the mid-point of differentiation (day 50) (Fig. 5.18).

At later stages of differentiation, significant differences were observed in PR and mature Müller glia marker expression in both cell lines. The expression of cone opsin markers (OPN-S/OPM-ML/ARR3) was seen to be both correctly localised in S1 at day 90 and 120 and showed significantly higher levels of gene expression at the latest point of differentiation in both H5 and S1 samples (Fig. 5.19).

In H5 samples cone opsin markers were similarly correctly positioned within the outer retinal tissue and at day 90 *ARR3* was significantly higher in the RPE-CM supplemented condition. Additionally, of all Sasai-based conditions tested, Rhodopsin was only detected in RPE-CM supplemented H5 samples.

The low magnitude of gene expression of PR markers, *ARR3*, *NRL* and *RCVRN* is surprising given the detection of OPN-ML, OPN-S and Rcvrn+ cells by IF analysis in H5 and S1 organoids at the day 90 stage. It was hypothesised that gene expression of cone PR specific markers would show an up-regulation prior to their detection by IF analysis however expression of ARR3 was low in all conditions. This might reflect the low proportion of PR cells generated within the overall cell number of the pooled organoid sample.

Unlike in the H5 sample generated with RPE-CM media, no rod opsin gene or protein expression was detected in any S1 samples, despite other mature markers being present. This may be due to a lack of this cell line capacity to generate rod PR cells. As the efficiency of Rho+ cells in H5 line was extremely low (<5 cells observed) it may also be due to the sample size being too small.

The addition of RPE-CM also had a positive impact on the generation of Müller glia cells. Müller glia marker expression was detected by both protein and gene analysis in S1 organoids with gene expression increasing to be significantly higher in the RPE-CM supplemented condition at day 120 as well as CRALBP+ cells present in the PR lamina of the organoids. In H5 organoids *RLBP1* expression was significantly higher at day 90 in the RPE-CM supplemented condition, which was the latest timepoint samples. Proactive effects on retinal tissue structure and PR and Müller glia marker expression are similar between the two cell lines however some key differences are seen. In terms of timing, H5 showed earlier upregulation of mature markers (*ARR3* and *RLBP1*) compared to S1.

Interneuron gene expression patterns also varied between cell lines, with *AP2A* significantly higher in RPE-CM condition in H5 organoids between days 42-90 and the un-supplemented condition peaking earlier at day 31. In S1 organoids *AP2A* expression peaks in both conditions between day 15-70 and there is no significant differences in magnitude due to RPE-CM supplementation.

As PRCKA is a marker for bipolar cells, it is expected to be expressed from day 43 onwards (Fig. 5.1). In S1 organoids this expression pattern is seen with both conditions being upregulated after day 42. In contrast, H5 organoids show expression peaks at day 42 for the un-supplemented condition, and peak expression in the RPE-CM condition is seen at day 90. As the day 70 timepoint was not assessed in H5 samples this decreases the resolution of the timing expression profiles.

Testing another marker for horizontal cells such as Calbindin would be useful for determining any effect of RPE-CM on horizontal cell formation as *PROX1* expression suggests it is disrupted in the S1 organoids with RPE-CM supplementation. Furthermore, it would be interesting to assess the presence of amacrine cells by IF analysis as *AP2A* expression is high compared to mature retina, in both cell lines, at a timepoint correlating to normal retinal cytogenesis.

Addition of RPE-CM in S1 organoid differentiation led to an earlier upregulation of MITF expression which peaks between at day 42-90 at approximately 3-fold that of the mature macaque retina and significantly higher than the un-supplemented condition. This is in contrast to H5 organoids which showed peak *MITF* expression in the RPE-CM condition at day 90. In the rhesus macaque *in vivo*, which has a similar gestation period to the cynomolgus macaque, the majority of RPE cytogenesis was found to occur from GD 27 − 85 with cell generation decreasing from GD 85 (Rapaport et al.

1995) (Table 1.2). Therefore, the expression profile seen in the S1 organoids with RPE-CM addition is the most aligned with gestational macaque development.

Limitations of these results include that S1 organoid gene expression analysis was performed from two independent biological repeat experiments, whereas a single experimental repeat was performed for H5 organoids. Therefore, the S1 results are more robust than those observed in H5 samples. These include the effect of RPE-CM addition on interneuron marker expression which is increased in H5 samples for *PRCKA* and *AP2A*, but not in S1 organoids. However, it does further support those significant results which are seen in both cell lines. The results suggest that RPE-CM addition has a positive effect on cone PR and Müller glia cell genesis as *ARR3* and *RLBP1* expression is significantly increased in both S1 and H5 samples at late stages of differentiation.

Overall, the addition of RPE-CM showed promising improvements to macaque RO differentiation. Based on these results it would be interesting to further increase the addition of RPE-CM to a higher ratio and test RPE-CM addition at a later timepoint, to investigate any further improvement that could be made to PR cell generation and retinal structure in macaque iPSC derived organoids.

5.4.5   Use of the IGF-1 method to improve macaque RO differentiation

In summary, these molecular analyses show that the IGF1 culture method is able to improve rod and cone PR-marker expression at appropriate times of development in both S1 and H5 organoids, in comparison to the Sasai protocol. This effect is heightened in the pooled culture condition compared with the 96-wp culture. These results are supported by the morphological observations of organoid development throughout the later stages of differentiation where clear, bright NE structures are maintained up to day 120 in H5 IGF1 samples (Fig. 5.23c).

In comparison, the effect on retinal differentiation using the IGF1 methods from the S1 cell line was positive but less pronounced. Morphological data showed similar generation of S1 organoids with retinal features throughout differentiation between the IGF1 and Sasai conditions (Fig. 5.23b). Protein expression analysis showed organoids derived both conditions to express retinal proteins at key stages throughout the differentiation timeline and at the latest stage of differentiation, day 120 (Fig. 5.29a).

The gene expression analysis supports these results to some extent showing no significant differences between S1 Sasai and IGF1 samples in expression of early retinal markers prior to day 50, *RAX* and *VSX2* (Fig. 5.24b). While in H5 samples both *RAX* and *VSX2* are significantly increased prior to day 50, i.e at timepoints aligning with NE development (Fig. 5.25b). In the expression of the PR progenitor marker *CRX*, and *RCVRN*, significantly higher expression is seen in both S1 and H5 IGF1

283

samples at timepoints aligned with gestational development (Fig. 5.26b, 5.27b). Furthermore, significantly higher expression of mature PR markers *RCVRN*, and *ARR3* is seen in IGF1 samples in both cell lines throughout the later stages of differentiation from day 50-120 (Fig. 5.28b, 5.29b, 5.30b, 5.31b). However, in H5 samples only, rod marker expression, shown by *RHO* and *NRL,* is significantly increased by the IGF1 condition.

These results indicates that the IGF1 method has a beneficial effect on PR development and organisation in both the S1 and H5 cell lines. This is interesting as it corroborates the results from using the IGF1 method successfully to maintain both cone and rod PR expression in human RO culture (Zerti et al., 2021, Dorgau et al., 2019). In both cell lines the retinal lamina was seen to be cone-rich with few (H5) or no (S1) rod cells evident which is not representative of the ratio of cone to rod PRs found in the macaque retina *in vivo*.

Longer periods of culture, beyond day 120, may be required to detect further development and overall representation of these cell types. It is possible that the culture media requires further optimisation to support rod cell growth from certain macaque iPSC lines.

These results show improvements to morphology, retinal cell generation and structure within macaque organoids however also highlight the non-uniformity of cell line responses to a given set of culture conditions. Further investigation into the efficacy of the method using the third macaque iPSC line, H1, would be inform these results further for the robustness of application of the technique.

Chapter 6

Chapter 6 General Discussion and Future Perspectives

Retinal degenerative diseases are extremely prevalent around the globe, affecting approximately 1 in 4000 people (Verbakel et al., 2018). This number is also set to rise, especially in regions with ageing populations (G. A. Stevens et al., 2013; Wong et al., 2014).

Current available treatments for retinal disease are limited and, in most cases, alleviate symptoms or the pace of disease onset without restoring sight significantly. In the cases of rare or heterogenous inherited retinal disease (IRDs), specific gene therapy treatments take time to develop and be approved for clinical use. These factors point to the significant need for better treatments and a quicker process of drug development while maintaining safety.

PSCs are a renewable source of cells with the capacity to differentiate into any retinal cell type which provides an *in vitro* model system for retinal research. Generating retinal tissue as a 3D RO enhances the cellular model by better replicating the *in vivo* tissue structure, improving cell maturity and allowing a functional light-response (Hallam et al., 2018; Zhong et al., 2014a).

PSC-derived ROs are a powerful technology that can also provide a source of retinal cells for transplantation studies, allow the recapitulation of disease phenotypes as well as modelling the retinal response to novel therapeutics.
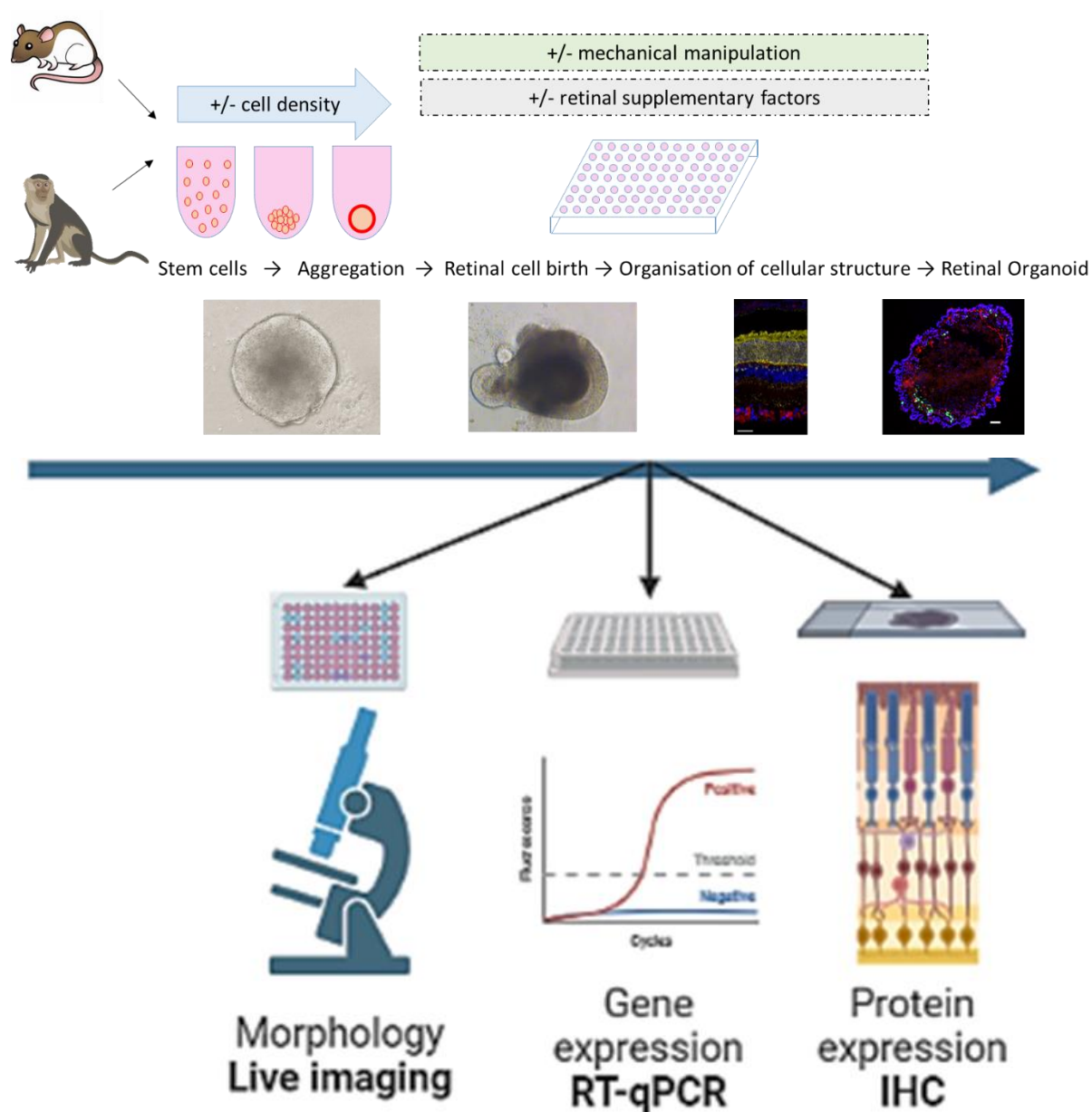
Figure 6.1. Graphical abstract summarising the project aims to differentiate rat and macaque stem cells in vitro over time and characterise the organoids throughout development using molecular and protein analyses.

This research project aimed to develop one application of PSCs for the treatment and alleviation of IRDs by generating *in vitro* animal RO models. These differentiation methods would be optimised to generate ROs which showed characteristic retinal morphology, gene and protein expression throughout development (Fig. 6.1). These models can be utilised for drug development and safety and toxicity studies and overall would reduce the use of live animals in pre-clinical research. In this

chapter I will summarise the conclusions, strengths and limitations of these results and discuss the further development of these methods.

6.1 Rat retinal organoid differentiations

The rat is the most commonly used rodent species in the drug development and safety assessment industry (Great Britain et al., 2020). More so than mouse, the rat is closer to modelling human development and disease due to its larger size (Aitman et al., 2008; Jacob & Kwitek, 2002). This has led to the widespread investigation of the rat in biomedical research and pre-clinical studies and many laboratory strains have been generated.

As there has been much optimisation of mouse and human RO differentiation methods, these provided the starting point for method development for rat (Decembrini et al., 2014; Eiraku & Sasai, 2012; Kruczek et al., 2017; Kuwahara et al., 2015; Völkner et al., 2016). Furthermore, previous research studies demonstrate a characterised profile of *in vitro* mammalian retinal development which can be used to assess method efficacy.

6.1.1   Conclusions from rat differentiation experiments

6.1.1.1 Testing serum-free embryoid body differentiation methods

As the biology and embryological development of rat and mouse occurs similarly, it was hypothesised that *in vivo* similarities, such as genetics, physiology, size and gestation length would translate to a similar responsiveness to *in vitro* cell differentiation methods.

In directed differentiation techniques, specific developmental pathways which are known to be instrumental in the patterning and specification of retinal tissue are targeted by applying exogenous growth factors and signalling molecules.

This starting point; applying the methods and principles of mouse and human RO differentiation protocols directly onto rat PSC lines, showed remarkable differences between the rat and mouse PSC lines at the earliest stages of differentiation. This was demonstrated by the application of the widely used mouse serum-free embryoid body with quick aggregation (SFEBq) method derived by Eiraku and Sasai (Eiraku & Sasai, 2012) and optimised by DiStefano et al. (DiStefano et al., 2017) to a riPSC (CM iPSC) and rESC (RRRC) line. In these experiments, the rat differentiation did not follow the expected pattern of retinal development with a lack of neuroepithelial (NE) tissue generation and a deterioration of organoid morphology. Beyond the initial stages (day 7 for riPSC) (day 1 for RRRC rESC) it became apparent that the ongoing retinal development in the rat PSC-derived organoids was not supported by the mouse differentiation methods.

This finding was in some ways supported by the literature as, to date, there have been no published data demonstrating the generation of 3D rat ROs, despite demand from the pharmaceutical industry to use them. The only publication to differentiate retinal cells from rat PSCs applies 3D culture up to day 10, after which cells are cultured as an adherent monolayer (Qu et al., 2015).

Despite the initial differences shown between rat and mouse PSC response, a combination of methods adapted from human, mouse and rat differentiation experiments, and novel method optimisations were tested and shown to improve rat retinal differentiation outcomes (Fig. 6.2).

Single cell Aggregation EB → NE formation → Retinal cell birth → Stratification of cell lamina
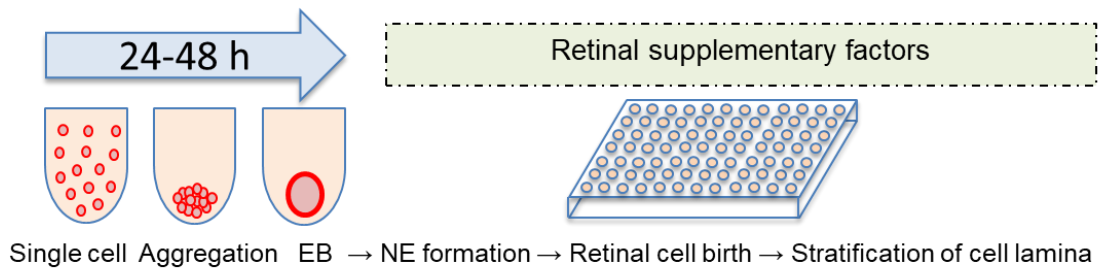
Figure 6.2. General schematic of the stages of the SFEBq method to generate stratified retinal tissue in a 96 well-plate. *Stem cells aggregate without serum within the first 48 hours after seeding in single cell suspension. An embryoid body (EB) is formed which is then exposed to retinal growth factors which prompt the development of retinal cells.*

The most successful results from the rESC differentiation experiments included the application of the rat-specific culture media with Knockout Serum Replacement (KSR) increased to 20%, Wnt pathway inhibitor IWR-1e and a lower Matrigel concentration of 1% (Qu et al., 2015). The rat EB and NE development was improved. This confirms and supports the published study and shows that species-specific optimisations are required for rat retinogenesis (Qu et al., 2015). The culture media composition of 20% KSR, Matrigel at 1% and IWR-1e also successfully generated self-organising optic cups from human ESC (Nakano et al., 2012). These similarities are promising as it confirms that retinal stimulating factors effective for human RO generation can be used for rat retinal differentiation.

The underlying reason why a higher KSR percentage is required in rat and human culture methods compared to mouse is not known. Using a higher KSR percentage may be effective for supporting rat and human PSC differentiation as it stimulates cell growth. KSR is a synthetic serum replacement protein source containing defined factors compositionally designed to enhance growth while replacing the commonly used foetal bovine serum (FBS). As such, it is nutrient rich and has been shown to increase cell proliferation in rat testicular cell culture (X. Zhang et al., 2017).

Further novel modifications were tested on rESC in chapter 4 (4.3.3.1). Following EB and NE formation, addition of the Sasai-based retinal maturation media allowed the maintenance of 3D rESC ROs beyond day 14. The retinal maturation media contains known retinal stimulants such as retinoic acid (RA), taurine, N2 supplement and the nutrient and growth factor-rich FBS (Eiraku & Sasai, 2012). The rESC-derived organoids showed some maintenance of retinal morphology and retinal gene and protein marker expression (Chx10, Rcvrn, RBPMS, CALB1, PROX1) at day 24 and 28. However, independent replicates of these experiments are required to confirm these effects.

6.1.1.2 Adherent plating strategy

Adherent plating has been used successfully to generate neural progenitor cells (NPCs) from rESC (Z. Wang et al., 2012). This study noted the difficulty of successfully differentiating rESC to EBs, noting low survival rates in the absence of LIF (Z. Wang et al., 2012). They overcame this by using feeder cell-conditioned media in the initial plating media and the hanging-drop plating method.

This approach was shown in chapter 4 (4.3.3.2) to generate NE cells with the capacity to differentiate into retinal cells (Fig. 6.2). As the neural retina is generated following the specification of the neural crest and NE (W. Heavner & Pevny, 2012), it was hypothesised that the early process of differentiation affecting the specification into NE cells would be common to both cortical and retinal progenitor cells.
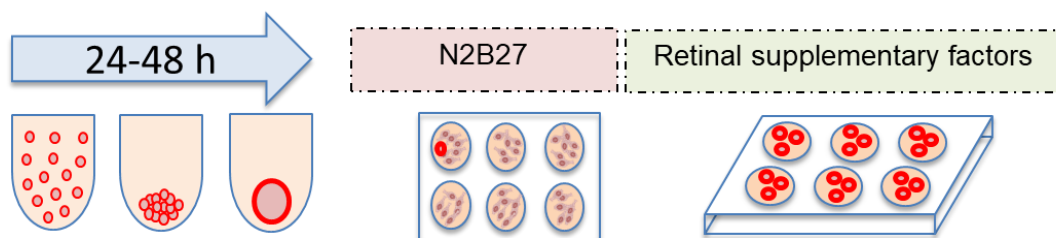
Figure 6.3. General schematic of the adherent retinal differentiation method to generate neuroepithelial (NE) stratified retinal tissue in 2D. NE cells are then transferred into low adhesion plates where they re-aggregate into a 3D structure.

This method robustly generated 3D EBs and branching bipolar cells expressing proliferative and neuronal markers, and, in some cases, neuron formation was observed. However, the addition of N2, RA, Taurine, IGF1 and SAG, was not found to be sufficient to induce retinal differentiation at later stages. Protein analysis for retinal markers showed a lack of mature PRs and cellular lamination and retinal gene expression levels were lower than previously discussed methods. Further independent replicates are required to confirm these results.

These experiments demonstrated the feasibility of using a validated rESC line for the early stages of NE differentiation and showed successful cellular re-aggregation from 2D to 3D. Demonstration of these properties is valuable for further method development and validates the Wang et al. study however, for the aim of retinal cell generation this approach was not successful. The timings for activation of retinal pathways may need optimisation to trigger an earlier commitment to a retinal fate. This could be supported by the earlier addition of retinal growth factors or signalling molecules which activate key eye-field transcription factors such as *LHX2* and *RAX*.

6.1.1.3 Retinal ganglion cell generation

What was consistently shown in multiple rat differentiation experiments, using both SFEBq and adherent methods, was the generation of retinal ganglion cells (RGCs) demonstrated by detection of RGC-specific markers; SNCG, Hu C/D and RBPMS. As all retinal neurons are specified from a population of retinal progenitor cells (RPCs) (Livesey & Cepko, 2001), this suggests that the initial process of RPC specification is occurring in the rESC-derived NE tissue. This also suggests that development of effective rat RO differentiation methods is dependent on optimisation of the mid and late stages when cell type specification, structural organisation and synaptogenesis is occurring.

Throughout this project two validated rat PSC lines (1 riPSC and 1 rESC) have shown some capacity for retinal differentiation and confirmed that signalling molecules physiologically active in the native retina can have the same proactive effect on *in vitro* rat retinal development.

6.1.2 Limitations of rat differentiation experiments

6.1.2.1 Perfusion and lack of non-neural tissue in the RO

Photoreceptor gene and protein expression was detected in rESC-derived organoids however, cell morphology and localisation within the organoid tissue did not show the organisation and morphology seen in mESC-derived ROs of a similar, or younger age.

A limitation of the RO model system in general is the lack of perfusion that is performed in the retina by vasculature. This non-neural system is important for the supply of oxygen and nutrients to the developing retinal tissue and highly metabolically active PRs (C.-H. Liu et al., 2017).

In vivo, the development of rat PRs occurs long-term over several postnatal weeks in concert with the development of the retinal vasculature and RPE (Rapaport et al., 2004; Stone et al., 1995). The RPE tissue plays an important role in the development of PRs, turnover of PR outer segments and supply of nutrients and oxygen to the NR (Bok, 1993; Redmond et al., 1998).

Some groups have begun to address this intrinsic limitation by expanding the human RO model to incorporate non-neural cells (Ghareeb et al., 2020). This includes the construction of a "retina-on-the-chip" integrated system using a multi-well chip with microfluidic channels to mimic the effects of perfusion and contact with the RPE (Achberger et al., 2019). This system showed significantly improved PR maturation and resistance to retinal toxicants and demonstrates one way the developmental proximity of RPE and vasculature can be replicated *in vitro*.

A lack of maturation was seen in the rESC-derived ROs beyond day 20. This could be improved by introducing factors in the culture environment to mimic the effects of angiogenesis, such as increased oxygen, improved nutrient circulation or VEGF. VEGF is secreted in the retina and can be used as a marker of retinal angiogenesis, and its expression is downregulated in the retina in response to hypoxia (Stone et al., 1995). Furthermore, the proactive effect of close RPE contact in other retinal studies (Gaur et al., 1992; N. Lin et al., 1996; Sheedlo & Turner, 1996b) suggests that RPE co-culture systems could be used to advance rat PR maturity *in vitro*.

6.1.2.2 Methodology

Full evaluation of the differentiation methods tested in this project was limited by a lack of independent biological repeats. Of significance is the possibility that, due to a lack of repeats, negative results may not be representative of the experimental outcomes.

Improved characterisation of the rat differentiation methods by investigating experimental repeats, testing other cell lines and further analysis of the most successful conditions would allow a more robust assessment of method efficacy.

This was begun in the final months of the project with a repeat of the rat differentiation methods for SFEBq method, growth factor supplementation and adherent plating. Analysis of retinal gene expression at timepoints earlier than day 28 would allow better assessment of the effect of retinal stimulant additions. Biological replicates of rat RO samples would allow improved statistical analysis and enable confident comparison of the optimised methods.

An additional challenge was the discovery that the rESC line used for the initial experimentation (XA ESC) was contaminated with mouse cells. As differences were subsequently shown between rESC and mESC response to retinal differentiation conditions, it is likely that the optimisation performed with the chimeric XA ESC line would have been targeted towards the requirements of mouse ESCs. Therefore, method optimisations discovered using these cells require re-testing on a validated rat PSC line.

While the subsequent method development performed with the validated rESC line (RRRC) is valuable to assess the species response, the aim of the project was to use iPSCs to generate the model system. Due to time constraints the optimised methods were not re-assessed on riPSC. As it has been shown that response to retinal differentiation methods and growth stimulants can be cell-line dependent, validation of any method requires testing in multiple cell lines (Chichagova et al., 2020; C. S. Cowan et al., 2020). This would provide valuable insight into the robustness of the methods and their suitability for use with riPSC.

6.1.2.3 Intrinsic differences in mouse and rat cell line responses

Further verification is required to fully determine whether the rESC response was different to the mESC differentiation due to species-specific differences or cell line differences however, there are interesting differences between the pluripotency and derivation of rat and mouse ESCs that have been reported and should be considered in future work.

Differences between rat and mouse at the early embryonic stages have been shown by transplantation of either mouse or rat epiblast to ectopic sites. While the mouse epiblast was found unable to regenerate parietal endoderm, the rat epiblast differentiated predominantly into parietal cells (P. Li et al., 2008; Nichols et al., 1998). When cultured *in vitro* rESC express high levels of trophoblast stem cell factors, have a higher level of genome instability and show lower efficiency of germ-line competence (Guo et al., 2009; Hong et al., 2011).

These early differences between the species were suggested as potential causes for the difficulty of derivation of genuine rESC lines using leukaemia inhibitory factor (LIF), which is sufficient to maintain pluripotency in mESC culture (P. Li et al., 2008). The successful generation of a genuine rESC line was first achieved in 2008, by the supplementation of 3 inhibitors (CHIR99021/PD184352/SU5402) which act on the GSK3, MEK and FGF pathways, respectively, and whose application blocks inductive differentiation cues (Buehr et al., 2008). The stabilisation of β-catenin effected by GSK3 inhibition was shown to be necessary to maintain rESC pluripotency while mESC can be maintained by a combination of GSK3 and MEK inhibition with LIF signalling (Meek et al., 2013). rESC, in contrast to mESC, exhibit higher levels of β-catenin signalling which influences their response to GSK3 inhibition and suggests why different culture conditions are required to maintain their pluripotency (Meek et al., 2013).

The epigenetic state of rESC has not yet been investigated, although it has in mouse (Barrera et al., 2008). Mapping the epigenetic state reveals the chromatin landscape and transcriptional activity and

can provide insight into the specification of cell-specific programs of expression. Potential differences between the epigenetic state of rESC and mESC genomes could be responsible for the variation between species to respond to the same environmental conditions in the differentiation protocols. Screening analysis and stem cell characterisation and profiling may therefore be useful to identify and validate appropriate rat PSC lines prior to differentiation.

6.1.3   Future work for rat differentiation experiments

6.1.3.1 Method optimisation

Further method development is required to generate mature 3D ROs from riPSCs. As differences between rESC and mESC differentiation have been suggested in this project, firstly this could be confirmed by analysing a replicate of the SFEBq method. Secondly, differentiation methods to stimulate rat retinogenesis may need to rely on novel methods, chemically directed signalling and genetic targeting approaches. This could be in the form of an edited cell line with inducible promoter for a key transcription factor such as *PAX6* or *RAX*, or the application of exogenous genetic constructs (Koo et al., 2012). As these techniques directly induce cell signalling pathways, they can be used to instigate cell specification, in comparison to methods relying on the self-organising principles of tissue development.

This project demonstrates some techniques which can improve the derivation of retinal cells from rat PSCs and provides an important starting point by highlighting targets for further method optimisation. These include 2D adherent amplification of RPCs, use of the "hanging-drop" method in suspension culture, and supplementation of retinal growth factors such as IGF1 and B27.

In rat development, key maturation events such as cell lamina separation, PR maturation and synaptogenesis occur postnatally and rat PRs are only observed to reach maturity at 2-3 post-natal weeks (Table 1.1) (Cruchten et al., 2017). This could suggest why full maturation of rat ROs *in vitro* is difficult to achieve. The RO culture environment might require further stimulation, for example from light sources or non-retinal cells to replicate the conditions required for retinal maturation. Early mouse retinal differentiation protocols highlighted the difficulty of extending viable culture length. This was partially overcome by method optimisations increasing oxygenation by using bioreactors, changin incubator conditions or dissecting organoids at late stages of differentiation (Table 1.3; Ito et al. 2017, Distefano et al. 2017, Ueda et al. 2018). These methods were not tested on rat PSC differentiations due to time limitations.

RPE-CM addition has been shown to aid PR maturation and retinal lamina organisation in the native rat retina and retinal explant cultures (N. Lin et al., 1996; Sheedlo & Turner, 1996b). It was hypothesised to improve rESC retinal differentiation in this project however, the primary rat RPE tissue which was obtained for this project was unusable due to infections in the culture. The addition of RPE-CM was also shown in macaque retinal differentiation experiments in this project to have a supportive effect on RO structure and improve the maintenance of mature retinal cells such as Müller glia and PRs. Due to these positive results, it would still be worth assessing the effect of RPE-CM or co-culture to improve rat RO differentiation.

The results from this project suggest that method optimisation in the mid and late stages of differentiation is required to improve rat RO development and extend viable culture times. This could be achieved by testing culture conditions shown to improve mouse differentiations such as bioreactors to improve nutrient circulation, or hyperoxia to better support the high metabolic demands of the developing retinal tissue.

In addition to improving the composition of retinal culture media the timing of signalling molecules addition is critical for affecting retinal method development. This has been shown in the timed application of T3 from day 37 in human RO differentiation when it caused a significant change to retinal structure and maintenance of lamination, however application from day 45 showed no significant difference (Eldred et al., 2018).

Finally, investigating different timings of media supplementation is important for further method development. The media additions tested in this project at a single timepoint, such as SAG and IGF1, which did not increase retinal gene expression may not represent the true effect as the optimal time window may have been missed.

6.1.3.2 Reproducibility and cell line screening

The use of validated iPSC lines as the source for ROs is important for the drug development industry. Widespread adoption of the model will depend on the availability of robust cell lines and iPSCs are largely more ethical, obtainable and subject to less intensive regulation than ESCs and primary tissue.

iPSC lines exhibit high differentiation variability due to genetic, epigenetic, reprogramming, culture conditions and other factors (Kilpinen et al., 2017; Kyttälä et al., 2016). Therefore, the most effective starting point might be the generation of a rat cell line library from independent tissue sources. Consequently, cell line characterisation and pre-screening for markers known to affect differentiation capacity, such as epigenetic markers, protein and gene expression could be

performed (Kilpinen et al., 2017). This profiling would be extremely informative and increase the chances for successful differentiation into the desired tissue type, by eliminating cell lines not suited for retinal specification.

This effect is clearly demonstrated in human RO differentiation where of 23 iPSC lines, only 17% were able to generate mature ROs (C. S. Cowan et al., 2020). There are a limited number of derived rat iPSC lines published by research institutions (Coppiello et al., 2017a; Liao et al., 2009; Merkl et al., 2013). Although these have been shown to have the capacity to generate teratomas and differentiate to hepatocytes, the generation and characterisation of further riPSC lines would increase the chances of retinal differentiation success and potentially identify markers which can improve the understanding of stem cell pluripotency and differentiation. In addition, discontinuation of unsuitable cell lines should increase the reproducibility of retinal differentiation experiments.

6.1.3.3 Potential for a rat RGC model
The generation of RGCs in the rat ROs derived with several methods was shown by the presence of RGC markers at appropriate times in development. The production of functional RGCs *in vitro*, even separated from the retina, may prove useful for pre-clinical studies. RGCs do not regenerate in the retina after injury and glaucoma is a leading cause of blindness worldwide resulting in damage and loss of RGCs (Soto et al., 2008). An RGC-rich organoid model would provide a platform on which to test compounds for the treatment of glaucoma, or as a source of RGCs for cell transplantation studies.

The RGC identity in the ROs could be further characterised using electrophysiology to determine if these cells are functional, responsive and capable of forming synaptic connections with other retinal cells. This has been demonstrated previously with human ROs (Hallam et al. 2017).

6.1.3.4 Potential for a rat RO model
As this project has demonstrated, there are significant challenges in generating new methods for differentiating complex retinal tissue from rat PSC. Additionally, methods must be tested on multiple cell lines to ensure their robustness and optimised accordingly. For the purposes of drug development, it may be sufficient to instead validate toxicity response in human ROs which have already been well characterised.

This project has presented results which suggest developmental differences between rat and mouse PSCs *in vitro*. The development of a rat RO model would be of interest in studying the developmental differences between mammalian species

6.1.4   Summary of rat differentiation outcomes

While rESC-derived organoids with a laminated retinal structure were not generated, the methods used to generate EBs, early-born retinal cells (RPCs and RGCs), and organoids with a retinal morphology have been developed and optimised in a rESC line.

The results from experimentation on another chimeric rat-mouse line confirmed the stimulatory action on retinal growth suggested by mouse and human differentiation research, such as the beneficial effects of supplementing B27, IGF1 and the use of pooled culture.

In light of the strengths and limitations of the experimental work, the rat differentiation outcomes suggest that rat PSCs have the capacity to be differentiated into retinal cells, however the cell culture conditions require further optimisation to generate a laminated structure and the full cellular diversity of the retina.

Differentiation of rat PSCs into 3D ROs has not yet been evidenced in published literature. Therefore, the data generated in this project provides a resource which can be used to inform future method development and will reduce the time and resources required to develop a robust rat-specific protocol.

From the results described in this report the generation of rat ROs for pre-clinical testing would not be straightforward. Therefore, the generation of more simple retinal models, or the use of mouse or human ROs should be sufficient to validate the RO model for pre-clinical testing.

6.1 Primate differentiation experiments

The cynomolgus macaque is currently the "gold standard" animal model for *in vivo* pre-clinical trials especially for gene therapy studies. The macaque is a valuable model for retinal cell transplantation therapy studies due to the trichromacy and similar ratio of PR subtypes shared by these diurnal primates and humans (Wikler & Rakić, 1990).

6.2.1 Conclusions from macaque differentiation experiments

To date, one publication has shown the successful translation of a human retinal differentiation method to generate a non-human primate (NHP) RO model from rhesus macaque iPSCs. Importantly, this shows the common response of macaque stem cells to human culture conditions, and the ability of macaque PSCs to differentiate and mature *in vitro* in response to known retinal cues.

The initial experiments in this project exposed cynomolgus macaque iPSCs to a human RO differentiation protocol, based on the self-organising method developed by Sasai et al. (Kuwahara et al., 2015; Nakano et al., 2012; Sasai et al., 2012). This approach successfully generated EBs, NR tissue and the expression of retinal cell markers and confirmed that conditions used to derive human ROs are capable of stimulating cynomolgus macaque iPSC retinal differentiation *in vitro*.

To improve the efficiency of the method and the maturity and diversity of the derived retinal cells, modifications were made to the Kuwahara et al. method including the timing and composition of media additions.

6.2.1.1 The effect of adjusting the timing of differentiation protocols

The macaque iPSC derived ROs showed an earlier staging of development than that expected for human retinal development, with advanced NE structures appearing by day 15. This is in line with the protracted development of the macaque eye in the embryo compared with human (Kiely et al., 1987; Vail et al., 1991). The advancement of culture media additions in the modified method (NHP-timing) was hypothesised to support the earlier generation of NE tissue however, this showed a limited effect on retinal gene expression. Key retinal markers *VSX2* and *RCVRN* showed earlier upregulation in one cell line (S1) with NHP-timing. The NHP-adjusted timing method did improve the maintenance of retinal morphology and phase-bright NE tissue, and the structural organisation of OPN-M and OPN-S expressing cells.

The results shown in the macaque-adjusted timing chapter are also supported by the study investigating rhesus macaque RO differentiation (Lopez, Kim, et al., 2021). The rhesus and cynomolgus macaque species have very similar gestation periods both with average lengths of 166

days (Silk et al., 1993). Similarly to humans, rhesus macaque gestation is grouped into three trimesters, with each lasting 55 days (1st trimester: day 0-55, 2nd trimester: day 55- 110, 3rd trimester: day 110 – 165) (Barry et al., 2006). The successful generation of rhesus macaque ROs expressing mature markers by day 120 is in accordance with the timeline seen in the cynomolgus iPSC differentiations and, somewhat surprisingly, this was not affected by moving the addition of culture media forward.

However, accelerating the timeline of differentiation improved RO morphology and the efficiency of differentiation at day 120 was between 30 – 40%. This is greater than resulting with the Sasai method with human timing and that of the two rhesus macaque cell lines derived with another method using human timing (Lopez, Kim, et al., 2021). While these results suggest that accelerating the timeline of differentiation methods does support the process of *in vitro* macaque retinogenesis and maintenance of retinal structures, further data is required to be conclusive.

The comparison of human to macaque RO development suggests that the earlier macaque retinogenesis is intrinsically regulated as the timeline and staging of marker expression and RO morphological development occurs at a similar pace to *in vivo* development (Vail et al., 1991) and an accelerated pace compared with human ROs (Capowski et al., 2018).

Similarly, Otani et al. showed that macaque ESCs differentiated *in vitro* towards cortical neurons exhibit more precocious development, in comparison with chimpanzee and gorilla PSCs; NHP species with longer gestation periods (Otani et al., 2016). Thus, earlier intrinsic regulation of key neuronal developmental processes has been demonstrated *in vitro*, which aligns with what is known about *in vivo* development.

The Lancaster group, also investigating *in vitro* cortical cytogenesis in primates, identified a key transcription factor, *ZEB2*, regulating the transition between symmetrical and neurogenic proliferation in NE cells (Benito-Kwiecinski et al., 2021). *ZEB2* was shown to be expressed later in human NE cells than in NHP species and was a driver of the change in cell proliferation. This study demonstrates a key determinant of developmental chronology in the primate CNS which is responsible for key evolutionary differences between humans and NHP species in brain size.

Interestingly, in both the cortical differentiation studies (Benito-Kwiecinski et al., 2021; Otani et al., 2016), and the rhesus macaque retinal differentiation study (Lopez, Kim, et al., 2021), the timing of the culture protocol was not altered between human and NHP species. Their results suggest that intrinsic mechanisms mediate the earlier timing of development more so than external environmental conditions.

Similarly to the cortex, retinal NE cells form a columnar lamina and proliferate symmetrically to generate RPCs, which subsequently differentiate into mature retinal neurons. Therefore, similar mechanisms may be involved in this process as shown in the cortical cells *in vitro*. Cortical organoid studies validate the use of *in vitro* organoids for comparative studies investigating the mechanism underpinning primate development and cell specification processes. Similarly, the macaque ROs generated in this project could be used to elucidate mechanisms and factors responsible for the chronology of retinal development and cell maturation in primates.

6.2.1.2 The addition of RPE conditioned media

The addition of RPE conditioned media (-CM) to the Sasai-based retinal maturation media was found to significantly improve retinal differentiation outcomes with two macaque iPSC lines. These data showed specific improvements to PR and Müller glia marker expression which is predicted by the literature (Dorgau et al., 2019; Pinzón-Duarte et al., 2000). The structure of the RO retinal lamina was also seen to be improved with the addition of RPE-CM from the mid-stage of differentiation, and the expression of early retinal markers was not significantly affected. This data supports the results from Dorgau et al. which showed a beneficial effect on rod PR generation, and no effect on early retinal markers (Dorgau et al., 2019). These results show that the beneficial effect of RPE-CM on PR development is common to both human and macaque retinal differentiation and is, to some extent, independent of the base culture media as the Dorgau et al. paper trialled the RPE-CM with an IGF1-based method.

The addition of RPE-CM at a ratio of 1:3 and from the timepoint of day 15 – 90 was the only variation analysed in this project. As RPE-CM is a limited resource, reducing the quantity required while maintaining positive retinal differentiation outcomes would be valuable. The expression of early retinal genes was not significantly affected in the RPE-CM conditions, so it would be informative to test RPE-CM addition at later timepoints to optimise its application.

6.2.1.3 The use of IGF1

The IGF1 method had been optimised for human iPSC and ESC differentiation to ROs where it showed a beneficial effect on increasing mature PR marker expression and maintaining structured retinal lamina at mature timepoints (Dorgau et al., 2019).

It was hypothesised that the method would similarly improve the macaque RO differentiation and support the maturation of PR cells. The application of the IGF1 method resulted in improved RO structure and PR gene expression (*RCVRN, ARR3, CRX*), compared to the Sasai method, in both macaque S1 and H5 lines. Additionally, it significantly increased Müller glia (*RLBP1*) and rod (*RHO*)

expression in H5-derived organoids and resulted in H5 organoids with phase-bright retinal morphology and a cone-rich retinal lamina at late stages (day 120) of differentiation.

Testing two macaque iPSC lines in parallel, showed some effects that were common to both lines, however also highlighted the cell line-specific effects, for example the presence of rod PR markers in H5 line which were not seen in the S1 samples.

One important finding from these experiments was the ability to generate cone PRs from macaque iPSCs readily, in a timeline approximating that of the macaque retina *in vivo*. The native macaque retina, and that of human, is rod-dominated and shares similar distributions and densities of cone PRs throughout the retina (Curcio et al., 1987). In the macaque retina, the ratio of S-cones was found to be ~10% to the 90% of M/L-cones (Wikler & Rakić, 1990). This distribution is not represented in the macaque RO tissue, where only cone PR expression occurs in clusters of OPN-S+ and OPN-ML+ cells.

Cellular specification in the retina occurs in a spatially determined manner with the peripheral retina lagging the specification and maturation of retinal cell types in the central regions(Hoshino et al., 2017; Vail et al., 1991). The generation of cones seen in the macaque ROs and lack of rod PRs could therefore, be suggestive of a central retinal phenotype which is typically cone dominated at early stages of development. Further assessment at timepoints beyond day 120 would be informative to investigate whether this phenotype has the capacity to mature further and develop rod PRs.

Additionally, the thyroid hormone signalling pathway has been shown to be instrumental in affecting the patterning and specification of cone subtypes in the primate retina (McNerney & Johnston, 2021). Eldred et al. showed that early addition of T3 from day 13 in the differentiation of human ROs prompted a transition and generation of M/L cones at the cost of S-cones (Eldred et al., 2018). The IGF1 method with NHP-timing tested with macaque iPSCs applied T3 in the differentiation media from day 18 onwards (Fig. 6.4). The number of S-cones was not quantified however, by visual inspection they were over-represented compared to the native retina, where around ~10% of cells are expected to be S-cones. This could be due to T3 being applied too late in differentiation.

Factors that have been shown to control the cone-rod PR specification have been discovered in knock-out mouse models. Notch1 is highly conserved in vertebrates and is present in RPCs (Cepko, 2015; Simionato et al., 2007). It has been implicated to inhibit PR differentiation, and its knock-out in mice resulted in an increase of cone PRs and loss of rods (Jadhav et al., 2006). This indicates its role in determining PR cell fate.

Accurate function and careful control of these genetic factors will be required in ROs to result in the correct pattern of cell specification in macaque ROs. Mediation in the timing of the application of T3 and Notch1 could be investigated in the differentiation conditions in order to generate an accurate representation of retinal cell diversity.

Strengths of the macaque experimentation was that the various retinal differentiation methods were evaluated independently in two or three cell lines. As cell line variability can affect method efficacy, it is essential to demonstrate robust results in more than one cell line.

The heterogeneity of RO differentiation, even within the same cell line, is well-known so in this project this was considered by assessing gene and protein analysis from two cell lines. The optimisations in the RPE-CM and IGF1 methods have been confirmed in two macaque iPSC lines suggesting a robust effect.

6.2.2   Limitations of macaque differentiation experiments

The lack of rod PRs generated in the macaque ROs produces a retinal structure which is not representative of the native primate retina, which usually consists of at least 90% rods (Szél et al., 1996). This may be due to the early application of RA in the maturation media, which is applied, in the Sasai methods with NHP-adjusted timing from day 15, and from day 18 in the IGF1 method with NHP timing.

In human RO differentiation experiments it was shown that early application of RA (from week 7) led to lower expression of rhodopsin in comparison to cultures supplemented with RA from week 10 (Zhong et al., 2014a). Even by adjusting the timing to NHP timelines, addition at week 10 in the human protocol corresponds to day 42 in an NHP-adjusted timing protocol.

In other studies investigating the differentiation of macaque retinal cells in 2D, RA/T was applied from day 90 to generate rhodopsin+/recoverin+ cells and in the generation of rhesus macaque 3D ROs, RA/T was applied from day 30-100 and rod marker expression and basic segment formation was observed from day 125 (Lopez, Kim, et al., 2021; Osakada et al., 2008).

These results suggest that rod PRs can be generated from macaque PSCs *in vitro* and that altering the timing of RA addition may be a way to affect this. Optimisation of this to would generate a more representative phenotype of the retina. However, the consistent generation of a cone-rich RO model would also be useful for modelling the cone-rich fovea.

Intrinsic cell line variation exists in retinal differentiation responsiveness. As a result RO differentiation efficiencies from different cell lines can vary with some lines unable to produce ROs and some generating different proportions of PRs when exposed to the same conditions (Chichagova et al., 2020; C. S. Cowan et al., 2020). This raises the interesting question of how many cell lines is it necessary to use in order to conclusively show an effect.

A third cell line (H1) was also exposed to macaque-timing adjusted differentiation methods and therefore analysis of these samples, which could not take place due to a lack of time, would provide informative data which could further confirm the method effects.

Representative cell markers of each retinal class (Retinal ganglion, amacrine, horizontal, bipolar, PR and MG) were detected in the most optimal macaque ROs, however, synaptogenesis and the full cellular diversity of retinal class sub-types was not assessed. Further characterisation of the retinal lamina structure and composition could be performed in order to assess the extent of the maturity and to determine where the differentiation methods should be further optimised. Other studies have used single cell transcriptomic approaches to assess the cellular diversity and timeline of retinal development which has been extremely informative for human RO staging and optimisation (Collin, Queen, et al., 2019; C. S. Cowan et al., 2020; Mellough, Collin, et al., 2019).

Similarly, this approach could be performed for macaque ROs to investigate the efficacy of *in vitro* retinal development.

6.2.3   Future work for macaque differentiation

The use of conditioned media to improve RO structure and cell expression is informative and shows one way to optimise RO culture. The main disadvantage is that, in this project RPE-CM was obtained from an explant tissue and its availability is dependent on a limited source of primary tissue.

An alternative would be to generate macaque RPE from iPSCs, to provide a sustainable source of RPE-CM without being dependent on primary tissue. This could also give rise to the creation of a co-culture system of iPSC-derived retina and RPE which may improve the maturity of the retinal lamina. This has been attempted with human iPSC model systems with some success. Incorporating non-retinal cells such as microglia, RPE and vasculature has already been explored in some human RO systems and shows the potential to improve the accuracy and function of the model (Achberger et al., 2019; Ghareeb et al., 2020).

The composition of RPE-CM used in these experiments was not defined and therefore key molecules which were beneficial in the maturation media are not known. It would accelerate the process of method development to identify the effective components which promote retinal development. These could then be acquired from synthetic sources and applied in the culture media.

To achieve this, molecular characterisation of the RPE-CM components via mass-spectrometry techniques could be performed. Following this, rigorous design-of-experiment studies could be performed which assess the components for their effect and optimal concentration for RO culture.

Another study investigated the addition of extra-cellular matrix proteins, laminins and growth factors secreted by the RPE on explant rat retinal culture. They showed that the effect of growth factors (TGF-β, PDGF, NGF of bFGF) in isolation, was less powerful than the addition of pure RPE-CM (Sheedlo & Turner, 1996b). This suggests there are undefined factors secreted by the RPE which are influential or that the combinatorial effect stimulates retinal growth. As suggested by other studies, adding RPE, or RPE-derived materials, to RO culture would be impactful on PR development and retinal maturation. These alternatives could be further investigated using macaque ROs.

To take this model to the next stage, it would be key to demonstrate the maturity of the retina by performing functional analysis such as recording electrical response to a light stimulus. This is a technique which has been used to characterise the maturity and function of human ROs (Hallam et al., 2018; Zhong et al., 2014a). This proves conclusively that the structure developed in the ROs is suitable as it allows the process of light transduction through the retinal synaptic connections to occur.

Finally, to show that the macaque ROs are suitable for use in pre-clinical studies, a toxicological evaluation to characterise the response of the macaque ROs to known retinal toxicants is required. This has recently been performed on iPSC-derived human ROs and successfully shows that retinal toxicants have the same physiological effect on RO tissue as on the native retina (Dorgau et al., 2022).

The macaque ROs can be used to generate a response to toxicants that can be directly compared to data collected from pre-clinical studies. In this way they can be used to validate the ROs as a model system and replace the use of live macaques in some pre-clinical studies.

6.2.4 Summary of macaque differentiation outcomes

The generation of cynomolgus macaque (*Macaca fascicularis*) ROs has not previously been published. This project therefore represents the first demonstration of cynomolgus macaque iPSC differentiation to 3D ROs and confirms that known retinal methods and growth factors can be used to stimulate *in vitro* retinogenesis from macaque iPSCs with modified methods and timing.

This has been shown to be effective in 3D suspension culture in a multi well plate format, which is amenable for drug development studies.

Further work should expand the characterisation of the model to determine the level of structural maturity, synaptogenesis and functionality in the macaque ROs. This will help evaluate the model and identify where the differentiation methods can be improved.

For the use of macaque ROs in drug development and safety assessment pre-clinical studies, further work is required to validate this novel platform. Given the challenges required to robustly validate and qualify the model it would be more straightforward, although still challenging, to instead work to validate the human RO model. This data would be most informative as they are to be used prior to clinical studies.

The development of NHP retinal organoids is of interest for studying the developmental differences between species, as has been shown by comparative primate studies with cortical organoids. NHP ROs provide a tool to study the mechanisms governing the timing of cell fate transition in the retina which would be of interest for modelling disease and development.

Appendices

Appendix A: Rat differentiation methods

C1
Sasai (PMID: 22179593)

D0 (100 ul per well)	
GMEM	
NEAA	0.1 mM
Pyruvate	1 mM
2-ME	0.1 M
KSR	1.50%
Pen/Strep	1.00%
D1 (20 ul per well)	
half change media	
Matrigel	2% v/v
D3/5	
half change media	
D7	
DMEM/F12, Glutamax	
N2	1%
Pen/Strep	1%
D9	
half change media	
D10	
DMEM/F12, Glutamax	
N2	1%
FCS	10%
Pen/Strep	1%
Taurine	1 mM
RA	0.5 uM
D14+	
Change medium every 3 days (-RA)	

C2/3
Takahashi (PMID: 29274337)

D0 (100 ul per well)	
GMEM	
NEAA	0.1 mM
Pyruvate	1 mM
2-ME	0.1 M
KSR	1.50%
Pen/Strep	1.00%
AGN193109	0.1 uM
D1 (20 ul per well)	
half change media	
Matrigel	2% v/v
D3/5/7	
half change media	
D9	
DMEM/F12, Glutamax	
N2	1%
Pen/Strep	1%
FBS	1%
D14	
DMEM/F12, Glutamax	
N2	1%
Pen/Strep	1%
FBS	1%
RA/9cisRA	0.5 uM
Taurine	1 mM
D17/20	
Change medium	
D23+	
DMEM/F12, Glutamax	

N2	1%
FBS	1%
Pen/Strep	1%

C4

Kuwahara (PMID: 28361307)

D0 (100 ul per well)	
GMEM	
NEAA	0.1 mM
Pyruvate	1 mM
2-ME	0.1 M
KSR	1.50%
Pen/Strep	1.00%
D1	
half change media	
D2	
BMP4	2.25 nM
D4 and D6	
half change media (no BMP4)	
D7	
DMEM/F12, Glutamax	
N2	1%
Pen/Strep	1%
D9	
half change media	
D10	
DMEM/F12, Glutamax	
N2	1%
FBS	10%
Pen/Strep	1%
Taurine	1 mM
RA	0.5 uM

C5

Ali (PMID: 28552606)

D0 (100 ul per well)	
GMEM	
NEAA	0.1mM
Sodium pyruvate	1mM
2-Me	0.1 M
KSR	1.50%
Pen/Strep	1.00%
D1 (20 ul per well)	
half change media	
Matrigel	2%
D3/5/7	
half change media	
D9	
DMEM/F12 Glutamax	
N2	1%
Pen/Strep	1%
D14+	
DMEM/F12 Glutamax	
N2	1%
Pen/Strep	1%
Taurine	1mM
RA	0.5 uM

D14+	
Change medium every 3 days (-RA)	

Appendix B: Macaque differentiation methods

C2.1

KUWHARA (PMID: 25695148)

D0	
IMDM	43.5%
Hams F12	43.5%
Glutamax	1.0%
Chemically defined lipid conc	1%
1-thioglycerol	450 uM
Pen/Strep	1%
KSR	10%
add ROCKi (Y-27632)	20 uM
D2/D4	
50% media add/change	
D6	
BMP4	1.5nM (55ng/mL)
D9/D12/D15	
50% media change	
D18-24	**IR media**
CHIR99021	3uM

C2.2

KUWAHARA + RPE-CM

D0	
IMDM	43.5%
Hams F12	43.5%
Glutamax	1.0%
Chemically defined lipid conc	1%
1-thioglycerol	450 uM
Pen/Strep	1%
KSR	10%
add ROCKi (Y-27632)	20 uM
D2/D4	
50% media add/change	
D6	
BMP4	1.5nM (55ng/mL)
D9/D12/D15	
50% media change	
D18-24	**IR media**
CHIR99021	3uM

SU5402	5uM
DMEM/F12, Glutamax	
N2	1%
FBS	10%
Pen/Strep	1%
D24+	
DMEM/F12, Glutamax	
N2	1%
Pen/Strep	1%
FBS	10%
Taurine	0.1mM
RA	0.5uM
feed 3x weekly	

SU5402	5uM
DMEM/F12, Glutamax	
N2	1%
FBS	10%
Pen/Strep	1%
D24+	
DMEM/F12, Glutamax	
add RPE-CM	1 in 3 with media
N2	1%
FBS	10%
Pen/Strep	1%
Taurine	0.1mM
RA	0.5uM
feed 3x weekly	

C2.3

KUWHARA (PMID: 25695148)

NHP timing

D0	
IMDM	43.5%
Hams F12	43.5%
Glutamax	1.0%
Chemically defined lipid conc	1%
1-thioglycerol	450 uM
Pen/Strep	1%
KSR	10%
add ROCKi (Y-27632)	20 uM

C2.4

KUWAHARA (NHP) + RPE-CM

D0	
IMDM	43.5%
Hams F12	43.5%
Glutamax	1.0%
Chemically defined lipid conc	1%
1-thioglycerol	450 uM
Pen/Strep	1%
KSR	10%
add ROCKi (Y-27632)	20 uM

D2/D3	
50% media add/change	
D4	
BMP4	1.5nM (55ng/mL)
D6/D9	
50% media change	
D11-15	**IR media**
CHIR99021	3uM
SU5402	5uM
DMEM/F12, Glutamax	
N2	1%
FBS	10%
Pen/Strep	1%
D15+	
DMEM/F12, Glutamax	
N2	1%
Pen/Strep	1%
FBS	10%
Taurine	0.1mM
RA	0.5uM
feed 3x weekly	

D2/D3	
50% media add/change	
D4	
BMP4	1.5nM (55ng/mL)
D6/D19	
50% media change	
D11-15	**IR media**
CHIR99021	3uM
SU5402	5uM
DMEM/F12, Glutamax	
N2	1%
FBS	10%
Pen/Strep	1%
D15+	
DMEM/F12, Glutamax	
add RPE-CM	1 in 3 with media
N2	1%
FBS	10%
Pen/Strep	1%
Taurine	0.1mM
RA	0.5uM
feed 3x weekly	

C3

IGF1 – NHP timing

D0	
DMEM/F12, Glutamax	
NEAA	1%
Pen/Strep	1%
B27	2%
KSR	20%
IGF-1	5ng/ml
D2/D4/D6/D9	
50% media add/change	
D11	
DMEM/F12, Glutamax	
NEAA	1%
Pen/Strep	1%
B27	2%
FBS	10%
IGF-1	5ng/ml
RA	0.5uM
Taurine	0.1mM
D13/D15	
50% media add/change	
D18+	
DMEM/F12, Glutamax	
NEAA	1%
Pen/Strep	1%
Lipids	1x
B27	2%
FBS	10%

N2	1%
IGF-1	10ng/ml
RA	0.5uM
Taurine	0.1mM
T3	40 ng/mL
feed 3x weekly	

Appendix C: Mouse differentiation methods

Sasai SFEBq   PMID: 22179593

D0 (100 ul per well)	
GMEM	
NEAA	0.1 mM
Pyruvate	1 mM
2-ME	0.1 mM
KSR	1.50%
Pen/Strep	1.00%
Y-27632	*5 uM*
D1 (20 ul per well)	
half change media	
Matrigel	2%
D3 and D5 (50 uL per well)	
half change media	
D7	
DMEM/F12, Glutamax	

DiStefano PMID: 29233554

D0 (100 ul per well)	
GMEM	
NEAA	0.1 mM/1x
Pyruvate	1 mM/1x
2-ME	0.1 mM/1x
KSR	1.50%
Pen/Strep	1.00%
Y-27632	*5 uM*
D1 (20 ul per well)	
half change media	
Matrigel	2%
D3 and D5 (50 uL per well)	
half change media	
D7	
DMEM/F12, Glutamax	

N2	1%
Pen/Strep	1%
D9	
half change media	
D10	
DMEM/F12, Glutamax	
N2	1%
FCS	10%
Pen/Strep	1%
Taurine	1 mM
RA	0.5 uM
D14+	
Change medium every 3 days (-RA)	

N2	1%
Pen/Strep	1%
2-ME	1x
D9	
half change media	
D10	
DMEM/F12, Glutamax	
N2	1%
2-ME	1x
Pen/Strep	1%
Taurine	1 mM
9-cis-retinal	0.5 uM
IGF-1	100 ng/mL
D18	
DMEM/F12, Glutamax	
N2	1%
2-ME	1x
Pen/Strep	1%
Taurine	1 mM
9-cis-retinal	0.5 uM
IGF-1	100 ng/mL
B27-VitA	1x
NEAA	1x
FBS	2%
D26+	
DMEM/F12, Glutamax	
N2	1%
2-ME	1x

Pen/Strep	1%
Taurine	1 mM
9-cis-retinal	0.5 uM
IGF-1	100 ng/mL
B27-VitA	1x
NEAA	1x
FBS	2%

References

Achberger, K., Probst, C., Haderspeck, J., Bolz, S., Rogal, J., Chuchuy, J., Nikolova, M., Cora, V., Antkowiak, L., Haq, W., Shen, N., Schenke-Layland, K., Ueffing, M., Liebau, S., & Loskill, P. (2019). Merging organoid and organ-on-a-chip technology to generate complex multi-layer tissue models in a human retina-on-a-chip platform. *ELife*, *8*, e46188. https://doi.org/10.7554/eLife.46188

Acland, G. M., Aguirre, G. D., Ray, J., Zhang, Q., Aleman, T. S., Cideciyan, A. V., Pearce-Kelling, S. E., Anand, V., Zeng, Y., Maguire, A. M., Jacobson, S. G., Hauswirth, W. W., & Bennett, J. (2001). Gene therapy restores vision in a canine model of childhood blindness. *Nature Genetics*, *28*(1), 92–95. https://doi.org/10.1038/ng0501-92

Aitman, T. J., Critser, J. K., Cuppen, E., Dominiczak, A., Fernandez-Suarez, X. M., Flint, J., Gauguier, D., Geurts, A. M., Gould, M., Harris, P. C., Holmdahl, R., Hubner, N., Izsvák, Z., Jacob, H. J., Kuramoto, T., Kwitek, A. E., Marrone, A., Mashimo, T., Moreno, C., … Worley, K. (2008). Progress and prospects in rat genetics: A community view. *Nature Genetics*, *40*(5), 516–522. https://doi.org/10.1038/ng.147

Akhtar, T., Xie, H., Khan, M. I., Zhao, H., Bao, J., Zhang, M., & Xue, T. (2019). Accelerated photoreceptor differentiation of hiPSC-derived retinal organoids by contact co-culture with retinal pigment epithelium. *Stem Cell Research*, *39*, 101491. https://doi.org/10.1016/j.scr.2019.101491

Al-Ubaidi, M. R., Naash, M. I., & Conley, S. M. (2013). A Perspective on the Role of the Extracellular Matrix in Progressive Retinal Degenerative Disorders. *Investigative Ophthalmology & Visual Science*, *54*(13), 8119–8124. https://doi.org/10.1167/iovs.13-13536

Ameri, H. (2018). Prospect of retinal gene therapy following commercialization of voretigene neparvovec-rzyl for retinal dystrophy mediated by RPE65 mutation. *Journal of Current Ophthalmology*, *30*(1), 1–2. https://doi.org/10.1016/j.joco.2018.01.006

Anchan, M., Reh, A., & Angello, J. (n.d.). *EGF and TGF-α Stimulate Retinal Neuroepithelial Cell Proliferation In Vitro*. 14.

Anchan, R. M., Reh, T. A., Angello, J., Balliet, A., & Walker, M. (1991). EGF and TGF-α stimulate retinal neuroepithelial cell proliferation in vitro. *Neuron*, *6*(6), 923–936. https://doi.org/10.1016/0896-6273(91)90233-P

Applebury, M. L., Antoch, M. P., Baxter, L. C., Chun, L. L. Y., Falk, J. D., Farhangfar, F., Kage, K., Krzystolik, M. G., Lyass, L. A., & Robbins, J. T. (2000). The Murine Cone Photoreceptor: A Single Cone Type Expresses Both S and M Opsins with Retinal Spatial Patterning. *Neuron*, *27*(3), 513–523. https://doi.org/10.1016/S0896-6273(00)00062-3

Assawachananont, J., Mandai, M., Okamoto, S., Yamada, C., Eiraku, M., Yonemura, S., Sasai, Y., & Takahashi, M. (2014). Transplantation of Embryonic and Induced Pluripotent Stem Cell-Derived 3D Retinal Sheets into Retinal Degenerative Mice. *Stem Cell Reports*, *2*(5), 662–674. https://doi.org/10.1016/j.stemcr.2014.03.011

Attwood, S. W., & Edel, M. J. (2019). iPS-Cell Technology and the Problem of Genetic Instability—Can It Ever Be Safe for Clinical Use? *Journal of Clinical Medicine*, *8*(3), Article 3. https://doi.org/10.3390/jcm8030288

Baden, T., Berens, P., Franke, K., Román Rosón, M., Bethge, M., & Euler, T. (2016). The functional diversity of retinal ganglion cells in the mouse. *Nature*, *529*(7586), 345–350. https://doi.org/10.1038/nature16468

Bailey, T. J., El-Hodiri, H., Zhang, L., Shah, R., Mathers, E. H., & Jamrich, M. (2004). Regulation of vertebrate eye development by Rx genes. *International Journal of Developmental Biology*, *48*(8–9), 761–770. https://doi.org/10.1387/ijdb.041878tb

Barber, A. C., Hippert, C., Duran, Y., West, E. L., Bainbridge, J. W. B., Warre-Cornish, K., Luhmann, U. F. O., Lakowski, J., Sowden, J. C., Ali, R. R., & Pearson, R. A. (2013). Repair of the degenerate

retina by photoreceptor transplantation. *Proceedings of the National Academy of Sciences*, *110*(1), 354–359. https://doi.org/10.1073/pnas.1212677110

Barnea-Cramer, A. O., Wang, W., Lu, S.-J., Singh, M. S., Luo, C., Huo, H., McClements, M. E., Barnard, A. R., MacLaren, R. E., & Lanza, R. (2016). Function of human pluripotent stem cell-derived photoreceptor progenitors in blind mice. *Scientific Reports*, *6*(1), Article 1. https://doi.org/10.1038/srep29784

Barrera, L. O., Li, Z., Smith, A. D., Arden, K. C., Cavenee, W. K., Zhang, M. Q., Green, R. D., & Ren, B. (2008). Genome-wide mapping and analysis of active promoters in mouse embryonic stem cells and adult organs. *Genome Research*, *18*(1), 46–59. https://doi.org/10.1101/gr.6654808

Barry, P. A., Lockridge, K. M., Salamat, S., Tinling, S. P., Yue, Y., Zhou, S. S., Gospe, S. M., Jr., Britt, W. J., & Tarantal, A. F. (2006). Nonhuman Primate Models of Intrauterine Cytomegalovirus Infection. *ILAR Journal*, *47*(1), 49–64. https://doi.org/10.1093/ilar.47.1.49

Bassett, E. A., & Wallace, V. A. (2012). Cell fate determination in the vertebrate retina. *Trends in Neurosciences*, *35*(9), 565–573. https://doi.org/10.1016/j.tins.2012.05.004

Bäumer, N., Marquardt, T., Stoykova, A., Spieler, D., Treichel, D., Ashery-Padan, R., & Gruss, P. (2003). Retinal pigmented epithelium determination requires the redundant activities of Pax2 and Pax6. *Development*, *130*(13), 2903–2915. https://doi.org/10.1242/dev.00450

Benito-Kwiecinski, S., Giandomenico, S. L., Sutcliffe, M., Riis, E. S., Freire-Pritchett, P., Kelava, I., Wunderlich, S., Martin, U., Wray, G. A., McDole, K., & Lancaster, M. A. (2021). An early cell shape transition drives evolutionary expansion of the human forebrain. *Cell*. https://doi.org/10.1016/j.cell.2021.02.050

Bernstein, S. L., Koo, J. H., Slater, B. J., Guo, Y., & Margolis, F. L. (2006). Analysis of optic nerve stroke by retinal Bex expression. *Molecular Vision*, *12*, 147–155.

Berson, E. L., Rosner, B., Sandberg, M. A., Weigel-DiFranco, C., Brockhurst, R. J., Hayes, K. C., Johnson, E. J., Anderson, E. J., Johnson, C. A., Gaudio, A. R., Willett, W. C., & Schaefer, E. J.

(2010). Clinical Trial of Lutein in Patients with Retinitis Pigmentosa Receiving Vitamin A.

Archives of Ophthalmology, *128*(4), 403–411.

https://doi.org/10.1001/archophthalmol.2010.32

Blanks, J. C., Adinolfi, A. M., & Lolley, R. N. (1974). Synaptogenesis in the photoreceptor terminal of

the mouse retina. *Journal of Comparative Neurology*, *156*(1), 81–93.

https://doi.org/10.1002/cne.901560107

Bodnarenko, S. R., Jeyarasasingam, G., & Chalupa, L. M. (1995). Development and regulation of

dendritic stratification in retinal ganglion cells by glutamate-mediated afferent activity.

Journal of Neuroscience, *15*(11), 7037–7045. https://doi.org/10.1523/JNEUROSCI.15-11-

07037.1995

Bok, D. (1993). The retinal pigment epithelium: A versatile partner in vision. *Journal of Cell Science.*

Supplement, *17*, 189–195.

Bottenstein, J. E., & Sato, G. H. (1979). Growth of a rat neuroblastoma cell line in serum-free

supplemented medium. *Proceedings of the National Academy of Sciences of the United*

States of America, *76*(1), 514–517.

Bringmann, A., Pannicke, T., Biedermann, B., Francke, M., Iandiev, I., Grosche, J., Wiedemann, P.,

Albrecht, J., & Reichenbach, A. (2009). Role of retinal glial cells in neurotransmitter uptake

and metabolism. *Neurochemistry International*, *54*(3), 143–160.

https://doi.org/10.1016/j.neuint.2008.10.014

Bringmann, A., Pannicke, T., Grosche, J., Francke, M., Wiedemann, P., Skatchkov, S. N., Osborne, N.

N., & Reichenbach, A. (2006). Müller cells in the healthy and diseased retina. *Progress in*

Retinal and Eye Research, *25*(4), 397–424. https://doi.org/10.1016/j.preteyeres.2006.05.003

Bringmann, A., Syrbe, S., Görner, K., Kacza, J., Francke, M., Wiedemann, P., & Reichenbach, A.

(2018). The primate fovea: Structure, function and development. *Progress in Retinal and Eye*

Research, *66*, 49–84. https://doi.org/10.1016/j.preteyeres.2018.03.006

Buehr, M., Meek, S., Blair, K., Yang, J., Ure, J., Silva, J., McLay, R., Hall, J., Ying, Q.-L., & Smith, A. (2008). Capture of Authentic Embryonic Stem Cells from Rat Blastocysts. *Cell*, *135*(7), 1287–1298. https://doi.org/10.1016/j.cell.2008.12.007

Buskin, A., Zhu, L., Chichagova, V., Basu, B., Mozaffari-Jovin, S., Dolan, D., Droop, A., Collin, J., Bronstein, R., Mehrotra, S., Farkas, M., Hilgen, G., White, K., Pan, K.-T., Treumann, A., Hallam, D., Bialas, K., Chung, G., Mellough, C., … Lako, M. (2018). Disrupted alternative splicing for genes implicated in splicing and ciliogenesis causes PRPF31 retinitis pigmentosa. *Nature Communications*, *9*(1), 4234. https://doi.org/10.1038/s41467-018-06448-y

Bytyqi, A. H., Bachmann, G., Rieke, M., Paraoanu, L. E., & Layer, P. G. (2007). Cell-by-cell reconstruction in reaggregates from neonatal gerbil retina begins from the inner retina and is promoted by retinal pigmented epithelium. *European Journal of Neuroscience*, *26*(6), 1560–1574. https://doi.org/10.1111/j.1460-9568.2007.05767.x

Caffé, A. R., Visser, H., Jansen, H. G., & Sanyal, S. (1989). Histotypic differentiation of neonatal mouse retina in organ culture. *Current Eye Research*, *8*(10), 1083–1092. https://doi.org/10.3109/02713688908997401

Canham, M. A., Van Deusen, A., Brison, D. R., De Sousa, P. A., Downie, J., Devito, L., Hewitt, Z. A., Ilic, D., Kimber, S. J., Moore, H. D., Murray, H., & Kunath, T. (2015). The Molecular Karyotype of 25 Clinical-Grade Human Embryonic Stem Cell Lines. *Scientific Reports*, *5*(1), 17258. https://doi.org/10.1038/srep17258

Capowski, E. E., Samimi, K., Mayerl, S. J., Phillips, M. J., Pinilla, I., Howden, S. E., Saha, J., Jansen, A. D., Edwards, K. L., Jager, L. D., Barlow, K., Valiauga, R., Erlichman, Z., Hagstrom, A., Sinha, D., Sluch, V. M., Chamling, X., Zack, D. J., Skala, M. C., & Gamm, D. M. (2018). Reproducibility and staging of 3D human retinal organoids across multiple pluripotent stem cell lines. *Development*, dev.171686. https://doi.org/10.1242/dev.171686

Carpenedo, R. L., Bratt-Leal, A. M., Marklein, R. A., Seaman, S. A., Bowen, N. J., McDonald, J. F., & McDevitt, T. C. (2009). Homogeneous and organized differentiation within embryoid bodies induced by microsphere-mediated delivery of small molecules. *Biomaterials*, *30*(13), 2507–2515. https://doi.org/10.1016/j.biomaterials.2009.01.007

Cepko, C. L. (2015). The Determination of Rod and Cone Photoreceptor Fate. *Annual Review of Vision Science*, *1*(1), 211–234. https://doi.org/10.1146/annurev-vision-090814-121657

Cheung, C. M. G., & Wong, T. Y. (2014). Is age-related macular degeneration a manifestation of systemic disease? New prospects for early intervention and treatment. *Journal of Internal Medicine*, *276*(2), 140–153. https://doi.org/10.1111/joim.12227

Chichagova, V., Dorgau, B., Felemban, M., Georgiou, M., Armstrong, L., & Lako, M. (2019). Differentiation of Retinal Organoids from Human Pluripotent Stem Cells. *Current Protocols in Stem Cell Biology*, *50*(1), e95. https://doi.org/10.1002/cpsc.95

Chichagova, V., Hilgen, G., Ghareeb, A., Georgiou, M., Carter, M., Sernagor, E., Lako, M., & Armstrong, L. (2020). Human iPSC differentiation to retinal organoids in response to IGF1 and BMP4 activation is line- and method-dependent. *STEM CELLS*, *38*(2), 195–201. https://doi.org/10.1002/stem.3116

Cideciyan, A. V., Jacobson, S. G., Beltran, W. A., Sumaroka, A., Swider, M., Iwabe, S., Roman, A. J., Olivares, M. B., Schwartz, S. B., Komáromy, A. M., Hauswirth, W. W., & Aguirre, G. D. (2013). Human retinal gene therapy for Leber congenital amaurosis shows advancing retinal degeneration despite enduring visual improvement. *Proceedings of the National Academy of Sciences of the United States of America*, *110*(6), E517–E525. https://doi.org/10.1073/pnas.1218933110

Close, J. L., Gumuscu, B., & Reh, T. A. (2005). Retinal neurons regulate proliferation of postnatal progenitors and Müller glia in the rat retina via TGFβ signaling. *Development*, *132*(13), 3015–3026. https://doi.org/10.1242/dev.01882

Collin, J., Queen, R., Zerti, D., Dorgau, B., Hussain, R., Coxhead, J., Cockell, S., & Lako, M. (2019). Deconstructing Retinal Organoids: Single Cell RNA-Seq Reveals the Cellular Components of Human Pluripotent Stem Cell-Derived Retina. *STEM CELLS*, *37*(5), 593–598. https://doi.org/10.1002/stem.2963

Collin, J., Zerti, D., Queen, R., Santos-Ferreira, T., Bauer, R., Coxhead, J., Hussain, R., Steel, D., Mellough, C., Ader, M., Sernagor, E., Armstrong, L., & Lako, M. (2019). CRX Expression in Pluripotent Stem Cell-Derived Photoreceptors Marks a Transplantable Subpopulation of Early Cones. *STEM CELLS*, *37*(5), 609–622. https://doi.org/10.1002/stem.2974

Coppiello, G., Abizanda, G., Aguado, N., Iglesias, E., Iglesias-Garcia, O., Lo Nigro, A., Prosper, F., & Aranguren, X. L. (2017a). Generation of a Sprague-Dawley-GFP rat iPS cell line. *Stem Cell Research*, *21*, 47–50. https://doi.org/10.1016/j.scr.2017.03.021

Coppiello, G., Abizanda, G., Aguado, N., Iglesias, E., Iglesias-Garcia, O., Lo Nigro, A., Prosper, F., & Aranguren, X. L. (2017b). Isolation and characterization of Sprague-Dawley and Wistar Kyoto GFP rat embryonic stem cells. *Stem Cell Research*, *21*, 40–43. https://doi.org/10.1016/j.scr.2017.03.020

Cora, V., Haderspeck, J., Antkowiak, L., Mattheus, U., Neckel, P. H., Mack, A. F., Bolz, S., Ueffing, M., Pashkovskaia, N., Achberger, K., & Liebau, S. (2019). A Cleared View on Retinal Organoids. *Cells*, *8*(5), Article 5. https://doi.org/10.3390/cells8050391

Cowan, C. A., Klimanskaya, I., McMahon, J., Atienza, J., Witmyer, J., Zucker, J. P., Wang, S., Morton, C. C., McMahon, A. P., Powers, D., & Melton, D. A. (2004). Derivation of Embryonic Stem-Cell Lines from Human Blastocysts. *New England Journal of Medicine*, *350*(13), 1353–1356. https://doi.org/10.1056/NEJMsr040330

Cowan, C. S., Renner, M., De Gennaro, M., Gross-Scherf, B., Goldblum, D., Hou, Y., Munz, M., Rodrigues, T. M., Krol, J., Szikra, T., Cuttat, R., Waldt, A., Papasaikas, P., Diggelmann, R., Patino-Alvarez, C. P., Galliker, P., Spirig, S. E., Pavlinic, D., Gerber-Hollbach, N., … Roska, B.

(2020). Cell Types of the Human Retina and Its Organoids at Single-Cell Resolution. *Cell*,

    182(6), 1623-1640.e34. https://doi.org/10.1016/j.cell.2020.08.013

Cowan, C. S., Renner, M., Gross-Scherf, B., Goldblum, D., Munz, M., Krol, J., Szikra, T., Papasaikas, P.,

    Cuttat, R., Waldt, A., Diggelmann, R., Patino-Alvarez, C. P., Gerber-Hollbach, N., Schuierer, S.,

    Hou, Y., Srdanovic, A., Balogh, M., Panero, R., Hasler, P. W., … Roska, B. (2019). Cell types of

    the human retina and its organoids at single-cell resolution: Developmental convergence,

    transcriptomic identity, and disease map. *BioRxiv*, 703348. https://doi.org/10.1101/703348

Cruchten, S. V., Vrolyk, V., Lepage, M.-F. P., Baudon, M., Voute, H., Schoofs, S., Haruna, J., Benoit-

    Biancamano, M.-O., Ruot, B., & Allegaert, K. (2017). Pre- and Postnatal Development of the

    Eye: A Species Comparison. *Birth Defects Research*, *109*(19), 1540–1567.

    https://doi.org/10.1002/bdr2.1100

Curcio, C. A., Sloan, K. R., Packer, O., Hendrickson, A. E., & Kalina, R. E. (1987). Distribution of Cones

    in Human and Monkey Retina: Individual Variability and Radial Asymmetry. *Science*,

    236(4801), 579–582. https://doi.org/10.1126/science.3576186

Cusato, K., Stagg, S. B., & Reese, B. E. (2001). Two phases of increased cell death in the inner retina

    following early elimination of the ganglion cell population. *Journal of Comparative

    Neurology*, *439*(4), 440–449. https://doi.org/10.1002/cne.1361

de Boni, L., Gasparoni, G., Haubenreich, C., Tierling, S., Schmitt, I., Peitz, M., Koch, P., Walter, J.,

    Wüllner, U., & Brüstle, O. (2018). DNA methylation alterations in iPSC- and hESC-derived

    neurons: Potential implications for neurological disease modeling. *Clinical Epigenetics*, *10*(1),

    13. https://doi.org/10.1186/s13148-018-0440-0

Decembrini, S., Koch, U., Radtke, F., Moulin, A., & Arsenijevic, Y. (2014). Derivation of Traceable and

    Transplantable Photoreceptors from Mouse Embryonic Stem Cells. *Stem Cell Reports*, *2*(6),

    853–865. https://doi.org/10.1016/j.stemcr.2014.04.010

Deng, W.-L., Gao, M.-L., Lei, X.-L., Lv, J.-N., Zhao, H., He, K.-W., Xia, X.-X., Li, L.-Y., Chen, Y.-C., Li, Y.-P., Pan, D., Xue, T., & Jin, Z.-B. (2018). Gene Correction Reverses Ciliopathy and Photoreceptor Loss in iPSC-Derived Retinal Organoids from Retinitis Pigmentosa Patients. *Stem Cell Reports*, *10*(4), 1267–1281. https://doi.org/10.1016/j.stemcr.2018.02.003

Diamond, J. S. (2017). Inhibitory Interneurons in the Retina: Types, Circuitry, and Function. *Annual Review of Vision Science*, *3*(1), 1–24. https://doi.org/10.1146/annurev-vision-102016-061345

DiStefano, T., Chen, H. Y., Panebianco, C., Kaya, K. D., Brooks, M. J., Gieser, L., Morgan, N. Y., Pohida, T., & Swaroop, A. (2017). Accelerated and Improved Differentiation of Retinal Organoids from Pluripotent Stem Cells in Rotating-Wall Vessel Bioreactors. *Stem Cell Reports*, *10*(1), 300–313. https://doi.org/10.1016/j.stemcr.2017.11.001

Dodson, K. H., Echevarria, F. D., Li, D., Sappington, R. M., & Edd, J. F. (2015). Retina-on-a-chip: A microfluidic platform for point access signaling studies. *Biomedical Microdevices*, *17*(6), 114. https://doi.org/10.1007/s10544-015-0019-x

Dorgau, B., Felemban, M., Hilgen, G., Kiening, M., Zerti, D., Hunt, N. C., Doherty, M., Whitfield, P., Hallam, D., White, K., Ding, Y., Krasnogor, N., Al-Aama, J., Asfour, H. Z., Sernagor, E., & Lako, M. (2019). Decellularised extracellular matrix-derived peptides from neural retina and retinal pigment epithelium enhance the expression of synaptic markers and light responsiveness of human pluripotent stem cell derived retinal organoids. *Biomaterials*, *199*, 63–75. https://doi.org/10.1016/j.biomaterials.2019.01.028

Dorgau, B., Georgiou, M., Chaudhary, A., Moya-Molina, M., Collin, J., Queen, R., Hilgen, G., Davey, T., Hewitt, P., Schmitt, M., Kustermann, S., Pognan, F., Steel, D. H., Sernagor, E., Armstrong, L., & Lako, M. (2022). Human Retinal Organoids Provide a Suitable Tool for Toxicological Investigations: A Comprehensive Validation Using Drugs and Compounds Affecting the Retina. *Stem Cells Translational Medicine*, *11*(2), 159–177. https://doi.org/10.1093/stcltm/szab010

Dutta, D., Heo, I., & Clevers, H. (2017). Disease Modeling in Stem Cell-Derived 3D Organoid Systems.

    Trends in Molecular Medicine, *23*(5), 393–410.

    https://doi.org/10.1016/j.molmed.2017.02.007

Dye, B. R., Hill, D. R., Ferguson, M. A., Tsai, Y.-H., Nagy, M. S., Dyal, R., Wells, J. M., Mayhew, C. N.,

    Nattiv, R., Klein, O. D., White, E. S., Deutsch, G. H., & Spence, J. R. (2015). In vitro generation

    of human pluripotent stem cell derived lung organoids. *ELife*, *4*, e05098.

    https://doi.org/10.7554/eLife.05098

Dyer, M. A., Livesey, F. J., Cepko, C. L., & Oliver, G. (2003). Prox1 function controls progenitor cell

    proliferation and horizontal cell genesis in the mammalian retina. *Nature Genetics*, *34*(1), 53.

    https://doi.org/10.1038/ng1144

Eiraku, M., & Sasai, Y. (2012). Mouse embryonic stem cell culture for generation of three-

    dimensional retinal and cortical tissues. *Nature Protocols*, *7*(1), 69–79.

    https://doi.org/10.1038/nprot.2011.429

Eiraku, M., Takata, N., Ishibashi, H., Kawada, M., Sakakura, E., Okuda, S., Sekiguchi, K., Adachi, T., &

    Sasai, Y. (2011). Self-organizing optic-cup morphogenesis in three-dimensional culture.

    Nature, *472*(7341), 51–56. https://doi.org/10.1038/nature09941

Ekström, P., & Johansson, K. (2003). Differentiation of ganglion cells and amacrine cells in the rat

    retina: Correlation with expression of HuC/D and GAP-43 proteins. *Developmental Brain*

    Research, *145*(1), 1–8. https://doi.org/10.1016/S0165-3806(03)00170-6

Eldred, K. C., Hadyniak, S. E., Hussey, K. A., Brenerman, B., Zhang, P.-W., Chamling, X., Sluch, V. M.,

    Welsbie, D. S., Hattar, S., Taylor, J., Wahlin, K., Zack, D. J., & JohnstonJr, R. J. (2018). Thyroid

    hormone signaling specifies cone subtypes in human retinal organoids. *Science*.

    https://doi.org/10.1126/science.aau6348

Eliasieh, K., Liets, L. C., & Chalupa, L. M. (2007). Cellular Reorganization in the Human Retina during Normal Aging. *Investigative Ophthalmology & Visual Science*, *48*(6), 2824–2830. https://doi.org/10.1167/iovs.06-1228

Evans, M. J., & Kaufman, M. H. (1981). Establishment in culture of pluripotential cells from mouse embryos. *Nature*, *292*(5819), 154. https://doi.org/10.1038/292154a0

Fadl, B. R., Brodie, S. A., Malasky, M., Boland, J. F., Kelly, M. C., Kelley, M. W., Boger, E., Fariss, R., Swaroop, A., & Campello, L. (2020). An optimized protocol for retina single-cell RNA sequencing. *Molecular Vision*, *26*, 705–717.

Fain, G. L., Hardie, R., & Laughlin, S. B. (2010). Phototransduction and the Evolution of Photoreceptors. *Current Biology*, *20*(3), R114–R124. https://doi.org/10.1016/j.cub.2009.12.006

Famiglietti, E. V., & Sundquist, S. J. (2010). Development of excitatory and inhibitory neurotransmitters in transitory cholinergic neurons, starburst amacrine cells, and GABAergic amacrine cells of rabbit retina, with implications for previsual and visual development of retinal ganglion cells. *Visual Neuroscience*, *27*(1–2), 19–42. https://doi.org/10.1017/S0952523810000052

Fariss, R. N., Li, Z.-Y., & Milam, A. H. (2000). Abnormalities in rod photoreceptors, amacrine cells, and horizontal cells in human retinas with retinitis pigmentosa. *American Journal of Ophthalmology*, *129*(2), 215–223. https://doi.org/10.1016/S0002-9394(99)00401-8

Felemban, M., Dorgau, B., Hunt, N. C., Hallam, D., Zerti, D., Bauer, R., Ding, Y., Collin, J., Steel, D., Krasnogor, N., Al-Aama, J., Lindsay, S., Mellough, C., & Lako, M. (2018). Extracellular matrix component expression in human pluripotent stem cell-derived retinal organoids recapitulates retinogenesis in vivo and reveals an important role for IMPG1 and CD44 in the development of photoreceptors and interphotoreceptor matrix. *Acta Biomaterialia*, *74*, 207–221. https://doi.org/10.1016/j.actbio.2018.05.023

Fernández-Nogales, M., Murcia-Belmonte, V., Chen, H. Y., & Herrera, E. (2019). The peripheral eye: A

neurogenic area with potential to treat retinal pathologies? *Progress in Retinal and Eye

Research*, *68*, 110–123. https://doi.org/10.1016/j.preteyeres.2018.09.001

Fisher, L. J. (1979). Development of retinal synaptic arrays in the inner plexiform layer of dark-reared

mice. *Development*, *54*(1), 219–227. https://doi.org/10.1242/dev.54.1.219

Fligor, C. M., Langer, K. B., Sridhar, A., Ren, Y., Shields, P. K., Edler, M. C., Ohlemacher, S. K., Sluch, V.

M., Zack, D. J., Zhang, C., Suter, D. M., & Meyer, J. S. (2018). Three-Dimensional Retinal

Organoids Facilitate the Investigation of Retinal Ganglion Cell Development, Organization

and Neurite Outgrowth from Human Pluripotent Stem Cells. *Scientific Reports*, *8*(1), 14520.

https://doi.org/10.1038/s41598-018-32871-8

Ford, K., & Feller, M. (2012). *Formation of Early Retinal Circuits in the Inner-Plexiform Layer*.

University of Utah Health Sciences Center. https://www.ncbi.nlm.nih.gov/books/NBK11547/

Fruttiger, M., Calver, A. R., Krüger, W. H., Mudhar, H. S., Michalovich, D., Takakura, N., Nishikawa, S.

I., & Richardson, W. D. (1996). PDGF Mediates a Neuron–Astrocyte Interaction in the

Developing Retina. *Neuron*, *17*(6), 1117–1131. https://doi.org/10.1016/S0896-

6273(00)80244-5

Fürtbauer, I., Schülke, O., Heistermann, M., & Ostner, J. (2010). Reproductive and Life History

Parameters of Wild Female Macaca assamensis. *International Journal of Primatology*, *31*(4),

501–517. https://doi.org/10.1007/s10764-010-9409-3

Garita-Hernandez, M., Lampič, M., Chaffiol, A., Guibbal, L., Routet, F., Santos-Ferreira, T., Gasparini,

S., Borsch, O., Gagliardi, G., Reichman, S., Picaud, S., Sahel, J.-A., Goureau, O., Ader, M.,

Dalkara, D., & Duebel, J. (2019). Restoration of visual function by transplantation of

optogenetically engineered photoreceptors. *Nature Communications*, *10*(1), 4524.

https://doi.org/10.1038/s41467-019-12330-2

Gasparini, S. J., Llonch, S., Borsch, O., & Ader, M. (2019). Transplantation of photoreceptors into the

degenerative retina: Current state and future perspectives. *Progress in Retinal and Eye*

Research, *69*, 1–37. https://doi.org/10.1016/j.preteyeres.2018.11.001

Gaur, V. P., Liu, Y., & Turner, J. E. (1992). RPE conditioned medium stimulates photoreceptor cell

survival, neurite outgrowth and differentiation in vitro. *Experimental Eye Research*, *54*(5),

645–659. https://doi.org/10.1016/0014-4835(92)90020-S

German, O. L., Buzzi, E., Rotstein, N. P., Rodríguez-Boulan, E., & Politi, L. E. (2008). Retinal pigment

epithelial cells promote spatial reorganization and differentiation of retina photoreceptors.

Journal of Neuroscience Research, *86*(16), 3503–3514. https://doi.org/10.1002/jnr.21813

Ghareeb, A. E., Lako, M., & Steel, D. H. (2020). Coculture techniques for modeling retinal

development and disease, and enabling regenerative medicine. *STEM CELLS Translational*

Medicine, *9*(12), 1531–1548. https://doi.org/10.1002/sctm.20-0201

Gjorevski, N., Ranga, A., & Lutolf, M. P. (2014). Bioengineering approaches to guide stem cell-based

organogenesis. *Development*, *141*(9), 1794–1804. https://doi.org/10.1242/dev.101048

Glubrecht, D. D., Kim, J.-H., Russell, L., Bamforth, J. S., & Godbout, R. (2009). Differential CRX and

OTX2 expression in human retina and retinoblastoma. *Journal of Neurochemistry*, *111*(1),

250–263. https://doi.org/10.1111/j.1471-4159.2009.06322.x

Gonzalez-Cordero, A., Kruczek, K., Naeem, A., Fernando, M., Kloc, M., Ribeiro, J., Goh, D., Duran, Y.,

Blackford, S. J. I., Abelleira-Hervas, L., Sampson, R. D., Shum, I. O., Branch, M. J., Gardner, P.

J., Sowden, J. C., Bainbridge, J. W. B., Smith, A. J., West, E. L., Pearson, R. A., & Ali, R. R.

(2017). Recapitulation of Human Retinal Development from Human Pluripotent Stem Cells

Generates Transplantable Populations of Cone Photoreceptors. *Stem Cell Reports*, *9*(3), 820–

837. https://doi.org/10.1016/j.stemcr.2017.07.022

Gonzalez-Cordero, A., West, E. L., Pearson, R. A., Duran, Y., Carvalho, L. S., Chu, C. J., Naeem, A.,

Blackford, S. J. I., Georgiadis, A., Lakowski, J., Hubank, M., Smith, A. J., Bainbridge, J. W. B.,

Sowden, J. C., & Ali, R. R. (2013). Photoreceptor precursors derived from three-dimensional embryonic stem cell cultures integrate and mature within adult degenerate retina. *Nature Biotechnology*, *31*(8), 741–747. https://doi.org/10.1038/nbt.2643

Gore, A., Li, Z., Fung, H.-L., Young, J. E., Agarwal, S., Antosiewicz-Bourget, J., Canto, I., Giorgetti, A., Israel, M. A., Kiskinis, E., Lee, J.-H., Loh, Y.-H., Manos, P. D., Montserrat, N., Panopoulos, A. D., Ruiz, S., Wilbert, M. L., Yu, J., Kirkness, E. F., … Zhang, K. (2011). Somatic coding mutations in human induced pluripotent stem cells. *Nature*, *471*(7336), Article 7336. https://doi.org/10.1038/nature09805

Goudreau, G., Petrou, P., Reneker, L. W., Graw, J., Löster, J., & Gruss, P. (2002). Mutually regulated expression of Pax6 and Six3 and its implications for the Pax6 haploinsufficient lens phenotype. *Proceedings of the National Academy of Sciences of the United States of America*, *99*(13), 8719–8724. https://doi.org/10.1073/pnas.132195699

Great Britain, Home Office, Great Britain, & Office for National Statistics. (2020). *Annual Statistics of Scientific Procedures on Living Animals, Great Britain 2019*.

Grünert, U., & Martin, P. R. (2020). Cell types and cell circuits in human and non-human primate retina. *Progress in Retinal and Eye Research*, *78*, 100844. https://doi.org/10.1016/j.preteyeres.2020.100844

Gu, S., Thompson, D. A., Srikumari, C. R. S., Lorenz, B., Finckh, U., Nicoletti, A., Murthy, K. R., Rathmann, M., Kumaramanickavel, G., Denton, M. J., & Gal, A. (1997). Mutations in RPE65 cause autosomal recessive childhood–onset severe retinal dystrophy. *Nature Genetics*, *17*(2), 194–197. https://doi.org/10.1038/ng1097-194

Guo, G., Yang, J., Nichols, J., Hall, J. S., Eyres, I., Mansfield, W., & Smith, A. (2009). Klf4 reverts developmentally programmed restriction of ground state pluripotency. *Development*, *136*(7), 1063–1069. https://doi.org/10.1242/dev.030957

Gust, J., & Reh, T. A. (2011). Adult Donor Rod Photoreceptors Integrate into the Mature Mouse

Retina. *Investigative Ophthalmology & Visual Science*, *52*(8), 5266–5272.

https://doi.org/10.1167/iovs.10-6329

Hallam, D., Hilgen, G., Dorgau, B., Zhu, L., Yu, M., Bojic, S., Hewitt, P., Schmitt, M., Uteng, M.,

Kustermann, S., Steel, D., Nicholds, M., Thomas, R., Treumann, A., Porter, A., Sernagor, E.,

Armstrong, L., & Lako, M. (2018). Human-Induced Pluripotent Stem Cells Generate Light

Responsive Retinal Organoids with Variable and Nutrient-Dependent Efficiency. *STEM CELLS*,

36(10), 1535–1551. https://doi.org/10.1002/stem.2883

Haridhasapavalan, K. K., Raina, K., Dey, C., Adhikari, P., & Thummer, R. P. (2020). An Insight into

Reprogramming Barriers to iPSC Generation. *Stem Cell Reviews and Reports*, *16*(1), 56–81.

https://doi.org/10.1007/s12015-019-09931-1

Hartong, D. T., Berson, E. L., & Dryja, T. P. (2006). Retinitis pigmentosa. *The Lancet*, *368*(9549), 1795–

1809. https://doi.org/10.1016/S0140-6736(06)69740-7

Haruta, M., Sasai, Y., Kawasaki, H., Amemiya, K., Ooto, S., Kitada, M., Suemori, H., Nakatsuji, N., Ide,

C., Honda, Y., & Takahashi, M. (2004). In Vitro and In Vivo Characterization of Pigment

Epithelial Cells Differentiated from Primate Embryonic Stem Cells. *Investigative*

Ophthalmology & Visual Science, *45*(3), 1020–1025. https://doi.org/10.1167/iovs.03-1034

Haverkamp, S., Ghosh, K. K., Hirano, A. A., & Wässle, H. (2003). Immunocytochemical Description of

Five Bipolar Cell Types of the Mouse Retina. *The Journal of Comparative Neurology*, *455*(4),

463. https://doi.org/10.1002/cne.10491

Haverkamp, S., Haeseleer, F., & Hendrickson, A. (2003). A comparison of immunocytochemical

markers to identify bipolar cell types in human and monkey retina. *Visual Neuroscience*,

20(6), 589–600. https://doi.org/10.1017/S0952523803206015

Haverkamp, S., & Wässle, H. (2000). Immunocytochemical analysis of the mouse retina. *Journal of Comparative Neurology*, *424*(1), 1–23. https://doi.org/10.1002/1096-9861(20000814)424:1<1::AID-CNE1>3.0.CO;2-V

Heavner, W. E., Andoniadou, C. L., & Pevny, L. H. (2014). Establishment of the neurogenic boundary of the mouse retina requires cooperation of SOX2 and WNT signaling. *Neural Development*, *9*. https://doi.org/10.1186/1749-8104-9-27

Heavner, W., & Pevny, L. (2012). Eye Development and Retinogenesis. *Cold Spring Harbor Perspectives in Biology*, *4*(12). https://doi.org/10.1101/cshperspect.a008391

Hendrickson, A. (1992). A morphological comparison of foveal development in man and monkey. *Eye*, *6*(2), 136–144. https://doi.org/10.1038/eye.1992.29

Hernandez-Sanchez, C., Lopez-Carranza, A., Alarcon, C., de La Rosa, E. J., & de Pablo, F. (1995). Autocrine/paracrine role of insulin-related growth factors in neurogenesis: Local expression and effects on cell proliferation and differentiation in retina. *Proceedings of the National Academy of Sciences*, *92*(21), 9834–9838. https://doi.org/10.1073/pnas.92.21.9834

Hinds, J. W., & Hinds, P. L. (1983). Development of retinal amacrine cells in the mouse embryo: Evidence for two modes of formation. *Journal of Comparative Neurology*, *213*(1), 1–23. https://doi.org/10.1002/cne.902130102

Hirami, Y., Osakada, F., Takahashi, K., Okita, K., Yamanaka, S., Ikeda, H., Yoshimura, N., & Takahashi, M. (2009). Generation of retinal cells from mouse and human induced pluripotent stem cells. *Neuroscience Letters*, *458*(3), 126–131. https://doi.org/10.1016/j.neulet.2009.04.035

Hong, J., He, H., & Weiss, M. L. (2011). Derivation and Characterization of Embryonic Stem Cells Lines Derived from Transgenic Fischer 344 and Dark Agouti Rats. *Stem Cells and Development*, *21*(9), 1571–1586. https://doi.org/10.1089/scd.2011.0370

Horsburgh, G. M., & Sefton, A. J. (1987). Cellular degeneration and synaptogenesis in the developing

retina of the rat. *Journal of Comparative Neurology*, *263*(4), 553–566.

https://doi.org/10.1002/cne.902630407

Hoshino, A., Ratnapriya, R., Brooks, M. J., Chaitankar, V., Wilken, M. S., Zhang, C., Starostik, M. R.,

Gieser, L., La Torre, A., Nishio, M., Bates, O., Walton, A., Bermingham-McDonogh, O., Glass,

I. A., Wong, R. O. L., Swaroop, A., & Reh, T. A. (2017). Molecular Anatomy of the Developing

Human Retina. *Developmental Cell*, *43*(6), 763-779.e4.

https://doi.org/10.1016/j.devcel.2017.10.029

Huang, J., Liu, Y., Oltean, A., & Beebe, D. C. (2015). Bmp4 from the Optic Vesicle Specifies Murine

Retina Formation. *Developmental Biology*, *402*(1), 119–126.

https://doi.org/10.1016/j.ydbio.2015.03.006

Huber, G., Heynen, S., Imsand, C., Hagen, F. vom, Muehlfriedel, R., Tanimoto, N., Feng, Y., Hammes,

H.-P., Grimm, C., Peichl, L., Seeliger, M. W., & Beck, S. C. (2010). Novel Rodent Models for

Macular Research. *PLOS ONE*, *5*(10), e13403. https://doi.org/10.1371/journal.pone.0013403

Hussein, S. M., Batada, N. N., Vuoristo, S., Ching, R. W., Autio, R., Närvä, E., Ng, S., Sourour, M.,

Hämäläinen, R., Olsson, C., Lundin, K., Mikkola, M., Trokovic, R., Peitz, M., Brüstle, O., Bazett-

Jones, D. P., Alitalo, K., Lahesmaa, R., Nagy, A., & Otonkoski, T. (2011). Copy number

variation and selection during reprogramming to pluripotency. *Nature*, *471*(7336), Article

7336. https://doi.org/10.1038/nature09871

Ientuile, R., Macaione, S., Russo, P., Pugliese, G., & Giorgio, R. M. D. (1984). Phenolic and tyrosyl ring

deiodination in thyroxine from rat retina during postnatal development. *European Journal of*

Biochemistry, *142*(1), 15–19. https://doi.org/10.1111/j.1432-1033.1984.tb08244.x

Ikeda, H., Osakada, F., Watanabe, K., Mizuseki, K., Haraguchi, T., Miyoshi, H., Kamiya, D., Honda, Y.,

Sasai, N., Yoshimura, N., Takahashi, M., & Sasai, Y. (2005). Generation of Rx+/Pax6+ neural

retinal precursors from embryonic stem cells. *Proceedings of the National Academy of Sciences*, *102*(32), 11331–11336. https://doi.org/10.1073/pnas.0500010102

Ikeda, Y., Nishiguchi, K. M., Miya, F., Shimozawa, N., Funatsu, J., Nakatake, S., Fujiwara, K., Tachibana, T., Murakami, Y., Hisatomi, T., Yoshida, S., Yasutomi, Y., Tsunoda, T., Nakazawa, T., Ishibashi, T., & Sonoda, K.-H. (2018). Discovery of a Cynomolgus Monkey Family With Retinitis Pigmentosa. *Investigative Ophthalmology & Visual Science*, *59*(2), 826–830. https://doi.org/10.1167/iovs.17-22958

Ikelle, L., Al-Ubaidi, M. R., & Naash, M. I. (2020). Pluripotent Stem Cells for the Treatment of Retinal Degeneration: Current Strategies and Future Directions. *Frontiers in Cell and Developmental Biology*, *8*, 743. https://doi.org/10.3389/fcell.2020.00743

Insinna, C., Daniele, L. L., Davis, J. A., Larsen, D. D., Kuemmel, C., Wang, J., Nikonov, S. S., Knox, B. E., & Pugh, E. N. (2012). An S-opsin knockin mouse (F81Y) reveals a role for the native ligand 11-cis retinal in cone opsin biosynthesis. *The Journal of Neuroscience*, *32*(23), 8094–8104. https://doi.org/10.1523/JNEUROSCI.0131-12.2012

Ito, S., Onishi, A., & Takahashi, M. (2017). Chemically-induced photoreceptor degeneration and protection in mouse iPSC-derived three-dimensional retinal organoids. *Stem Cell Research*, *24*, 94–101. https://doi.org/10.1016/j.scr.2017.08.018

Jacob, H. J., & Kwitek, A. E. (2002). Rat genetics: Attaching physiology and pharmacology to the genome. *Nature Reviews. Genetics*, *3*(1), 33–42. https://doi.org/10.1038/nrg702

Jacobs, G. H. (1993). The Distribution and Nature of Colour Vision Among the Mammals. *Biological Reviews*, *68*(3), 413–471. https://doi.org/10.1111/j.1469-185X.1993.tb00738.x

Jacobs, G. H., Fenwick, J. A., & Williams, G. A. (2001). Cone-based vision of rats for ultraviolet and visible lights. *Journal of Experimental Biology*, *204*(14), 2439–2446.

Jacobs, G. H., Neitz, J., & Deegan, J. F. (1991). Retinal receptors in rodents maximally sensitive to ultraviolet light. *Nature*, *353*(6345), 655–656. https://doi.org/10.1038/353655a0

Jadhav, A. P., Cho, S.-H., & Cepko, C. L. (2006). Notch activity permits retinal cells to progress

through multiple progenitor states and acquire a stem cell property. *Proceedings of the*

National Academy of Sciences of the United States of America, *103*(50), 18998–19003.

https://doi.org/10.1073/pnas.0608155103

Jeon, C.-J., Strettoi, E., & Masland, R. H. (1998). The Major Cell Populations of the Mouse Retina.

Journal of Neuroscience, *18*(21), 8936–8946. https://doi.org/10.1523/JNEUROSCI.18-21-

08936.1998

Joachim, N., Kifley, A., Colijn, J. M., Lee, K. E., Buitendijk, G. H. S., Klein, B. E. K., Myers, C., Meuer, S.

M., Tan, A. G., Flood, V., Schoufour, J. D., Franco, O. H., Holliday, E. G., Attia, J., Liew, G.,

Iyengar, S. K., de Jong, P. T. V. M., Hofman, A., Vingerling, J. R., … Wang, J. J. (2018). Joint

Contribution of Genetic Susceptibility and Modifiable Factors to the Progression of Age-

Related Macular Degeneration over 10 Years: The Three Continent AMD Consortium Report.

Ophthalmology. Retina, *2*(7), 684–693. https://doi.org/10.1016/j.oret.2017.10.019

Johansson, B. M., & Wiles, M. V. (1995). Evidence for involvement of activin A and bone

morphogenetic protein 4 in mammalian mesoderm and hematopoietic development.

Molecular and Cellular Biology, *15*(1), 141–151. https://doi.org/10.1128/MCB.15.1.141

Kaarniranta, K., Salminen, A., Haapasalo, A., Soininen, H., & Hiltunen, M. (2011). Age-Related

Macular Degeneration (AMD): Alzheimer's Disease in the Eye? *Journal of Alzheimer's*

Disease, *24*(4), 615–631. https://doi.org/10.3233/JAD-2011-101908

Kawamura, T., Suzuki, J., Wang, Y. V., Menendez, S., Morera, L. B., Raya, A., Wahl, G. M., &

Belmonte, J. C. I. (2009). Linking the p53 tumour suppressor pathway to somatic cell

reprogramming. *Nature*, *460*(7259), 1140–1144. https://doi.org/10.1038/nature08311

Kelley, M. W., Williams, R. C., Turner, J. K., Creech-Kraft, J. M., & Reh, T. A. (1999). Retinoic acid

promotes rod photoreceptor differentiation in rat retina in vivo. *NeuroReport*, *10*(11), 2389–

2394.

Kiely, P. M., Gillard-Crewther, S., Nathan, J., Brennan, N. A., Efron, N., & Madigan, M. (1987). A

comparison of ocular development of the Cynomolgus monkey and man. *Clinical Vision*

Sciences, *1*(3), Article 3.

Kilb, W., & Fukuda, A. (2017). Taurine as an Essential Neuromodulator during Perinatal Cortical

Development. *Frontiers in Cellular Neuroscience*, *11*.

https://doi.org/10.3389/fncel.2017.00328

Kilpinen, H., Goncalves, A., Leha, A., Afzal, V., Alasoo, K., Ashford, S., Bala, S., Bensaddek, D., Casale,

F. P., Culley, O. J., Danecek, P., Faulconbridge, A., Harrison, P. W., Kathuria, A., McCarthy, D.,

McCarthy, S. A., Meleckyte, R., Memari, Y., Moens, N., … Gaffney, D. J. (2017). Common

genetic variation drives molecular heterogeneity in human iPSCs. *Nature*, *546*(7658), 370–

375. https://doi.org/10.1038/nature22403

Kim, I.-B., Lee, E.-J., Kim, M.-K., Park, D.-K., & Chun, M.-H. (2000). Choline acetyltransferase-

immunoreactive neurons in the developing rat retina. *Journal of Comparative Neurology*,

427(4), 604–616. https://doi.org/10.1002/1096-9861(20001127)427:4<604::AID-

CNE8>3.0.CO;2-C

Kim, S., Lowe, A., Dharmat, R., Lee, S., Owen, L. A., Wang, J., Shakoor, A., Li, Y., Morgan, D. J., Hejazi,

A. A., Cvekl, A., DeAngelis, M. M., Zhou, Z. J., Chen, R., & Liu, W. (2019). Generation,

transcriptome profiling, and functional validation of cone-rich human retinal organoids.

Proceedings of the National Academy of Sciences, *116*(22), 10824–10833.

https://doi.org/10.1073/pnas.1901572116

King, H. D. (1913). Some Anomalies in the Gestation of the Albino Rat (Mus Norvegicus Albinus).

Biological Bulletin, *24*(6), 377–391. JSTOR. https://doi.org/10.2307/1536051

Klein, R., Peto, T., Bird, A., & Vannewkirk, M. R. (2004). The epidemiology of age-related macular

degeneration. *American Journal of Ophthalmology*, *137*(3), 486–495.

https://doi.org/10.1016/j.ajo.2003.11.069

Komeima, K., Rogers, B. S., & Campochiaro, P. A. (2007). Antioxidants slow photoreceptor cell death in mouse models of retinitis pigmentosa. *Journal of Cellular Physiology*, *213*(3), 809–815. https://doi.org/10.1002/jcp.21152

Komeima, K., Rogers, B. S., Lu, L., & Campochiaro, P. A. (2006). Antioxidants reduce cone cell death in a model of retinitis pigmentosa. *Proceedings of the National Academy of Sciences*, *103*(30), 11300–11305. https://doi.org/10.1073/pnas.0604056103

Koo, B.-K., Stange, D. E., Sato, T., Karthaus, W., Farin, H. F., Huch, M., van Es, J. H., & Clevers, H. (2012). Controlled gene expression in primary *Lgr5* organoid cultures. *Nature Methods*, *9*(1), 81–83. https://doi.org/10.1038/nmeth.1802

Kruczek, K., Gonzalez-Cordero, A., Goh, D., Naeem, A., Jonikas, M., Blackford, S. J. I., Kloc, M., Duran, Y., Georgiadis, A., Sampson, R. D., Maswood, R. N., Smith, A. J., Decembrini, S., Arsenijevic, Y., Sowden, J. C., Pearson, R. A., West, E. L., & Ali, R. R. (2017). Differentiation and Transplantation of Embryonic Stem Cell-Derived Cone Photoreceptors into a Mouse Model of End-Stage Retinal Degeneration. *Stem Cell Reports*, *8*(6), 1659–1674. https://doi.org/10.1016/j.stemcr.2017.04.030

Kuwabara, T., & Weidman, T. A. (1974). Development of the Prenatal Rat Retina. *Investigative Ophthalmology & Visual Science*, *13*(10), 725–739.

Kuwahara, A., Ozone, C., Nakano, T., Saito, K., Eiraku, M., & Sasai, Y. (2015). Generation of a ciliary margin-like stem cell niche from self-organizing human retinal tissue. *Nature Communications*, *6*, 6286. https://doi.org/10.1038/ncomms7286

Kyttälä, A., Moraghebi, R., Valensisi, C., Kettunen, J., Andrus, C., Pasumarthy, K. K., Nakanishi, M., Nishimura, K., Ohtaka, M., Weltner, J., Van Handel, B., Parkkonen, O., Sinisalo, J., Jalanko, A., Hawkins, R. D., Woods, N.-B., Otonkoski, T., & Trokovic, R. (2016). Genetic Variability Overrides the Impact of Parental Cell Type and Determines iPSC Differentiation Potential. *Stem Cell Reports*, *6*(2), 200–212. https://doi.org/10.1016/j.stemcr.2015.12.009

Lam, P. T., Gutierrez, C., Rio-Tsonis, K. D., & Robinson, M. L. (2019). Generation of a Retina Reporter
hiPSC Line to Label Progenitor, Ganglion, and Photoreceptor Cell Types. *BioRxiv*, 658963.
https://doi.org/10.1101/658963

Lamba, D. A., Karl, M. O., Ware, C. B., & Reh, T. A. (2006). Efficient generation of retinal progenitor
cells from human embryonic stem cells. *Proceedings of the National Academy of Sciences*,
103(34), 12769–12774. https://doi.org/10.1073/pnas.0601990103

Lancaster, M. A., & Knoblich, J. A. (2014). Organogenesis in a dish: Modeling development and
disease using organoid technologies. *Science*, *345*(6194), 1247125.
https://doi.org/10.1126/science.1247125

Lancaster, M. A., Renner, M., Martin, C.-A., Wenzel, D., Bicknell, L. S., Hurles, M. E., Homfray, T.,
Penninger, J. M., Jackson, A. P., & Knoblich, J. A. (2013). Cerebral organoids model human
brain development and microcephaly. *Nature*, *501*(7467), 373–379.
https://doi.org/10.1038/nature12517

Land, M. F., & Nilsson, D.-E. (2012). *Animal Eyes*. Oxford University Press.

Lane, A., Jovanovic, K., Shortall, C., Ottaviani, D., Panes, A. B., Schwarz, N., Guarascio, R., Hayes, M.
J., Palfi, A., Chadderton, N., Farrar, G. J., Hardcastle, A. J., & Cheetham, M. E. (2020).
Modeling and Rescue of RP2 Retinitis Pigmentosa Using iPSC-Derived Retinal Organoids.
Stem Cell Reports, *15*(1), 67–79. https://doi.org/10.1016/j.stemcr.2020.05.007

Levine*, E. M., Fuhrmann, S., & Reh**, T. A. (2000). Soluble factors and the development of rod
photoreceptors. *Cellular and Molecular Life Sciences CMLS*, *57*(2), 224–234.
https://doi.org/10.1007/PL00000686

Li, P., Tong, C., Mehrian-Shai, R., Jia, L., Wu, N., Yan, Y., Maxson, R. E., Schulze, E. N., Song, H., Hsieh,
C.-L., Pera, M. F., & Ying, Q.-L. (2008). Germline Competent Embryonic Stem Cells Derived
from Rat Blastocysts. *Cell*, *135*(7), 1299–1310. https://doi.org/10.1016/j.cell.2008.12.006

Li, W., Wei, W., Zhu, S., Zhu, J., Shi, Y., Lin, T., Hao, E., Hayek, A., Deng, H., & Ding, S. (2009).

Generation of Rat and Human Induced Pluripotent Stem Cells by Combining Genetic

Reprogramming and Chemical Inhibitors. *Cell Stem Cell*, *4*(1), 16–19.

https://doi.org/10.1016/j.stem.2008.11.014

Li, Y., Liu, M., Yan, Y., & Yang, S.-T. (2014). Neural differentiation from pluripotent stem cells: The

role of natural and synthetic extracellular matrix. *World Journal of Stem Cells*, *6*(1), 11–23.

https://doi.org/10.4252/wjsc.v6.i1.11

Liao, J., Cui, C., Chen, S., Ren, J., Chen, J., Gao, Y., Li, H., Jia, N., Cheng, L., Xiao, H., & Xiao, L. (2009).

Generation of Induced Pluripotent Stem Cell Lines from Adult Rat Cells. *Cell Stem Cell*, *4*(1),

11–15. https://doi.org/10.1016/j.stem.2008.11.013

Lillien, L., & Cepko, C. (n.d.). *Control of proliferation in the retina: Temporal changes in*

responsiveness to FGF and TGFa. 14.

Lillien, L., & Cepko, C. (1992). Control of proliferation in the retina: Temporal changes in

responsiveness to FGF and TGF alpha. *Development*, *115*(1), 253–266.

https://doi.org/10.1242/dev.115.1.253

Lin, N., Fan, W., Sheedlo, H. J., Aschenbrenner, J. E., & Turner, J. E. (1996). Photoreceptor repair in

response to RPE transplants in RCS rats: Outer segment regeneration. *Current Eye Research*,

15(10), 1069–1077. https://doi.org/10.3109/02713689609017657

Lin, Y., Ouchi, Y., Satoh, S., & Watanabe, S. (2009). Sox2 Plays a Role in the Induction of Amacrine

and Müller Glial Cells in Mouse Retinal Progenitor Cells. *Investigative Ophthalmology &*

Visual Science, *50*(1), 68–74. https://doi.org/10.1167/iovs.07-1619

Lister, R., Pelizzola, M., Kida, Y. S., Hawkins, R. D., Nery, J. R., Hon, G., Antosiewicz-Bourget, J.,

O'Malley, R., Castanon, R., Klugman, S., Downes, M., Yu, R., Stewart, R., Ren, B., Thomson, J.

A., Evans, R. M., & Ecker, J. R. (2011). Hotspots of aberrant epigenomic reprogramming in

human induced pluripotent stem cells. *Nature*, *471*(7336), Article 7336.

https://doi.org/10.1038/nature09798

Liu, C.-H., Wang, Z., Sun, Y., & Chen, J. (2017). Animal models of ocular angiogenesis: From

development to pathologies. *The FASEB Journal*, *31*(11), 4665–4681.

https://doi.org/10.1096/fj.201700336R

Liu, H., Zhu, F., Yong, J., Zhang, P., Hou, P., Li, H., Jiang, W., Cai, J., Liu, M., Cui, K., Qu, X., Xiang, T., Lu,

D., Chi, X., Gao, G., Ji, W., Ding, M., & Deng, H. (2008). Generation of Induced Pluripotent

Stem Cells from Adult Rhesus Monkey Fibroblasts. *Cell Stem Cell*, *3*(6), 587–590.

https://doi.org/10.1016/j.stem.2008.10.014

Livak, K. J., & Schmittgen, T. D. (2001). Analysis of Relative Gene Expression Data Using Real-Time

Quantitative PCR and the 2−ΔΔCT Method. *Methods*, *25*(4), 402–408.

https://doi.org/10.1006/meth.2001.1262

Livesey, F. J., & Cepko, C. L. (2001). Vertebrate neural cell-fate determination: Lessons from the

retina. *Nature Reviews Neuroscience*, *2*(2), 109. https://doi.org/10.1038/35053522

Livne-bar, I., Pacal, M., Cheung, M. C., Hankin, M., Trogadis, J., Chen, D., Dorval, K. M., & Bremner, R.

(2006). Chx10 is required to block photoreceptor differentiation but is dispensable for

progenitor proliferation in the postnatal retina. *Proceedings of the National Academy of*

Sciences, *103*(13), 4988–4993. https://doi.org/10.1073/pnas.0600083103

Lopez, A. J., Kim, S., Qian, X., Rogers, J., Stout, J. T., Thomasy, S. M., Torre, A. L., Chen, R., & Moshiri,

A. (2021). Retinal organoids derived from rhesus macaque iPSCs undergo accelerated

differentiation compared to human stem cells. *BioRxiv*, 2021.05.25.445693.

https://doi.org/10.1101/2021.05.25.445693

Lopez, A. J., Sangbae, K., Thomasy, S. M., Miltner, A., Rogers, J., Stout, T., Torre, A. L., Chen, R., &

Moshiri, A. (2021). Retinal organoids generated from rhesus macaque (Macaca Mulatta)

induced pluripotent stem cells demonstrate mature photoreceptors and rods. *Investigative Ophthalmology & Visual Science*, *62*(8), 3156–3156.

Lukovic, D., Artero Castro, A., Delgado, A. B. G., Bernal, M. de los A. M., Luna Pelaez, N., Díez Lloret, A., Perez Espejo, R., Kamenarova, K., Fernández Sánchez, L., Cuenca, N., Cortón, M., Avila Fernandez, A., Sorkio, A., Skottman, H., Ayuso, C., Erceg, S., & Bhattacharya, S. S. (2015). Human iPSC derived disease model of MERTK-associated retinitis pigmentosa. *Scientific Reports*, *5*, 12910. https://doi.org/10.1038/srep12910

Luni, C., Serena, E., & Elvassore, N. (2014). Human-on-chip for therapy development and fundamental science. *Current Opinion in Biotechnology*, *25*, 45–50. https://doi.org/10.1016/j.copbio.2013.08.015

Luo, D.-G., Su, C.-Y., & Yau, K.-W. (2009). Photoreceptors: Physiology. In L. R. Squire (Ed.), *Encyclopedia of Neuroscience* (pp. 677–686). Academic Press. https://doi.org/10.1016/B978-008045046-9.00913-X

Mandai, M., Fujii, M., Hashiguchi, T., Sunagawa, G. A., Ito, S., Sun, J., Kaneko, J., Sho, J., Yamada, C., & Takahashi, M. (2017). IPSC-Derived Retina Transplants Improve Vision in rd1 End-Stage Retinal-Degeneration Mice. *Stem Cell Reports*, *8*(1), 69–83. https://doi.org/10.1016/j.stemcr.2016.12.008

Marlhens, F., Bareil, C., Griffoin, J.-M., Zrenner, E., Amalric, P., Eliaou, C., Liu, S.-Y., Harris, E., Redmond, T. M., Arnaud, B., Claustres, M., & Hamel, C. P. (1997). Mutations in RPE65 cause Leber's congenital amaurosis. *Nature Genetics*, *17*(2), 139–141. https://doi.org/10.1038/ng1097-139

Martinez-Morales, J. R., & Wittbrodt, J. (2009). Shaping the vertebrate eye. *Current Opinion in Genetics & Development*, *19*(5), 511–517. https://doi.org/10.1016/j.gde.2009.08.003

Matthias, R., Afrim, B., Florian, F., & Paul G, L. (2018). Reconstructing Mammalian Retinal Tissue: Wnt3a Regulates Laminar Polarity in Retinal Spheroids from Neonatal Mongolian Rats, while

RPE Promotes Cell Differentiation. *International Journal of Stem Cell Research & Therapy*, *5*(1). https://doi.org/10.23937/2469-570X/1410051

McClements, M. E., Staurenghi, F., MacLaren, R. E., & Cehajic-Kapetanovic, J. (2020). Optogenetic Gene Therapy for the Degenerate Retina: Recent Advances. *Frontiers in Neuroscience*, *0*. https://doi.org/10.3389/fnins.2020.570909

McCracken, K. W., Catá, E. M., Crawford, C. M., Sinagoga, K. L., Schumacher, M., Rockich, B. E., Tsai, Y.-H., Mayhew, C. N., Spence, J. R., Zavros, Y., & Wells, J. M. (2014). Modelling human development and disease in pluripotent stem-cell-derived gastric organoids. *Nature*, *516*(7531), 400–404. https://doi.org/10.1038/nature13863

McGinnis, J. F., Stepanik, P. L., Chen, W., Elias, R., Cao, W., & Lerious, V. (1999). Unique retina cell phenotypes revealed by immunological analysis of recoverin expression in rat retina cells. *Journal of Neuroscience Research*, *55*(2), 252–260. https://doi.org/10.1002/(SICI)1097-4547(19990115)55:2<252::AID-JNR13>3.0.CO;2-N

McKay, J. S., Steele, S. J., Ahmed, G., Johnson, E., & Ratcliffe, K. (2009). An antibody panel for immunohistochemical analysis of the retina in Davidson's-fixed, paraffin-embedded eyes of rats. *Experimental and Toxicologic Pathology*, *61*(2), 91–100. https://doi.org/10.1016/j.etp.2008.06.005

McNerney, C., & Johnston, R. J. (2021). Thyroid hormone signaling specifies cone photoreceptor subtypes during eye development: Insights from model organisms and human stem cell-derived retinal organoids. *Vitamins and Hormones*, *116*, 51–90. https://doi.org/10.1016/bs.vh.2021.03.001

Meek, S., Wei, J., Sutherland, L., Nilges, B., Buehr, M., Tomlinson, S. R., Thomson, A. J., & Burdon, T. (2013). Tuning of β-catenin activity is required to stabilize self-renewal of rat embryonic stem cells. *Stem Cells*, *31*(10), 2104–2115. https://doi.org/10.1002/stem.1466

Meinhardt, A., Eberle, D., Tazaki, A., Ranga, A., Niesche, M., Wilsch-Bräuninger, M., Stec, A., Schackert, G., Lutolf, M., & Tanaka, E. M. (2014). 3D Reconstitution of the Patterned Neural Tube from Embryonic Stem Cells. *Stem Cell Reports*, *3*(6), 987–999. https://doi.org/10.1016/j.stemcr.2014.09.020

Melguizo-Sanchis, D., Xu, Y., Taheem, D., Yu, M., Tilgner, K., Barta, T., Gassner, K., Anyfantis, G., Wan, T., Elango, R., Alharthi, S., El-Harouni, A. A., Przyborski, S., Adam, S., Saretzki, G., Samarasinghe, S., Armstrong, L., & Lako, M. (2018). IPSC modeling of severe aplastic anemia reveals impaired differentiation and telomere shortening in blood progenitors. *Cell Death & Disease*, *9*(2), 1–16. https://doi.org/10.1038/s41419-017-0141-1

Mellough, C. B., Bauer, R., Collin, J., Dorgau, B., Zerti, D., Dolan, D. W. P., Jones, C. M., Izuogu, O. G., Yu, M., Hallam, D., Steyn, J. S., White, K., Steel, D. H., Santibanez-Koref, M., Elliott, D. J., Jackson, M. S., Lindsay, S., Grellscheid, S., & Lako, M. (2019). An integrated transcriptional analysis of the developing human retina. *Development*, *146*(2), dev169474. https://doi.org/10.1242/dev.169474

Mellough, C. B., Collin, J., Khazim, M., White, K., Sernagor, E., Steel, D. H. W., & Lako, M. (2015). IGF-1 Signaling Plays an Important Role in the Formation of Three-Dimensional Laminated Neural Retina and Other Ocular Structures From Human Embryonic Stem Cells. *STEM CELLS*, *33*(8), 2416–2430. https://doi.org/10.1002/stem.2023

Mellough, C. B., Collin, J., Queen, R., Hilgen, G., Dorgau, B., Zerti, D., Felemban, M., White, K., Sernagor, E., & Lako, M. (2019). Systematic Comparison of Retinal Organoid Differentiation from Human Pluripotent Stem Cells Reveals Stage Specific, Cell Line, and Methodological Differences. *STEM CELLS Translational Medicine*. https://doi.org/10.1002/sctm.18-0267

Mellough, C. B., Sernagor, E., Moreno-Gimeno, I., Steel, D. H. W., & Lako, M. (2012). Efficient Stage-Specific Differentiation of Human Pluripotent Stem Cells Toward Retinal Photoreceptor Cells. *STEM CELLS*, *30*(4), 673–686. https://doi.org/10.1002/stem.1037

Merkl, C., Saalfrank, A., Riesen, N., Kühn, R., Pertek, A., Eser, S., Hardt, M. S., Kind, A., Saur, D., Wurst, W., Iglesias, A., & Schnieke, A. (2013). Efficient Generation of Rat Induced Pluripotent Stem Cells Using a Non-Viral Inducible Vector. *PLOS ONE*, *8*(1), e55170. https://doi.org/10.1371/journal.pone.0055170

Mestas, J., & Hughes, C. C. W. (2004). Of Mice and Not Men: Differences between Mouse and Human Immunology. *The Journal of Immunology*, *172*(5), 2731–2738. https://doi.org/10.4049/jimmunol.172.5.2731

Meyer, J. S., Howden, S. E., Wallace, K. A., Verhoeven, A. D., Wright, L. S., Capowski, E. E., Pinilla, I., Martin, J. M., Tian, S., Stewart, R., Pattnaik, B., Thomson, J. A., & Gamm, D. M. (2011). Optic Vesicle-like Structures Derived from Human Pluripotent Stem Cells Facilitate a Customized Approach to Retinal Disease Treatment. *STEM CELLS*, *29*(8), 1206–1218. https://doi.org/10.1002/stem.674

Meyer, J. S., Shearer, R. L., Capowski, E. E., Wright, L. S., Wallace, K. A., McMillan, E. L., Zhang, S.-C., & Gamm, D. M. (2009). Modeling early retinal development with human embryonic and induced pluripotent stem cells. *Proceedings of the National Academy of Sciences*, *106*(39), 16698–16703. https://doi.org/10.1073/pnas.0905245106

Mills, E. A., & Goldman, D. (2017). The Regulation of Notch Signaling in Retinal Development and Regeneration. *Current Pathobiology Reports*, *5*(4), 323–331. https://doi.org/10.1007/s40139-017-0153-7

Miraldi Utz, V., Coussa, R. G., Antaki, F., & Traboulsi, E. I. (2018). Gene therapy for RPE65-related retinal disease. *Ophthalmic Genetics*, *39*(6), 671–677. https://doi.org/10.1080/13816810.2018.1533027

Mitalipov, S., Kuo, H.-C., Byrne, J., Clepper, L., Meisner, L., Johnson, J., Zeier, R., & Wolf, D. (2006). Isolation and Characterization of Novel Rhesus Monkey Embryonic Stem Cell Lines. *STEM CELLS*, *24*(10), 2177–2186. https://doi.org/10.1634/stemcells.2006-0125

Morgan, J. L., Schubert, T., & Wong, R. O. (2008). Developmental patterning of glutamatergic

synapses onto retinal ganglion cells. *Neural Development*, *3*(1), 8.

https://doi.org/10.1186/1749-8104-3-8

Moshiri, A., Chen, R., Kim, S., Harris, R. A., Li, Y., Raveendran, M., Davis, S., Liang, Q., Pomerantz, O.,

Wang, J., Garzel, L., Cameron, A., Yiu, G., Stout, J. T., Huang, Y., Murphy, C. J., Roberts, J.,

Gopalakrishna, K. N., Boyd, K., … Thomasy, S. M. (2019). A nonhuman primate model of

inherited retinal disease. *The Journal of Clinical Investigation*, *129*(2), 863–874.

https://doi.org/10.1172/JCI123980

Muranishi, Y., Terada, K., & Furukawa, T. (2012). An essential role for Rax in retina and

neuroendocrine system development. *Development, Growth & Differentiation*, *54*(3), 341–

348. https://doi.org/10.1111/j.1440-169X.2012.01337.x

Murray, S. A., Morgan, J. L., Kane, C., Sharma, Y., Heffner, C. S., Lake, J., & Donahue, L. R. (2010).

Mouse Gestation Length Is Genetically Determined. *PLoS ONE*, *5*(8).

https://doi.org/10.1371/journal.pone.0012418

Nakano, T., Ando, S., Takata, N., Kawada, M., Muguruma, K., Sekiguchi, K., Saito, K., Yonemura, S.,

Eiraku, M., & Sasai, Y. (2012). Self-Formation of Optic Cups and Storable Stratified Neural

Retina from Human ESCs. *Cell Stem Cell*, *10*(6), 771–785.

https://doi.org/10.1016/j.stem.2012.05.009

Nasir-Ahmad, S., Lee, S. C. S., Martin, P. R., & Grünert, U. (2021). Identification of retinal ganglion cell

types expressing the transcription factor Satb2 in three primate species. *Journal of

Comparative Neurology*, *529*(10), 2727–2749. https://doi.org/10.1002/cne.25120

Nasu, M., Takata, N., Danjo, T., Sakaguchi, H., Kadoshima, T., Futaki, S., Sekiguchi, K., Eiraku, M., &

Sasai, Y. (2012). Robust Formation and Maintenance of Continuous Stratified Cortical

Neuroepithelium by Laminin-Containing Matrix in Mouse ES Cell Culture. *PLOS ONE*, *7*(12),

e53024. https://doi.org/10.1371/journal.pone.0053024

Neugebauer, K. M., Emmett, C. J., Venstrom, K. A., & Reichardt, L. F. (1991). Vitronectin and

thrombospondin promote retinal neurite outgrowth: Developmental regulation and role of

integrins. *Neuron*, *6*(3), 345–358. https://doi.org/10.1016/0896-6273(91)90244-T

Ng, L., Ma, M., Curran, T., & Forrest, D. (2009). Developmental expression of thyroid hormone

receptor β2 protein in cone photoreceptors in the mouse. *Neuroreport*, *20*(6), 627–631.

https://doi.org/10.1097/WNR.0b013e32832a2c63

Nichols, J., & Smith, A. (2009). Naive and Primed Pluripotent States. *Cell Stem Cell*, *4*(6), 487–492.

https://doi.org/10.1016/j.stem.2009.05.015

Nichols, J., Zevnik, B., Anastassiadis, K., Niwa, H., Klewe-Nebenius, D., Chambers, I., Schöler, H., &

Smith, A. (1998). Formation of pluripotent stem cells in the mammalian embryo depends on

the POU transcription factor Oct4. *Cell*, *95*(3), 379–391. https://doi.org/10.1016/s0092-

8674(00)81769-9

Nowak, J. Z. (2006). Age-related macular degeneration (AMD): Pathogenesis and therapy.

Pharmacological Reports : PR, *58*(3), 353–363.

Ohkubo, Y., Chiang, C., & Rubenstein, J. L. R. (2002). Coordinate regulation and synergistic actions of

BMP4, SHH and FGF8 in the rostral prosencephalon regulate morphogenesis of the

telencephalic and optic vesicles. *Neuroscience*, *111*(1), 1–17. https://doi.org/10.1016/S0306-

4522(01)00616-9

Oku, H., Ikeda, T., Honma, Y., Sotozono, C., Nishida, K., Nakamura, Y., Kida, T., & Kinoshita, S. (2002).

Gene Expression of Neurotrophins and Their High-Affinity Trk Receptors in Cultured Human

Müller Cells. *Ophthalmic Research*, *34*(1), 38–42. https://doi.org/10.1159/000048323

Olney, J. W. (1968). An Electron Microscopic Study of Synapse Formation, Receptor Outer Segment

Development, and other Aspects of Developing Mouse Retina. *Investigative Ophthalmology

& Visual Science*, *7*(3), 250–268.

Ortega, J. A., Sirois, C. L., Memi, F., Glidden, N., & Zecevic, N. (2017). Oxygen Levels Regulate the

Development of Human Cortical Radial Glia Cells. *Cerebral Cortex (New York, NY)*, *27*(7),

3736–3751. https://doi.org/10.1093/cercor/bhw194

Osafune, K., Caron, L., Borowiak, M., Martinez, R. J., Fitz-Gerald, C. S., Sato, Y., Cowan, C. A., Chien, K.

R., & Melton, D. A. (2008). Marked differences in differentiation propensity among human

embryonic stem cell lines. *Nature Biotechnology*, *26*(3), Article 3.

https://doi.org/10.1038/nbt1383

Osakada, F., Ikeda, H., Mandai, M., Wataya, T., Watanabe, K., Yoshimura, N., Akaike, A., Sasai, Y., &

Takahashi, M. (2008). Toward the generation of rod and cone photoreceptors from mouse,

monkey and human embryonic stem cells. *Nature Biotechnology*, *26*(2), 215–224.

https://doi.org/10.1038/nbt1384

Osakada, F., Jin, Z.-B., Hirami, Y., Ikeda, H., Danjyo, T., Watanabe, K., Sasai, Y., & Takahashi, M.

(2009). In vitro differentiation of retinal cells from human pluripotent stem cells by small-

molecule induction. *Journal of Cell Science*, *122*(17), 3169–3179.

https://doi.org/10.1242/jcs.050393

Otani, T., Marchetto, M. C., Gage, F. H., Simons, B. D., & Livesey, F. J. (2016). 2D and 3D Stem Cell

Models of Primate Cortical Development Identify Species-Specific Differences in Progenitor

Behavior Contributing to Brain Size. *Cell Stem Cell*, *18*(4), 467–480.

https://doi.org/10.1016/j.stem.2016.03.003

Palczewski, K. (2006). G Protein–Coupled Receptor Rhodopsin. *Annual Review of Biochemistry*, *75*,

743–767. https://doi.org/10.1146/annurev.biochem.75.103004.142743

Parfitt, D. A., Lane, A., Ramsden, C., Jovanovic, K., Coffey, P. J., Hardcastle, A. J., & Cheetham, M. E.

(2016). Using induced pluripotent stems cells to understand retinal ciliopathy disease

mechanisms and develop therapies. *Biochemical Society Transactions*, *44*(5), 1245–1251.

https://doi.org/10.1042/BST20160156

Pearson, R. A., Barber, A. C., Rizzi, M., Hippert, C., Xue, T., West, E. L., Duran, Y., Smith, A. J., Chuang, J. Z., Azam, S. A., Luhmann, U. F. O., Benucci, A., Sung, C. H., Bainbridge, J. W., Carandini, M., Yau, K.-W., Sowden, J. C., & Ali, R. R. (2012). Restoration of vision after transplantation of photoreceptors. *Nature*, *485*(7396), 99–103. https://doi.org/10.1038/nature10997

Pearson, R. A., Gonzalez-Cordero, A., West, E. L., Ribeiro, J. R., Aghaizu, N., Goh, D., Sampson, R. D., Georgiadis, A., Waldron, P. V., Duran, Y., Naeem, A., Kloc, M., Cristante, E., Kruczek, K., Warre-Cornish, K., Sowden, J. C., Smith, A. J., & Ali, R. R. (2016). Donor and host photoreceptors engage in material transfer following transplantation of post-mitotic photoreceptor precursors. *Nature Communications*, *7*(1), 13029. https://doi.org/10.1038/ncomms13029

Pellissier, L. P., Quinn, P. M., Alves, C. H., Vos, R. M., Klooster, J., Flannery, J. G., Heimel, J. A., & Wijnholds, J. (2015). Gene therapy into photoreceptors and Müller glial cells restores retinal structure and function in CRB1 retinitis pigmentosa mouse models. *Human Molecular Genetics*, *24*(11), 3104–3118. https://doi.org/10.1093/hmg/ddv062

Penha, F. M., Rodrigues, E. B., Maia, M., Furlani, B. A., Regatieri, C., Melo, G. B., Octaviano Magalhães, J., Manzano, R., & Farah, M. E. (2010). Retinal and Ocular Toxicity in Ocular Application of Drugs and Chemicals – Part II: Retinal Toxicity of Current and New Drugs. *Ophthalmic Research*, *44*(4), 205–224. https://doi.org/10.1159/000316695

Pérez de Sevilla Müller, L., Azar, S. S., de los Santos, J., & Brecha, N. C. (2017). Prox1 Is a Marker for AII Amacrine Cells in the Mouse Retina. *Frontiers in Neuroanatomy*, *11*. https://doi.org/10.3389/fnana.2017.00039

Perry, V. H., & Walker, M. (1980). Morphology of cells in the ganglion cell layer during development of the rat retina. *Proceedings of the Royal Society of London. Series B, Biological Sciences*, *208*(1173), 433–445. https://doi.org/10.1098/rspb.1980.0061

Picaud, S., Dalkara, D., Marazova, K., Goureau, O., Roska, B., & Sahel, J.-A. (2019). The primate model for understanding and restoring vision. *Proceedings of the National Academy of Sciences*, *116*(52), 26280–26287. https://doi.org/10.1073/pnas.1902292116

Pinzón-Duarte, G., Kohler, K., Arango-González, B., & Guenther, E. (2000). Cell differentiation, synaptogenesis, and influence of the retinal pigment epithelium in a rat neonatal organotypic retina culture. *Vision Research*, *40*(25), 3455–3465. https://doi.org/10.1016/S0042-6989(00)00185-1

Qin, D., Li, W., Zhang, J., & Pei, D. (2007). Direct generation of ES-like cells from unmodified mouse embryonic fibroblasts by Oct4/Sox2/Myc/Klf4. *Cell Research*, *17*(11), 959–962. https://doi.org/10.1038/cr.2007.92

Qu, Z., Guan, Y., Cui, L., Song, J., Gu, J., Zhao, H., Xu, L., Lu, L., Jin, Y., & Xu, G.-T. (2015). Transplantation of rat embryonic stem cell-derived retinal progenitor cells preserves the retinal structure and function in rat retinal degeneration. *Stem Cell Research & Therapy*, *6*(1), 219. https://doi.org/10.1186/s13287-015-0207-x

Raedler, A., & Sievers, J. (1975). The development of the visual system of the albino rat. *Advances in Anatomy, Embryology, and Cell Biology*, *50*(3), 3–88.

Rapaport, D. H., Rakic, P., Yasamura, D., & LaVail, M. M. (1995). Genesis of the retinal pigment epithelium in the macaque monkey. *Journal of Comparative Neurology*, *363*(3), 359–376. https://doi.org/10.1002/cne.903630303

Rapaport, D. H., Wong, L. L., Wood, E. D., Yasumura, D., & LaVail, M. M. (2004). Timing and topography of cell genesis in the rat retina. *Journal of Comparative Neurology*, *474*(2), 304–324. https://doi.org/10.1002/cne.20134

Rayon, T., & Briscoe, J. (2021). Cross-species comparisons and *in vitro* models to study tempo in development and homeostasis. *Interface Focus*, *11*(3), rsfs.2020.0069, 20200069. https://doi.org/10.1098/rsfs.2020.0069

Redmond, T. M., Yu, S., Lee, E., Bok, D., Hamasaki, D., Chen, N., Goletz, P., Ma, J.-X., Crouch, R. K., &

Pfeifer, K. (1998). Rpe65 is necessary for production of 11- cis -vitamin A in the retinal visual

cycle. *Nature Genetics*, *20*(4), 344–351. https://doi.org/10.1038/3813

Regent, F., Chen, H. Y., Kelley, R. A., Qu, Z., Swaroop, A., & Li, T. (2020). A simple and efficient

method for generating human retinal organoids. *Molecular Vision*, *26*, 97–105.

Reichenbach, A., & Bringmann, A. (2013). New functions of Müller cells. *Glia*, *61*(5), 651–678.

https://doi.org/10.1002/glia.22477

Remington, L. A. (2012). Chapter 4—Retina. In L. A. Remington (Ed.), *Clinical Anatomy and

Physiology of the Visual System (Third Edition)* (pp. 61–92). Butterworth-Heinemann.

https://doi.org/10.1016/B978-1-4377-1926-0.10004-9

Ripps, H., & Shen, W. (2012). Review: Taurine: A "very essential" amino acid. *Molecular Vision*, *18*,

2673–2686.

Rochefort, N. L., Garaschuk, O., Milos, R.-I., Narushima, M., Marandi, N., Pichler, B., Kovalchuk, Y., &

Konnerth, A. (2009). Sparsification of neuronal activity in the visual cortex at eye-opening.

Proceedings of the National Academy of Sciences, *106*(35), 15049–15054.

https://doi.org/10.1073/pnas.0907660106

Rodrigues, M., Waldbillig, R. J., Rajagopalan, S., Hackett, J., LeRoith, D., & Chader, G. J. (1988).

Retinal insulin receptors: Localization using a polyclonal anti-insulin receptor antibody. *Brain

Research*, *443*(1), 389–394. https://doi.org/10.1016/0006-8993(88)91639-3

Rodrigues, M., Xin, X., Jee, K., Babapoor-Farrokhran, S., Kashiwabuchi, F., Ma, T., Bhutto, I., Hassan,

S. J., Daoud, Y., Baranano, D., Solomon, S., Lutty, G., Semenza, G. L., Montaner, S., & Sodhi,

A. (2013). VEGF Secreted by Hypoxic Müller Cells Induces MMP-2 Expression and Activity in

Endothelial Cells to Promote Retinal Neovascularization in Proliferative Diabetic

Retinopathy. *Diabetes*, *62*(11), 3863–3873. https://doi.org/10.2337/db13-0014

Rodriguez, A. R., Müller, L. P. de S., & Brecha, N. C. (2014). The RNA binding protein RBPMS is a

    selective marker of ganglion cells in the mammalian retina. *Journal of Comparative*

    Neurology, *522*(6), 1411–1443. https://doi.org/10.1002/cne.23521

Roost, M. S., Slieker, R. C., Bialecka, M., van Iperen, L., Gomes Fernandes, M. M., He, N., Suchiman,

    H. E. D., Szuhai, K., Carlotti, F., de Koning, E. J. P., Mummery, C. L., Heijmans, B. T., & Chuva

    de Sousa Lopes, S. M. (2017). DNA methylation and transcriptional trajectories during

    human development and reprogramming of isogenic pluripotent stem cells. *Nature*

    Communications, *8*(1), 908. https://doi.org/10.1038/s41467-017-01077-3

Rosenfeld, P. J., Rich, R. M., & Lalwani, G. A. (2006). Ranibizumab: Phase III clinical trial results.

    Ophthalmology Clinics of North America, *19*(3), 361–372.

    https://doi.org/10.1016/j.ohc.2006.05.009

Rouwkema, J., Koopman, B. F. J. M., Blitterswijk, C. A. V., Dhert, W. J. A., & Malda, J. (2009). Supply

    of Nutrients to Cells in Engineered Tissues. *Biotechnology and Genetic Engineering Reviews*,

    26(1), 163–178. https://doi.org/10.5661/bger-26-163

Sahel, J.-A., Boulanger-Scemama, E., Pagot, C., Arleo, A., Galluppi, F., Martel, J. N., Esposti, S. D.,

    Delaux, A., de Saint Aubert, J.-B., de Montleau, C., Gutman, E., Audo, I., Duebel, J., Picaud, S.,

    Dalkara, D., Blouin, L., Taiel, M., & Roska, B. (2021). Partial recovery of visual function in a

    blind patient after optogenetic therapy. *Nature Medicine*, *27*(7), 1223–1229.

    https://doi.org/10.1038/s41591-021-01351-4

Samson, M., Emerson, M. M., & Cepko, C. L. (2009). Robust Marking of Photoreceptor Cells and

    Pinealocytes with Several Reporters under Control of the Crx Gene. *Developmental*

    Dynamics : An Official Publication of the American Association of Anatomists, *238*(12), 3218–

    3225. https://doi.org/10.1002/dvdy.22138

Santos, A., Humayun, M. S., de Juan, E., Jr, Greenburg, R. J., Marsh, M. J., Klock, I. B., & Milam, A. H.

    (1997). Preservation of the Inner Retina in Retinitis Pigmentosa: A Morphometric Analysis.

Archives of Ophthalmology, *115*(4), 511–515.

https://doi.org/10.1001/archopht.1997.01100150513011

Sasai, Y., Eiraku, M., & Suga, H. (2012). In vitro organogenesis in three dimensions: Self-organising

stem cells. *Development*, *139*(22), 4111–4121. https://doi.org/10.1242/dev.079590

Schnichels, S., Kiebler, T., Hurst, J., Maliha, A. M., Löscher, M., Dick, H. B., Bartz-Schmidt, K.-U., &

Joachim, S. C. (2019). Retinal Organ Cultures as Alternative Research Models: *Alternatives to

Laboratory Animals*. https://doi.org/10.1177/0261192919840092

Sefton, A. J., Dreher, B., Harvey, A. R., & Martin, P. R. (2015). Chapter 30—Visual System. In G.

Paxinos (Ed.), *The Rat Nervous System (Fourth Edition)* (pp. 947–983). Academic Press.

https://doi.org/10.1016/B978-0-12-374245-2.00030-9

Sernagor, E., Eglen, S. J., & Wong, R. O. L. (2001). Development of Retinal Ganglion Cell Structure and

Function. *Progress in Retinal and Eye Research*, *20*(2), 139–174.

https://doi.org/10.1016/S1350-9462(00)00024-0

Sevilla-Romero, E., Muñoz, A., & Pinazo-Durán, M. D. (2002). Low Thyroid Hormone Levels Impair

the Perinatal Development of the Rat Retina. *Ophthalmic Research*, *34*(4), 181–191.

https://doi.org/10.1159/000063885

Shamir, E. R., & Ewald, A. J. (2014). Three-dimensional organotypic culture: Experimental models of

mammalian biology and disease. *Nature Reviews Molecular Cell Biology*, *15*(10), 647–664.

https://doi.org/10.1038/nrm3873

Shanks, M. E., Downes, S. M., Copley, R. R., Lise, S., Broxholme, J., Hudspith, K. A., Kwasniewska, A.,

Davies, W. I., Hankins, M. W., Packham, E. R., Clouston, P., Seller, A., Wilkie, A. O., Taylor, J.

C., Ragoussis, J., & Németh, A. H. (2013). Next-generation sequencing (NGS) as a diagnostic

tool for retinal degeneration reveals a much higher detection rate in early-onset disease.

European Journal of Human Genetics, *21*(3), 274–280.

https://doi.org/10.1038/ejhg.2012.172

Sharma, R. K., O'Leary, T. E., Fields, C. M., & Johnson, D. A. (2003). Development of the outer retina

in the mouse. *Developmental Brain Research*, *145*(1), 93–105.

https://doi.org/10.1016/S0165-3806(03)00217-7

Shattuck, M. R., Satkoski-Trask, J., Deinard, A., Tito, R. Y., Smith, D. G., Melnick, D. J., & Malhi, R. S.

(2014). Patterns of genetic variation and the role of selection in HTR1A and HTR1B in

macaques (Macaca). *BMC Genetics*, *15*(1), 116. https://doi.org/10.1186/s12863-014-0116-5

Shaw, P. X., Stiles, T., Douglas, C., Ho, D., Fan, W., Du, H., & Xiao, X. (2016). Oxidative stress, innate

immunity, and age-related macular degeneration. *AIMS Molecular Science*, *3*(2), 196–221.

https://doi.org/10.3934/molsci.2016.2.196

Sheedlo, H. J., & Turner, J. E. (1996a). Influence of a retinal pigment epithelial cell factor(s) on rat

retinal progenitor cells. *Developmental Brain Research*, *93*(1), 88–99.

https://doi.org/10.1016/0165-3806(96)00008-9

Sheedlo, H. J., & Turner, J. E. (1996b). Influence of a retinal pigment epithelial cell factor(s) on rat

retinal progenitor cells. *Developmental Brain Research*, *93*(1), 88–99.

https://doi.org/10.1016/0165-3806(96)00008-9

Shibata, S., Hayashi, R., Okubo, T., Kudo, Y., Katayama, T., Ishikawa, Y., Toga, J., Yagi, E., Honma, Y.,

Quantock, A. J., Sekiguchi, K., & Nishida, K. (2018). Selective Laminin-Directed Differentiation

of Human Induced Pluripotent Stem Cells into Distinct Ocular Lineages. *Cell Reports*, *25*(6),

1668-1679.e5. https://doi.org/10.1016/j.celrep.2018.10.032

Shimozawa, N. (2016). Cynomolgus Monkey Induced Pluripotent Stem Cells Generated By Using

Allogeneic Genes. In K. Turksen & A. Nagy (Eds.), *Induced Pluripotent Stem (iPS) Cells:*

Methods and Protocols (pp. 173–182). Springer New York.

https://doi.org/10.1007/7651_2014_137

Sieving, P. A., Caruso, R. C., Tao, W., Coleman, H. R., Thompson, D. J. S., Fullmer, K. R., & Bush, R. A.

(2006). Ciliary neurotrophic factor (CNTF) for human retinal degeneration: Phase I trial of

CNTF delivered by encapsulated cell intraocular implants. *Proceedings of the National Academy of Sciences of the United States of America*, *103*(10), 3896–3901. https://doi.org/10.1073/pnas.0600236103

Silk, J., Short, J., Roberts, J., & Kusnitz, J. (1993). Gestation length in rhesus macaques (Macaca mulatta). *International Journal of Primatology*, *14*(1), 95–104. https://doi.org/10.1007/BF02196505

Silverman, S. M., & Wong, W. T. (2018). Microglia in the Retina: Roles in Development, Maturity, and Disease. *Annual Review of Vision Science*, *4*(1), 45–77. https://doi.org/10.1146/annurev-vision-091517-034425

Simionato, E., Ledent, V., Richards, G., Thomas-Chollier, M., Kerner, P., Coornaert, D., Degnan, B. M., & Vervoort, M. (2007). Origin and diversification of the basic helix-loop-helix gene family in metazoans: Insights from comparative genomics. *BMC Evolutionary Biology*, *7*(1), 33. https://doi.org/10.1186/1471-2148-7-33

Singh, D., Wang, S.-B., Xia, T., Tainsh, L., Ghiassi-Nejad, M., Xu, T., Peng, S., Adelman, R. A., & Rizzolo, L. J. (2018). A biodegradable scaffold enhances differentiation of embryonic stem cells into a thick sheet of retinal cells. *Biomaterials*, *154*, 158–168. https://doi.org/10.1016/j.biomaterials.2017.10.052

Singh, R. K., Winkler, P. A., Binette, F., Petersen-Jones, S. M., & Nasonkin, I. O. (2021). Comparison of Developmental Dynamics in Human Fetal Retina and Human Pluripotent Stem Cell-Derived Retinal Tissue. *Stem Cells and Development*, *30*(8), 399–417. https://doi.org/10.1089/scd.2020.0085

Smith, A. G., Heath, J. K., Donaldson, D. D., Wong, G. G., Moreau, J., Stahl, M., & Rogers, D. (1988). Inhibition of pluripotential embryonic stem cell differentiation by purified polypeptides. *Nature*, *336*(6200), 688. https://doi.org/10.1038/336688a0

Sorrentino, F. S., Allkabes, M., Salsini, G., Bonifazzi, C., & Perri, P. (2016). The importance of glial cells in the homeostasis of the retinal microenvironment and their pivotal role in the course of diabetic retinopathy. *Life Sciences*, *162*, 54–59. https://doi.org/10.1016/j.lfs.2016.08.001

Soto, I., Oglesby, E., Buckingham, B. P., Son, J. L., Roberson, E. D. O., Steele, M. R., Inman, D. M., Vetter, M. L., Horner, P. J., & Marsh-Armstrong, N. (2008). Retinal Ganglion Cells Downregulate Gene Expression and Lose Their Axons within the Optic Nerve Head in a Mouse Glaucoma Model. *Journal of Neuroscience*, *28*(2), 548–561. https://doi.org/10.1523/JNEUROSCI.3714-07.2008

Sridhar, A., Hoshino, A., Finkbeiner, C. R., Chitsazan, A., Dai, L., Haugan, A. K., Eschenbacher, K. M., Jackson, D. L., Trapnell, C., Bermingham-McDonogh, O., Glass, I., & Reh, T. A. (2020). Single-Cell Transcriptomic Comparison of Human Fetal Retina, hPSC-Derived Retinal Organoids, and Long-Term Retinal Cultures. *Cell Reports*, *30*(5), 1644-1659.e4. https://doi.org/10.1016/j.celrep.2020.01.007

Steinmetz, J. D., Bourne, R. R. A., Briant, P. S., Flaxman, S. R., Taylor, H. R. B., Jonas, J. B., Abdoli, A. A., Abrha, W. A., Abualhasan, A., Abu-Gharbieh, E. G., Adal, T. G., Afshin, A., Ahmadieh, H., Alemayehu, W., Alemzadeh, S. A. S., Alfaar, A. S., Alipour, V., Androudi, S., Arabloo, J., … Vos, T. (2021). Causes of blindness and vision impairment in 2020 and trends over 30 years, and prevalence of avoidable blindness in relation to VISION 2020: The Right to Sight: an analysis for the Global Burden of Disease Study. *The Lancet Global Health*, *9*(2), e144–e160. https://doi.org/10.1016/S2214-109X(20)30489-7

Stevens, G. A., White, R. A., Flaxman, S. R., Price, H., Jonas, J. B., Keeffe, J., Leasher, J., Naidoo, K., Pesudovs, K., Resnikoff, S., Taylor, H., & Bourne, R. R. A. (2013). Global Prevalence of Vision Impairment and Blindness: Magnitude and Temporal Trends, 1990–2010. *Ophthalmology*, *120*(12), 2377–2384. https://doi.org/10.1016/j.ophtha.2013.05.025

Stevens, L. C. (1970). The development of transplantable teratocarcinomas from intratesticular

grafts of pre- and postimplantation mouse embryos. *Developmental Biology*, *21*(3), 364–382.

https://doi.org/10.1016/0012-1606(70)90130-2

Stone, J., Itin, A., Alon, T., Pe'er, J., Gnessin, H., Chan-Ling, T., & Keshet, E. (1995). Development of

retinal vasculature is mediated by hypoxia-induced vascular endothelial growth factor

(VEGF) expression by neuroglia. *Journal of Neuroscience*, *15*(7), 4738–4747.

https://doi.org/10.1523/JNEUROSCI.15-07-04738.1995

Streilein, J. W. (2003). Ocular immune privilege: Therapeutic opportunities from an experiment of

nature. *Nature Reviews Immunology*, *3*(11), Article 11. https://doi.org/10.1038/nri1224

Subirada, P. V., Paz, M. C., Ridano, M. E., Lorenc, V. E., Vaglienti, M. V., Barcelona, P. F., Luna, J. D., &

Sánchez, M. C. (2018). A journey into the retina: Müller glia commanding survival and death.

European Journal of Neuroscience, *47*(12), 1429–1443. https://doi.org/10.1111/ejn.13965

Sung, C.-H., & Chuang, J.-Z. (2010). The cell biology of vision. *The Journal of Cell Biology*, *190*(6), 953–

963. https://doi.org/10.1083/jcb.201006020

Szél, Á., Röhlich, P., Caffé, A. R., & van Veen, T. (1996). Distribution of cone photoreceptors in the

mammalian retina. *Microscopy Research and Technique*, *35*(6), 445–462.

https://doi.org/10.1002/(SICI)1097-0029(19961215)35:6<445::AID-JEMT4>3.0.CO;2-H

Takahashi, K., & Yamanaka, S. (2006). Induction of Pluripotent Stem Cells from Mouse Embryonic

and Adult Fibroblast Cultures by Defined Factors. *Cell*, *126*(4), 663–676.

https://doi.org/10.1016/j.cell.2006.07.024

Takasato, M., Er, P. X., Chiu, H. S., Maier, B., Baillie, G. J., Ferguson, C., Parton, R. G., Wolvetang, E. J.,

Roost, M. S., Chuva de Sousa Lopes, S. M., & Little, M. H. (2015). Kidney organoids from

human iPS cells contain multiple lineages and model human nephrogenesis. *Nature*,

526(7574), 564–568. https://doi.org/10.1038/nature15695

Takebe, T., Sekine, K., Enomura, M., Koike, H., Kimura, M., Ogaeri, T., Zhang, R.-R., Ueno, Y., Zheng,

    Y.-W., Koike, N., Aoyama, S., Adachi, Y., & Taniguchi, H. (2013). Vascularized and functional

    human liver from an iPSC-derived organ bud transplant. *Nature*, *499*(7459), 481–484.

    https://doi.org/10.1038/nature12271

Thomson, J. A., Itskovitz-Eldor, J., Shapiro, S. S., Waknitz, M. A., Swiergiel, J. J., Marshall, V. S., &

    Jones, J. M. (1998). Embryonic Stem Cell Lines Derived from Human Blastocysts. *Science*,

    282(5391), 1145–1147. https://doi.org/10.1126/science.282.5391.1145

Townes-Anderson, E., & Raviola, G. (1981). The formation and distribution of intercellular junctions

    in the rhesus monkey optic cup: The early development of the cilio-iridic and sensory

    retinas. *Developmental Biology*, *85*(1), 209–232. https://doi.org/10.1016/0012-

    1606(81)90252-9

Tsang, S. H., Aycinena, A. R. P., & Sharma, T. (2018). Ciliopathy: Alström Syndrome. In S. H. Tsang &

    T. Sharma (Eds.), *Atlas of Inherited Retinal Diseases* (pp. 179–180). Springer International

    Publishing. https://doi.org/10.1007/978-3-319-95046-4_35

Ueda, K., Onishi, A., Ito, S., Nakamura, M., & Takahashi, M. (2018). Generation of three-dimensional

    retinal organoids expressing rhodopsin and S- and M-cone opsins from mouse stem cells.

    Biochemical and Biophysical Research Communications, *495*(4), 2595–2601.

    https://doi.org/10.1016/j.bbrc.2017.12.092

Vail, M. M. la, Rapaport, D. H., & Rakic, P. (1991). Cytogenesis in the monkey retina. *Journal of

    Comparative Neurology*, *309*(1), 86–114. https://doi.org/10.1002/cne.903090107

van Velthoven, M. E. J., Faber, D. J., Verbraak, F. D., van Leeuwen, T. G., & de Smet, M. D. (2007).

    Recent developments in optical coherence tomography for imaging the retina. *Progress in

    Retinal and Eye Research*, *26*(1), 57–77. https://doi.org/10.1016/j.preteyeres.2006.10.002

Vandenberghe, L. H., & Auricchio, A. (2012). Novel adeno-associated viral vectors for retinal gene

    therapy. *Gene Therapy*, *19*(2), 162–168. https://doi.org/10.1038/gt.2011.151

Verbakel, S. K., van Huet, R. A. C., Boon, C. J. F., den Hollander, A. I., Collin, R. W. J., Klaver, C. C. W.,

    Hoyng, C. B., Roepman, R., & Klevering, B. J. (2018). Non-syndromic retinitis pigmentosa.

    Progress in Retinal and Eye Research, *66*, 157–186.

    https://doi.org/10.1016/j.preteyeres.2018.03.005

Völkner, M., Zschätzsch, M., Rostovskaya, M., Overall, R. W., Busskamp, V., Anastassiadis, K., & Karl,

    M. O. (2016). Retinal Organoids from Pluripotent Stem Cells Efficiently Recapitulate

    Retinogenesis. *Stem Cell Reports*, *6*(4), 525–538.

    https://doi.org/10.1016/j.stemcr.2016.03.001

Voronina, V. A., Kozhemyakina, E. A., O'Kernick, C. M., Kahn, N. D., Wenger, S. L., Linberg, J. V.,

    Schneider, A. S., & Mathers, P. H. (2004). Mutations in the human RAX homeobox gene in a

    patient with anophthalmia and sclerocornea. *Human Molecular Genetics*, *13*(3), 315–322.

    https://doi.org/10.1093/hmg/ddh025

Wagstaff, P. E., ten Asbroek, A. L. M. A., ten Brink, J. B., Jansonius, N. M., & Bergen, A. A. B. (2021).

    An alternative approach to produce versatile retinal organoids with accelerated ganglion cell

    development. *Scientific Reports*, *11*(1), 1101. https://doi.org/10.1038/s41598-020-79651-x

Waldbillig, R. J., Pfeffer, B. A., Schoen, T. J., Adler, A. A., Shen-Orr, Z., Scavo, L., ERoith, D., & Chader,

    G. J. (1991). Evidence for an Insulin-Like Growth Factor Autocrine-Paracrine System in the

    Retinal Photoreceptor-Pigment Epithelial Cell Complex. *Journal of Neurochemistry*, *57*(5),

    1522–1533. https://doi.org/10.1111/j.1471-4159.1991.tb06347.x

Wan, Q.-F., & Heidelberger, R. (2011). Synaptic release at mammalian bipolar cell terminals. *Visual*

    Neuroscience, *28*(1), 109–119. https://doi.org/10.1017/S0952523810000453

Wang, A.-G., Yen, M.-Y., Hsu, W.-M., & Fann, M.-J. (2006). Induction of vitronectin and integrin

    alphav in the retina after optic nerve injury. *Molecular Vision*, *12*, 76–84.

Wang, Y., Dakubo, G. D., Thurig, S., Mazerolle, C. J., & Wallace, V. A. (2005). Retinal ganglion cell-

    derived sonic hedgehog locally controls proliferation and the timing of RGC development in

the embryonic mouse retina. *Development*, *132*(22), 5103–5113.

https://doi.org/10.1242/dev.02096

Wang, Z., Sheng, C., Li, T., Teng, F., Sang, L., Cao, F., Wang, Z., Zhu, W., Li, W., Zhao, X., Liu, Z., Wang,

L., & Zhou, Q. (2012). Generation of Tripotent Neural Progenitor Cells from Rat Embryonic

Stem Cells. *Journal of Genetics and Genomics*, *39*(12), 643–651.

https://doi.org/10.1016/j.jgg.2012.07.013

Warre-Cornish, K., Barber, A. C., Sowden, J. C., Ali, R. R., & Pearson, R. A. (2013). Migration,

Integration and Maturation of Photoreceptor Precursors Following Transplantation in the

Mouse Retina. *Stem Cells and Development*, *23*(9), 941–954.

https://doi.org/10.1089/scd.2013.0471

Watson, C. (2012). Chapter 25—Visual System. In C. Watson, G. Paxinos, & L. Puelles (Eds.), *The*

Mouse Nervous System (pp. 646–652). Academic Press. https://doi.org/10.1016/B978-0-12-

369497-3.10025-1

West, E. L., Pearson, R. A., Barker, S. E., Luhmann, U. F. O., Maclaren, R. E., Barber, A. C., Duran, Y.,

Smith, A. J., Sowden, J. C., & Ali, R. R. (2010). Long-Term Survival of Photoreceptors

Transplanted into the Adult Murine Neural Retina Requires Immune Modulation. *STEM*

CELLS, *28*(11), 1997–2007. https://doi.org/10.1002/stem.520

Wikler, K. C., & Rakić, P. (1990). Distribution of photoreceptor subtypes in the retina of diurnal and

nocturnal primates. *The Journal of Neuroscience : The Official Journal of the Society for*

Neuroscience, *10*(10), 3390–3401. https://doi.org/10.1523/JNEUROSCI.10-10-03390.1990

Wobus, A. M., Guan, K., Yang, H.-T., & Boheler, K. R. (2002). Embryonic Stem Cells as a Model to

Study Cardiac, Skeletal Muscle, and Vascular Smooth Muscle Cell Differentiation. In K.

Turksen (Ed.), *Embryonic Stem Cells: Methods and Protocols* (pp. 127–156). Springer New

York. https://doi.org/10.1385/1-59259-241-4:127

Wobus, A. M., Wallukat, G., & Hescheler, J. (1991). Pluripotent mouse embryonic stem cells are able to differentiate into cardiomyocytes expressing chronotropic responses to adrenergic and cholinergic agents and Ca2+ channel blockers. *Differentiation*, *48*(3), 173–182. https://doi.org/10.1111/j.1432-0436.1991.tb00255.x

Wong, W. L., Su, X., Li, X., Cheung, C. M. G., Klein, R., Cheng, C.-Y., & Wong, T. Y. (2014). Global prevalence of age-related macular degeneration and disease burden projection for 2020 and 2040: A systematic review and meta-analysis. *The Lancet Global Health*, *2*(2), e106–e116. https://doi.org/10.1016/S2214-109X(13)70145-1

Wu, Z., Chen, J., Ren, J., Bao, L., Liao, J., Cui, C., Rao, L., Li, H., Gu, Y., Dai, H., Zhu, H., Teng, X., Cheng, L., & Xiao, L. (2009). Generation of Pig Induced Pluripotent Stem Cells with a Drug-Inducible System. *Journal of Molecular Cell Biology*, *1*(1), 46–54. https://doi.org/10.1093/jmcb/mjp003

Wu, Z., Chen, J., Ren, J., Bao, L., Liao, J., Cui, C., Rao, L., Li, H., Gu, Y., Dai, H., Zhu, H., Teng, X., Cheng, L., & Xiao, L. (2010). Generation of Pig-Induced Pluripotent Stem Cells with a Drug-Inducible System. *Journal of Molecular Cell Biology*, *2*(2), 104–104. https://doi.org/10.1093/jmcb/mjq004

Wunderlich, S., Haase, A., Merkert, S., Beier, J., Schwanke, K., Schambach, A., Glage, S., Göhring, G., Curnow, E. C., & Martin, U. (2012). Induction of Pluripotent Stem Cells from a Cynomolgus Monkey Using a Polycistronic Simian Immunodeficiency Virus–Based Vector, Differentiation Toward Functional Cardiomyocytes, and Generation of Stably Expressing Reporter Lines. *Cellular Reprogramming*, *14*(6), 471–484. https://doi.org/10.1089/cell.2012.0041

Xiang, M. (2013). Intrinsic control of mammalian retinogenesis. *Cellular and Molecular Life Sciences*, *70*(14), 2519–2532. https://doi.org/10.1007/s00018-012-1183-2

Xu, X., Wu, J., Yu, X., Tang, Y., Tang, X., & Shentu, X. (2020). Regional differences in the global burden of age-related macular degeneration. *BMC Public Health*, *20*(1), 410. https://doi.org/10.1186/s12889-020-8445-y

Xue, X., Sun, Y., Resto-Irizarry, A., Yuan, Y., Aw Yong, K. M., Zheng, Y., Weng, S., Shao, Y., Chai, Y., Studer, L., & Fu, J. (2018). Mechanics-guided embryonic patterning of neuroectoderm tissue from human pluripotent stem cells. *Nature Materials*, *17*(7), 633–641. https://doi.org/10.1038/s41563-018-0082-9

Yan, W., Laboulaye, M. A., Tran, N. M., Whitney, I. E., Benhar, I., & Sanes, J. R. (2020). Mouse Retinal Cell Atlas: Molecular Identification of over Sixty Amacrine Cell Types. *Journal of Neuroscience*, *40*(27), 5177–5195. https://doi.org/10.1523/JNEUROSCI.0471-20.2020

Yang, X.-L. (2004). Characterization of receptors for glutamate and GABA in retinal neurons. *Progress in Neurobiology*, *73*(2), 127–150. https://doi.org/10.1016/j.pneurobio.2004.04.002

Yau, K.-W., & Hardie, R. C. (2009). Phototransduction Motifs and Variations. *Cell*, *139*(2), 246–264. https://doi.org/10.1016/j.cell.2009.09.029

Ying, Q.-L., Wray, J., Nichols, J., Batlle-Morera, L., Doble, B., Woodgett, J., Cohen, P., & Smith, A. (2008). The ground state of embryonic stem cell self-renewal. *Nature*, *453*(7194), 519–523. https://doi.org/10.1038/nature06968

Yoshida, N., Ikeda, Y., Notomi, S., Ishikawa, K., Murakami, Y., Hisatomi, T., Enaida, H., & Ishibashi, T. (2013). Clinical Evidence of Sustained Chronic Inflammatory Reaction in Retinitis Pigmentosa. *Ophthalmology*, *120*(1), 100–105. https://doi.org/10.1016/j.ophtha.2012.07.006

Young, G. T., Gutteridge, A., Fox, H. D., Wilbrey, A. L., Cao, L., Cho, L. T., Brown, A. R., Benn, C. L., Kammonen, L. R., Friedman, J. H., Bictash, M., Whiting, P., Bilsland, J. G., & Stevens, E. B. (2014). Characterizing Human Stem Cell–derived Sensory Neurons at the Single-cell Level

Reveals Their Ion Channel Expression and Utility in Pain Research. *Molecular Therapy*, *22*(8), 1530–1543. https://doi.org/10.1038/mt.2014.86

Young, T. L., & Cepko, C. L. (2004). A role for ligand-gated ion channels in rod photoreceptor development. *Neuron*, *41*(6), 867–879. https://doi.org/10.1016/s0896-6273(04)00141-2

Yourey, P. A., Gohari, S., Su, J. L., & Alderson, R. F. (2000). Vascular Endothelial Cell Growth Factors Promote the *In Vitro* Development of Rat Photoreceptor Cells. *The Journal of Neuroscience*, *20*(18), 6781–6788. https://doi.org/10.1523/JNEUROSCI.20-18-06781.2000

Yu, J., Vodyanik, M. A., Smuga-Otto, K., Antosiewicz-Bourget, J., Frane, J. L., Tian, S., Nie, J., Jonsdottir, G. A., Ruotti, V., Stewart, R., Slukvin, I. I., & Thomson, J. A. (2007). Induced Pluripotent Stem Cell Lines Derived from Human Somatic Cells. *Science*, *318*(5858), 1917–1920. https://doi.org/10.1126/science.1151526

Yue, F., Johkura, K., Shirasawa, S., Yokoyama, T., Inoue, Y., Tomotsune, D., & Sasaki, K. (2010). Differentiation of primate ES cells into retinal cells induced by ES cell-derived pigmented cells. *Biochemical and Biophysical Research Communications*, *394*(4), 877–883. https://doi.org/10.1016/j.bbrc.2010.03.008

Zerti, D., Collin, J., Queen, R., Cockell, S. J., & Lako, M. (2020). Understanding the complexity of retina and pluripotent stem cell derived retinal organoids with single cell RNA sequencing: Current progress, remaining challenges and future prospective. *Current Eye Research*, *45*(3), 385–396. https://doi.org/10.1080/02713683.2019.1697453

Zerti, D., Dorgau, B., Felemban, M., Ghareeb, A. E., Yu, M., Ding, Y., Krasnogor, N., & Lako, M. (2020). Developing a simple method to enhance the generation of cone and rod photoreceptors in pluripotent stem cell-derived retinal organoids. *STEM CELLS*, *38*(1), 45–51. https://doi.org/10.1002/stem.3082

Zerti, D., Hilgen, G., Dorgau, B., Collin, J., Ader, M., Armstrong, L., Sernagor, E., & Lako, M. (2021). Transplanted pluripotent stem cell-derived photoreceptor precursors elicit conventional and

unusual light responses in mice with advanced retinal degeneration. *STEM CELLS*, *39*(7),

882–896. https://doi.org/10.1002/stem.3365

Zhang, K., Zhang, L., & Weinreb, R. N. (2012). Ophthalmic drug discovery: Novel targets and

mechanisms for retinal diseases and glaucoma. *Nature Reviews Drug Discovery*, *11*(7), 541–

559. https://doi.org/10.1038/nrd3745

Zhang, S. S.-M., Fu, X.-Y., & Barnstable, C. J. (2002). Molecular Aspects of Vertebrate Retinal

Development. *Molecular Neurobiology*, *26*(2–3), 137–152.

https://doi.org/10.1385/MN:26:2-3:137

Zhang, X., Wang, L., Zhang, X., Ren, L., Shi, W., Tian, Y., Zhu, J., & Zhang, T. (2017). The use of

KnockOut serum replacement (KSR) in three dimensional rat testicular cells co-culture

model: An improved male reproductive toxicity testing system. *Food and Chemical

Toxicology*, *106*, 487–495. https://doi.org/10.1016/j.fct.2017.05.001

Zhao, L., Wang, Z., Liu, Y., Song, Y., Li, Y., Laties, A. M., & Wen, R. (2007). Translocation of the retinal

pigment epithelium and formation of sub-retinal pigment epithelium deposit induced by

subretinal deposit. *Molecular Vision*, *13*, 873–880.

Zhong, X., Gutierrez, C., Xue, T., Hampton, C., Vergara, M. N., Cao, L.-H., Peters, A., Park, T. S.,

Zambidis, E. T., Meyer, J. S., Gamm, D. M., Yau, K.-W., & Canto-Soler, M. V. (2014a).

Generation of three-dimensional retinal tissue with functional photoreceptors from human

iPSCs. *Nature Communications*, *5*, 4047. https://doi.org/10.1038/ncomms5047

Zhong, X., Gutierrez, C., Xue, T., Hampton, C., Vergara, M. N., Cao, L.-H., Peters, A., Park, T. S.,

Zambidis, E. T., Meyer, J. S., Gamm, D. M., Yau, K.-W., & Canto-Soler, M. V. (2014b).

Generation of three-dimensional retinal tissue with functional photoreceptors from human

iPSCs. *Nature Communications*, *5*, 4047.

Zuber, M. E., Gestri, G., Viczian, A. S., Barsacchi, G., & Harris, W. A. (2003). Specification of the

vertebrate eye by a network of eye field transcription factors. *Development*, *130*(21), 5155–

5167. https://doi.org/10.1242/dev.00723